Modulating intracellular Ca^{2+} signalling using recombinant fragments of the human cardiac ryanodine receptor (RyR2)

Debra L. Fry

Department of Cardiology
School of Medicine,
Wales Heart Research Institute,
Cardiff University

Supervisors:
Dr. C. H. George
Professor F. A. Lai

CARDIFF UNIVERSITY
PRIFYSGOL CAERDYDD

ProQuest LLC
789 East Eisenhower Parkway
P.O. Box 1346
Ann Arbor, MI 48106-1346

Publications and published abstracts

Clack, A.I., **Fry, D.L.**, Thomas, N.L., Lai, F.A., and George, C.H. (2009). An L433P arrhythmia-linked mutation in RyR2 uncouples agonist-evoked Ca^{2+} release fro homeostatic Ca^{2+} cycling. Biophysics meeting 2009.

George, C.H., **Fry, D.L.**, Jundi, H., Barberini, S.R., and Lai, F.A. (2008). Physical interaction between discrete domains of the cardiac ryanodine receptor is a pivotal mechanism of channel regulation. ESC Winter Research Meeting 2008.

Jundi, H., **Fry, D.L.**, Barberini, S.R., Lai, F.A., and George, C.H. (2008). Suppression of arrhythmogenic Ca^{2+} fluxes in cardiac cells using fragments of human RyR2. Biophysics meeting 2008.

Fry,D.L., Jundi, H., Thomas, N.L., Lai, F.A., and George, C.H. (2007). Modulating intracellular Ca^{2+} signalling using recombinant fragments of the human cardiac ryanodine receptor (RyR2). Biophysics meeting 2007.

George, C.H., Jundi, H., Thomas, N.L., **Fry, D.L.**, and Lai, F.A. (2007). Ryanodine receptors and ventricular arrhythmias: emerging trends in mutations, mechanisms and therapies. J. Mol. Cell Cardiol. 42(1): 34-50.

Acknowledgements

I would like to send special thanks to my supervisor Dr. Christopher George, to whom I am indebted to for all his guidance, advice and of course patience in helping me accomplish this work. Thanks also to Professor Tony Lai for supporting my project and lending helpful comments when appropriate, and to Dr. Spyros Zissimopoulos and Dr. Lowri Thomas for their helpful advice. Thanks to Dr. Lisa Gray for all her help and assistance in flow cytometry, and also to Dr. Chris Pepper for performing FACS analysis. All figures in Chapters 3-7 were generated from my own data, except Figure 3.17 and Appendix I (Dr. Chris George) and Figure 7.10 (Hala Jundi). I would also like to thank Cardiff University, School of Medicine for financially supporting my PhD.

Thanks to Hala Jundi, Lowri Thomas, Laila Guzadhur and Naadiya Docrat for always understanding the situation, for keeping me smiling and for all the laid-back conversations when I needed them, you kept me grounded! Also thanks to everyone at the Wales Heart Research Institute for making my time there one to remember.

And last of all special thanks to Steven Barberini and my parents Susan and Graham Fry for always being there to point me in the right direction, providing cool-head advice, as was often required and for believing in me, all my love.

Abstract

Interaction between discrete domains of the cardiac ryanodine receptor (RyR2) has emerged as a pivotal mechanism regulating channel function. RyR2 mutations perturb conformational intra-molecular constraints that are linked to dysregulated Ca^{2+} release. Previous work from this laboratory identified an interacting- or I-domain of human RyR2 that mediates interaction between the large cytoplasmic assembly and the transmembrane (TM) domain of RyR2. Bioinformatic approaches revealed striking structural homology between sub-fragments of the RyR2 I-domain and I-domain-like regions of inositol 1,4,5-trisphosphate receptors (IP_3R). Acute expression of I-domain sub-fragments in human embryonic kidney (HEK) cells (where the rank order of expression is $IP_3R2 > IP_3R1$) was associated with profound loss of cell viability predominantly via apoptosis. This increase in apoptosis was linked to altered Ca^{2+} cycling (measured using a novel index of Ca^{2+} signal variability) and a remarkable loss of carbachol-evoked Ca^{2+} release. Intriguingly, increased apoptosis and perturbed Ca^{2+} handling was also observed in neighbouring cells that did not express recombinant I-domain proteins - a phenomenon termed the bystander effect. The bystander effect is likely mediated by transfer of signalling molecules via direct cell-to-cell coupling (gap junctions) and via diffusible mediators (extracellular route). This thesis supports the novel concept that IP_3R-mediated Ca^{2+} handling and cellular phenotype can be exquisitely tuned by recombinant fragments of RyR2.

Table of contents

Table of contents 5
Abbreviations 1
Figure Index 7
Table Index 10
Chapter 1 General Introduction 12
1.1. The cardiac ryanodine receptor (RyR2) *12*
1.1.1. Structure and function 15
1.1.2. Targeted phosphorylation of RyR2 16
1.1.3. Channel regulation 21
1.1.3.1. Physiological modulators 21
1.1.3.2. Redox modification 22
1.1.3.3. Pharmacological regulators 23
1.1.4. RyR:RyR inter-tetrameric interaction (arrays) 25
1.1.5. RyR:LTCC organisation 27
1.1.6. RyR intra-subunit interaction 28
1.1.7. Non-contractile aspects of RyR2 function 29
1.2. Excitation-contraction (EC) coupling in the heart *30*
1.2.1. Ultrastructure of cardiac muscle 30
1.2.2. Cardiac action potential 31
1.2.3. Beta- adrenergic (β-AR) pathway 32
1.2.4. CICR and EC coupling 33
1.3. Macromolecular Ca^{2+} signalling network *35*
1.4. Ca^{2+} dysregulation and pathology *44*
1.4.1. Arrhythmic diseases 44
1.4.1.1. Catecholaminergic polymorphic ventricular tachycardia (CPVT) and arrhythmogenic right ventricular cardiomyopathy (ARVC) 44
1.4.1.2. RyR2 mutations 45
1.4.1.3. Heart failure 48
1.4.2. Mechanisms of RyR2-linked arrhythmia 49
1.4.2.1. Defective interdomain interaction 49
1.4.2.2. PKA hyper-phosphorylation of RyR2 and FKBP12.6 dissociation 51
1.4.2.3. SR Ca^{2+} and luminal Ca^{2+} sensitivity 52
1.4.3. Targeting RyR2 as a therapeutic intervention 53
1.4.3.1. Targeting intra-molecular instability 54
1.4.3.2. Targeting redox modification 54
1.5. SR Ca^{2+} release – a second player *56*
1.5.1. Inositol trisphosphate receptor (IP_3R) 56
1.5.1.1. IP_3R channel regulation 60
1.5.1.2. IP_3R phosphorylation 62
1.5.2. Functional and structural similarities between RyR and IP_3R 63
1.6. Thesis principle *64*

Chapter 2 General Materials and Methods **66**

2.1. Materials *66*
2.1.1. Microbiology reagents 66
2.1.2. Molecular biology reagents 67
2.1.2.1. PCR and sequencing 67
2.1.2.2. Agarose gel electrophoresis 68
2.1.2.3. DNA restriction enzymes 68
2.1.2.4. Protein preparation, SDS-PAGE and Western blot 69
2.1.2.5. Antibodies 69
2.1.3. Cell Culture Reagents 71
2.1.3.1. Cell culture assay reagents and kits 71
2.1.4. Ca^{2+} imaging reagents 72

2.2. Methods *74*
2.2.1. Detecting recombinant proteins 74
2.2.1.1. mRFP as a fluorescent fusion protein 75
2.2.1.2. eGFP as a fluorescent fusion protein 75
2.2.2. DNA Cloning 75
2.2.2.1. Generation of plasmid DNA encoding RyR2 I-domain 75
2.2.2.2. Generation of plasmid DNA encoding full-length RyR2 76
2.2.3. Plasmid DNA propagation 77
2.2.3.1. Propagation of I-domain plasmid DNA 77
2.2.3.2. Ultra violet (UV) spectrophotometry 79
2.2.4. Agarose gel electrophoresis 79
2.2.4.1. DNA gel extraction 80
2.2.5. Restriction enzyme digestion 80
2.2.6. PCR and DNA sequencing 81
2.2.7. Mammalian cell culture 84
2.2.7.1. Human embryonic kidney 293 cells (HEK293) 84
2.2.7.2. HL-1 cardiomyocytes 85
2.2.7.3. DNA transfection 86
2.2.7.4. Flow cytometry & fluorescence activated cell sorting (FACS) 88
2.2.8. Confocal laser scanning microscopy (CLSM) 90
2.2.8.1. Fluorescence analysis of fixed cells expressing I-domain 91
2.2.8.2. Immunofluorescent analysis of fixed cells expressing IP_3R 91
2.2.8.3. Intracellular Ca^{2+} imaging 91
2.2.9. Sodium dodecyl sulphate polyacrylamide gel electrophoresis (SDS-PAGE) and Western blotting 94
2.2.9.1. Protein isolation from HEK cells 94
2.2.9.2. SDS-PAGE 96
2.2.9.3. Protein transfer and Western blot 98
2.2.9.4. Protein Stain 99
2.2.9.5. Densitometric quantification of protein and immunoblot signals 99
2.2.10. Statistical Analysis 100

Chapter 3 Phenotypic characterisation of cells expressing recombinant I-domain **102**

3.1. Introduction *102*
3.1.1. Intrinsic interdomain interaction regulates RyR channel function 102
3.1.2. Characterisation of the interacting domain (I-domain) 106
3.1.3. Investigating RyR structure/function using cellular expression systems 110
3.1.3.1. Transient recombinant protein expression 110
3.1.3.2. Stable recombinant protein expression 111

3.1.4. Objective 112
3.2. Methods *113*
3.2.1. Cloning strategy of I-domain constructs 113
3.2.2. HEK transfection with mRFP tagged I-domain constructs 117
3.2.3. Assessment of cell proliferation and metabolism 117
3.2.4. Assessing cell viability using Trypan blue 120
3.2.5. Immunoblotting of recombinant protein isolated from HEK cells 121
3.2.6. G418-mediated selection of cells expressing recombinant I-domain 121
3.3. Results *125*
3.3.1. Generation of I-domain constructs 125
3.3.2. I-domain localisation is not dependent on cellular expression of RyR2 125
3.3.3. Prolonged I-domain expression profoundly alters cell phenotype 130
3.3.4. I-domain expression is associated with reduced cell viability 132
3.3.5. I-domain expression reduces cell proliferation 133
3.3.6. Cellular metabolism was altered in cells expressing recombinant I-domain 133
3.3.7. I-domain elimination was confirmed by immunoblot 136
3.3.8. I-domain elimination and associated toxicity was independent of expression vector 136
3.4. Discussion *139*
3.4.1. Expression of recombinant I-domain subfragments exhibited unexpected cellular localisation and phenotypic alteration 139
3.4.2. Reduced cell viability correlated with expression of recombinant I-domain protein 140
Chapter 4 I-domain expression induces apoptosis 142
4.1. Introduction *142*
4.1.1. Routes of cell demise 142
4.1.2. Objective 144
4.2. Methods *145*
4.2.1. Flow cytometric quantification of mRFP-expressing cell populations 145
4.2.2. FACS enrichment of cell populations expressing recombinant ID protein 145
4.2.3. Analysis of mode of death in cell populations 146
4.2.3.1. Control for Ca^{2+}-linked apoptosis 147
4.3. Results *149*
4.3.1. Flow cytometry reveals a potential link between I-domain expression and apoptosis 149
4.3.2. Fluorescence activated cell sorting (FACS) failed to enrich recombinant I-domain expression 151
4.3.3. I-domain expression induced apoptotic cell death 154
4.4. Discussion *158*
4.4.1. Constitutive cellular I-domain expression triggers apoptosis 158
4.4.2. I-domain associated abnormal phenotype was extended to neighbouring untransfected cells (NUCs) 159
Chapter 5 Investigating the effects of I-domain expression on Ca^{2+} release channels in HEK cells 161
5.1. Introduction *161*
5.1.1. Ca^{2+} dependent cell death pathways 161
5.1.2. The role of IP_3R in apoptosis 162
5.1.3. Monitoring intracellular Ca^{2+} signalling using fluorescent Ca^{2+} indicators 165

5.1.4. Objective 166

5.2. Methods *167*
5.2.1. Cellular Ca^{2+} imaging using fluo-4 and CLSM 167
5.2.2. Analysis of agonist-induced Ca^{2+} transients 167
5.2.2.1. Ca^{2+} transient characterisation 170
5.2.3. Understanding the effect of PMT voltage on fluorescent signals 172
5.2.4. Using thapsigargin to estimate ER Ca^{2+} store content 173
5.2.5. Calibration of resting Ca^{2+} levels 173
5.2.6. Immunoblot and immunofluorescence analysis of Ca^{2+} handling proteins 174
5.2.7. Generation of ^{eGFP}RyR2 plasmid DNA 175
5.2.8. RyR2:ID^B co-transfection into HEK cells 176
5.2.9. Immuno-localisation of RyR2 and ID^B in HEK cells 176
5.2.10. Elucidating ID^B function in the presence of recombinant RyR2 176

5.3 Results *178*
5.3.1. PMT voltage is a critical determinant of fluorescence signal intensity 178
5.3.2. I-domain expression alters cellular Ca^{2+} handling 179
5.3.2.1. Recombinant I-domain expression does not significantly elevate $[Ca^{2+}]_i$ 179
5.3.2.2. Cells expressing I-domain constructs exhibit reduced ER Ca^{2+} load 180
5.3.3. I-domain expression reduced IP_3R agonist responses 180
5.3.4 Alterations in cellular levels of Ca^{2+} handling proteins following I-domain expression 188
5.3.4.1 Altered expression of ER Ca^{2+} handling proteins following I-domain expression 188
5.3.4.2. I-domain co-localises with IP_3R type 1 but not type 2 190
5.3.4.3. ID^B downregulates IP_3R type 1, but not type 2 – a cellular analysis 194

5.4. Discussion *196*
5.4.1. I-domain expression alters intracellular Ca^{2+} handling 196
5.4.2. Expression of recombinant I-domain revealed NUC death via the 'bystander effect' 198

Chapter 6 Exploring the subtleties of intracellular Ca^{2+} handling – assessment of Ca^{2+} signal variability 200

6.1. Introduction *200*
6.1.1. Assessment of cellular Ca^{2+} handling 200
6.1.2. Objective 202

6.2. Methods *203*
6.2.1. Analysis of temporal Ca^{2+} cycling 203
6.2.1.1. Quantification of Ca^{2+} signal variability 203
6.2.2. Ca^{2+} signal variability in RyR2:ID^B expressing HEK cells 205

6.3. Results *206*
6.3.1. Assessment and determination of Ca^{2+} signal variability 206
6.3.1.1. Why variance-based methods cannot be used to decode intracellular Ca^{2+} signal variability in these experiments 206
6.3.2. Elevated SV^m was exhibited by I-domain expressing cells 210
6.3.3. ID expression suppressed IP_3R-dependent post-activational Ca^{2+} signal variability 211
6.3.4. ID^B does not alter carbachol-evoked responses in HEK cells 212
6.3.5. ID^B does not modulate post-activational RyR2 Ca^{2+} signalling 213

6.4. Discussion *215*

6.4.1. Determination of Ca^{2+} signal variability using SV^m 215
6.4.2. Altered Ca^{2+} signal variability induced by the I-domain 215
6.4.3. ID^B increases basal Ca^{2+} signal variability of RyR2 216

Chapter 7 Elucidating signalling pathways underpinning ID^B cytotoxicity 218

7.1. Introduction 218
7.1.1. The mechanisms of cell-to-cell communication 218
7.1.2. Intercellular signal transduction mechanisms 220
7.1.3. Direct cell-to-cell coupling via gap junctions 222
7.1.4. Cell signalling mediated by connexin hemichannels 222
7.1.5. Objective 223

7.2. Methods 225
7.2.1. Confocal analysis of Ca^{2+} handling following ID^B expression 225
7.2.1.1. Design of media transfer assays 225
7.2.1.2. Hydrolysis of extracellular ATP using apyrase 226
7.2.1.3. Scavenging reactive oxygen species (ROS) using edaravone 226
7.2.2. Measurement of extracellular ATP 227

7.3. Results 228
7.3.1. ID^B media transfer did not alter Ca^{2+} handling 228
7.3.2. Extracellular ATP was unaltered in cells expressing ID^B 230
7.3.2.1. Hydrolysis of extracellular ATP did not affect intracellular Ca^{2+} handling in bystander cells 231
7.3.3. Scavenging free radicals did not rescue dysfunctional Ca^{2+} handling in ID^B transfected cells 232
7.3.4. HEK cells communicate via gap junctions 232

7.4. Discussion 234
7.4.1. Bystander cell death was not mediated by ATP 234
7.4.2. ROS did not mediate the bystander effect 235

Chapter 8 General Discussion 237

8.1. Localisation of I-domain constructs is not dependent on cellular expression of RyR2 237

8.2. I-domain expression induced apoptosis 237

8.3. IP_3R agonist-induced responses are profoundly diminished by I-domain constructs. 238

8.4. Decoding of intracellular Ca^{2+} handling 240

8.5. I-domain expression and the bystander effect 240

8.6. Pathways underlying ID^B induced cytotoxicity 241

8.7. Further work and future direction 242

8.8 Practical limitations 242

Appendix I 245

Appendix II 253

Appendix III 255

Bibliography 258

Abbreviations

2D	two dimensional
3D	three dimensional
A	adenine
Å	Ångström
α	alpha
a.a.	amino acid
AC	adenylate cyclase
AF	atrial fibrillation
AKAP	A kinase anchoring protein
Akt	protein kinase B
AM	acetoxymethyl
ANOVA	analysis of variance
AOBS	acousto-optical beam splitter
APAF	apoptosis activating factor
ARVC	arrhythmogenic right ventricular cardiomyopathy
ARVD	arrhythmogenic right ventricular dysplasia
ATP	adenosine trisphosphate
β	beta
β-AR	beta adrenergic receptor/pathway
BCA	bicinchoninic acid
BFP	blue fluorescent protein
BSA	bovine serum albumin
C	cytosine
Ca^{2+}	ionised (free) calcium
$[Ca^{2+}]_i$	intracellular free calcium concentration
cADPR	cyclic adenine diphosphate ribose
CaM	Calmodulin
CaMKII	calcium/calmodulin-dependent protein kinase
CAMP	cyclic adenine monophosphate
$CaPO_4$	calcium phosphate
CARP	carbonic anhydrase related protein
CCD	central core disease
cDMEM	complete Dulbecco's modified Eagle medium
cDNA	complementary DNA
CFP	cyan fluorescent protein
CGA	chromogranin A
CGB	chromogranin B
CHO	Chinese hamster ovary cells

CICR	calcium-induced calcium release
Cl^-	chloride ion
CLSM	confocal laser-scanning microscopy
CM	cardiomyocyte
CMV	cytomegalovirus
CoV	coefficient of variation
CPVT	catecholaminergic polymorphic ventricular tachycardia
CSQ	calsequestrin
Cu^{2+}	copper
Cy3	cyanine 3
°C	degrees (Celsius)
DAD	delayed after-depolarisation
DAG	diacylglycerol
dATP	deoxyadenosine triphosphate
ddNTP	dideoxynucleotide triphosphate
dF/dT	change in fluorescence over time (gradient or 'drift')
DICR	depolarisation-induced calcium release
DMEM	Dulbecco's modified Eagle medium
DMSO	dimethyl sulphoxide
DNA	deoxyribonucleic acid
DNase	deoxyribonuclease
dNTP	deoxynucleotide triphosphate
DP	domain peptide
DPSS	diode-pumped solid-state laser
DR1-3	divergent regions 1-3
DsRed	*Discosoma sp.* red fluorescent protein
DTT	dithiothreitol
EAD	early after-depolarisation
ECC	excitation-contraction coupling
EC	excitation contraction
ECG	electrocardiogram
EDTA	ethylenediaminetetraacetic acid
EGTA	ethyleneglycoltetraacetic acid
eGFP	enhanced green fluorescent protein
EM	electron microscopy
ER	endoplasmic reticulum
EtBr	ethidium bromide
FACS	fluorescence activated cell sorting
FBS	foetal bovine serum
FKBP	FK506 binding protein
F	fluorescent signal at any time

FM	femtomoles per litre
F_{min}	minimum fluorescent signal
F_{max}	maximum fluorescent signal
FP	fluorescent protein
FRET	fluorescence resonance energy transfer
FSC	forward scatter
g	gravity
G	gram
G	guanine
γ	gamma
G418	geneticin 418 sulphate
GFN	gelatin / fibronectin
GFP	green fluorescent protein
GSH/GSSG	glutathione
H	hour
H_2O	water
H_2O_2	hydrogen peroxide
HCl	hydrogen chloride
HBSS	hepes buffered salt solution
HCl	hydrochloric acid
HEK	human embryonic kidney cells
HF	heart failure
HRP	horse radish peroxidase
I_{Ca}	inward calcium current
ICD	implantable cardiac defibrillator
ID	interacting domain; 3722-4610
ID^A	interacting domain A; 3722-4353
ID^B	interacting domain B; 4353-4499
ID^C	interacting domain C; 4353-4610
I-domain	ID, ID^A, ID^B, ID^C
I_{CRAC}	calcium release activated current
IICR	IP_3-induced calcium release
IP_3	inositol trisphosphate
IP_3R	inositol trisphosphate receptor
IRBIT	IP_3 binding protein released with IP_3
JCN	junctin
K^+	ionised (free) potassium
KCl	potassium chloride
K_d	dissociation constant
KDS	potassium dodecyl sulphate
KDa	kilo Dalton

KH_2PO_4	potassium dihydrogen phosphate
KI	knock-in
KO	knock-out
L	litre
LB	Luria-Bertani
LIZ	leucine/isoleucine zipper
LQTS	long Q-T syndrome
LTCC	L-type calcium channel
LY	Lucifer yellow
M	moles per litre
mAKAP	muscle A kinase anchoring protein
MCS	multiple cloning site
MH	malignant hyperthermia
min	minute
ml	millilitre
mM	millimoles per litre
MOPS	morpholinopropane sulfonic acid
mRFP	monomeric red fluorescent protein
MW	molecular weight
N	nucleus
Na^+	ionised (free) sodium
Na_2HPO_4	disodium phosphate anhydrous
NAADP	nicotinic acid adenine dinucleotide phosphate
$NADH/NAD^+$	nicotinamide adenine dinucleotides
NaOH	sodium hydroxide
NaCl	sodium chloride
NCX	sodium calcium exchanger
ND	not determined
nm	nanometre
nM	nanomoles per litre
NO	nitric oxide
NUC	neighbouring untransfected cells
$O_2^{\bullet-}$	superoxide anion radicals
OD	optical density
$OH^{\bullet}$	hydroxyl radicals
PBS	phosphate buffered saline
PCR	polymerase chain reaction
PCD	programmed cell death
PDE	phosphodiesterase
pH	-log concentration of H^+ ions
PIP_2	phosphatidyl inositol bisphosphate

PKA	cAMP-dependent protein kinase
PKB	protein kinase B
PKC	protein kinase C
PKG	protein kinase G
PLB	phospholamban
PLC	phospholipase C
pM	picomoles per litre
PM	plasma membrane
PMA	phorbol 12-myristate 13-acetate
PMCA	plasma membrane calcium ATPase
PMT	photomultiplier tube
PNS	post-nuclear supernatant
P_o	channel open probability
PP1	protein phosphatase 1
PP2A	protein phosphatase 2a
PTP	permeability transition pore
PVC	premature ventricular contraction
PVDF	polyvinylidene difluoride
rL/L	recombinant Luciferin/Luciferase
ROI	region of interest
RNase	ribonuclease
RNS	reactive nitrogen species
ROS	reactive oxygen species
RPM	rotations per minute
RSV	relative signal variability
RT	room temperature
rTdT	recombinant terminal deoxynucleotidyl transferase
RyR	ryanodine receptor
RyR1	skeletal muscle ryanodine receptor (type 1)
RyR2	cardiac muscle ryanodine receptor (type 2)
RyR3	ryanodine receptor (type 3)
S2808	serine 2808
S2815	serine 2815
SCD	sudden cardiac death
SD	standard deviation
SDS	sodium dodecyl sulphate
SDS-PAGE	sodium dodecyl sulphate polyacrylamide gel electrophoresis
Sec	second
SEM	standard error of the mean
SERCA	sarco/endoplasmic reticulum calcium ATPase
SOC	store operated channels

SOICR	store overload-induced calcium release
SOPMA	self-optimised prediction method with alignment
SR	sarcoplasmic reticulum
SSC	side scatter
SV	signal variability
SV_A	pre-agonist signal variability
SV_B	post-agonist signal variability
SV^m	signal variability normalised to mean fluorescence
T	thymine
TA	transmembrane assembly
TAE	tris-acetate-EDTA
TBS	tris-buffered saline
TBS-T	tris-buffered saline and 0.1% (v/v) Tween-20
TEMED	tetramethylethylenediamine
TM	transmembrane domain
TRD	triadin
TRITC	tetramethyl rhodamine isothiocyanate
µl	microlitre
µm	micrometer
UV	ultraviolet
VF	ventricular fibrillation
VGCC	voltage gated calcium channels
VT	ventricular tachycardia
v/v	volume by volume
WT	wild-type
w/v	weight by volume
YFP	yellow fluorescent protein

Figure Index

Chapter	Figure	Title
1	1.1	Three dimensional reconstruction of RyR2
	1.2	Targeted phosphorylation of RyR2
	1.3	Proposed RyR2 phosphorylation sites
	1.4	RyR2 Ca^{2+} binding sites
	1.5	Physical association of RyR tetramers
	1.6	Functional coupling of RyR tetramers
	1.7	Skeletal and cardiac arrangements of LTCC and RyR channels
	1.8	RyR2 array-formation displaying potential I-domain epitopes and FKBP binding site
	1.9	Cardiac muscle ultrastructure
	1.10	Phases of the cardiac action potential (AP)
	1.11	Calcium-induced calcium release (CICR) triggers muscle contraction
	1.12	Macromolecular Ca^{2+} signalling network
	1.13	CPVT-linked RyR2 mutations cluster within functional domains
	1.14	Store-overload induced calcium release (SOICR)
	1.15	Schematic representation of IP_3R structure (based on mouse IP_3R1)
2	2.1	DNA ladder for agarose gel electrophoresis
	2.2	Typical DNA sequence trace
	2.3	HEK293 cells
	2.4	HL-1 cardiomyocytes
	2.5	Principle of Effectene-based transfection
	2.6	Schematic representation of flow cytometric and FACS analysis
	2.7	SP5 confocal laser-scanning microscopy (CLSM) principle
	2.8	BSA protein assay standard
	2.9	SDS-PAGE and protein transfer
3	3.1	Schematic representation of RyR 'unzipping' hypothesis
	3.2	Mutations in RyR1 and RyR2 map to sites of interdomain interaction
	3.3	Sites of intra-molecular interaction
	3.4	I-domain conformation and the loci of disease-linked mutations
	3.5	pmRFP-C1 restriction enzyme map
	3.6	Schematic representation of pmRFP-C1 I-domain plasmid construction and I-domain constructs in relation to the predicted RyR2 transmembrane domain topology
	3.7	Identification of pmRFP-C1 I-domain cloning by restriction digestion

	3.8	Sequencing of I-domain constructs in pmRFP-C1
	3.9	Absorbance measurements at 560nm and 600nm of alamarBlue in cDMEM (10% v/v)
	3.10	alamarBlue measurement of cell proliferation
	3.11	Cell viability using Trypan blue
	3.12	G418 and hygromycin dose-dependent elimination of non-resistant cell populations
	3.13	Cloning strategy for I-domain into pcDNA3.1 hygromycin
	3.14	Restriction digestion of pcDNA3.1 I-domain constructs
	3.15	Transient transfection of I-domain constructs in HEK293 cells
	3.16	Cellular localisation of I-domain constructs in HEK and HL-1 cells
	3.17	C15Y, a CFP:YFP tandem expressed in HL-1 cardiomyocytes exhibits pronounced nuclear localisation
	3.18	Comparison of cytoplasmic and nuclear fluorescence
	3.19	Effect of I-domain expression on cell size
	3.20	Cellular phenotypic observations
	3.21	Cell viability following I-domain transfection
	3.22	Proliferation of HEK, mRFP and I-domain expressing cells
	3.23	Cell metabolism assessed by alamarBlue
	3.24	Progressive elimination of I-domain confirmed by immunoblotting
	3.25	Phenotype of HEK cells expressing mRFP and ID^B in pcDNA3.1
4	**4.1**	Intrinsic and extrinsic apoptosis pathways
	4.2	Flow cytometric quantification and phenotypic analysis during I-domain elimination
	4.3	FACS enrichment of ID and mRFP-positive cell populations
	4.4	FACS histograms of mRFP-expressing cell populations
	4.5	I-domain expression was associated with an increase in apoptosis
	4.6	PMA-induced apoptosis in HEK cells
	4.7	I-domain expression induces apoptosis
5	**5.1**	Ca^{2+}-associated apoptosis pathways
	5.2	Schematic representation of signalling pathways triggered by carbachol
	5.3	Carbachol-induced Ca^{2+} transients in HEK cells loaded with fluo-4
	5.4	Heterogeneity of carbachol-evoked Ca^{2+} transients
	5.5	Schematic representation of analysis parameters implemented in assessment of Ca^{2+} release
	5.6	Fluorescence intensity depends on voltage
	5.7	Typical thapsigargin response
	5.8	pcDNA3-^{eGFP}RyR2 plasmid

	5.9	Snapshot of HEK cells expressing RyR2:ID^B exposed to 10mM caffeine
	5.10	Voltages used for Ca^{2+} imaging experiments on I-domain cells
	5.11	Elevated $[Ca^{2+}]_i$ in mRFP and I-domain expressing cells
	5.12	ER Ca^{2+} load estimated by thapsigargin
	5.13	Absence of agonist-induced responses in ID^C expressing cells and NUC
	5.14	Non-responsive transfected cells and NUCs to carbachol
	5.15	Distance of NUC from transfected cells was not associated with the magnitude of Ca^{2+} release evoked by 1mM carbachol
	5.16	Transient types of carbachol and caffeine responsive cells
	5.17	Characterisation of 1mM carbachol-induced Ca^{2+} release in I-domain expressing HEK cells and NUCs
	5.18	Mean carbachol-evoked response against mean thapsigargin-evoked response
	5.19	Endogenous levels of IP_3R1, IP_3R2, SERCA2 and calreticulin
	5.20	Immunofluorescence of endogenous levels of IP_3R1 in mRFP and I-domain expressing cells
	5.21	RyR2:ID^B co-localisation
	5.22	IP_3R2 does not co-localise with I-domain fragments
	5.23	I-domain and IP_3R type 1 and type 2 co-localisation
	5.24	ID^B expression is associated with the downregulation of IP_3R1 in single cells
6	**6.1**	Versatility of Ca^{2+} signalling
	6.2	Variability in Ca^{2+} signals
	6.3	Definition of signal variability (SV)
	6.4	Calculation of RSV and the utility of SV^m
	6.5	Example Ca^{2+} traces displaying 'drift' or gradient (dF/dT)
	6.6	Correlation between commonly used operations and fluorescence signals
	6.7	Correlation between common indices of signal variability and gradient (dF/dT), or 'drift'
	6.8	Signal variability (SV) normalised to mean fluorescence (SV^m) is independent of fluorescence and gradient (dF/dT)
	6.9	SV^m is elevated in I-domain expressing cells and NUC, and in cells co-expressing RyR2:ID^B
	6.10	RSV of carbachol-induced Ca^{2+} release (1mM) in I-domain expressing HEK cells and neighbouring untransfected cells (NUC)
	6.11	RSV and peak carbachol-induced transient height of ID^B expressing cells
	6.12	RSV of cells exposed to caffeine
	6.13	ID^B does not alter caffeine-induced RSV in HEK cells

7	7.1	Gap junction and hemichannel formation
	7.2	Schematic of media transfer experiments
	7.3	Structure of edaravone
	7.4	SV^m of cells exposed to 24-h ID^B media for 1, 6 and 24 h
	7.5	Cell viability following mRFP and ID^B media transfer
	7.6	ATP standard curve
	7.7	ATP released by ID^B expressing cells normalised to mRFP
	7.8	Apyrase exposed mRFP and ID^B cells
	7.9	Edaravone exposed mRFP and ID^B cells
	7.10	Lucifer yellow (LY) dye transfer in HEK cells
8	8.1	Schematical representation of I-domain-induced intracellular Ca^{2+} dysregulation

Table Index

Chapter	Table	Title
1	1.1	Summary of differences between the three RyR isoforms
	1.2	Summary of RyR genetically modified mice
	1.3	Functional modulation of RyR2 by phosphorylation
	1.4	Functional modulation of RyR2 by dephosphorylation
	1.5	RyR physiological and pharmacological regulators
	1.6	Summary of functional studies exploring the roles of EC coupling-related proteins
	1.7	Characterisation of RyR2 mutations
	1.8	Functional characteristics of IP_3R isoforms
	1.9	Functional and physical association of key proteins in IP_3R regulation
	1.10	Main physiological and pharmacological regulators of IP_3R
	1.11	Functional regulation of IP_3R by kinases and phosphatases
2	2.1	Restriction enzymes and recognition sequences
	2.2	Restriction enzyme reactions
	2.3	PCR reaction
	2.4	Composition of SDS-PAGE separating and stacking mini-gels
3	3.1	Nomenclature and functional basis of I-domain constructs

Chapter 1

General Introduction

Chapter 1 General Introduction

1.1. The cardiac ryanodine receptor (RyR2)

The ryanodine receptor (RyR) is the largest known membrane protein (~2.3MDa) located on the sarco-/endoplasmic reticulum (SR/ER) of both muscle and non-muscle cells (Lai *et al.*, 1988; Fleischer and Inui, 1989). RyRs are intracellular ion channels that release Ca^{2+} from intracellular stores to regulate a vast number of cellular processes that includes muscle contraction, neuronal function and fertilisation (Miyazaki *et al.*, 1992; Furuichi *et al.*, 1993; Gorza *et al.*, 1993; Newton *et al.*, 1994; Fujino *et al.*, 1995; Giannini *et al.*, 1995).

The RyR is a tetrameric protein, where each subunit is comprised of ~5000 amino acids. The cytosolic N-terminus and luminal C-terminus constitute approximately 90% and 10% of the protein structure, respectively (Tunwell *et al.*, 1996) (See Figure 1.1). Three RyR isoforms have been identified (RyR1, RyR2 and RyR3) that bear functional and structural similarity; however, despite relatively high sequence homology (~66%), isoform-specific differences underpin their relative function and tissue distribution (Otsu *et al.*, 1990; Fill and Copello, 2002; Xiao *et al.*, 2002; Meissner, 2004). These functional differences between RyR1, 2 and 3 are possibly mediated by three regions of sequence divergence (DR1, 2 and 3) and are summarised in Table 1.1.

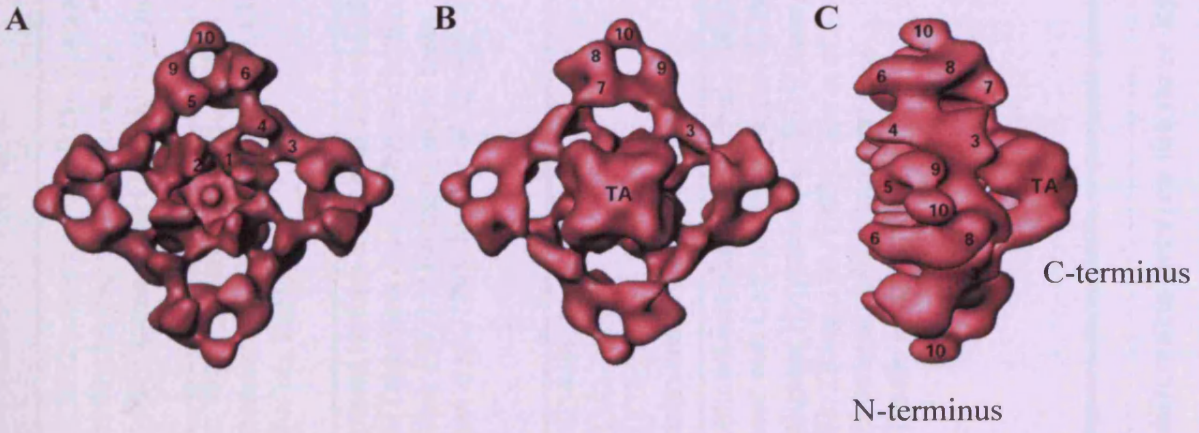

Figure 1.1 Three-dimensional reconstruction of RyR2

Three-dimensional (3D) reconstruction of RyR2 obtained by cryo-electron microscopy (cryo-EM) studies and single particle image processing, a technique that generates a 3D image based on the averaging of thousands of images. Perspectives displayed are **A**, cytoplasmic; **B**, transmembrane assembly (TA); **C**, side view. Numerical arrangements (1-10) represent established structural globular-shaped domains (Radermacher *et al.*, 1994) in the folded 3D protein structure of RyR2 although the primary sequences that form these structures remain unknown.

Modified from Sharma *et al.* 2006.

	RyR1	RyR2	RyR3
Monomer size	Human: 5032 amino acids, 564kDa (Zorzato *et al.*, 1990); Mouse: 5035 amino acids; Rabbit: 5037 amino acids, (Takeshima *et al.*, 1989)	Human: 4967 amino acids, 565kDa (Tunwell *et al.*, 1996); Mouse: 4966 amino acids; Rabbit: 4969 amino acids, 565kDa (Otsu *et al.*, 1990)	Human: 4870 amino acids, 552kDa (Leeb and Brenig, 1998); Mouse: 4888 amino acids; Rabbit: 4872 amino acids, 552kDa (Hakamata *et al.*, 1992)
Gene locus	Human: 19q13 (MacKenzie *et al.*, 1990; MacLennan *et al.*, 1990); Mouse: 7A2-7A3 (Mattei *et al.*, 1994)	Human: 1q42-43 (Otsu *et al.*, 1993; Swan *et al.*, 1999) Mouse: 13A1-13A2 (Mattei *et al.*, 1994)	Human: 15q14-15 (Sorrentino *et al.*, 1993); Mouse: 2E5-2F3 (Mattei *et al.*, 1994)
Expression distribution	Predominant isoform in skeletal and smooth muscle (Takeshima *et al.*, 1989; Sorrentino and Volpe, 1993). Also expressed in brain (Giannini *et al.*, 1995; Mori *et al.*, 2000)	Predominantly expressed in cardiac muscle (Lai *et al.*, 1987; Lai *et al.*, 1988; Sorrentino and Volpe, 1993) and brain (Giannini *et al.*, 1995; Mori *et al.*, 2000)	Always co-localised with other isoforms, RyR3 has a low expression yet broad tissue distribution including brain (Lai *et al.*, 1992; Giannini *et al.*, 1995; Mori *et al.*, 2000) and diaphragm (Sorrentino and Volpe, 1993; Jeyakumar *et al.*, 1998)
Divergent Regions (DR1-3) in human RyR	**DR1:** 4254-4631 **DR2:** 1342-1403 **DR3:** 1872-1923 (Sorrentino and Volpe, 1993)	**DR1:** 4210-4562 (Liu *et al.*, 2002) **DR2:** 1353-1397 (Liu *et al.*, 2004) **DR3:** 1852-1890 (Sorrentino and Volpe, 1993; Zhang *et al.*, 2003)	**DR1**: 4100-4400 (Williams *et al.*, 2001) **DR2**: absent (Williams *et al.*, 2001) **DR3**: undefined (Coronado *et al.*, 1994; Marziali *et al.*, 1996)
Number of gene mutations linked to disease	>80 dominant mutations (Zhou *et al.*, 2006) associated with Central Core Disease (CCD) and Malignant Hyperthermia (MH) (Quane *et al.*, 1993; Zhang *et al.*, 1993; Zhou *et al.*, 2006; Zhou *et al.*, 2007; Anderson *et al.*, 2008; Tanabe *et al.*, 2008).	>71 (Inherited arrhythmias database). Catecholamine polymorphic ventricular tachycardia (CPVT) (Priori *et al.*, 2001). Arrhythmogenic right ventricular dysplasia (ARVD2) (Tiso *et al.*, 2001). Heart failure (HF) (Brillantes *et al.*, 1992; Schumacher *et al.*, 1995). HF has not yet been linked to mutations. Clinical phenotypes such as sino-atrial (SA) node & atrio-ventricular (AV) node dysfunction and atrial fibrillation (AF) (Bhuiyan *et al.*, 2007b).	> 40 (Dettling *et al.*, 2004), however no direct link to disease. Putative association with Alzheimer's disease (Kelliher *et al.*, 1999; O'Neill *et al.*, 2001).

Table 1.1. Summary of differences between the three RyR isoforms

	Knock-out mouse models	Transgenic/knock-in mouse models
RyR1	Severe skeletal abnormalities and perinatal death in mice lacking functional RyR1 (Takeshima *et al.*, 1994a)	Mice homozygous for MH mutation Y522S exhibited skeletal defects and perinatal death, whereas heterozygousity causes muscle dysfunction and MH susceptibility (Chelu *et al.*, 2006; Durham *et al.*, 2008)
		Heterozygous mice harbouring the R163C mutation displayed MH phenotype (Yang *et al.*, 2006a)
RyR2	Death at embryonic day 10 in mice lacking RyR2 gene (Takeshima *et al.*, 1998)	Mice harbouring CPVT mutation R4496C were predisposed to caffeine/isoproterenol- induced VT and VF (Cerrone *et al.*, 2005; Liu *et al.*, 2006)
		R176Q mutation induced VT and cardiomyopathy (Kannankeril *et al.*, 2006)
		Ex vivo hearts from heterozygous and homozygous P2328S mice mutation displayed VT (Goddard *et al.*, 2008)
		Mice harbouring three amino acid mutations in RyR2 CaM binding site (W3587A/ L3591D/ F3603A) died by day 16. Hearts displayed reduced CaM inhibition, decreased RyR2 protein and disrupted Ca^{2+} cycling (Yamaguchi *et al.*, 2007)
		RyR2-S2808A mutant mice were moderately less vulnerable to HF progression attributable to ablated S2808 PKA phosphorylation site (Wehrens *et al.*, 2006), but this has not been reproduced by others (Benkusky *et al.*, 2007)
RyR3	No gross abnormalities but evidence of neurological dysfunction as a result of increased locomotor activity (Takeshima *et al.*, 1996)	Not characterised

Table 1.2. Summary of RyR genetically modified mice

1.1.1. Structure and function

RyRs were first visualised as 'foot structures' on the SR (Campbell *et al.*, 1980; Franzini-Armstrong, 1980) that formed a junctional complex with voltage-gated Ca^{2+} channels (VGCC) on T-tubules (Lai *et al.*, 1987; Block *et al.*, 1988). RyRs were subsequently identified following specific high-affinity binding of the alkaloid ryanodine (isolated from the South American shrub *Ryania speciosa)* (Pessa h *et al.*, 1985). The pivotal role of RyR channels is summarised in Table 1.2.

RyRs are characterised by structural and functional complexity. The N- and C-terminal domains are host to a myriad of regulatory binding sites critical for normal function. Dynamic modulation of the channels is attributable to a number of distinct functional domains that reside within the RyR N-terminus, whereas the predominant function of the C-terminus is to form the Ca^{2+} releasing pore (MacKrill, 1999). The pore is approximately 3Å wide (Tu *et al.*, 1994) and 10.4Å long (Tinker and Williams, 1995) and is proposed to comprise between six and ten transmembrane (TM) spanning domains per monomer (Zorzato et al., 1990; Tunwell et al., 1996; Du et al., 2002b). The confusion as to the precise number of TM domains has stemmed from their identification via hydropathy analysis. Although latter studies have used experimental strategies to address this issue (Du et al., 2002a) it is difficult to predict whether hydrophobic-rich regions actually embed within the membrane or are non-integral 'membrane associated' domains. It has been suggested that a number of the TM domains in the 10TM model proposed by Zorzato *et al.* (Zorzato *et al.*, 1990) formed hairpin loops and did not span the entire membrane (Balshaw et al., 1999; Williams et al., 2001; Du et al., 2002a). The precise RyR TM arrangement remains unclear, although current imaging-based research predicts assemblies comprising more than 10 domains (Takeshima et al., 1989; Zorzato et al., 1990; Tunwell et al., 1996; Du et al., 2002a; Ludtke et al., 2005; Samso et al., 2005).

RyRs are possibly retained in ER/SR membranes by a TM retention signal localised to residues 4918-4943 in RyR1 (Bhat and Ma, 2002b). This putative retention motif lies within a distal TM domain (Takeshima *et al.*, 1989) conserved across RyR isoforms and species (Takeshima *et al.*, 1994b). In contrast, compelling findings place the membrane retention signal within the first TM domain (Meur *et al.*, 2007), which is consistent with IP_3R targeting to the ER (via TM1 and 2) (Parker *et al.*, 2004). Taken together, this indicates a structural significance of the first two TM domains in membrane retention. The significance of these TM domains is considered further in Chapter 3.

1.1.2. Targeted phosphorylation of RyR2

RyR channels are substrates for a wide range of kinases and phosphatases (Figure 1.2 and Tables 1.3 and 1.4). Three highly conserved regions on the cytoplasmic face of RyR2 serve as kinase and phosphatase attachment sites, referred to as leucine/isoleucine zipper (LIZ) motifs (Marx *et al.*, 2001b). Ca^{2+}/calmodulin-dependent protein kinase II (CaMKII) and cAMP-dependent protein kinase A (PKA) are intricately involved in RyR regulation, although the precise details as to how they regulate RyR is of much dispute (Wehrens *et al.*, 2004b; Ai *et al.*, 2005; Xiao *et al.*, 2005; Guo *et al.*, 2006; Ferrero *et al.*, 2007).

PKA. Tetrameric protein (two regulatory/two catalytic subunits) (Foss *et al.*, 1994). Associates with mAKAP and binds RyR2 via LIZ3 (Colledge and Scott, 1999). During adrenergic stress, PKA phosphorylates RyR2 increasing P_o and enhancing contractility (Marx *et al.*, 2000).

S2808 and S2815 phosphorylation sites in hRyR2. S2808 and S2815 are proposed PKA and CaMKII sites respectively (Marx *et al.*, 2000; Wehrens *et al.*, 2004b). S2030 has also been suggested as a PKA site (Xiao *et al.*, 2005). Additional CaMKII sites also proposed (Rodriguez *et al.*, 2003).

PP2A and PP1 bind RyR2 via adaptor proteins PR130 (LIZ2) and Spinophilin (LIZ1), respectively (Bers, 2004). Dephosphorylates RyR2 channels (Zhao *et al.*, 1998) to regulate closed state (Marx *et al.*, 2000). PP1 also suggested to increase P_o (Terentyev *et al.*, 2003).

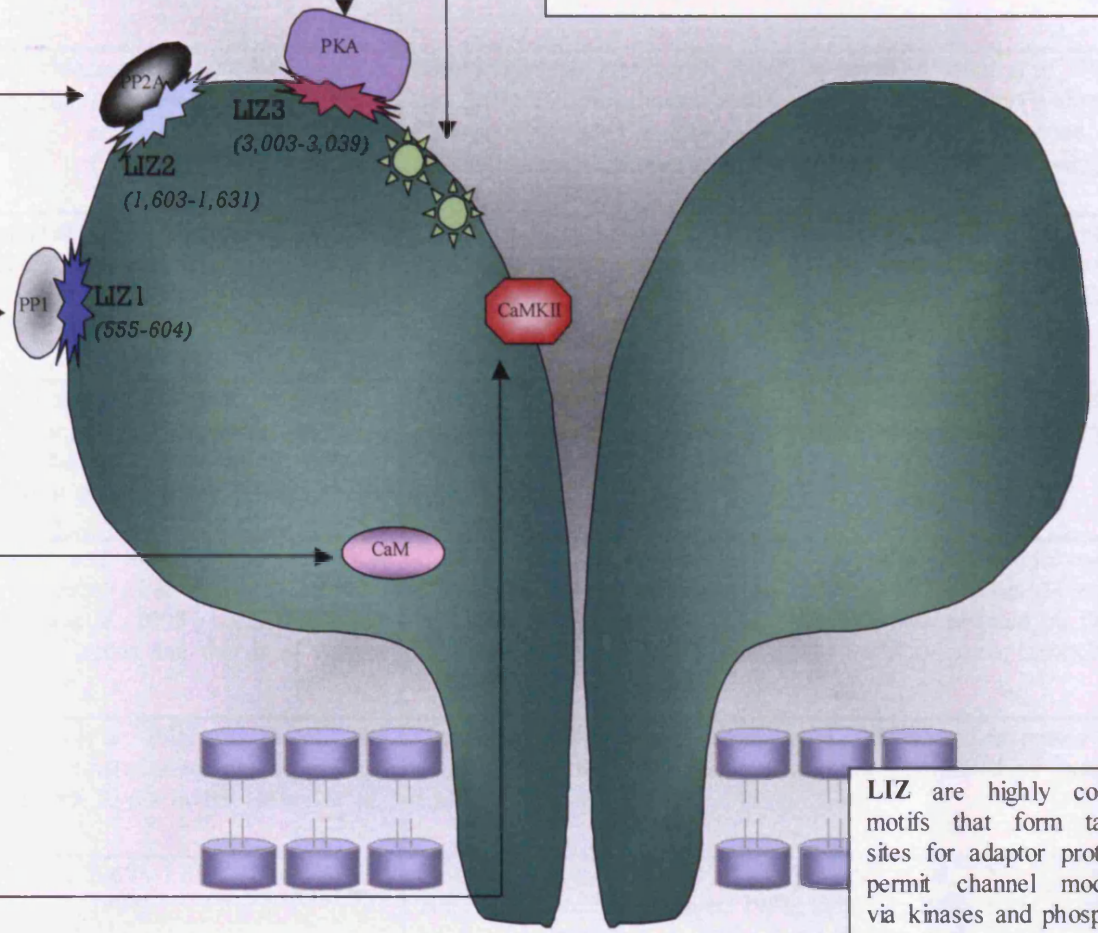

CaM binds to multiple sites on RyR2 (Balshaw *et al.*, 2001), and has both activating and inactivating functions depending on Ca^{2+} concentration (Balshaw *et al.*, 2001; Rodney *et al.*, 2001; Yamaguchi *et al.*, 2003).

CaMKII phosphorylation of RyR2 increases Ca^{2+} sensitivity and P_o (Witcher *et al.*, 1991; Wehrens *et al.*, 2004b). CaMKII activity depends on presence of Ca^{2+}/calmodulin complexes (Pitt, 2007).

LIZ are highly conserved motifs that form targeting sites for adaptor proteins to permit channel modulation via kinases and phosphatases (Marx *et al.*, 2001b).

Figure 1.2 Targeted phosphorylation of RyR2

Schematic respresentation of modulatory RyR2 phosphorylation and dephosphorylation sites.

	PKA	CaMKII
Size/structure/ isoforms	Regulatory and catalytic subunit sizes as follows: RIα 49kDa, RIβ 54-55kDa, RIIα 51kDa, RIIβ 53kDa and all C subunits (α, β and γ) were 40kDa (Foss *et al.*, 1994)	Four subunits of 50-62kDa (Colbran *et al.*, 1989): α, β, δ and γ, of which δ associates with RyR2 (Currie *et al.*, 2004).
RyR2 (de-) phosphorylation sites	S2808 in human and mouse, S2809 in rabbit (Marx *et al.*, 2000; Rodriguez *et al.*, 2003). S2030 in human and mouse, and S2031 in rabbit (Xiao *et al.*, 2005)	S2808 in human and mouse, S2809 in rabbit (Witcher *et al.*, 1991; Rodriguez *et al.*, 2003). S2814 in human and mouse, S2815 in rabbit (Wehrens *et al.*, 2004b). However, >8 CaMKII sites per monomer have been proposed. Stoichiometry of CaMKII phosphorylation is at least 4 times that of PKA (Rodriguez *et al.*, 2003; Stange *et al.*, 2003)
Effect on RyR2	Increased P_o (Takasago *et al.*, 1991; Uehara *et al.*, 2002; Reiken *et al.*, 2003b), which was suggested to be via S2808/9 phosphorylation that caused FKBP12.6 dissociation (Marx *et al.*, 2000). Although this is controversial (Jiang *et al.*, 2002b; Xiao *et al.*, 2004; Xiao *et al.*, 2006; Benkusky *et al.*, 2007)	Increased P_o (Currie *et al.*, 2004; Ferrero *et al.*, 2007) but not via FKBP12.6 dissociation (Wehrens *et al.*, 2004b). Also reported to decrease P_o (Lokuta *et al.*, 1995). CaMKII decreased SR store load that was reversed by CaMKII inhibition (Ai *et al.*, 2005).
Transgenic animals	Ablation of proposed PKA phosphorylation site (S2808) was suggested to protect from heart failure (Wehrens *et al.*, 2006), however this was inconsistent with another study that showed that ablation of the PKA site in mice did not alter β-AR response, nor did it protect animals from stress-induced cardiac defects (Benkusky *et al.*, 2007).	Mice with chronic myocardial CaMKII inhibition exhibited reduced action potential duration, increased PKA activity and a greater LTCC current (Li *et al.*, 2006)
Cell-based studies	PKA directly activated RyR2 (Hohenegger and Suko, 1993), but PKA inhibition did not reduce spontaneous Ca^{2+} release (Ai *et al.*, 2005). S2808/9 was targeted by PKA and CaMKII (Rodriguez *et al.*, 2003), but S2030/1 was PKA specific (Xiao *et al.*, 2005; Xiao *et al.*, 2006), but this is of current dispute (Wehrens *et al.*, 2006)	CaMKII achieved maximum RyR2 phosphorylation (Hohenegger and Suko, 1993), which was associated with increased Ca^{2+} release (Ai *et al.*, 2005; Guo *et al.*, 2006; Kohlhaas *et al.*, 2006). S2808/9 was targeted by PKA and CaMKII (Rodriguez *et al.*, 2003) whereas S2814/5 was unique to CaMKII (Wehrens *et al.*, 2004b)
Single RyR channels in lipid bilayers	Phosphorylation at S2808 increased P_o (Uehara *et al.*, 2002) due to enhanced Ca^{2+} sensitivity (Valdivia *et al.*, 1995), that eliminated subconductance states (Carter *et al.*, 2006). PKA was associated with RyR2 in HF (Marx *et al.*, 2000)	CaMKII both increased (Wehrens *et al.*, 2004b) and decreased RyR2 P_o (Lokuta *et al.*, 1995). RyR2 was equivalently phosphorylated by exogenous PKA and CaMKII (Hain *et al.*, 1995)
Modulation of other EC coupling proteins	Range of targets included NCX (Yeung *et al.*, 2007), LTCC (Haase *et al.*, 1993), PLB (Colyer, 1998), Sorcin (Lokuta *et al.*, 1997)	Extensive targets included LTCC (Grueter *et al.*, 2006; Lee *et al.*, 2006; Pitt, 2007), SERCA/PLB (Colyer, 1998; Li *et al.*, 2006; Picht *et al.*, 2007), PKCα , NCX. (Vila-Petroff *et al.*, 2007), β-AR (Curran *et al.*, 2007)

Table 1.3. Functional modulation of RyR2 by phosphorylation

	PP1	PP2A
Size/structure	Approximately 160kDa (MacDougall *et al.*, 1991) with a catalytic subunit of 36kDa (Bodalina *et al.*, 2005)	Catalytic subunit of 36kDa (Bodalina *et al.*, 2005) and regulatory subunit of 65kDa (Gergs *et al.*, 2004)
RyR2 (de-) phosphorylation sites via adaptor proteins	Binds to RyR2 LIZ1 via spinophilin (Marx *et al.*, 2001b)	Binds to RyR2 LIZ2 via PR130 (Marx *et al.*, 2001b)
Effect on RyR2	Reversed phosphorylation of RyR induced by PKA (Marx *et al.*, 2001b; Bers, 2004), although elevated phosphatase levels increased P_o and depleted SR Ca^{2+} (Terentyev *et al.*, 2003)	As per PP1
Transgenic animals	Cardiac-specific overexpression of PP1 and PP2a catalytic subunits resulted in impaired contractility, dilated cardiomyopathy and death (Carr *et al.*, 2002; Gergs *et al.*, 2004)	As per PP1
Cell-based studies	Increased Ca^{2+} spark frequency and depleted SR stores (Terentyev *et al.*, 2003). Reduced CaMKII phosphorylation *in vitro* (Guo *et al.*, 2006)	As per PP1
Single RyR channels in lipid bilayers	Decreased PP1 phosphorylation activated RyR2 by a route distinct from PKA (Carter *et al.*, 2006), however PP1 also increased RyR P_o (Terentyev *et al.*, 2003; Carter *et al.*, 2006).	PP1 and PP2A dissociated from RyR2 in HF (Marx *et al.*, 2000), but remained intact following acute β-AR phosphorylation of RyR2 (Reiken *et al.*, 2003a).
Modulation of other EC coupling proteins	PP1 dephosphorylated PLB, inhibiting SERCA function (Berrebi-Bertrand *et al.*, 1998)	PP2A reduced P_o of LTCC (Groschner *et al.*, 1996)

Table 1.4. Functional modulation of RyR2 by dephosphorylation

Note that protein kinase and phosphatase modulation regulates other components of EC coupling and is not restricted to RyR.

Although the controversy surrounding RyR phosphorylation may, in part, be due to different experimental conditions, it is also likely to mirror the diverse functional consequences of phosphorylation at numerous sites. Figure 1.3 illustrates the range of kinase target sites on RyR2, which, in combination with the large number of other regulatory phosphorylation sites underscores the potential plasticity of channel modulation.

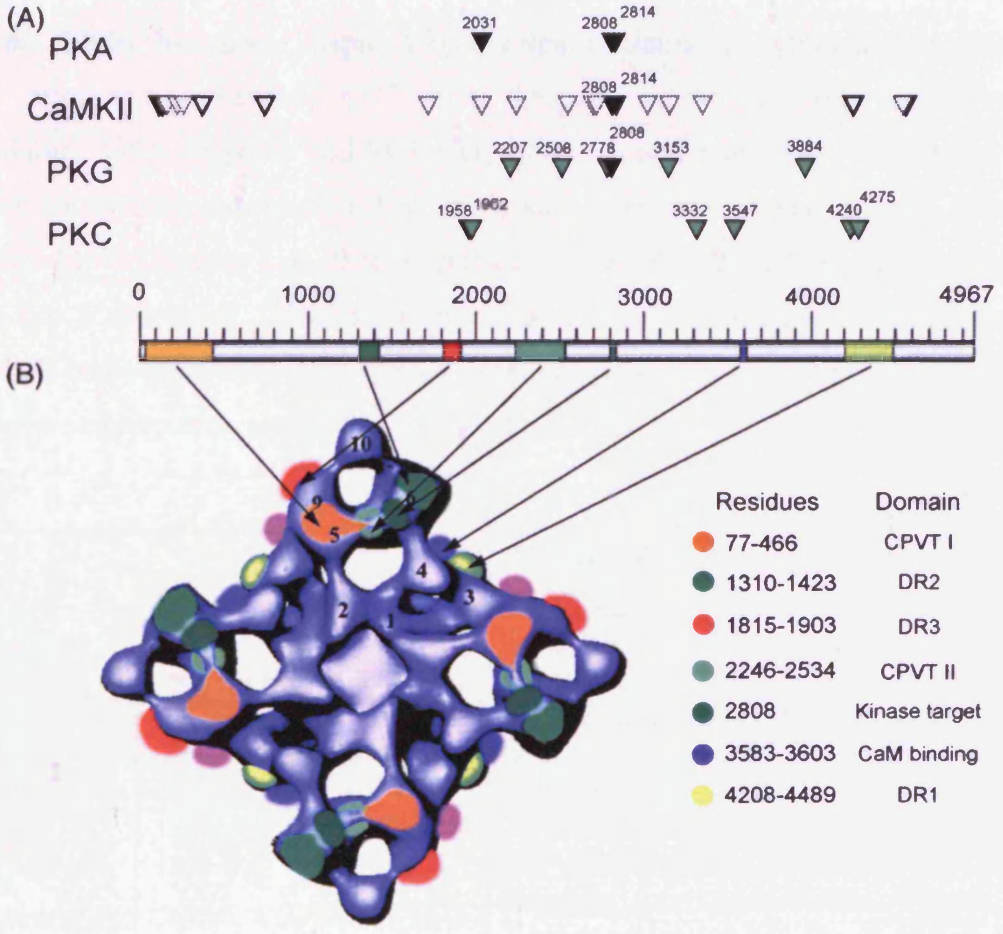

Figure 1.3 Proposed RyR2 phosphorylation sites

Schematic depicting the localisation of experimentally defined and predicted sites of phosphorylation by PKA, CaMKII, PKG and PKC (A) and how these epitopes may map onto the 3D structure (B). Black triangles represent phosphorylation sites determined experimentally, while other triangles represent sites predicted using Markov models (coloured triangles are based on 100% confidence, unfilled dotted line triangles are CaMKII sites based on 95% confidence, unfilled solid line triangles are both CaMKII and PKA sites based on 95% confidence). Domain numbering is explained in Figure 1.1.

From George, 2008.

1.1.3. Channel regulation

1.1.3.1. Physiological modulators

The combined action of the ions Ca^{2+} and Mg^{2+}, and ATP exquisitely modulate RyR channel function. RyR regulation by Ca^{2+} involves the finely-tuned interplay between Ca^{2+} sensing sites on both luminal and cytoplasmic domains. A model based on a luminal RyR Ca^{2+} activation site was proposed (Sitsapesan and Williams, 1994; Gyorke and Gyorke, 1998; Ching *et al.*, 2000), but this is disputed by the demonstration of cytoplasmic activation and inhibitory sites via a luminal Ca^{2+} 'flow-through' mechanism (Herrmann-Frank and Lehmann-Horn, 1996; Tripathy and Meissner, 1996; Xu and Meissner, 1998). More recently it has been shown that cytoplasmic Ca^{2+} activation sites are targeted by both luminal and cytoplasmic Ca^{2+} (Figure 1.4) that implicates a novel high-affinity cytoplasmic Ca^{2+} activation site (Laver *et al.*, 2007a). Furthermore, the same group have also suggested that RyR channels can differentiate between Ca^{2+} that has passed through their own pore and Ca^{2+} released from neighbouring channels (Laver *et al.*, 2004).

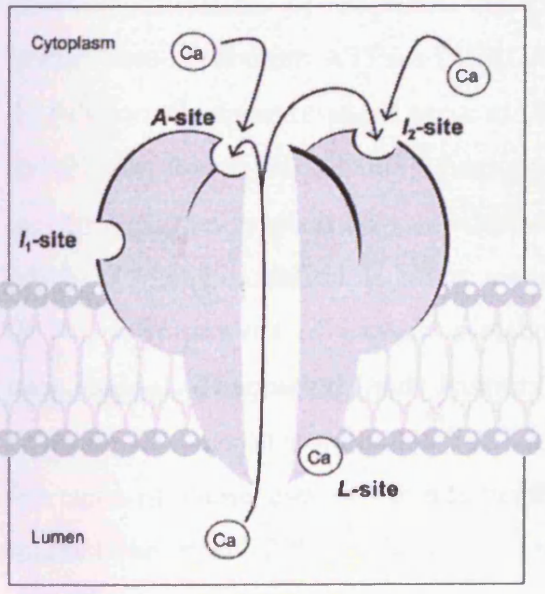

Figure 1.4 RyR2 Ca^{2+} binding sites

Ca^{2+} regulation of RyR2 via three binding sites; luminal Ca^{2+} activation site (or L-site), cytoplasmic activation site (or A-site) and cytoplasmic inactivation site (I_2-site). The I_1 site refers to a dual Ca^{2+}/Mg^{2+} cytoplasmic inhibitory site. RyR2 is activated upon Ca^{2+} interacting with the L-site. Cytoplasmic sites are subsequently accessible to Ca^{2+} flow through the channel that triggers either further activation via the A-site or channel closure via the I_2-site, a mechanism described as Ca^{2+} feed-through.

From Laver, 2007.

The spatio-temporal versatility of Ca^{2+} signalling permits the regulation of diverse cellular processes via dynamic changes in intracellular Ca^{2+} concentrations. Ca^{2+} signalling is dependent on amplitude, duration and localisation of RyR Ca^{2+} release events, in addition to the number of channels recruited. Modest rises in intracellular Ca^{2+} evoke localised Ca^{2+} release, via CICR, through single RyR channels, referred to as a Ca^{2+} quark (Lipp and Niggli,

1996). Propagative co-activation of ~20 RyR units ('cluster') will release a large localised Ca^{2+} transient, termed a Ca^{2+} spark. Further coordinated Ca^{2+} release, sequentially recruiting adjacent RyR clusters, will produce whole-cell Ca^{2+} transients and waves (Keizer and Smith, 1998).

Modulation of RyR by Mg^{2+} is imposed via two distinct mechanisms; channel inhibition at millimolar concentrations and channel activation at micromolar concentrations (Hymel *et al.*, 1988; Laver *et al.*, 1997). The dual control of both RyR1 and RyR2 channel function by Ca^{2+} and Mg^{2+} have long been recognised (Hymel *et al.*, 1988; Williams, 1992; Meissner, 1994; Chen *et al.*, 1997; Kawano, 1998), and are summarised in Table 1.5. However, the precise mechanics of this regulation are highly controversial, and may have resulted from differences in experimental conditions, such as ionic concentration, redox environment and pH, and/or the precise functional status of RyR under study.

1.1.3.2. Redox modification

Redox-modification of proteins including RyR, L-type Ca^{2+} channel (LTCC) and sarco-/endoplasmic reticulum ATPase (SERCA) is emerging as a hugely relevant mode of EC coupling modulation. Cysteine residues serve as target sites for oxidation (Aracena-Parks *et al.*, 2006; Zima and Blatter, 2006; Hool, 2008). Each monomer of RyR1 and RyR2 is composed of 100 and 89 cysteine residues respectively; of which about 20-30% are 'free' i.e. they have reactive sulphydryl groups. Protein oxidation is often mediated by mitochondrial-derived reactive oxygen species (ROS), a by-product of oxygen metabolism that are fundamental mediators of cellular signal transduction (Thannickal and Fanburg, 2000). Enhanced metabolic activity and increased cytosolic Ca^{2+} elevates mitochondrial Ca^{2+} that promotes ROS production. It has been shown that this chain of events can lead to augmented RyR2 Ca^{2+} release that manifests as spontaneous Ca^{2+} sparks (Yan *et al.*, 2008). The close spatial proximity of mitochondria to the SR facilitates this signalling loop.

The involvement of ROS in oxidative stress and pathology has been documented (Hool, 2006; Valko *et al.*, 2007). ROS arise in three forms: hydrogen peroxide (H_2O_2), superoxide anion radicals ($O_2^{\bullet-}$) and hydroxyl radicals ($OH^{\bullet}$). ROS-induced oxidation increases RyR sensitivity to Ca^{2+} and ATP activation, in addition to attenuating Mg^{2+} inhibition of the channel (Bull *et al.*, 2007). ROS are not only produced by respiratory processes but also through signalling molecules,

that include nicotinic acid adenine dinucleotide phosphate (NAADP), nicotinamide adenine dinucleotides ($NADH/NAD^+$), glutathione (GSH/GSSG), cyclic guanosine monophosphate (cGMP) and cyclic ADP ribose (cADPR, formed from NAD by $O_2^{\bullet-}$) (Kumasaka *et al.*, 1999). ROS generated by NADPH oxidase is proposed to increase channel activity by RyR2 S-glutathionylation, a redox-sensitive modification characterised by the formation of GSH-disulphide bonds between GSSG and protein thiol groups (Sanchez *et al.*, 2008). Furthermore, reactive nitrogen species (RNS) exert nitrosative stress through nitric oxide (NO) production, which induces RyR S-nitrosylation that is reported to activate RyRs (Anzai *et al.*, 2000). S-nitrosylation of RyR1 residue cysteine 3635 has been reported, as mutation rendered the channel non-responsive to NO (Sun *et al.*, 2001). RyR2 is endogenously S-nitrosylated (Xu *et al.*, 1998), and reduced S-nitrosylation has been associated with diastolic Ca^{2+} leak (Gonzalez *et al.*, 2007).

1.1.3.3. Pharmacological regulators

Pharmacological agents including caffeine and ryanodine have been widely used to probe RyR modulation. Although neither could be considered physiological modulators, their broad utility as 'research tools' in experimental studies is summarised in Table 1.5. Ryanodine only binds to channels in an open conformation therefore it is often used to assess the extent of channel activity. In addition, the rate of ryanodine binding and dissociation from the channel provides information on functional state, i.e. the ryanodine binds faster at greater P_o, whereas decreasing P_o correlates with a slower dissociation rate (Du *et al.*, 2001; Butanda-Ochoa *et al.*, 2006).

Caffeine is a methylxanthine derivative with a rapid yet reversible activating action on RyR channels and hence is useful in quantifying RyR Ca^{2+} release. Caffeine sensitises RyR channels to Ca^{2+} activation, however it is not a specific agonist, and some effects may be due to phosphodiesterase (PDE) inhibition (Butcher and Sutherland, 1962).

Physiological	RyR regulation
Ca^{2+}	Activated and inhibited by μM and mM Ca^{2+}, respectively (Chen *et al.*, 1997). RyR2 has a greater sensitivity to Ca^{2+} than RyR1 (Williams, 1992; Meissner, 1994).
Mg^{2+}	Potent inhibitor of RyR at mM concentrations (Hymel *et al.*, 1988; Chen *et al.*, 1997; Kawano, 1998). Unlike RyR1, RyR2 is inhibited by luminal Mg^{2+} (Laver, 2007). Defective RyR1 Mg^{2+} is associated with MH phenotype (Laver *et al.*, 1997; Steele and Duke, 2007).
ATP	RyR1 exhibits phosphorylation dependent ATP activation (Hymel *et al.*, 1988; Chen *et al.*, 1997) (Butanda-Ochoa *et al.*, 2006) and exhibits a greater sensitivity than RyR2 (Williams, 1992; Meissner, 1994; Copello *et al.*, 2002). ATP stabilises RyR2 in open conformation (Chan *et al.*, 2003) and facilitates Ca^{2+} activation (Hymel *et al.*, 1988).
NAADP NADH/NAD^+	NAADP activates RyRs (Gerasimenko *et al.*, 2003), whilst inhibition is mediated by the reducing agent NADH, but this effect can be reversed by NAD^+ (Zima *et al.*, 2004).
cADPR	cADPR evokes RyR Ca^{2+} release (Gerasimenko *et al.*, 2003) via weak competition for an ATP binding site (Sitsapesan *et al.*, 1994). However, high cytoplasmic levels of ATP may render RyRs insensitive to cADPR. cADPR may regulate RyRs via indirect mechanisms (Copello *et al.*, 2001).
GSH/GSSG	GSH inhibits RyRs via reduction, while GSSG stimulates via oxidation. Redox regulation by GSH/GSSG altered the affinity of CaM for RyR2 (Balshaw *et al.*, 2001). GSSG involved in S-glutathionylation of RyR2 (Sanchez *et al.*, 2008)
NO	NO activates RyR by S-nitrosylation at >1 cysteine residue (Stoyanovsky *et al.*, 1997)
Pharmacological	
Caffeine	Caffeine activates RyRs (Chen *et al.*, 1997) via increasing Ca^{2+} sensitivity (Butanda-Ochoa *et al.*, 2006). More potently activates RyR2 than other RyR isoforms (Zimanyi and Pessah, 1991).
Ryanodine	At lower doses (nM to μM) ryanodine binds to a single site (a.a. 4863) on open RyR1 (Michalak *et al.*, 1988; Wang *et al.*, 2003) and multiple sites on RyR2 (Michalak *et al.*, 1988) that results in a partially conducting (subconductance) state (Hymel *et al.*, 1988; Fill and Copello, 2002). Higher concentrations (mM) lock RyRs in a closed formation (Zimanyi *et al.*, 1992; Fessenden *et al.*, 2001) that sensitise channels to Ca^{2+} activation (Du *et al.*, 2001; Masumiya *et al.*, 2001).

Table 1.5. RyR physiological and pharmacological regulators

1.1.4. RyR:RyR inter-tetrameric interaction (arrays)

In situ RyRs are arranged in complex arrays in which neighbouring units physically and functionally interact via their large cytoplasmic domains (Hu *et al.*, 2005a; Yin *et al.*, 2005a; Liang *et al.*, 2006) (Figure 1.5). RyR organisation into arrays permits simultaneous agonist responses, a mechanism that may help to explain the phenomenon of coupled gating (Marx *et al.*, 2001a) (Figure 1.6). Coupled gating is thought to be an essential attribute in cardiac muscle, through which synchronous contraction during systole can be achieved, or to mediate rapid restoration of resting Ca^{2+} levels. Depletion of luminal Ca^{2+} was shown to destabilise channel coupling and induced rapid synchronous termination of Ca^{2+} release (Gaburjakova and Gaburjakova, 2008).

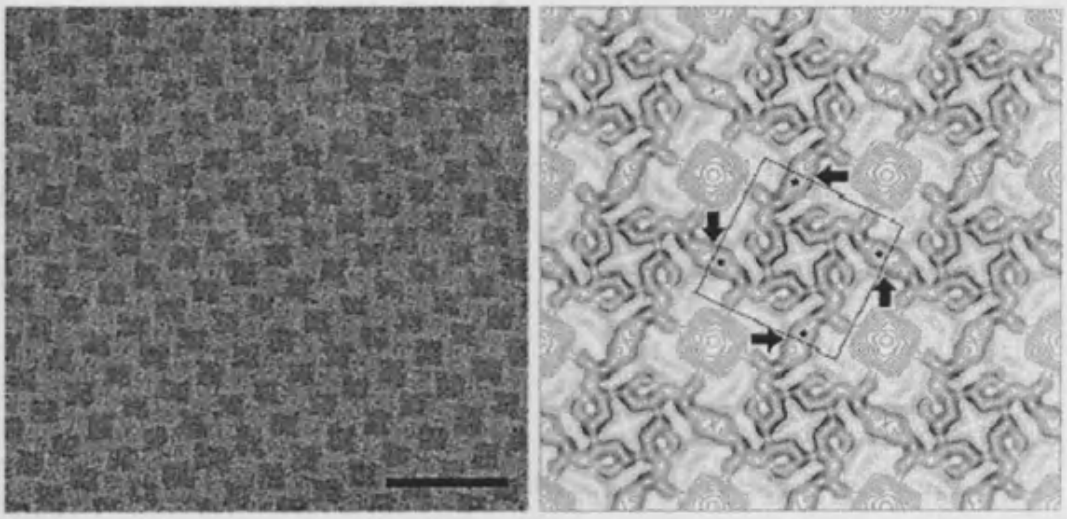

Figure 1.5. Physical association of RyR tetramers

Physical coupling between RyR tetramers in the checkerboard array. An electron micrograph of the cytoplasmic face of organised RyRs (left panel) and a projection map of RyR inter-molecular interaction following image processing (right panel). Arrows indicate physical coupling between adjacent RyR units now thought to be mediated by domain 6. Scale bar is 100nm.

Adapted from Yin *et al.*, 2005.

Channel-associated proteins have also been proposed to stabilise coupled gating of RyRs. Initially it was proposed that the RyR accessory proteins (immunophilins) FKBP12 and 12.6 (see Figure 1.8 and 1.12) mediated coupled gating of adjacent RyR channels (Ondrias *et al.*, 1998; Gaburjakova *et al.*, 2001; Marx *et al.*, 2001a) since RyR2 devoid of its ability to bind FKBP12.6 exhibited an increased channel P_o and uncoupled gating (Wehrens *et al.*, 2003). However, these studies were discounted by Hu *et al.* (Hu *et al.*, 2005b), and RyR visualisation studies did not corroborate the site of FKBP binding and that of RyR tetramer interaction (domain 9 and 6 respectively) (Figure 1.8) (Wagenknecht *et al.*, 1996; Yin *et al.*, 2005a; Yin *et al.*, 2005b; Sharma *et al.*, 2006). Furthermore, the gating properties of single RyR2 channels from FKBP12.6-deficient mice displayed no difference to wild type (Xiao *et al.*, 2007). Therefore, given this evidence it is extremely unlikely that FKBP acts as the 'glue' between tetramers. However, it is worth noting that chronic expression of FKBP12.6 suppressed RyR2-dependent Ca^{2+} fluxes and restored cellular phenotype in CHO cells (George *et al.*, 2003b), indicating a potential signalling role for the FKBP:RyR2 complex.

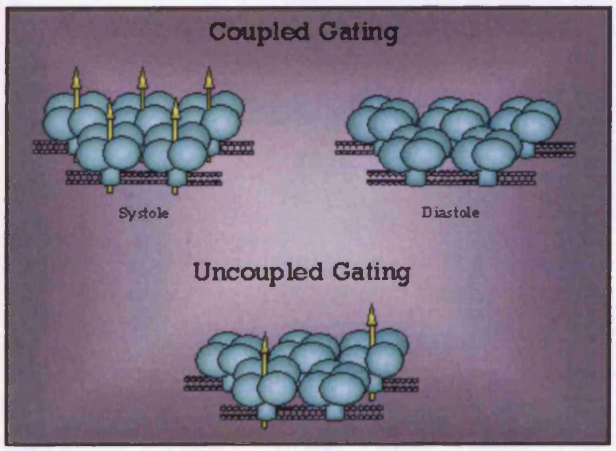

Figure 1.6. Functional coupling between RyR2 tetramers

In the heart, synchronous Ca^{2+} release is enabled by coupled RyR units (systole). Inter-tetrameric interaction also permits the coordinated termination of Ca^{2+} release (diastole). 'Uncoupling' of RyR channels is considered a pathological event. Yellow arrows represent Ca^{2+} release.

1.1.5. RyR:LTCC organisation

In addition to forming arrays with 'self' (Section 1.1.4), RyR1 display intimate physical coupling with LTCC (Block *et al.*, 1988; Flucher and Franzini-Armstrong, 1996; Paolini *et al.*, 2004). Direct interaction between RyR1 and LTCC in skeletal muscle generates high-speed Ca^{2+} signals required for contraction (Cheng *et al.*, 2005) that facilitate the activation of RyR1 by depolarisation-induced Ca^{2+} release (DICR). In contrast, LTCC assume a more irregular arrangement in cardiac muscle (Takekura *et al.*, 2004) (Figure 1.7), and no physical (direct) interaction with RyR2 has been documented (Lu *et al.*, 1994). This more random formation facilitates slower fine-tuned synchronous SR Ca^{2+} release compared to skeletal muscle (Bers, 2002). Ultimately, these differences in RyR:LTCC structural organisation reflect the distinct requirements of EC coupling in both muscles.

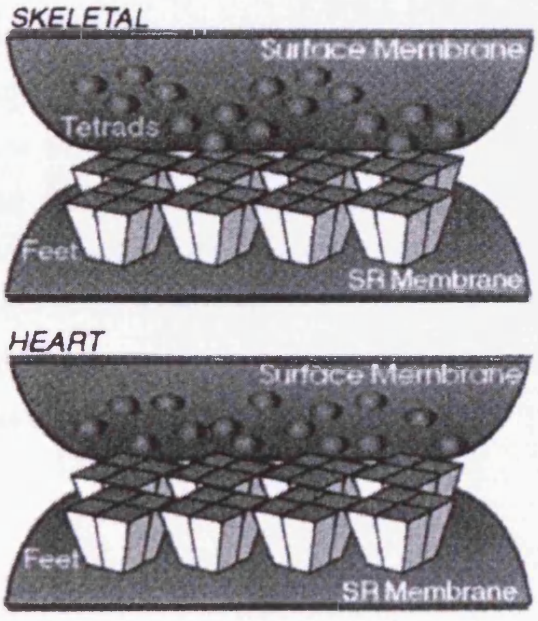

Figure 1.7. Skeletal and cardiac arrangements of LTCC and RyR channels

Note that LTCCs are arranged in clusters of four or 'tetrads' in skeletal muscule whereas cardiac muscle exhibits a more irregular pattern.

From Flucher *et al.*, 1996

1.1.6. RyR intra-subunit interaction

Interdomain interaction within ion channels has emerged as a novel mode of regulation, whereby extrinsic stimuli received via cytoplasmic and luminal sensing sites, are transduced to the TM domain to effect Ca^{2+} pore opening and closing (Yamamoto *et al.*, 2000; Ikemoto and Yamamoto, 2002; George *et al.*, 2004; Kobayashi *et al.*, 2004; George *et al.*, 2006). A similar mechanism has also been reported in both IP_3R (Uchida *et al.*, 2003) and voltage gated shaker K^+ channels (Schulteis *et al.*, 1996; Yao *et al.*, 2000).

Ikemoto and colleagues utilised lipid bilayers to study the effect of synthetic RyR peptides (corresponding to discrete epitopes within RyR1 and RyR2) on single RyR channel function in order to investigate the nature of RyR intramolecular (interdomain) interactions (Yamamoto *et al.*, 2000; Shtifman *et al.*, 2002; Oda *et al.*, 2005; Bannister *et al.*, 2007; Hamada *et al.*, 2007b). Peptides were also applied to permeabilised muscle fibres to assess the dynamics of individual Ca^{2+} release events. Their work pioneered the concept that interactions between cytoplasmic RyR domains profoundly modulated channel activity. Consistent with these studies, George and colleagues identified a region of RyR2 (amino acids 3722-4610) termed the interacting domain or I-domain, which mediated functional interactions between N- and C-terminal regions of RyR2 (George *et al.*, 2004). Moreover, arrhythmia-linked I-domain mutations caused defective interdomain interactions that triggered aberrant Ca^{2+} release. The I-domain overlaps with DR1, which has been localised to the vicinity of domain 3 and as such it is likely to be accessible to cytoplasmic modulation (Figure 1.8). The mechanisms and functional consequences of interdomain interaction are central to this thesis and the above concepts are more fully appraised in Chapter 3.

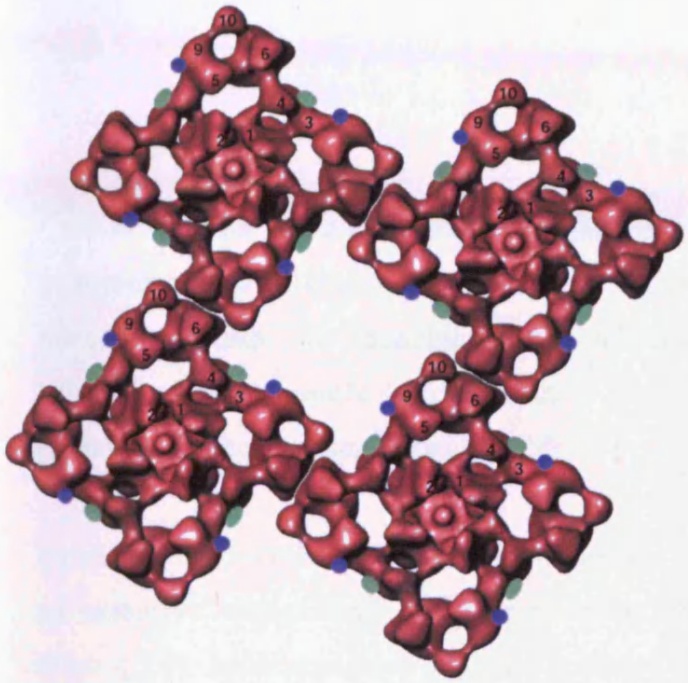

Figure 1.8. RyR2 array-formation displaying potential I-domain epitopes and FKBP binding site

RyR2 complexes displaying putative localisation of I-domain (green, based on the localisation of DR1) and FKBP binding (blue) (Wagenknecht *et al.*, 1996).

Modified from Sharma *et al.*, 2006.

1.1.7. Non-contractile aspects of RyR2 function

The broad distribution of RyR isoforms in both contractile and non-contractile tissues points to their diverse functionality in an array of physiological events, which are not restricted to muscular contraction (Giannini *et al.*, 1995). Such 'non-contractile' functions include excitation-secretion coupling in endocrine cells and neurons and roles in long-term memory development (Zhao *et al.*, 2000). Notably, in a neural context, there is preliminary evidence that RyR2 dysfunction in the brain is linked to epilepsy (Lehnart *et al.*, 2008). In skeletal and cardiac muscle, RyR2 are also localised to nuclear membranes where they are proposed to participate in nuclear Ca^{2+} signalling and gene transcription (Guatimosim *et al.*, 2008).

1.2. Excitation-contraction (EC) coupling in the heart

1.2.1. Ultrastructure of cardiac muscle

Cardiac muscle is composed of highly specialised cells known as cardiomyocytes (approximately 20x100μm) that form fibres via longitudinal co-association at structures called intercalated disks. The branching nature of cardiomyocytes reinforces the tight association between adjacent muscle fibres, which is fundamental in action potential transmission and global cardiac contraction (Ruegg, 1990).

Cardiomyocytes contain actin-myosin filaments (the basic unit of contraction) surrounded by an extensive endoplasmic reticular network, known as the sarcoplasmic reticulum (SR) (Figure 1.9). Mononucleated cells are enclosed by the sarcolemma (cell membrane) and the association between the SR and invaginations of the sarcolemma, referred to as transverse tubules (T-tubules), is central to muscle contraction (Ayettey and Navaratnam, 1978). Cardiomyocytes also contain numerous mitochondria, reflecting the huge metabolic demand during continuous contractile cycles (Carafoli, 2002).

Muscle contraction is initiated by cross-bridge formation between actin and myosin filaments, during which the intrinsic ATPase activity of the myosin head enables the sliding motion of actin and myosin components. However, cross-bridge formation is dependent upon a Ca^{2+} linked conformational change in troponin C (a Ca^{2+} binding protein) that is triggered by a rapid transient rise in intracellular Ca^{2+} (Ruegg, 1990; Davis *et al.*, 2007). Elevated Ca^{2+} levels induce a conformational change within troponin C that triggers actin and myosin cross-bridging, instigating global cellular contraction (systole) (Takeshima *et al.*, 1998; Bers, 2002; Fill and Copello, 2002; Meissner, 2004). Subsequent Ca^{2+} extrusion from the cell dissociates Ca^{2+} from troponin C returning the cell to diastole (Bers, 2002).

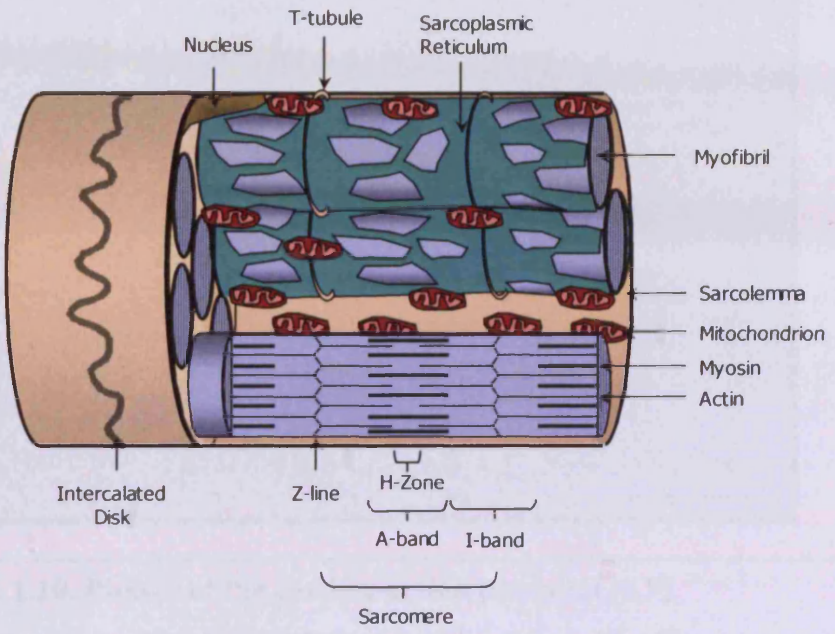

Figure 1.9. Cardiac muscle ultrastructure

T-tubules are regularly spaced in-line with sarcomere Z-lines. The sarcolemma surrounds the cardiomyocyte and forms extensive folds at cell-to-cell junctions, which constitute the intercalated disks. The sarcomere is separated into functional units: H-zone, A-band and I-band. Adjacent sarcomeres meet at the Z-line.

1.2.2. Cardiac action potential

Cardiomyocytes have a resting electrostatic potential across their membranes (typically -85mV) attributable to the non-equivalent fluxes of Na^+ and K^+ ions. Membrane depolarisation, triggered by the massive inward influx of Na^+ ions through surface membrane Na^+ channels instigates the action potential (AP) and raises the membrane potential to approximately 50mV. *In vivo*, the AP is triggered by the pacemaker cells of the sinoatrial (SA) node and is transmitted via the atrioventricular (AV) node to the bundle of His and Purkinje fibres that branch around the base of the ventricles. The ionic fluxes occurring throughout the AP are defined by five key phases (Figure 1.10).

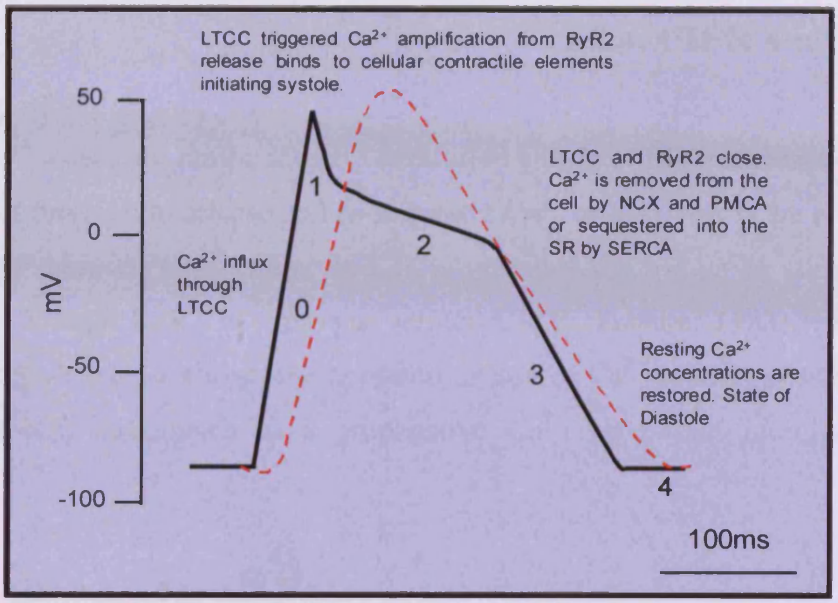

Figure 1.10. Phases of the cardiac action potential (AP)

Phase 0: cell-membrane depolarisation (Na^+ influx, K^+ efflux).
Phase 1: net outward current caused by Na^+ channel ($Na_v1.5$) closure.
Phase 2: plateau sustained by inward Ca^{2+} (LTCC) and outward K^+ movement (several channels).
Phase 3: net outward current caused by K^+ efflux alone. Ionic balance is restored via ion pumps that return membrane potential to ~-85mV (**Phase 4**).
The corresponding movements of Ca^{2+} are described on the figure (red dashed line, modified from Bers and Despa, 2006).

1.2.3. Beta- adrenergic (β-AR) pathway

Activation of the β-AR pathway via the sympathetic nervous system increases cardiac output during episodes of stress, by enhancing both the magnitude of cardiac contraction (inotropy) and heart rate (chronotropy), often referred to as the 'fight or flight' response. Adrenaline or noradrenaline agonise β-adrenoceptors that couple via G-proteins to adenylate cyclase (AC) leading to increased cellular levels of cAMP. Localised cAMP concentrations stimulate PKA, which modifies the phosphorylation status of numerous EC coupling proteins (Bers, 2002; Berridge *et al.*, 2003; Eisner *et al.*, 2006). This modulation of EC-coupling machinery by microdomain-targeted phosphorylation enables a rapid functional adaptation in contractile performance in response to increased demand. Macromolecular complexes also allow the generation of highly localised signalling regions in which channels can be exposed to localised environments without interference from other cellular compartments.

1.2.4. CICR and EC coupling

Intracellular Ca^{2+} stores are maintained by controlled gating of SR membrane proteins RyR2 and SERCA that function to release and re-sequester Ca^{2+} respectively (Chu *et al.*, 1998; Sato *et al.*, 1998). AP-induced Ca^{2+} entry via LTCC provides the trigger to stimulate a greater release of Ca^{2+} through RyR2 in a process termed CICR (Fabiato, 1983) (Figure 1.11). As described in Section 1.1.3.1 above, the temporal unison of Ca^{2+} sparks (possibly via coupled gating mechanisms) culminates in a propagative Ca^{2+} wave that recruits neighbouring

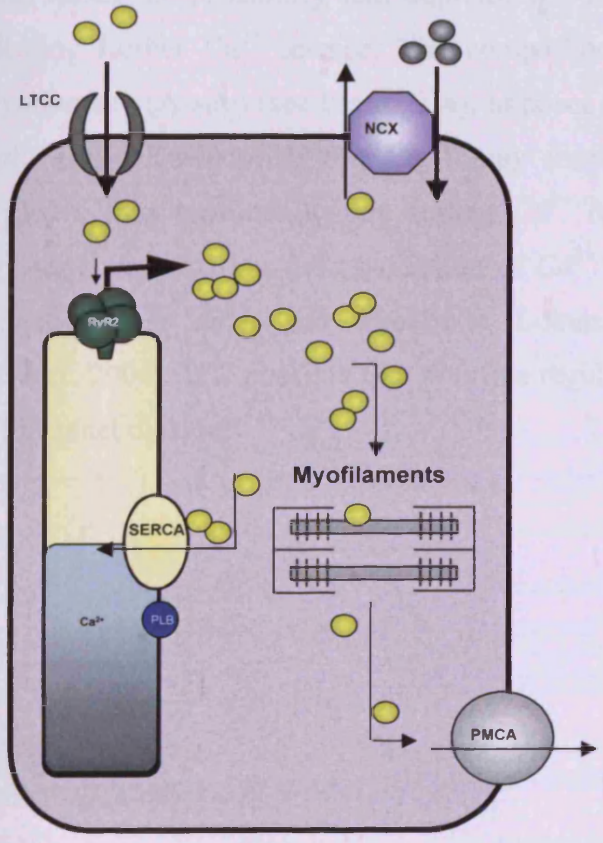

Figure 1.11. CICR triggers muscle contraction

Schematic representation of the physiological process of CICR. Ca^{2+} influx via LTCC activates a greater release of Ca^{2+} from the SR via RyR2. Increased cytoplasmic Ca^{2+} induces a conformational change within myofilaments that triggers contraction (systole). Diastole is restored by Ca^{2+} efflux mechanisms including those dependent on NCX, PMCA and SERCA. Yellow and grey spheres represent Ca^{2+} and Na^{+} respectively.

complexes via CICR (Keizer and Smith, 1998) and raises global cytoplasmic Ca^{2+} from ~100nM to 1μM. The physiological process that converts electrical stimulation into coordinated cellular contraction is termed EC coupling. The efficiency of EC coupling is dependent on the relative amplification of I_{Ca} mediated by CICR (Lai *et al.*, 1988; Fill and Copello, 2002; Marban, 2002; Wehrens and Marks, 2004), and is expressed as EC coupling gain (Wier and Balke, 1999).

Mechanisms governing termination of RyR Ca^{2+} release events are incompletely understood. Previous studies have proposed a number of mechanisms, such as coupled gating, luminal Ca^{2+}, Mg^{2+} inhibition and channel modulation via accessory proteins. Various effectors including FKBP have been implicated in promoting coupled gating, but as discussed above in Section 1.1.4, it is unlikely to directly contribute to Ca^{2+} release termination. A key role of luminal Ca^{2+} in regulating coupled gating is emerging, and it has been suggested that lowered luminal Ca^{2+} can terminate Ca^{2+} release by de-stabilising channel coupling (Gaburjakova and Gaburjakova, 2008). In addition, luminal Ca^{2+} has also been reported to increase RyR sensitivity to cytoplasmic Ca^{2+} activation (Gyorke and Gyorke, 1998; Ching *et al.*, 2000), which raises the possibility that depleted SR Ca^{2+} could de-sensitise the receptor, thereby inhibiting further Ca^{2+} release. The competitive binding of Mg^{2+} to a cytoplasmic Ca^{2+} activation site (A-site) (see Figure 1.4), imposes an inhibitory effect on RyR channels (Laver *et al.*, 1997; Kawano, 1998). Mg^{2+} may displace Ca^{2+} at the A-site following channel activation, thus terminating any further Ca^{2+} release. Channel inactivation has also been proposed to result from the association of Ca^{2+} regulatory proteins and molecules with the channel, such as sorcin and calmodulin (Lokuta *et al.*, 1997; Meyers *et al.*, 2003; Xu and Meissner, 2004). It is possible that multiple regulatory mechanisms contribute to orchestrated Ca^{2+} channel closure.

1.3. Macromolecular Ca^{2+} signalling network

RyR2 acts as a scaffold, associated with a vast network of proteins, pumps and exchangers. The precisely co-ordinated interplay between the components of this network exquisitely regulate intracellular Ca^{2+} (Kranias and Bers, 2007; Bers, 2008). The macromolecular Ca^{2+} signalling network encompasses two inter-linked modes of Ca^{2+} regulation, that which physically associates with and regulates RyR (illustrated in Figure 1.12), and the larger Ca^{2+} handling network (outlined in Table 1.6), which controls Ca^{2+} cycling throughout the cell.

Plasmalemmal ion channels such as LTCC regulate Ca^{2+} influx into the cytosol, whereas the Na^{+} Ca^{2+} exchanger (NCX), and the plasma membrane calcium ATPase (PMCA) control Ca^{2+} efflux mechanisms, maintaining intracellular Ca^{2+} homeostasis (Bers and Perez-Reyes, 1999; Bers and Weber, 2002). The tight control of SR Ca^{2+} concentrations is maintained by Ca^{2+} release via RyR2, and restoration of luminal free Ca^{2+} via the SERCA pump (Bers, 2002). Both RyR2 and SERCA function is modulated by the binding of various accessory proteins. The binding of the immunophillin FKBP12.6 (FKBP12 in skeletal muscle) to the RyR2 cytosolic domain has been proposed to stabilise the channel preventing diastolic Ca^{2+} leak (Timerman et al., 1996; Marx et al., 2000). Another cytosolic protein that interacts with and regulates the RyR2 is sorcin. Sorcin is a 22kDa Ca^{2+} binding protein that binds RyR2 with high affinity reducing channel activity (Lokuta et al., 1997). Luminally, the RyR2 is modulated by association with the SR Ca^{2+} buffering protein calsequestrin (CSQ), which can bind up to 50 Ca^{2+} ions per molecule (Beard et al., 2004). CSQ traffics Ca^{2+} ions to the RyR during systole facilitating Ca^{2+} release. RyR2 and CSQ form a quaternary complex with the accessory proteins, junctin and triadin, both of which share similar sequence homology and are proposed to mediate interactions between CSQ and RyR2 governing Ca^{2+} release (Zhang et al., 1997; Beard et al., 2005). Similar to CSQ, calreticulin is also a luminal Ca^{2+} binding protein expresed primarily in embryonic cells, but has a lower (approximately 50%) Ca^{2+} binding capacity compared to CSQ (Treves et al., 1990; Milner et al., 1992; Nakamura et al., 2001). Calreticulin will be discussed further in Chapter 5. The function of SERCA in relinquishing cytosolic Ca^{2+} back to the SR after systole is regulated by the phosphoprotein phospholamban (PLB). PLB binding to SERCA inhibits Ca^{2+} uptake into the SR during systole, while PLB phosphorylation during diastole results in its dissociation, enabling Ca^{2+} to be relinquished to the SR in preparation for the next cardiac cycle (Toyofuku et al., 1994; MacLennan et al., 1997). See Figure 1.12 and Table 1.6 for more details on all the aforementioned Ca^{2+}-associated proteins.

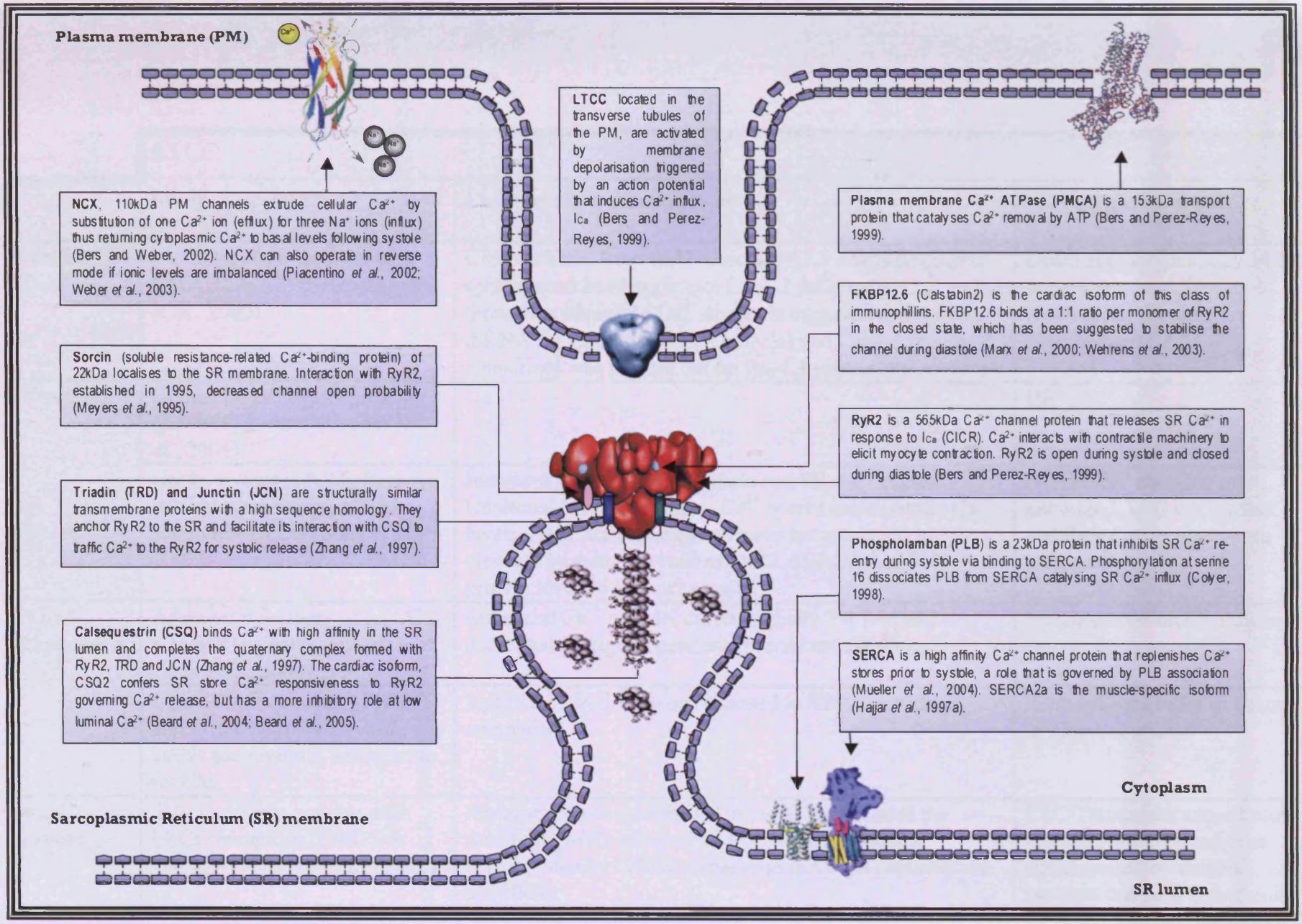

Figure 1.12. Schematic illustration of the macromolecular Ca^{2+} signalling network

	LTCC		
	Study	**Ca^{2+} handling Observations**	**Phenotypic consequence**
Knock-Out	Homozygous knock-out of LTCC ($Ca_V1.2$) (Seisenberger *et al.*, 2000)	CMs obtained from embryonic day 12.5 hearts displayed spontaneous beating despite $Ca_V1.2$ deficiency. Ca^{2+} influx through unidentified Ca^{2+} channels triggered contraction. mRNA for $Ca_V1.1$ (skeletal muscle) and $Ca_V1.3$ (neuro-endocrine) was present but no $Ca_V1.1$ protein was detected	Death at embryonic day 14.5 suggesting that LTCC is required for normal development
Transgenic	Human LTCC overexpression (2.8-fold) in mice (Groner *et al.*, 2004)		HF
	Cardiomyocytes (CM) from mice overexpressing the α1 subunit of LTCC (Song *et al.*, 2002)	Increased Ca^{2+} influx amplitude and SR Ca^{2+} release. Unaltered SR Ca^{2+} content, Ca^{2+} sparks and diastolic Ca^{2+} levels. NCX activity was increased accompanied by elevated protein expression. RyR2, SERCA and PLB protein levels were unchanged	Normal EC coupling gain, although LTCC Ca^{2+} influx and RyR Ca^{2+} release were increased.
Viral expression	Adenoviral delivery of LTCC β subunits to young adult rat CM (Wei *et al.*, 2000).	Enhanced Ca^{2+} channel current density 3-4 fold and decreased voltage-dependent channel inactivation	Increased contractile function
	LTCC double mutant (T1039Y and Q1043M) (Walsh *et al.*, 2007) adenovirally delivered to rat CM.	I_{Ca} reduced by 35% when exposed to dihydropyridine compound	Reduced sensitivity of channels to dihydropyridine
Case report	Two paediatric patients with LTCC mutations (G402S or G406R) (Splawski *et al.*, 2005)	Mutations prolonged the QT interval and reduced the sensitivity of the channel to deactivation, a finding corroborated by G406R expression in CHOs (Splawski *et al.*, 2004).	LTCC mutations caused multi-system Timothy syndrome characterised by autism, syncope and fatal arrhythmia

	NCX		
	Study	**Ca^{2+} handling Observations**	**Phenotypic consequence**
Knock-Out	NCX1 ablation in mice (Reuter *et al.*, 2003).	Ca^{2+} transients are maintained at rest but upon stimulation cells displayed increased diastolic Ca^{2+} and reduced Ca^{2+} transients. No up-regulation of the sarcolemmal Ca^{2+} pump was observed	Embryonic lethality; heart tube analysis showed diminished SR membranes. (Cardiac specific ablation in mice was viable, see 'Tissue-specific' below)
Transgenic	Homozygous NCX overexpression (3-fold) in mice (Reuter *et al.*, 2004; Pott *et al.*, 2007a)	Enhanced Ca^{2+} extrusion and prolonged action potential. Increased LTCC amplitude and slower inactivation of the current, unchanged SR Ca^{2+} load but reduced SR Ca^{2+} release. No difference in RyR2 levels	Decreased EC coupling gain (see Section 1.2.4) that resulted in cardiac hypertrophy and enhanced susceptibility to heart failure
Tissue-Specific	Cardiac specific knock-out of NCX1 in 80-90% of murine CM (Henderson *et al.*, 2004; Imahashi *et al.*, 2005; Pott *et al.*, 2005; Pott *et al.*, 2007b; Pott *et al.*, 2007c; Pott *et al.*, 2007d)	Unaltered resting Ca^{2+}, SR Ca^{2+} content and Ca^{2+} transient amplitude, but a reduced transient decay, shortened action potential and a 50% reduction in LTCC current. Mice exhibit an increase in EC coupling gain. PMCA, SERCA, CSQ and LTCC protein levels were unchanged, despite a reduction in LTCC current. No compensation for NCX1 by NCX2 or 3.	Mice survived to adulthood and exhibited only a modest reduction in cardiac contractility. No cardiac hypertrophy and hearts were protected against ischemia-reperfusion injury due to absence of reverse-mode (inward) NCX Ca^{2+} currents
	Cardiac-specific NCX overexpressing mice (Terracciano *et al.*, 1998)	Increased SR Ca^{2+} content. No difference in protein expression of SERCA2a, PLB or CSQ	
Viral expression	NCX overexpressing rabbit CM (Ranu *et al.*, 2002).	Lowered systolic and diastolic Ca^{2+} levels, amplitude of contraction and depleted SR stores	Depressed contractility
	Adenoviral-induced NCX overexpression in rabbit CM (Schillinger *et al.*, 2000)	Reduced SR load and frequency of shortening. Protein levels of SERCA, PLB and CSQ unchanged	Depressed contractility

	SERCA		
	Study	**Ca^{2+} handling Observations**	**Phenotypic consequence**
Knock-Out	Heterozygous SERCA2a KO mice (Talukder *et al.*, 2008)	Lower systolic and higher diastolic intracellular Ca^{2+}. Reduced SERCA2a protein levels	Reduced contractility
Transgenic	Mice overexpressing rat SERCA2 protein (Dillmann, 1998)	Increased SR load, Ca^{2+} transient release and myocyte re-lengthening.	Improved contractility
	Mouse model with SERCA2a replaced by SERCA2b (Vangheluwe *et al.*, 2006)		Cardiac hypertrophy
Tissue-Specific	SERCA2a overexpression in rat hearts (Maier *et al.*, 2005)	Myocytes displayed a 2-fold increase in SR Ca^{2+} stores and reduced trans-sarcolemmal Ca^{2+} flux (LTCC and NCX). Trend (ns) towards reduced levels of LTCC and NCX.	Improved contractility
Viral expression	SERCA2a overexpression in rabbit CM (Terracciano *et al.*, 2002).	Increased SR Ca^{2+} stores, but decreased action potential duration and Ca^{2+} entry through LTCC	
	SERCA2a overexpression (Davia *et al.*, 2001).	Increased SR Ca^{2+} content and enhanced amplitude of contraction during stimulation	Enhanced contractile function
	SERCA expression in myocytes from hypertrophied hearts (Reilly *et al.*, 2001)		Improved cardiac function in hypertrophic myocytes
	SERCA overexpression in ventricular CMs from human HF model (del Monte *et al.*, 1999).	Increased both SERCA expression and activity that increased cell shortening. Lower diastolic Ca^{2+} and higher systolic Ca^{2+} was observed when SERCA was overexpressed	Improved contractility in failing CMs
	SERCA1 overexpression in neonatal and adult rat CMs (Zhang *et al.*, 2001)	SERCA1 infection caused 4-fold higher protein expression in neonatal and adult rat CMs	Apoptosis in neonatal cells, which was not observed in adult CMs

	PLB		
	Study	**Ca^{2+} handling Observations**	**Phenotypic consequence**
Knock-Out	PLB deficient mice (Chu *et al.*, 1998)	Increased SERCA activity and contractile function. Normal SERCA, CSQ or NCX protein levels, although RyR2 expression was down-regulated	Enhanced contractile function and reduced catecholamine responses consistent with previous studies (Luo *et al.*, 1994). Down-regulated RyR2 may be a compensatory mechanism for increased SERCA activity.
	Isolated CM from PLB-knock out mice (Li *et al.*, 1998)	Increased Ca^{2+} store load and SERCA activity but reduced NCX activity, despite unaltered NCX protein expression. Normal actin expression.	Increased re-filling of SR stores (may cause SR overload and aberrant Ca^{2+} release).
	PLB deficient mouse CM (Santana *et al.*, 1997)	LTCC Ca^{2+} current amplitude was unchanged but SR Ca^{2+} transient was increased, enhancing EC coupling gain. Increased SR Ca^{2+} load, frequency and amplitude of spontaneous Ca^{2+} sparks suggest an increased RyR sensitivity to Ca^{2+}	Increased SR load and sensitised RyR Ca^{2+} activation that could result in diastolic Ca^{2+} leak
Knock-In	Mouse model of overexpressed mutant PLB (R9C) (Gramolini *et al.*, 2007)	Increased diastolic Ca^{2+} levels and decreased contractile function. Increased expression of cytoskeletal and Ca^{2+} binding proteins.	Dilated cardiomyopathy from 8 weeks that resulted in death by ~20 weeks
	Mouse model of mutant PLB (V49G) overexpression (Haghighi *et al.*, 2001)	Reduced Ca^{2+} uptake leading to decreased cell shortening and re-lengthening. Increased rate of Ca^{2+} transient decay. Significantly depressed cardiac function and β-AR response.	Hypertrophy, dilated cardiomyopathy and death by 6 months in male mice. Female mice exhibited hypertrophy by 3 months but normal systolic function up to one year.
Tissue-Specific	Mouse model of PLB deletion of Arg-14 (Haghighi *et al.*, 2006) (*)	PLB mutant chronically suppressed SERCA affinity for Ca^{2+}, decreasing re-sequestration of Ca^{2+} to the SR.	Increased heart size due to ventricular dilation, myocyte disarray and myocardial fibrosis, consistent with dilated cardiomyopathy observed in human carriers of Arg14 deletion. Overexpression of mutant in mice resulted in premature death, findings observed in human patients (#).
Viral expression	PLB overexpression in rat CM (Davia *et al.*, 1999)	Reduced SR Ca^{2+} stores, reduced transient amplitude and increased transient decay time. Normal SERCA2a expression.	Diminished contractility
	T116G point mutation in rat CM and HEK293 cells (Haghighi *et al.*, 2003)	Mutant PLB exhibited a loss of function: it failed to decrease cell shortening, lower SR transient amplitude and reduce the affinity of SERCA for Ca^{2+}, characteristic of WT PLB. Diminished PLB expression, consistent with human patients. Human patients also had reduced SERCA expression but unchanged CSQ levels.	Mutation introduces a premature stop codon resulting in non-functional protein, which, in humans causes severe dilated cardiomyopathy.
	Mutant PLB expression in failing rabbit CM (Ziolo *et al.*, 2005)	Increased Ca^{2+} transient amplitude and rate of decay. Increased SR load and enhanced force-frequency response. No changes in SERCA or NCX protein expression	Mutant PLB inhibition of endogenous PLB increased SERCA activity and restored contractile function in failing myocytes
Case-study	Individuals homozygous for T116G mutation that introduced premature stop codon (Haghighi *et al.*, 2003)	PLB mRNA was reduced by 50% whereas no PLB protein was detected.	Dilated cardiomyopathy and heart failure requiring a heart transplant between adolescence and adulthood. Contrary results to those from PLB deficient mice (Chu *et al.*, 1998).
	Hereditary deletion of PLB Arg-14 (Haghighi *et al.*, 2006)(#)	Chronic suppression of SERCA activity	No reported homozygosity. Heterozygous individuals exhibited contractile dysfunction, ventricular arrhythmias that predisposed them to HF and premature death. Findings that were corroborated in mice (*).

	CSQ		
	Study	**Ca^{2+} handling observations**	**Phenotypic consequence**
Knock-Out	Tissue specific only		
Knock-In	Mice carrying D307H mutation (Song *et al.*, 2007)	Decreased SR load, slower transient release and Ca^{2+} re-uptake. Stimulation induced reduced Ca^{2+} transients, elevated cytosolic Ca^{2+} and spontaneous Ca^{2+} release. Reduced CSQ, but increased calreticulin and RyR2 (unaltered phosphorylation). Unaltered levels of FKBP12.6.	Mutation induced similar phenotype to cardiac specific CSQ KO mice (*). Structurally normal but mice exhibited ventricular arrhythmias, cardiac hypertrophy and reduced contractile function.
Transgenic	Mice overexpressing CSQ (Knollmann *et al.*, 2000)		Developed contractile dysfunction after 60 days with a survival rate of only 40% by 6 months
Tissue-Specific	Cardiac CSQ (CSQ2) null mice (Knollmann *et al.*, 2006) (*)	Myocytes had an increased SR volume. Catecholamine exposure caused diastolic Ca^{2+} leak. Decreased expression of JCN & TRD	Normal contractility at rest, but under stress mice phenocopied human arrhythmias
	20-fold overexpression of cardiac CSQ in mice (Sato *et al.*, 1998)	Enhanced SR Ca^{2+} but reduced Ca^{2+} transient amplitude, cell shortening and re-lengthening. SERCA, PLB and calreticulin protein expression was up-regulated, but no change in RyR, JCN or TRD	Cardiac hypertrophy
	2-6 fold overexpression of cardiac CSQ D307H (Dirksen *et al.*, 2007)	Reduced SR transient amplitude and duration and increased Ca^{2+} spark frequency. Upon stimulation CM displayed spontaneous Ca^{2+} oscillations that resulted in DADs	Structurally normal hearts devoid of cardiac hypertrophy with intact ventricular contractility. Stress-evoked mice phenocopied human CPVT by developing arrhythmias such as non-sustained polymorphic VT
	10 fold overexpression of cardiac CSQ in mice (Jones *et al.*, 1998)	Suppressed frequency and amplitude of Ca^{2+} sparks. Increased (10-fold) SR Ca^{2+} release (following caffeine administration) and NCX current. RyR, JCN and TRD were down-regulated but SERCA and PLB were unaltered.	Severe cardiac hypertrophy associated with a 2-fold increase in cell size and heart mass.
Adenoviral	CSQ overexpression in rabbit CM (Miller *et al.*, 2005)	Increased SR Ca^{2+} content, LTCC current and Ca^{2+} transient amplitude, but reduced EC coupling gain. Increased expression (50%) of CSQ. No increase in LTCC subunit expression despite enhanced LTCC current	
	CSQ overexpression (3.5-fold) and reduced expression (30%) in rat CM (Kubalova *et al.*, 2004)	Ca^{2+} wave amplitude, period between waves and recovery of basal SR Ca^{2+} was increased in overexpressing CM. The opposite was observed in reduced CSQ CM. SR load was unchanged in both instances. No change in SERCA and PLB protein levels	Reduced CSQ increased levels of free Ca^{2+} and reduced the occurrence of spontaneous Ca^{2+} waves. Increased CSQ slowed recovery of free SR Ca^{2+} reducing the frequency of Ca^{2+} waves.
	4-fold overexpression of D307H canine CSQ in rat CM (Viatchenko-Karpinski *et al.*, 2004)	Reduced SR Ca^{2+} and lowered transient amplitude, duration and time to peak.	Isoproterenol exposed mutant myocytes displayed spontaneous oscillations and DADs
Case-study	Individuals harbouring CSQ D307H mutation (Eldar *et al.*, 2002; Lahat *et al.*, 2004)		Predisposition to autosomal recessive form of CPVT
	Individuals harbouring CSQ nonsense mutations (Postma *et al.*, 2002).		All three CSQ mutations induced a premature stop codon resulting in phenotypically similar forms of CPVT

	JCN		
	Study	**Ca^{2+} handling observations**	**Phenotypic consequence**
Knock-Out	Junctin ablation in mice (Yuan *et al.*, 2007)	Unaltered LTCC current, but enhanced NCX current. Increased fractional shortening, Ca^{2+} transient amplitude (54%), SR load and Ca^{2+} spark frequency/amplitude. Transients had a shorter decay. No significant changes in protein expression of CSQ, TRD, SERCA, PLB, FKBP12.6, LTCC or RyR S2808 phosphorylation. However NCX protein levels increased by 70%.	Increased cardiac function, but PVC and VT triggered by DADs upon stimulation. 25% of mice died by 3 months with no cardiac structural abnormalities.
Transgenic	CM of mice overexpressing canine JCN (Zhang *et al.*, 2001)		Increased association between SR and T-tubules. Junctional SR is narrower and CSQ more compact
	A remarkable 24-29-fold overexpression of canine JCN in mice (Hong *et al.*, 2002)	RyR2 and TRD down-regulation while LTCC was up-regulated	Bradycardia, atrial fibrillation and fibrosis.
Tissue-Specific	Cardiac-specific JCN overexpression in mice (Kirchhefer *et al.*, 2006)	Decreased SR Ca^{2+} content and Ca^{2+} spark frequency. Down-regulated NCX expression and increased phosphorylation of RyR2 at S2808	
Viral expression	Adenoviral overexpression of JCN in rat CM (Gergs *et al.*, 2007)	Decreased SR transient amplitude	Reduced contractility

	TRD		
	Study	**Ca^{2+} handling observations**	**Phenotypic consequence**
Knock-Out	Skeletal and cardiac TRD knock-out mice (Shen *et al.*, 2007).	Increased basal Ca^{2+} and reduced Ca^{2+} transients in skeletal muscle. Junctin and CSQ down-regulation in skeletal muscle	No obvious skeletal contractile dysfunction.
Transgenic	5-fold TRD overexpression in mice (Kirchhefer *et al.*, 2001)	Myocytes had a slower Ca^{2+} transient decay. Down-regulated RyR2 and JCN but unaltered SERCA and PLB levels	Reduced contractility, cell shortening and re-lengthening
	Mice overexpressing TRD 2.9-fold (Kirchhof *et al.*, 2007)	Normal JCN protein levels	Repetitive VT at heart rate > 600bpm
Tissue-Specific	Cardiac specific overexpression of TRD in mice (Kirchhefer *et al.*, 2004)	Increased SR Ca^{2+} content, peak transient height and transient decay	Decreased cardiac contractility
Adenoviral	TRD overexpression in rat CM (Terentyev *et al.*, 2005)	Increased frequency but decreased amplitude of Ca^{2+} sparks, lowered SR Ca^{2+}stores and increased RyR2 P_o	Stimulation-evoked arrhythmic oscillations

Table 1.6. Summary of functional studies exploring the roles of EC coupling-related proteins

1.4. Ca^{2+} dysregulation and pathology

1.4.1. Arrhythmic diseases

Arrhythmia describes an irregular cardiac sinus rhythm, such as tachycardia and bradycardia (increased and decreased heart rate, respectively) (Bhuiyan *et al.*, 2007b). Arrhythmic conditions include: premature ventricular contractions (PVC), polymorphic tachycardia, atrial fibrillation (AF) and ventricular fibrillation (VF), the latter usually preceding sudden cardiac death (SCD) (Francis *et al.*, 2005; Vest *et al.*, 2005; Pizzuto *et al.*, 2006; Yano *et al.*, 2006). Rhythmic disturbances are intrinsically linked to perturbed fluxes of Na^+, K^+ and Ca^{2+} ions and often arise as a consequence of defects in EC coupling. The following section appraises some of the mechanisms linked to EC coupling dysfunction in arrhythmia.

1.4.1.1. Catecholaminergic polymorphic ventricular tachycardia (CPVT) and arrhythmogenic right ventricular cardiomyopathy (ARVC)

Catecholaminergic polymorphic ventricular tachycardia (CPVT) is a genetic disease characterised by catecholamine-induced arrhythmic episodes. Due to the nature of the disease, CPVT usually only manifests following exercise or stress. Susceptible individuals experience palpitations and syncope, which frequently lead to death. In many individuals, their first CPVT episode is fatal (Priori *et al.*, 2002; Laitinen *et al.*, 2003) highlighting the need for preventative therapies (e.g. implantable cardioverter defibrillators [ICD]). CPVT exists in autosomal dominant (Priori *et al.*, 2002; Brini, 2004) and recessive forms (Lahat and Eldar, 2002) (CPVT1 and CPVT2 respectively). CPVT1 has been mapped to the RyR2 gene on chromosome 1q42-43 (Swan *et al.*, 1999), whereas CPVT2 is linked to the CSQ2 gene located on the short arm of chromosome 1 (1p13-21) (Lahat *et al.*, 2004). CPVT is frequently confused with a phenotypically similar disease called arrhythmogenic right ventricular cardiomyopathy (ARVC2), but unlike CPVT that occurs in the absence of structural heart disease, ARVC2 presents with a fibro-fatty structural thickening of the right ventricular wall (Tiso *et al.*, 2001; Scheinman and Lam, 2006). Although ARVC2 has been suggested to arise as a consequence of RyR2 mutation (Tiso *et al.*, 2001), this is contentious. In addition, the existence of another highly malignant autosomal recessive form of CPVT has been mapped to

an alternative locus on chromosome 7 (7p14-22), but the protein products of this rather large chromosomal region remains to be defined (Bhuiyan *et al.*, 2007a).

CPVT2 was initially characterised in Bedouin families and resulted from a single point mutation in CSQ (D307H) (i.e. the replacement of Asp (negatively charged) with His (positively charged) (Lahat *et al.*, 2001; Eldar *et al.*, 2002; Lahat and Eldar, 2002). Mice carrying the D307H mutation exhibited contractile abnormalities and stress-induced arrhythmias (Dirksen *et al.*, 2007; Song *et al.*, 2007) (see Table 1.6). The phenotype of CSQ2-null mice was entirely consistent with the human phenotype in patients lacking functional CSQ2 (Postma *et al.*, 2002).

1.4.1.2. RyR2 mutations

Mutation-induced RyR2 dysfunction perturbs intracellular Ca^{2+} cycling that results in irregular electrical episodes known as delayed after depolarisations (DADs). Ca^{2+} leak through destabilised RyR2 channels atypically triggers Ca^{2+} extrusion via NCX that induces Na^{+} influx. This abnormal depolarisation, termed DAD, may if sufficiently large or frequent, degenerate into VF (Priori and Corr, 1990; Paavola *et al.*, 2007).

Altered RyR2 function underpins CPVT and heart failure (HF) (Priori *et al.*, 2002; Wehrens and Marks, 2002; Wehrens *et al.*, 2006). Over seventy RyR2 mutations have been identified to date (Laitinen *et al.*, 2001; Priori *et al.*, 2002; Tester *et al.*, 2004; Postma *et al.*, 2005; Nishio *et al.*, 2008), however controversy surrounds the precise basis through which these mutations induce RyR2 dysregulation (Ikemoto and Yamamoto, 2002; Wehrens *et al.*, 2003; Jiang *et al.*, 2004b; George *et al.*, 2006; Terentyev *et al.*, 2006). Marks and colleagues propose that mutations 'weaken' the complex formed by RyR2 and FKBP12.6, which destabilises the channel and induces Ca^{2+} leak (Marx *et al.*, 2000; Wehrens *et al.*, 2003). However, several groups (including our own) contest this hypothesis (George *et al.*, 2005; Jiang *et al.*, 2005; Xiao *et al.*, 2005; Liu *et al.*, 2006; Xiao *et al.*, 2007).

The functional characterisation of published RyR2 mutations has lagged behind the speed at which they have been identified. To date, only twelve mutations have been functionally characterised (~15% of all those reported) (Table 1.7) with most of these revealing a gain of

function phenotype whereby the mutation appears to sensitise the channel to Ca^{2+} release by a number of potential mechanisms (Jiang *et al.*, 2002a; George *et al.*, 2003a; Lehnart *et al.*, 2004; Kannankeril *et al.*, 2006). Notably, $L^{433}P$ was the first mutation to exhibit reduced Ca^{2+} sensitivity (Thomas *et al.*, 2004), a finding that was disputed by Jiang and colleagues (Jiang *et al.*, 2005) who subsequently characterised $A^{4860}G$ as a loss-of-function mutation based on its diminished activation by luminal Ca^{2+} and normal activation by cytosolic Ca^{2+} and caffeine (Jiang *et al.*, 2007). The $A^{4860}G$ mutation is located in a distal TM region of RyR2 that encompasses the pore inner helix, a region proposed to be critical in channel activation and gating (Wang *et al.*, 2004). The $I^{4867}M$ mutation also resides in this region, but has a functionally diverse phenotype from $A^{4860}G$ (Jiang *et al.*, 2005). In addition, $A^{4860}G$ was found to induce catecholaminergic idiopathic ventricular fibrillation in a 7-year old male, while a 9-year old female harbouring the $S^{2246}L$ mutation exhibited the same disease manifestation (Priori *et al.*, 2002). Subsequent characterisation determined $S^{2246}L$ to be a gain-of-function mutation (George *et al.*, 2003a; Jiang *et al.*, 2005), inconsistent with $A^{4860}G$. These findings underline the potential functional heterogeneity of RyR2-linked pathologies. The ramifications of functional heterogeneity of mutant RyR2 for developing anti-arrhythmic therapies are substantial and have been reviewed elsewhere (Thomas *et al.*, 2007).

The disproportionate clustering of almost 40% of published RyR2 mutations in the I-domain (representing just ~18% of the RyR2 polypeptide) underscores the critical functional role of this region. Figure 1.13 displays CPVT-linked RyR2 mutations and their relative clustering within functional domains. The severe R4497C I-domain mutation has been studied intensively and the arrhythmic phenotype has recently been reproduced in $R^{4496}C$ mutant mice (Cerrone *et al.*, 2005; Liu *et al.*, 2006). Other mouse models harbouring RyR2 mutations have also been recently generated (Kannankeril *et al.*, 2006; Lehnart *et al.*, 2008). In addition, Mark's laboratory has suggested that R2474S not only predisposed mice to VT and SCD, but also induced epileptic episodes (Lehnart *et al.*, 2008). It is debatable whether mice carrying CPVT-linked mutations accurately mimic the causative arrhythmic mechanisms underlying the diseased phenotypes in humans, particularly when considering the species differences in EC coupling (Griffiths, 1999; Takagishi *et al.*, 2000; Hintz *et al.*, 2002). Nevertheless, these animal models represent a powerful approach to studying the molecular basis of fatal arrhythmias.

Mutation	Functional characterisation	
	Lipid bilayer and cell models	**Animal models**
R176Q	Unaffected basal Ca^{2+} but reduced Ca^{2+} dependent inhibition when co-expressed with T2504M (Thomas *et al.*, 2005)	Spontaneous Ca^{2+} oscillations that resulted in VT (Kannankeril *et al.*, 2006)
	Sustained high cytoplasmic Ca^{2+} levels following stimulation (Thomas *et al.*, 2004)	
	Enhanced SOICR and luminal Ca^{2+} sensitivity, unaltered FKBP12.6 association (Jiang *et al.*, 2005)	
L433P	Unaffected basal Ca^{2+} but reduced Ca^{2+} dependent inhibition (Thomas *et al.*, 2005)	
	Only mutation suggested to induce a loss of function, although cytoplasmic Ca^{2+} was sustained following stimulation (Thomas *et al.*, 2004)	
	Enhanced SOICR and luminal Ca^{2+} sensitivity, unaltered FKBP12.6 association (Jiang *et al.*, 2005)	
S2246L	Normal basal Ca^{2+}, but augmented Ca^{2+} release upon activation, unaltered FKBP12.6 association (George *et al.*, 2003a)	
	Defective interdomain interaction destabilised channel (George *et al.*, 2006)	
	Enhanced SOICR and luminal Ca^{2+} sensitivity, unaltered FKBP12.6 association (Jiang *et al.*, 2005)	
P2328S	Increased Ca^{2+} sensitivity and reduced affinity for FKBP12.6 (Lehnart *et al.*, 2004) causing polymorphic tachycardia (Laitinen *et al.*, 2001)	
N2386I	Unaffected basal Ca^{2+} but reduced Ca^{2+} dependent inhibition (Thomas *et al.*, 2005)	
	Sustained high cytoplasmic Ca^{2+} levels following stimulation (Thomas *et al.*, 2004)	
R2474S	Enhanced SOICR and luminal Ca^{2+} sensitivity, unaltered FKBP12.6 association (Jiang *et al.*, 2005)	Caused spontaneous seizures, exercise-induced VT and SCD (Lehnart *et al.*, 2008)
T2504M	Unaffected basal Ca^{2+} but reduced Ca^{2+} dependent inhibition when co-expressed with R176Q (Thomas *et al.*, 2005)	
	Sustained high cytoplasmic Ca^{2+} levels following stimulation (Thomas *et al.*, 2004)	
	Enhanced SOICR and luminal Ca^{2+} sensitivity, unaltered FKBP12.6 association (Jiang *et al.*, 2005)	
N4104K	Normal basal Ca^{2+}, but augmented Ca^{2+} release upon activation, unaltered FKBP12.6 association (George *et al.*, 2003a)	
	Defective interdomain interaction destabilised channel (George *et al.*, 2006)	
Q4201R	Increased Ca^{2+} sensitivity and reduced affinity for FKBP12.6 (Lehnart *et al.*, 2004) causing polymorphic tachycardia (Laitinen *et al.*, 2001)	
	Controversial demonstration of enhanced SOICR and luminal Ca^{2+} sensitivity and unaltered FKBP12.6 association (Jiang *et al.*, 2005).	
R4496C (mouse) R4497C (Human)	Increased Ca^{2+} sensitivity and Ca^{2+} oscillations (Jiang *et al.*, 2002a)	Predisposed heart to VT and VF (Cerrone *et al.*, 2005), without FKBP12.6 dissociation (Liu *et al.*, 2006)
	Normal basal Ca^{2+}, but augmented Ca^{2+} release upon activation, unaltered FKBP12.6 association (George *et al.*, 2003a)	
	Defective interdomain interaction destabilised channel (George *et al.*, 2006)	
I4867M	Enhanced SOICR and luminal Ca^{2+} sensitivity, unaltered FKBP12.6 association (Jiang *et al.*, 2005)	
V4653F	Increased Ca^{2+} sensitivity and reduced affinity for FKBP12.6 (Lehnart *et al.*, 2004) causing polymorphic tachycardia (Laitinen *et al.*, 2001)	

Table 1.7. Functional characterisation of RyR2 mutations

1.4.1.3. Heart failure

Heart Failure (HF) is a life-threatening disease characterised by a prolonged decline in cardiac contractility due to defective intracellular Ca^{2+} signalling. HF can arise through degenerative conditions such as cardiopathology, ischemia and hypertension, and is often characterised by a reduced SR load arising as a consequence of RyR2 Ca^{2+} leak (Shannon *et al.*, 2003; Ai *et al.*, 2005; Lehnart, 2007).

Marks and colleagues claimed that the pathogenesis of HF specifically resulted from hyper-phosphorylation of RyR2 at S2808, which dissociates FKBP12.6 and induces Ca^{2+} leak (see Section 1.4.5.2). This high profile, yet contentious theory has been proposed as a unifying pathologenic mechanism underlying both HF and CPVT (Wehrens *et al.*, 2005a). In view that HF encompasses multiple components of the EC coupling machinery including NCX and SERCA (Hajjar *et al.*, 1997; Terentyev *et al.*, 2003; Hoshijima, 2005; Maier *et al.*, 2005), and that CPVT has been linked to functionally diverse mutations throughout both RyR2 and CSQ (Priori *et al.*, 2002; Laitinen *et al.*, 2003; Lahat *et al.*, 2004), it is difficult to reconcile fully that two distinct diseases arising via separate modes of dysfunction have the same mechanistic basis.

The precise interplay of EC coupling components is central to Ca^{2+} homeostasis and normal contractile function (see Section 1.2.4). Human HF is characterised by a reduced SR load, probably resulting from a combination of increased NCX activity over-compensating for reduced cellular levels of SERCA (Shannon *et al.*, 2003). However, 'leaky' RyR2 channels are also the hallmark of human HF and are observed experimentally in 'failing myocytes' as an increased frequency of Ca^{2+} sparks (Kubalova *et al.*, 2005). Other mechanisms also contribute to Ca^{2+} dysfunction in heart failure. It has been reported that reduced PLB phosphorylation in failing cardiac cells maintained the inhibitory action on SERCA, which also reduced cellular SR load (Sande *et al.*, 2002). Furthermore, reduced EC coupling gain in HF is attributable to dysfunctional RyR2 gating and a decreased proximity of LTCC and RyR2 channels. Transverse tubule migration from the cardiomyocyte Z-line (see Figure 1.9) caused isolated 'orphaned' RyR2 channels that resulted in dyssynchronous Ca^{2+} sparks and Ca^{2+} cycling interference (Song *et al.*, 2006). Similarly, isolated RyR2 channels, referred to as 'rogue receptors', independently decoded and responded to Ca^{2+} signals, thus failing to participate in coordinated channel activity (Sobie *et al.*, 2006).

1.4.2. Mechanisms of RyR2-linked arrhythmia

1.4.2.1. Defective interdomain interaction

Intra-molecular interactions within RyR2 are critical for normal channel function (section 1.1.6), which can be destabilised as a consequence of mutation (e.g. in CPVT) (George *et al.*, 2006; Yano *et al.*, 2006) or following years of chronic dysregulation (e.g. in HF). Despite the different aetiologies of these diseases, it is emerging that defective domain interaction may be a common mechanistic basis underlying RyR2 dysfunction (Oda *et al.*, 2005; Yano *et al.*, 2005a; George *et al.*, 2006). In agreement with the hypothesis that RyR instability may be considered a generalised mechanism of channel dysfunction, defective inter-domain interactions within RyR1 underlie malignant hyperthermia (MH). The mutational clustering discussed in Section 1.4.3 is striking when considering that the mutation-rich domains are regions involved in domain interaction (Figure 1.13). This concept is explored more fully in Chapter 3.

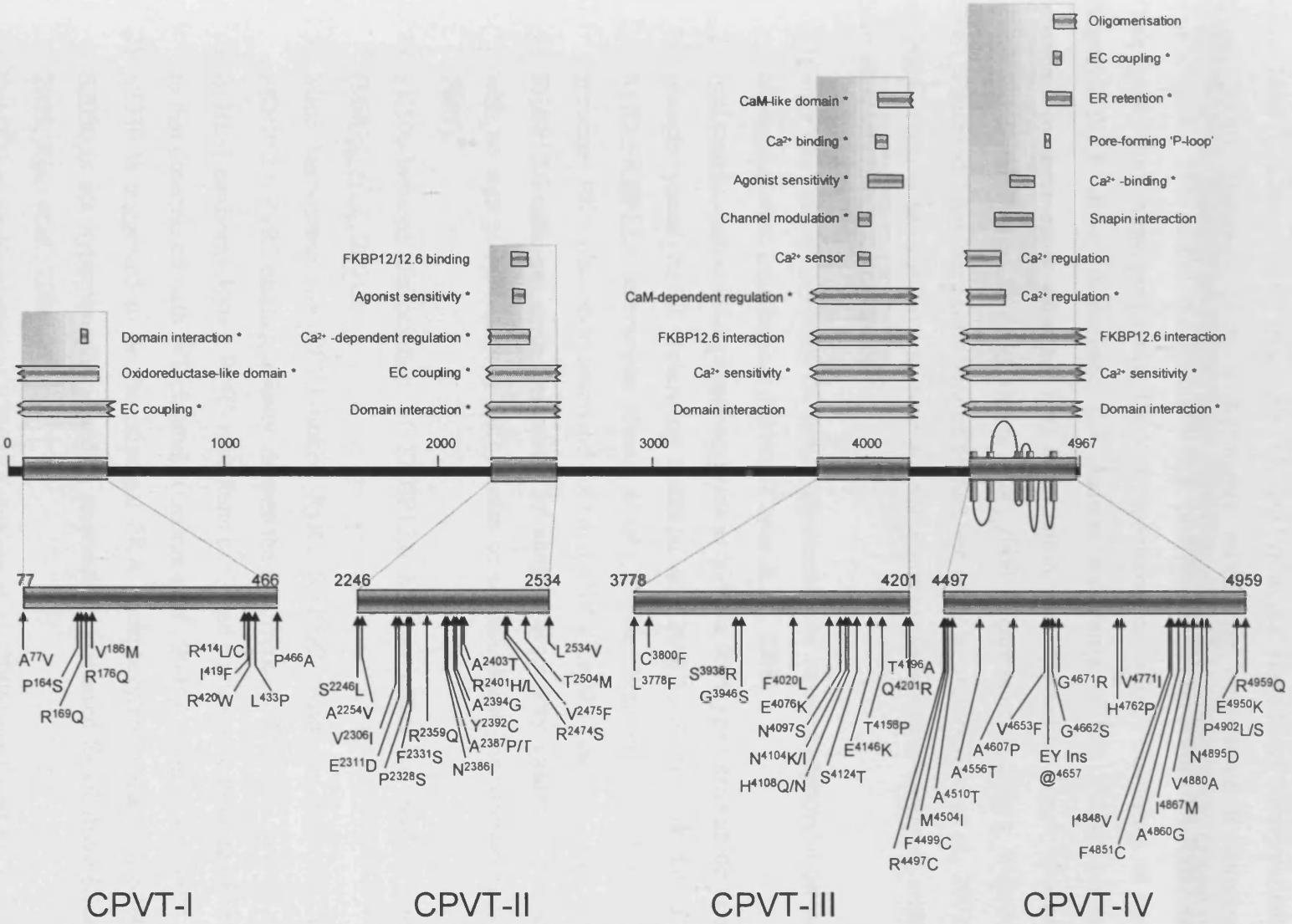

Figure 1.13. CPVT-linked RyR2 mutations cluster within functional domains

Arrhythmogenic RyR2 mutations that cluster into four discrete regions of the protein (CPVT I-IV) are associated with intramolecular regulation of Ca^{2+} release and altered EC-coupling. Text denoted * refers to analysis based on RyR1.

Modified from George *et al.*, 2007.

1.4.2.2. PKA hyper-phosphorylation of RyR2 and FKBP12.6 dissociation

The term 'hyper-phosphorylation' was used to describe the status of PKA phosphorylation at serine 2808 (S2808) of RyR2 in samples obtained from end-stage heart failure patients (Marx *et al.*, 2000). However, it is a thoroughly misleading term since it corresponds to approximately 75% of full-stoichiometry (e.g. phospho-S2808 on 3 out of 4 RyR2 subunits). Their model further proposed that PKA 'hyper-phosphorylation', occurring as a result of increased β-AR drive, dissociated the channel stabilising protein FKBP12.6 (renamed calstabin2 by these same authors). This dissociation was reported to trigger abnormal Ca^{2+} release via destabilisation of RyR2 (Marx *et al.*, 2000; Wehrens *et al.*, 2005a; Wehrens *et al.*, 2006). This model has been corroborated by just one other laboratory (Doi *et al.*, 2002; Oda *et al.*, 2005; Yano *et al.*, 2005b) and there are numerous inconsistencies emerging with studies from other laboratories. For example:

1) 75% PKA phosphorylation of S2808 represented the basal phosphorylation status and corresponded to low channel activity (Carter *et al.*, 2006).
2) Full stoichiometric PKA phosphorylation at S2808 (100%) or introduction of a pseudo phosphorylated RyR2 (following mutation of S2808 to Asp), both failed to alter RyR2:FKBP12.6 interaction (Jiang *et al.*, 2002b; Xiao *et al.*, 2004). Similarly, sustained PKA phosphorylation did not elicit SR Ca^{2+} leak (Tokuhisa *et al.*, 2006)
3) FKBP12.6-deficient mice generated by another laboratory exhibited normal RyR2 with no sign of spontaneous Ca^{2+} release or stress-induced arrhythmias (Xiao *et al.*, 2007).
4) FK506-induced dissociation of FKBP12.6 had no effect on cardiac contraction (Milting *et al.*, 2001).
5) Mice harbouring the CPVT-linked RyR2 R4496C mutation displayed unaltered FKBP12.6:RyR2 binding affinity, despite the occurrence of DADs (Liu *et al.*, 2006).
6) In HL-1 cardiomyocytes, RyR2 mutations exhibited comparable binding of FKBP12.6 to that determined with WT channels (George *et al.*, 2003a; Jiang *et al.*, 2005).
7) S2030 is suggested to be the principal PKA phosphorylation site (not S2808), and S2030 is not hyperphosphorylated in response to increased β-AR drive (Xiao *et al.*, 2005; Xiao *et al.*, 2006).
8) CaMKII phosphorylation at S2808 (Kohlhaas *et al.*, 2006) mediated SR Ca^{2+} leak via a mechanism independent of FKBP12.6 (Ai *et al.*, 2005; Guo *et al.*, 2006).

9) Ablation of the S2808 phosphorylation site in mice did not alter β-AR response, nor did it protect the mice from stress-induced episodes (Benkusky *et al.*, 2007).

Taken together, these findings do not support the central role of FKBP12.6 as a 'stabilising protein', nor do they support the theory that PKA is the only kinase responsible for inducing Ca^{2+} leak in HF and CPVT.

1.4.2.3. SR Ca^{2+} and luminal Ca^{2+} sensitivity

As shown in Figure 1.13, the majority of CPVT-linked RyR2 mutations map to the cytoplasmic domain. Thus, it has proven difficult to reconcile the occurrence of cytoplasmic mutations with the strong regulation of RyR2 by luminal Ca^{2+} environments. A mechanism that provided a potential answer to the 'cytoplasmic mutations' versus 'luminal regulation' conundrum has been put forward. In a mechanism termed store-overload-induced-calcium-release, or SOICR, Chen's lab showed that abnormal Ca^{2+} release though mutant RyR2 was linked to an increased sensitivity to SR Ca^{2+} store content (Jiang *et al.*, 2004a; Xiao *et al.*, 2004; Jiang *et al.*, 2005) (Figure 1.14). The group proposed that during periods of increased adrenergic drive, RyR2 mutations increase channel sensitivity to luminal Ca^{2+}, resulting in abnormal Ca^{2+} leak. This was proposed as a common mechanism underlying the dysfunction of all gain-of-function CPVT-linked RyR2 mutations. However, not all RyR2 mutations are gain of function (e.g. $L^{433}P$) and recently the $A^{4860}G$ mutation was found to impose reduced luminal Ca^{2+} sensitivity and a lower propensity for SOICR (Jiang *et al.*, 2007).

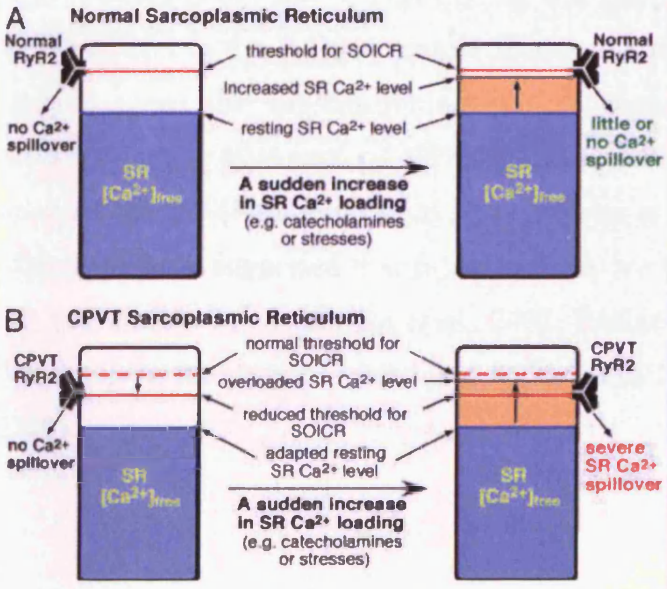

Figure 1.14. Store-overload induced calcium release (SOICR)

Both normal (A) and CPVT (B) SR Ca^{2+} load at rest (left panels) and following exercise/stress (right panels) are displayed. The red bar position signifies the relative SOICR threshold determined by RyR2, which is reduced in CPVT patients (B). The blue area represents SR free Ca^{2+}, whereas the orange area depicts increased SR-free Ca^{2+} resulting from exercise or stress. In normal RyR2, either at rest or during stress, this level is below the threshold set by SOICR. However, in mutant RyR2, following stress, Ca^{2+} leak can occur due to Ca^{2+} load rising above the SOICR threshold. Ca^{2+} leak can trigger arrhythmia through the generation of DADs. From Jiang *et al.*, 2004.

1.4.3. Targeting RyR2 as a therapeutic intervention

Currently treatments for arrhythmic conditions are limited. The predominant use of pharmacological agents that modify ion channel function is a cost-effective but sub-optimal treatment and most individuals with severe or recurrent arrhythmias are candidates for implantable mechanical devices.

To date, implantable cardioverter defibrillators (ICDs) (Keating and Sanguinetti, 2001; Dai and Yu, 2005; Francis *et al.*, 2005) are by far the most successful therapy for normalising arrhythmic episodes (Hentati *et al.*, 2003; Werner *et al.*, 2004; Napolitano and Priori, 2006). ICDs operate through monitoring cardiac rate and rhythm, and the detection of rhythmic irregularities triggers corrective therapy in the form of electrical pulses. However, ICDs are hugely expensive and are not indicated for use in all patients, particularly children. Consequently there is a clear need for new, more effective and safe alternative anti-arrhythmic strategies.

β-blockers have been used in the treatment of arrhythmias for many years and they have become the main pharmacological regime in the clinical management of CPVT. As discussed, CPVT manifests under episodes of stress and increased adrenergic drive, therefore attenuation of the β-AR response appears to be a valid strategy. In clinical trials, β-blocker therapy has been found fairly successful in reducing the occurrence of arrhythmias (Priori *et al.*, 2002). However, due to the functional heterogeneity of CPVT and its incomplete penetrance, β-blockade was inconsistent and only partially controlled arrhythmic episodes (Sumitomo *et al.*, 2003; Postma *et al.*, 2005). This finding was corroborated by incomplete protection afforded by β-blockers in the R4496C mouse model of CPVT (Cerrone *et al.*, 2005). A more recent study suggests the implementation of Ca^{2+} channel blockers increases the efficacy of β-blockers in the treatment of CPVT (Rosso *et al.*, 2007), consistent with findings from previous studies (Sumitomo *et al.*, 2003; Swan *et al.*, 2005). The two groups of Marks and Matsuzaki have suggested that β-blockers restore the association of RyR2 and FKBP12.6 in HF, preventing Ca^{2+} leak (Doi *et al.*, 2002; Reiken *et al.*, 2003c) but the beneficial effects of β-blockers in the absence of restored RyR2:FKBP12.6 binding should also be noted (George, 2008).

1.4.3.1. Targeting intra-molecular instability

Novel drugs, such as JTV519 (K201), are currently under development for the treatment of arrhythmic conditions (Kohno et al., 2003; Wehrens et al., 2004a). JTV519 was first introduced by Kaneko in 1997 (Kaneko et al., 1997) and was adopted for use as an RyR2-centred therapeutic approach by Matsuzaki's lab (Kohno et al., 2003). Following these early promising studies, it has since been promoted by Andrew Marks as the 'universal' treatment for all RyR2-related diseases, based on its apparent rescuing of the interaction between RyR2 and FKBP12.6 (Wehrens et al., 2004a; Wehrens et al., 2005b). The authors argued for an unequivocal role for FKBP12.6 re-binding to RyR2 to restore normal Ca^{2+} cycling, and showed that JTV519 had no beneficial effect in the absence of FKBP12.6. In contrast, JTV519 modulated several EC coupling proteins including SERCA (James, 2007) and K^+ channels (Nakaya et al., 2000) that suggested a lack of target specificity for RyR2. However, this broad targeting of JTV519 may underpin its successful implementation as a cardioprotective agent (Lehnart et al., 2004; Wehrens et al., 2004a; Wehrens et al., 2005b). Following on from the disastrous outcomes resulting from targeting single ion channels (Echt et al., 1991; Starmer et al., 1991), the markedly anti-arrhythmic effects of JTV519 emphasise that future pharmacological interventions should seek to modify the EC coupling network and not concentrate on the potentially hazardous targeting of single molecules.

1.4.3.2. Targeting redox modification

Redox sensitivity of RyR channels poses a novel therapeutic target. As previously discussed, ROS play an important physiological role in signal transduction within cells, however, they also function in the development of pathological conditions (Davidson and Duchen, 2006; Hool, 2006). Carvedilol, a mixed action β-blocker with free radical scavenger effects corrected defective inter-domain interactions and normalised contractility in canine heart failure (Mochizuki *et al.*, 2007). Likewise, edaravone (MCI-186), a potent free radical scavenger, was reported to reduce cell and tissue damage as a result of ROS. It has also been associated with improved cardiac function following myocardial infarction (Onogi *et al.*, 2006), and stabilising RyR inter-domain interactions in canine heart failure (Yano *et al.*, 2005a). However, the therapeutic effects of this compound are not limited to cardiovascular diseases, it has also been successfully implemented in a range of oxidative-stress related conditions and is clinically licensed for use in reducing the extent of tissue damage following

neurological ischemia (stroke) (Ito *et al.*, 2005; Asai *et al.*, 2007; Niyaz *et al.*, 2007; Ito *et al.*, 2008). Edaravone also has anti-apoptotic qualities by means of enhancing intracellular survival signalling cascades (Asai *et al.*, 2007; Niyaz *et al.*, 2007). However, edaravone may also generate ROS by reacting with a pterin (organic compound) derivative, the products of which triggered gross cell death (Arai *et al.*, 2008). Consequently the use of edaravone in a cardiac context requires the generation of careful, trial-based data in population studies. Edaravone is discussed further in Chapter 7.

1.5. SR Ca^{2+} release – a second player

1.5.1. Inositol trisphosphate receptor (IP_3R)

Inositol trisphosphate receptors (IP_3R) are a family of tetrameric Ca^{2+} release channels (Mignery *et al.*, 1989; Taylor and Richardson, 1991; Berridge, 1993) Three isoforms of IP_3R have been identified (IP_3R1, 2 and 3), which display an overall sequence homology of approximately 70% (Mackrill *et al.*, 1997) (Table 1.8). At least one isoform of IP_3R is present in all cells, although the relative expression and distribution is isoform-, tissue-type- and function- dependent (Vermassen *et al.*, 2004). IP_3Rs are crucial for both general and localised Ca^{2+}-mediated cellular signalling pathways, such as gene expression and regulation (Powell *et al.*, 2001; Cardenas *et al.*, 2005), fertilisation (Miyazaki *et al.*, 1992), apoptosis (Sugawara *et al.*, 1997; Hajnoczky *et al.*, 2000) and vital other processes (Berridge, 1993). Their wide distribution in exocrine tissues also underlies a role in secretory functions throughout the body (Fujino *et al.*, 1995; Futatsugi *et al.*, 2005).

The involvement of IP_3R in cardiac contraction was originally hypothesised in 1993 following the marked expression of IP_3R 'clusters' in Purkinje cells (Gorza *et al.*, 1993), a role that has been corroborated by recent studies (Zima and Blatter, 2004; Li *et al.*, 2005). However, as cardiomyocyte IP_3R mRNA levels are 50-fold lower than RyR2 mRNA (Moschella and Marks, 1993), the fundamental contribution of IP_3R-dependent signalling to EC coupling has been largely overlooked. Nevertheless, recent compelling findings have shown that IP_3R2, the most abundant IP_3R isoform expressed in the heart, localises to the nuclear envelope (NE) and the SR, and is involved in Ca^{2+}-dependent processes such as gene transcription and signal transduction (Zima *et al.*, 2007). Moreover, IP_3R may activate RyR2 via Ca^{2+}-release events increasing Ca^{2+} concentrations in the locality of RyR2 (Zima and Blatter, 2004; Domeier *et al.*, 2008). Despite conflicting reports (MacMillan *et al.*, 2005), this concept is appealing considering IP_3R2 and RyR2 co-localise in the SR, and that RyR2 are known to be primed by localised Ca^{2+} environments (i.e. the basis of CICR).

IP_3R are also composed of a large cytoplasmic N-terminus that constitutes ~85% of the protein, and a smaller transmembrane region that forms the Ca^{2+} releasing pore (Taylor and Richardson, 1991). Like RyR, IP_3Rs are modulated by a vast array of regulators on both luminal and cytoplasmic faces (Table 1.9). The N-terminal residues 1-604 of IP_3R1 bind IP_3,

which was enhanced by deletion of a 'suppressor' domain' (a.a. 1-225) (Yoshikawa *et al.*, 1996; Yoshikawa *et al.*, 1999) (Figure 1.15). The N-terminus is reported to be involved in channel gating via interaction with a conserved cysteine residue in the TM domain (2613 in IP_3R1) (Uchida *et al.*, 2003), which supports the functional intra-molecular interactions demonstrated in other studies (Boehning and Joseph, 2000; Schug and Joseph, 2006). Furthermore, mutation-linked disruption of the IP_3R pore inactivated the channel (Schug *et al.*, 2008). Following IP_3 binding to the receptor, activation signals are transduced via the N-terminal and internal coupling domains to the gatekeeper domain, which causes a conformation change in the TM assembly that opens the channel (Figure 1.15). IP_3R have six putative transmembrane (TM) spanning domains (Figure 1.15), of which TM1 and 2 are documented as essential for ER membrane retention (Parker *et al.*, 2004). Various IP_3R domains have been determined at a resolution (~2Å, (Bosanac *et al.*, 2002; Bosanac *et al.*, 2005)) superior to that presently obtained for RyR. Thus, in view of the high structural homology of RyR and IP_3R (60-70%, Appendix I) it is anticipated that ongoing structural studies of IP_3R may provide valuable insights into the relationship between RyR structure and function.

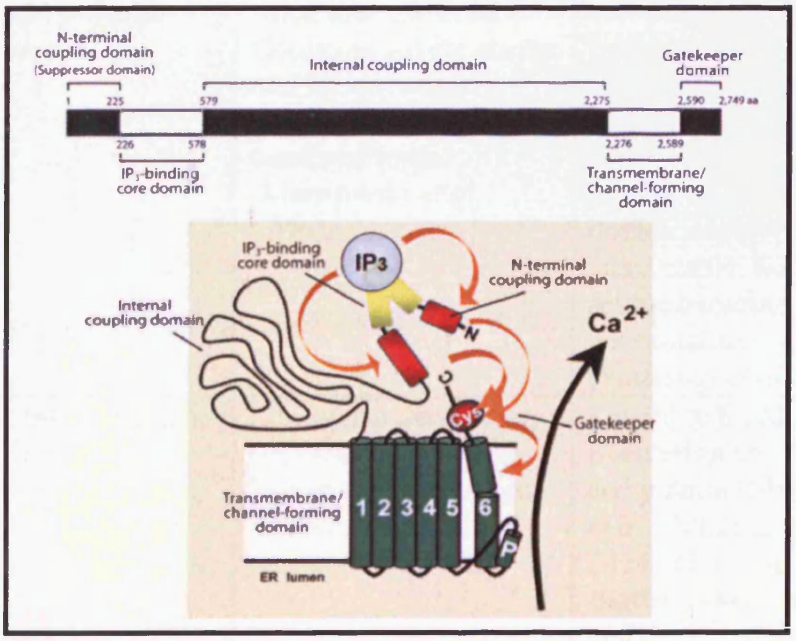

Figure 1.15. Schematic representation of IP_3R structure

The IP_3R **(shown here based on mouse IP_3R1)** is composed of an N-terminal cytoplasmic IP_3-binding domain (β-trefoil), C-terminal channel domain (α-helical) and an intermediate regulatory/coupling domain. IP_3 binds to the N-terminus which elicits a conformational change via coupling domains that activates the channel.

From Mikoshiba, 2007.

	IP_3R1	IP_3R2	IP_3R3
Size	Human: 2695 amino acids (Yamada *et al.*, 1994) 220kDa (Yamada *et al.*, 1994)	Human: 2701 amino acids (Sudhof *et al.*, 1991; Yamamoto-Hino *et al.*, 1994) 270kDa (Li *et al.*, 2005)	Human: 2671 amino acids (Yamada *et al.*, 1994; Yamamoto-Hino *et al.*, 1994) 240kDa (Yamamoto-Hino *et al.*, 1995)
Gene Location	Human: 3p25-26 (Yamada *et al.*, 1994)	Human: 12p11 (Yamada *et al.*, 1994)	Human: 6p21 (Yamada *et al.*, 1994)
Expression & Distribution	Brain and smooth muscle (Yoshida and Imai, 1997) and throughout the CNS (Furuichi *et al.*, 1993). Detected in smooth ER and outer nuclear membrane (Yoshida and Imai, 1997).	Predominant cardiac isoform (Zima *et al.*, 2007), expressed six times higher in atrial myocytes than ventricular (Lipp *et al.*, 2000). Also expressed in liver, testis, lung, spleen and pancreas (Yoshida and Imai, 1997). Localised to cardiomyocyte nuclear envelope (Bare *et al.*, 2005).	Widespread tissue distribution but expression was higher in pancreas, intestine, lung and brain (Yoshida and Imai, 1997). Co-localised with mitochondria (Mendes *et al.*, 2005).
Mutations/ Polymorphisms and animal models	Most IP_3R1-null mice were embryonic lethal. Mice that survived displayed severe ataxia and seizures that caused death within weeks of birth (Matsumoto *et al.*, 1996).	IP_3R2-deficient mice were viable with no compensatory changes in either IP_3R1 or IP_3R3. RyR, NCX and SERCA expression was unaltered (Li *et al.*, 2005). IP_3R2 and 3 double knock-out mice were viable, but had severe exocrine abnormalities (Futatsugi *et al.*, 2005).	IP_3R3 deficient mice displayed abnormal taste perception (Hisatsune *et al.*, 2007). Natural polymorphism, P335L, affected intracellular Ca^{2+} signalling by reducing IP_3 binding and IICR (Kim *et al.*, 2005).
Link to Disease	Long-term depression (Inoue *et al.*, 1998). Epilepsy (Matsumoto and Nagata, 1999).	Linked to atrial fibrillation and arrhythmia (Mackenzie *et al.*, 2002; Guo *et al.*, 2004; Zima and Blatter, 2004; Li *et al.*, 2005)	

Table 1.8. Functional characteristics of IP_3R isoforms

	IP_3R
CaM	Inhibited IP_3-mediated Ca^{2+} release in all IP_3R isoforms independent of Ca^{2+} (Patel *et al.*, 1999; Adkins *et al.*, 2000)
IRBIT (IP_3 binding protein released with IP_3)	Competes with IP_3 for IP_3-binding core on IP_3R (Ando *et al.*, 2006) but was released from IP_3R upon IP_3 binding. IRBIT bound to IP_3R in phosphorylated form and was only dissociated by IP_3 during IICR (Ando *et al.*, 2003)
CABP1 (IP_3R Ca^{2+} binding protein)	CABP1 bound with high affinity (~25nM) to IP_3 binding region of all IP_3R isoforms, and increased P_o (Yang *et al.*, 2002). Conversely, CABP1 was reported to reduce IICR (Kasri *et al.*, 2004)
ERp44	ERp44 is a luminal IP_3R binding protein of 44kDa that interacted with the third luminal loop variable region of IP_3R1, an association dependent on redox state. As this region was not conserved throughout isoforms, interaction does not occur with IP_3R2 or 3. Decreased luminal Ca^{2+} concentration increased ERp44 interaction with IP_3R1 that attenuated channel response to IP_3 and subsequently prevented store depletion (Higo *et al.*, 2005).
Chromogranin A/B (CGA/CGB)	Both CGA and B are high-capacity, low-affinity luminal Ca^{2+} storage proteins. CGA and B interacted with the conserved region of the third luminal loop of all three IP_3R isoforms (Kang *et al.*, 2007), but interaction with CGB was stronger than CGA (Thrower *et al.*, 2003). CGA and B increased IP_3R activity (Higo *et al.*, 2005)
Homer	Binds a proline-rich region in N-terminal suppressor region of IP_3R and may physically couple IP_3Rs to metabotropic glutamate receptors (involved in IP_3 and PKC production) (Tu *et al.*, 1998)
Cytochrome C	Cytochrome C binding blocked Ca^{2+} dependent inhibition of IP_3R, causing uncontrolled Ca^{2+} release. Sustained intracellular Ca^{2+} concentrations triggered global cytochrome C release from mitochondria, which induced apoptosis (Boehning *et al.*, 2003; Sedlak and Snyder, 2006)
Carbonic-anhydrase related protein (CARP)	CARP bound to the modulatory domain of IP_3R1, which reduced IP_3 affinity, and inhibited IP_3 binding (Hirota *et al.*, 2003)
FKBP	FKBP12 bound to the internal coupling domain of IP_3R (Cameron *et al.*, 1997). Agonist-induced Ca^{2+} release was unaffected by FKBP12 (Bultynck *et al.*, 2001)

Table 1.9. Functional and physical association of key proteins in IP_3R regulation

1.5.1.1. IP_3R channel regulation

IP_3R are primarily regulated by second messengers Ca^{2+} and IP_3, as well as Mg^{2+} and ATP (Table 1.10). However, receptor function is also modulated by protein interactions (Table 1.9) and phosphorylation (Table 1.11) (Choe and Ehrlich, 2006). Extracellular stimuli are conveyed via G-protein coupled receptors (GPCR) in the plasma membrane, which activate phospholipase C (PLC). PLC stimulates hydrolysis of phosphatidyl inositol bisphosphate (PIP2) into IP_3 and diacylglycerol (DAG), which participate in distinct, yet interconnected signalling events. IP_3 induces conformational-dependent Ca^{2+} release (IICR) directly through IP_3R (Mikoshiba *et al.*, 1994) whereas DAG may activate IP_3R indirectly via downstream PKC-mediated events (Mikoshiba *et al.*, 1994; Arguin *et al.*, 2007; Mikoshiba, 2007).

Like RyR, IP_3R are organised into lattice-like arrays and can function either individually or in synchronised clusters. A possible functional consequence of IP_3R array formation is that the dynamic range of IICR from ER stores may be precisely tuned by the magnitude of the stimuli. Localised Ca^{2+} signalling events arise through single channel activation termed a Ca^{2+} 'blip' which are synchronised into clusters termed Ca^{2+} 'puffs' that are analogous to a RyR-mediated 'spark'. Co-ordinated 'puffs' can trigger propagative Ca^{2+} waves (Keizer and Smith, 1998). In addition, IP_3R1 harbouring a mutation (K508A) that prevented an IP_3-induced conformational change was also found to inhibit cluster formation and Ca^{2+} release (Tateishi *et al.*, 2005; Chalmers *et al.*, 2006). These findings, in line with previous studies, suggest that both intra-molecular and inter-protein communication is vital for normal channel function.

	IP_3R
Physiological	
IP_3	IP_3R1 and 2 bind IP_3 with high affinity (K_d ~50 and 15nM respectively) (Sudhof *et al.*, 1991). IP_3R2 is most sensitive isoform to IP_3 (Miyakawa *et al.*, 1999) and mobilised significantly more Ca^{2+} than IP_3R1 (Ramos-Franco *et al.*, 1998). IP_3R3 is least sensitive isoform to IP_3 (K_d~160nM) (Miyakawa *et al.*, 1999).
Ca^{2+}	IP_3R1, but not IP_3R2 was inhibited by mM cytoplasmic Ca^{2+} levels, (Ramos-Franco *et al.*, 1998). All IP_3Rs were inhibited by mM luminal Ca^{2+}, yet stimulated by μM luminal Ca^{2+}. IP_3R3 is the least sensitive isoform to Ca^{2+}. Ca^{2+} inhibition of IP_3Rs is inversely related to cytoplasmic IP_3 concentration (Miyakawa *et al.*, 1999).
Mg^{2+}	Mg^{2+} inhibited IP_3R and did not compete with IP_3 or Ca^{2+} for binding sites (Volpe and Vezu, 1993; White *et al.*, 1993), but this is controversial (Van Delden *et al.*, 1993)
ATP	Consensus ATP binding site between isoforms suggested a similar action on all IP_3R isoforms (Yoshida and Imai, 1997) but rank order of IP_3R sensitivity is $IP_3R1 > IP_3R2 > IP_3R3$ (Miyakawa *et al.*, 1999; Maes *et al.*, 2000). ATP increased IP_3R P_o, however, in the absence of ATP, higher $[Ca^{2+}]_i$ was required for channel activation.
cADPR	Contrasting to its actions on RyR, cADPR inhibited IICR (Missiaen *et al.*, 1998).
Pharmacological	
Carbachol	Carbachol (a muscarinic receptor agonist widely used experimentally to stimulate IP_3R) increases IP_3 concentrations by GPCR activation of PLC (Arguin *et al.*, 2007; Caron *et al.*, 2007; Chaloux *et al.*, 2007; Regimbald-Dumas *et al.*, 2007). Carbachol-triggered Ca^{2+} release through PKC-phosphorylated IP_3R was reduced (Arguin *et al.*, 2007).
Heparin	Heparin blocks IP_3R function ($IP_3R3 > IP_3R1$/ IP_3R2) and competitively inhibits IP_3 binding (White *et al.*, 1993; Ramos-Franco *et al.*, 1998; Zima and Blatter, 2004; Zima *et al.*, 2007)
Thimerosal	Oxidative agents potentially modulate IP_3R function through enhancing receptor sensitivity to IP_3. Redox state can modulate binding of the luminal protein ERp44.

Table 1.10. Main physiological and pharmacological regulators of IP_3R

1.5.1.2. IP_3R phosphorylation

IP_3R is a substrate for phosphorylation by an array of phosphatases and kinases, which, like RyR imposes a potentially huge functional plasticity on IP_3R regulation (Table 1.11). For example, IP_3R1 phosphorylation by PKA at S1589 and S1755 increased receptor sensitivity to IP_3, whereas targeting of PKG to identical sites inhibited IICR. In addition, CaMKII phosphorylation was reported to diminish IP_3 responses, but this function was suggested to underlie a negative feedback mechanism that modulated Ca^{2+} oscillations (Zhu *et al.*, 1996). A further kinase, protein kinase B (PKB, also termed Akt) binds to a C-terminal tail sequence present across all IP_3R isoforms (Khan *et al.*, 2006) and is proposed to modulate the binding of apoptosis-related proteins (Szado *et al.*, 2008).

	IP_3R
CaMKII	Phosphorylation reduced IP_3R P_o (Ferris *et al.*, 1991; Bare *et al.*, 2005).
PKA	Phosphorylation increased IP_3R activity (Chaloux *et al.*, 2007; Regimbald-Dumas *et al.*, 2007) and sensitivity to IP_3 (Tang *et al.*, 2003). IP_3R1 is more sensitive to PKA phosphorylation than type 2 or 3 (Murthy and Zhou, 2003).
PKB	Phosphorylation reduced Ca^{2+} efflux, which was associated with a lower susceptibility to apoptosis (Szado *et al.*, 2008).
PKC	Phosphorylation was increased by Ca^{2+} and DAG (Ferris *et al.*, 1991), and was associated with a decreased response to IICR and carbachol stimulation (Arguin *et al.*, 2007; Caron *et al.*, 2007).
PKG	Phosphorylation inhibited IICR (Murthy and Zhou, 2003)
PP1/PP2A	Dephosphorylation reversed PKA phosphorylation via the same site (a.a. 1251-1287) (Tang *et al.*, 2003), and regulated interactions between IP_3R and IRBIT, influencing IICR (Devogelaere *et al.*, 2007).

Table 1.11. Functional regulation of IP_3R by kinases and phosphatases

1.5.2. Functional and structural similarities between RyR and IP_3R

As described above, although RyR and IP_3R constitute distinct intracellular Ca^{2+} release channels, they exhibit some similarities with respect to expression profiles and tissue restriction, modes of channel regulation and 'domain-based' structural organisation. Both are homotetrameric channels comprised of a large N-terminus that protrudes into the cytoplasm, and a comparably smaller C-terminus that forms the Ca^{2+} pore (Taylor and Richardson, 1991; Coronado *et al.*, 1994). In addition, there is a pronounced degree of structural similarity that belies rather limited sequence homology between the IP_3R and RyR channel families (Lai *et al.*, 1987; Lai *et al.*, 1988; Mignery *et al.*, 1989; Mignery *et al.*, 1990), (see Appendix I). The activities of both receptor families are modulated by discrete interdomain interactions (Yamamoto *et al.*, 2000; Uchida *et al.*, 2003; George *et al.*, 2004), which are also sensitive to interactions with accessory proteins (e.g. FKBP and CaM), localised phosphorylation events and redox environments (Ferris *et al.*, 1991; Ai *et al.*, 2005; Aracena-Parks *et al.*, 2006; Joseph *et al.*, 2006; Mochizuki *et al.*, 2007). Taken together, these characteristics provide a basis for cross-communication between receptor families, and is a concept that has been explored by various laboratories (Lipp *et al.*, 2000; George *et al.*, 2003b; McCarron *et al.*, 2003; MacMillan *et al.*, 2005; Domeier *et al.*, 2008).

1.6. Thesis principle

Discrete RyR2 protein domains interact to functionally regulate channel gating. RyR2 mutations (CPVT) and chronic maladaptive responses in cardiac cells (HF) have been proposed to disrupt intra-molecular interactions, thereby impairing channel regulation, and leading to gross abnormalities in cellular Ca^{2+} handling.

The I-domain is an important region that mediates interactions within RyR2. A bioinformatic approach revealed that IP_3R contain putative structural motifs similar to those of the RyR2 I-domain (Appendix I). Based on the pioneering *in vitro* studies of Ikemoto and colleagues, I hypothesised that the I-domain (and sub- fragments therein) could exquisitely modulate Ca^{2+} release channel function (RyR2 and IP_3R) in a cellular context. The central tenet of this technique is that domain-targeted peptides can structurally and functionally interact with RyR via homologous sequences and modulate channel function. A similar approach demonstrated the feasibility of modulating IP_3R function (Varnai *et al.*, 2005). This thesis presents the first characterisation of the phenotypic and functional consequences of manipulating cellular Ca^{2+} using recombinant I-domain fragments in living cells. Subsequently it aims to determine the nature and mode of cell damage induced by I-domain expression, and if this is a result of perturbed IP_3R Ca^{2+} signalling, whether under stimulated or resting conditions. This thesis will also assess the effect of I-domain transfection on neighbouring non-expressing cells; in particular investigating the contribution of various cell signalling pathways.

Chapter 2

General Materials and Methods

Chapter 2 General Materials and Methods

2.1. Materials

All reagents used were stored at room temperature (RT) unless otherwise stated.

2.1.1. Microbiology reagents

- XL-10 Gold® Ultracompetent cells (Stratagene). Stored at -80°C.
- Luria-Bertani (LB) broth (1% (w/v) tryptone, 0.5% (w/v) NaCl, 0.5% (w/v) yeast extract). Autoclaved and cooled to 37°C prior to antibiotic addition.
- Agar plates: LB broth with 1.5% (w/v) agar. Autoclaved and cooled to 50°C prior to antibiotic addition. Plates were made fresh.
- NZY broth: 1.6% (w/v) NZ medium, 0.5% (w/v) yeast extract. Autoclaved.
- Wizard® *Plus* SV Minipreps DNA Purification System (Promega) including:
    - Wizard® *Plus* SV Cell Resuspension Solution
        - 50mM Tris-HCl, 10mM EDTA, 100µg/ml RNase A (to limit contamination by RNA); pH7.5
    - Wizard® *Plus* SV Cell Lysis Solution
        - 0.2M NaOH and 1% SDS (w/v)
    - Wizard® *Plus* SV Neutralisation Solution
        - 4.09M guanidine hydrochloride, 0.759M potassium acetate, 2.12M glacial acetic acid; pH4.2
    - Wizard® *Plus* SV Column Wash Solution
        - 60mM potassium acetate, 8.3mM Tris-HCl, 40µM EDTA, 60 ethanol; pH 7.5
- Plasmid Maxi Kit (Qiagen®) including:
    - Resuspension buffer, P1
        - 50mM Tris-HCl, 10mM EDTA, 100µg/ml RNase A; pH8.0
    - Cell Lysis buffer, P2
        - 0.2M NaOH and 1% SDS (w/v)
    - Neutralisation buffer, P3
        - 3M potassium acetate; pH5.5
    - Equilibration buffer, QBT

- 750mM NaCl, 50mM MOPS pH 7.0, 15% isopropanol (v/v), 0.15% Triton® X-100 (v/v)

- Column Wash buffer, QC
  - 1M NaCl, 50mM MOPS pH 7.0, 15% isopropanol (v/v)
- Elution buffer, QF
  - 1.25M NaCl, 50mM Tris-HCl pH8.5, 15% isopropanol (v/v)

- QIAquick Gel Extraction Kit (Qiagen®)
  - Proprietary QIAquick agarose liquefying buffer (QG) containing guanidine isothiocyanate.
  - Proprietary QIAquick wash buffer (PE) containing 70% (v/v) ethanol.
  - Elution buffer, EB
    - 10mM Tris-HCl; pH8.5

2.1.2. Molecular biology reagents

2.1.2.1. PCR and sequencing

- Rapid DNA ligation kit (Roche)
  - ATP-containing T4 DNA ligation buffer, 2x concentrated.
  - DNA dilution buffer, 5x concentrated
  - T4 DNA ligase, 5U/µl
- Taq DNA Polymerase in buffer B (Promega). Stored at -20°C.
- Big Dye® sequencing mix (Applied Biosystems). Stored at -20°C.
- Sequencing primers for PCR :
  - SPFOR12713 (TTTGAAATGCAGCTGGCG) (forward: pmRFP-C1 ID[A]), binding RyR2 12713-12730.
  - 24R (GGACCAATGGTAGCAGCTA) (reverse: pmRFP-C1 ID[A]), binding RyR2 11375-11393.
  - BF13403 (ACAGATACGGAGAACCAG) (forward: pmRFP-C1 ID[B&C]), binding RyR2 13403-13420.
  - SPREV13343 (AACCCAGTCCCCATGCCTGAGGTGCA) (reverse: pmRFP-C1 ID[B&C]), binding RyR2 13318-13343.

2.1.2.2. Agarose gel electrophoresis

- Agarose powder (ultra-pure, Eurogentec)
- 1x TAE buffer: 40mM Tris, 20mM glacial acetic acid, 1mM EDTA.
- Ethidium Bromide (EtBr), aqueous solution at 10mg/ml (Sigma-Aldrich).
- 1kb DNA ladder (Invitrogen). Stored at -20°C.
- Agarose gel loading buffer: 50% glycerol (v/v), 50% 1xTAE buffer (v/v) and Orange G (sufficient for colour change to yellow/orange).

2.1.2.3. DNA restriction enzymes

All restriction enzymes were purchased from New England BioLabs and were stored at -20°C:

Restriction enzyme	Restriction site recognised	Optimal digest temperature
Bam HI	5'-G|GATCC-3'	37°C
Bgl II	5'-A|GATCT-3'	37°C
Eco RI	5'-G|AATTC-3'	37°C
Hind III	5'-A|AGCTT-3'	37°C
Nhe I	5'-G|CTAGC-3'	37°C
Pvu II	5'-CAG|CTG-3'	37°C
Sal I	5'-G|TCGAC-3'*	37°C
Xba I	5'-T|CTAGA-3'	37°C
Xho I	5'-C|TCGAG-3'*	37°C

Table 2.1. Restriction enzymes and recognition sequences

* Compatible overhang permits T4-ligase mediated ligation of *SalI* / *XhoI* ends

2.1.2.4. Protein preparation, SDS-PAGE and Western blot

- Proprietary protease inhibitor cocktail: 1x protease inhibitor cocktail tablet (Roche) dissolved in 20mM Tris, 5mM EDTA and 0.05% (v/v) Triton-X-100 (25ml total volume), adjusted to pH7.4 with HCl.
- 1.5M Tris, pH8.8 adjusted with HCl.
- 0.5M Tris: pH6.8 adjusted with HCl.
- Ammonium persulphate (10% (w/v)), freshly prepared.
- TEMED (Sigma-Aldrich).
- Acrylamide/Bisacrylamide solution (ratio of 37.5:1), 40% (Bio-Rad). Stored at 4°C.
- 5x SDS loading buffer: 250mM Tris pH6.8, 50% (v/v) glycerol, 10% (w/v) SDS, 0.5% (w/v) bromophenol blue. Heated to 50°C prior to 10% (v/v) β-mercaptoethanol addition and loading.
- 1x SDS-PAGE running buffer: 25mM Tris, 250mM glycine, 0.1% (w/v) SDS.
- Pre-stained Kaleidoscope molecular weight markers (BioRad). Stored at -20°C.
- Semi-dry transfer buffer: 48mM Tris, 39mM glycine, 0.037% (w/v) SDS and 20% (v/v) methanol.
- 1x Tris-buffered saline (TBS): 20mM Tris, 137mM NaCl, adjusted to pH7.5 with HCl.
- 1x TBS-T: 0.1% (v/v) Tween-20 in 1x TBS, adjusted to pH7.5 with HCl.
- Milk blocking solution: 5% (w/v) non-fat dried milk in TBS-T.
- Imperial™ protein stain (Pierce). An optimised solution of Coomassie Brilliant Blue ™ R250 dye

2.1.2.5. Antibodies

2.1.2.5.1. Primary antibodies

- *Living Colours® DsRed polyclonal antibody* (Clontech, Takara). Rabbit antiserum raised against whole recombinant protein DsRed-express (an

optimised variant of *Discosoma* sp. red fluorescent protein). Used at 1:750 for Western blot. Stored at -20°C.

- *IP_3R1* (Affinity Bioreagents). Rabbit antiserum raised against a synthetic peptide in the N-terminus of IP_3R1 ((1829) KKKDDEVDRDAPSRKKAKE (1848). Used at 1:1000 for Western blot and immunofluorescence. Stored at -20°C, specific for type 1.
- *IP_3R2* (e-15) (Santa Cruz Biotech). Goat antiserum raised against an unspecified peptide specific to human IP_3R2. Used at 1:200 for Western blot and immunofluorescence. Stored at 4°C.
- *SERCA2* (Affinity Bioreagents). IgG1 mouse monoclonal antibody clone IID8 raised against native human SERCA2. Used at 1:2,500 for Western blot. Stored at -20°C.
- *Calreticulin.* Rabbit polyclonal antiserum generated against the entire recombinant protein, provided by Dr. D. Llewellyn, Cardiff University. Used at 1:1,000 for Western blot. Stored at -20°C.

2.1.2.5.2. Secondary antibodies

- Goat anti-rabbit: Horseradish peroxidase conjugated (Santa Cruz Biotechnology). Used at 1:10,000 for Western blot. Stored at 4°C.
- Rabbit anti-mouse: Horseradish peroxidase conjugated (Santa Cruz Biotechnology). Used at 1:5,000 for Western blot. Stored at 4°C.
- Donkey anti-goat: Horseradish peroxidase conjugated (Santa Cruz Biotechnology). Used at 1:10,000 for Western blot. Stored at 4°C.
- Goat anti-rabbit: Alexa Fluor® 488 conjugated (Molecular Probes, Invitrogen). Used at 1:2,000 for immunofluorescence. Stored at -20°C.
- Donkey anti-goat: Alexa Fluor® 488 conjugated (Molecular Probes, Invitrogen). Used at 1:1,000 for immunofluorescence. Stored at 4°C.

2.1.3. Cell Culture Reagents

- Dulbecco's modified Eagle medium (DMEM) containing 4.5g/L L-glucose was supplemented with filter sterilised 10% (v/v) foetal bovine serum (FBS), 1% (v/v) 2mM glutamine and 100μg/ml penicillin/streptomycin (supplemented medium referred to as complete DMEM [cDMEM]) (all from Invitrogen). Stored at 4°C and pre-warmed to 37°C prior to use.
- Claycomb medium (SAFC Biosciences) supplemented with filter sterilised 10% (v/v) foetal bovine serum (FBS), 1% (v/v) 10mM norepinephrine, 1% (v/v) 2mM glutamine and 100μg/ml penicillin/streptomycin (supplemented medium referred to as complete Claycomb). Stored at 4°C and pre-warmed to 37°C prior to use.
- 1x Trypsin-EDTA in Hepes buffered salt solution (HBSS) (Invitrogen), stored at -20°C.
- Poly-L-lysine, 0.1% (w/v) solution (Invitrogen) for pre-coating cultureware. Stored at 4°C.
- Gelatin-fibronectin (GFN) (1mg fibronectin in 79ml 0.02% gelatin). Fibronectin supplied by Sigma-Aldrich. Filter sterilised and stored at -20°C.
- Cell freezing-down solution: FBS containing 10% (v/v) dimethyl sulphoxide (DMSO), filter sterilised into 1ml aliquots stored at -20°C.
- Isotonic NaCl solution, 0.9% (w/v) (Baxter Medical Supplies).
- Phosphate buffered saline (PBS), pH7.4: 137mM NaCl, 2.7mM KCl, 4.3mM Na_2HPO_4, 1.4mM KH_2PO_4, pH adjusted using HCl.
- Cell fixing reagent: 4% (v/v) paraformaldehyde in PBS. Freshly prepared.
- Effectene non-liposomal lipid-based cell transfection reagent (Qiagen): Used as per manufacturers instructions. Stored at 4°C.

2.1.3.1. Cell culture assay reagents and kits

- Proprietary alamarBlue™ reagent (Abd Serotec): used at 10% (v/v) in cDMEM prepared fresh. Stored at 4°C.

- Trypan Blue™ reagent (Sigma-Aldrich), 0.4%: Used as an addition of 0.1ml to 0.5ml $1x10^5$ cell suspension in PBS pH7.4.
- DeadEnd™ Tunel System (Promega): Used as per manufacturers instructions. Stored at -20°C.
    - Equilibration buffer
        - 200mM potassium cacodylate pH6.6
        - 25mM Tris-HCl pH6.6
        - 0.2mM DTT
        - 0.25mg/ml BSA
        - 2.5mM cobalt chloride
    - Nucleotide mix
        - 50μM fluorescein-12-dUTP
        - 100μM dATP
        - 10mM Tris-HCl pH7.6
        - 1mM EDTA
    - Terminal deoxynucleotidyl transferase, recombinant enzyme (rTdT)
    - 20x SSC pH7.2
        - 175.4 mg/ml NaCl
        - 88.2 mg/ml sodium citrate
- ENLITEN® rLuciferase/Luciferin reagent (Promega): Used as per manufacturers instructions. Stored at -20°C.
    - Reconstitution buffer
    - rLuciferin/Luciferase reagent
    - Proprietary composition but working reagent contains unknown amounts of luciferase, D-luciferin, Tris-acetate buffer (pH7.75), EDTA, magnesium acetate, BSA, DTT and 0.02% sodium azide (preservative).

2.1.4. Ca^{2+} imaging reagents

- Poly-L-lysine pre-coated 30mm coverslip chambers (MatTek Corporation).
- Fluo-4 acetoxymethyl (AM) ester (Molecular Probes, Invitrogen): Dissolved in 20% (w/v) pluronic acid F-127 in DMSO to give a stock concentration of

3.2mM. Stored at -20°C. Fluo-4AM was used at 5μM following dilution in unsupplemented culture media.

- Carbamyl chloride (carbachol) (Sigma-Aldrich): Freshly prepared 10mM stock in DMEM.
- Caffeine (Sigma-Aldrich): Freshly prepared 100mM stock in unsupplemented DMEM. Stock solutions were diluted in unsupplemented DMEM to a working concentration of 10mM.
- Thapsigargin (Sigma-Aldrich): Prepared 1mM stock in DMSO and stored in 20μl aliquots at -20°C. Used at a final concentration of 5μM.
- Ionomycin (Sigma-Aldrich): Prepared 1mM stock in DMSO and stored in 50μl aliquots at -20°C. Used at a final concentration of 1μM.
- Edaravone (MCI-186) (Sigma-Aldrich): Prepared 1M stock in DMSO and stored in 100μl aliquots at -20°C.
- Apyrase, grade I isolated from potato (Sigma-Aldrich): Prepared 100U/ml stock in water and stored in 100μl aliquots at -20°C. Used a working concentration of 10U/ml.
- Phorbol 12-myristate 13-acetate (PMA) (Sigma-Aldrich): Prepared 250μM stock in DMSO and stored in 300μl aliquots at -20°C. Stock solutions were diluted in unsupplemented DMEM to give working concentrations of 10, 1, 0.1 and 0.01μM.

2.2. Methods

2.2.1. Detecting recombinant proteins

The use of inherently fluorescent proteins (FPs) that require no accessory cofactors for fluorescence (e.g. green fluorescent protein (GFP)) has become commonplace over the past two decades (Chalfie *et al.*, 1994; Zhang *et al.*, 1996; Baird *et al.*, 2000; Campbell *et al.*, 2002). Their widespread implementation in protein imaging studies is due to a number of advantageous features including the ready availability of plasmid DNA encoding spectral variants, a relative lack of adverse effects on the intracellular environment and a structural stability that precludes photobleaching. Current molecular biological techniques make it a relatively simple task to fuse a FP to the amino- or carboxyl-terminus of a recombinant protein of interest, and as such these approaches have become the method of choice in most laboratories for the detection and visualisation of recombinant proteins in living cells.

Green fluorescent protein (GFP) was discovered in 1961 as a trace contaminant during the isolation and purification of the Ca^{2+}-sensitive protein aequorin from *Aequorea victoria* jellyfish (Shimomura *et al.*, 1962, 1963). Since its adaptation for research purposes throughout the 1990s, selective mutagenesis of GFP has resulted in the generation of large numbers of spectrally distinct variants that emit in the blue-green region of the spectrum including yellow- (YFP), blue- (BFP) and cyan- (CFP) fluorescent proteins (Shaner *et al.*, 2007). The isolation of the first red fluorophore, DsRed from a coral of the *Discosoma* Sp. (Baird *et al.*, 2000; Fradkov *et al.*, 2000) has significantly augmented the spectral range of FPs. Although DsRed is potentially useful since it is spectrally distinct from tags based on A. victoria's GFP, its fluorescence is entirely dependent on homo-tetramerisation and thus its utility as a fusion tag is limited. This problem was largely negated by mutagenesis of the oligomerisation domain of DsRed that resulted in the generation of a panel of monomeric red fluorescent proteins (mRFPs) with small but distinct alterations in their excitation and emission profiles (such as mCherry, mTomato, mMelon) (Shaner *et al.*, 2004; Muller-Taubenberger *et al.*, 2006; Shaner *et al.*, 2007). The mRFP used extensively in this thesis is the 'first-generation' mRFP originally derived from DsRed mutagenesis. The excitation and emission profile of mRFP and DsRed are

585nm/608nm and 558/583nm respectively and can both be easily distinguished from eGFP tagged RyR2 and cellular Ca^{2+} monitored with green fluorescent dyes (excitation 485-495nm and emission 510-520nm).

2.2.1.1. mRFP as a fluorescent fusion protein

Monomeric red fluorescent protein (mRFP) (Campbell *et al.*, 2002) was derived from tetrameric DsRed by thirty-three point mutations. Its inherent rapid green-red maturation rate (>10 times faster than DsRed), significantly smaller size (682bp compared to >2700bp) and monomericity improved protein manipulation and makes it far more suited for use as a red fusion tag in this project (see Section 3.2.1).

2.2.1.2. eGFP as a fluorescent fusion protein

Enhanced green fluorescent protein (eGFP) was derived from GFP by two key point mutations (F64L and S65T) that resulted in an increased photostability and an augmented excitation peak that was shifted to 488nm, ideal for excitation with the argon laser commonly fitted on confocal microscopes. eGFP has been extensively used as a fusion tag in many studies performed in our laboratory (see Section 5.2.7).

2.2.2. DNA Cloning

2.2.2.1. Generation of plasmid DNA encoding RyR2 I-domain

RyR2 fragments corresponding to the I-domain (a.a. 3722-4610), ID^A (a.a. 3722-4353), ID^B (a.a. 4353-4499) and ID^C (a.a. 4353-4610) containing engineered *Eco* RI (5') and *Xho* I (3') flanking restriction sites were sub-cloned from pET29b (kindly provided by H. Jundi, WHRI) into pmRFP-C1 using an 'in-frame' *Eco*RI and *Xho* I/*Sal*I strategy. Restriction fragments of the anticipated size were gel extracted using the QIAquick gel extraction kit (Qiagen) (Section 2.2.4.1). Ligation was done using

the Rapid DNA ligation kit (Roche) and a 3:1 insert-to-vector molar ratio with 50ng vector. The 1x DNA dilution buffer was added to pre-mixed vector and insert DNA up to a total volume of 25µl. T4 DNA ligation buffer (25µl) was then added to the reaction followed by the addition of 1µl T4 DNA ligase. The ligation mix was incubated overnight at 16°C. This strategy placed the I-domain constructs in frame at the C-terminus of mRFP (see Figures 3.6 and 3.7, Chapter 3).

2.2.2.2. Generation of plasmid DNA encoding full-length RyR2

Human RyR2 fused at the C-terminus of eGFP was provided by Dr. Christopher George and was generated by the amplification of a cassette containing the CMV-promoter and entire reading frame of eGFP from peGFP-C3 (Clontech) using oligonucleotide primers containing *Mlu* I and *Spe* I. The CMV-eGFP cassette replaced the CMV region in pcDNA3 (Invitrogen) at the *Mlu* I and *Spe* I sites. (See Section 5.2.7) (George *et al.*, 2003a).

2.2.3. Plasmid DNA propagation

2.2.3.1. Propagation of I-domain plasmid DNA

Bacterial transformation and subsequent isolation of plasmid DNA enables the production of large quantities of highly pure DNA suitable for eukaryotic cell transfection. Bacteria are an appropriate host as they replicate exogenous plasmid DNA with high fidelity independent of the bacterial genome, enabling it to be easily isolated.

The ultracompetent XL-10 Gold® Epicurian coli (E. coli) strain (Stratagene) was used due to its high transformation efficiency and stability for plasmid replication. George and colleagues previously showed that XL-10 was the only commercially available strain capable of propagating full-length RyR2 (George et al., 2003). XL-10s were 'primed' with the reducing agent β-mercaptoethanol (2μl 0.5M per 50μl bacteria for 10 min on ice) to facilitate plasmid ingress through the bacterial wall. XL-10s were incubated with 10ng of plasmid DNA on ice for 30 min, then 'heat-shocked' at 42°C for 30 sec (optimum temperature for DNA uptake into E. coli) before returning to ice for 2 min. NZY media (a rich antibiotic-free broth) (700μl) was added to the cells and incubated at 37°C for 1h with gentle rotary agitation at 225rpm to permit the development of antibiotic resistance. Following the incubation period, 100μl bacterial culture and 100μl 5-fold concentrated culture were spread over two agar plates containing 25μg/ml kanamycin prior to incubation at 37°C for >15h until colony formation.

Typically between 5 and 10 colonies (1-2mm diameter) were selected and further cultured for ~15h in 3ml of Luria-Bertani (LB) media supplemented with 25μg/ml kanamycin. Upon visible culture 'thickening' 1ml was pelleted (1 min, 14,000xg) and recombinant DNA isolation was performed using the Wizard® SV plasmid purification system (Promega). To the remaining culture, 2ml of fresh antibiotic-supplemented LB broth was added to limit plateau-phase bacterial culture that may cause DNA recombination or degradation. Briefly, bacterial pellets were resuspended in 250μl resuspension reagent prior to a 3 min lysis using the lysis reagent. Addition of a high-salt neutralisation solution (350μl) precipitated cell debris and other

contaminating protein via precipitation of potassium dodecyl sulphate (KDS), which was subsequently removed by centrifugation (10 min, 14,000rpm). The cleared lysate was carefully removed from each sample and applied to a mini spin-column containing a silica gel DNA binding membrane that retains DNA based on charge. Impurities were removed from the column by two washes with an 80% ethanol buffer and DNA was eluted from the column using 10mM Tris pH8.5 (typically 30µl). To verify the recombinant plasmid, isolated DNA was digested using Pvu II or *Pst* I restriction enzyme digestion for 2h at 37°C and the resulting fragments were analysed using agarose gel electrophoresis (Section 2.2.4). Large-scale ('Maxi-prep') plasmid isolation was carried out if the correct restriction fragments were observed. Typically, 90-100% of colonies displayed the correct DNA restriction analysis.

Autoclaved LB broth (250-500ml; 25µg/ml kanamycin) was inoculated with 1ml of a discrete mini-culture (see above) and incubated overnight at 37°C with agitation at 225rpm. After 16-20h, cultures were centrifuged (10 min, 8,000 xg) in an Avanti J.25 (Beckman) pre-cooled to 4°C. Bacterial pellets were treated using the Qiagen® Plasmid Maxi Kit that consisted of 10ml resuspension reagent, 10ml cell lysis buffer and 10ml neutralisation (see Materials above). Following the neutralisation step samples were stored on ice for 30 min to increase precipitation of contaminants that were subsequently removed by centrifugation (45 min, 20,000 xg) at 4°C. Cleared lysate was applied to a large Q-500 silica gel column, before being washed twice with a high ethanol buffer, and elution of plasmid DNA using elution buffer (EB, 15ml). The addition of 0.7 volumes of 100% isopropranol precipitated the DNA to increase the final concentration and yield. DNA was centrifuged (20,000xg) at 4°C for 10 min, washed with 70% ethanol before a final 5 min spin (20,000xg) at 4°C. The DNA precipitate was air-dried and dissolved in 750µl 10mM Tris pH8.0. DNA purity and concentration was determined by UV spectrophotometry. DNA restriction mapping using *Pvu* II or *Pst* I enzymes was used to validate the integrity of the plasmid DNA as described above.

2.2.3.2. Ultra violet (UV) spectrophotometry

UV spectrophotometry is a technique that quantitates light passage through a sample at a given wavelength, determining the relative DNA/protein concentration based on the amount of light absorbed. DNA exhibits peak absorbance at 260nm; an A_{260} value of 1 corresponds to 50μg/ml of double stranded DNA. Sample purity can be determined by dividing the A_{260} value by the A_{280} (peak absorbance of protein contaminants); a sample was considered of high purity between 1.8 and 2.5. DNA was diluted 1:50 and assayed on a Perkin-Elmer MBA 2000 spectrophotometer using a quartz cuvette.

2.2.4. Agarose gel electrophoresis

Agarose gel electrophoresis robustly separates DNA based on size, utilising the porosity of the matrix formed by agarose and the negative charge of DNA. The percentage of agarose gel used depends on the molecular weight of DNA to be separated. A high percentage gel (e.g. 2.5-3.5% (w/v) agarose) is used for improved resolution of low molecular weight DNA due to the low porosity matrix. Conversely a lower percentage gel (e.g. 1% (w/v) agarose) is typically used to separate higher molecular weight DNA. Ethidium bromide (EtBr, diluted to a final concentration of 0.2ug per ml of agarose gel) is used to visualise DNA since it fluoresces upon intercalating with DNA. Consequently, larger DNA fragments will bind more EtBr so fluorescence is due to both amount **and** size of DNA.

Gels were prepared by heating agarose powder (ultra-pure, Eurogentec) in 1x TAE buffer to boiling point. Mixture was then cooled to 50°C for the addition of EtBr before pouring into a pre-assembled gel tray. Gels were allowed to set for >30 min prior to use. DNA samples were prepared with 30% (v/v) loading buffer prior to loading into the pre-formed wells of the gel. DNA samples were analysed alongside a molecular weight marker that consists of fragmented DNA of pre-determined sizes (Figure 2.1) for accurate size identification. The migration of negatively charged

DNA toward the anode was driven by an applied potential difference (usually 10V per cm of gel). Gels were exposed to UV trans-illumination to visualise EtBr fluorescence and images were captured using a Bio-Rad system (Gel Doc), Hamamatsu camera and Quantity One analysis software.

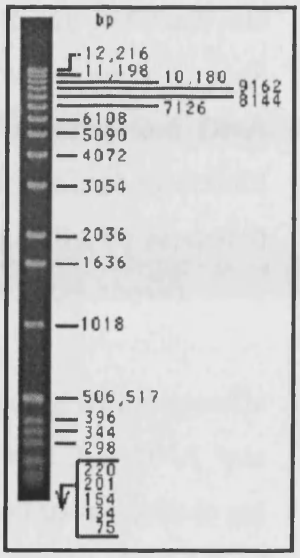

Figure 2.1. DNA ladder for agarose gel electrophoresis

DNA ladder (1kb, 0.5µg) loaded on a 0.9% agarose gel. DNA stained with ethidium bromide.

Image modified from Invitrogen datasheet

2.2.4.1. DNA gel extraction

Gel extraction of DNA was achieved using the QIAquick gel extraction kit (Qiagen). Gel slices of ~100mg were excised using a clean, sharp scalpel and were dissolved in 3 'gel volumes' of QG buffer at 50°C for 10 min (i.e. 300µl QG added to 100mg gel slice). The buffer has an intrinsic pH indicator that changes colour from yellow to violet if pH is not optimal for DNA binding (≤ pH7.5) and if necessary pH was adjusted by the addition of 10µl 3M sodium acetate. Isopropanol (1 'gel volume') was added to the sample and inverted five times for mixing and precipitation of DNA to provide a higher yield. The dissolved gel was applied to a QIAquick spin column and centrifuged for 2 min at 14,000 rpm to bind DNA. Two PE buffer wash steps, the first of 750µl and the second of 250µl, were applied to eliminate contaminants. DNA was eluted from the column in buffer EB (30µl). A small amount (typically 10% of recovered DNA) was run on a 1.0% agarose gel for analysis.

2.2.5. Restriction enzyme digestion

Restriction endonucleases are enzymes produced by bacteria that cleave double-stranded DNA at specific sequences, usually palindromic sequences of 6 nucleotide base-pairs (Table 2.1). Restriction enzymes, that are named according to the host

bacterial strain, serve as a defence mechanism in bacteria as they cleave and inactivate foreign DNA. Their characterisation and isolation from bacteria was a break-through in molecular biology that enabled the development of gene cloning and DNA manipulation. They also serve as a diagnostic tool in the determination of successful cloning as they cleave specific DNA fragments that can subsequently be separated and analysed using techniques including agarose gel electrophoresis (see above).

Restriction enzymes were selected based on their recognition sequence within specific plasmid DNA. The typical digestion reaction is displayed in Table 2.2. DNA was digested at 37°C for 2h (see Table 2.1) and products were visualised using agarose gel electrophoresis.

Restriction Digest	
Plasmid DNA	0.5-1μg
Restriction enzyme (5U/μl)	1μl
10X buffer*	2.5μl
Distilled H_2O	to 25μl

Table 2.2. Restriction enzyme reaction

*Buffer appropriate to specific restriction enzyme. In the case of DNA digestion using two enzymes simultaneously, a manufacturer-recommended buffer suitable for both enzymes was used.

2.2.6. PCR and DNA sequencing

Sequencing of cloned plasmid DNA is the unequivocal test that no undesired insertions, deletions or mutations have been introduced. The polymerase chain reaction (PCR) amplification of DNA consists of three key stages. First the double stranded DNA is heat-denatured to separate the strands that serve as templates for subsequent strand formation. Primers (small single stranded DNA sequences typically

10-24 bases) are designed for their complementary base pairing with the template DNA and anneal at the 3' end of each strand, flanking the region to be amplified. The DNA is extended by the enzymic incorporation of deoxynucleotide triphosphates (dNTPs) in the 5' to 3' direction. There are numerous thermostable DNA polymerases suitable for use in PCR (e.g. *Taq* polymerase originally isolated from the bacterial strain *Thermus aquaticus*). The sequencing system commercially available via Applied Biosystems uses a proprietary 'proof-reading' AmpliTaq formulation to minimise incorrect base incorporation.

Various sequencing methods have been described; however the most frequently used is the chain-terminator developed by Fred Sanger (Sanger *et al.*, 1977). Nowadays, DNA sequencing uses PCR to amplify DNA incorporating dideoxynucleotides (ddNTPs) in addition to the standard dNTPs in the PCR reaction. ddNTPs lack the 3'-OH group that is essential for the formation of phosphodiester bonds between adjacent bases required for DNA elongation and thus the enzymic incorporation of a ddNTP terminates the nascent elongation of the DNA strand. Subsequently DNA amplified in the presence of mixes of dNTP and ddNTP will be synthesised in lengths of one-nucleotide increments encompassing the whole of the template DNA. The size and fluorescence of each sequence determines the location of each base in the chain. In the BigDye system presently used each ddNTP (adenine (A), cytosine (C), guanine (G) and thymine (T)) is labelled with a spectrally distinct dye that permits the products of the sequencing reaction to be analysed using laser-based excitation and emission from one lane of a sequencing-grade agarose gel at one base-pair resolution. DNA sequencing results are provided in a trace format that is converted to text alignment as displayed in Figure 2.2.

PCR reactions of 10µl were set up as displayed in Table 2.3. Template DNA was amplified using a pre-determined optimal cycle on a PCR machine (Perkin-Elmer) that consisted of 25 cycles of 1) Denaturation; 96°C, 30 sec 2) Annealing; 50°C,15 sec and 3) Elongation; 60°C, 4 min.

PCR reaction	
Plasmid DNA	0.5μg
Sense/anti-sense primer (3.2pM)	1μl
5x Sequencing buffer	2μl
Big Dye® sequencing mix	4μl
Distilled H_2O	to 10μl

Table 2.3. PCR reaction

Following amplification, DNA was precipitated by mixing with 80μl of 75% isopropanol (20 min, RT) prior to centrifugation (14,000rpm, 15 min). The pellet was washed once using with 250μl of 75% isopropanol before a final 15 min spin at 14,000rpm. Isopropanol was aspirated from the pellet that was then air-dried. All sequence analysis was performed via the Central Biotechnology Service (CBS) of Cardiff University's Medical School.

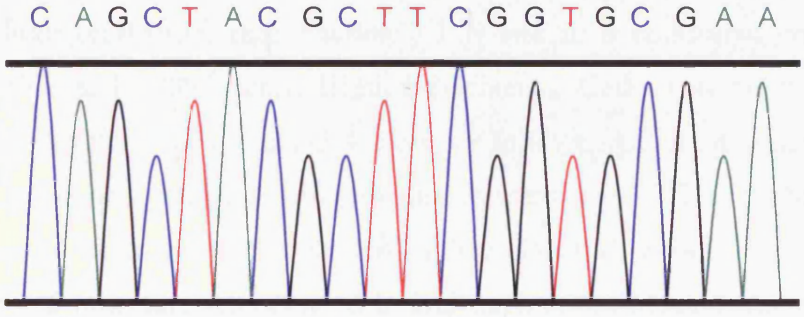

Figure 2.2. Typical DNA sequence trace

Example DNA sequencing trace, produced using the chain-terminator method. C=cytosine (blue), G= guanine (black), A=adenine (green), T=thymine (red).

2.2.7. Mammalian cell culture

2.2.7.1. Human embryonic kidney 293 cells (HEK293)

Human embryonic kidney derived cells (HEK293, ATCC#CRL-1573) (Figure 2.3) are adherent cells of epithelial origin generated as an immortalised cell line by transformation with adenovirus-5 DNA (~4.5kb insert) (Graham *et al.*, 1977; Louis *et al.*, 1997). The HEK cell line has been successfully implemented in our laboratory (Thomas *et al.*, 2004; Thomas *et al.*, 2005) and elsewhere (Kong *et al.*, 2007; Tester *et al.*, 2007) for the characterisation of recombinant RyR2. The high transfectability of this cell line coupled with the endogenous expression of IP_3R subtypes and the absence of RyR2 made it a suitable cell model for studying the phenotypic effects of RyR2 I-domain expression.

Figure 2.3. HEK293 cells
Bright-field confocal image of HEK293 cells at 63x magnification. Scale bar represents 25μm.

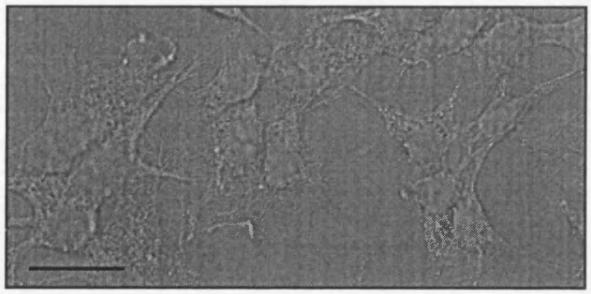

HEK cells (of > passage 100) were maintained in complete Dulbecco's Modified Eagle Medium (cDMEM) (see Section 2.1.3) and in a controlled environment of 37°C, 5% CO_2 and 100% humidification (Heraeus). Cells were routinely passaged upon confluency (typically every 3-4 days) as follows. Adherent cells were washed twice with saline and detached using trypsin (5mg/ml) and EDTA (5mM) for 2 min at 37°C. Detached cells were resuspended in 5ml cDMEM, pelleted by centrifugation (1,500 xg for 5 min) and resuspended in 5ml fresh cDMEM. A small volume of this suspension (~10μl) was used for haemocytometric counting (Neubauer haemocytometer (Reichert, USA)), and an appropriate number of cells were seeded in fresh cultureware followed by continued incubation at 37°C. All tissue culture was carried out in a Class I Microflow containment hood.

Cell cryopreservation was carried out in freezing-down media (FCS, 90% (v/v), DMSO, 10% (v/v)). Cells (~$5x10^6$) were trypsin-detached and pelleted as above and resuspended in 1ml of cold freezing-down media in labelled sealed (gas-tight) screw top cryo-vials (NUNC, UK). Vials were controlled-cooled to -80°C using 1-2cm of insulating tissue paper prior to longer-term storage in liquid nitrogen. To re-establish cultures from stocks, cells were rapidly thawed by hand and taken up into a syringe containing 5ml pre-warmed cDMEM followed by pelleting by centrifugation (1,500 xg, 5 min). Cells were resuspended in 6ml cDMEM and seeded in a $25cm^2$ flask, prior to fresh media being exchanged after 4h.

2.2.7.2. HL-1 cardiomyocytes

HL-1 cardiomyocytes (Figure 2.4) are adherent cells obtained from the AT-1 atrial cardiomyocyte tumour lineage mouse model (Claycomb *et al.*, 1998). HL-1 cells are a valuable tool for studying protein expression against a background of endogenous RyR2 and other EC coupling proteins including CSQ and FKBP12.6. HL-1 cells spontaneously contract while maintaining adult cardiomyocyte phenotype even after repeated passages.

Figure 2.4. HL-1 cardiomyocytes
Bright-field confocal image of HL-1 cells at 63x magnification.
Scale bar represents 25µm.

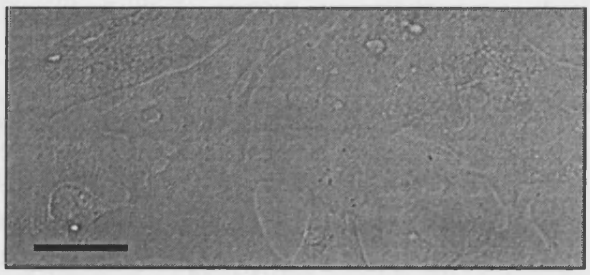

HL-1 cells (of passage 87) were grown on gelatin-fibronectin (GFN) coated flasks and maintained in Claycomb media (JRH Biosciences) supplemented as described in section 2.1.3. Upon confluency the cells were split using 0.1% trypsin/EDTA to the next passage or prepared for experiments. Unlike HEK, HL-1s were cultured to superconfluency (typically 2-3 days after initial confluency) prior to split. They require propagation at a density of 1:3 in order to preserve cardiomyocytic cell

phenotype and avoid reversion to a non-contractile 'fibroblastic' state that results in the loss of many EC coupling proteins (George *et al.*, 2003a).

2.2.7.3. DNA transfection

DNA transfection introduces recombinant DNA of a gene of interest into a eukaryotic cell for the purpose of investigating its function. Multiple methods have been established and have evolved over the past few decades. Calcium phosphate ($CaPO_4$) transfection was one of the first techniques to demonstrate a robust applicability (Chen and Okayama, 1987) whereby a precipitate is formed between plasmid DNA, calcium chloride and phosphate over several min that is then readily accepted by cells via endocytosis. The disadvantage of this method is its comparative toxicity and non-specific effects on cellular phenotype. Other more gentle methods of transfection utilise lipid-based delivery of DNA into cells, a technique referred to as lipofection. The negatively charged (anionic) DNA forms a lipid complex (usually with cationic lipids) that enters eukaryotic cells via fusion with the phospholipid cell membrane (Felgner *et al.*, 1987). Effectene (Qiagen) is a novel lipid-based method that utilises an enhancer to condense the DNA prior to the formation of DNA-lipid complexes (Figure 2.5). In addition, the compatibility of the Effectene protocol with serum-containing medium means that it is less toxic to cells than other lipid-based delivery methods that require the removal of serum during and after the transfection procedure.

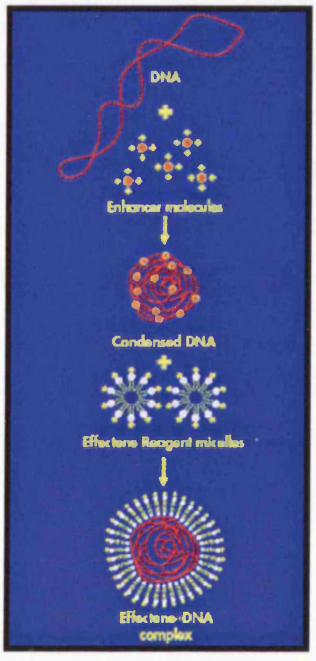

Figure 2.5. Principle of Effectene-based transfection

Effectene is a non-liposomal lipid-based reagent. DNA is first condensed by the Effectene enhancer that enables it to be coated by the cationic Effectene reagent for incorporation into eukaryotic cells. Effectene achieves high levels of transfection efficiency (typically >30%) and requires 5-fold less DNA than $CaPO_4$ and other lipid-based techniques.

Schematic representation obtained from Qiagen datasheet.

HEK cells were maintained as described in Section 2.2.7.1. HEK were cultured in 6 well plates or on poly-L-lysine coverslip chambers (MatTek Corporation) at a density of $5x10^5$ or $5x10^4$ respectively (~70% confluency) 2h prior to transfection. One Effectene transfection was sufficient for 1 well of a 6-well plate or 6-7 coverslip chambers. DNA (0.8μg) was made to a final volume of 100μl with EC buffer before the addition of 6.4μl enhancer followed by vortex (10s). The transfection mix was incubated at RT for 5 min before the addition of 20μl Effectene and subsequent vortex (10s) and incubation (10 min, RT). During the 10 min incubation, media was removed from the cells and replaced with fresh cDMEM (1.2 ml per well or 150μl applied in a meniscus per coverslip chamber). cDMEM (600μl) was added to the transfection mixture, and after a brief mix was gently applied drop-wise to cells. All transfection mixture was added to one well of a 6-well plate or 100μl was added in a meniscus per coverslip chamber. Cells were left overnight at 37°C and fresh media was applied the following day. The level of cell transfection was assessed by the appearance of fluorescently-tagged recombinant proteins in cells after 24h using a Zeiss Axiovert 200 fluorescent microscope, (Section 2.2.7.3.2).

2.2.7.3.1. Preparation of fixed cells for imaging studies

In order to preserve recombinant protein fluorescence, 48h post-transfection cells were washed twice in PBS (pH7.4) and fixed using paraformaldehyde (4% (v/v)) / PBS solution (10 min). Fixed cells were rehydrated (PBS (pH7.4), 2h) and briefly rinsed in distilled H_2O prior to mounting on ethanol-cleaned microscope slides in FluoSave™ (Calbiochem), a reagent that preserves the fluorescence of mounted cells. Slides were dried at RT away from light for 30 min before storage at 4°C. Slides were viewed within seven days of processing.

2.2.7.3.2. Fluorescence microscopy for transfected cell visualisation

The *in situ* visualisation of recombinant I-domain tagged to mRFP was performed on a Zeiss Axiovert 200 fluorescent microscope. Images were obtained using 10x, 20x and 40x objectives, a condenser set at phase 0 and DAPI (brightfield images) and Cy3 (mRFP fluorescence) filter sets. The Cy3 filter set permitted excitation and emission wavelengths at 528-552nm and 578-637nm respectively. All imaging parameters including camera exposure and autofocus were controlled using Axiovert software.

2.2.7.4. Flow cytometry & fluorescence activated cell sorting (FACS)

Flow cytometry is a powerful technique that enables the precise quantification of levels of cellular fluorescence either via antibody-mediated labelling or following expression of a recombinant fluorescent protein. The cell stream is rapidly passed under high hydrodynamic pressure at 1-10 thousand events/sec through a laser beam that excites the fluorophore with the resulting emission filtered through an appropriate filter and captured by a photomultiplier tube (PMT) (Figure 2.6). In addition, important information is collected as to how discrete cell populations scatter light, which is related to physical cell characteristics. In particular, forward scattering (FSC) is defined by cell size and the extent of side scattering is related to cell granularity. Although flow cytometry is predominantly used as an analytical technique, some apparatus enable the isolation of distinct cell populations that are characterised by discrete fluorescent emissions or morphological features. This latter technique is referred to as fluorescence activated cell sorting (FACS).

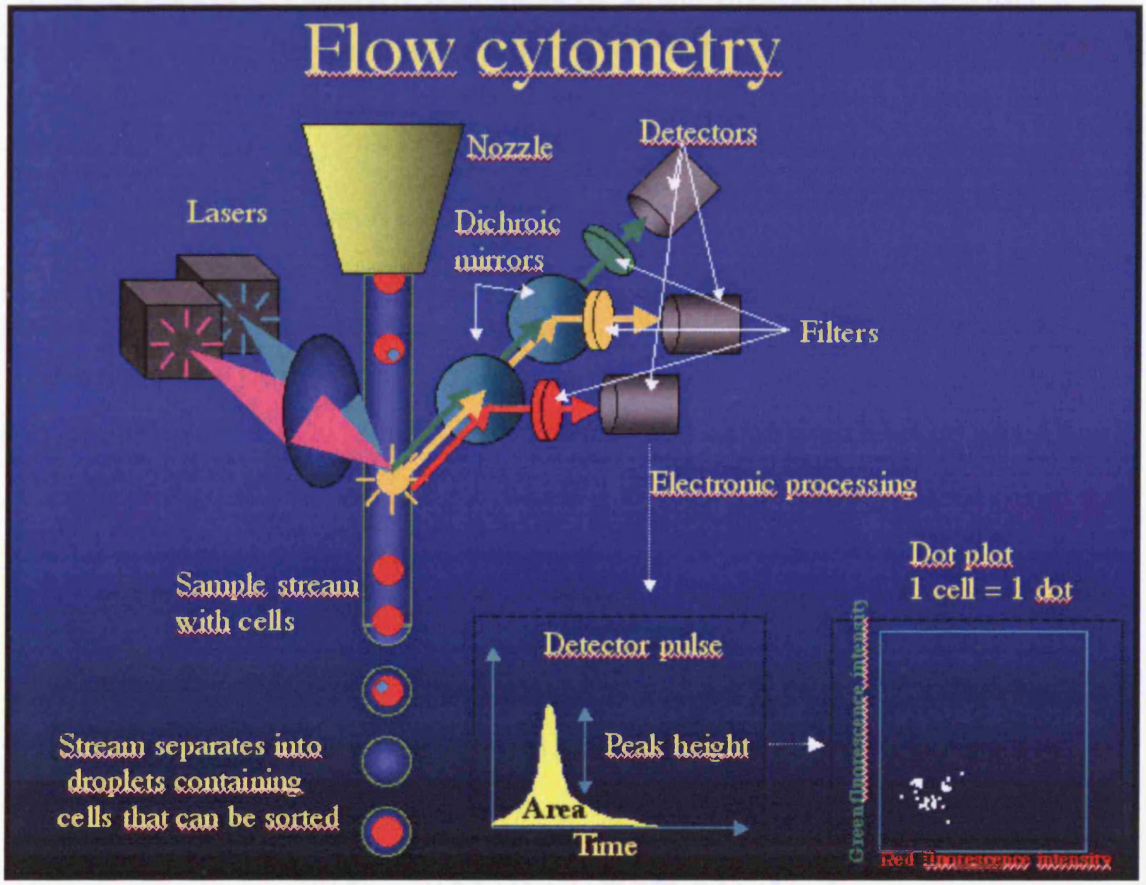

Figure 2.6. Schematic representation of flow cytometric and FACS analysis

Cells are hydro-dynamically dispensed in a stream that is interrogated by a laser. The pattern of scattered light provides information on cell size and granularity. In addition, fluorescently labelled cells also emit light of a specific wavelength depending on the fluorophore. Dichroic mirrors chosen to suit the particular fluorophore in use deflect the light through an optical filter that is collected by a detector. In cell-sorting mode, the stream of cells is vibrated to separate them into one-cell droplets. Cells that emit light at the desired wavelength can be isolated from the stream by applying a charge and electrostatically deflecting them into a collection tube.

Image obtained from: http://www.rudbeck.uu.se/cellanalys/flowpic.html

2.2.8. Confocal laser scanning microscopy (CLSM)

CLSM enables 'optical sections' to be visualised in a sample by capturing emitted light from individual focal planes. Excitation of fluorophores occurs via high-powered lasers that emit at discrete wavelengths (e.g. Argon lasers emits lights in the blue-green range at 454, 488, 496 and 514nm) and fluorophore detection is via sensitive PMTs. The central premise of confocal microscopy is that a restrictive aperture prevents out of focus light from reaching the PMT (see Figure 2.7). The SP5 Confocal microscope (Leica Microsystems) was used for live cell experiments, and in experiments using paraformaldehyde-fixed cells. The acquisition of digital images was performed using 8bit scaling i.e. fluorescence intensity is scaled between 0-256 arbitrary units.

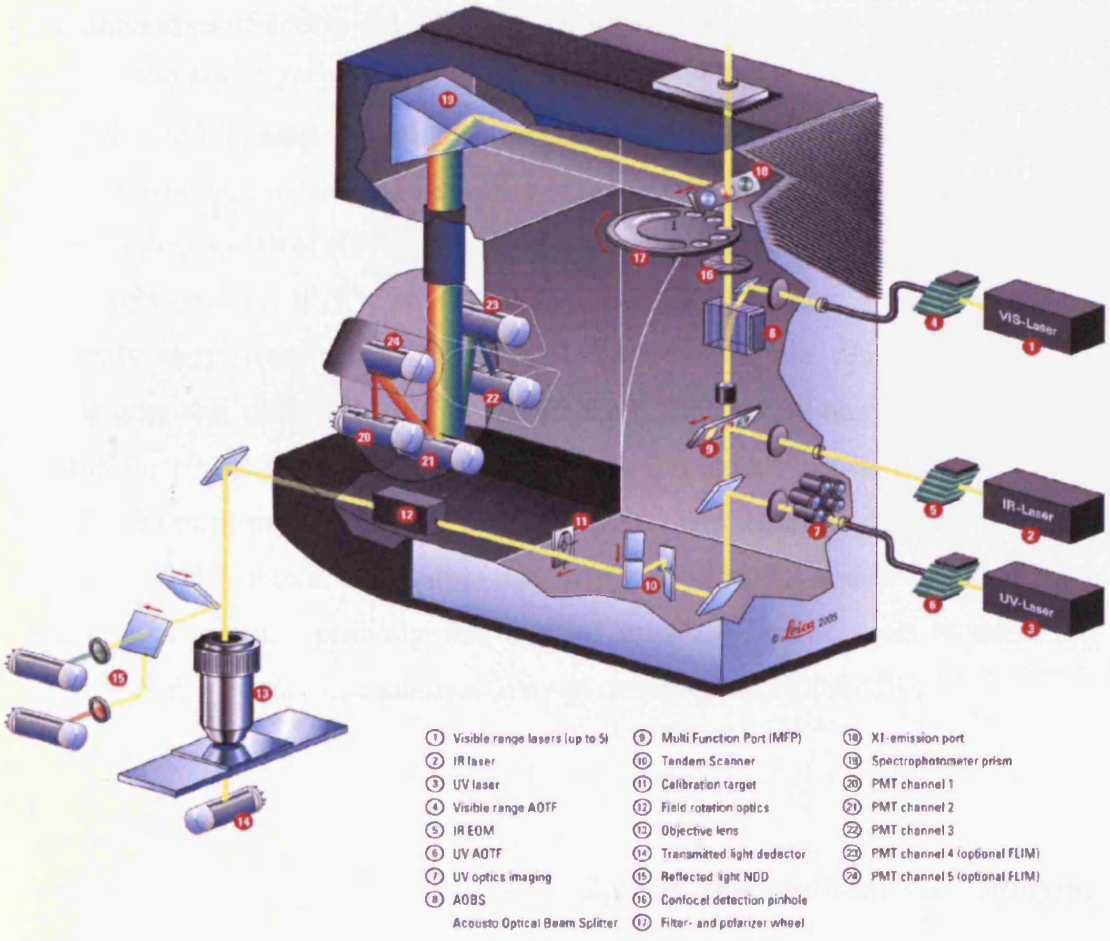

Figure 2.7. SP5 CLSM principle

The laser is focussed through a pinhole aperture and is tunelled to the objective via acousto-optical beam splitting (AOBS). Fluorescence emission of the sample is passed through a second pinhole (the diameter of which is precisely matched to the particular objective used) that restricts out-of-focus light en route to detection via a PMT. The PMT converts light into an electical signal that is recorded by the computer. Images were typically recorded at 512x512 pixel resoultion.

Taken from *www.zmb.uzh.ch/resources/download/CLSM.pdf*

2.2.8.1. Fluorescence analysis of fixed cells expressing I-domain

Paraformaldehyde-fixed cells mounted on glass coverslips were warmed to RT and were visualised using the resonance scanning (SP5) confocal microscope (Leica Microsystems) through a 63x 1.23 numerical aperture oil immersion objective. The 561 He:Ne laser line at 20% power was used for the visualisation of mRFP, with the PMT set to detect emission at 600-630nm. At least 30 images from 5-10 fields of view were taken per transfection.

2.2.8.2. Immunofluorescent analysis of fixed cells expressing IP_3R

Immunodetection of endogenous IP_3R types 1 and 2 in HEK293 cells using isoform-specific antibodies (Section 2.1.2.5) was performed as follows. Cells were fixed, rehydrated (Section 2.2.7.3.1) and permeabilised with 0.1% Triton X-100 in PBS (pH7.4) (30 min, RT) away from light. Coverslips were washed with PBS (pH7.4) (2x 10 min) followed by blocking non-specific immunoreactivity using a solution of 10% (v/v) FBS in PBS for 1h at RT. Following the blocking step, cells were incubated with primary antibodies to IP_3R1 or IP_3R2 for >15h at 4°C (see Materials above). Subsequently they were washed (2x PBS, 20 min) before applying secondary antibodies goat anti rabbit:Alexa Fluor® 488 for IP_3R1, and donkey anti goat:Alexa Fluor® 488 for IP_3R2 for >15h at 4°C. Cells were thoroughly washed with PBS (3 x 10 min, 2 x 20 min) prior to rinsing in distilled H_2O and then mounting as described in Section 2.2.7.3.1 above. Coverslips that were processed as above except that the incubation with primary antibody was omitted were used as controls to determine non-specific (background) immunoreactivity of the secondary antibodies.

2.2.8.3. Intracellular Ca^{2+} imaging

HEK cells were seeded under a meniscus of cDMEM at a density of $5x10^4$ on pre-coated poly-L-lysine coverslip chambers (MatTek Corporation) 2h prior to transfection using Effectene (Qiagen). Two days after transfection cells were

visualised for intracellular Ca^{2+} imaging experiments using CLSM. Cells were loaded under a 100µl meniscus of unsupplemented DMEM containing the Ca^{2+} indicator dye fluo-4AM (5µM in 20% (w/v) pluronic acid F-127) and incubated at 37°C for 60 min. Chambers were flooded with unsupplemented DMEM (2ml) and incubated for a further 10 min prior to imaging. The Ca^{2+}-dependent fluorescence of fluo-4 was visualised using the 488nm laser line from an argon laser (set at 20% source power) focussed through a 63x 1.23 numerical aperture oil immersion objective and PMT detection at 510-540nm. A diode-pumped solid-state laser (DPSS) emitting at 561nm was used to excite recombinant mRFP-tagged proteins and fluorescence was detected at 600-630nm. The two-channel data were recorded at 200 ms intervals for 120 sec duration (600 frames/experiment) at a 512x512 pixel resolution. The z-axis is less than 1µm, and therefore less than the thickness of a cell. Following an experimental series, 5-20 cells were selected (per coverslip) by an elliptical area of ~40μm^2 (termed a region of interest (ROI)).

Calibration of resting fluorescence is described in Section 5.2.4. The K_d value used was based on the published value from Molecular Probes, Invitrogen (345nM). Thomas *et al.* have determined the K_d of various Ca^{2+} dyes (Thomas et al., 2000), however the value established for fluo-4 (K_d=1000nM) gives unusually high resting Ca^{2+} values. Therefore, as previous studies have used the K_d value determined by Invitrogen (Collier et al., 2000; Peluso et al., 2001; Iwata et al., 2004) this value was seen as appropriate for use in my studies.

2.2.8.3.1. Chemical-induced responses

Experiments were structured to either incorporate the addition of a known pharmacological modulator of intracellular Ca^{2+} signalling (Chapter 5) or to analyse signal variability in the Ca^{2+} dependent fluo-4 traces in the absence of any addition to cells (Chapter 6). Data obtained prior to the addition of a modulator (first 300 frames) was used to estimate resting fluo-4 dependent Ca^{2+} signals. Following addition of a pharmacological agent, a comprehensive analysis of Ca^{2+} signals including peak Ca^{2+} transient height, time to peak, and rate of transient decay (shown in Chapter 5, Figure 5.5) was performed. Chemical-induced responses are described in Chapter 5:

carbachol (Section 5.2.2), thapsigargin (Section 5.2.3), ionomycin (Section 5.2.4), and caffeine (Section 5.2.9).

2.2.8.3.2. Analysis of Ca^{2+} signal variability

Signal variability (termed noise analysis in much of the literature although this is technically incorrect) defines the amplitude and temporal variation in Ca^{2+} signals. Analysis of signal variability represents a powerful tool to investigate the minutiae of cellular Ca^{2+} handling including the effects of agonists on the Ca^{2+} cycling within a cell, or to compare variations in basal Ca^{2+} signals between different cells and following different experimental conditions. Chapter 6 describes the precise derivation of mathematical operations used to calculate signal variability in this thesis.

2.2.9. Sodium dodecyl sulphate polyacrylamide gel electrophoresis (SDS-PAGE) and Western blotting

SDS-PAGE is a technique that separates detergent-denatured proteins in a sample based on relative molecular weight. Proteins are initially mixed with SDS that in addition to denaturing the polypeptides gives each protein a negative charge that is proportional to its size, and that can be distinguished in an electrophoretic field. Following SDS-PAGE, the separated proteins can either be stained using a protein-binding dye (e.g. Coomassie or Imperial^{TM} stain) or transferred to a membrane for detection using protein-specific antibodies (known as immuno- or Western blotting). All SDS-PAGE and Western blotting experiments were carried out using standard published techniques (Laemmli, 1970; Burnette, 1981).

2.2.9.1. Protein isolation from HEK cells

For SDS-PAGE experiments, cells at days 1 to 4 post-transfection were trypsin-detached, pelleted and stored at –80°C. Pellets were resuspended in a hypo-osmotic protein inhibitor cocktail (see Materials) and passed ~15 times through a syringe attached to a 21G- 26G needle to homogenise the cells and begin disrupting surface membranes. Suspensions were then subjected to freeze-thaw sonication (5-10 cycles using liquid nitrogen and a waterbath sonication tank) to breakdown remaining cells. This detergent-free technique is not sufficient to breakdown nuclear membranes and therefore leaves nuclei intact, which can be removed by centrifugation (1500 xg, 10 min) leaving the post-nuclear supernatant (PNS). Microsomal fractions were obtained by centrifugation of PNS at 55,000rpm for 45 min at 4°C using an Optima^{TM} microcentrifuge (Beckman Coulter). The concentration of total protein in post-nuclear supernatants (containing cytoplasmic and microsomal fractions) and in microsomal fractions was determined using the BCA^{TM} protein assay reagents (Pierce) (See section 2.2.9.1.1).

2.2.9.1.1. Protein assay

Protein concentration was measured using the BCA™ protein assay (Pierce) that utilises the colour change of the assay reagent to a blue/violet- complex by the reduction of Cu^{2+} to Cu^{+} by protein in an alkaline medium. Peptides of three or more amino acids chelate Cu^{+} ions in the presence of sodium potassium tartrate to form the complex. The intensity of the colour change is proportional to the number of peptide bonds in the sample and is therefore a reflection of total protein concentration. The complex absorbs light at 560nm that can be detected using spectrophotometry techniques. The quantification is carried out in parallel with control concentrations of bovine serum albumin (BSA) protein of 0, 125, 250, 500, 750, 1000, 1500 and 2000µg/ml in order to calibrate the absorbance of the reagent to the levels of protein present. Total sample protein concentration can then be determined by measuring absorbance at 560nm and extrapolating the concentration from the fitted regression equation (Figure 2.8A).

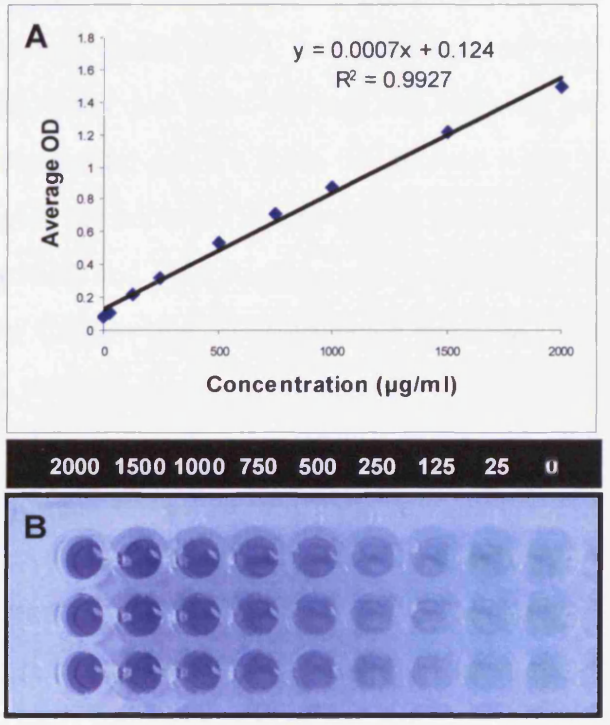

Figure 2.8. BSA protein assay standard

A. Line plot of average optical density (OD) against protein concentration, where the R^2 value of approximately 1 demonstrates rigorous correlation. Each point represents the average of three samples. BCA calibration was performed for every protein measurement

B. Protein assay standard reactions in triplicates following a 30 min incubation at 37°C. Increased protein concentration correlates with more pronounced colour change, as shown in A.

Both the BSA standards and samples were assayed in triplicates using a 96-well plate protocol as recommended by the manufacturer (Figure 2.8B). Working BCA reagent

(200µl) was added to each test well and incubated at 37°C for 30 min to allow complex formation. Typically, samples were diluted at 1:50 to obtain a concentration of 500-1000µg/ml. Absorbance was measured at 560nm using a plate reader (Labsystems Multiskan EX) and Genesis analysis software.

2.2.9.2. SDS-PAGE

SDS-PAGE gels consisting of different percentages of acrylamide were prepared using the Bio-Rad Proteome 2 mini casting chamber (assembled according to manufacturer's instructions) and were of a 10 well, 1.5 mm thickness and 10cm x 7cm size. The separating gel was prepared as described in Table 2.4 (with the percentage acrylamide dictated by the size of the protein under study), and then layered with water. Once the separating gel was set the water was removed and the stacking gel (Table 2.4) was poured over the pre-set separating gel. To form the sample wells, a 10-well comb was inserted, avoiding trapping air bubbles (Figure 2.9A). The final gel composition was approximately 70% separating and 30% stacking gel. The purpose of the stack is to ensure all protein samples migrate the same distance prior to their separation in the resolution gel, which is enabled by the slow migration of glycine behind protein samples at pH6.8. The stacking gel was allowed to set for >2h, the comb was removed, gels were secured in the gel apparatus (Bio-Rad) and submerged in 1x SDS-PAGE running buffer. Protein samples were incubated with a 20% (v/v) final concentration of 5x Laemmli SDS sample buffer for 3 min at 95 °C, centrifuged at 14,000rpm before loading onto the gel. Total protein (50-400µg) (up to final volume in Laemmli loading buffer of 20-25µl) was loaded onto the gel alongside an appropriate molecular weight marker. Gels were subjected to electrophoresis at a constant current of 30mA for 2-4h using a Bio-Rad Proteome 2 mini electrophoresis chamber and power-pack (Figure 2.9B). Protein separation was visualised with Imperial stain (Bio-Rad) as detailed in Section 2.2.9.4. Alternatively gels were transferred onto polyvinylidene difluoride (PVDF) membranes for Western blot (Section 2.2.9.3).

Separating Gel	4%	6%	10%	12%
Distilled H_2O	6345	5845	4845	4345
Tris-HCl pH8.8, 1.5M	2500	2500	2500	2500
SDS, 10% (w/v)	100	100	100	100
Acrylamide/Bis (37.5:1), 40%	1000	1500	2500	3000
TEMED	5	5	5	5
Ammonium persulphate, 10% (w/v)	50	50	50	50
Stacking Gel	4%			
Distilled H_2O	3170			
Tris-HCl pH6.8, 0.5M	1250			
SDS, 10% (w/v)	50			
Acrylamide/Bis (37.5:1), 40%	500			
TEMED	2.5			
Ammonium persulphate, 10% (w/v)	25			

Table 2.4. Composition of SDS-PAGE separating and stacking mini-gels

Quantities are in µl and the total volume is sufficient for one 1.5mm thick mini-gel.

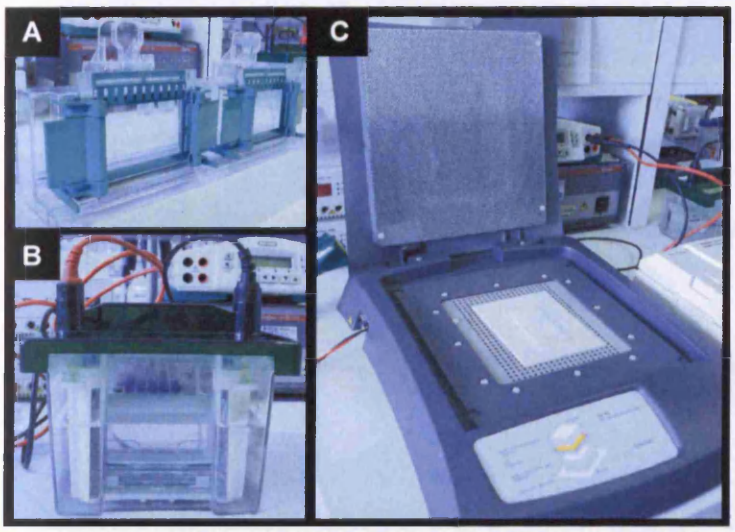

Figure 2.9. SDS-PAGE and protein transfer

A. Mini-gels were secured in SDS-PAGE apparatus; comb was inserted into stacking gel to form wells.

B. Samples were loaded onto both mini-gels, which were then assembled in the electrophoresis tank.

C. Proteins were transferred onto PVDF membrane using semi-dry transfer apparatus.

2.2.9.3. Protein transfer and Western blot

Proteins were transferred from an SDS-PAGE gel to a PVDF membrane (Immobilon-P, Millipore) using a semi-dry transfer apparatus (Hoefer) (Figure 2.9C). PVDF membranes were initially exposed to a 30 sec methanol soak to render the membrane hydrophilic before use, prior to a 20 min equilibration in semi-dry transfer buffer. Protein transfer was carried out at 300mA, limited to 25V, for 1-2h. The high hydrophobicity of PVDF membranes means that proteins are retained by hydrophobic interactions alone. Membranes were briefly rinsed in distilled H_2O before incubation in blocking buffer consisting of 5% (w/v) non-fat dried milk protein (Marvel) in TBS-T buffer for 1h at RT or >15h at 4°C. The membrane was incubated with primary antibody (diluted as recommended by the manufacturer) in blocking buffer overnight at 4°C, and then washed with blocking buffer (2 x 10 min, 4 x 5 min). The secondary antibody, conjugated to horseradish peroxidase (HRP) was similarly diluted in blocking buffer (typically 1:10,000) and applied to the membrane for 2h at RT. The membrane was then thoroughly washed with TBS-T (2 x 10 min, 4 x 5 min). Immuno-labelled proteins were visualised using enhanced chemiluminescence (ECL, GE Healthcare) and exposed to X-ray film (Hyperfilm, GE Healthcare) for a range of exposure intervals, dependent on the intensity of the chemiluminescent signal. The film was developed using a FujiFilm automated image developer.

2.2.9.4. Protein Stain

Imperial stain (Bio-Rad) is a coomassie stain that exhibits greater sensitivity in protein detection than other commercially available protein stains. It was used for visualising protein profiles and to permit densitometric analysis of proteins separated by SDS-PAGE. Following SDS-PAGE, gels were briefly washed in distilled H_2O before staining for 2-3h at RT until optimal colour development. Gels were de-stained by washing overnight in distilled H_2O. Gel imaging and densitometric analysis was carried out using a Bio-Rad GS710 scanner controlled by Quantity One software. All gels and exposed Hyperfilm from Western blotting experiments were scanned at 300dpi using a densitometer (GS-700, Bio-Rad). For permanent record, gels were dried on a horizontal slab gel drier (Hoefer) fitted with a vacuum pump for 1-2h at 75°C.

2.2.9.5. Densitometric quantification of protein and immunoblot signals

Densitometry quantifies the intensity of protein bands either following dye-based staining or immunoblotting techniques. Images obtained as described in 2.2.9.4 were saved and analysed as raw data files (*.1sc) using Quantity One software. Densitometric quantification was carried out by defining the optical intensity (measured in density per pixel) of an equal area around the band(s) of interest. Background correction was carried out using the automated background correction function applied to regions of the image that did not contain any protein-specific signal (enabling normalisation of individual lanes). All densitometry comparisons were based on equivalent amounts of protein added to each lane, and raw pixel data from I-domain bands were normalised to control (HEK). Following analysis images were archived using a standard HP 7000 desktop scanner.

Transmissive and reflective scans were automatically calibrated using the GS-700 Biorad calibration step tablet and Quantity One software.

2.2.10. Statistical Analysis

Unless stated, all data in this thesis is derived from at least 3 separate observations and is expressed as mean ± standard error of the mean (SEM), where SEM is defined as standard deviation / $\sqrt{(n-1)}$ (n=number of observations or measurements). Data were considered statistically significant if $p<0.05$. Significance between normally distributed data sets (tested using Prism (version 3.0, GraphPad) corresponding to control and experimental observations were tested using the unpaired student's *t* test. Where stated, datasets of equal variance were also analysed by ANOVA. All graphs were constructed using GraphPad Prism software, and linear and non-linear regression equations were derived by best-fitting methods using the software.

Chapter 3

Chapter 3 Phenotypic characterisation of cells expressing recombinant I-domain

3.1. Introduction

As outlined in Section 1.6, the objective of this project was to investigate the functional consequences of cellular I-domain expression, both in the absence and presence of endogenous RyR2, with the prospect of manipulating intracellular Ca^{2+} environments using I-domain peptide probes. 'Tuning' Ca^{2+} environments has recently been demonstrated to modulate cell phenotype and susceptibility to cell death (George *et al.*, 2007). In addition, Varnai and colleagues used a molecular approach and an inverted microscope to demonstrate that the recombinant ligand-binding domain of IP_3R1 tethered to an ER-retention signal could 'tune' IP_3R Ca^{2+} release, the functional modulation of which was fully dependent on the proximity of recombinant protein to the ER membrane. The authors fused the ligand-binding domain to mRFP, and confirmed the localisation of ER tethered constructs by confocal microscopy. (Varnai *et al.*, 2005). These findings inspired the current project and therefore this chapter begins by describing the cloning and expression of the I-domain in mammalian cells to provide an insight into recombinant protein localisation and effect of expression on cell phenotype, prior to functional studies that are presented later in this thesis.

3.1.1. Intrinsic interdomain interaction regulates RyR channel function

The molecular basis underlying dysfunctional Ca^{2+} release as a result of RyR2 mutation, and acquired defects such as HF is incompletely understood. A number of mechanisms have been proposed including SOICR and RyR2 hyperphosphorylation by PKA (discussed in Section 1.4.5.2); however, defective interdomain interaction has more recently emerged as a possible mechanism underpinning abnormal Ca^{2+} handling.

In 1996, Zorzato *et al.* first proposed the regulatory function of intramolecular interactions within RyR using an N-terminal antibody (a.a335-341) that interacted with RyR a.a.3010-3225, and increased channel activity (Zorzato *et al.*, 1996). Yamamoto and colleagues described additional sites of interaction by using domain peptides (DP) that corresponded to RyR sequences (~35a.a.) to assess changes in RyR channel functionality (Yamamoto *et al.*, 2000; Ikemoto and Yamamoto, 2002; Shtifman *et al.*, 2002; Kobayashi *et al.*, 2004; Oda *et al.*, 2005). Intimate interaction between two distinct regions of RyR1, located within N-terminal and central domains (DP1, a.a.590-609 and DP4, a.a.2442-2477 respectively) altered the functional state of the channel (Yamamoto *et al.*, 2000; Shtifman *et al.*, 2002; Bannister *et al.*, 2007), and recently, other RyR1 functional interaction sites have been identified (Oda *et al.*, 2005; Hamada *et al.*, 2007b; Laver *et al.*, 2007b; Mochizuki *et al.*, 2007) (Figure 3.2).

Although intrinsic channel regulation was initially proposed as a mechanism underpinning RyR1 function (Yamamoto *et al.*, 2000), it has since been applied to RyR2 (George *et al.*, 2004; Oda *et al.*, 2005). Addition of either DPc10 or DPc15 (a.a.2460-2495 and a.a.4752-4773 respectively) to cardiomyocytes activated RyR2 (Oda *et al.*, 2005; Laver *et al.*, 2007b), confirming that interactions within the cardiac isoform regulated channel function, which has since been corroborated by other studies (Hamada *et al.*, 2007b; Gangopadhyay and Ikemoto, 2008). These findings strongly support the concept that intramolecular interactions within RyR govern its functional state, (Figure 3.1). The close association of paired interacting sub-domains within RyRs form a 'domain switch' that results in a 'zipped' conformation, thus stabilising the closed channel in the non-activated state (Figure 3.1). During activation, EC coupling induces a decreased affinity between interacting domains ('domain unzipping') that permits controlled channel opening and Ca^{2+} release (Ikemoto and Yamamoto, 2002) (Figure 3.1). RyR2 mutations have been suggested to interfere with these interactions by reducing conformational constraints between interacting sub-domains, which promotes abnormal 'unzipping'. Mutation-induced weakening of interdomain interactions has been demonstrated (George *et al.*, 2006; Murayama *et al.*, 2006) and is proposed to underlie channelopathies such as CPVT and ARVD (George *et al.*, 2006; Yang *et al.*, 2006b) (Figure 3.1). Furthermore, RyR mutational hot-spots are confined to distinct sites in N-terminal, central, and C-

terminal domains, which coincide with currently identified regions of intramolecular interaction, shown in Figure 3.2, suggesting a functional basis for mutation clusters.

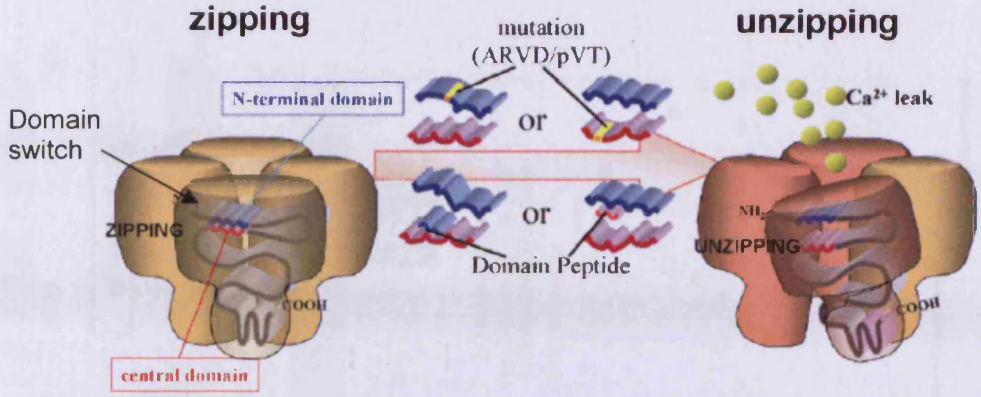

Figure 3.1. Schematic representation of RyR 'unzipping' hypothesis

RyR channels are stabilised when interacting domains that form a 'domain switch' are closely associated in the 'zipped' conformation. RyR2 mutations can induce channel de-stabilisation, termed domain 'unzipping', which was experimentally reproduced using domain peptides

Taken from Yano et al., 2005b

However, the scope of domain interaction sites is still emerging, and more work is needed to clearly understand the molecular basis of channel dysfunction arising from specific mutational loci (see Chapter 1 section 1.4.2.1).

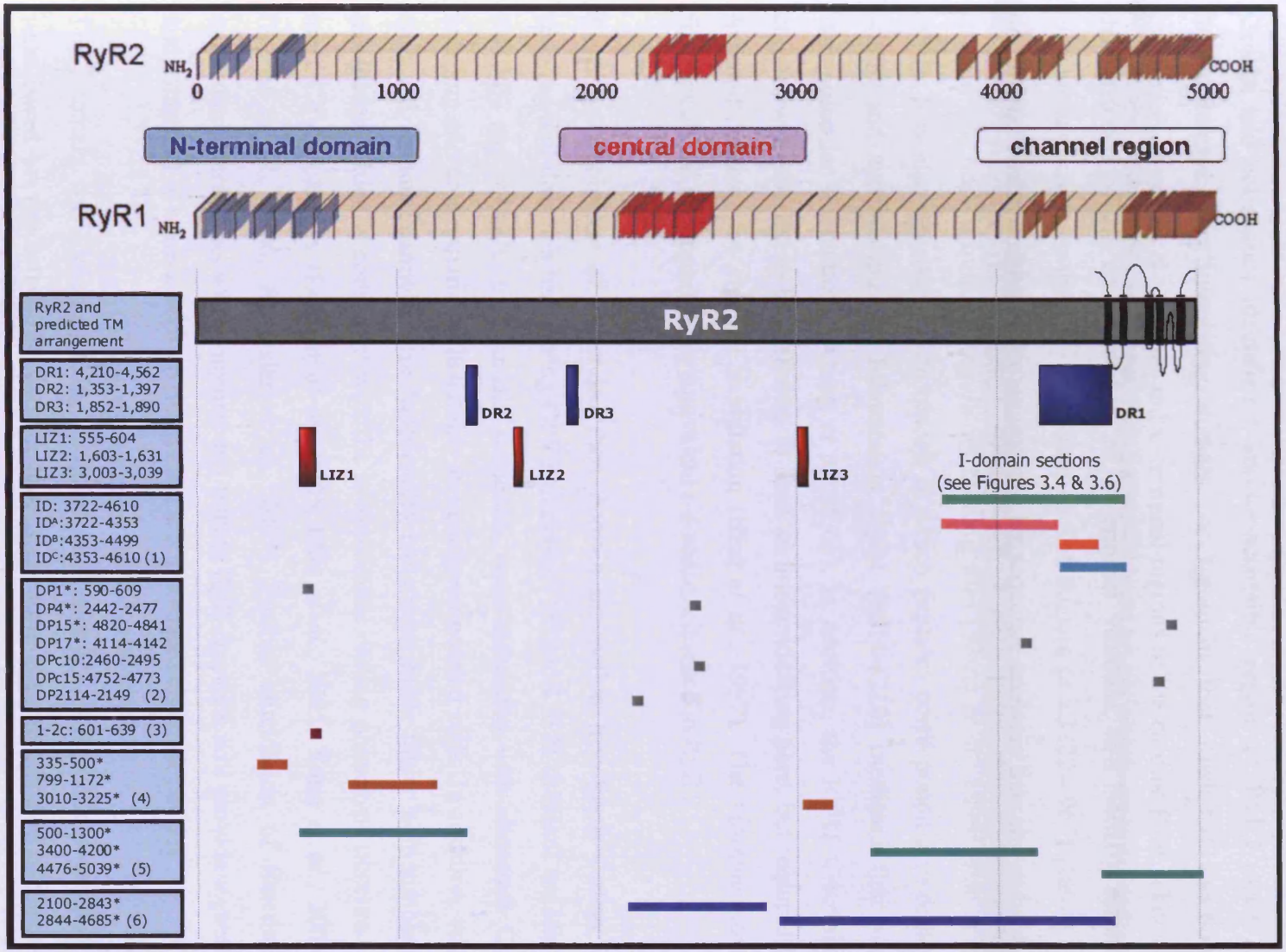

Figure 3.2. Mutation distribution in RyR1 and RyR2 map to sites of interdomain interaction

Disease-linked mutations cluster in RyR1 and RyR2 interacting domains as published: 1 (George *et al.*, 2004; George *et al.*, 2006), 2 (Yamamoto *et al.*, 2000; Ikemoto and Yamamoto, 2002; Oda *et al.*, 2005; Hamada *et al.*, 2007b), 3 (El-Hayek *et al.*, 1999), 4 (Zorzato *et al.*, 1996), 5 (Chen *et al.*, 1993) and 6 (Wu *et al.*, 1997). Also included are RyR2 regions of sequence diversity (DR) and sites of leucine/isoleucine zippers (LIZ). *refers to findings obtained with RyR1. DP refers to domain peptides used to probe sites of domain interaction. RyR mutations adapted from Yano *et al.*, 2006

3.1.2. Characterisation of the interacting domain (I-domain)

George and colleagues identified a surface-accessible region of RyR2 (a.a.3722-4610), termed the 'interacting domain' or I-domain that mediated functional interactions between N-terminal and C-terminal regions of the cardiac RyR. This was demonstrated when co-expression of N-terminal residues (a.a.1-4610) restored caffeine sensitivity to the Ca^{2+} pore forming TM domain (a.a.3722-4967) (George *et al.*, 2004). These findings were augmented by sequence analysis that showed the I-domain was host to multiple regulatory binding sites (Wang *et al.*, 1996; Bhat *et al.*, 1997). It is also consistent with reports in which peptides corresponding to regions within and surrounding the I-domain in RyR1 (3614-4210) mediated functional intramolecular interactions (Xiong *et al.*, 2006). In addition, the RyR1 C-terminal domain was reported to be sufficient to form an ion-conducting pore, but required N-terminal residues for channel modulation (Bhat *et al.*, 1997). The aforementioned findings are all in support of an equivalent I-domain sequence in RyR1.

Recently, George *et al.* extended their domain interaction hypothesis further by showing that domains harbouring CPVT mutations (S2246L in N-terminal sequence, N4104K and R4497C in I-domain sequence) were associated with abnormal Ca^{2+} handling and conformational instability in agonist-stimulated cells. In addition, wild-type and mutant channels were functionally indistinguishable under non-stimulated conditions, which is consistent with the asymptomatic resting phenotype observed in most CPVT patients (Lehnart *et al.*, 2005; Oda *et al.*, 2005; Yano *et al.*, 2005a; George *et al.*, 2006; Bannister *et al.*, 2007). Further elucidation of functional molecular interactions within normal and mutant RyR channels will provide a greater understanding of normal RyR conformation and associated channelopathies.

The I-domain was identified using confocal microscopy, and RyR2 sequences used were based on predicted TM domain topologies from the laboratories of Lai and MacLennan (Zorzato et al., 1990; Tunwell et al., 1996; Du et al., 2002a), and sequences with a proposed involvement in ionic sensitivity and channel gating (George *et al.*, 2004), detailed below. The 6TM model, according to Tunwell *et al.* adapted with the nomenclature of Du *et al.* is displayed in Figure 3.3.

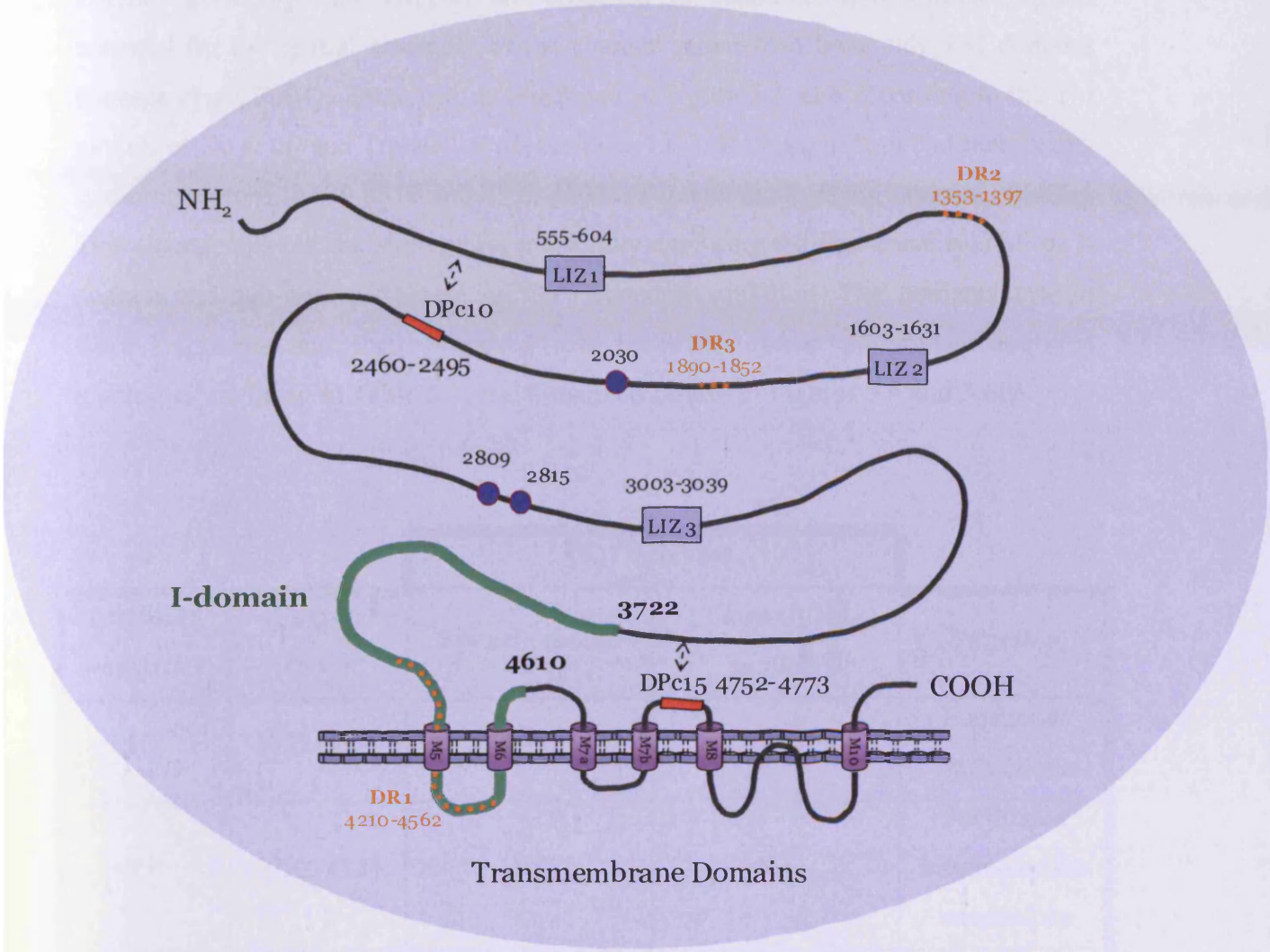

Figure 3.3. Sites of intra-molecular interaction

Conformational representation of RyR2 revealing sites potentially involved in intrinsic channel regulation. The location of cardiac domain peptides DPc10 and DPc15 demonstrates the plausibility of an association between disparate protein sequences (illustrated by dashed arrows). Similarly, the I-domain (3722-4610, displayed in green) also shows an arrangement that may facilitate self-association. The I-domain incorporates the first two predicted TM domains. TM domains are termed M5, M6, M7a, M7b, M8 and M10, as published by Du *et al.* in 2002. Sites of divergent regions (DR1-3), LIZ motifs (LIZ1-3) and reported phosphorylation loci (blue circles) are also labelled.

Based on this TM topology, I-domain residues downstream of 4450 are likely involved in TM domain assembly, whereas amino acids 3722-4450 (reported by Zorzato to incorporate TM1-4) are proposed to constitute hydrophobic regions essential for the spatial assembly of the channel rather than bona fide TM domains (George *et al.*, 2004). Therefore, as illustrated in Figure 3.3, and according to the TM models of Du *et al.* and Tunwell *et al.*, residues 4353-4610 are host to two membrane-spanning regions (4499-4519 and 4572-4593) (Tunwell et al., 1996; Du et al., 2002a). This chapter sets out the strategy for more fully exploring the functional role of the I-domain and sub-regions therein on Ca^{2+} channel regulation. The nomenclature of these fragments and their proposed role based on functional studies and TM topologies are listed in Table 3.1, and illustrated further in Figures 3.4 and 3.6B:

		TM domains		
I-domain construct	**Region (a.a.)**	**Zorzato model**	**Tunwell/Du models**	**Function**
ID	3722-4610	1-6	1-2	Functional interactions
ID^A	3722-4353	1-4	None	Facilitated intramolecular interactions
ID^B	4353-4499	None	None	Facilitated intramolecular interactions
ID^C	4353-4610	5-6	1-2	Increased channel functionality

Table 3.1. Nomenclature and functional basis of I-domain constructs

I-domain construct nomenclature, the numbers of predicted TM domains that they encompass, and their proposed function as suggested by George *et al.*, 2004. Note that ID^B is the only I-domain section that does not have any proposed TM domains.

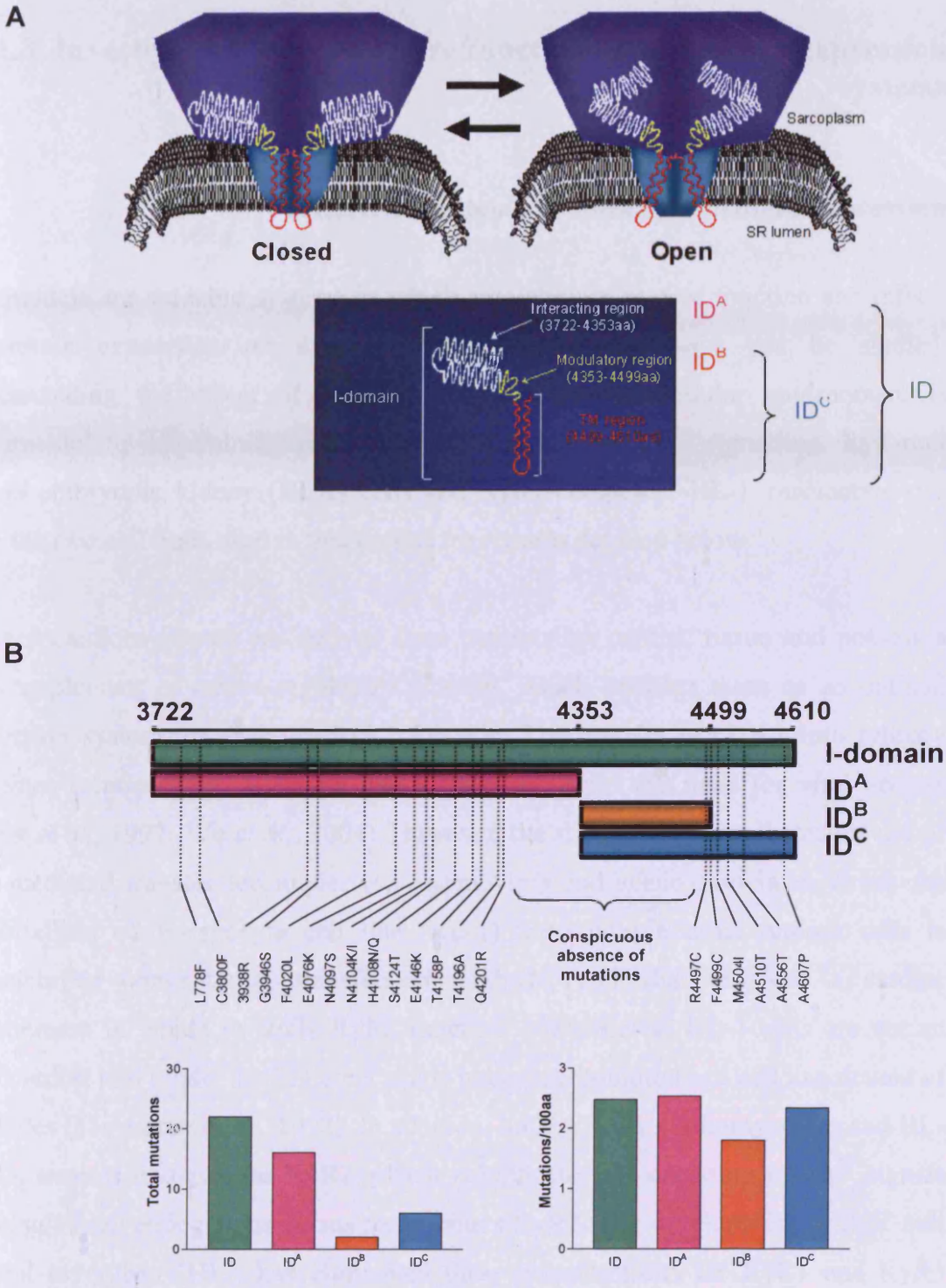

Figure 3.4. I-domain conformation and the loci of disease-linked mutations

A. The I-domain was divided into three distinct regions: interacting (ID^A), modulatory (ID^B) and TM-containing ID^C. ID^C is composed of the modulatory region (ID^B) plus two putative TM domains. Figure adapted from George and Lai, 2007. Reported mutations in each I-domain section (left bar graph) is adjusted for the number of mutations per 100 amino acids (right bar graph). Interestingly the majority of ID^B is largely devoid of mutations, and the two reported mutations arise in the distal three amino acids (2% of the sequence). It could be argued that the paucity of mutations in ID^B reflects that mutations within this region may be lethal.

3.1.3. Investigating RyR structure/function using cellular expression systems

3.1.3.1. Transient recombinant protein expression

Cell models are valuable systems in which recombinant protein function and effects of protein expression on dynamic cell signalling pathways can be studied. Understanding the effect of I-domain expression in a cellular environment is fundamental to determining precisely how it modulates Ca^{2+} signalling. RyR-null human embryonic kidney (HEK) cells and RyR2-competent HL-1 cardiomyocytes were the two cell lines used in this project for reasons detailed below.

Primary cardiomyocytes are derived from mammalian cardiac tissue and possess a full complement of cardio-regulatory proteins, which presents them as an optimal expression system for studying RyR2 function. The transfer of cDNA into primary cell lines is remarkably difficult, and usually stipulates the need for viral vectors (Hajjar *et al.*, 1997; Wu *et al.*, 2004). However, the size of RyR2 precludes the use of viral-mediated transfer techniques (e.g. adenovirus and adeno-associated virus). An immortalised cardiomyocyte cell line (HL-1) from murine atrial tumour cells is amenable to conventional transfection methods, and also provides a cardiac environment in which to study RyR2 function. Nevertheless HL-1 cells are not an ideal cardiac cell model as they are a single nucleated immortalised cell line devoid of T-tubules (Claycomb *et al.*, 1998). In addition, both primary cardiomyocytes and HL-1 cells express endogenous RyR2, which complicates the decoding of Ca^{2+} signals that result from endogenous versus recombinant RyR2. The development of RyR-null skeletal myotubes (1B5) has eliminated these complications for RyR1 and RyR3 functional studies (Moore *et al.*, 1998); however, currently no cardiomyocyte cell model lacking endogenous RyR2 has been generated. In light of these issues, RyR-deficient cell models have been implemented for recombinant RyR2 study. The use of RyR-null cell models has enabled the detection of functional differences between wild type and mutant RyR2 that may have been overlooked if assessed in cells with a background of endogenous RyR (Thomas *et al.*, 2004; Thomas *et al.*, 2005; Paavola *et al.*, 2007). Recombinant RyR2 channels expressed in RyR-null HEK cells have

been shown to exhibit comparable Ca^{2+} and caffeine activation to channels obtained from native tissue (Chen *et al.*, 1997). In addition, mutation-induced channel instability documented by George and colleagues was comparable in both RyR2 proficient and deficient cell models (George *et al.*, 2006) validating the use of RyR null expression systems, which also suggests that RyR2 regulation may not be completely dependent on cardiac-specific proteins.

Expression of recombinant RyR2 has been investigated in a number of RyR2-null cell models including HEK, Chinese hamster ovary (CHO) and green monkey fibroblast (COS-7) cells (Bhat and Ma, 2002a; Treves et al., 2002; Xiao et al., 2002; George et al., 2003c; George et al., 2006; George et al., 2007; Jiang et al., 2007), and are still widely used for this purpose. HEK are regularly used by virtue of their high transfection efficiency, tolerance to expression of the large size of RyR protein, and their human origin. It should, however, be noted that some laboratories have detected discrete levels of RyR in low passage (<25) HEK cells (Querfurth *et al.*, 1998; Luo *et al.*, 2005), and although other laboratories have disputed the endogenous expression of RyR in HEK (Gao *et al.*, 1997; Du and MacLennan, 1998; Tong *et al.*, 1999; Jiang *et al.*, 2002a) low passage HEK cells were not used in this project to negate this issue.

3.1.3.2. Stable recombinant protein expression

Transient expression of recombinant proteins provides temporary (~48h) assessment of protein function. However, in order to investigate the long-term consequences of protein expression, stable cell lines are usually generated. Stable protein expression employs antibiotic selection to eliminate cells lacking the permanent integration of recombinant DNA at a transcriptionally active locus. Stable expression of RyR2 in both CHO and HEK cells has been previously documented, although it is associated with increased toxicity at higher expression levels (Bhat *et al.*, 1999; Pan *et al.*, 2000; Rossi *et al.*, 2002; George *et al.*, 2003c). This prompted the development of inducible stable systems that enable precise control of RyR2 expression levels (George *et al.*, 2004; Jiang *et al.*, 2007; Stewart *et al.*, 2008). In addition, the development of novel systems such as the Flp-In system (using mammalian cell lines that enable site-

specific DNA integration) has further facilitated the generation of potentially cytotoxic stable cell lines and has been shown to be useful in the inducible expression of RyR2 (Jiang *et al.*, 2005; Jiang *et al.*, 2007).

3.1.4. Objective

This chapter describes the generation of I-domain constructs, and characterises the resultant phenotypes following their transient expression in HEK and HL-1 cell models.

3.2. Methods

3.2.1. Cloning strategy of I-domain constructs

The fluorescent proteins eGFP and DsRed have both been implemented in our laboratory as fusion proteins in confocal imaging studies (George *et al.*, 2004), however the reasons for using monomeric red fluorescent protein (mRFP) in favour of eGFP and DsRed are detailed in Section 2.2.1.

mRFP was a gift from Professor R.Y. Tsien (University of California at San Diego [UCSD]). The mRFP expression vector, pmRFP-C1 (Figure 3.5), was generated by H.L. Roderick (Babraham Institute, Cambridge), following *Nhe* I and *Hind* III excision of mRFP from the pRSET bacterial expression vector (Campbell *et al.*, 2002) and subsequent sub-cloning into the peGFP-C3 plasmid (Takara Biosciences, Japan) by direct substitution of mRPF for eGFP.

RyR2 DNA fragments corresponding to the I-domain (a.a.3722-4610) and regions within (ID^A, 3722-4353; ID^B, 4353-4499; ID^C, 4353-4610) were cloned into pmRFP-C1 in frame with the open reading frame of mRFP, shown schematically in Figure 3.6 using methods described in Section 2.2.2.1. DNA fragments of the correct sizes (mRFP 4648bp, I-domain 2648bp; ID^A 1899bp; ID^B 445bp; ID^C 749bp) were excised from the gel, purified and cloned into pmRFP-C1 as described elsewhere (Section 2.2.2.1). Figure 3.7 displays the predicted DNA digest patterns of I-domain constructs in pmRFP-C1. Sequencing traces are displayed in Figure 3.8.

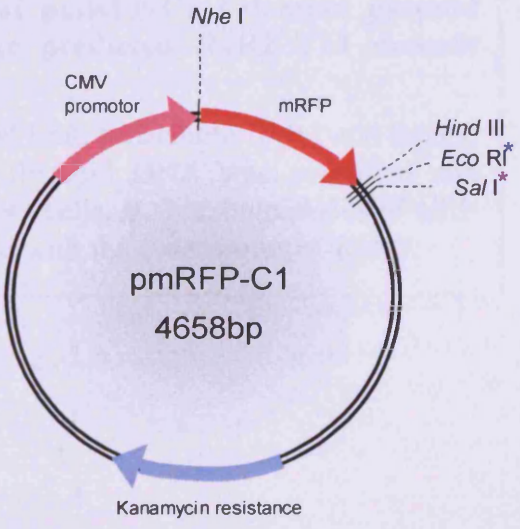

Figure 3.5. pmRFP-C1 restriction enzyme map

mRFP (red arrow) expression is driven by the CMV promoter (pink arrow). *Eco* RI and *Sal* I restriction sites located in the multiple cloning site (MCS) (used for cloning of I-domain) are indicated (*) directly following the mRFP sequence. The resistance gene is kanamycin (pale blue arrow). See Appendix II for detailed pmRFP-C1 sequence.

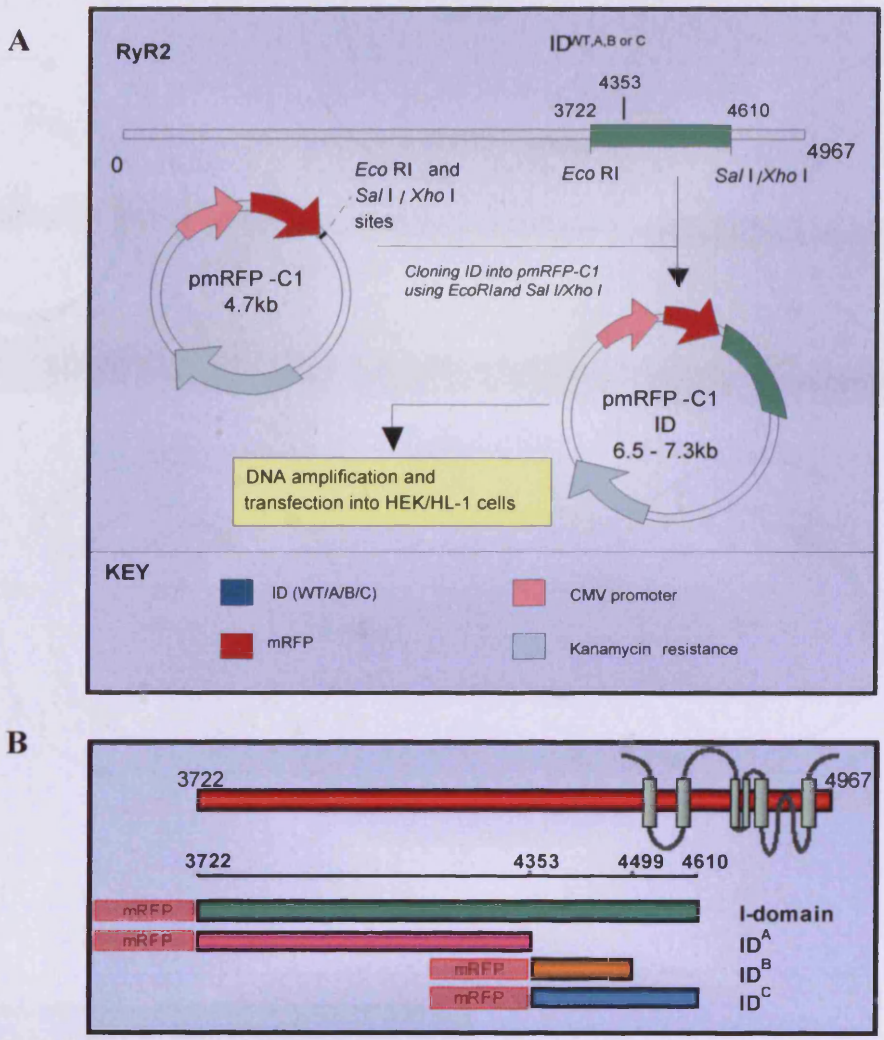

Figure 3.6. Schematic representation of pmRFP-C1 I-domain plasmid construction and their relation to the predicted RyR2 TM domain topology

A. I-domain constructs were PCR amplified from full-length RyR2 and ligated into pmRFP-C1 with *Eco* RI & *Xho* I. Plasmid DNA was amplified and sequenced prior to transfection into HEK293 cells. **B**. The boundaries of all I-domain constructs are indicated and aligned with the C-terminus of RyR2.

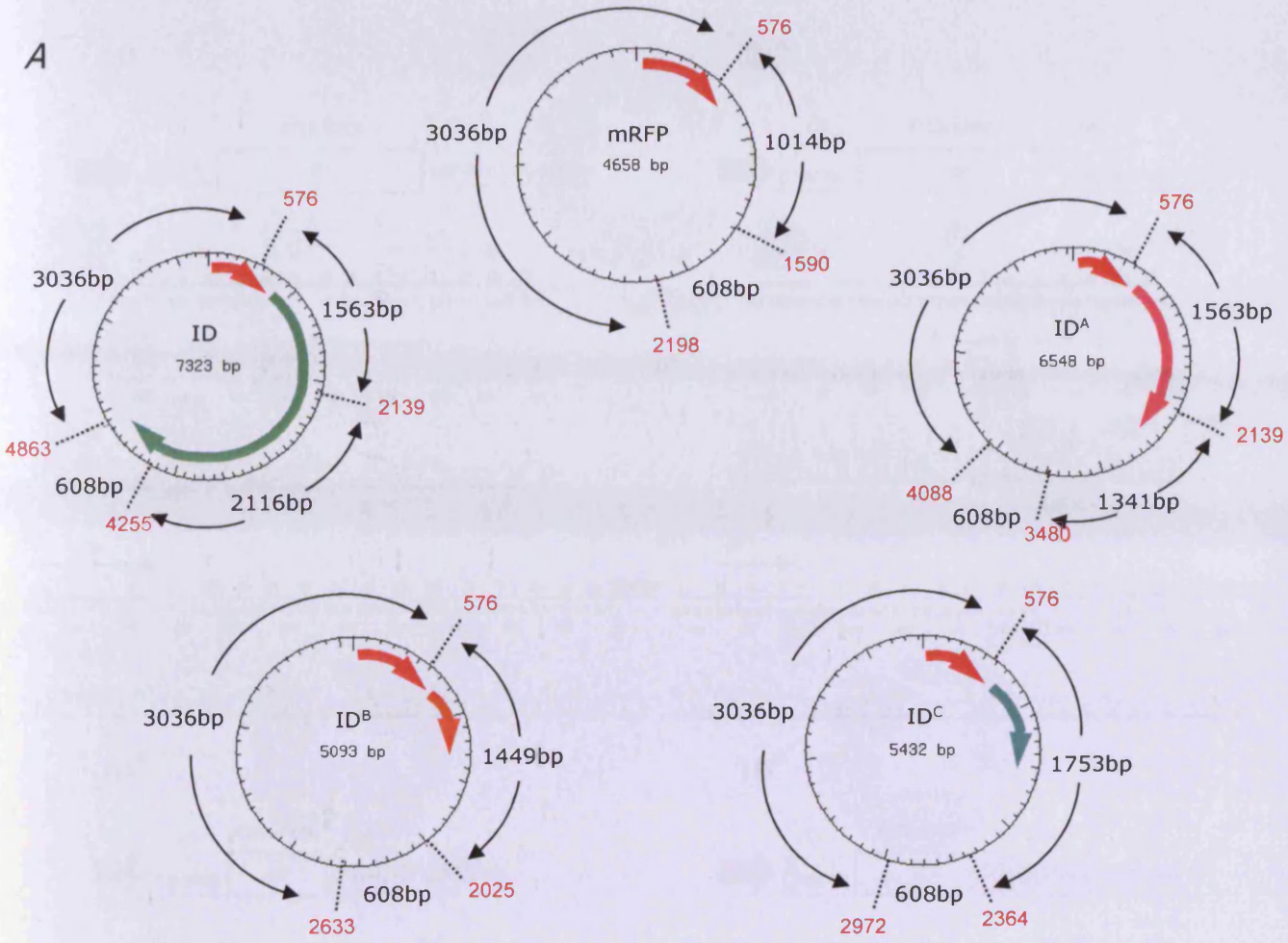

B

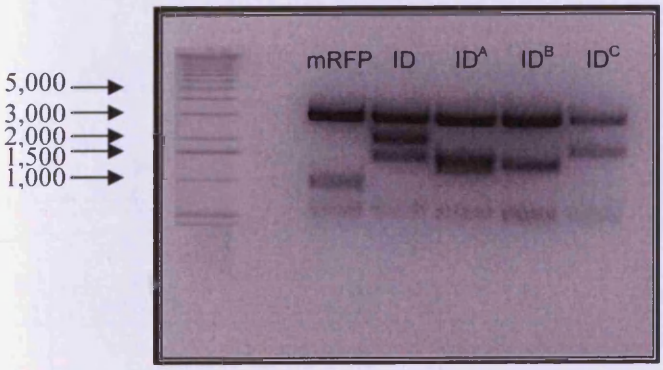

C

mRFP	ID	IDA	IDB	IDC
3036bp	3036bp	3036bp	3036bp	3036bp
1014bp	2116bp	1563bp	1449bp	1753bp
608bp	1563bp	1341bp	608bp	608bp
	608bp	608bp		

Figure 3.7. Identification of pmRFP-C1 I-domain cloning by restriction digestion

A. Restriction maps of pmRFP-C1 I-domain sections using *Pvu* II (restriction sites are represented by dashed lines). Expected fragment size is shown between restriction sites. **B.** Electrophoretic mobility resolved restriction fragments from pmRFP-C1 I-domain digestion as shown in A. **C.** Expected *Pvu* II cleavage fragments.

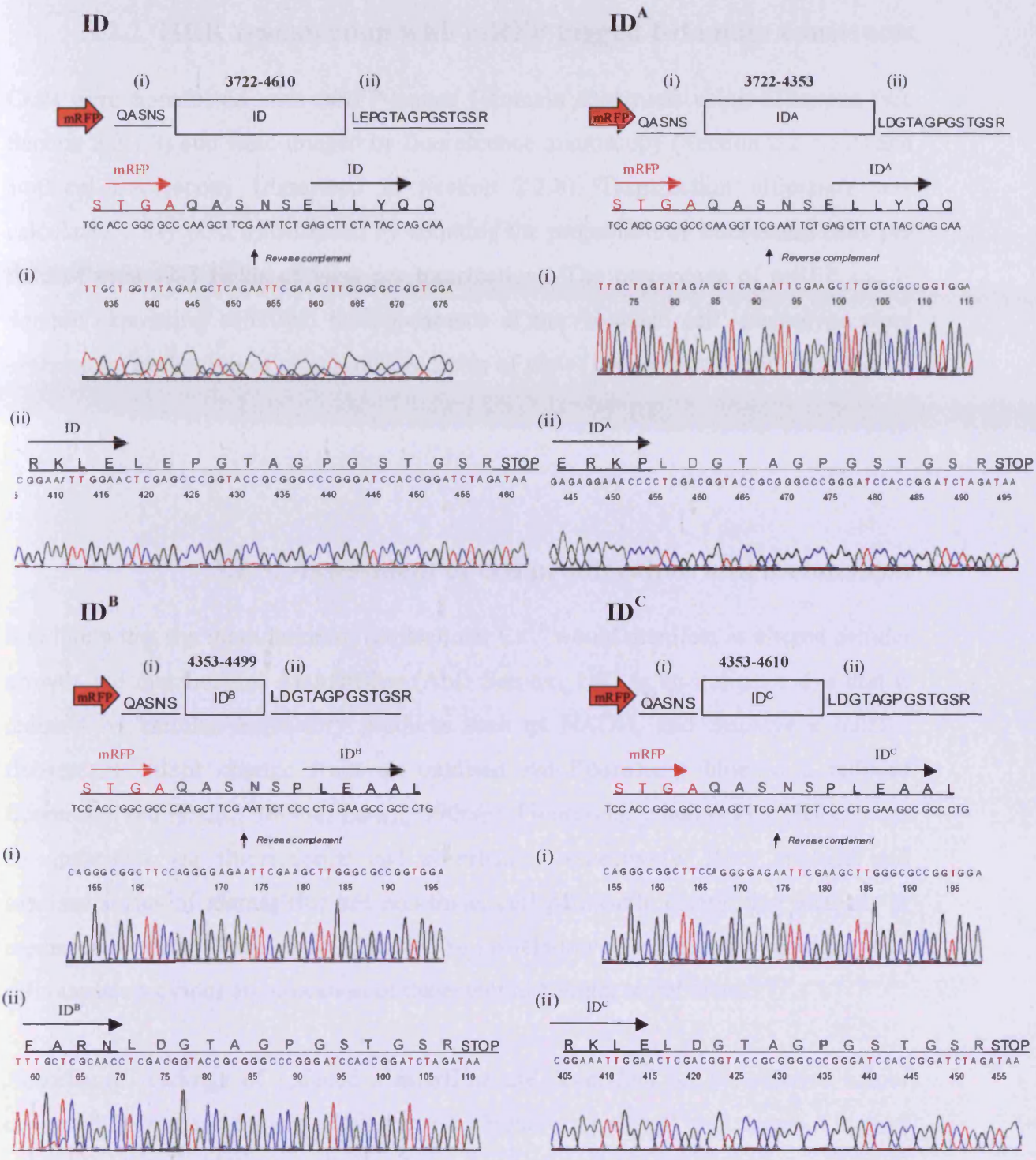

Figure 3.8. Sequencing of I-domain constructs in pmRFP-C1

Top panels display the predicted linker sequences either side of I-domain constructs, labelled as 5' (i) and 3' (ii). Middle and bottom panels are electropherograms displaying the 5' (i) and 3' (ii) ligation sites of I-domain cloning into pmRFP-C1. Middle panels display 5' sequencing trace obtained using the sense strand of DNA as a template and was subsequently reverse complemented to obtain coding amino acid sequence. Amino acids that code for mRFP and I-domain are highlighted. Lower panels display the 3' sequencing trace obtained by using the antisense DNA strand as template. Coding amino acids are displayed above the trace and the residues corresponding to the I-domain are indicated. Linker sequences are shown in grey.

3.2.2. HEK transfection with mRFP tagged I-domain constructs

Cells were transfected with mRFP-tagged I-domain constructs using Effectene (see Section 2.2.7.3) and were imaged by fluorescence microscopy (Section 2.2.7.3.2) and confocal microscopy (described in Section 2.2.8). Transfection efficiency was calculated 1 day post transfection by counting the proportion of fluorescent cells per field of view (2-3 fields of view per transfection). The percentage of mRFP and I-domain expressing cells and the appearance of the 'rounded cell' phenotype were assessed by evaluation of representative fields of view (1-4 days post-transfection).

3.2.3. Assessment of cell proliferation and metabolism

It is likely that the modulation of intracellular Ca^{2+} would manifest as altered cellular growth and metabolism. AlamarBlue (AbD Serotec, UK) is an indicator dye that is reduced by cellular respiratory products such as NADH, and displays a relative fluorescent colour change from an oxidised non-fluorescent blue to a reduced fluorescent red (Ex_{max}, 560nm; Em_{max}, 590nm). Fluorescence and colour changes can be quantified via fluorescence and absorbance respectively. Both reduced and oxidised forms of alamarBlue are non-toxic, cell permeable (permitting analysis of media) and stable (Pettit *et al.*, 2005). The correlation of alamarBlue readings with cell number provides an indication of the extent of cellular metabolism.

Absorbance readings of reduced alamarBlue are dependent on the relative colour change at 560nm and 600nm. However, the pH indicator phenol red is present in most culture media, and this perceptively changes colour over 4 days and can significantly influence absorbance readings at 560nm (Figure 3.9). To preclude this issue, and since changing culture media was not a practical option (e.g. phenol red-free media), the fluorescence route was pursued instead.

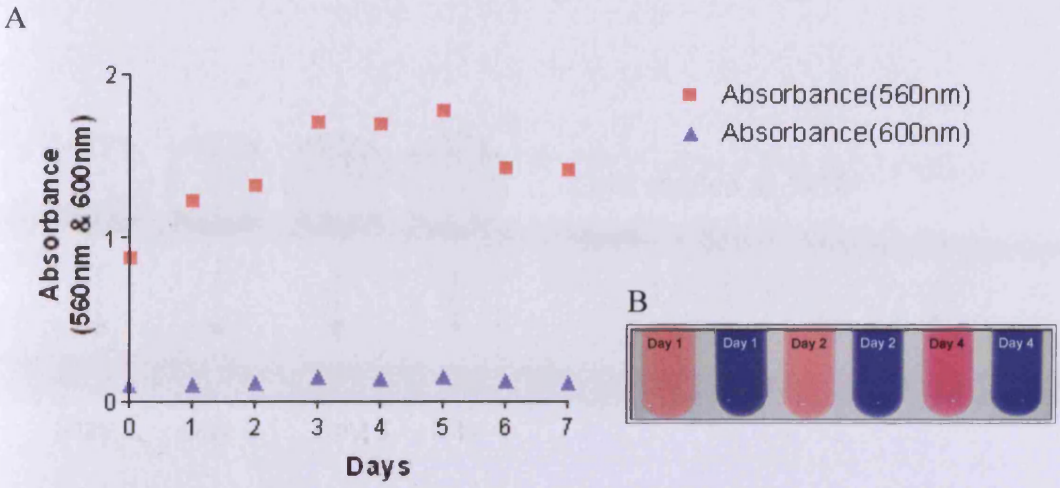

Figure 3.9. Absorbance measurements at 560nm and 600nm of alamarBlue in cDMEM (10% v/v)

A. The pH of cDMEM (indicated by phenol red) is not stable over seven days, which dramatically altered absorbance measurements at 560nm. n=1. **B.** Images showing media colour of both cDMEM and cDMEM with alamarBlue at 1, 2 and 4 days after DMEM supplementation.

HEK cells and recombinant protein (I-domain/mRFP) expressing cells were seeded 4h post-transfection into four wells of a six well plate at a density of 5 $x10^4$ (one plate per construct, n=4) that also included two empty control wells (for cDMEM and cDMEM-alamarBlue). Three duplicate plates were set up for analysis on consecutive days (D1-4). Cells were exposed to alamarBlue in 2ml cDMEM (10% v/v) for 4 h at 24, 48, 72 and 96 h time points. Media (2 x 0.5ml) was removed from each well into 1ml cuvettes and immediately assayed using a LS50B fluorometer (Perkin-Elmer), with excitation and emission at 545nm and 590nm respectively, see Figure 3.10. Following experiments, cells were counted and paired with alamarBlue fluorescence readings to calculate cellular metabolism per 10,000 cells. Cell growth of HEK, mRFP and I-domain expressing cells was also quantified via daily haemocytometric counts over 4 days following transfection. Cells seeded 4 h after transfection (density of $5x10^4$) were labelled as day 0. Cell counts for day 1 were performed 20h later (i.e. 24h post-transfection), and subsequent daily counts performed at 24h intervals until day 4.

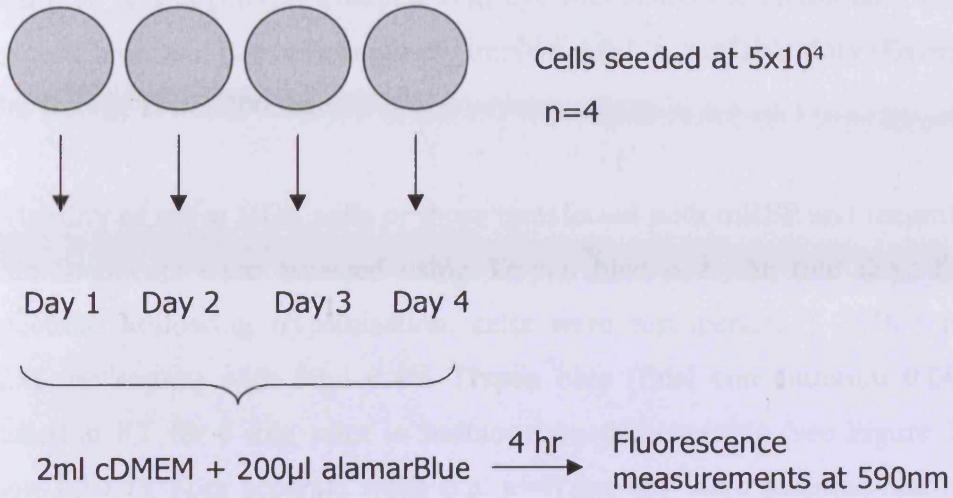

Figure 3.10. Protocol for alamarBlue measurement of cell proliferation

alamarBlue (in cDMEM) was applied to cells for 4h at 1-4 days post transfection, then analysed for fluorescence at 590nm

3.2.4. Assessing cell viability using Trypan blue

The proportion of dead or dying cells within a cell population as a result of apoptosis and necrosis can be determined using cell viability assays, such as Trypan blue. Trypan blue is a negatively charged vital dye that stains the membranes of dead or dying cells blue, and has been routinely implemented in our laboratory (George *et al.*, 2003a; George *et al.*, 2003b).

The viability of naïve HEK cells or those transfected with mRFP and recombinant I-domain fragments were assessed using Trypan blue over the four days following transfection. Following trypsinisation, cells were resuspended (~$2x10^5$) in 250µl DMEM (no serum) with 50µl 0.4% Trypan blue (final concentration 0.08%) and incubated at RT for 5 min prior to haemocytometric counting (see Figure 3.11 and Section 2.2.7.1). Four separate wells (i.e. n=4) per day were assessed and each cell suspension was read in duplicate. Cells visibly stained blue were counted as non-viable.

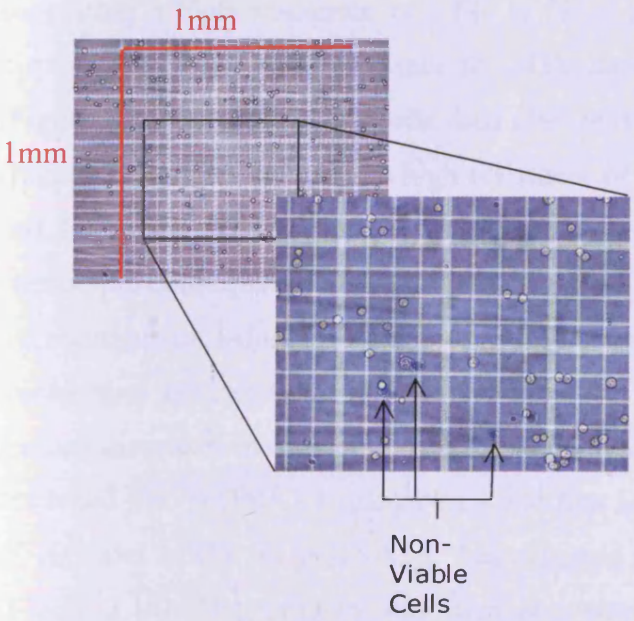

Figure 3.11. Cell viability using Trypan blue

Haemocytometer slide displaying both viable (clear) and non-viable (blue) cell populations. The 0.1µl grid (1mm x 1mm x 0.1mm) is composed of a 5 x 5 arrangement (with a 4x4 inner demarkation).

3.2.5. Immunoblotting of recombinant protein isolated from HEK cells

HEK cells (1-10x10^6) were harvested 1 to 4 days post-transfection and pelleted for protein isolation as described in Section 2.2.9.1. SDS-PAGE and Western blotting experiments were carried out on 100μg of cellular post-nuclear supernatant (PNS) using standard published techniques (Laemmli and Quittner, 1974; Burnette, 1981) (Section 2.2.9). Membranes were probed with a polyclonal antibody to DsRed (Clontech) (used at 1:750) that reacts with the mRFP fusion tag (Section 2.1.2.5.1).

3.2.6. G418-mediated selection of cells expressing recombinant I-domain

Cellular expression of the neomycin gene confers resistance to geneticin (G418 sulphate), a potent inhibitor of protein synthesis. G418 concentrations ranging from 0.2mg/ml and 1mg/ml have been administered to HEK cells to select stable expression of recombinant proteins (Stetzer *et al.*, 1996; Rintoul *et al.*, 2001; Rossi *et al.*, 2002; Chapman *et al.*, 2005; Hanson *et al.*, 2008b), although higher concentrations have been used (Kunapuli *et al.*, 1997; Dassanayake *et al.*, 2007) suggesting a high resistance of HEK to G418 selection. In this project, HEK cells displayed a remarkable resistance to G418, surviving for 14 days in 2mg/ml G418 (Figure 3.12A), while HL-1 cells died after only 2 days exposure to 500μg/ml G418 (Figure 3.12B). In light of the high resistance of HEK to G418 selection, both mRFP and ID^B were re-cloned into a hygromycin vector in order to confirm that any phenotypic consequences following their expression via pmRFP-C1 was due solely to the recombinant I-domain fragments. For this study, ID^B was used because of its high transfection efficiency in comparison to other I-domain constructs, and for other reasons discussed in Section 5.3.3. ID^B and mRFP were excised from pmRFP-C1 and re-cloned into pcDNA3.1 using *Nhe* I and *Kpn* I, See Figure 3.13. Successful cloning of ID^B and mRFP in pcDNA3.1 was assessed by restriction digestion with *EcoR*I (Figure 3.14). Hygromycin was used at a concentration of 200μg/ml, which was sufficient to select for stable expression while preventing rapid cell loss. Similar to G418, hygromycin is also a potent inhibitor of protein synthesis. Prior to cloning, a

dose-dependence curve was conducted on HEK cells to ensure that hygromycin would eliminate non-resistant cell populations, and also to determine a suitable working concentration (Figure 3.12C). Surviving cells were counted using haemocytometry as described in Section 2.2.7.1. A low seeding density was used to prevent the cells becoming confluent over the duration of the experiments since G418 only works if the cells are actively growing. Similarly, HEK cells were seeded at a density of $1x10^5$ in wells of a 6-well plate and exposed to increasing concentrations of hygromycin (0, 200, 500, 800 and 1000μg/ml) for 2 days (n=3 per dose). A higher seeding density was used attributable to the rapid loss of cells induced by hygromycin. Cells remaining after 2 days were harvested and counted by haemocytometry (Section 2.2.7.1), shown in Figure 3.12.

Note that the cells used here were HEK293 and not the variant 293T cell line, which are HEK293 cells transformed by the T-antigen from the SV40 virus that confers G418 resistance (Lebkowski *et al.*, 1985; Stewart and Bacchetti, 1991) and thus the high level of G418 resistance was unexpected.

A. HEK G418

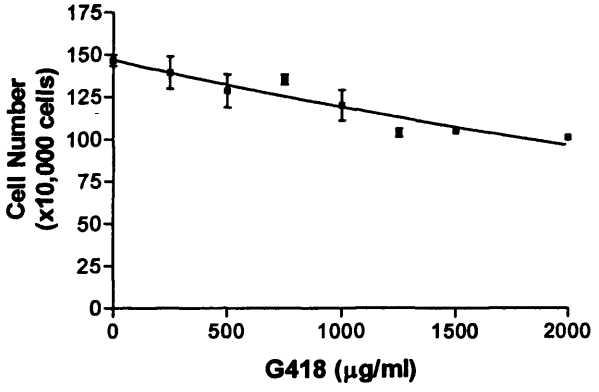

B. HL-1 G418

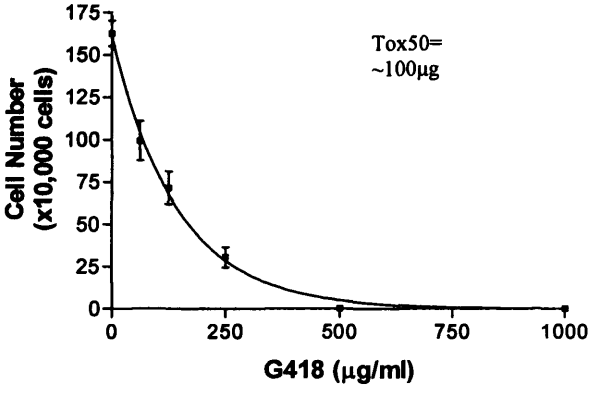

Figure 3.12. G418 and hygromycin dose-dependent elimination of non-resistant cell populations

A. HEK cell exposure to G418 (0-2 mg/ml) for 14 days failed to effectively select cells, whereas HL-1 cell exposure to G418 (0-1 mg/ml) over 2 days resulted in a rapid elimination of cells (**B**). **C**. HEK cell exposure to hygromycin (0-1 mg/ml over 2 days also resulted in rapid cell death. Tox50 (dose at which antibiotic kills 50% of cells) is displayed on graphs B and C. n=3 for each dose.

C. HEK hygromycin

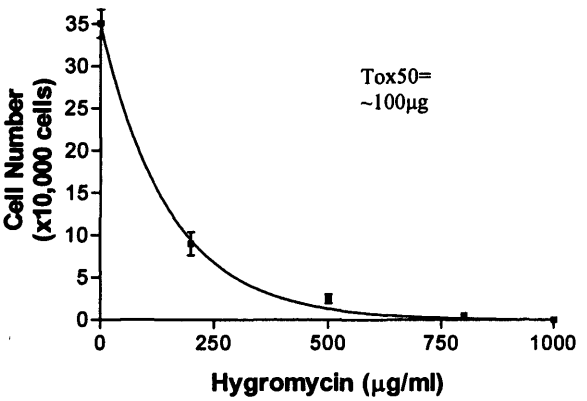

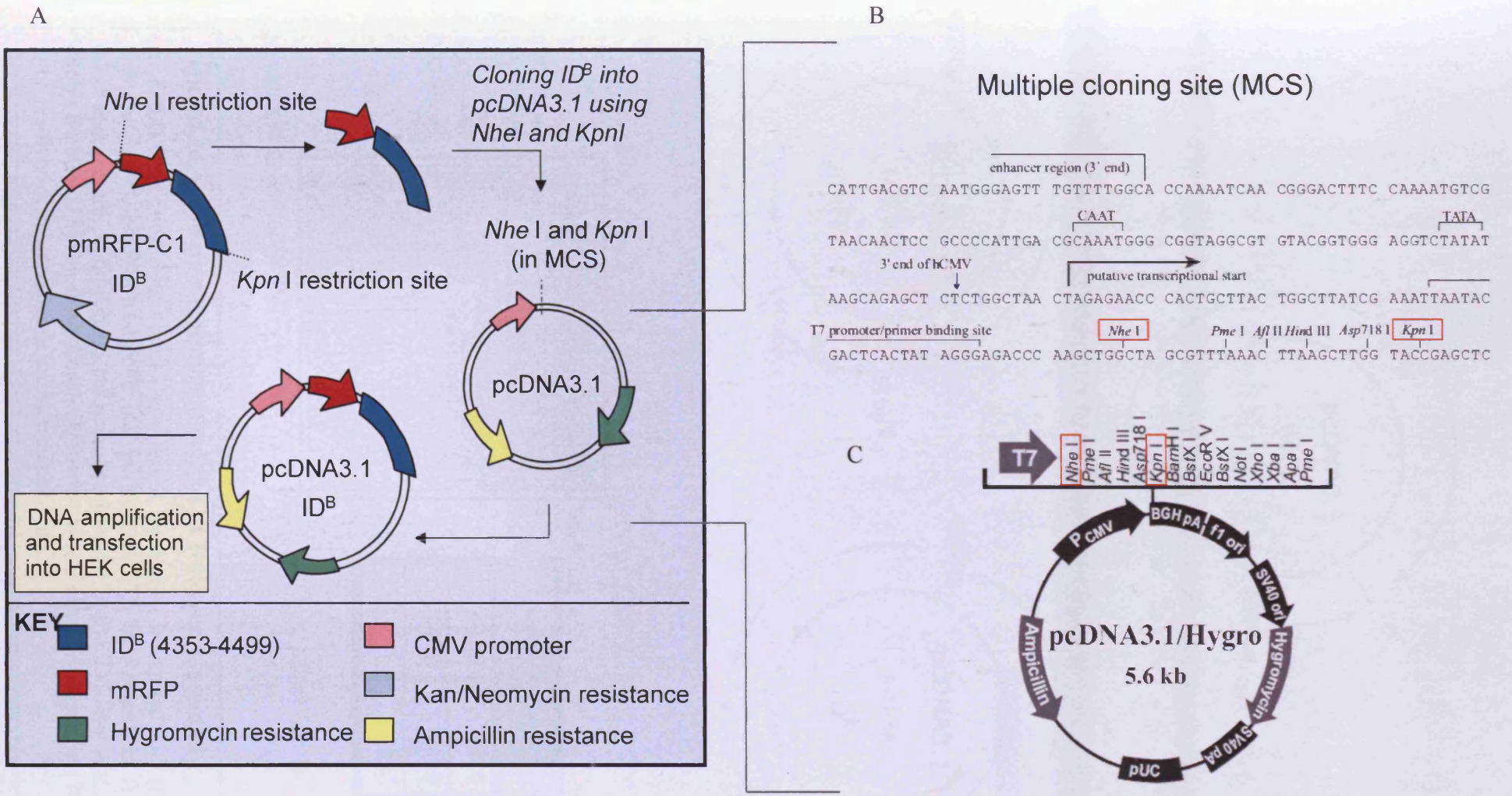

Figure 3.13. Cloning strategy for sub-cloning I-domain into pcDNA3.1 hygromycin

A. Schematic representation of ID^B-mRFP and mRFP cloning into pcDNA3.1. Both constructs were excised from pmRFP-C1 and re-cloned into pcDNA3.1 using *Nhe* I and *Kpn* I (cutting at bases 4 and 711, and 4 and 1146 of pmRFP-C1 for mRFP and ID^B respectively). **B.** pcDNA3.1 multiple cloning site (MCS) and **C.** Plasmid map displaying MCS, *Nhe* I and *Kpn* I restriction sites are highlighted. See Appendix III for full pcDNA3.1 map.

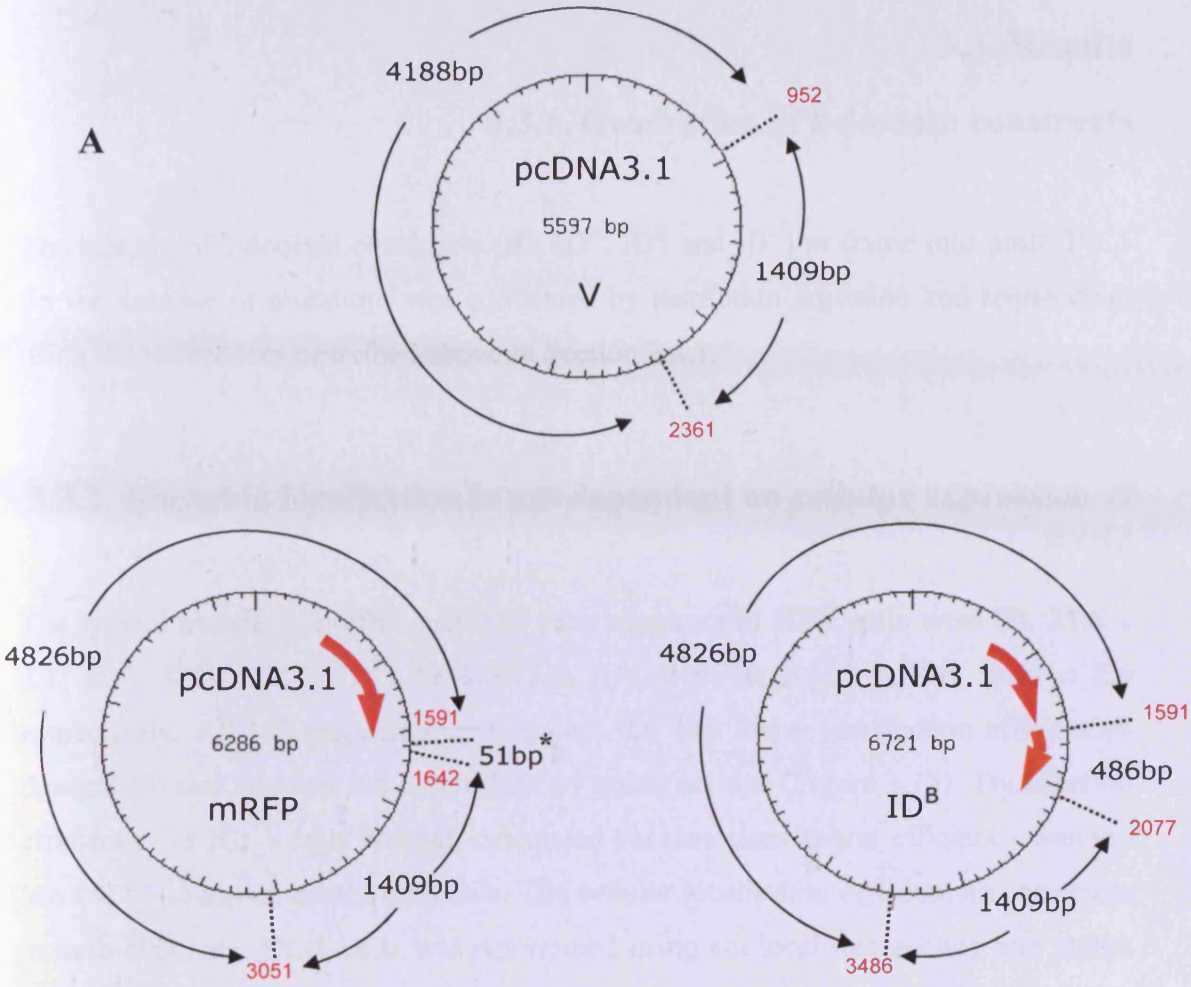

B

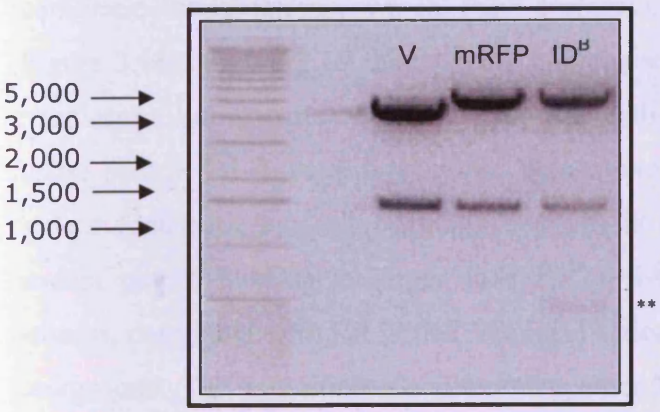

C

Vector	mRFP	ID^B
4188	4826	4826
1409	1409	1409
	51*	486

Figure 3.14. Restriction digestion of pcDNA3.1 I-domain constructs

A. *EcoR*I restriction digest sites (represented by dashed lines) and loci (red figures) in pcDNA3.1 (V), pcDNA3.1-mRFP and pcDNA3.1-ID^B. **B.** Restriction fragments on a 0.8% agarose gel. A faint band (**) can be observed in the ID^B lane that represents the 486bp fragment. *51bp band from pcDNA3.1-mRFP digestion with *Eco* RI is too small to be resolved. Expected bands are summarised in **C.**

3.3. Results

3.3.1. Generation of I-domain constructs

The cloning of I-domain constructs (ID, ID^A, ID^B and ID^C) in frame into pmRFP-C1 (in the absence of mutation) was confirmed by restriction digestion and sequencing, using the procedures described above in Section 3.2.1.

3.3.2. I-domain localisation is not dependent on cellular expression of RyR2

The typical transfection efficiencies of each construct in HEK cells were ID, 25% ± 2.1; ID^A, 38% ± 2.5; ID^B, 52% ± 2.7; ID^C, 40% ± 2 and mRFP, 56% ± 2.6 respectively. All I-domain fragments except ID^B had lower transfection efficiencies than mRFP and this was not determined by construct size (Figure 3.15). Transfection efficiency for HL-1 cells was not calculated because transfection efficiency was too low (<1%) to obtain meaningful data. The cellular localisation of I-domain constructs in both HEK and HL-1 cells was determined using confocal microscopy and unlike mRFP, all I-domain constructs were excluded from the nucleus (Figure 3.16). However, it should be noted that I-domain constructs did also appear to target nuclear membrane invaginations, which may correspond to the nucleoplasmic reticulum (Figure 3.16). Figure 3.17 displays the homogeneous expression in both nuclear and cytoplasmic compartments of the cyan and yellow fluorescent protein (CFP:YFP) fusion pair in HL-1 cardiomyocytes. This figure is good evidence that the lack of nuclear localisation of all I-domain sections is not due to size limitations, as the tandem pair (~55kDa) is larger than ID^B (~44kDa). Further distinct localisation patterns, consistent with ER lattice-like localisation were observed independent of cell background. This is particularly interesting since HL-1 and HEK are RyR2 sufficient and null respectively. In addition, note the highly punctuated pattern of ID^C that was displayed in both cell types (Figure 3.16). The relative fluorescence intensity per pixel was expressed as a ratio of cytoplasmic to nuclear fluorescence (Figure 3.18) and represents the semi-quantitative measurement of nuclear exclusion exhibited by all I-domain sections. The high level of fluorescence calculated for ID^C is skewed by the dense fluorescent aggregates (Figure 3.16).

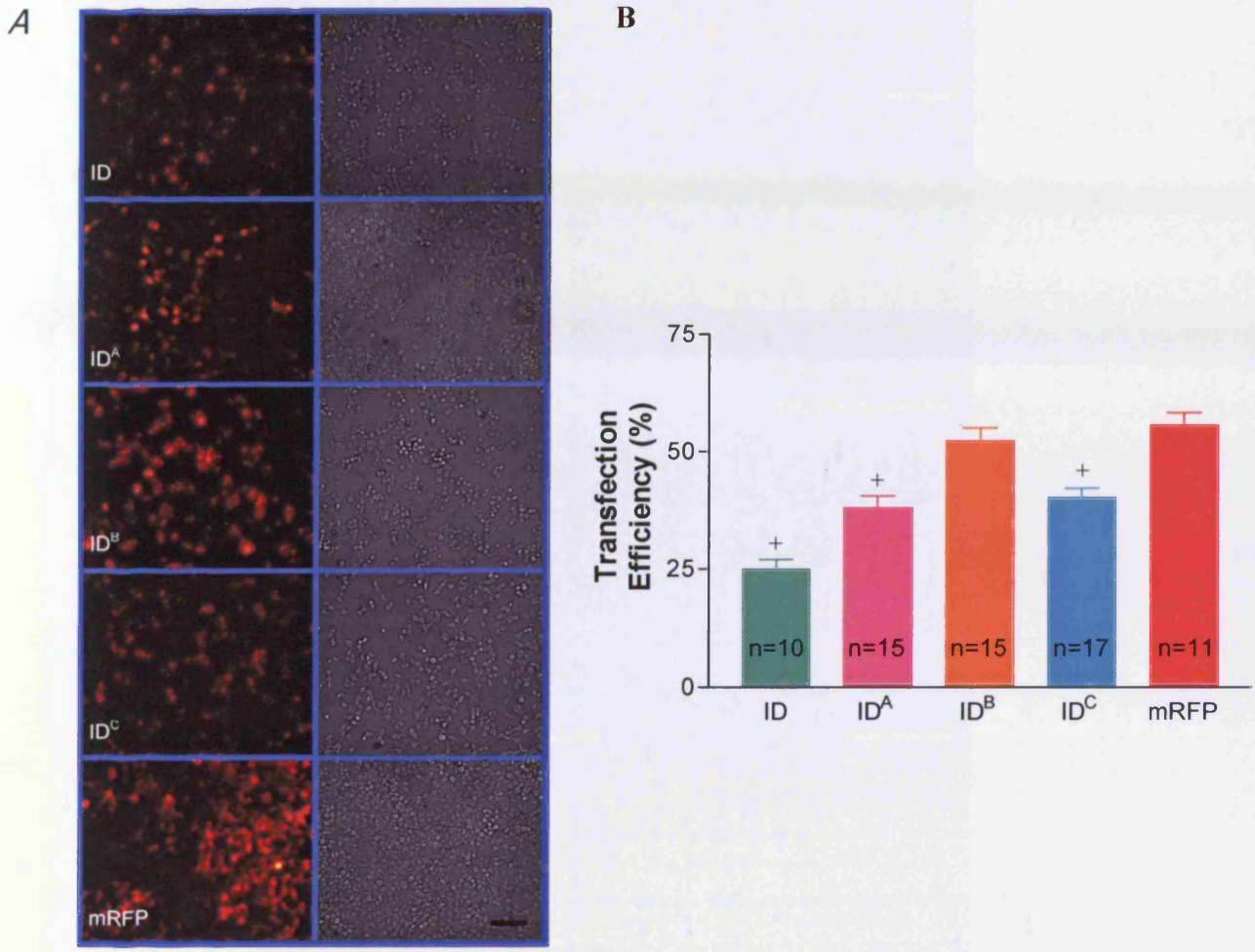

Figure 3.15. Transient transfection of I-domain constructs in HEK cells

A. Typical fields of view of transfected cells at 10x magnification. Left panels represent fluorescent images and right panels are the corresponding phase images. Scale bar represents 50μm. **B.** Standard transfection efficiencies, n represents the average of 2-3 fields of view per transfection. $^{+}p<0.001$ compared to mRFP expressing cell populations.

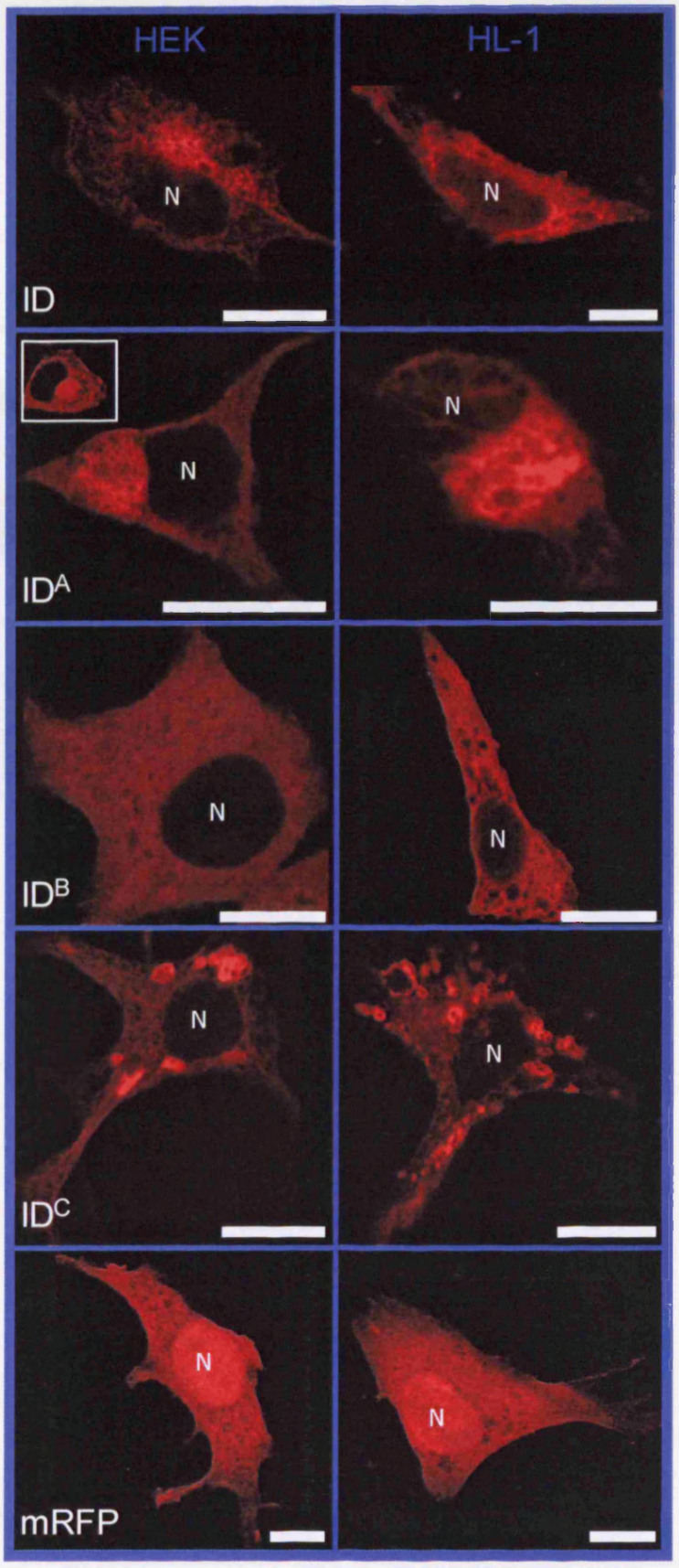

Figure 3.16. Cellular localisation of I-domain constructs in HEK and HL-1 cells

Confocal images of HEK and HL-1 cells 48h after transient transfection with mRFP and I-domain constructs. Images are representative of typical localisation profiles. Inset in ID^A panel displays Golgi staining of a HEK cell (Triantafilou and Triantafilou, 2004) using TRITC conjugated Concanavalin A (a lectin that specifically binds to mannosyl groups in the Golgi). N = nucleus. Scale bars represent 10μm.

A

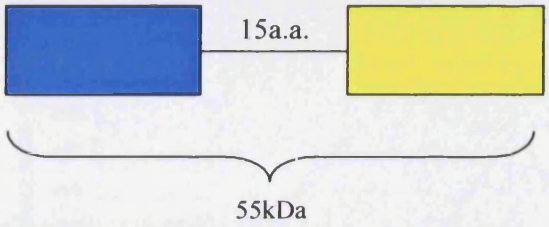

B

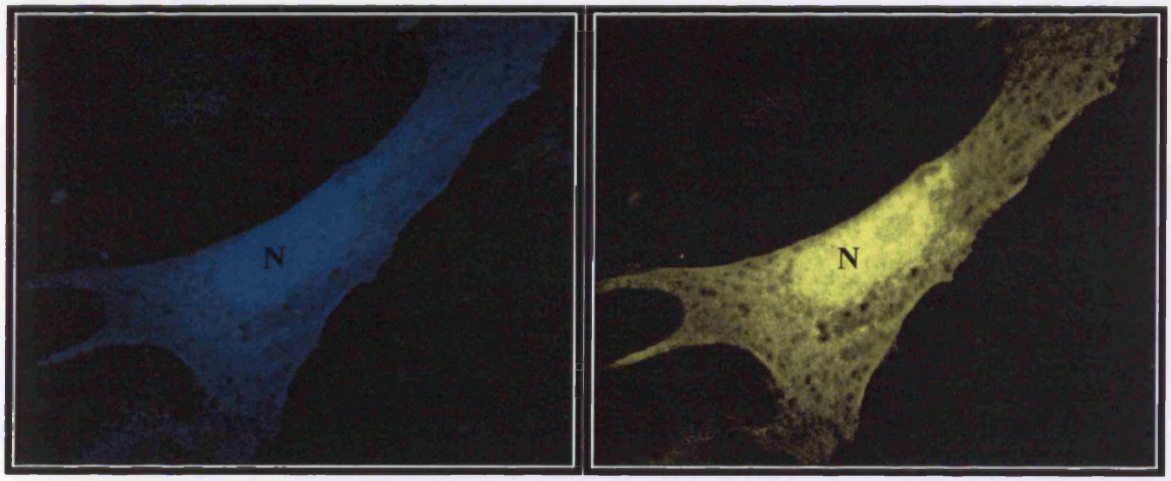

Figure 3.17. C15Y, a 55kDa CFP:YFP tandem expressed in HL-1 cardiomyocytes exhibits pronounced nuclear localisation

A. CFP and YFP tandem pair separated by 15a.a. linker sequence CSSCARARDAAVATM. **B.** Confocal images of a HL-1 cell transfected with CFP:YFP tandem fluorescent protein pair. Figure generated by Dr. Chris George.

HEK

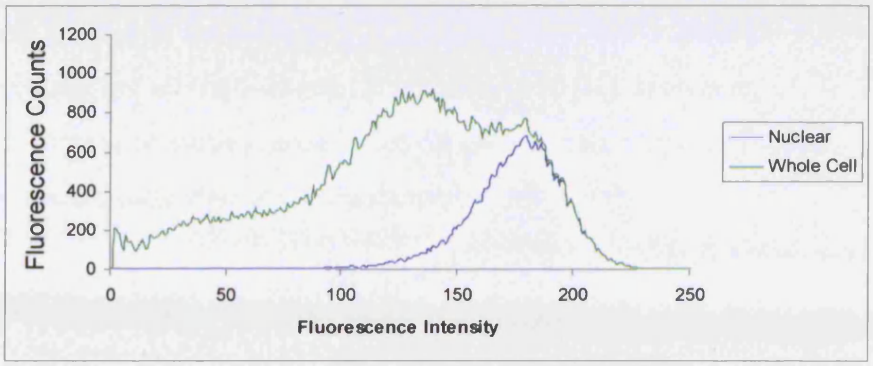

HL-1

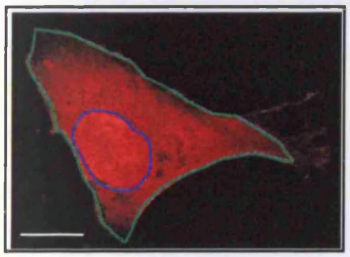

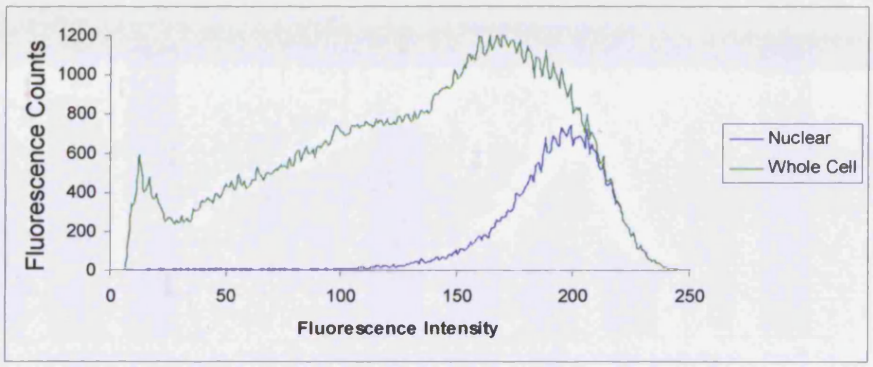

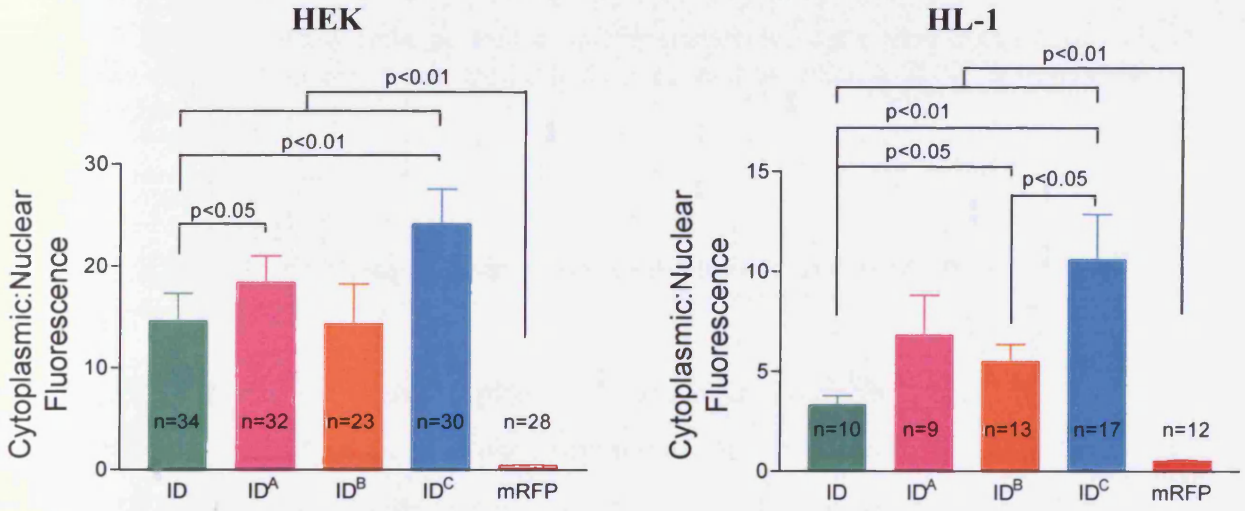

Figure 3.18. Comparison of cytoplasmic and nuclear localisation of recombinant proteins

Whole-cell and nuclear regions were selected, and total fluorescent counts were calculated for both whole cell and nucleus (scale bar = 10μm), which is represented by the area under the curve. Cytoplasmic counts were determined by subtracting nuclear fluorescent counts from whole cell counts. A ratio of average cytoplasmic fluorescence to nuclear fluorescence was obtained per cell (lower panels). Data is plotted as mean ± SEM, n represents number of cells.

HEK cell size, measured by surface area, was also significantly reduced following I-domain expression compared to control cells (Figure 3.19). Similarly, HL-1 mRFP cells were larger than cells expressing all the I-domain fragments ($p<0.01$). However, it cannot be ruled out that reduction in surface area is due to greater cell depth as I-domain expressing cells become less adherent. All cells measured were viable.

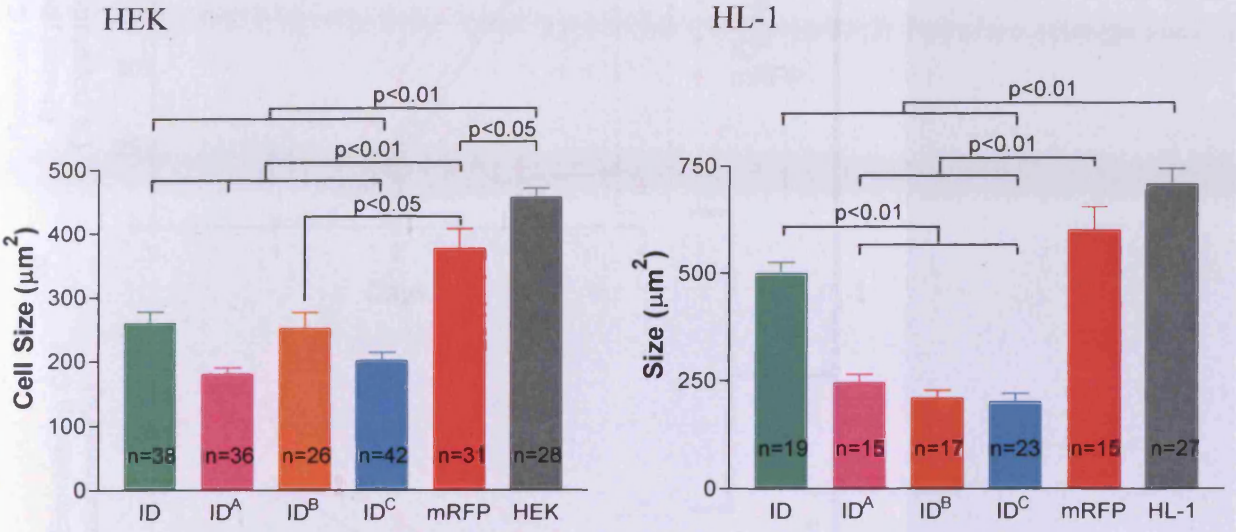

Figure 3.19. Effect of I-domain expression on cell size

WT HEK and HL-1 cells, as well as mRFP-transfected cells were significantly larger than all I-domain expressing cells. Data is plotted as mean ± SEM, n represents the number of cells.

3.3.3. Prolonged I-domain expression profoundly alters cell phenotype

Since cell size was significantly reduced by transient I-domain expression, other phenotypic consequences of I-domain expression were monitored using confocal microscopy for 4 days post-transfection. It was noted that an increasing number of I-domain expressing cells began to exhibit a 'rounded cell' phenotype compared with mRFP cells over the course of the 4 day protocol shown in Figure 3.20. The percentage of mRFP expressing cells was significantly greater than those expressing I-domain on days 2-4 ($p<0.01$) and exhibited a significantly lower proportion of 'rounded cells' ($p<0.01$, days 2-4) as determined by visual assessment of phenotype.

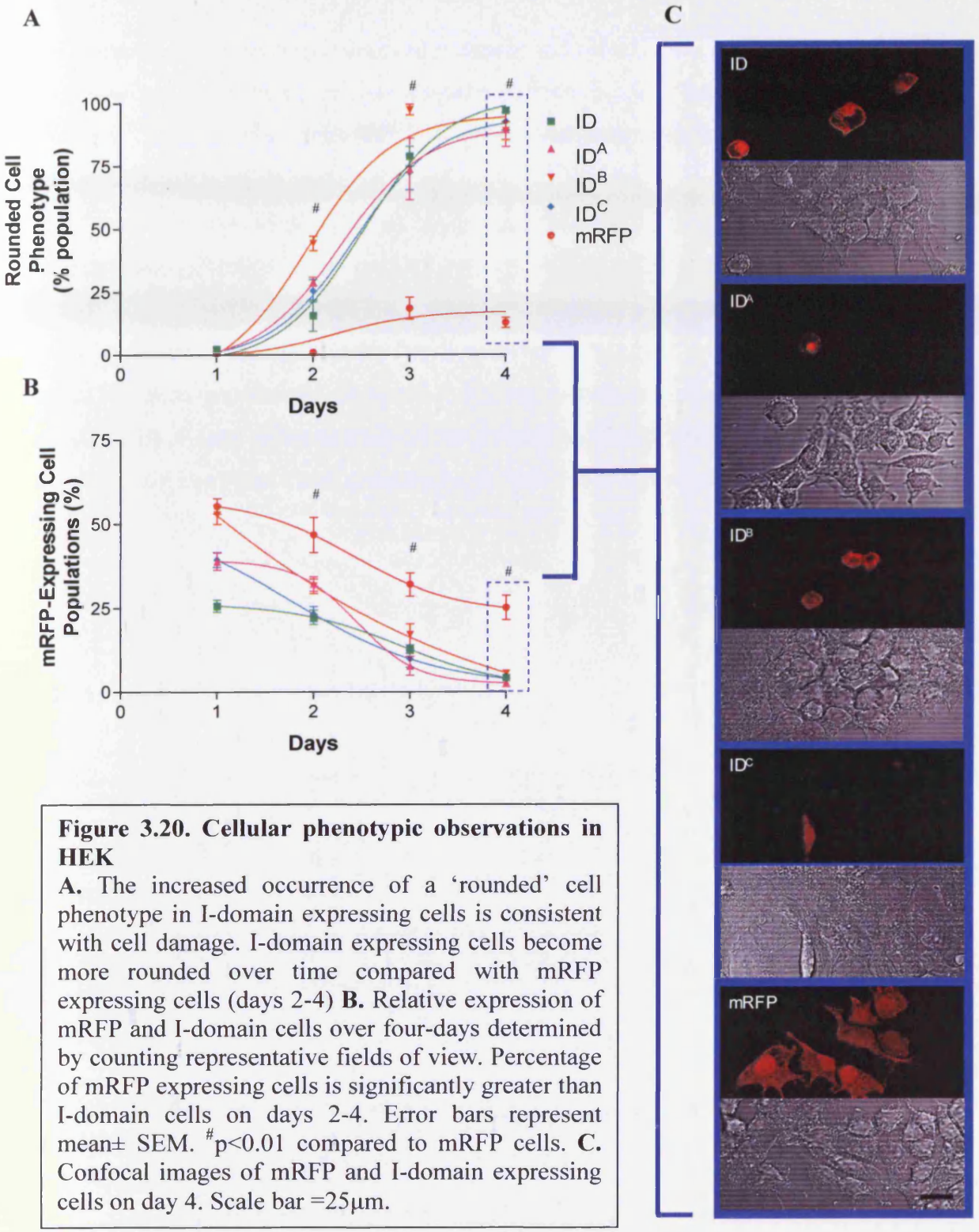

Figure 3.20. Cellular phenotypic observations in HEK

A. The increased occurrence of a 'rounded' cell phenotype in I-domain expressing cells is consistent with cell damage. I-domain expressing cells become more rounded over time compared with mRFP expressing cells (days 2-4) **B.** Relative expression of mRFP and I-domain cells over four-days determined by counting representative fields of view. Percentage of mRFP expressing cells is significantly greater than I-domain cells on days 2-4. Error bars represent mean± SEM. $^{\#}p<0.01$ compared to mRFP cells. **C.** Confocal images of mRFP and I-domain expressing cells on day 4. Scale bar =25μm.

3.3.4. I-domain expression is associated with reduced cell viability

The 'rounded cell' phenotype observed routinely and robustly in I-domain expressing cells was consistent with cellular damage (Figure 3.20). Therefore in order to determine whether the 'rounded cell' phenotype was indicative of increased cytotoxicity, cell viability was determined using Trypan blue.

There was no difference in cell viability between WT or mRFP-expressing HEK cells (Figure 3.21). However, 2 and 3 days post-transfection, I-domain expressing cells were characterised by significantly lower viability than mRFP-expressing cells. On day 2, I-domain populations displayed 2-3 times more non-viable cells than mRFP and HEK. By 4 days post-transfection, the proportion of non-viable cells transfected with I-domain constructs was comparable to both HEK and mRFP (p=NS) (Figure 3.21).

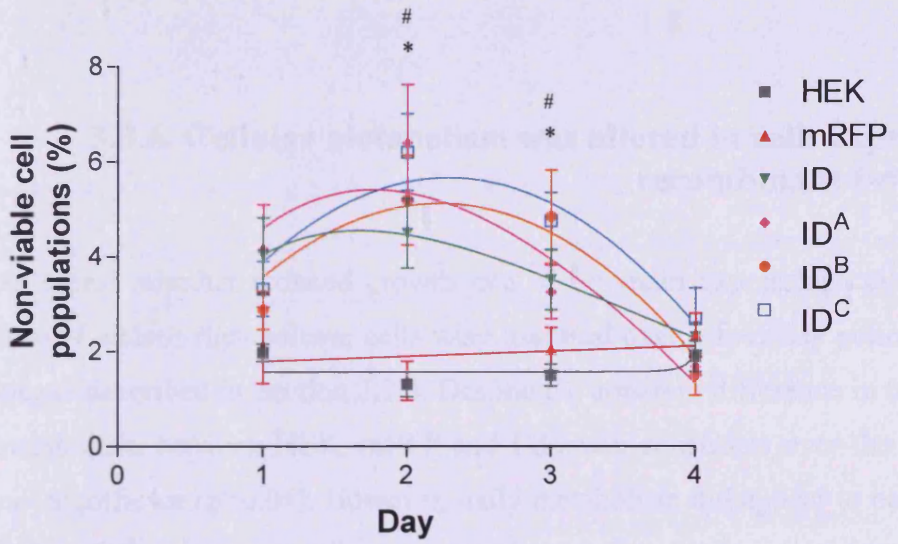

Figure 3.21. Cell viability following I-domain transfection in HEK cells

The non-viable cell populations in HEKwt, mRFP and I-domain transfected cells following transfection, expressed as a percentage of total cells. *$p<0.05$ and #$p<0.01$ compared to mRFP expressing cells. n = 4 for each construct.

3.3.5. I-domain expression reduces cell proliferation

When considering the reduced cell viability and altered cell phenotype following I-domain transfection (Figures 3.19, 3.20 and 3.21) it was pertinent to investigate cell proliferation and metabolism over the same period. Cells seeded at the same density were imaged on days 1-4 (Figure 3.22A). There were less adherent cells on day 1 in I-domain- and mRFP-transfected populations than HEK cells ($p<0.01$) and notably ID^C adherence was even lower still (Figure 3.22B). The low adherence of mRFP cells following transfection suggests that transfection itself may subsequently play a role in the toxic phenotype. In light of the lower adherence of transfected cells, cell counts on days 2-4 were normalised to day 1 cell numbers for each construct (Figure 3.22C). Cell proliferation rates were suppressed on day 2 in ID^{A-C} ($p<0.01$) transfected cells, on day 3 in ID^C ($p<0.05$) and on day 4 in ID, ID^A ($p<0.05$) and ID^C ($p<0.01$) compared to mRFP transfected cells (Figure 3.22C).

3.3.6. Cellular metabolism was altered in cells expressing recombinant I-domain

In order to assess whether reduced growth rate of I-domain expressing cells was a consequence of altered metabolism, cells were assessed over a four day period using alamarBlue, as described in Section 3.2.3. Despite the apparent difference in trends in cellular metabolism between HEK, mRFP and I-domain constructs over the 4 days, this was not significant ($p>0.05$). However, daily metabolism did appear to be altered in ID^A, ID^B and ID^C expressing cells most notably at 1, 2 and 3 days post-transfection compared to HEK and mRFP cells (Figure 3.23). More specifically, the metabolism of ID^{A-C} cells was suppressed on day 1 ($p<0.01$), yet elevated on day 2 (ID^A, $p<0.05$; ID^B and ID^C, $p<0.01$) when compared with mRFP-expressing cells. Metabolism on day 3 was only significantly different between ID^C and mRFP ($p<0.05$). Day 4 metabolism was significantly higher for both ID^A and ID^C ($p<0.01$) than mRFP cells, see Figure 3.23.

A

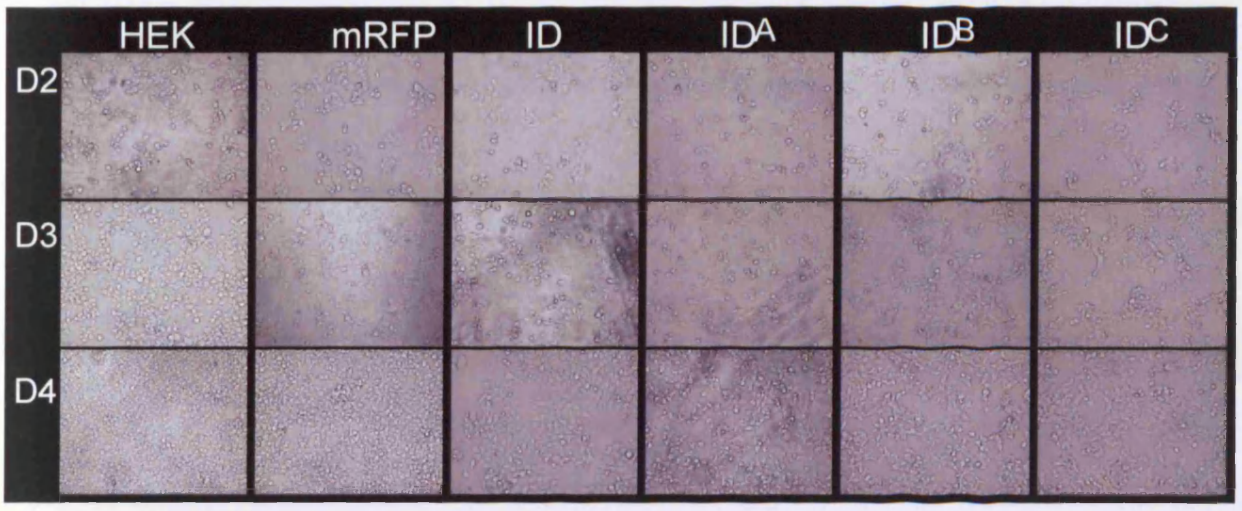

B

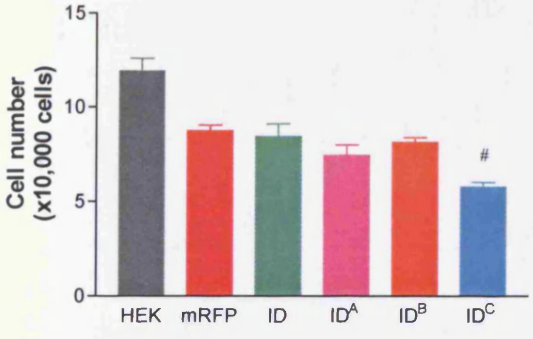

C

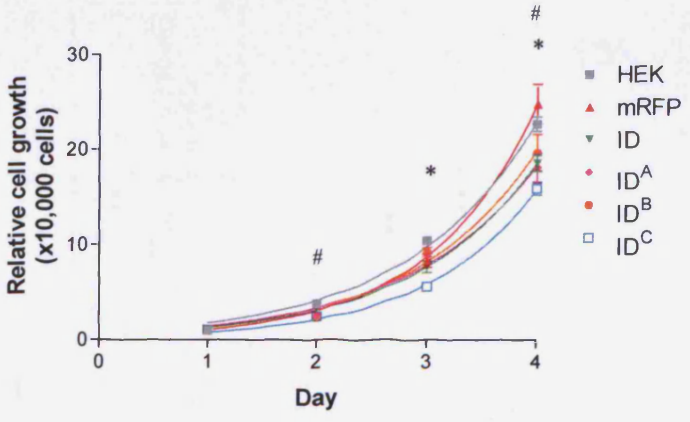

Figure 3.22. Proliferation of WT HEK, mRFP and I-domain expressing cells

A. Images obtained at day 2, day 3 and day 4 from seeding $5x10^4$ cells per well. **B.** Proportion of adherent cells 20h after seeding ($5x10^4$), $^{\#}p<0.01$ compared to mRFP, n = 4. **C.** Cell growth based on daily cell counts per 10,000 cells standardised to day one cell counts. Statistical significance compared to mRFP: Day 2, $^{\#}p<0.01$ ID^{A-C}; Day 3, $*p<0.05$ ID^{C}; Day 4, $^{\#}p<0.01$ ID^{C} and $*p<0.05$ ID & ID^{A}. n=4 for each cell line.

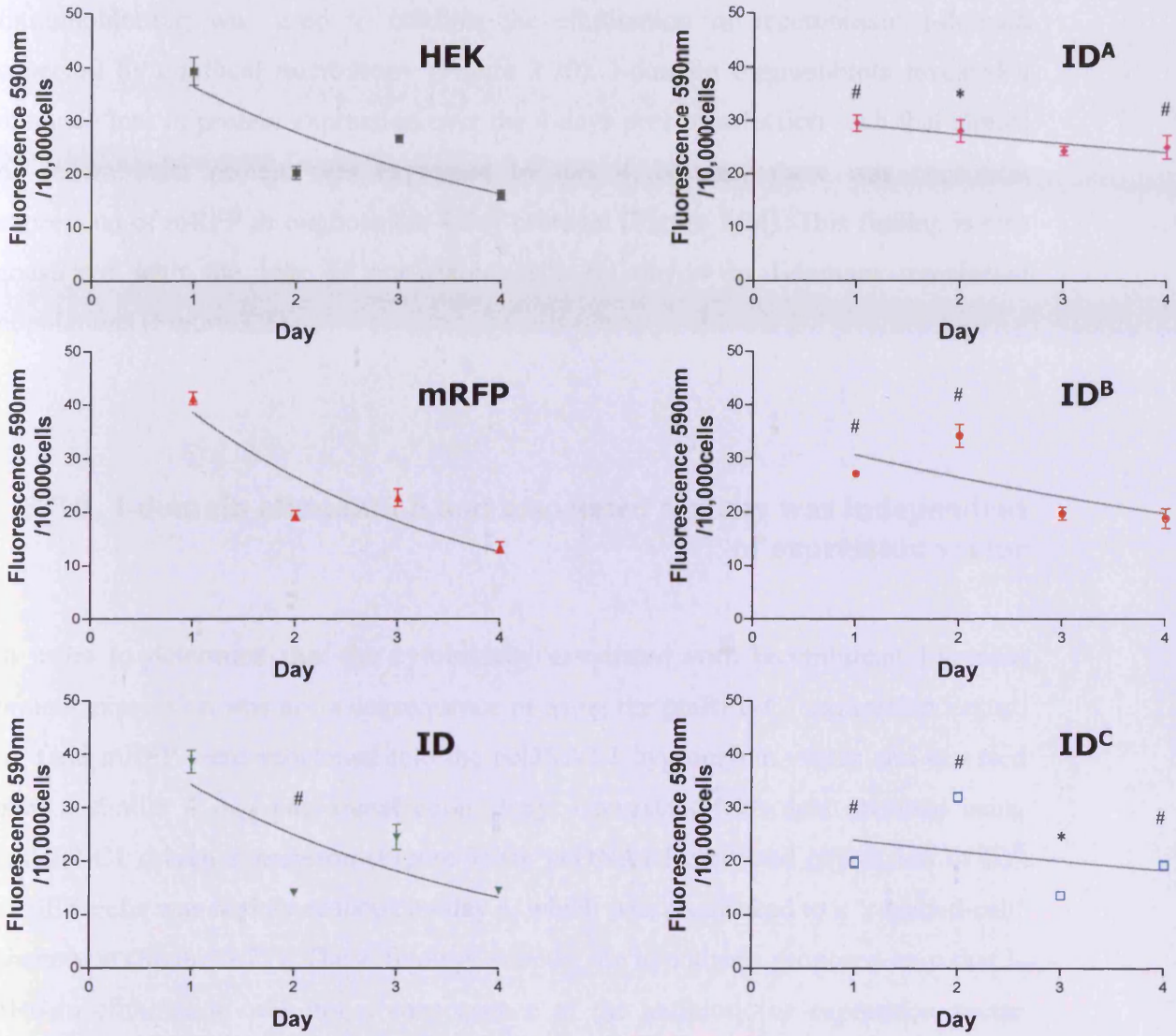

Figure 3.23. HEK Cell metabolism assessed by alamarBlue

WT HEK and mRFP metabolism was not significantly different on any day, however ID, ID^A, ID^B and ID^C all displayed altered metabolism compared to cells transfected with mRFP on different days. n=4 for each cell line. $^{\#}p<0.01$ and $^{*}p<0.05$ compared to mRFP on the same day.

3.3.7. I-domain elimination was confirmed by immunoblot

Immunoblotting was used to confirm the elimination of recombinant I-domain observed by confocal microscopy (Figure 3.20). I-domain immunoblots revealed a dramatic loss in protein expression over the 4 days post-transfection such that almost no recombinant protein was expressed by day 4. Notably there was consistent expression of mRFP throughout the 4 day protocol (Figure 3.24). This finding is also consistent with the loss of non-viable cells by day 4 in I-domain transfected populations (Figure 3.21).

3.3.8. I-domain elimination and associated toxicity was independent of expression vector

In order to determine that the cytotoxicity associated with recombinant I-domain protein expression was not a consequence of using the pmRFP-C1 expression vector, ID^B and mRFP were subcloned into the pcDNA3.1 hygromycin vector and assessed over a similar 4 day post-transfection study. Consistent with data obtained using pmRFP-C1 driven expression (Figure 3.20), pcDNA3.1-mediated expression of ID^B in HEK cells was rapidly reduced by day 4, which was also linked to a 'rounded-cell' phenotype (Figure 3.25). These findings support the hypothesis proposed here that I-domain elimination was not a consequence of the antibiotic or expression vector system employed. In view of the data that I-domain expression could not be maintained past day 3-4 because of confounding toxicity issues, the failure of G418 selection of I-domain in pmRFP-C1 did not negatively impact on subsequent experiments.

A

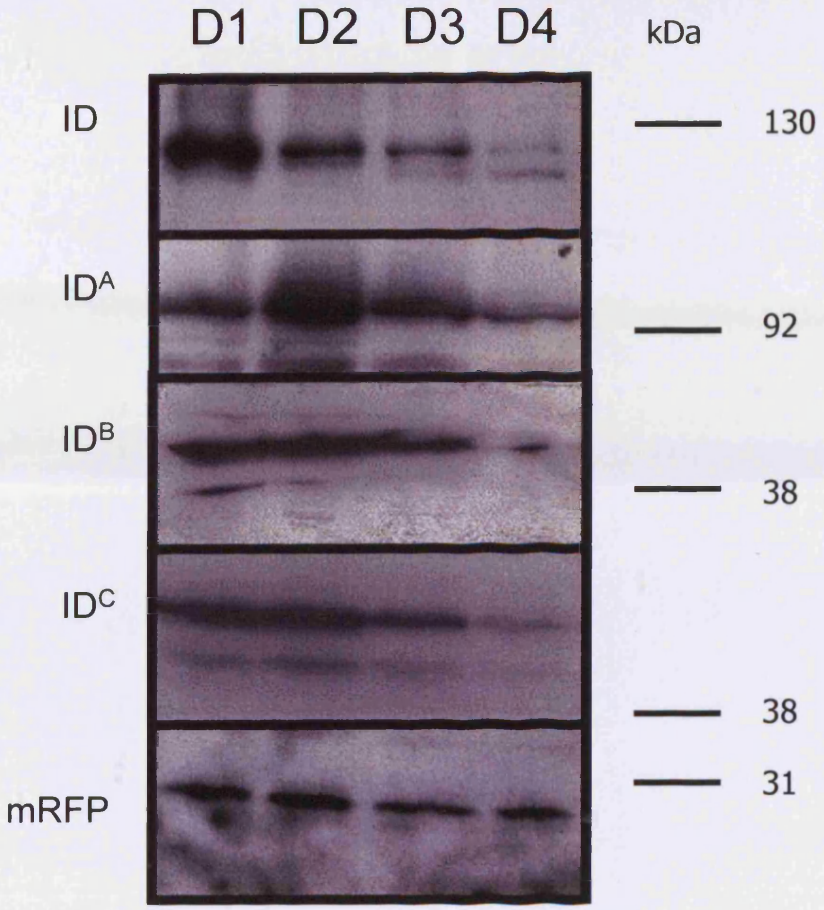

B

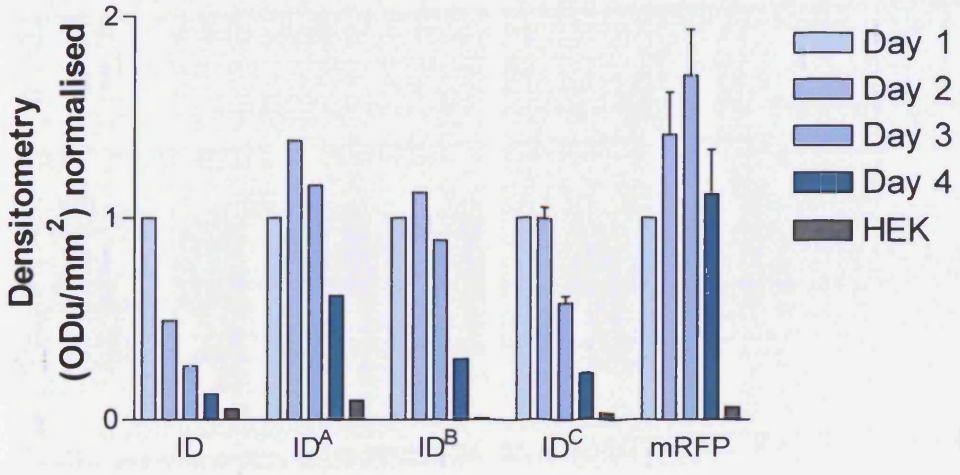

Figure 3.24. Progressive elimination of I-domain confirmed by immunoblotting of HEK cell PNS

A. Immunoblots displaying bands obtained for ID (129kDa), ID^A (99kDa), ID^B (44kDa) and ID^C (57kDa) on days 1-4 (lanes 1-4). mRFP alone is represented by a 27kDa band. Blots were based on 100µg of total protein per lane. **B.** Densitometric quantification of I-domain blots on days 1 to 4 normalised to day 1. HEK cells served as a null-I-domain control. n=1 for ID, ID^A and ID^B, n=3 for ID^C and mRFP.

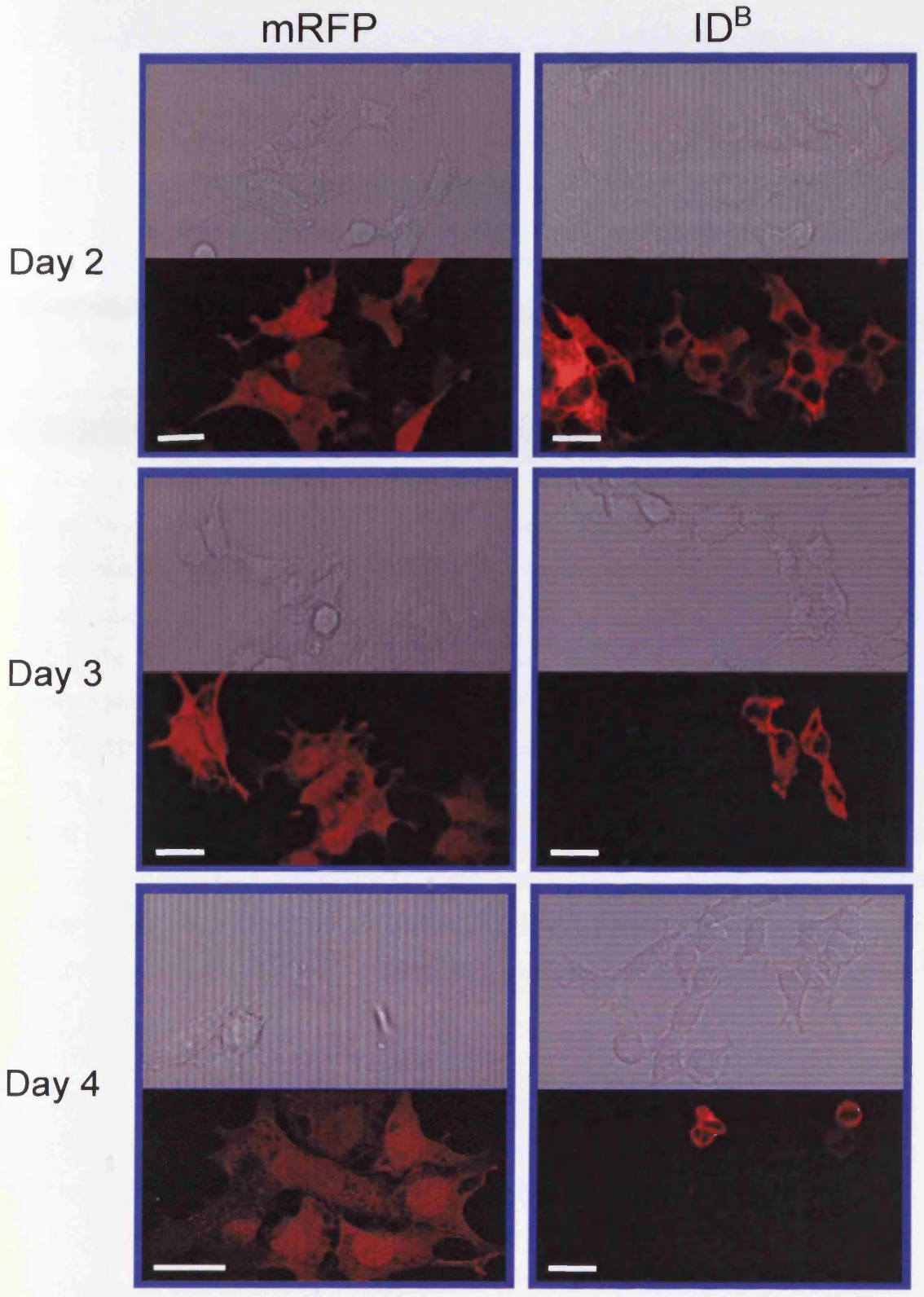

Figure 3.25. Phenotype of HEK cells expressing mRFP and ID^B via pcDNA3.1

Confocal images of mRFP and ID^B expressing cells on days 2-4. Cells transfected with mRFP display a 'healthy' phenotype after four days expression, however ID^B cells exhibit the rounded 'unhealthy' phenotype comparable to that seen with pmRFP-C1. Scale bar =25μm.

3.4. Discussion

3.4.1. Expression of recombinant I-domain subfragments exhibited unexpected cellular localisation and phenotypic alteration

I-domain expression was distinct from the homogenous cellular expression of mRFP (Figure 3.16) indicating that this subcellular localisation results from I-domain-mediated targeting. Nuclear exclusion of ID^B (44kDa) appeared not to have been a consequence of I-domain construct size since the CFP:YFP fusion protein pair (with a molecular weight of 55kDa) was homogeneously distributed throughout HL-1 cells (Figure 3.17). In addition, expression of DsRed, a large tetrameric fluorescent protein of more than 100kDa resulted in homogeneous cellular expression (Hess *et al.*, 2003). In light of these findings, it would appear that nuclear exclusion is not a function of size and most likely is a consequence of an undetermined signal in the I-domain sequence. The lattice-like distribution characterised by ID is typical of RyR expression in the ER (Bhat and Ma, 2002a; Treves et al., 2002; George et al., 2003b; Thomas et al., 2004). Similar localisations have been reported for truncated RyR2 sequences encoding residues 3722-4967 and 4485-4967, but not N-terminal residues 1-3722 and 1-4353 (George *et al.*, 2004). Considering that a.a.4499 represents the first TM in the putative TM arrangement of RyR2 (Tunwell *et al.*, 1996), this characteristic lattice-like expression pattern may be a function of membrane-spanning domains. In addition, results obtained for ID^C suggest that its aggregation, which did not occur with ID^B, implies that residues 4499-4610 may be entirely responsible for this marked clustering of recombinant protein, and could be a function of proximal membrane spanning sequences. The random aggregate formation and lack of specificity of ID^C for intracellular structures indicates a possible self-interaction within this sequence. Such self-association has also been reported in the C-terminus of the IP_3R (Galvan *et al.*, 1999; Magnino *et al.*, 2001). This concept could be explained by the inherent hydrophobicity of ID^C promoting self-association, which is prevented by interactions within full-length ID. In view of the initial objectives of this thesis, the aberrant localisation of ID^C would preclude its use as a probe to target ER membranes. Importantly, the observed membrane targeting of I-domain constructs in the absence of RyR2 suggests association with other membrane proteins. Appendix I suggests that structural and functional similarity between RyR2 and IP_3R Ca^{2+} channels may partly explain this finding.

Both ID and ID^A encompass a hydrophobic span of <50 amino acids (after TM4, at a.a.4337 (Zorzato *et al.*, 1990)) that potentially form a TM hairpin loop (Du *et al.*, 2004). This

structure has been suggested to mediate membrane association and is consistent with our data showing moderately dense localisation of both ID and ID^A in a peri-nuclear environment. A similar staining pattern of Golgi in HEK has also been shown (Triantafilou and Triantafilou, 2004), which supports the hypothesis that ID and ID^A may associate with the Golgi apparatus (Figure 3.16).

3.4.2. Reduced cell viability correlated with expression of recombinant I-domain protein

Together with cell rounding, reduced size and other characteristics described above, transient expression of I-domain sections also reduced cell viability, which was not observed with expression of mRFP (Figure 3.21). Notably, these phenotypic alterations correlated closely with the levels of recombinant I-domain proteins expressed in these cell populations. By day 4, viable cell populations were comparable to control cells (Figure 3.21), which is consistent with rapid loss of I-domain expression (Figure 3.24).

The findings of this chapter revealed a profound toxicity associated with I-domain expression. The demonstration that cell viability returned to 'normal' levels following I-domain elimination corroborated these findings.

The following chapters aim to extend the present findings and delineate the signalling mechanisms involved in these phenomena.

Chapter 4

Chapter 4 I-domain expression induces apoptosis

4.1. Introduction

Chapter 3 showed a distinct association of I-domain expression with cellular cytotoxicity. Specifically, cytotoxic I-domain expression was associated with an abnormal cell phenotype including reduced cell size and altered metabolism. Furthermore, recombinant I-domain expressing cells were rapidly eliminated by 4 days post-transfection. This chapter explores the basis of these findings by investigating the precise mode of I-domain induced cell death using complementary techniques including flow cytometry and confocal imaging.

4.1.1. Routes of cell demise

Four morphologically distinct cell death pathways have been characterised: apoptosis, apoptosis-like programmed cell death (PCD), necrosis and necrosis-like PCD (Leist and Jaattela, 2001). However, studies have also demonstrated that cells can 'switch' between, or integrate components of different cell death paradigms (Leist *et al.*, 1997; Leist *et al.*, 1999; Nicotera and Melino, 2004), underlining the plasticity of this signalling cascade.

Apoptosis (Greek for 'falling off') was initially adopted as a general term to describe PCD and can be triggered by either intrinsic or extrinsic stimuli. Intrinsic pathways are initiated by the release of cytochrome c from mitochondria (see Chapter 5), whereas extrinsic apoptosis is typically initiated by stimuli received via death receptors on the cell membrane (Figure 4.1). Apoptosis is characterised by phosphatidylserine exposure (an early indicator of apoptosis) and caspase-induced breakdown of the cytoskeleton, which causes cell shrinkage, chromatin condensation and DNA cleavage ('laddering'). Caspases are a large family of cysteine protease enzymes responsible for protein breakdown in cells undergoing apoptosis. Thirteen caspases have been identified to date that are grouped into either initiator and effector caspases (Earnshaw *et al.*, 1999) (Figure 4.1). Zeiosis or 'blebbing' of the cell membrane is a distinguishable hallmark of apoptosis that results in cell separation into

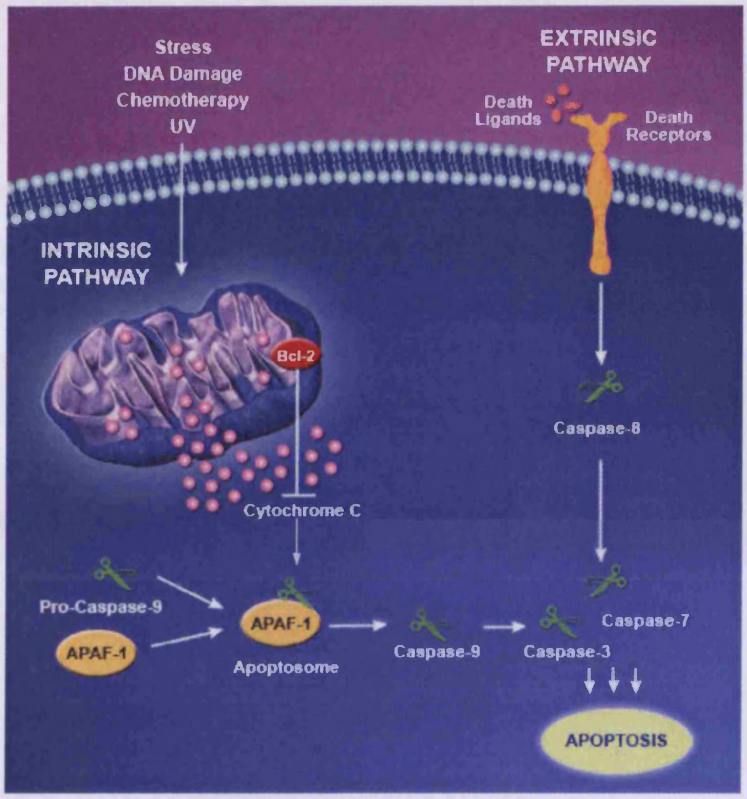

Figure 4.1. Intrinsic and extrinsic apoptosis pathways

Apoptosis can be initiated via two distinct pathways. Intrinsic pathways are mediated by cell damage that triggers the release of cytochrome c from mitochondria, which activates initiator caspases such as caspase 9 and apoptosis activating factors (APAF-1). Initiator caspases activate effector caspases such as caspase 3. The role of Bcl-2 in apoptosis will be addressed in Chapter 5. Extrinsic pathways are initiated by extracellular stimuli, which result in the activation of initiator caspase 8 that subsequently activates effector caspase 7 committing the cell to apoptosis.

Adapted from (Zaffaroni *et al.*, 2005)

several vesicles referred to as 'apoptotic bodies' (Cohen *et al.*, 1992). The translocation of phosphatidylserine from the inner to the outer leaflet of the plasma membrane permits recognition and removal of apoptotic bodies by nearby macrophages (Verhoven *et al.*, 1995). Apoptosis-like PCD exhibits characteristics similar to apoptosis, such as phosphatidylserine translocation and zeiosis, however, unlike 'typical' apoptosis: it is a caspase-independent form of cell death distinguished by incomplete chromatin condensation (Didenko *et al.*, 2002).

In contrast, cell necrosis was initially defined as 'non-programmed' cell death due to acute cellular injury or infection that triggered an inflammatory response (Trump and

Berezesky, 1992). However, necrosis can also result from disrupted cell signalling pathways by molecules such as ROS (Waring, 2005), as a consequence of mutation in apoptotic proteins (Chautan *et al.*, 1999), and even by aborted apoptosis via caspase inhibitors or anti-apoptotic proteins such as Bcl-2 (Leist *et al.*, 1997; Melino *et al.*, 1997; Leist *et al.*, 1999). This distinct necrotic cell death pathway is termed necrosis-like PCD and although it is morphologically identified by the absence of chromatin condensation and apoptotic body formation (Henriquez *et al.*, 2008), it can also exhibit characteristics consistent with apoptosis such as phosphatidylserine translocation (Brouckaert *et al.*, 2004).

4.1.2. Objective

The objective of this chapter was to determine the nature and mode of cell damage induced by I-domain expression that was reported in Chapter 3.

4.2. Methods

4.2.1. Flow cytometric quantification of mRFP-expressing cell populations

Following on from immunoblot analysis that showed a progressive loss of recombinant I-domain protein over 4 days post-transfection, flow cytometry was used to more precisely determine the loss of I-domain expressing cells. Cells (~$5x10^5$) were resuspended in 0.5ml PBS pH7.4 and sorted at a rate of 1,000 events/s, sorting up to 20,000 events using a FACSCalibur system (BD Biosciences). In addition to fluorescence measurements, flow cytometry also provides information on cell phenotype by virtue of forward scatter (FSC) and side scatter (SSC). FSC identifies changes in cell size, while SSC conveys alterations in cell granularity. A greater SSC is exhibited by apoptosing cells due to morphological changes (Pepper *et al.*, 1998; Sandstrom *et al.*, 2000). The relative fluorescence, FSC and SSC of recombinant protein expressing cells was determined on each day (1 to 4 days post-transfection). Cells expressing mRFP were also exposed to 0.01-1μM concentrations of PMA (as described in Section 4.2.3) and analysed by flow cytometry to compare cell size and granularity following PMA-induced apoptosis. Analysis was performed using WinMDI version 2.8.

4.2.2. FACS enrichment of cell populations expressing recombinant ID protein

Stable cell lines are achieved via culture and maintenance of transfected cells in the presence of a selection agent that depends on the resistance gene encoded for in the expression vector. Generation of stable cell lines often results in the survival of antibiotic resistant cells that lack recombinant protein due to 'switching off' the recombinant protein of interest expression but retaining resistance (Zhang *et al.*, 2006). Fusion of recombinant proteins with a fluorescent tag permits the identification of cell populations that express recombinant protein, and also serves to facilitate

positive cell selection using a variety of techniques. Fluorescence activated cell sorting (FACS) has proven to be a hugely successful and sensitive technique for enriching stable recombinant protein expressing populations (George *et al.*, 2003c; Zhang *et al.*, 2006).

As discussed in Section 3.2.6, G418 failed to positively select for cells expressing recombinant I-domain, but was used in this chapter to retain cell populations expressing I-domain that were subsequently to be selected via FACS. Cells expressing mRFP and mRFP-tagged ID were cultured in cDMEM supplemented with 500μg/ml G418 from 24 hours post-transfection to maintain selective pressure, then sequentially propagated to >1 x 10^7 cells/ml (~7 days) for FACS (MoFlo, Dako Cytomation). mRFP-positive cells exhibiting fluorescence greater than 10-fold above non-expressing cells were selected using a 543nm laser line. ID and mRFP expressing cell suspensions (~1x10^7) were sorted at <10,000 cells/second and collected in 2ml cDMEM in one well of a six-well plate. Media was immediately supplemented with 500μg/ml G418 after FACS and cells were returned to culture. Cellular fluorescence was observed daily on an Axiovert 2000 fluorescent microscope (see Section 2.2.7.3.2 and Figure 3.15A). ID and mRFP cells were then propagated (up to ~1x10^7) for a second sort to further enrich recombinant protein expressing cells. I-domain cells were sorted alongside cells expressing mRFP alone, which served as a positive control for selection. Data was analysed using Dako Summit (Version 4.3).

4.2.3. Analysis of mode of death in cell populations

Many kits and reagents are available for detection of various stages of apoptosis using either morphological or biochemical markers, such as DNA fragmentation, phosphatidylserine translocation and caspase activation. Despite there being many factors that promote apoptosis, DNA fragmentation is a hallmark of end-stage apoptosis. This can be readily detected *in situ* using commercially available DNA end-labelling systems, as previously demonstrated (George *et al.*, 2003b). The DeadEnd™ Fluorometric TUNEL (TdT-mediated dUTP Nick-end labelling) System (Promega) was used, that catalytically incorporates fluorescein-12-dUTP at the 3'-OH

end of fragmented DNA, utilising recombinant Terminal Deoxynucleotidyl Transferase (rTdT) since this system has been routinely used in our laboratory.

Cells expressing mRFP and I-domain constructs were seeded onto coverslip chambers following transfection at days 1-4. Cells were fixed in 4% (v/v) paraformaldehyde and rehydrated in PBS pH7.4 (see Section 2.2.7.3.1), and permeabilised in 0.1% (v/v) Triton-X100 in PBS for 30 minutes at RT. Following permeabilisation, cells were washed twice in PBS for 5 minutes and then incubated with 100µl equilibration buffer for 10 minutes. After equilibration, 50µl rTdT buffer was added (consisting of equilibration buffer, 45µl; nucleotide mix, 5µl and rTdT enzyme, 1µl), then were covered with the provided plastic coverslips to prevent drying out and incubated for one hour at 37°C. A 20x SSC salt solution (see Section 2.1.3.1) was diluted to 2x and applied to cells for 15 minutes at RT to terminate the reaction. Cells were washed three times in PBS for 5 minutes to remove unincorporated fluorescein-12-dUTP, mounted with FluoSave™ as previously described and stored at 4°C for up to a week prior to imaging. Additional cells were also treated with 100µg/ml DNase I for 30 minutes as a positive control for DNA fragmentation, prior to proceeding with the TUNEL system.

Green-channel images (TUNEL/fluorescein) were laid over red-channel images (mRFP-tagged recombinant protein) and the degree of transparency was adjusted to 60% green: 40% red using Adobe Photoshop software. The TUNEL system is not quantitative and therefore does not enable the comparison of the extent of apoptosis in different cells within or between each field of view.

4.2.3.1. Control for Ca^{2+}-linked apoptosis

Phorbol 12-myristate 13-acetate (PMA) activates protein kinase C (PKC), a Ca^{2+} dependent protein kinase family of intracellular mediators (Park *et al.*, 2001; Kim *et al.*, 2003; Zong *et al.*, 2004) involved in cell growth, differentiation and apoptosis (Basu and Miura, 2002). PMA induces the translocation of various PKC isoforms to the cell membrane (Chen *et al.*, 1995a; Lin and Chen, 1998), which triggers apoptosis

via isoform-specific mechanisms (Mandil *et al.*, 2001; Gutcher *et al.*, 2003). PMA enabled the assessment of the extent of apoptosis that resulted from Ca^{2+} associated pathways. PMA concentrations of 0.01 - 1 μM have previously been implemented to induce apoptosis in HEK cells (Kim *et al.*, 2003; Zong *et al.*, 2004). Cells expressing mRFP were incubated with 0, 0.01, 0.1 and 1 μM PMA in unsupplemented DMEM (as serum interferes with PMA associated pathways) for 1.5 hours, equilibrated in cDMEM for 4 hours then fixed, rehydrated and processed for the DeadEnd™ TUNEL system as described above.

4.3. Results

4.3.1. Flow cytometry reveals a potential link between I-domain expression and apoptosis

The loss of recombinant I-domain expression over 4 days post-transfection was previously shown by immunoblotting analysis (Figure 3.24). Here flow cytometry was employed to quantitate the reduction in protein expression using mRFP fluorescence at the cellular level. Cells expressing both recombinant I-domain and mRFP were subjected to flow cytometry 1-4 days following transfection. Flow cytometric fluorescent counts for all I-domain constructs were normalised to mRFP day 1. The percentage of cells expressing mRFP alone was significantly greater than all I-domain expressing cells both 3 and 4 days post-transfection ($p<0.05$). In addition, flow cytometric analysis of I-domain expressing cells also reflected morphological changes induced by I-domain expression. Figure 4.2A regions i and ii denote untransfected cells (fluorescence below an arbitrary threshold of 150 fluorescent units) and recombinant protein expressing cells (fluorescence above this arbitrary threshold) respectively, in the same cell suspension. Importantly, the analysis of these separate populations revealed that both I-domain expressing and non-expressing cells exhibited a greater SSC than did populations of mRFP cells. Note the striking positive relationship between ID^B fluorescence and magnitude of SSC when compared to that obtained with mRFP (Figure 4.2A). Figure 4.2Bi and ii clearly display that both transfected I-domain populations and cells with a low fluorescence (i.e. cells with low or non-detectable expression of the same recombinant protein) have a significantly increased granularity on both 1 and 2 days post transfection compared to mRFP transfected cells. *Figure 4.2 thus provides compelling evidence that I-domain-induced cellular damage was not only restricted to cells expressing recombinant protein, but also adversely affected untransfected cells within the same cell populations.*

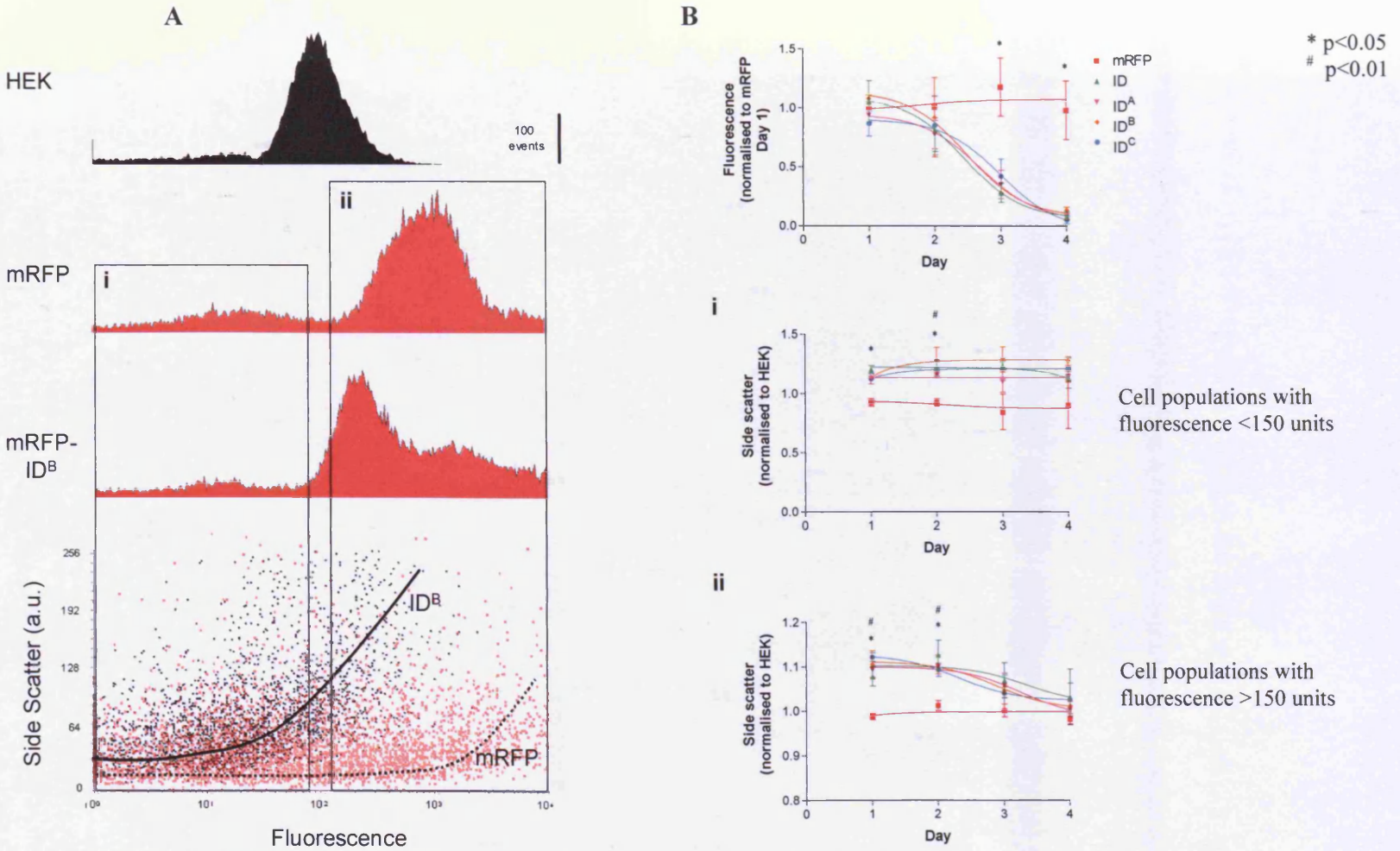

Figure 4.2. Flow cytometric quantification and phenotypic analysis during I-domain elimination

A. Flow cytometric histograms represent data from day 2 HEK, mRFP and ID^B expressing populations, and clearly display that mRFP and ID^B exhibit greater fluorescence than HEK (region ii). SSC for both mRFP and ID^B populations is depicted in the lower panel, aligned against relative fluorescence, displaying a higher SSC of ID^B cells than mRFP cells, within both non-fluorescent (i) and fluorescent (ii) cell populations. **B.** Upper right panel displays flow cytometric selection of mRFP expressing cell populations over a 4 day period following transfection. The SSC of the non-fluorescent cell population is displayed in the middle panel corresponding to cells typical of population (i) in panel A, and SSC of cells exhibiting greater than threshold fluorescence (>150 fluorescent units) is shown in the bottom panel (ii). Day 1 *$p<0.05$ for ID and ID^B, #$p<0.01$ for ID^A and ID^C; day 2 *$p<0.05$ for ID, ID^B and ID^C, #$p<0.01$ ID^A; day 3 and 4 $p>0.05$. A similar trend was also observed in NUCs compared to mRFP NUCs: day 1 *$p<0.05$ for ID, ID^A, ID^B and ID^C; day 2 *$p<0.05$ for ID, ID^A and ID^B, #$p<0.01$ ID^C. n=2, error bars represent mean± SD.

4.3.2. Fluorescence activated cell sorting (FACS) failed to enrich recombinant I-domain expression

Following transient expression of I-domain constructs (Chapter 3), the selection of cells positively expressing recombinant protein was required in order to more fully assess the relationship between recombinant I-domain expression and cellular phenotype/cytotoxicity. Our strategy aimed to generate stable I-domain expressing cells in order to assess the more chronic effect of I-domain expression. G418 was used to maintain plasmid selection and FACS was employed to positively select ID expressing cells (detailed in Section 3.2.6). Although immunoblotting experiments had revealed a dramatic loss of recombinant I-domain protein by day 4 (Figure 3.24), protein levels were not completely eliminated. In our approach, the focus was on enriching isolated cell populations that maintained expression of detectable levels of recombinant ID protein. Only the full-length ID construct was used in these experiments to provide an insight into whether this was a viable approach. FACS successfully enriched mRFP-positive cell populations that were able to maintain high levels of protein expression (Figure 4.3A and B). In contrast, and despite selecting around 30,000 expressing cells (Figure 4.3C), bona fide I-domain expressing cells could not be maintained, and consequently a progressive loss in ID expressing cells over time was determined (Figure 4.3C and D). Time between sorts was shorter for ID cells than mRFP cells (8 and 10 days respectively) due to the time required to obtain sufficient cells to sort and as a consequence of the rapid loss of ID. In addition, as discussed in Section 4.2.1, FACS also has a robust utility in investigating alterations in cell phenotype that accompanied changes in I-domain expression using FSC which represents cell size, and SSC which represents cell granularity. Figures 4.3 and 4.4 show the loss of mRFP fluorescence in ID populations between the first and second sort correlated with a decrease in cell size and granularity. Despite an increase in cell granularity observed in mRFP cells between first and second sorts, cells did not display a toxic phenotype (Figure 3.20). It is also important to note that after the first sort, ID transfected cells displayed greater granularity (Figure 4.3C) than mRFP cells implying more cell damage. Interestingly, despite few cells retaining ID expression at both first and second sorts (33440 and 657 respectively), a high number of ID transfected cells exhibited a SSC of >100 (68601 and 6914 respectively). In contrast,

a SSC of >100 was displayed by fewer mRFP transfected cells (Figure 4.3A) compared to those retaining expression of recombinant mRFP protein (Figures 4.3B). FSC and SSC of ID transfected cells displayed a marked reduction between first and second sorts, which is the inverse observed with mRFP transfected cells. The reduced FSC and SSC following the second sort of ID, not observed with mRFP (Figures 4.3 and 4.4), was fully consistent with ID elimination (Figures 3.20 and 3.24).

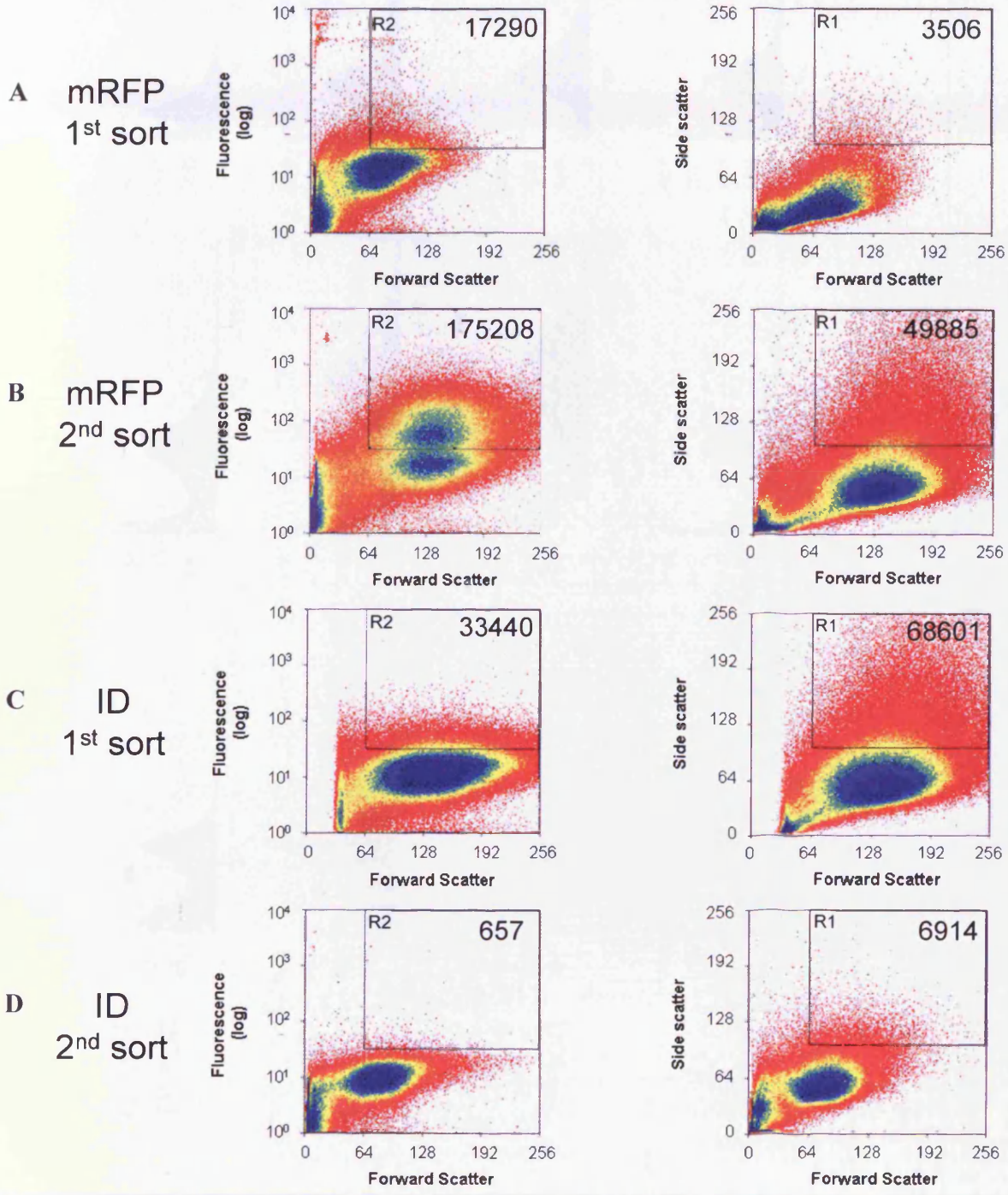

Figure 4.3. FACS enrichment of ID and mRFP-positive cell populations

mRFP expressing HEK cells and mRFP-tagged ID were selected by mRFP fluorescence (high angle scatter). FSC and SSC provide information on cell size and granularity respectively. R2 gate defines cell populations exhibiting >30 fluorescence units and a FSC of >64 arbitrary units. R1 gate defines cell populations characterised by SSC >100 and FSC >64, and indicates total number of cells within gate. Only ID and mRFP were assessed in this manner.

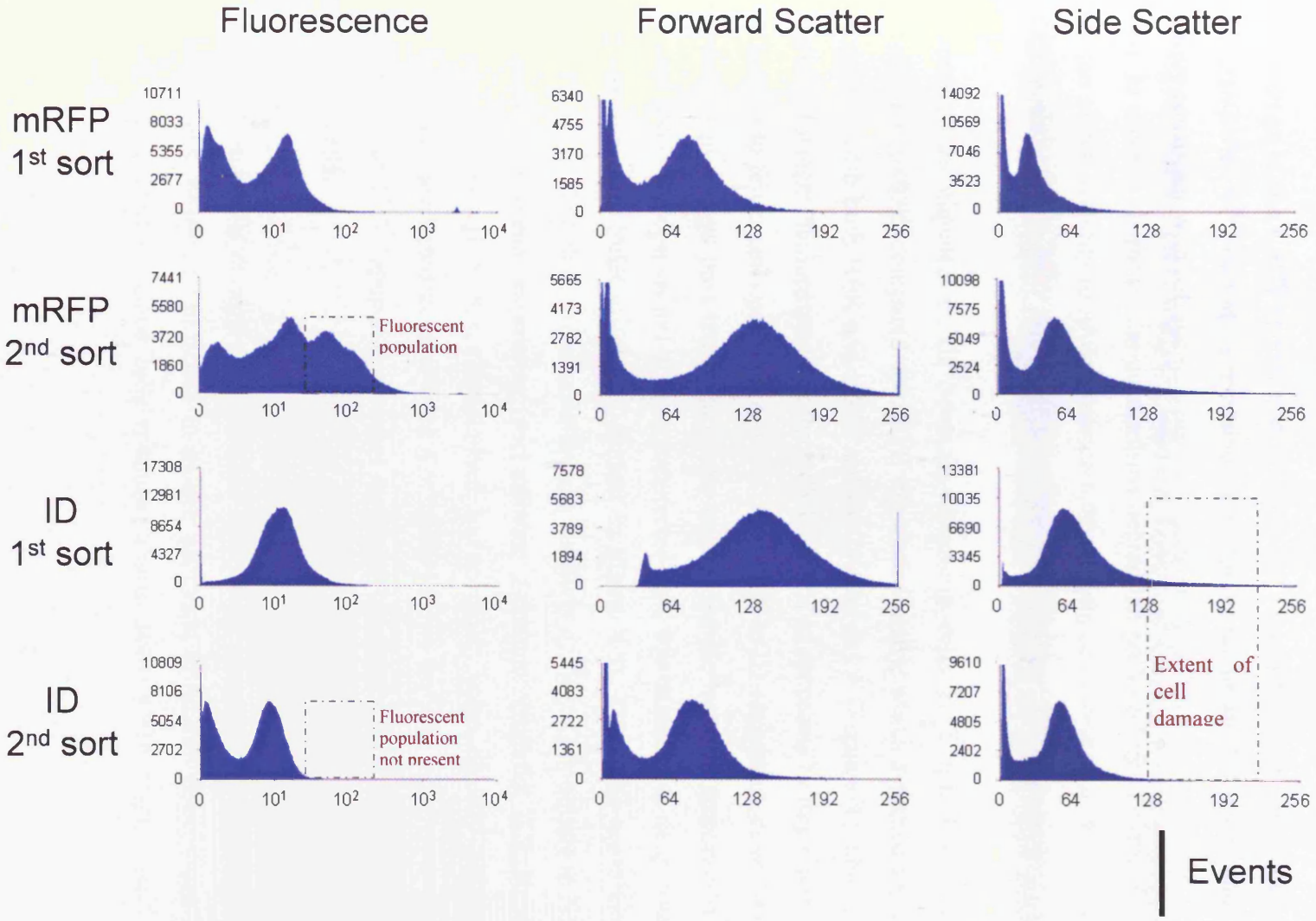

Figure 4.4. FACS histograms of mRFP-expressing cell populations

Data from Figure 4.3 plotted against total counts (y-axis) in histogram format. Fluorescence histograms clearly display an enrichment of mRFP cells between the first (day 13) and second sort (+ 18 days), whereas a loss of fluorescence is observed in ID cells between first and second sorts (day 8 and + 10 days respectively). Only ID and mRFP were assessed in this manner.

4.3.3. I-domain expression induced apoptotic cell death

The findings of the FACS experiments (Figures 4.2 to 4.4) demonstrate an increased cell granularity of I-domain expressing cells compared to mRFP cells, which is entirely consistent with cell damage observed previously (Figures 3.19, 3.20, 3.21 and 3.25). In order to delineate the mechanisms behind the profound phenotypic changes and loss of cell viability following I-domain expression, cells were analysed for levels of apoptosis.

Apoptosis was elevated in all I-domain-expressing cells at 2 and 3 days post-transfection ($p<0.05$ compared to mRFP transfected cells), which returned to levels comparable with both HEK and mRFP cells (~2%) by day 6 (Figures 4.5 and 4.7A). Brightfield images demonstrate that the reduced levels of apoptosis by day 6 were not attributable to fewer cells per field of view. Apoptosis in ID expressing cells was not determined at 6 days post transfection due to low sample number. Importantly the elevated level of apoptosis in I-domain transfected cells was extended to neighbouring untransfected cells (NUCs) (clearly evident in Figure 4.5). This fully corroborated flow cytometric data that also demonstrated a similarly damaged phenotype in NUCs as observed in cells expressing recombinant I-domain (Figures 4.2 to 4.4). Furthermore, not all NUCs characterised by apoptosis were directly physically coupled with transfected cells (Figure 4.5, white arrows in 'merged' day 2 panel), suggesting that NUC apoptosis was not mediated by direct contact with I-domain expressing cells.

Figures 4.6 and 4.7B display a proportional increase in apoptosis with higher PMA concentrations, however this failed to induce apoptosis in all cell populations (see Section 4.4.1). DNase treated cells exhibited almost 100% DNA fragmentation as expected.

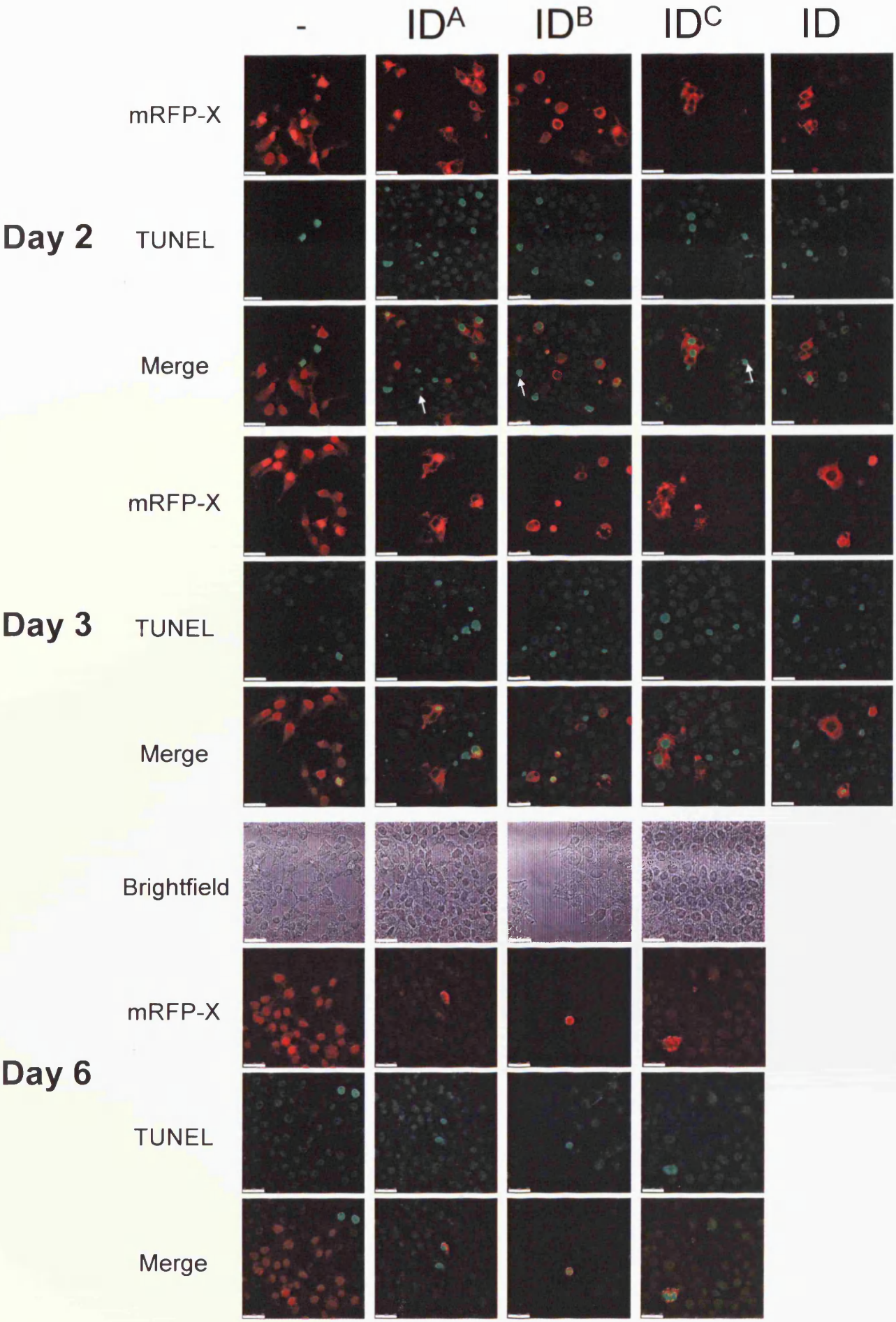

Figure 4.5. I-domain expression was associated with an increase in apoptosis

A. Confocal images of brightfield, mRFP channel, TUNEL displaying degree of apoptosis and TUNEL-mRFP channel merge. White arrows in the merged panel of day 2 indicate apoptotic NUCs that are not coupled to a transfected cell. Scale bar =25μm.

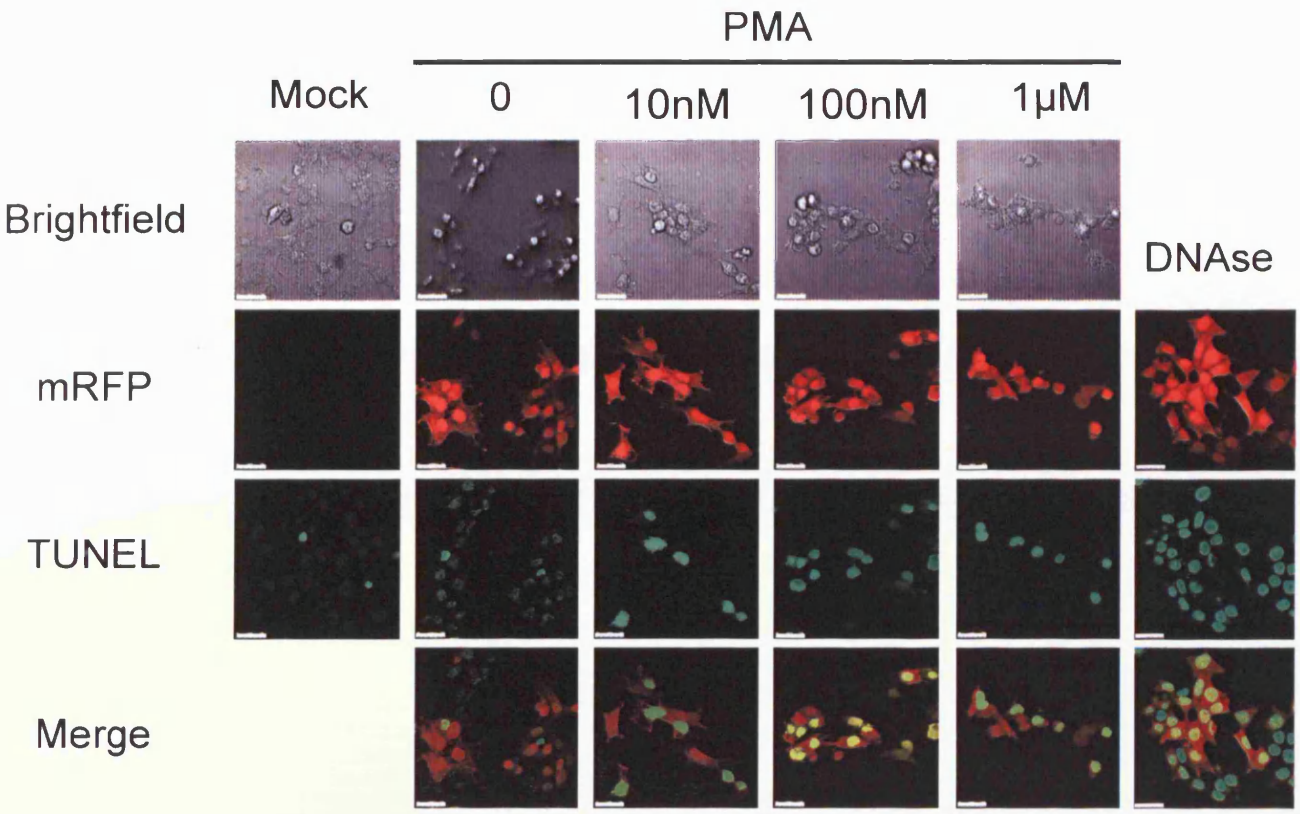

Figure 4.6. PMA-induced apoptosis in HEK cells

Confocal images displaying apoptosis in mRFP-expressing cells induced by Ca^{2+}-linked mechanisms (PMA) or physical DNA damage (fragmentation using DNase I). Images displayed for each construct are brightfield, red channel (mRFP fluorescence) and green channel (TUNEL/fluorescein). Lower panels display 'merge' of green and red channels. Scale bar =25μm.

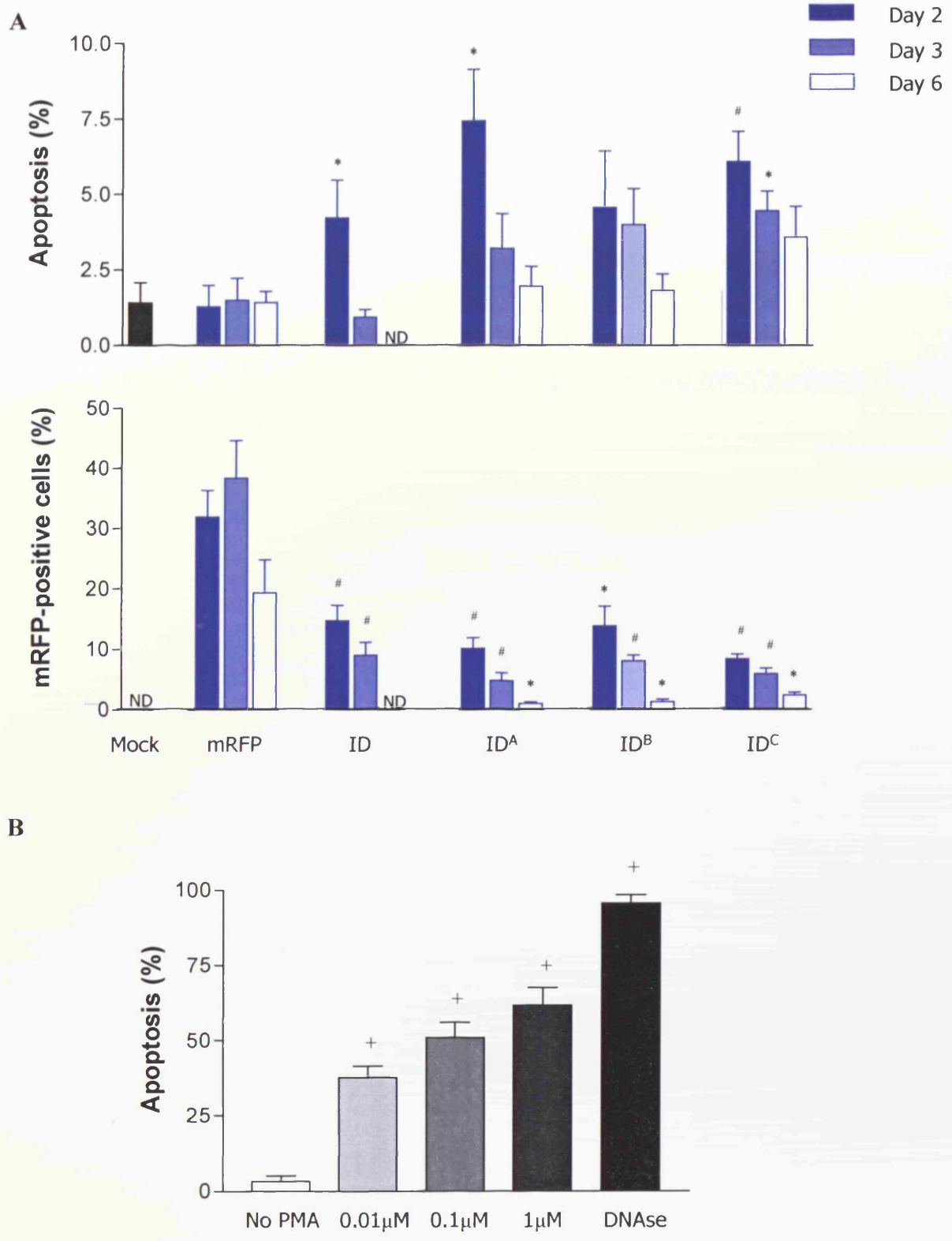

Figure 4.7. I-domain expression induces apoptosis

A. The extent of apoptosis in mRFP and I-domain transfected HEK cells (upper panel) and the corresponding percentage of mRFP-positive cell populations (lower panel), *$p<0.05$ and $^{\#}p<0.01$ when compared to mRFP expressing cells. Mock refers to transfection without DNA. **B.** Extent of apoptosis in mRFP expressing cells exposed to PMA (0.01-1μM) or DNase treated cells, $^{+}p<0.001$ compared to mRFP cells not exposed to PMA. ND = not determined.

4.4. Discussion

4.4.1. Constitutive cellular I-domain expression triggers apoptosis

This chapter describes attempts to generate stable expression of I-domain constructs, however it failed to produce any viable expressing cells. Stable high-level expression of RyR2 in CHO cells has previously been shown to be cytotoxic, which was avoided by selection of discrete clonally-derived cells expressing lower levels of recombinant protein (George *et al.*, 2003c). However, selection of low-level I-domain expression was not achieved because FACS followed by subsequent culture did not enrich ID-expressing populations (Figures 4.3 and 4.4). Using an inducible stable expression system may overcome these problems but was not suitable for this study since it was only intended to provide an insight into chronic constitutive I-domain expression. FACS data in Figure 4.2 demonstrated that loss of I-domain correlated with fewer damaged cells, which suggests that cellular survival is linked to the elimination of I-domain populations. This is also entirely consistent with the findings in Chapter 3, whereby viable cell populations were comparable to control cells by 4 days post-transfection (Figure 3.21) after the majority of recombinant I-domain expressing cells were eliminated. Interestingly, another study conducted in HEK cells whereby transfection of HtrA2 (serine protease) induced apoptotic morphological changes that included cells shrinkage and rounding (Suzuki *et al.*, 2001). These findings are fully consistent with the changes observed in this and the previous chapter (Figures 3.21 and 4.5).

The extent of apoptosis (Figures 4.5 and 4.7A) and reduced cell viability (Figure 3.21) following I-domain transfection were comparable. However, in view that cell viability using Trypan blue does not discriminate between necrosis and apoptosis, it would appear that I-domain cytotoxicity was predominantly via apoptosis rather than necrosis. Nevertheless, necrosis probably contributes to the overall extent of cytotoxicity measured in this thesis. As discussed in Section 4.2.3.1, PMA was used to induce Ca^{2+}-dependent apoptosis in view of the central role of RyR2 in Ca^{2+} signalling and the possibility that I-domain induces apoptosis via Ca^{2+} dependent mechanisms (to be addressed in Chapter 5). Previously it was shown that a 30 minute incubation with 0.01μM PMA was sufficient to drive ANX-1 nuclear translocation (Kim *et al.*, 2003). However, the group only measured this characteristic marker of apoptosis, and did not assess whether apoptosis was fully evoked. With reference to findings of this chapter (Figures 4.6 and 4.7B), a 1.5 hour incubation with 0.01μM PMA and 4 hours equilibration in complete media resulted in DNA fragmentation in ~40% of cells

(Figure 4.7B). Therefore it is likely that the time frame of these present experiments may have only been sufficient for 40% apoptosis and accordingly, a longer time duration may be required to observe 100% programmed cell death.

It should also be noted that a large number of mRFP cells displayed a greater FSC and SSC following second FACS (Figures 4.3 and 4.4), which suggests that prolonged expression of mRFP is not completely benign and does alter cell phenotype. However, transient expression of mRFP is largely compatible with cell viability (Figures 3.21, 4.5 and 4.7A) therefore these changes associated with chronic mRFP expression did not present any limitations in the context of these experiments.

4.4.2. I-domain associated abnormal phenotype was extended to neighbouring untransfected cells (NUCs)

Analysis of cell granularity using flow cytometry indicated a greater proportion of damaged cells following I-domain expression (Figure 4.2), which was consistent with findings from apoptosis experiments (Figure 4.5 and 4.7A). In addition, these studies also revealed an intriguing finding that I-domain expression not only compromised cell phenotype in transfected cells, but also was detrimental to NUCs irrespective of contact with a transfected cell (Figures 4.2 and 4.4). This fascinating finding provided the first glimpse that cellular cross-talk may be triggered by I-domain expression, and that abnormal signalling in a transfected cell could in some way be transmitted to its neighbours. Chapter 7 addresses these issues in more detail.

The profound toxicity and rapid elimination of recombinant I-domain constructs prompted further investigation into the underlying mechanisms of I-domain induced cell demise, which is the focus of the next chapter.

Chapter 5

Chapter 5 Investigating the effects of I-domain expression on Ca^{2+} release channels in HEK cells

5.1. Introduction

As previously discussed, Ca^{2+} plays an essential role in normal cellular homeostasis and signalling. However, the complex interplay of Ca^{2+} signalling components is also a critical determinant in the progression and mode of cell death (Trump and Berezesky, 1992, 1996; Pan *et al.*, 2000). In view of the findings of Chapters 3 and 4, particularly that expression of recombinant I-domain was associated with lower cell viability and increased levels of apoptosis, it was important to elucidate the mechanistic basis of altered viability and metabolism in cells expressing I-domain fragments. The intimate association of Ca^{2+} signalling and cell death pathways is highly documented but is particularly centred on the involvement of IP_3R (Gutstein and Marks, 1997; Szalai *et al.*, 1999). This is particularly relevant to this thesis considering that HEK cells only express IP_3R Ca^{2+} release channels, and not RyR. Given that this data presented here is consistent with Ca^{2+}-linked apoptosis in I-domain expressing cells, and a possible role for cellular cross-talk with neighbouring cells, it was hypothesised that perturbed cellular Ca^{2+} cycling may underlie I-domain-linked cell death. This chapter aims to specifically determine the involvement of Ca^{2+} signalling pathways, and their perturbation in I-domain cytotoxicity.

5.1.1. Ca^{2+} dependent cell death pathways

Perturbations in intracellular Ca^{2+} have been intimately linked with cell damage (Hajnoczky *et al.*, 2000; Pan *et al.*, 2000; Schwab *et al.*, 2002; Orrenius *et al.*, 2003; Lim *et al.*, 2008). Depletion of ER Ca^{2+} stores and increased cytoplasmic Ca^{2+} flux in CHO cells expressing recombinant RyR increased apoptosis (Pan *et al.*, 2000; George *et al.*, 2003b). Likewise, sustained high intracellular Ca^{2+} concentrations in thymocytes and hepatoma cells initiated events that also induced apoptosis (Tsukamoto and Kaneko, 1993; Jiang *et al.*, 1994). NCX and PMCA ion pumps in

cardiomyocytes and PC12 cells have been demonstrated to rapidly remove high intracellular Ca^{2+} into the extracellular environment, thus restoring lower resting Ca^{2+} concentrations (Garcia *et al.*, 2001; Miyamoto *et al.*, 2005). However, caspases have been shown to cleave both ion pumps during apoptosis, which results in the toxic accumulation of intracellular Ca^{2+} (Paszty *et al.*, 2002; Schwab *et al.*, 2002; Bano *et al.*, 2007; Paszty *et al.*, 2007). Similarly, cardiac myocytes from embryonic mice devoid of NCX1 displayed altered Ca^{2+} handling and apoptosis (Wakimoto *et al.*, 2000). In addition, perturbed Ca^{2+} homeostasis as a result of ion channel cleavage was found to induce necrotic cell death (Schwab *et al.*, 2002). The fine balance between apoptosis and necrosis has been proposed to be dependent on levels of ATP (Leist *et al.*, 1997; Leist *et al.*, 1999), which places mitochondria and cell metabolic pathways central to the execution of cell death programmes.

Apoptosis can also arise through an imbalance in cellular protein expression, particularly components of the Ca^{2+} signalling machinery (referred to as the Ca^{2+} signalosome). For example, Bobe and colleagues demonstrated that both increased and reduced ER load, attributable to overexpression of various SERCA isoforms, triggered ER stress and induced apoptosis (Bobe *et al.*, 2004; Chaabane *et al.*, 2006). Similarly calreticulin overexpression increased intracellular Ca^{2+}, which was associated with reduced and elevated activity of the anti- and pro-apoptotic proteins Bcl-2 and Bax respectively (Lim *et al.*, 2008). In addition, low-level expression of Bcl-2 protects against apoptosis, whereas high-level expression spontaneously induced apoptosis in a Ca^{2+}- and redox-dependent manner (Hanson *et al.*, 2008a).

5.1.2. The role of IP_3R in apoptosis

IP_3Rs are central to the progression of apoptosis (Boehning *et al.*, 2003; Wang and El-Deiry, 2004; Boehning *et al.*, 2005; Mendes *et al.*, 2005). Sugawara and colleagues were the first to report that IP_3R-deficient chicken DT40 B-lymphocytes were resistant to apoptosis (Sugawara *et al.*, 1997), and manoeuvres intended to promote apoptosis in these cells failed to activate caspases 3 and 9 (Tantral *et al.*, 2004). These findings suggest that IP_3R are intimately involved in caspase-dependent apoptosis

(See Figures 4.1 and 5.1). All IP_3R isoforms have been reported to preferentially transmit Ca^{2+} signals into mitochondria (Mendes *et al.*, 2005) inducing mitochondrial Ca^{2+} overload and cytochrome C release (Boehning *et al.*, 2003) that triggers apoptosis (Boehning *et al.*, 2003; Mendes *et al.*, 2005). In addition, depletion of ER Ca^{2+} induces influx via the plasma membrane Ca^{2+} channels, including store-operated channels (SOC) or Ca^{2+}-release activated current (I_{crac}), due to an association between these channels and IP_3R on the ER (Kiselyov *et al.*, 1998). This association could further elevate $[Ca^{2+}]_i$ promoting the progression of apoptosis.

IP_3R expression is reported to be upregulated in HF and there is an association between increased apoptosis and pathological severity (Gutstein and Marks, 1997). Similarly, IP_3R have also been linked to the onset of arrhythmia (Mackenzie *et al.*, 2002; Proven *et al.*, 2006). Due to the abundance of endogenous RyR2 in cardiomyocytes in comparison to IP_3R, these cardiopathological roles of IP_3R are likely to be influenced by intracellular cross-talk with RyR2 (White and McGeown, 2002; George *et al.*, 2003b).

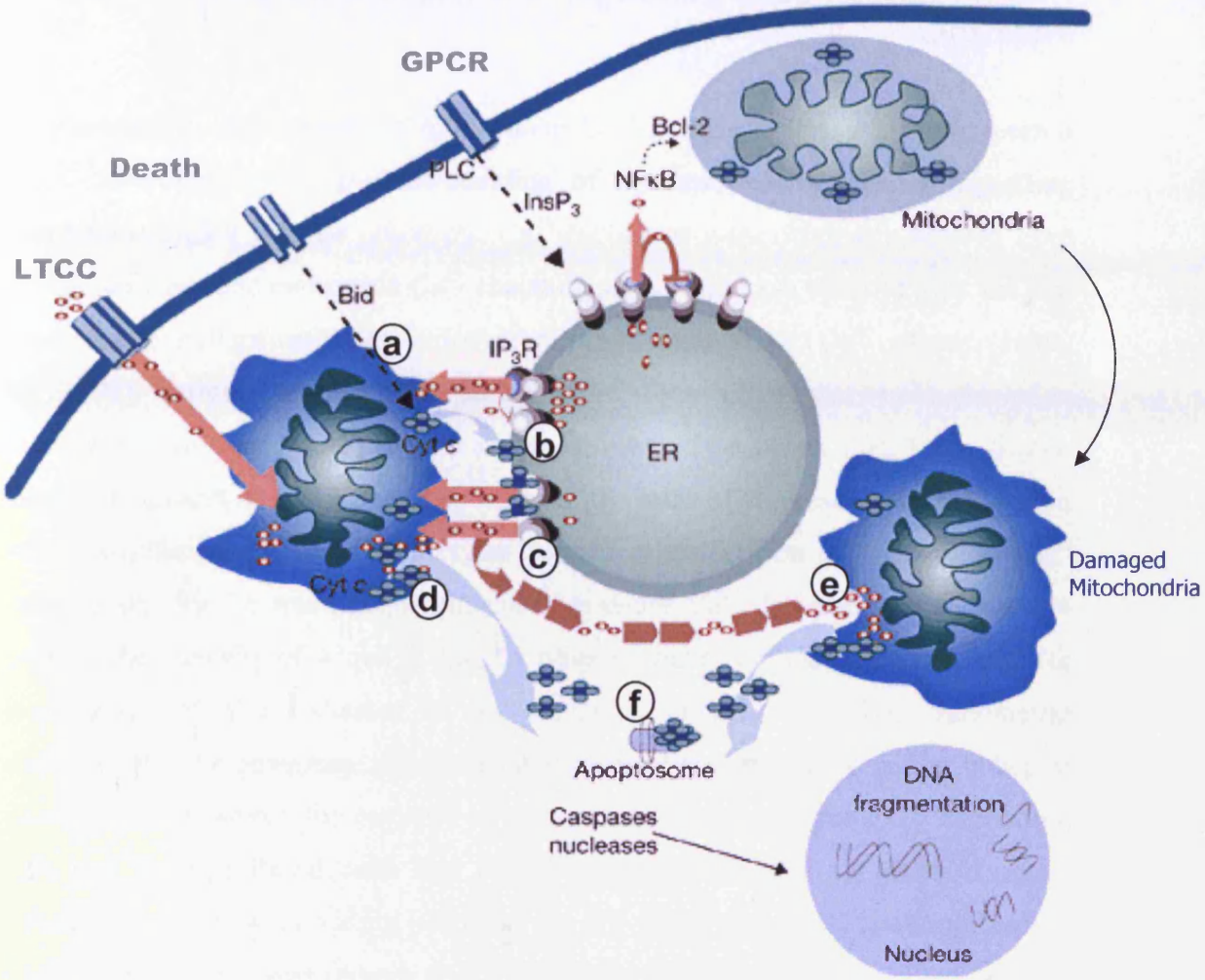

Figure 5.1. Ca^{2+}-associated apoptosis pathways

Schematic representation of the intimate association between Ca^{2+} signalling and the initiation of apoptosis. Activation of plasma membrane Ca^{2+} channels (such as LTCC) or G-protein coupled receptors (GPCR) induce IP_3R Ca^{2+} release, which can elevate mitochondrial Ca^{2+} and initiate Ca^{2+}-induced apoptosis cascades. High mitochondrial Ca^{2+} alters its membrane permeability, which triggers cytochrome C release **(a)** that binds to IP_3R **(b)**, enhancing IP_3R Ca^{2+} release **(c)**. Subsequently a global rise in cytosolic Ca^{2+} levels **(d)** triggers high mitochondrial Ca^{2+} concentrations that cause global cytochrome C release from mitochondria **(e)**, i.e. a feed-forward mechanism. Cytosolic cytochrome C induces apoptosome formation, promoting late-stage apoptosis via caspase 9 activation **(f)** and finalising the apoptosis cascade by DNA cleavage. In addition, the pro-apoptotic protein Bid can be activated via so-called death receptors (cell surface receptors such as tumour-necrosis factor receptor), which induce ROS formation by specific targeting of mitochondria, thus promoting cell death (Ding *et al.*, 2004). Furthermore IP_3R also have a role in promoting cell survival via activation of proteins such as the transcription factor NF-kappa B and anti-apoptosis protein Bcl-2.

Adapted from Mattson and Chan, 2003

5.1.3. Monitoring intracellular Ca^{2+} signalling using fluorescent Ca^{2+} indicators

The quantitative measurement of intracellular Ca^{2+} cycling in living cells has been a pivotal development in the understanding of dynamic spatiotemporal signalling underlying complex cellular processes. Ca^{2+} indicators were originally derived from BAPTA (a membrane permeable Ca^{2+} chelating agent) and have evolved over the past 30 years into indispensable tools for monitoring intracellular Ca^{2+} events (Tsien, 1980, 1992). Various Ca^{2+} indicators are commercially available and can be classed as either ratiometric, such as Fura-2 or single-wavelength, such as fluo-3 and fluo-4. Ratiometric indicators can be used to measure the ratio of fluorescent signals at two distinct wavelengths, which enables the precise quantification of changes in Ca^{2+} concentration. Single wavelength indicators measure Ca^{2+} fluorescence at a single emission, the intensity of which is directly proportional to both ambient Ca^{2+} and the concentration of the indicator at sub-saturating levels. Therefore, ratiometric indicators offer the advantage of eliminating artefacts that may arise due to indicator concentration. However, the majority of ratiometric indicators require UV excitation, which can damage living cells and increase autofluorescence. In addition, many confocal microscopes (including our own) are not fitted with a UV laser, precluding the use of ratiometric dyes (Niggli *et al.*, 1994; Novak and Rabinovitch, 1994; Sako *et al.*, 1997). Single wavelength indicators, such as fluo-3 and fluo-4, are preferred due to their non-destructive and effective implementation in live cell confocal microscopy studies using an argon laser (Gee *et al.*, 2000). Following cellular incorporation of the non–fluorescent acetoxymethyl (AM) conjugated form of the dye via facilitated passive uptake of the dye, the free (fluorescent) indicator is released into the cytoplasm by the hydrolysing action of endogenous esterases. In addition, removal of acetoxymethyl ester groups restores the hydrophobic properties of the dye, thus preventing leakage from the cell (Gee *et al.*, 2000). Fluo-4 was synthesised from fluo-3 by the direct substitution of two fluorine molecules for two chlorines, which shifted the excitation maxima to the left (from 506nm to 494nm). This alteration improved fluorescence emission using an argon laser (488nm) (Mattson and Chan, 2003), providing a more intense fluorescence signal at equivalent dye and Ca^{2+} concentration. The left shift in emission maximum (526nm to 516nm) also permits a

lower incidence of spectral overlap when used in combination with dyes that emit in the red spectrum (e.g. mRFP). Fluo-4 also has a higher affinity for Ca^{2+} than fluo-3 (Kd of 345nM compared to 390nM) and a greater dynamic range (Gee *et al.*, 2000).

5.1.4. Objective

In light of the crucial role of perturbed Ca^{2+} cycling via IP_3R in triggering apoptosis, this chapter investigates whether I-domain constructs pathologically alter cellular IP_3R-dependent Ca^{2+} handling in HEK cells that ultimately leads to their demise.

5.2. Methods

5.2.1. Cellular Ca^{2+} imaging using fluo-4 and CLSM

Intracellular Ca^{2+} measurements were performed on both fluo-4 loaded resting (non-stimulated) and agonist-induced cells using an SP5 confocal microscope. Cells were loaded under a 100µl meniscus of fluo-4 (5µM in 20% w/v pluronic acid F-12) in unsupplemented DMEM and incubated at 37°C for 60 minutes. Coverslip chambers were flooded with 2ml unsupplemented DMEM and further incubated at 37°C for 10 minutes (to allow for additional fluo-4 de-esterification) prior to imaging.

5.2.2. Analysis of agonist-induced Ca^{2+} transients

Agonist-activation of Ca^{2+} dependent pathways has revealed Ca^{2+} handling dysfunction, such as via stimulation of mutant RyR2 using caffeine (Thomas *et al.*, 2005), and activation of pathways that trigger IP_3-induced Ca^{2+} release by carbachol (Luo *et al.*, 2001; Futatsugi *et al.*, 2005). Carbachol (carbamylcholine, Figure 5.2) is a stable analogue of acetylcholine (Nathanson *et al.*, 1978; Fedorov and Cherkasova, 1997) that stimulates endogenous cell surface acetylcholine muscarinic G-protein coupled receptors (GPCR), resulting in a cascade of events that raises intracellular levels of IP_3 (Figure 5.2). Carbachol is widely implemented in Ca^{2+} imaging experiments (Conklin *et al.*, 1992; Honda *et al.*, 1994; Schachter *et al.*, 1997; Tojyo *et al.*, 1997; Mundell and Benovic, 2000; MacMillan *et al.*, 2005).

Basal fluorescent signals were recorded for 60s (300 frames) prior to the addition of carbachol (1µM-1mM dissolved in unsupplemented DMEM). To avoid confounding issues of cellular responses to successive carbachol additions, each dose was administered to cell populations on separate coverslips (n>5 coverslips). Figure 5.3 displays a typical field of view of WT HEK cells in the right panel, before (A) and after (B) carbachol (1mM) addition. Coloured halos represent selected cellular regions of interest (~30µm), data from which was used to generate the transient response graphs in the left panel. Note the heterogeneity of the carbachol-induced response in HEK cells (Figure 5.3), which was observed at all carbachol doses.

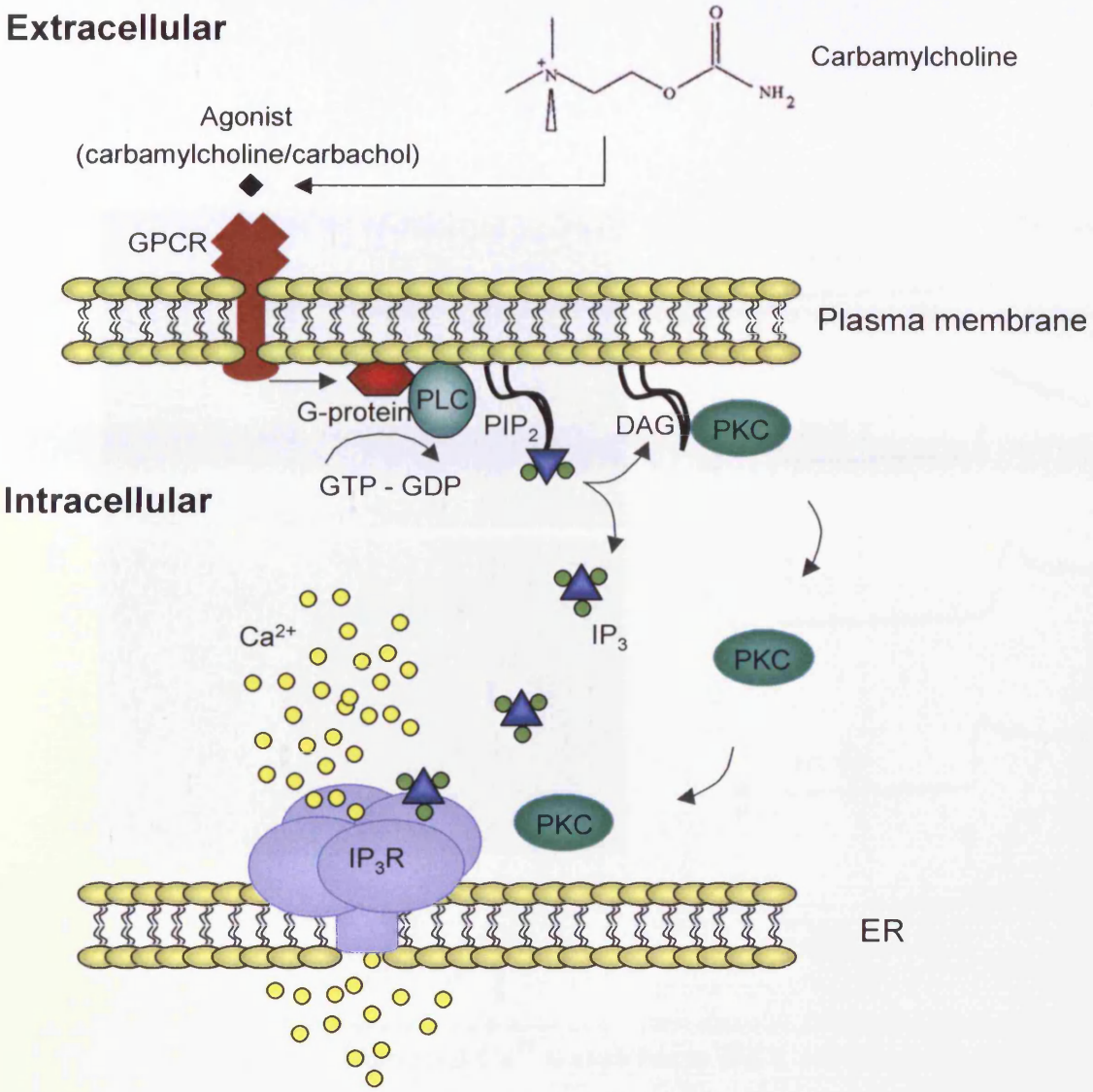

Figure 5.2. Schematic representation of signalling pathways triggered by carbachol

Carbachol stimulation of muscarinic G-protein coupled receptors (GPCR) activates G-protein, which by conversion of GTP to GDP triggers the hydrolysis of phosphatidylinositol-4,5-bisphosphate (PIP_2) by phospholipase C (PLC) to IP_3 and diacylglycerol (DAG). IP_3 induces the release of stored Ca^{2+} via the IP_3R, while DAG activates protein kinase C (PKC) that phosphorylates downstream proteins (including IP_3R).

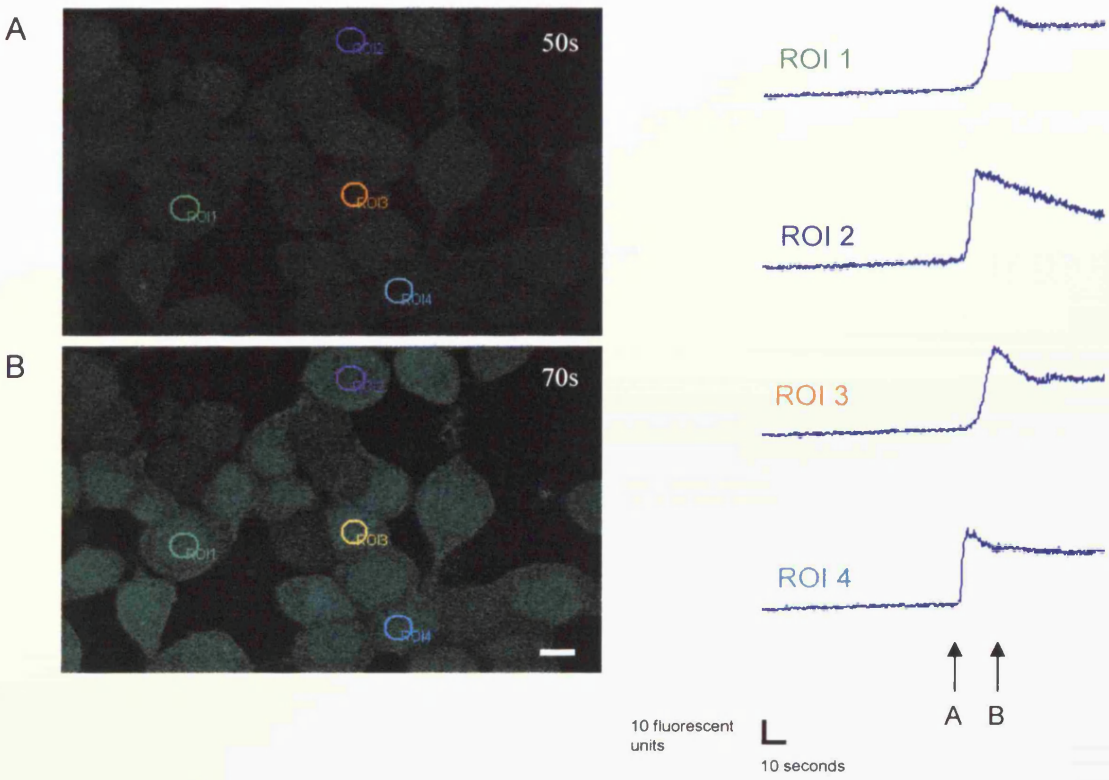

Figure 5.3. Carbachol-induced Ca^{2+} transients in HEK cells loaded with fluo-4

A. Fluo-4 fluorescence before 1mM carbachol addition. **B**. Fluorescent image acquired after carbachol addition. Regions of interest (ROI) are highlighted, and the corresponding transients representative of the Ca^{2+} dependent change in fluo-4 fluorescence are depicted in the left panel. Scale bar represents 10μm. Four ROI are displayed for illustration purposes, however typically 10-20 ROI were selected per experiment depending on number of cells per field of view.

5.2.2.1. Ca^{2+} transient characterisation

Carbachol-evoked Ca^{2+} transients were heterogeneous in profile and were characterised as described in Figure 5.4.

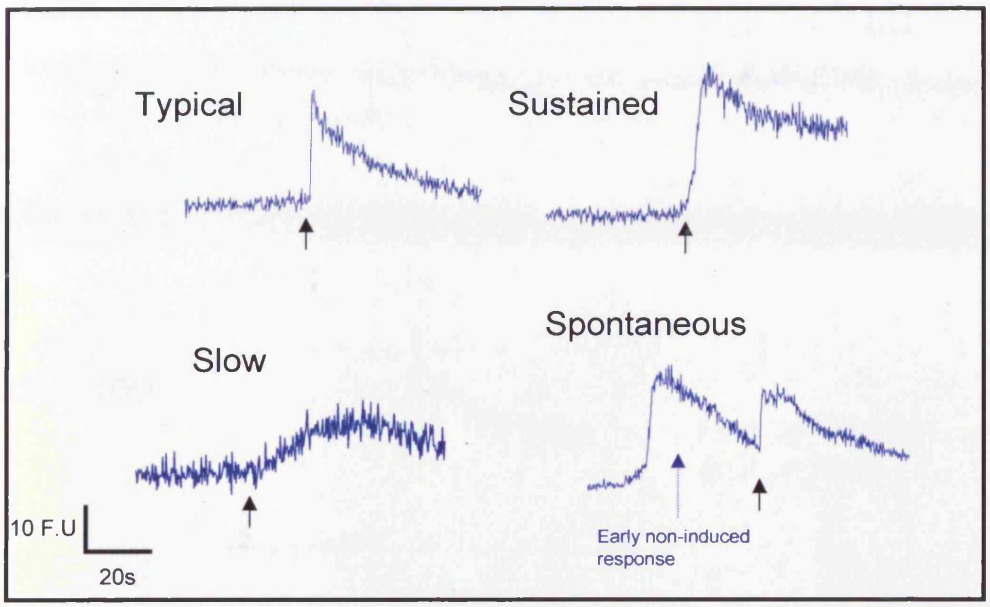

Figure 5.4. Heterogeneity of carbachol-evoked Ca^{2+} transients
Characteristic carbachol-induced Ca^{2+} transients observed. Spontaneous transients occurred prior to addition of agonist, and were not used for analysis.

In this thesis, a Ca^{2+} transient is defined as a Ca^{2+}-associated fluorescent increase greater than 10% of the basal fluorescence. The analysis parameters of Ca^{2+} transient were:

I. Basal fluorescence: the average resting fluo-4 fluorescence obtained from the first minute (300 frames) before agonist addition.
II. Peak Ca^{2+} release: the relative increase in fluo-4 fluorescence following agonist addition, measured as a percentage increase from basal fluorescence.
III. Rate of Ca^{2+} release: the relative increase in fluo-4 fluorescence over time, from basal to peak fluorescence.
IV. Rate of transient decay: the relative decrease in fluo-4 fluorescence over time, from peak fluorescence until the trace plateaued

The analysis parameters are displayed in Figure 5.5.

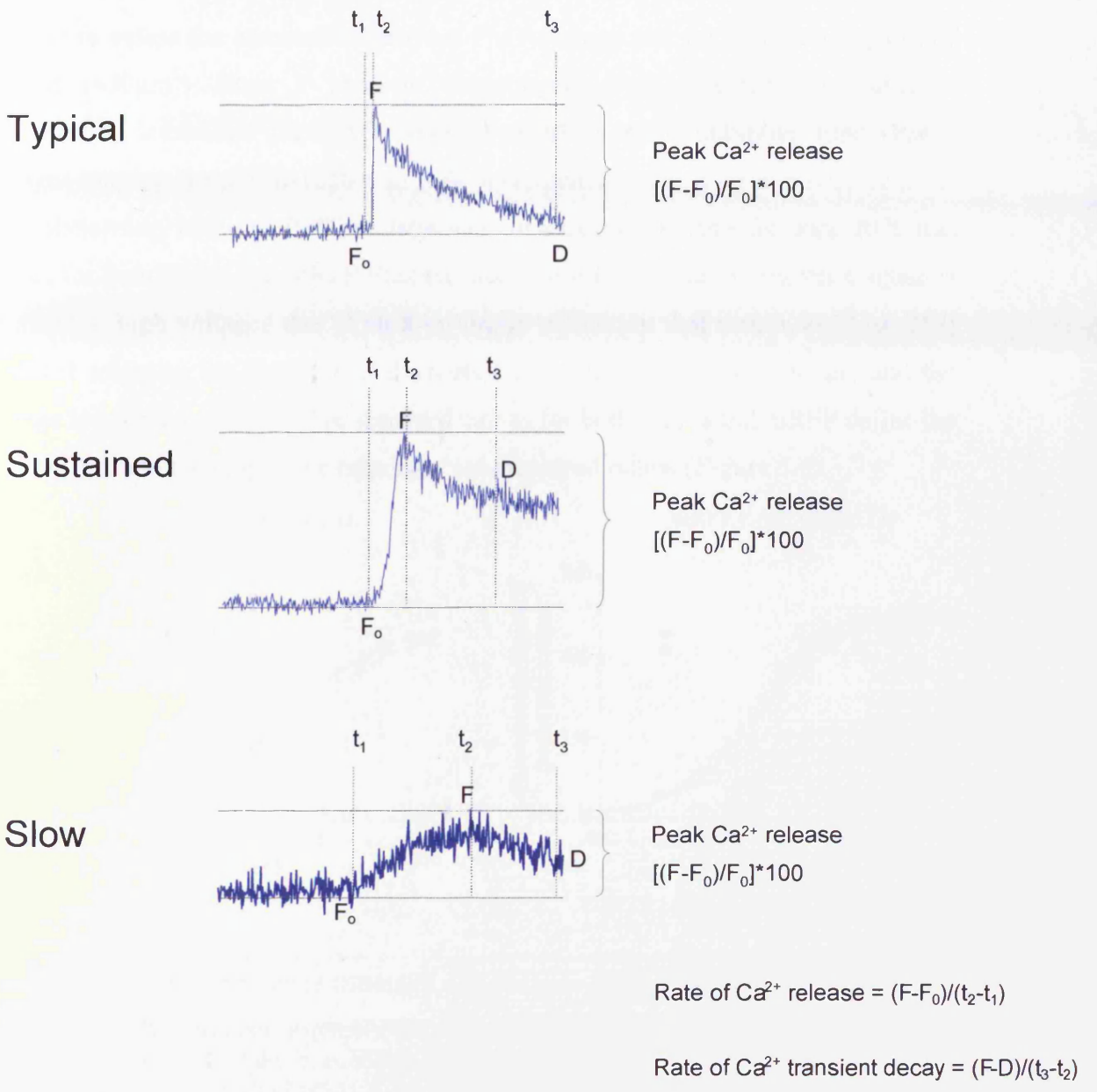

Figure 5.5. Schematic representation of analysis parameters implemented in assessment of Ca^{2+} release

F_0 = basal fluorescence, F = peak fluorescence, D = fluorescence after transient decay, t_1 = time immediately before response, t_2 = time at fluorescence peak, t_3 = time after transient decay.

5.2.3. Understanding the effect of PMT voltage on fluorescent signals

In order to assess the association between PMT voltage and fluorescence, regions of interest (~30μm^2) from 3 separate experiments were selected. The average fluorescence intensities per pixel were obtained at photomultiplier tube (PMT) voltages ranging from 500-1250V in 50V increments, using a laser power of 20%. The relationship between PMT voltage and fluorescent intensity for each ROI was plotted for both fluo-4 and mRFP fluorescence (see below). The fluorescence signal is saturated at high voltages due to an 8-bit image resolution that results in 2^8 (or 256) levels of intensity for each pixel. Each ROI is represented by a grey line and the average is overlaid in black. The standard curves for both fluo-4 and mRFP define the relationship, and the respective equations are displayed below (Figure 5.6).

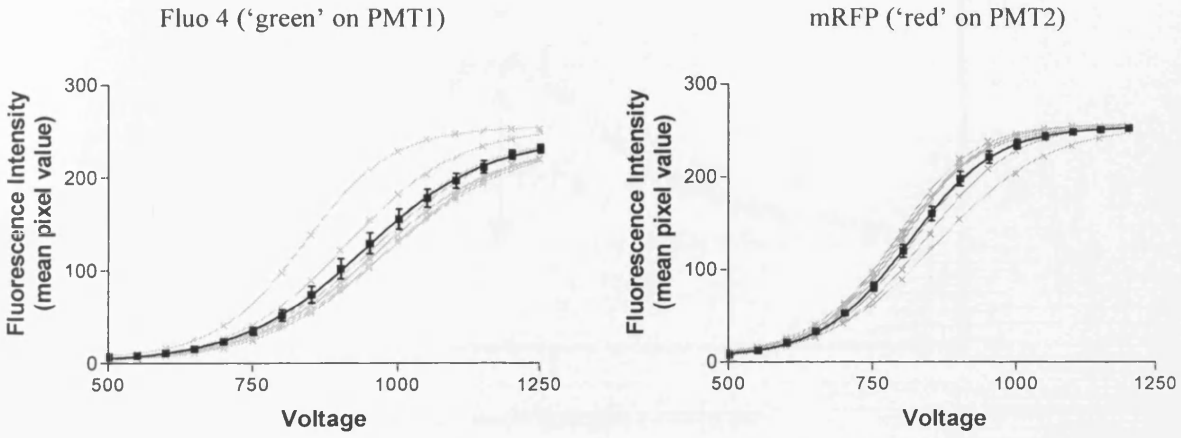

Figure 5.6. Fluorescence intensity dependence on voltage

Relative fluorescence intensity plotted against PMT voltage, n=8 for both mRFP and fluo-4. The data was fitted to a Boltzmann equation yielding non-linear regression of y=0.4347+(241.3 - 0.4347)/(1+exp((939.1 - x)/106.2)) for fluo-4 and y=6.728+(255.4 - 6.728)/(1+exp((810.2 - x)/75.36)) for mRFP.

5.2.4. Using thapsigargin to estimate ER Ca^{2+} store content

In light of the dependence of intracellular Ca^{2+} release on ER/SR store load (Ranu *et al.*, 2002; Terentyev *et al.*, 2003; Maier *et al.*, 2005), ER Ca^{2+} content was assessed. Thapsigargin is a selective blocker of SERCA with a low K_d (dissociation constant) that enables it to passively deplete the entire ER/SR store (Thastrup *et al.*, 1990). In most cells, this passive depletion manifests as a Ca^{2+} transient as a result of the steep gradient between ER Ca^{2+} (mM) and cytosolic Ca^{2+} (nM). Thapsigargin (5μM) was applied to WT HEK cells and those expressing mRFP and I-domain to estimate total ER Ca^{2+}. Live cell imaging was performed as described in Section 2.2.8.3. A typical thapsigargin response trace is displayed below in Figure 5.7.

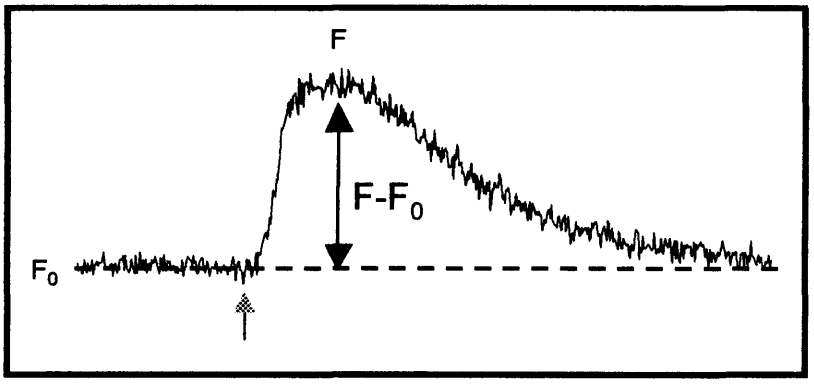

Figure 5.7. Typical thapsigargin response

Addition of thapsigargin induced a transient rise in $[Ca^{2+}]_i$ ($F-F_0$), which was measured as a percentage increase in fluorescence (F) from basal (F_0): $(F-F_0)/F_0*100$. Thapsigargin addition is indicated by the grey arrow.

5.2.5. Calibration of resting Ca^{2+} levels

Ionomycin is a pore-forming ionophore which mobilises $[Ca^{2+}]_i$ independent of cellular expression of RyR and IP_3R. In the presence of extracellular Ca^{2+}, ionomycin can be used to calibrate the Ca^{2+}-dependent fluorescence of fluo-4. Ionomycin (1μM) was applied to cells following 30 sec imaging of basal fluo-4 fluorescence. Resting

$[Ca^{2+}]_i$ concentration was then calculated using the following equation (Grynkiewicz *et al.*, 1985):

$$[Ca^{2+}] = K_d (F-F_{min})/(F_{max}-F)$$

Where K_d, the dissociation constant for the rate of Ca^{2+} dissociation from fluo-4 was taken from the published value of 345nM (Molecular Probes, Invitrogen). F_{min} and F_{max} represent minimum and maximum fluorescent signals respectively, and F represents fluorescent signal at any time. F_{max} was the peak fluorescence after addition of ionomycin (1μM) and F_{min} was the lowest fluorescent value determined in the presence of the Ca^{2+}-chelating agent EGTA (20mM).

5.2.6. Immunoblot and immunofluorescence analysis of Ca^{2+} handling proteins

The rank order of IP_3R subtype expression in HEK cells is reported to be IP_3R2 >IP_3R1 >IP_3R3 (Wojcikiewicz, 1995; Kaznacheyeva *et al.*, 1998). The endogenous expression levels of IP_3R2 was detected 2 days post-transfection in microsomal fractions obtained from HEK, mRFP- and ID^B-expressing cells (see Section 5.3.4.1). IP_3R1, SERCA2 and calreticulin were detected in post-nuclear supernatant (PNS) in cells 2 days post-transfection. SDS-PAGE and immunoblotting procedures were performed as described in Section 2.2.9. SERCA and calreticulin (65-125kDa) were analysed using 10% gels, whereas IP_3R (~220kDa for IP_3R1; ~270kDa for IP_3R2) was analysed using 6% gels. Membranes were probed with primary antibodies as detailed in Section 2.1.2.5.1.

Cells were assessed by immunofluorescence for localisation of I-domain constructs in relation to endogenous IP_3R, in order to yield any insights as to whether interaction between I-domain and IP_3R may underlie the Ca^{2+}-linked cytotoxicity of I-domain expression. Cells expressing mRFP and I-domain constructs were fixed 2 days post-transfection and processed for CLSM (see Section 2.2.8). At least 30 fields of view were obtained per construct. Red (mRFP-tagged) and green (IP_3R isoforms) channels

were overlaid and quantified using the co-localisation module of Imaris Bitplane (version 6.0) (performed by Dr. Chris George).

5.2.7. Generation of ^{eGFP}RyR2 plasmid DNA

Enhanced green fluorescent protein (eGFP) was derived from GFP by two point mutations and additional silent mutations that resulted in an increased mammalian expression photostability and an excitation peak shift to 488nm that increased its fluorescent signal following argon laser excitation (Zhang *et al.*, 1996). eGFP has a maximum excitation and emission spectra of 488nm and 512nm respectively, and has been successfully used in RyR2 studies in our laboratory. eGFP fusion to the N-terminus of RyR2 does not compromise channel function (Thomas *et al.*, 2004; Thomas *et al.*, 2005). Dr Chris George provided pcDNA3 containing human RyR2 tagged with eGFP. ^{eGFP}RyR2 expression was driven by the CMV promotor and the protein product produced was 16.531 kb (~560kDa). See Figure 5.8.

Figure 5.8. pcDNA3-^{eGFP}RyR2 plasmid

eGFP (green arrow) is tagged to the N-terminus of human RyR2 (grey arrow). The two sequences are separated by a four amino acid linker sequence (Thr-Ser-Gly-Ser). ^{eGFP}RyR2 expression is driven by the CMV promoter and the resistance genes encoded are ampicillin and neomycin. See Appendix III for detailed vector map.

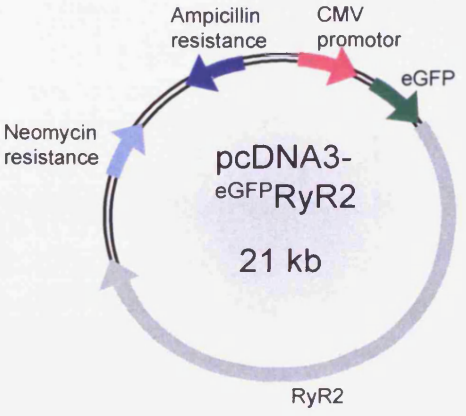

RyR2 DNA was propagated in XL-10 Ultracompetent *E. Coli* and purified using Qiagen Maxiprep Purification Kit (Qiagen), see Section 2.2.2.3. DNA was digested with *Hind* III, *Eco* RI, *Bgl* II and *Bam* HI and analysed using 1% (w/v) agarose gel electrophoresis to confirm the validity of the plasmid.

5.2.8. RyR2:ID^B co-transfection into HEK cells

HEK cells were transfected on coverslip chambers with ^{eGFP}RyR2 by the Effectene protocol (Section 2.2.7.3). Following a 6h incubation at 37°C, the same coverslip was transfected with ID^B and incubated overnight at 37°C. Following 24 h post-transfection the coverslips were flooded with cDMEM and left for a further 24 h prior to fixing for fluorescence imaging (Section 2.2.8.1) or loaded for Ca^{2+} imaging experiments (Section 2.2.8.3).

5.2.9. Immuno-localisation of RyR2 and ID^B in HEK cells

Cells co-expressing ^{eGFP}RyR2 and ID^B were fixed 2 days post-transfection and visualised using SP5 CLSM (Section 2.2.8). At least 30 fields of view representative of distinct cell populations were obtained. Red and green channels were overlaid and quantified using the co-localisation module of Imaris Bitplane (version 6.0) (performed by Dr. Chris George).

5.2.10. Elucidating ID^B function in the presence of recombinant RyR2

Ca^{2+} signalling in cells co-expressing RyR2 and ID^B were analysed 2 days post-transfection. Cells transfected with RyR2 alone were used as controls. Caffeine-induced responses identified cells transfected with RyR2, as these cells could not be distinguished due to the overlapping fluorescence of fluo-4 and eGFP. Since eGFP fluorescence is not affected by caffeine addition (Thomas *et al.*, 2004) all fluorescent changes are due to fluo-4. ID^B expressing cells were visualised via their inherent 'red' fluorescence (Figure 5.9). These parameters permitted the identification of different populations: ID^B alone, RyR2:ID^B, RyR2 alone (without ID^B) that were termed RyR2:ID$^B_{NUC}$. Figure 5.9 displays a snapshot of RyR2:ID^B co-transfected cells immediately before and after 10mM caffeine addition. These experiments were

specifically aimed to study the effect of ID^B on RyR2 channel function therefore cells that were non-responsive to caffeine were not analysed (cells 'A' in Figure 5.9).

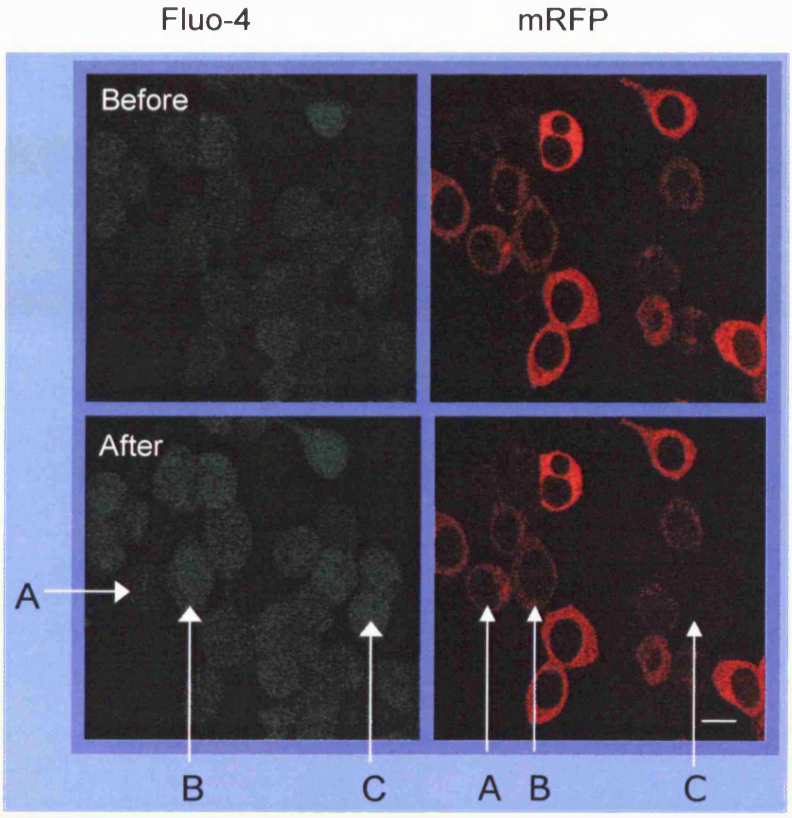

Figure 5.9. Snapshot of HEK cells expressing RyR2:ID^B exposed to 10mM caffeine

Top panels display fluo4 and mRFP channels of the same field of view prior to caffeine (10mM) addition; lower panels display the same cells immediately after caffeine addition. The three different cells are designated by A (ID^B expressing only), B (RyR2:ID^B expressing) and C (RyR2 expressing, ID^B_{NUC}). Scale bar = 10μm.

5.3 Results

5.3.1. PMT voltage is a critical determinant of fluorescence signal intensity

Given the dependency of fluorescence signal intensity on voltage (Figure 5.6), experimental data acquired at different voltages would need correcting using the equations given in Figure 5.6. However, all experiments performed in this thesis were done at comparable voltages and less than 750V (Figure 5.10). The linear relationship between voltage and fluorescence exists at >750V (Figure 5.6). Consequently our experimental protocol/set-up negated the need to correct fluorescent signals post-acquisition.

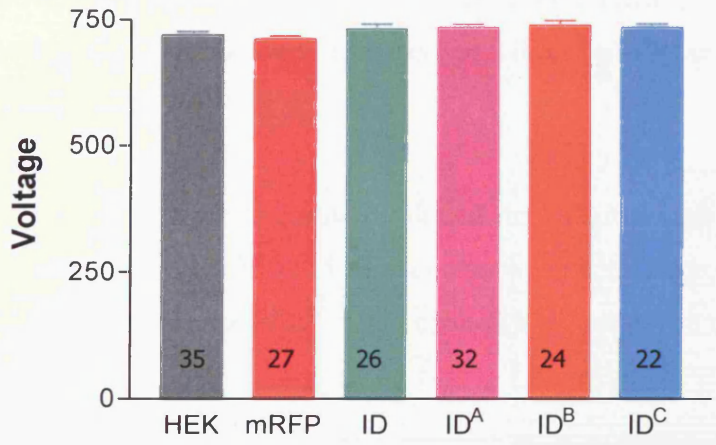

Figure 5.10. Voltages used for Ca^{2+} imaging experiments on I-domain cells in this thesis

n = the number of separate experiments that comprised the entire data set described in this thesis. There were no significant differences ($p>0.05$) between voltages used for all I-domain experiments compared to those used for mRFP expressing cells (analysed by ANOVA).

5.3.2. I-domain expression alters cellular Ca^{2+} handling

As discussed previously, HEK cells are RyR2-null, which precludes the use of caffeine to study Ca^{2+} mobilisation (Tong *et al.*, 1999). However, HEK cells express endogenous IP_3R Ca^{2+} release channels, which have an active role in Ca^{2+}-dependent apoptosis, as already discussed. Therefore carbachol was administered to I-domain and mRFP expressing cells in order to trigger muscarinic receptors on the cell surface, stimulating a cascade of events resulting in activation of IP_3R, as displayed in Figure 5.2. Cells co-expressing RyR2 and ID^B activated by caffeine were used for comparison.

5.3.2.1. Recombinant I-domain expression does not significantly elevate $[Ca^{2+}]_i$

In light of reports that elevated intracellular Ca^{2+} concentrations are associated with cell death (Gutstein and Marks, 1997; Garcia *et al.*, 2001; Tantral *et al.*, 2004; Lim *et al.*, 2008), resting Ca^{2+} levels were assessed in HEK, mRFP and recombinant I-domain expressing cells.

The expression of recombinant I-domain induced persistently high $[Ca^{2+}]_i$, although there were no statistically significant differences between cells expressing I-domain or mRFP. It is possible that elevated Ca^{2+} may occur as a consequence of transfection.

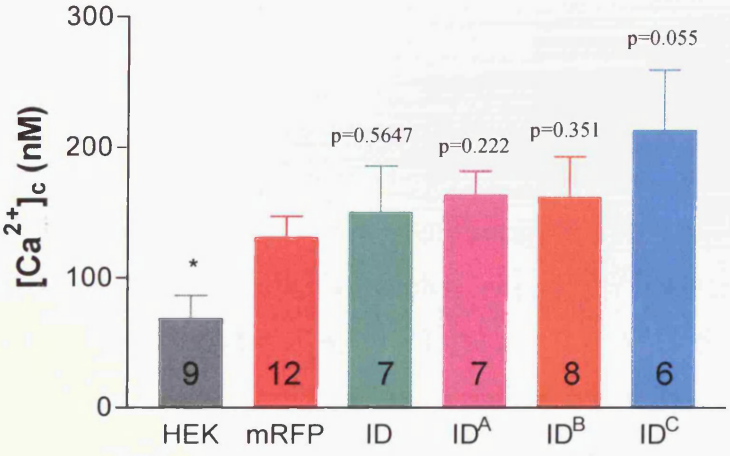

Figure 5.11. Elevated $[Ca^{2+}]_i$ in mRFP and I-domain expressing cells

Basal Ca^{2+} in I-domain and mRFP cells was determined following ionomycin calibration of fluo-4. $^*p<0.05$ compared to mRFP expressing cells, n number is displayed inside each bar and represents separate experiments.

5.3.2.2. Cells expressing I-domain constructs exhibit reduced ER Ca^{2+} load

In order to ascertain whether alterations in intracellular stores contributed to I-domain associated cytotoxicity, thapsigargin was applied to HEK, mRFP and I-domain cells to estimate ER Ca^{2+} load. Thapsigargin experiments revealed that I-domain expression was associated with lower ER Ca^{2+}. Remarkably this phenomenon was observed in both transfected cells and NUCs (Figure 5.12).

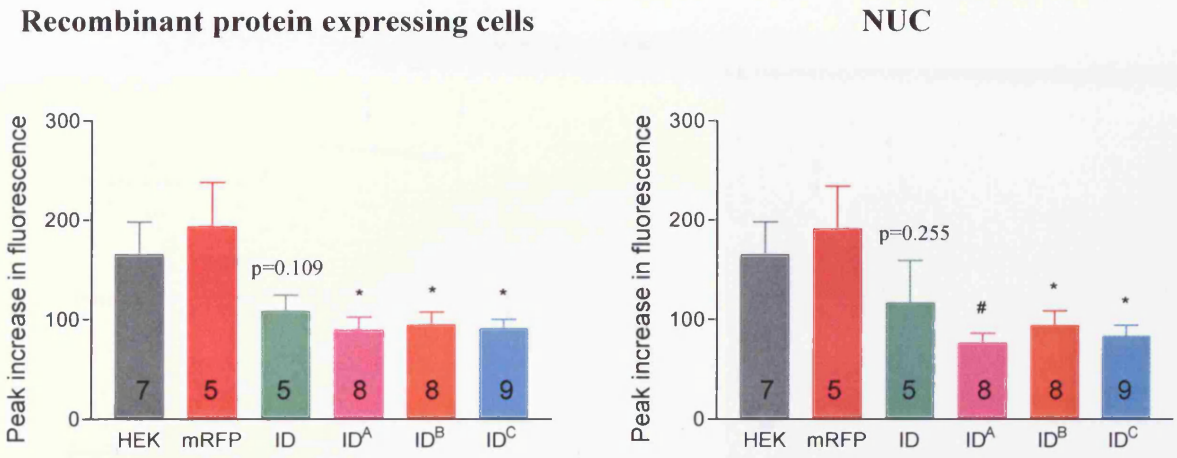

Figure 5.12. ER Ca^{2+} load estimated by thapsigargin

*$p<0.05$ and #$p<0.01$ compared to mRFP-expressing cells and mRFP NUC. Data obtained from >5 separate coverslips per cell type. n number is displayed inside each bar and represents separate experiments.

5.3.3. I-domain expression reduced IP_3R agonist responses

Cells transfected with all I-domain constructs, except for ID^B, were characterised by markedly decreased dose-dependent carbachol-induced Ca^{2+} release when compared to mRFP cells, which was observed at both 1mM and 0.1mM carbachol doses (Figure 5.14). Lower carbachol doses (0.001-0.01mM) did not evoke Ca^{2+} release in I-domain and mRFP expressing cells (Figure 5.14). Interestingly the reduced Ca^{2+} responsiveness of I-domain expressing cells was also broadly exhibited by NUCs, although significance was only reached at the highest dose of carbachol used (1mM)

in ID^C transfected cells (Figure 5.14). Figure 5.13 displays a typical field of view of cells transfected with ID^C, note that both transfected cells and NUCs exhibit diminished carbachol-induced responses. Loss of Ca^{2+} response is most dramatic for ID and ID^C (Figure 5.14), and are the only regions encoding putative transmembrane sequences (Figure 3.4 and 3.6). In contrast, ID^B expression did not reduce carbachol-induced Ca^{2+} responses, and interestingly the proportion of non-responsive ID^B cells was comparable to mRFP at all carbachol doses (Figure 5.14).

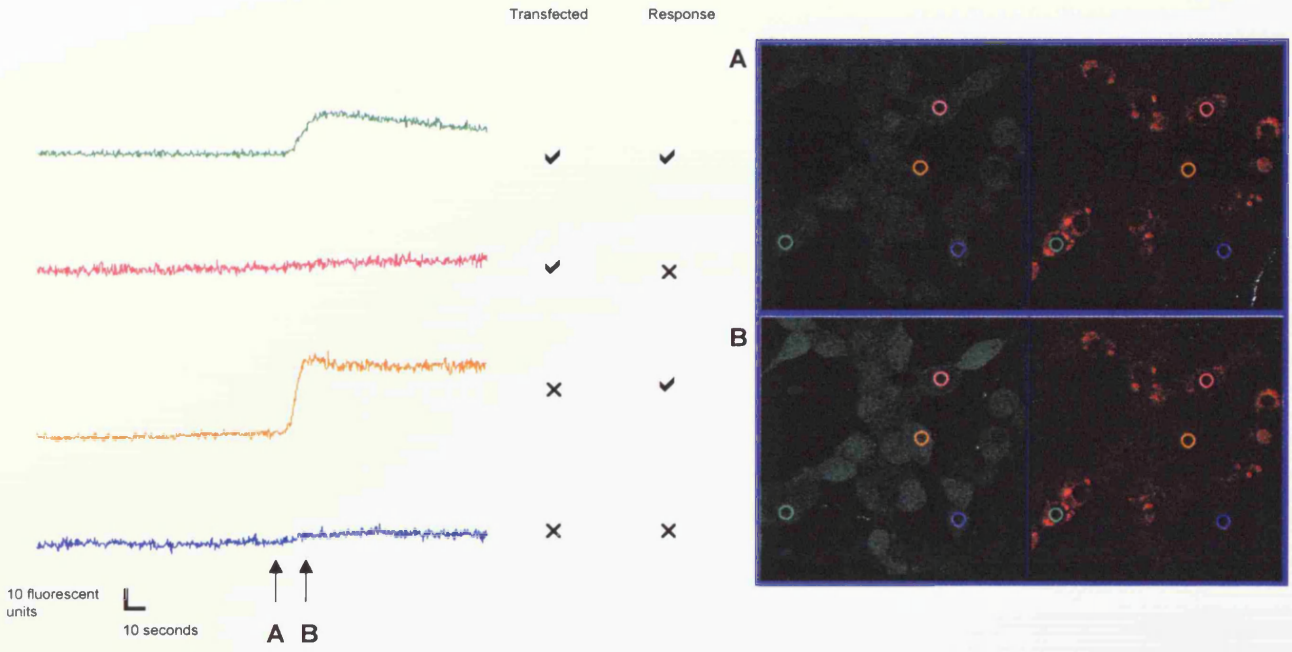

Figure 5.13. Absence of agonist-induced responses in ID^C expressing cells and NUC

Left panels display Ca^{2+} traces from cells selected in the right confocal panel that were exposed to 1mM carbachol. Coloured halos correspond to ID^C expressing cells and NUC. Both ID^C expressing cells and NUC are non-responsive to carbachol (pink and blue halos for ID^C expressing and NUC respectively). A corresponds to time before carbachol addition, whereas B corresponds to time directly after carbachol addition.

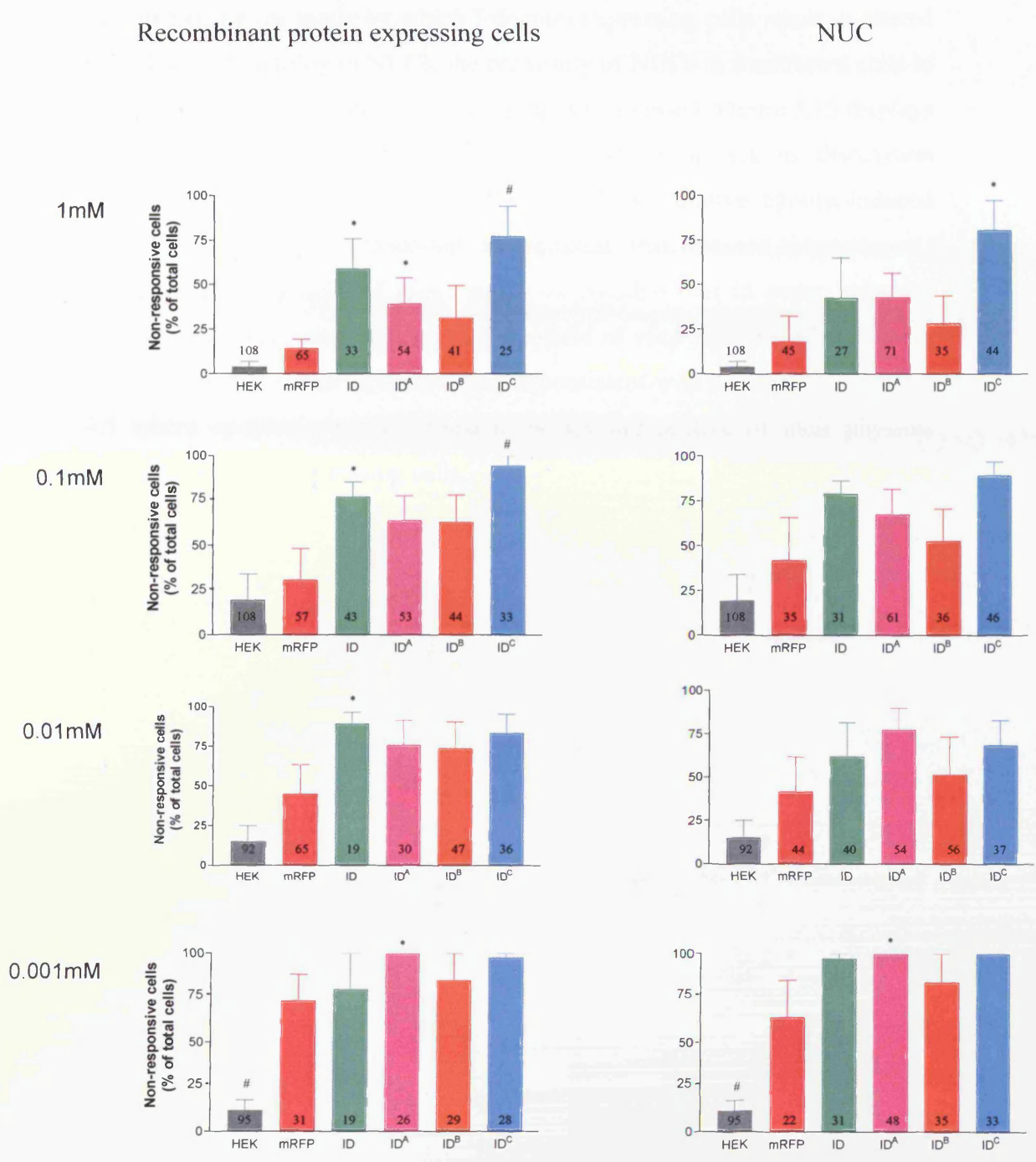

Figure 5.14. Non-responsive transfected cells and NUCs to carbachol.

Cells that did not exhibit agonist-induced Ca^{2+} release were analysed. Left panels represent recombinant protein expressing cells and right panels display the NUC responses from the same fields of view. *$p<0.05$, $^{\#}p<0.01$ compared to mRFP cells for recombinant protein expressing cells and mRFP NUC for I-domain NUC.

In order to investigate the mode by which I-domain expressing cells result in altered signalling and loss of viability in NUCs, the proximity of NUCs to transfected cells in the context of the carbachol-induced Ca^{2+} transient was assessed. Figure 5.15 displays scatterplots for all I-domain constructs, and demonstrates a lack of association between NUC distance from a transfected cell and the relative agonist-induced response (F/F_0). Although, it is important to recognise that distance measurements were limited to within a field of view, and it is possible that in some instances recombinant protein-expressing cells outside the field of view may have been closer than those assessed. Nevertheless, this finding is consistent with the data presented in Figure 4.5 where apoptosis was observed in NUCs irrespective of their physical association with I-domain expressing cells.

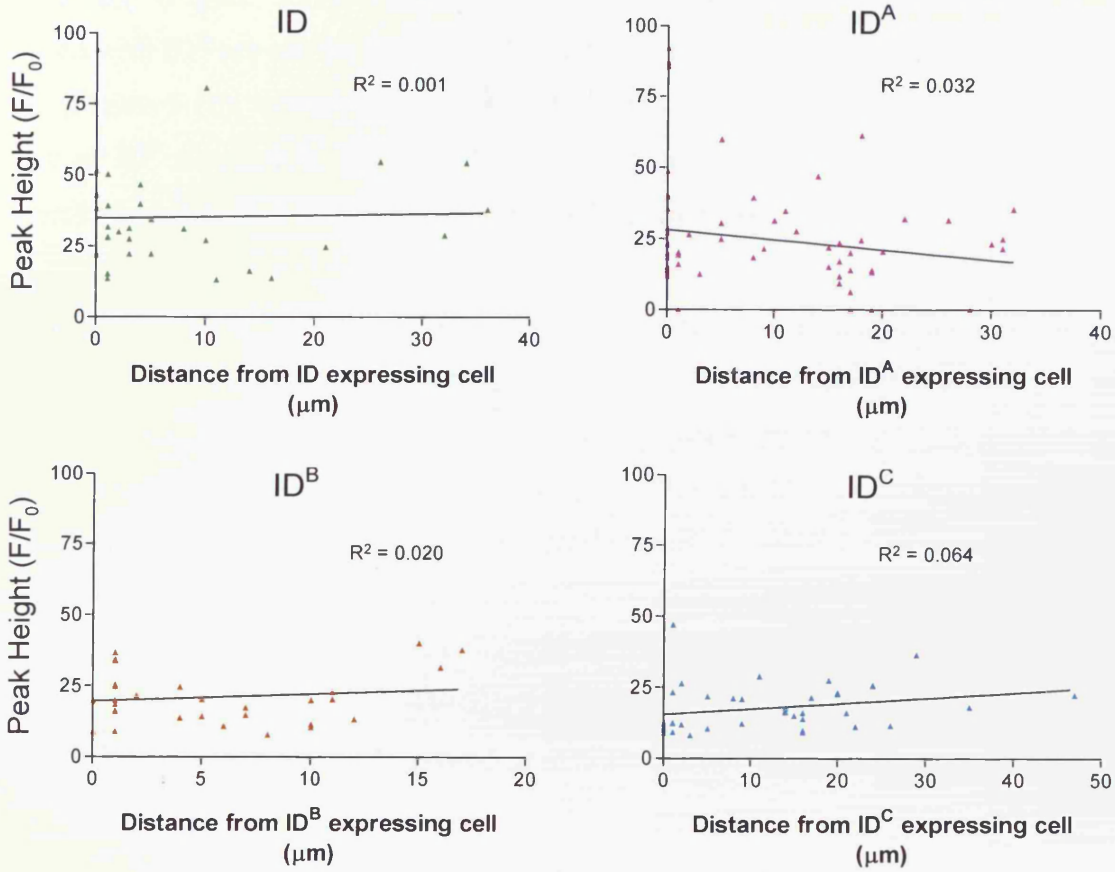

Figure 5.15. Distance of NUC from transfected cells was not associated with the magnitude of Ca^{2+} release evoked by 1mM carbachol

Scatter plots for all I-domain constructs, displaying a lack of correlation between carbachol-evoked responses in NUC and their distance from a transfected cell. Each point represents a cell. R^2 values are displayed on each graph.

Although a large proportion of I-domain transfected cells were non-responsive to carbachol (Figure 5.14), I-domain expressing cells in which Ca^{2+} transients persisted were analysed. Characterisation of transients induced by 1mM and 0.1mM carbachol revealed a broadly similar distribution of transient types (characterised in Figures 5.4 and 5.5) in mRFP and I-domain expressing cells (Figure 5.16). In line with this analysis, RyR2 and RyR2:ID^B caffeine-induced Ca^{2+} transients were also characterised. Transient types were broadly comparable between RyR2 and RyR2:ID^B, however more sustained transients were displayed by RyR2 only. More notable were the fewer typical transients exhibited by RyR2:ID^B_{NUC} than both RyR2 and RyR2:ID^B (Figure 5.16). Furthermore, an interesting finding was that three RyR2:ID^B co-expressing cells exhibited spontaneous Ca^{2+} transients prior to caffeine addition, which was not observed in either RyR2 only expressing cells or RyR2:ID^B_{NUC} (Figure 5.16). The distribution of transient types following RyR2 activation with ID^B are similar to those exhibited by activation of IP_3R in the presence of ID^B (Figure 5.16), which were also broadly comparable to transient types in the absence of ID^B expression. These findings suggest that I-domain constructs do not alter these characteristics of agonist-induced Ca^{2+} transients.

In order to evaluate the modulation of the temporal aspects of Ca^{2+} transients induced by 1mM carbachol, a detailed assessment of peak Ca^{2+} release, rate of Ca^{2+} release and rate of Ca^{2+} transient decay was performed, as displayed in Figure 5.17. The robust peak height of Ca^{2+} transients evoked by 1mM carbachol were reduced in ID expressing cells compared with those expressing mRFP, whereas no significant difference was observed with any other I-domain fragment or with any NUC. Rate of Ca^{2+} release was lower in ID cells compared to mRFP cells, and in ID^A and ID^B NUCs compared to mRFP NUCs ($p<0.01$). The rate of Ca^{2+} transient decay was lower in ID and ID^A expressing cells compared to mRFP, and this observation extended to ID^A NUCs. ID^C expression was tempered by marked cytotoxicity demonstrated by the few cells (7) responsive to 1mM carbachol.

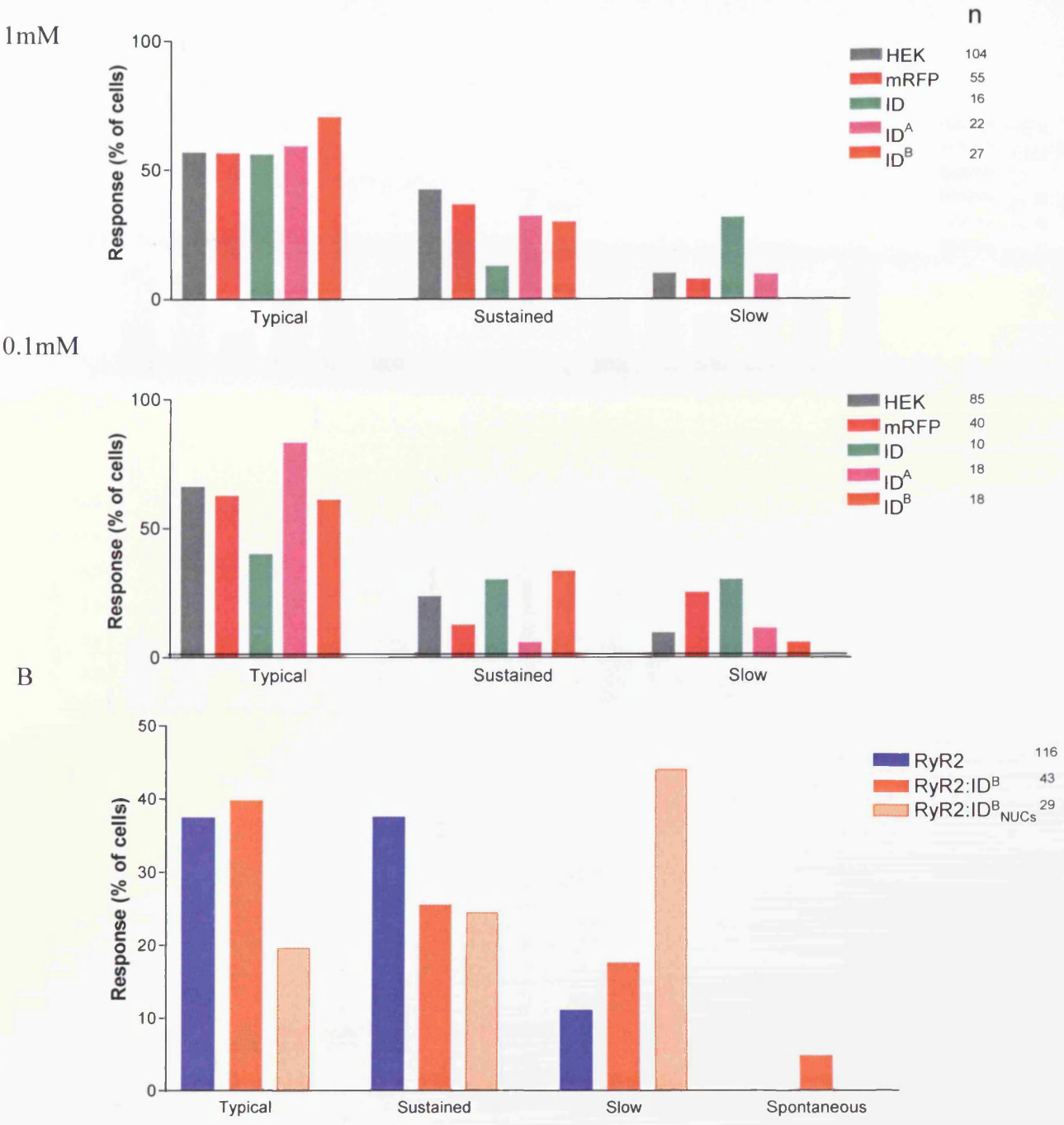

Figure 5.16. Transient types of carbachol and caffeine responsive cells

A. HEK, mRFP and I-domain expressing cells displayed similar response types to 1mM (upper panel) and 0.1mM carbachol (lower panel). ID^C transient types were not determined due to very few responding cells to either carbachol dose. n= number of cells analysed. **B.** Caffeine-induced (10mM) transient types of HEK cells expressing RyR2 alone, RyR2:ID^B and RyR2:ID^B_{NUC} represented as a percentage of total cells. Data obtained from at least 15 separate fields of view per construct; n is representative of cell number.

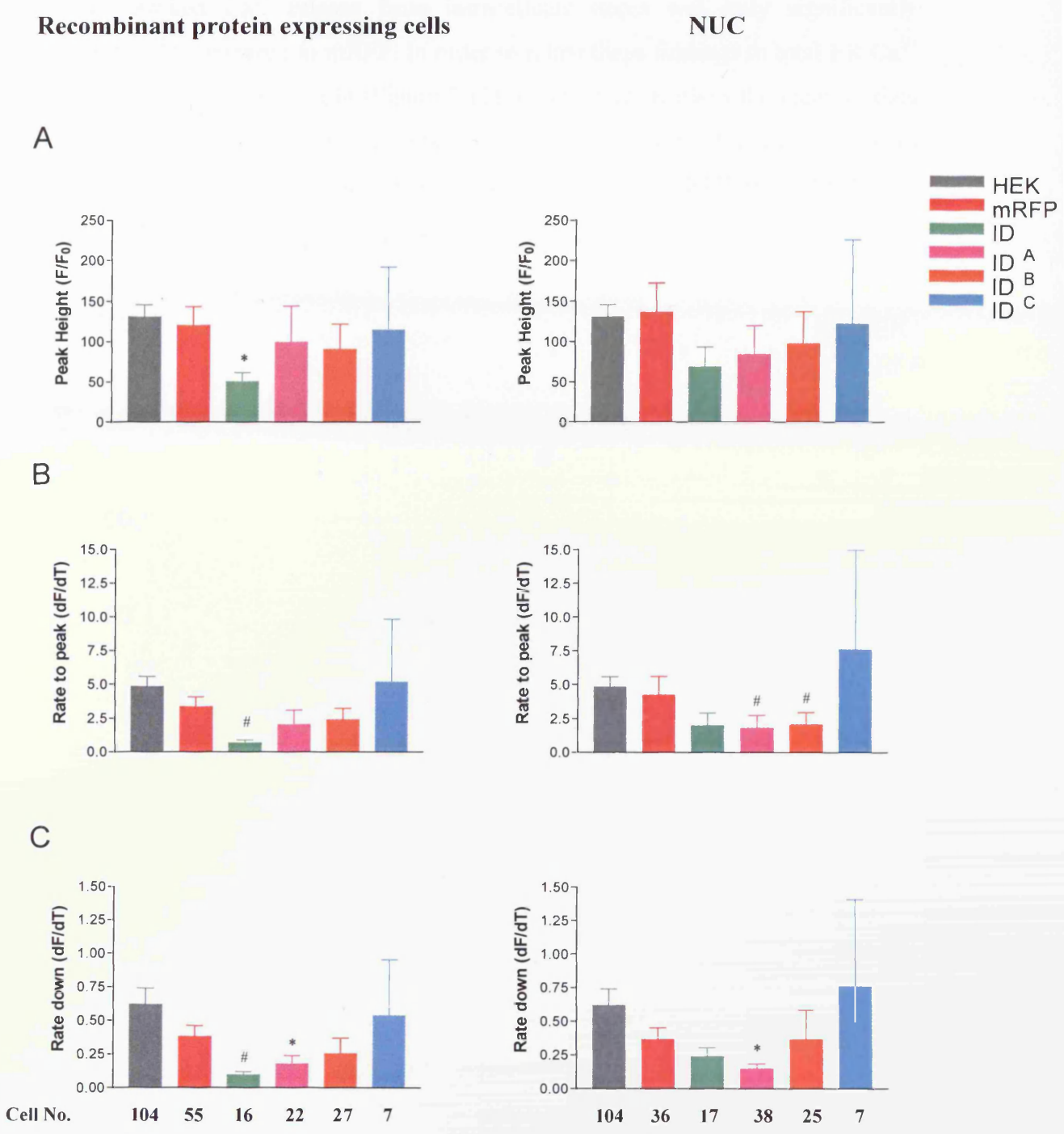

Figure 5.17. Characterisation of 1mM carbachol-induced Ca^{2+} release in I-domain expressing HEK cells and NUCs

Peak height (A), rate to peak (B) and rate of decay (C) characteristics of carbachol-induced responses of HEK, mRFP and I-domain expressing cells and NUC. $^{*}p<0.05$ and $^{\#}p<0.01$ compared to mRFP cells and mRFP NUC. Data is plotted as average±SEM. Cell no. represents the total number of responsive cells from which the data was acquired.

Carbachol-evoked Ca^{2+} release from intracellular stores was only significantly different for ID compared to mRFP. In order to relate these findings to total ER Ca^{2+} stores estimated by thapsigargin (Figure 5.12), Figure 5.18 displays the mean of data obtained from carbachol (1mM) experiments plotted against the mean of data obtained from thapsigargin experiments. Note that HEK and mRFP are distinct from I-domain constructs.

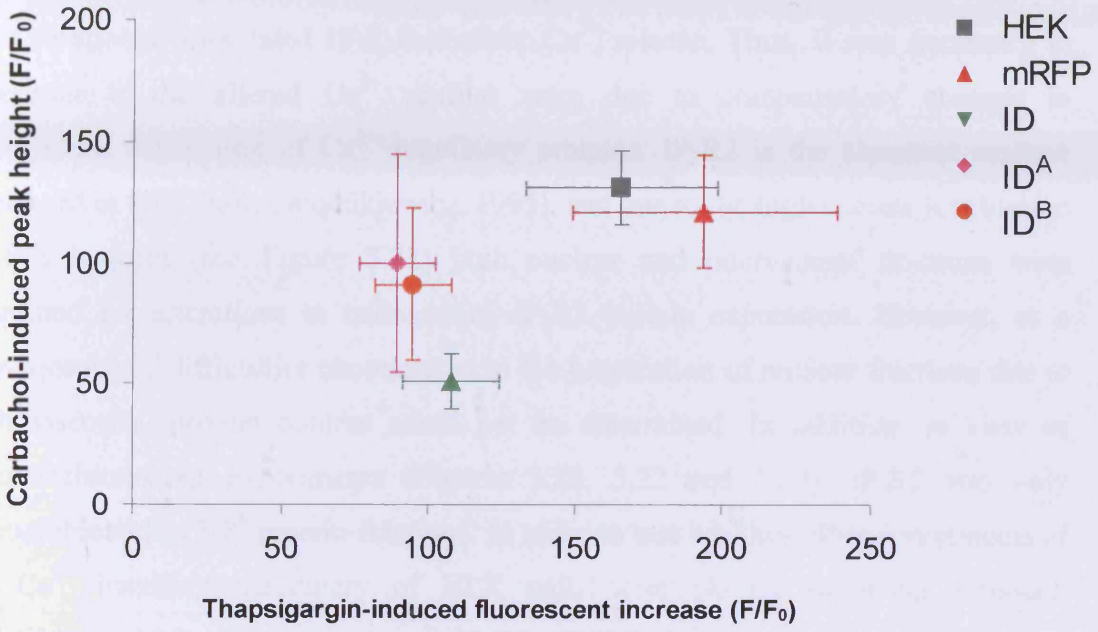

Figure 5.18. Mean carbachol-evoked response against mean thapsigargin-evoked response

Carbachol-evoked responses (1mM) were plotted against thapsigargin (5μM) for HEK, mRFP and I-domain constructs. ID^C was not included due to low n-numbers for carbachol-evoked Ca^{2+} release.

5.3.4 Alterations in cellular levels of Ca^{2+} handling proteins following I-domain expression

5.3.4.1 Altered expression of ER Ca^{2+} handling proteins following I-domain expression

Figures 5.14 and 5.17 showed that in day 2 cells (when expression of I-domain constructs was highest) some I-domain fragments modulated the responsiveness of cells to agonist-stimulated IP_3R-dependent Ca^{2+} release. Thus, it was necessary to determine if the altered Ca^{2+} profiles were due to compensatory changes in endogenous expression of Ca^{2+} regulatory proteins. IP_3R2 is the abundant isoform expressed in HEK cells (Wojcikiewicz, 1995), and due to the high nuclear localisation of this isoform (see Figure 5.22) both nuclear and microsomal fractions were examined for alterations in endogenous IP_3R2 protein expression. However, as a consequence of difficulties encountered in the preparation of nuclear fractions due to high viscosity, protein content could not be determined. In addition, in view of immunofluorescent experiments (Figures 5.20, 5.22 and 5.23), IP_3R2 was only immunoblotted in ID^B protein fractions. In order to test whether other components of the Ca^{2+} handling machinery of HEK cells were altered following I-domain transfection, endogenous levels of IP_3R1, SERCA2 and calreticulin were also examined. There was no difference in expression of IP_3R1, IP_3R2, SERCA or calreticulin following transfection with I-domain constructs ($p>0.05$) (Figure 5.19).

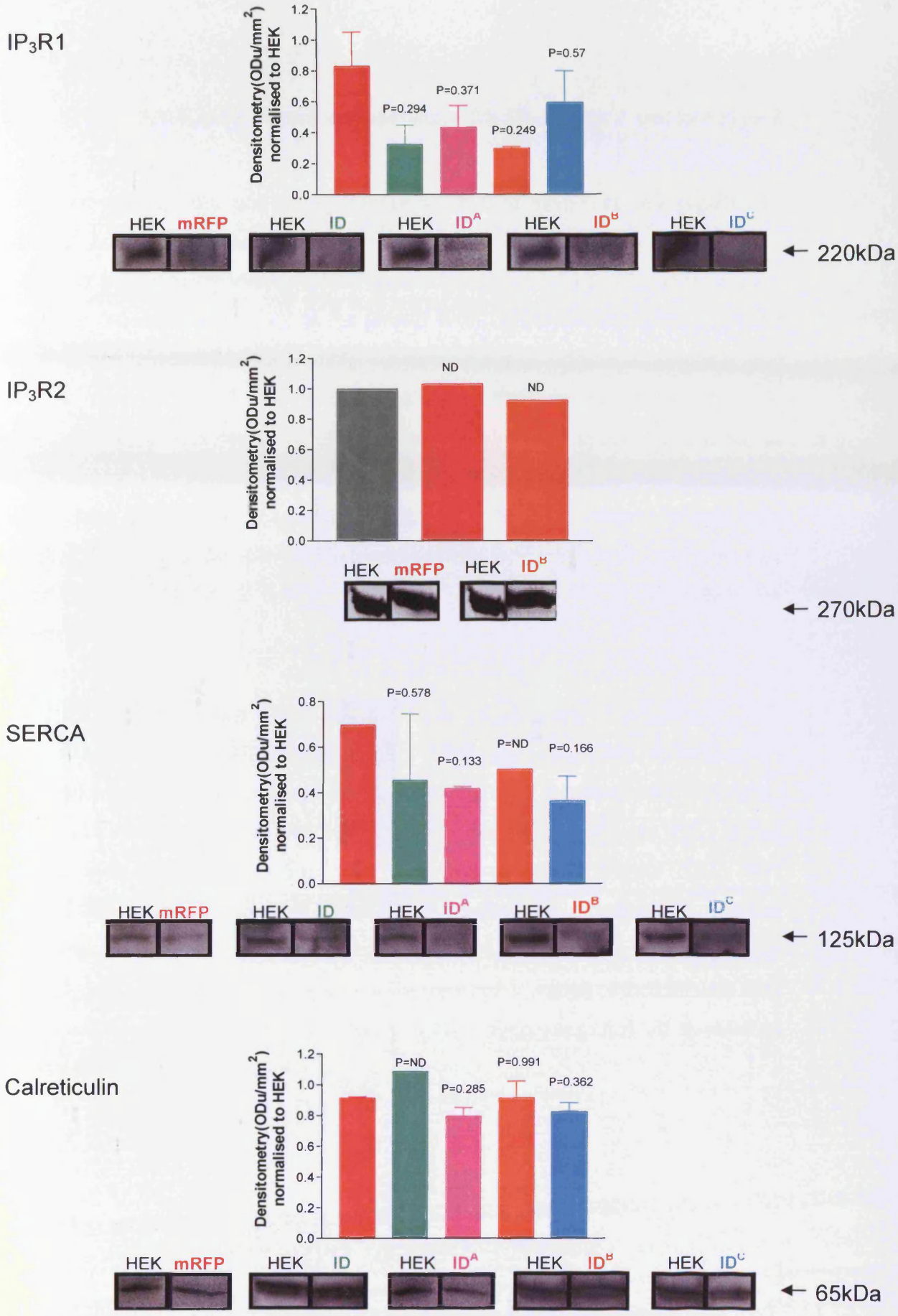

Figure 5.19. Endogenous levels of IP_3R1, IP_3R2, SERCA2 and calreticulin

Immunoblots of IP_3R1 (200µg total protein), IP_3R2 (100µg total protein), SERCA2 (100µg total protein) and calreticulin (100µg total protein) 2 days post-transfection. The calculated molecular weight of calreticulin is ~47kDa but runs atypically at ~65kDa due to endogenous glycosylation. ID^B did not alter IP_3R2 expression 2 days post-transfection. n=3 for IP_3R1, SERCA and calreticulin. n=1 for IP_3R2 therefore p was not determined (ND).

5.3.4.2. I-domain co-localises with IP_3R type 1 but not type 2

Immunoblot analysis did not reveal a reduced level of IP_3R1 in cell populations expressing I-domain (Figure 5.19), however, in view of the reduced carbachol responses of I-domain expressing cells (Figure 5.14) there could still be an interaction between the I-domain and IP_3R1 at the protein level. Therefore endogenous protein levels were also assessed in single cells. Co-localisation of I-domain constructs with both IP_3R type 1 and 2 was assessed using CLSM (Figures 5.20 and 5.22, respectively). IP_3R1 was mainly localised within cytoplasmic compartments, however IP_3R2 displayed predominant nuclear localisation. IP_3R1 expression was assumed to be lower than IP_3R2, since it required a higher voltage to observe localisation, although it should be noted that IP_3R-isoform specific antibodies have a different titre /affinity (Section 2.1.2.5.1), which could have affected the required voltage for visualisation.

ID^B and ID, and to a lesser extent ID^C displayed predominant co-localisation with IP_3R1 whereas ID^A did not (Figures 5.23). There was very little co-localisation between all I-domain constructs and IP_3R2 in cytoplasmic compartments (~25-30%, Figures 5.23). Furthermore, the high level of co-localisation of ID^B with IP_3R1 is also consistent with its co-localisation with recombinant RyR2 (Figure 5.21). ID^B expression did not appear to inhibit RyR2 Ca^{2+} release, however the use of fluo-4 meant that non-functional RyR2 channels could not be identified. Nevertheless about 20-30% of cells per field of view were caffeine responsive, which correlates well with the expected transfection efficiency (Figure 5.21B) suggesting that all transfected cells were expressing functional RyR2.

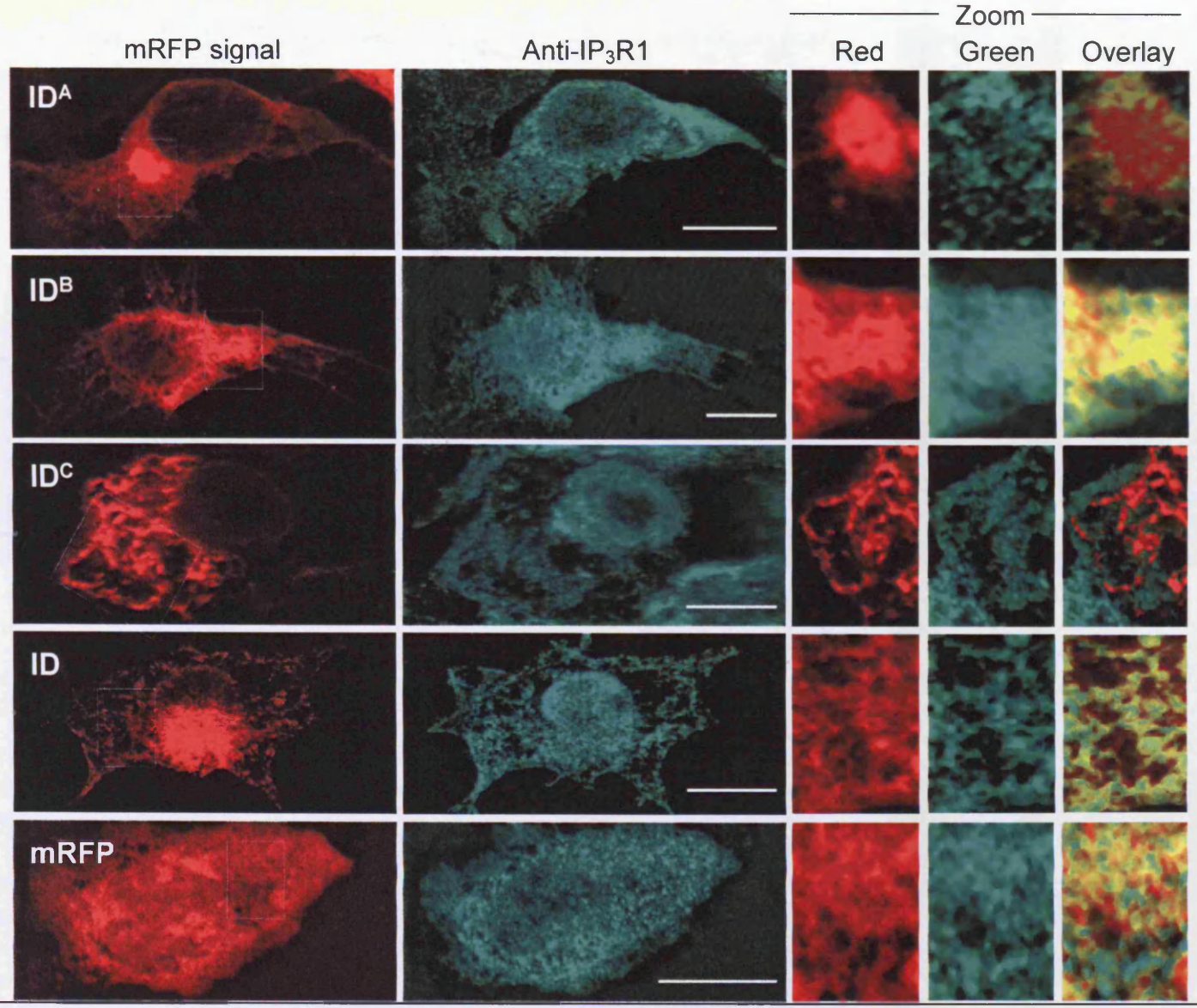

Figure 5.20. Immunofluorescence of endogenous IP_3R1 in mRFP and I-domain expressing cells

Confocal images of IP_3R1 in I-domain and mRFP expressing cells two days post-transfection. Right panels display the boxed 'zoomed-in' regions shown in the left panels, in both red and green channels, and the overlay of both channels. Scale bar represents 10μm. Number of cells analysed: mRFP, 18; ID, 14; ID^A, 13; ID^B, 22; ID^C, 39.

Given the structural homology between the I-domain of RyR2 and motifs within IP_3R (Appendix I), and the above finding that ID^B potentially interacted with IP_3R1 and not IP_3R2, it was important to determine the co-localisation between ^{eGFP}RyR2 and mRFP-tagged ID^B. Immunofluorescence revealed an approximately 75% co-localisation of both constructs, displayed in Figure 5.21.

A

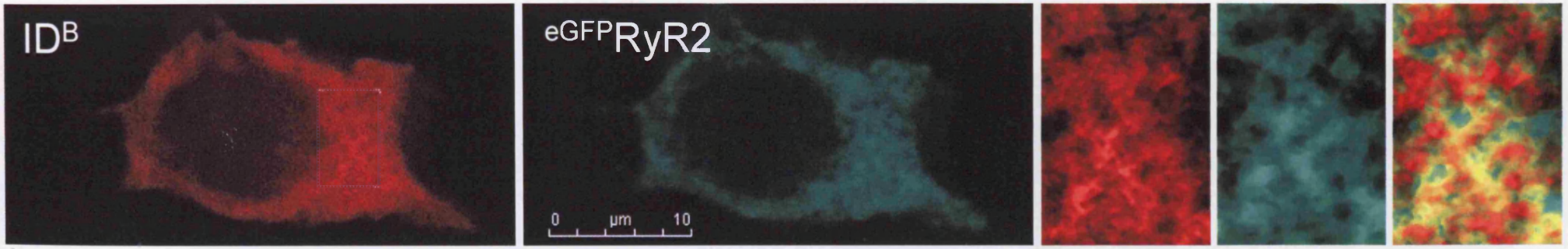

Figure 5.21. RyR2:ID^B co-localisation

A. HEK cells co-expressing RyR2 and ID^B were analysed by CLSM. Left two panels display typical cellular localisation of $^{mRFP}ID^B$ and ^{eGFP}RyR2 channels. The boxed 'zoomed-in' region selected in the ID^B panel are magnified in the 'zoomed in' panels corresponding to ID^B (red), ^{eGFP}RyR2 (green) and the merged image (far right). Data is representative of those obtained from 66 cells, scale bar represents 10µm. **B.** Transfection efficiency for cells co-transfected with ID^B and RyR2 (representative of 8 separate fields of view). Total number of caffeine responsive cells (representative of 14 fields of view) is comparable to the number of RyR2 transfected cells indicating that ID^B does not inhibit RyR2 function.

B

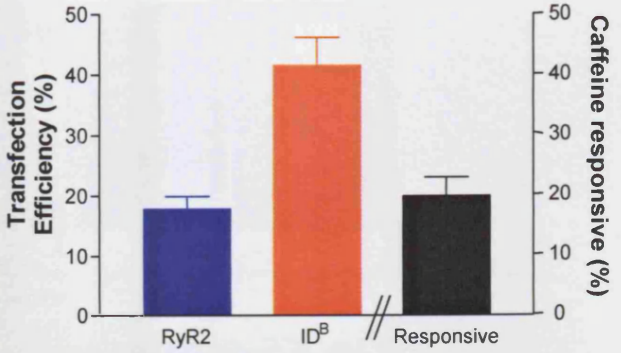

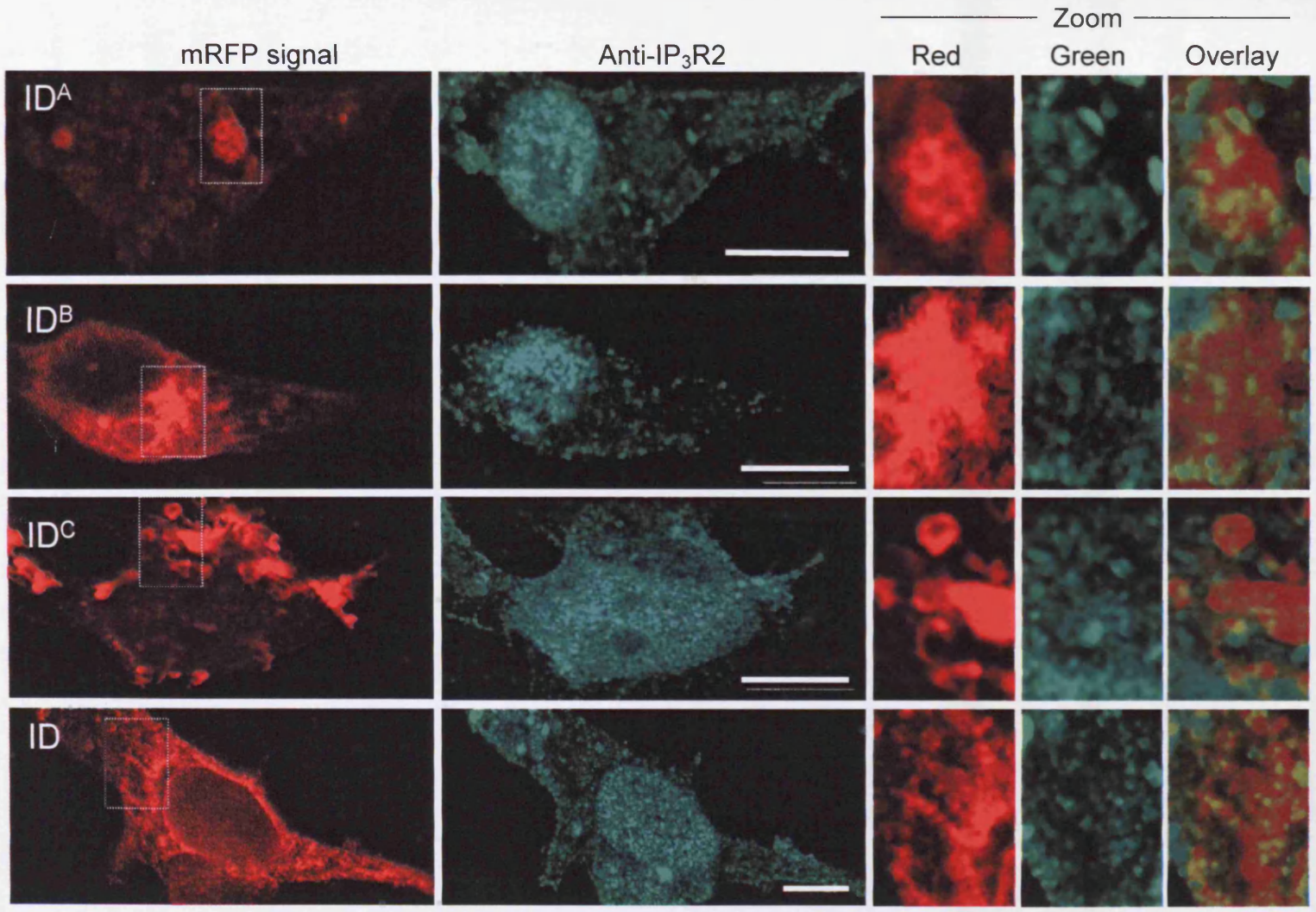

Figure 5.22. IP_3R2 does not co-localise with I-domain fragments

Confocal images of IP_3R2 in cells two days post-transfection. Expression was predominantly observed in the nucleus. Right panels display boxed 'zoomed-in' region in individual red and green channels, and the overlay of both channels. Scale bar is 10μm. Number of cells analysed: ID, 28; ID^A, 33; ID^B, 49; ID^C, 28.

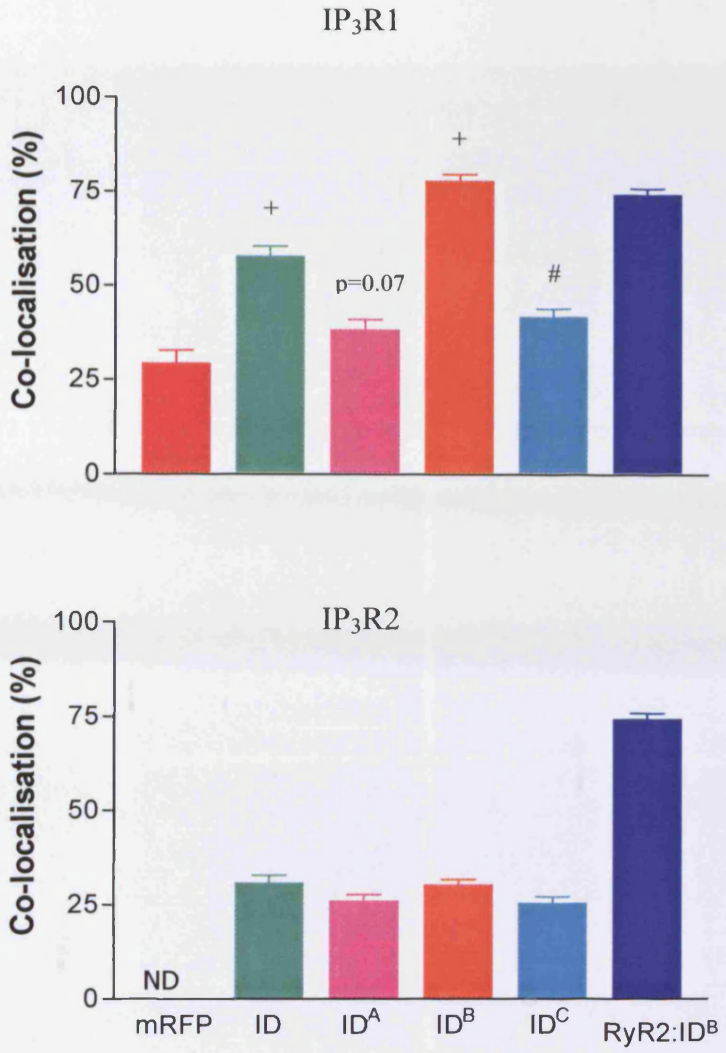

Figure 5.23. I-domain and IP_3R type 1 and type 2 co-localisation

IP_3R type 1 (top panel) and 2 (bottom panel) co-localisation with mRFP and I-domain constructs. $^{\#}p<0.01$ and $^{+}p<0.001$ compared to mRFP co-localisation. Blue bar represents RyR2:ID^B co-localisation.

5.3.4.3. ID^B downregulates IP_3R type 1, but not type 2 – a cellular analysis

The trend toward reduced levels of IP_3R1 in cell populations following I-domain expression (Figure 5.19) was more pronounced at the single cell level using immunofluorescence analysis. In single cells, the levels of IP_3R type-1 were inversely proportional to ID^B expression levels (Figure 5.24). In contrast, mRFP expression had no effect on cellular levels of IP_3R1 expression (Figures 5.19 and 5.24), and likewise ID^B did not alter IP_3R2 expression (Figure 5.24).

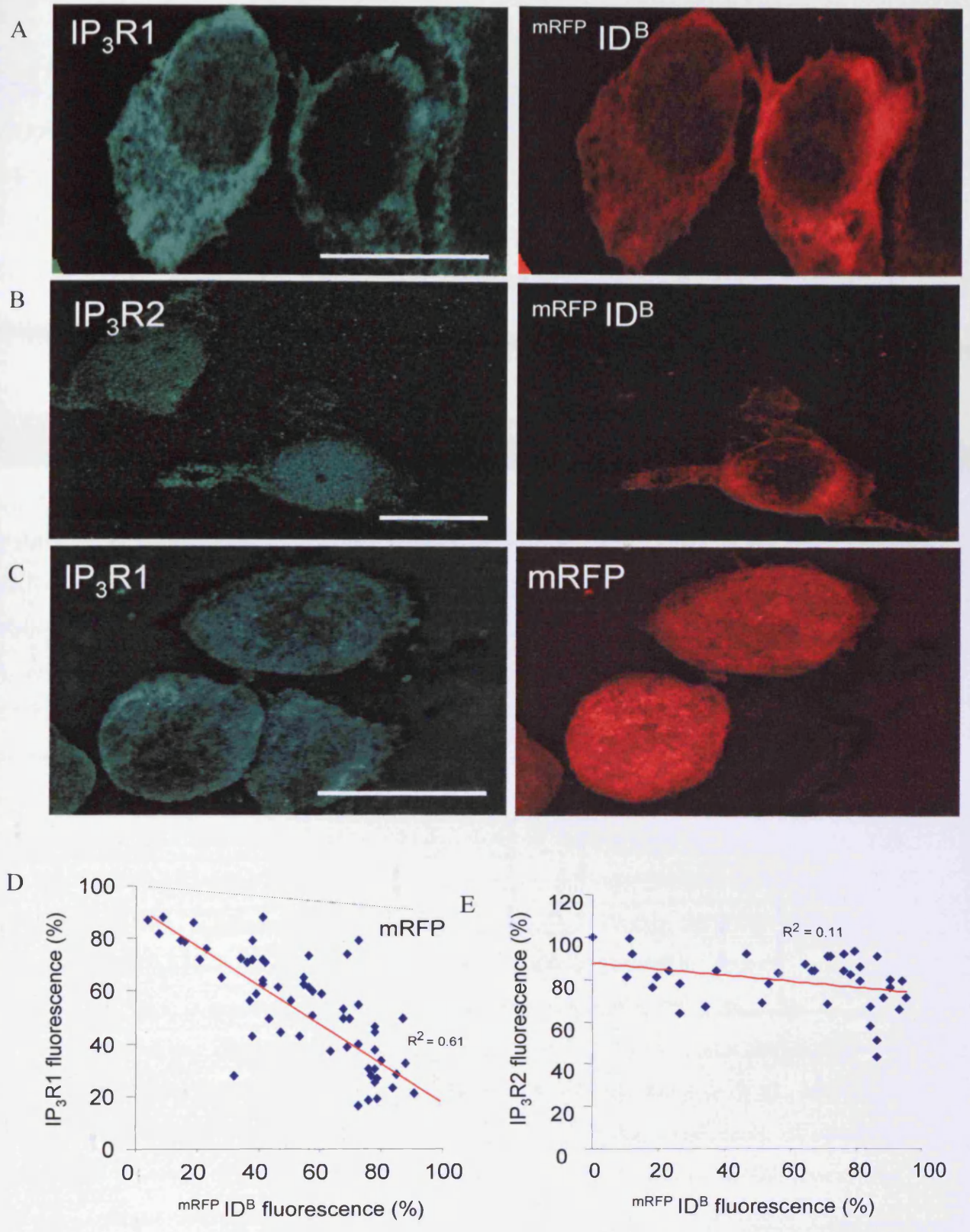

Figure 5.24. ID^B expression is associated with the downregulation of IP_3R1 in single cells

Relative fluorescence of $^{mRFP}ID^B$ with antibody-labelled (fluorescein) IP_3R1 **(A)** and IP_3R2 **(B)**, and cells expressing mRFP with IP_3R1 **(C)**. Scatter plot of endogenous IP_3R1 **(D)** and IP_3R2 expression **(E)** against recombinant ID^B expression. Trendline for IP_3R1 in cells transfected with mRFP is shown in **D**. In D and E each data point represents one cell (IP_3R1, n=61; IP_3R2 n=39). Scale bar is 20μm.

5.4. Discussion

Chapters 3 and 4 provided evidence that I-domain expression was detrimental to cell phenotype and was not compatible with cell viability. The present chapter extended these findings, and explored the basis of these findings in the context of cellular Ca^{2+} handling using confocal microscopy.

5.4.1. I-domain expression alters intracellular Ca^{2+} handling

The complex interplay of Ca^{2+} signals from IP_3R and mitochondria are fundamental to the control of cell survival and cell death pathways, and altered resting $[Ca^{2+}]_i$ or ER Ca^{2+} can upset Ca^{2+} homeostasis. This chapter revealed that I-domain expression was associated with a lower ER Ca^{2+} load, however this was not substantiated by altered expression of IP_3R1, IP_3R2 or SERCA (Figures 5.12, 5.19 and 5.24). Significance for lower expression of IP_3R1 could potentially be gained upon increasing n numbers, however time limitations precluded these further experiments. In addition, with regard to IP_3R2 immunoblot analysis, it should also be noted that no assessment could be made from an n of 1. Conceptually, lower ER Ca^{2+} content in combination with unaltered calreticulin expression would diminish the Ca^{2+} available for carbachol-induced release. In addition, reduced agonist responses in some I-domain cells (see Figures 5.14 and 5.17 for lack of clear trend) could be attributable to inhibition of IP_3R activity by depleted ER stores (Figure 5.12). Also, a possible explanation for these findings may involve caspase-3 degradation. Activation of caspase-3 during apoptosis induces the specific cleavage of IP_3R1 by binding to a conserved site at a.a.1888-1891 (Assefa *et al.*, 2004). IP_3R1 cleavage is reported to cause continual Ca^{2+} leak from ER stores thus elevating $[Ca^{2+}]_i$ (Nakayama et al., 2004). In addition, IP_3 binding to IP_3R type 1 was demonstrated to result in the ubiquitination and degradation of the receptor (Wojcikiewicz et al., 1994; Zhu and Wojcikiewicz, 2000). Furthermore, the IP_3R1 isoform is also sensitive to extracellular ATP activation whereas IP_3R2 is unaffected (Miyakawa *et al.*, 1999), which could also promote Ca^{2+} release through uncleaved IP_3R1 channels. Trump and colleagues suggested that elevated $[Ca^{2+}]_i$ preceded apoptotic and necrotic events (Trump and Berezesky, 1996; Trump *et al.*, 1997). In line with this, other laboratories demonstrated that prolonged elevation of $[Ca^{2+}]_i$ as a result of persistent intracellular store depletion triggered apoptosis (Jiang *et al.*, 1994; Szalai *et al.*, 1999; Hajnoczky *et al.*, 2000; Demaurex and Distelhorst, 2003; Cardozo *et al.*, 2005). Nevertheless, although $[Ca^{2+}]_i$ was relatively high in I-domain expressing cells

(Figure 5.11), this was also observed in cells transfected with mRFP, in which levels of apoptosis were not significantly different from WT HEK. Therefore the data suggests that the presence of elevated Ca^{2+} may not be a determinant of whether a cell undergoes apoptosis or not.

The findings of this chapter indicate that I-domain expression triggered programmed cell death by interference or disruption of intracellular Ca^{2+} homeostasis. Some I-domain constructs reduced IP_3R agonist responses, however, no clear trend emerged. For example, ID^B expression did not alter peak height, rate up or rate of transient decay, yet cellular expression was still associated with lower ER Ca^{2+} (Figure 5.12) and reduced cell viability (Figure 3.21). Although ID^B expression did not affect agonist-induced responses it did alter Ca^{2+} handling, and these findings indicate that the associated cytotoxicity may be due to altered basal Ca^{2+} signals (signal variability). Chapter 6 explores the possibility that it is the precise way in which Ca^{2+} levels are perturbed that may underlie the phenotypic observations described in this thesis.

Despite the data above showing that I-domain expression was linked to elevated levels of apoptosis, the possibility that I-domain expression could have resulted in the activation of anti-apoptotic pathways cannot be ruled out. The anti-apoptotic protein Bcl-2 lowers $[Ca^{2+}]_i$ in response to apoptotic stimuli, either by decreasing ER Ca^{2+} to reduce the magnitude of Ca^{2+} release or by inhibition of IP_3R opening. These effects are concentration dependent; low levels are protective, whereas high levels can induce organelle fragmentation and cause cell death through Ca^{2+} and ROS dependent pathways (Hanson *et al.*, 2008a; Hanson *et al.*, 2008b). Although it is possible that altered levels of Bcl-2 following I-domain expression could upset cellular Ca^{2+} balance and alter cell sensitivity to apoptosis, Bcl-2 expression has not been determined in this project. Nevertheless, the data presented in this chapter suggests that the activation of pro-apoptotic pathways exceeds the triggering of anti-apoptotic mechanisms.

Boehning and others demonstrated the inhibition of apoptosis via disruption of cytochrome C and IP_3R interaction using a peptide targeting the cytochrome C binding site in IP_3R C-terminus (2621-2636) (Boehning *et al.*, 2005). Interestingly ten amino acids of this sequence share a 60% and 70% identity with C-terminal regions (at a locus 300 amino acids upstream of the I-domain) in rat and human RyR2 and rat RyR1 respectively. However, previous studies have suggested an interaction between residues within the I-domain and C-terminal

tail regions of RyR2 (Hamada *et al.*, 2007b) and the schematic model of RyR2 conformation (Figure 3.6) suggests how such an interaction is feasible. A recent study revealed that the addition of synthetic prion (disease-inducing protein) peptides to cells depleted ER Ca^{2+} via IP_3R and RyR, which raised $[Ca^{2+}]_i$. Elevated cytosolic Ca^{2+} triggered apoptosis, which was associated with depleted GSH and an increase in free radicals (Ferreiro *et al.*, 2008). In addition to RyR and IP_3R, recent research has suggested the existence of a novel intracellular Ca^{2+}-release channel that is sensitive to NAADP activation, and is widely distributed on intracellular organelles including the ER (Mandi and Bak, 2008). This novel finding suggests an even greater plasticity of the Ca^{2+} signalosome and could provide an alternative but as yet unexplored Ca^{2+}-dependent route of cell death following I-domain expression.

5.4.2. Expression of recombinant I-domain revealed NUC death via the 'bystander effect'

Data in this chapter demonstrated a lack of correlation between NUC distance from transfected cells and the relative agonist-induced response (Figure 5.15). This was consistent with increased levels of apoptosis observed in NUCs that were not physically coupled to I-domain expressing cells (Figure 4.5). Both these observations suggest that the NUC phenotype is not induced by cell-to-cell contact, but more likely it is due to a freely diffusible signalling molecule. The concept that I-domain expression alters transcellular communication via diffusible effectors forms the basis of Chapter 7.

Chapter 6

Chapter 6 Exploring the subtleties of intracellular Ca^{2+} handling – assessment of Ca^{2+} signal variability

6.1. Introduction

Chapter 5 indicated that Ca^{2+} handling characteristics in cells expressing recombinant I-domain were altered, however analysis of carbachol-induced transients failed to reveal any clear pattern that could be linked to apoptosis. George *et al.* showed previously that cytotoxicity was invoked by abnormal ER-to-cytoplasmic Ca^{2+} fluxes in the absence of persistently elevated $[Ca^{2+}]_i$ (George *et al.*, 2003b). This chapter focuses on the precise dissection of basal cellular Ca^{2+} signals to provide clues as to the specific perturbations in Ca^{2+} signalling that may underpin I-domain linked cytotoxicity.

6.1.1. Assessment of cellular Ca^{2+} handling

The spatio-temporal nature of Ca^{2+} signals is a fundamental aspect of cellular signalling, and subtle changes in Ca^{2+} coding determine cellular functions and promotion of cell survival or death pathways (Jiang *et al.*, 1994; Lipp and Niggli, 1996; Petersen and Burdakova, 2002). Therefore, decoding the amplitude and temporal variability in cellular Ca^{2+} handling can provide clues into cell health and normal function, and as such has become a useful tool in the diagnosis of pathological perturbations in Ca^{2+} signals (George *et al.*, 2003b; George *et al.*, 2007; Shuba Ia, 2007).

An extraordinary feature of Ca^{2+} signalling is the way in which Ca^{2+} is able to exert this control on diverse processes simultaneously within the same cell. Localised or elementary Ca^{2+} events arise by either Ca^{2+} release from intracellular stores or via influx of extracellular Ca^{2+}, which controls cell processes such as cell division, mitochondrial metabolism and vesicle secretion whereas co-ordinated intracellular Ca^{2+} release via IP_3R triggers a global intracellular Ca^{2+} wave that controls gene

transcription and cell proliferation (see Figure 6.1). Elementary or global Ca^{2+} events can control these processes either by spontaneous Ca^{2+} transients, or by repetitive Ca^{2+} signals, referred to as Ca^{2+} oscillations.

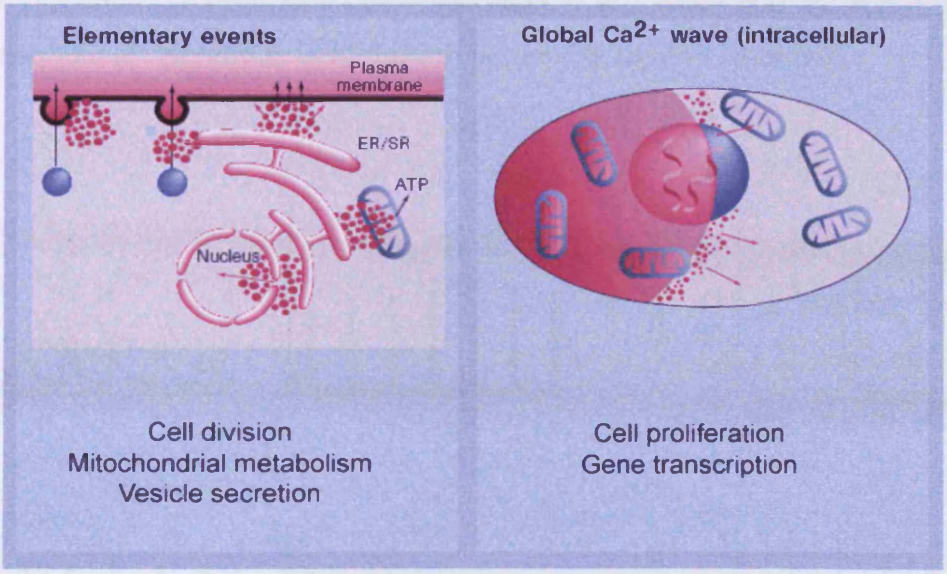

Figure 6.1. Versatility of Ca^{2+} signalling

Differential regulation of Ca^{2+} underpins a range of cellular processes, either via specific delivery of elementary Ca^{2+} events or co-ordinated recruitment of elementary events resulting in a Ca^{2+} wave.

Adapted from Berridge *et al.*, 1998

Various different temporal patterns of Ca^{2+} oscillations have been reported, each dictating a precise cell function or process. These include regular peaks (termed 'spiking'), low and high peak oscillations, and periodic/chaotic signals (termed 'bursting') (Schuster *et al.*, 2002) (Figure 6.2). Ca^{2+} oscillations can convey different signals depending on their frequency and amplitude (Dolmetsch *et al.*, 1997; Dolmetsch *et al.*, 1998). Furthermore, Schuster *et al.* demonstrated in a theoretical model that controlling specific temporal dynamics of Ca^{2+} signalling could independently regulate two proteins involved in distinct cellular processes (Schuster *et al.*, 2005).

George and colleagues demonstrated that decoding of spatio-temporal intracellular Ca^{2+} signals provided invaluable insights into pathologies that arise as a result of dysfunctional Ca^{2+} cycling (George *et al.*, 2003b; George *et al.*, 2006; George *et al.*, 2007), which has since been demonstrated by other studies (Uhlen, 2004; Weisleder

and Ma, 2006; Bray *et al.*, 2007; Colella *et al.*, 2008). A number of methods exist to enable a more informed understanding of cellular Ca^{2+} handling and to permit exquisite decoding and quantification of Ca^{2+} signals (Wood and Cadusch, 2005; George *et al.*, 2006; George *et al.*, 2007; Colella *et al.*, 2008) and the application of these mathematical operations to biological systems is rapidly emerging.

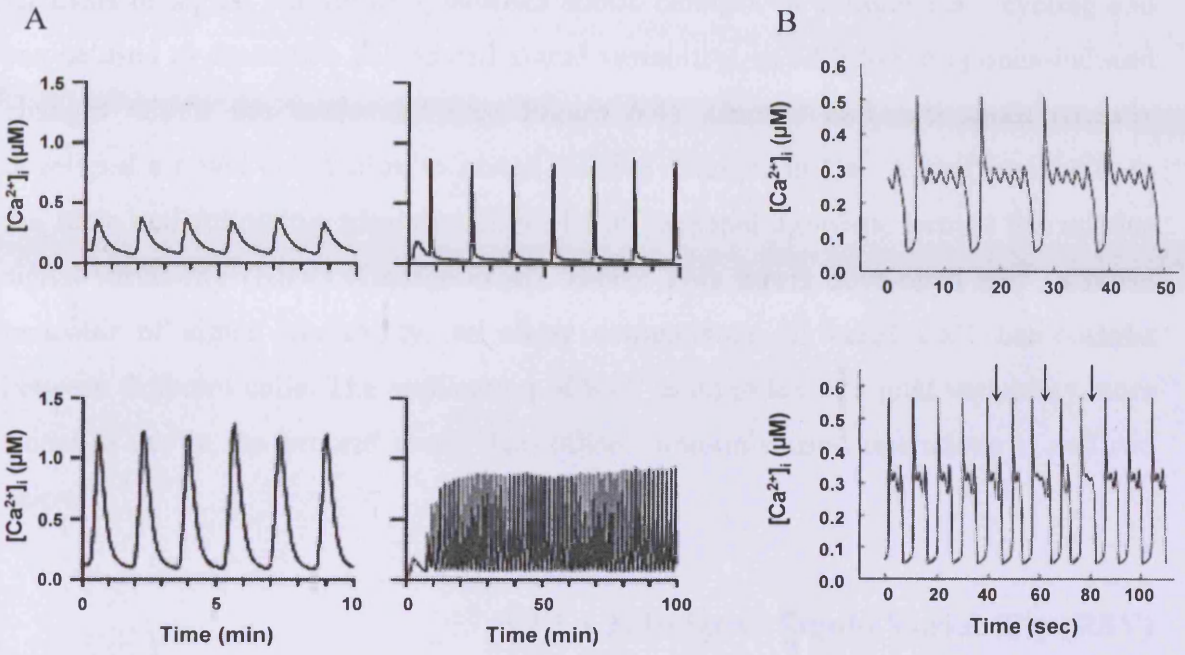

Figure 6.2. Variability in Ca^{2+} signals

A. Ca^{2+} oscillations in the form of regular peaks ('spiking'), varying in amplitude and temporal dynamics. Slower oscillations such as those in the top left panel control cell proliferation, whereas rapid oscillations (bottom right panel) control gene transcription (Dolmetsch *et al.*, 1998). **B.** Ca^{2+} signals in high and low peak oscillations (top panel), and periodic or chaotic signals (bottom panel), referred to as 'bursting' (Schuster *et al.*, 2002). Note the irregular oscillations (arrows).
Data from Dolmetsch *et al.*, 1998, and Schuster *et al.*, 2002.

6.1.2. Objective

The present chapter elucidates the precise nature of Ca^{2+} signal variability in cells expressing recombinant I-domain fragments. In view of the extremely high toxicity associated with the expression of ID and ID^{C} (Figures 5.14 and 5.17), this chapter focuses exclusively on the effect of ID^{B} expression on basal cellular Ca^{2+} handling.

6.2. Methods

6.2.1. Analysis of temporal Ca^{2+} cycling

6.2.1.1. Quantification of Ca^{2+} signal variability

Analysis of signal variability quantifies subtle changes in cellular Ca^{2+} cycling and can be used to determine cell-to-cell signal variability, in addition to agonist-induced changes within the same cell (see Figure 6.4). George and colleagues recently developed a novel calculation to assess relative changes in Ca^{2+} signal variability in the same cell following administration of Ca^{2+} channel agonists, termed the relative signal variability (RSV) (George *et al.*, 2006). This thesis developed SV^m, a novel indicator of signal variability, to allow comparisons in basal Ca^{2+} homeostasis between different cells. The application of SV^m as an index of signal variability more suited to use in the present study than other commonly used operations is outlined below.

6.2.1.1.1. Relative Signal Variability (RSV)

RSV is calculated by comparing the sum of point-to-point differences in Ca^{2+} signals following cellular activation (i.e. by Ca^{2+} agonists) to pre-activation signals **in the same trace** (George *et al.*, 2006). Figure 6.3 displays the definition of signal variability (SV). SV can also be used to compare point-to-point variations in the intensity values of Ca^{2+} signals between traces from separate experiments, provided that they are normalised to mean fluorescence. Therefore, the RSV was used for analysis of agonist-induced transients where $RSV= (SV_B-SV_A)/SV_A*100$, where SV_B and SV_A are post- and pre- agonist signal variabilities, respectively (Figure 6.4A). In this thesis, the analysis of Ca^{2+} traces between **different** non-stimulated cells was performed using signal variability (SV) normalised to mean fluorescence (SV^m), Figure 6.4B.

For a set of k intensity values; $x_1, x_2, x_3 \ldots\ldots x_k$

$$SV= \sum_{n=1}^{n=k-1} | (x_{n+1} - x_n) |$$

Figure 6.3. Definition of SV

SV is the sum of the moduli of the differences between successive intensity values.

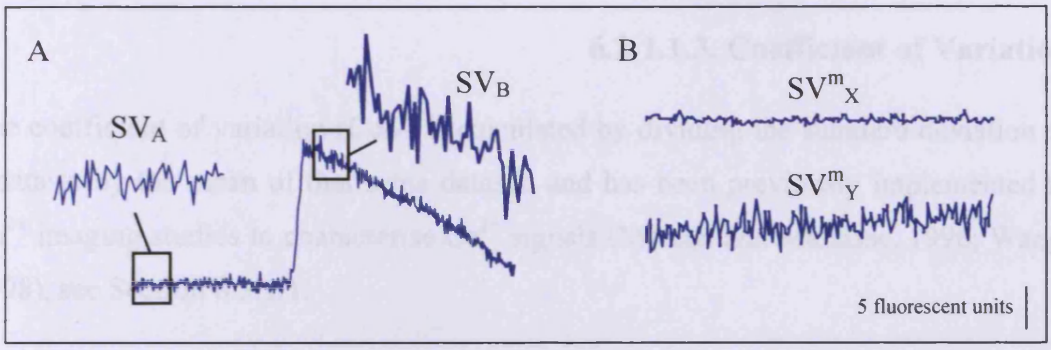

Figure 6.4. Calculation of RSV and the utility of SV^m

RSV can be used to measure the relative change in cellular Ca^{2+} handling before (SV_A) and after (SV_B) agonist administration in the same cell **(A)**, whereas SV^m compares the amplitude and temporal variation of resting Ca^{2+} in two separate cells (X and Y) normalised to their respective mean (SV^m), SV^m_X and SV^m_Y **(B)**. SV = signal variability.

The rather limited utility of some commonly used indices of signal variability are clearly demonstrated in Section 6.3.1.1, and their calculations are summarised below.

6.2.1.1.2. F-Ratio test

F-ratio compares the variance (the square of the standard deviation) between two discrete sets of data obtained from experimental cells (Y) (e.g. mRFP-expressing cells) to wild-type cells (X) (e.g. WT HEK cells) by means of simple division. In our experiments the variance of Ca^{2+} signals from Y cells was compared with the variance of signals from X cells.

$$\text{F-ratio} = \frac{\text{Variance of Y}}{\text{Variance of X}}$$

The F-ratio is generally used on log transformed data and has been implemented to measure Ca^{2+} signal variability previously within our laboratory (George *et al.*, 2006). See Section 6.3.1.1.

6.2.1.1.3. Coefficient of Variation

The coefficient of variation (CoV) is calculated by dividing the standard deviation of a dataset by the mean of that same dataset, and has been previously implemented in Ca^{2+} imaging studies to characterise Ca^{2+} signals (Mercan and Malaisse, 1996; Wang, 1998), see Section 6.3.1.1.

$$CoV = \frac{\text{Standard deviation}}{\text{Mean}}$$

6.2.2. Ca^{2+} signal variability in RyR2:ID^B expressing HEK cells

SV^m of cells expressing RyR2 and RyR2:ID^B was determined as described in Section 6.3.1.1. Caffeine was used to evoke Ca^{2+} release via recombinant RyR2 through a mechanism that increases the Ca^{2+} sensitivity of the channel (see Section 1.1.3.3). SV^m of basal Ca^{2+} signal variability and RSV of pre- and post- caffeine addition Ca^{2+} signals were assessed. Caffeine (10mM dissolved in unsupplemented DMEM) was applied during Ca^{2+} imaging experiments to HEK cells expressing RyR2, and cells co-expressing RyR2:ID^B. Data was acquired as described in Section 2.2.8.3.

6.3. Results

6.3.1. Assessment and determination of Ca^{2+} signal variability

6.3.1.1. Why variance-based methods cannot be used to decode intracellular Ca^{2+} signal variability in these experiments

Analysis of variability in Ca^{2+} signals can be used to determine the amplitude and spatiotemporal aspects of Ca^{2+} signalling in single cells. Methods of analysis used to monitor cellular Ca^{2+} signalling comprise relative signal variability (RSV), F-ratio and coefficient of variation (CoV) (Smith *et al.*, 1998; Wang, 1998; George *et al.*, 2006; George *et al.*, 2007). As described above, there is not a *single* method that represents the best tool for studying dysfunctional Ca^{2+} signalling under non-stimulated conditions.

In keeping with standard statistical and mathematical operations, initial assessment of Ca^{2+} signal variability was performed using both standard deviation and variance. The analysis revealed a striking and expected correlation between signal variability and relative fluorescence intensity (Figure 6.6A and B) that was partly negated by normalisation, either by considering the mean value (CoV) or by log transforming the data (Figure 6.6C and D). However, neither is ideal. This is particularly evident when considering the relationship between both CoV and log variance with 'drift' or gradient (dF/dT) in the acquired fluorescent signal (Figure 6.7). Despite only a very small change in dF/dT (<0.04), it precluded analysis using CoV or on log transformed data. Since small gradients in the fluorescence signal is frequently observed in CLSM experiments (see Figure 6.5), and it was crucial to choose a method of analysis that was not compromised by such 'drift'. Therefore two options presented themselves: either to set a threshold of gradient above which data would be eliminated, or to identify a more robust method for assessing Ca^{2+} signal variability. Elimination of data would have sacrificed a large number of data points and hence was ruled out, stipulating the need for a new analytical tool.

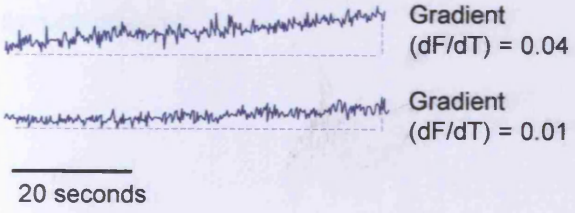

Figure 6.5. Example Ca^{2+} traces displaying 'drift' or gradient (dF/dT)

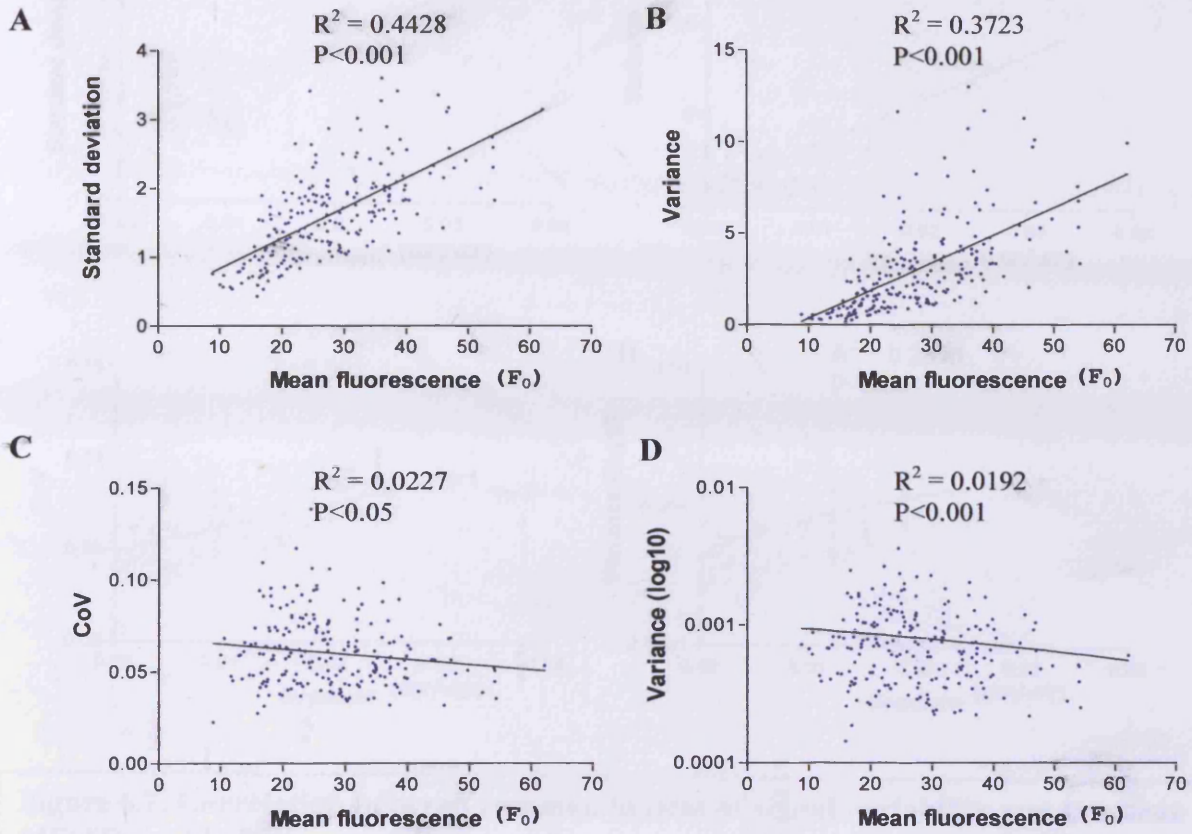

Figure 6.6. Correlation between commonly used operations and fluorescence signals

Increased basal fluorescence was associated with enhanced variability, determined by standard deviation **(A)** and variance **(B)**. This marked positive correlation was reduced by normalising standard deviation to relative resting fluorescence (i.e. deriving CoV), and log transforming the data prior to calculating the variance, **(C)** and **(D)** respectively.

The F-ratio has been previously implemented in analysis of Ca^{2+} signal variability to quantitatively compare the variance of Ca^{2+} traces under non-stimulated conditions. However, in light of its dependence on variance, which is somewhat proportional to the 'drift' in the experimental data, it was not suitable for analysis of the data presented here.

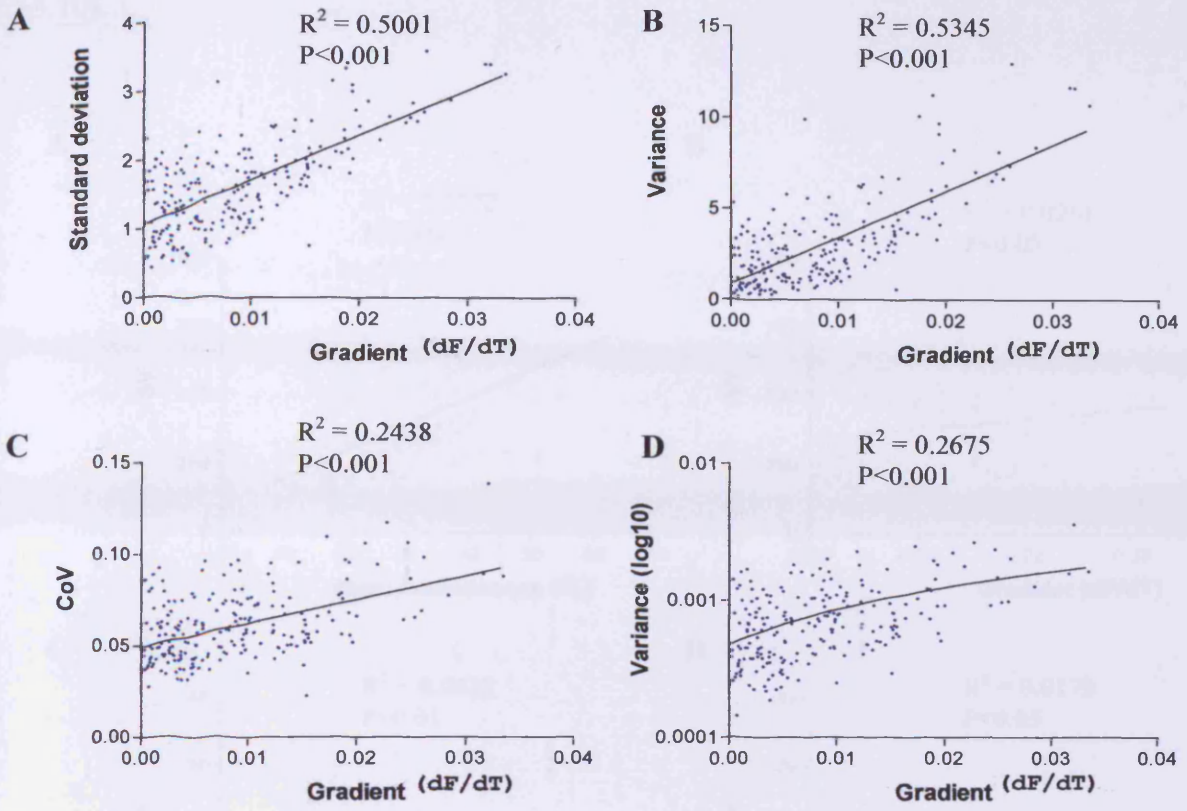

Figure 6.7. Correlation between common indices of signal variability and gradient (dF/dT), or 'drift'

Gradient in the fluorescent signal was associated with an increase in variability, determined by standard deviation **(A)**, variance **(B)**, CoV **(C)** and log transformed variance **(D)**.

George and colleagues previously identified the RSV as a tool to measure relative changes in signal variability induced by agonist administration. The RSV compares the sum of point-to-point changes between pre- and post-agonist events (described in Section 6.2.1.1.1) and is independent of gradient. Consequently, RSV can be applied where F-ratio, standard deviation and CoV cannot. However, SV is significantly influenced by basal fluorescence (Figure 6.8A), hence required normalisation to relative fluorescence. SV^m displayed little relationship with fluorescence or gradient (Figure 6.8C and D) and was subsequently determined to be the most suitable parameter to assess basal cellular Ca^{2+} handling as it negated the need to eliminate data due to fluorescence-dependent gradient. It is important to re-emphasise that although fluorescence is affected by voltage, as discussed in Section 5.2.3 this does

not apply to the data presented in this thesis due to voltage limited to <750V (Figure 5.10).

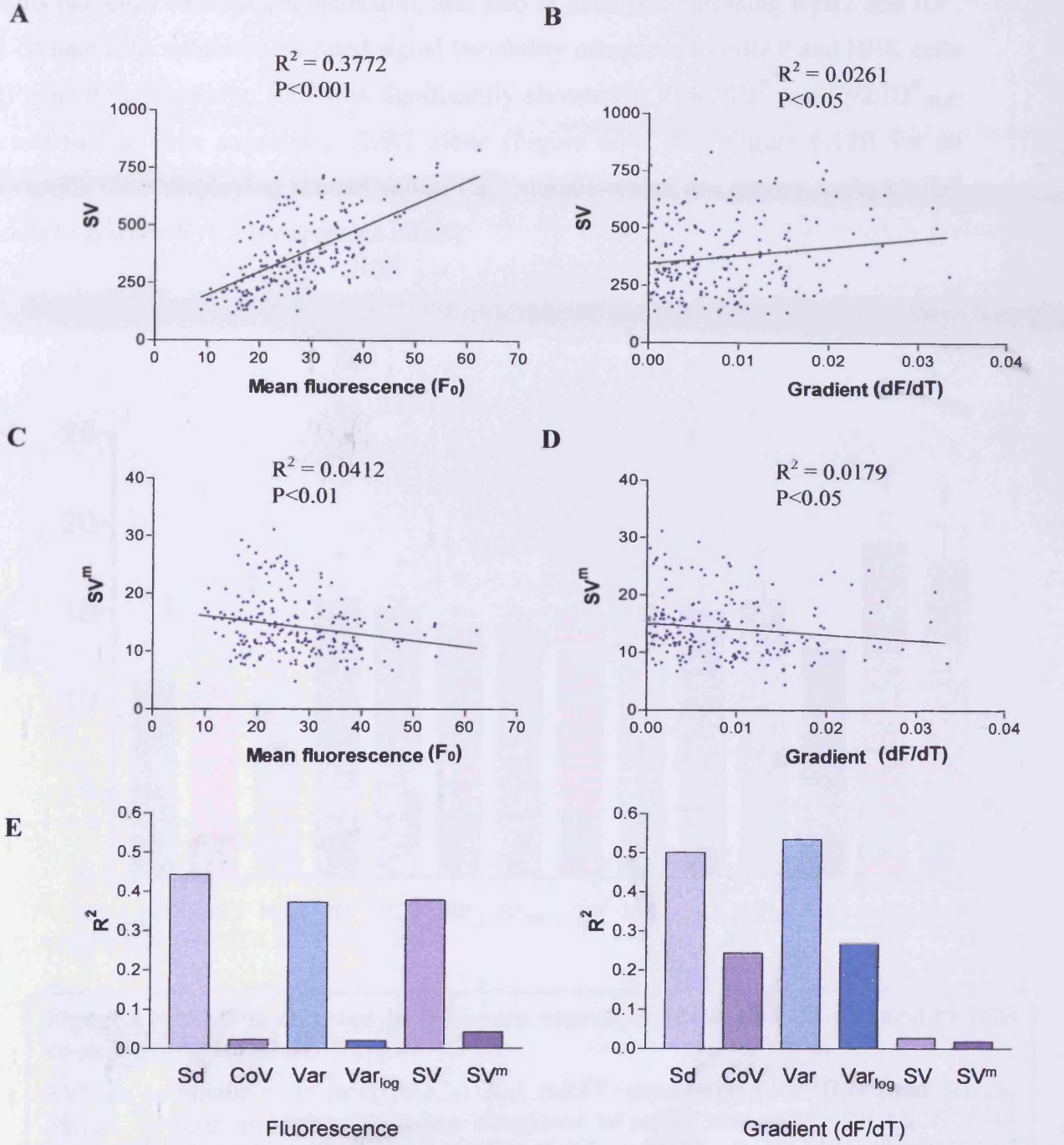

Figure 6.8. Signal variability (SV) divided by mean fluorescence (SV^m) is independent of fluorescence and gradient (dF/dT)

Scatter plots of data obtained from HEK cells (n=221) showing the relationship between SV with mean fluorescence **(A)** and gradient **(B)**, and the normalised SV obtained by dividing SV by mean fluorescence (SV^m), against mean fluorescence **(C)** and gradient **(D)**. **E** displays the R^2 values of all parameters analysed against fluorescence (left panel) and gradient (right panel). Sd=standard deviation; CoV=coefficient of variation; Var=variance; Var_{log}=log of variance.

6.3.2. Elevated SV^m was exhibited by I-domain expressing cells

SV^m was implemented to assess basal Ca^{2+} signal variability in mRFP and I-domain cells two days following transfection, and also in cells co-expressing RyR2 and ID^B. I-domain cells exhibited elevated signal variability compared to mRFP and HEK cells (Figure 6.9). Similarly, SV^m was significantly elevated in RyR2:ID^B and Ry2:$ID^B{}_{NUC}$ compared to cells expressing RyR2 alone (Figure 6.9). (See Figure 6.12B for an example trace displaying pre-activation Ca^{2+} signals which are greater in RyR2:ID^B cells than when RyR2 is expressed alone).

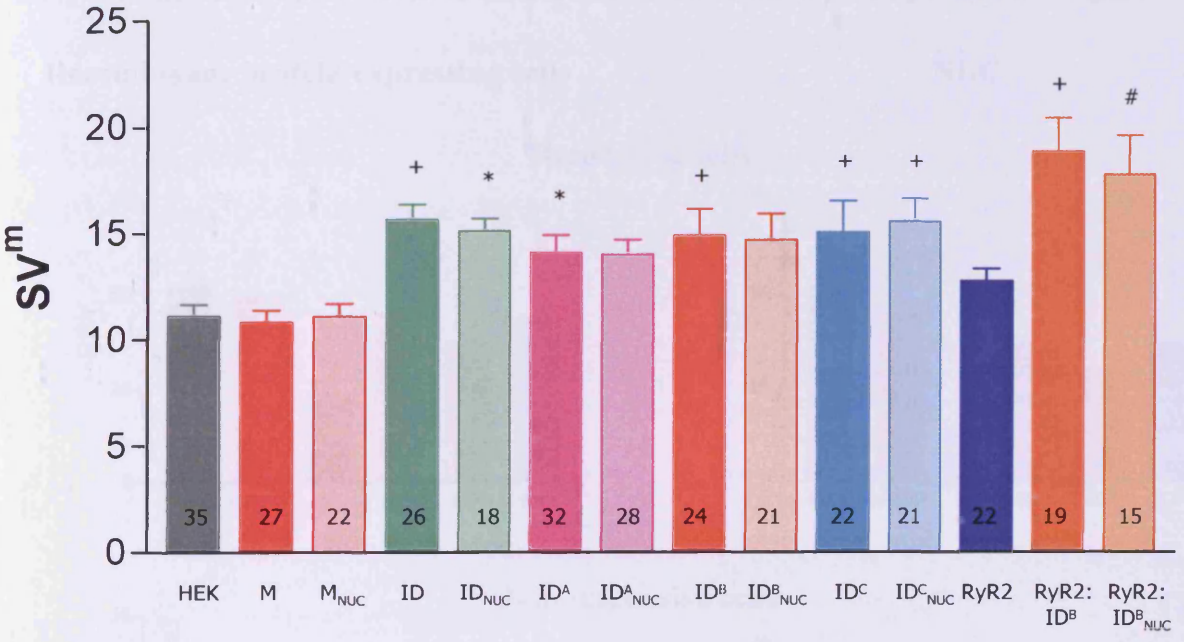

Figure 6.9. SV^m is elevated in I-domain expressing cells and NUCs, and in cells co-expressing RyR2:ID^B

SV^m in I-domain cells (and NUCs) and mRFP expressing cells (M) (and NUCs, M_{NUC}). $^*p<0.05$ and $^+p<0.001$ when compared to mRFP and mRFP NUCs. SV^m of RyR2:ID^B expressing cells is compared to those expressing RyR2 alone, $^\#p<0.01$ and $^+p<0.001$. Number of coverslips analysed are given in each bar.

6.3.3. ID expression suppressed IP_3R-dependent post-activational Ca^{2+} signal variability

Following the results of Chapter 5, carbachol-induced Ca^{2+} transients were analysed for pre- and post-activational signal variability. The relative signal variability (RSV), as detailed above, is a valuable tool for assessing alterations in post-activational Ca^{2+} signals. The RSV was calculated in cells that either did or did not exhibit transient Ca^{2+} release in response to 1mM carbachol (responsive and non-responsive cells, respectively) (see Figure 5.14). The RSV of responsive ID expressing cells and ID NUCs (but no other I-domain fragment) was significantly lower than that of mRFP and mRFP NUCs respectively ($p<0.05$) (Figure 6.10). In addition, the RSV in non-responding cells was not significantly different between any of the constructs (Figure 6.10). Therefore it is reasonable to conclude that the relative post-agonist Ca^{2+} signals

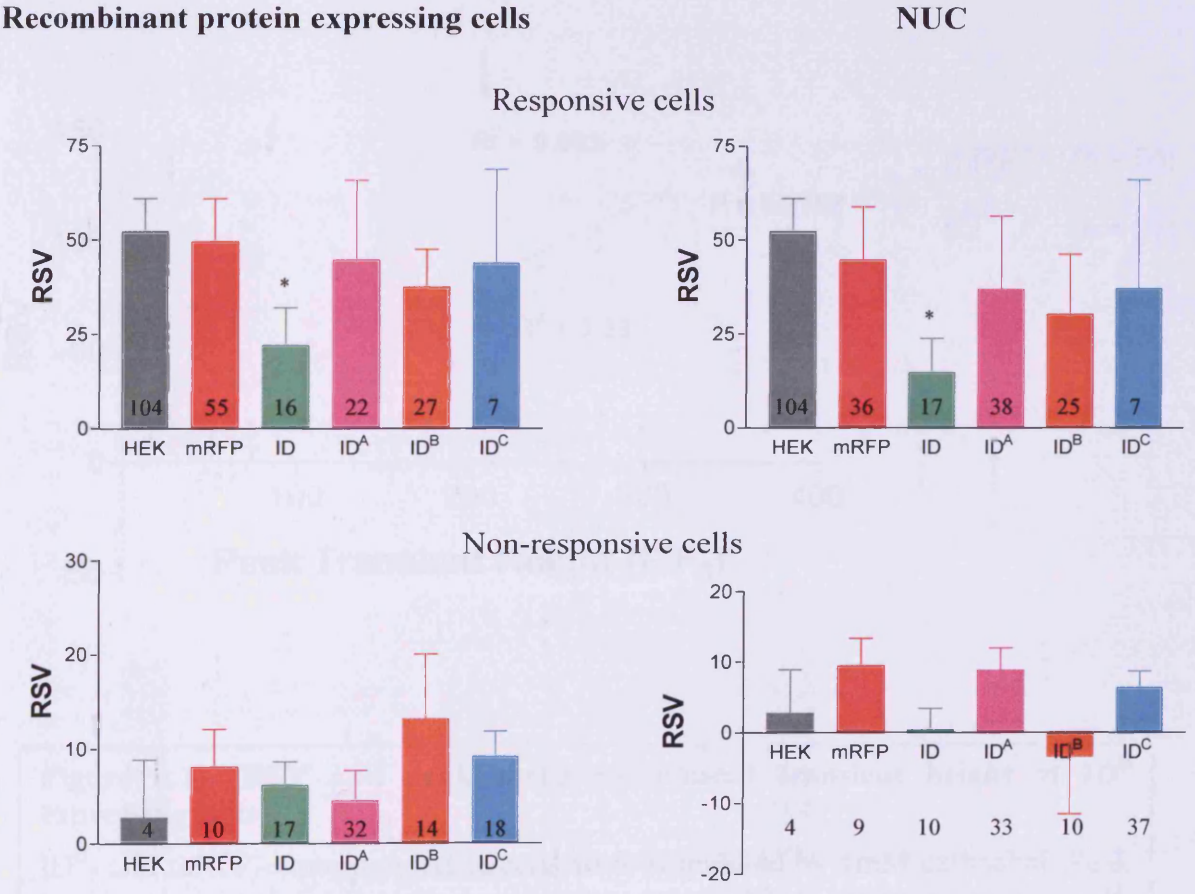

Figure 6.10. RSV of carbachol-induced Ca^{2+} release (1mM) in I-domain expressing HEK cells and NUCs

RSV of agonist-induced responses of HEK, mRFP and I-domain expressing cells and NUCs. Top panels represent the RSV of responsive cells, lower panels represent non-responsive cell RSV. $^{*}p<0.05$ compared to mRFP expressing cells or $mRFP_{NUC}$. Data is plotted as mean±SEM. Cell number data acquired from is displayed in the bars.

in cells were largely unaffected by I-domain transfection, which is consistent with Figures 6.11 and 6.13. Moreover, the data suggests that RSV is not a determinant of whether a cell responds to agonist or not.

6.3.4. ID^B does not alter carbachol-evoked responses in HEK cells

Carbachol-evoked Ca^{2+} signals were largely unaffected by ID^B expression as shown in Figure 6.10 (also see Chapter 5). These findings are confirmed by the similar correlations between agonist-induced transient height and relative post-agonist signal variability when compared to mRFP cells (Figure 6.11).

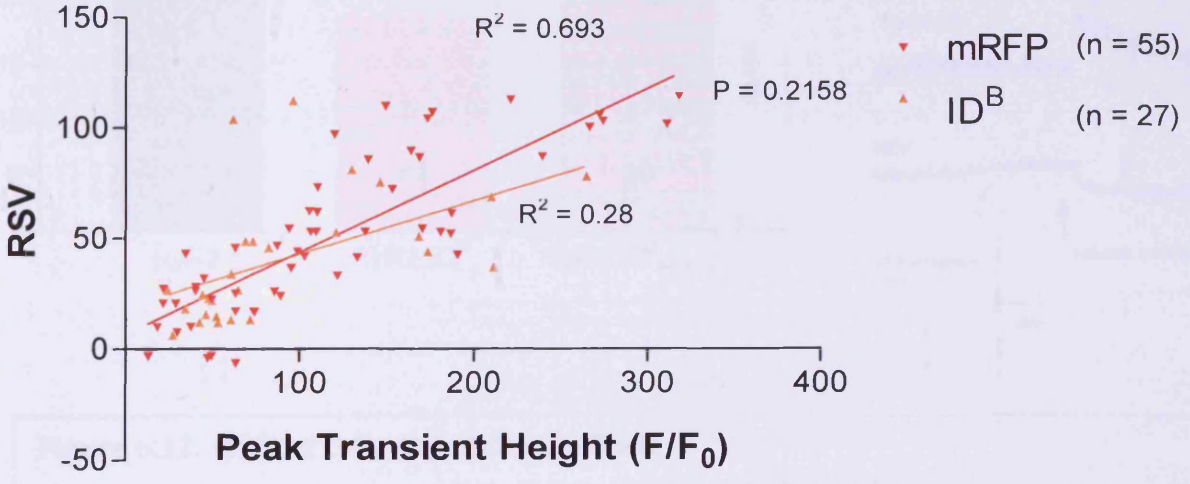

Figure 6.11. RSV and peak carbachol-induced transient height of ID^B expressing cells

ID^B- and mRFP-expressing HEK cells were stimulated by 1mM carbachol. Peak transient height (F/F_0) is plotted against respective RSV for every responsive cell, represented by each point.

6.3.5. ID^B does not modulate post-activational RyR2 Ca^{2+} signalling

Following exposure to 10mM caffeine, RyR2:ID^B co-expressing cells were analysed for agonist-induced responses using RSV (as discussed in Section 6.2.1.1.1). The RSV in RyR2, RyR2:ID^B and RyR2:ID^B_{NUC} cells did not reveal an effect of ID^B on RyR2 (Figure 6.12A). Representative traces of RyR2 and RyR2:ID^B are displayed in Figure 6.12B, note the greater signal variability both before and after caffeine addition.

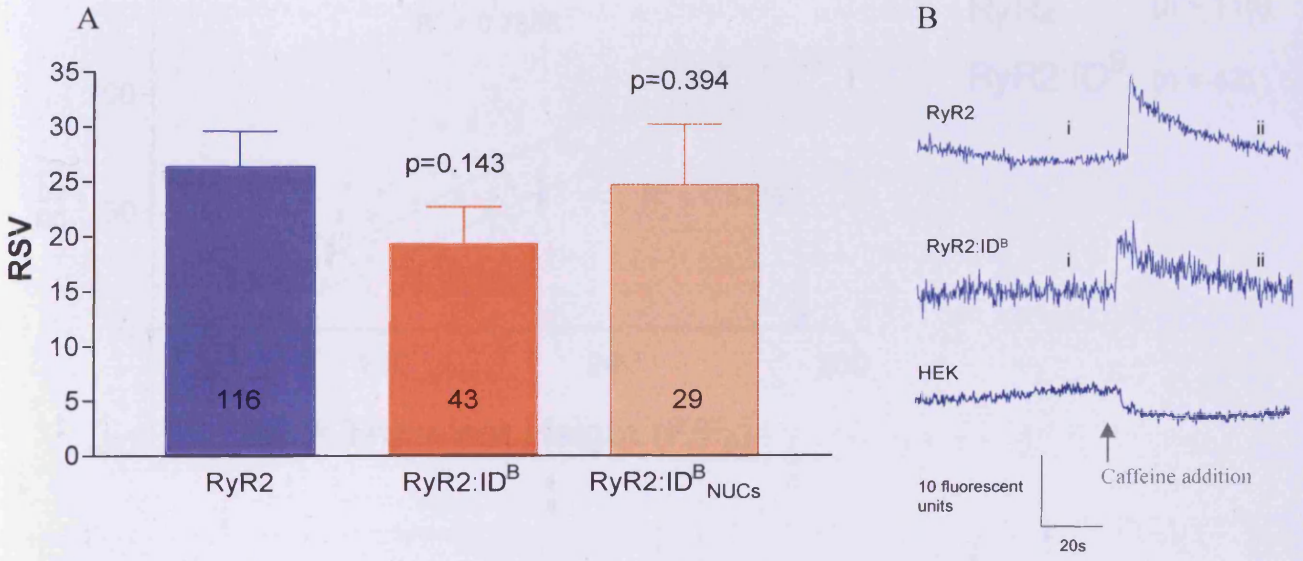

Figure 6.12. RSV of cells exposed to caffeine

A. The RSV for cells expressing RyR2 alone or RyR2:ID^B following exposure to 10mM caffeine was calculated. Data is plotted as mean±SEM ($p>0.05$). The number in each bar represents number of cells, and was obtained from 22 coverslips of RyR2, 19 coverslips of RyR2:ID^B and 15 coverslips of RyR2:ID^B_{NUC}. **B.** Representative traces of RyR2, RyR2:ID^B and HEK cells exposed to 10mM caffeine. HEK cell Ca^{2+} trace displays that HEK are not responsive to caffeine.

RSV was also assessed in relation to peak Ca^{2+} transient height induced by caffeine (similar to analysis with carbachol, Figure 6.11). RSV of both RyR2:ID^B and RyR2 alone was similarly proportional to peak transient height (F/F_0) (Figure 6.13), suggesting that ID^B did not alter caffeine-evoked signalling via RyR2. This data is consistent with the effect of ID^B on IP_3R-mediated signalling (Figure 6.10 and 6.11).

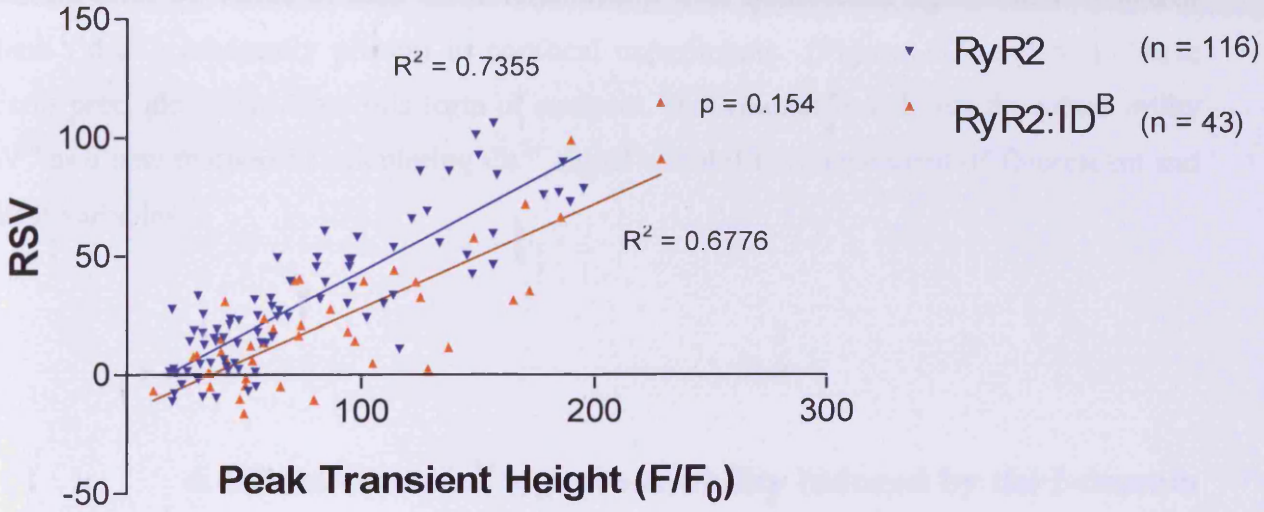

Figure 6.13. ID^B does not alter caffeine-induced RSV in HEK cells

RyR2:ID^B and RyR2 co-expressing HEK cells were stimulated by 10mM caffeine administration. Peak transient height (F/F_0) is plotted against respective RSV for each responsive cell expressing either RyR2 alone or RyR2:ID^B. Each point represents data obtained from a single cell.

6.4. Discussion

6.4.1. Determination of Ca^{2+} signal variability using SV^m

In light of the findings of Chapter 5 that cellular expression of I-domain constructs, in particular ID^B, did not alter agonist-induced Ca^{2+} responses, it was necessary to decode basal intracellular Ca^{2+} signals to provide an insight into the cytotoxicity associated with I-domain expression. This project initially considered the use of (i) standard deviation, (ii) CoV and (iii) F-ratio using log-transformed variances. However, these operations would have caused significant error by virtue of their close relationship with fluorescent signal intensity and/or gradient ('drift') inherently present in confocal experiments (Figures 6.6 and 6.7). These concerns precluded them from this form of analysis. This chapter has shown the robust utility of SV^m as a new method of calculating Ca^{2+} signal variability independent of fluorescent and gradient variables.

6.4.2. Altered Ca^{2+} signal variability induced by the I-domain

Calculation of SV^m revealed a link between I-domain expression and increased Ca^{2+} signal variability compared to mRFP cells (Figure 6.9), which suggested that the I-domain induced perturbations in normal cellular Ca^{2+} cycling. SV^m was also comparable between I-domain transfected cells and NUCs (Figure 6.9), which further corroborates a distinct signalling mechanism by which transfected cells are coupled to their neighbours; this is explored more fully in Chapter 7. Altered Ca^{2+} cycling in NUCs suggests that this mechanism may be associated with Ca^{2+}-dependent pathways, however this is yet to be determined.

6.4.3. ID^B increases basal Ca^{2+} signal variability of RyR2

RyR2 studies described in this chapter were performed in order to gain an insight into whether the co-localisation of ID^B with RyR2 (Chapter 5) functionally modulated RyR2. ID^B did not modulate RyR2 function following agonist exposure (Figures 6.12 and 6.13). However, a marked increase in basal Ca^{2+} signal variability was exhibited following transfection of RyR2 with ID^B that was not observed when cells were transfected with RyR2 alone (Figure 6.9). This either suggests that ID^B functionally interacts with RyR2 via homologous sequences, or its expression could perturb some other aspect of the Ca^{2+} signalling pathway. A further study would be to assess the effect of ID^B expression on mutation-harbouring RyR2. In addition, in light that only ID suppressed RSV following IP_3R activation (Figure 6.10), it would therefore be interesting to assess the effect of ID expression on RyR2-evoked Ca^{2+} responses. However, time limitations precluded these interesting further investigations.

Chapter 7

Chapter 7 Elucidating signalling pathways underpinning ID^B cytotoxicity

7.1. Introduction

As discussed in Chapters 5 and 6, I-domain cytotoxicity results from perturbed Ca^{2+} handling and cell death. Intriguingly, these phenomena were also observed in neighbouring cells that did not express the recombinant protein (termed NUCs). Importantly, Figures 5.15 and 4.5 provided compelling evidence that this communication was not solely mediated by direct cell-to-cell contact.

The similar phenotypic manifestation and cell death observed in NUCs (Figures 4.3 and 4.4), a characteristic of I-domain transfected populations, has been reported previously (Kettman and Skarvall, 1974; Hamada *et al.*, 2007a) and termed the 'bystander effect'. The bystander effect can be conferred via signalling molecules such as ROS or ATP (Lyng *et al.*, 2002a; Vines *et al.*, 2008), and may invoke cell surface channels such as hemichannels/gap junctions (Jiang and Gu, 2005; Udawatte and Ripps, 2005). This chapter aims to delineate the signal transduction mechanisms underpinning the profoundly abnormal phenotype of NUCs.

7.1.1. The mechanisms of cell-to-cell communication

The altered cell phenotype (Figure 4.2), Ca^{2+} signalling (Figures 5.12, 5.14 and 6.9) and cell death (Figure 4.5) observed in NUCs was typical of a 'bystander effect'. This term describes the activation of cell death pathways in 'untreated' cells that is attributable to signals received from neighbouring 'treated' cells. It has recently been associated with cells exposed to ionising radiation (Lyng *et al.*, 2002a; Grifalconi *et al.*, 2007), although it was first reported in the 1970s in relation to the primary immune response (Kettman and Skarvall, 1974). An accumulating body of research proposed that secretion of factors into the media from irradiated cells can induce cell death signals in non-irradiated cells. In addition, cells incubated with conditioned media from irradiated cells displayed altered Ca^{2+} fluxes, increased ROS production

and diminished mitochondrial membrane potential (Lyng *et al.*, 2000, 2002b). This finding indicates that a diffusible signalling molecule was released into the media by irradiated cells that caused oxidative stress in non-irradiated cells. Furthermore, expression of a 30a.a. region of the transcriptional co-regulator (interacting factor-3) in cancer cells resulted in death of both expressing and non-expressing cells (Das *et al.*, 2007). The authors suggested that cell death occurred via two distinct pathways; first that apoptosis was initiated in cells expressing the recombinant protein, and second that recombinant protein expressing cells released a soluble factor (such as ROS) into the media that induced apoptosis in non-expressing cells via the bystander effect. In addition, transfer of media from these transfected cells to 'naïve' cells (not previously exposed to noxious stimuli) also induced apoptosis (Das *et al.*, 2007). Similarly, Grifalconi *et al.* reported that cells exposed to media removed from irradiated cells displayed an increase in non-viable and apoptotic cell populations. These cytotoxic effects were proposed to arise through the release of a soluble factor into the media, which was inconsistent with the effects of ROS (Grifalconi *et al.*, 2007), suggesting that other soluble effectors are responsible for the bystander effect.

Bystander cell death has been proposed to be mediated by gap junctions and/or hemichannels (Cusato *et al.*, 2003). Wilson and colleagues demonstrated that dye transfer between adjacent cells was maintained during apoptosis (Wilson *et al.*, 2000) indicating that cell-to-cell communication remains intact during this mode of cell demise, and that death signals can be conveyed to adjacent healthy cells irrespective of physical contact. However, the size of the cell death signalling protein cytochrome C and the caspase family of enzymes precludes them from passing through the junctional pore and mediating this signalling cascade (Cusato *et al.*, 2006). Nevertheless, messengers such as ATP and ROS are able to freely pass through hemichannels, and have been suggested to be involved in extracellular signalling (De Vuyst *et al.*, 2006; Stamatakis and Mantzaris, 2006; Das *et al.*, 2007). In addition, considering that Ca^{2+} dysregulation has been associated with the bystander effect (Lin *et al.*, 1998), it is entirely feasible that Ca^{2+} pathways are involved in promoting and delivering cell death signals.

7.1.2. Intercellular signal transduction mechanisms

Chapters 5 and 6 described the effect of I-domain expression on basal intracellular Ca^{2+} signalling, and this project also revealed that the I-domain induced a profoundly altered phenotype in NUCs. In view of these findings, the scope of this thesis was broadened in order to determine the *intercellular* signal transduction mechanisms that may have altered Ca^{2+} signalling and caused death in neighbouring cells.

Indirect inter-cellular communication is dependent on signal transduction pathways mediated by molecules such as ATP and reactive oxygen species (ROS). Many studies have reported that ATP can act as an extracellular messenger to modulate an extensive range of processes from signalling in the brain and CNS (Deitmer *et al.*, 2006; North and Verkhratsky, 2006; Stamatakis and Mantzaris, 2006) to respiratory muscle function (Govindaraju *et al.*, 2005) and immune responses (Hasko *et al.*, 2000). Cells typically maintain intracellular ATP concentrations in the millimolar range, and need to release <2% in order to elicit an effect on neighbouring cells (Gordon, 1986; Braet *et al.*, 2004). ATP release is via the stimulation of G-protein coupled receptors (GPCR) such as P2Y receptors, which are sensitive to nucleotide activation (Chen *et al.*, 1995b; Ostrom *et al.*, 2000). Various messengers such as Ca^{2+} and IP_3 have been reported to trigger ATP release, which in turn can increase Ca^{2+} concentrations, and hence acts as a diffusible feedback circuit (Ostrom *et al.*, 2000; Braet *et al.*, 2004; Stamatakis and Mantzaris, 2006; Katsuragi *et al.*, 2008). This intricate control is facilitated by the physical and physiological association between the ER and mitochondria, which also enables the bi-directional transfer of Ca^{2+} that regulates both cell survival and cell death pathways. Recycling of Ca^{2+} from mitochondria back to the ER via SERCA can prevent ER store depletion (Arnaudeau *et al.*, 2001), whereas the fine-tuned decoding of ER Ca^{2+} signals by mitochondria regulates cellular metabolism (Hajnoczky *et al.*, 1995; Csordas *et al.*, 2006) and PCD (Rizzuto *et al.*, 1993). Intracellular ATP concentrations have been demonstrated to control whether a cell is committed to apoptosis or becomes necrotic (Nicotera *et al.*, 1998). Specifically, depletion of intracellular ATP results in cell damage and the initiation of cell death pathways (Eguchi *et al.*, 1997; Nanavaty *et al.*, 2002). This process could also be responsible for cell death in surrounding cells, since ATP released from dying cells can promote apoptosis in neighbouring cells (Bulanova *et*

al., 2005; Noguchi *et al.*, 2008). Therefore two ATP-dependent routes of cell death, either ATP haemorrhage or ATP-induced signalling, could underpin the cytotoxicity that was associated with I-domain transfection.

Reactive oxygen species (ROS) (see Section 1.1.3.2) are actively involved in signal transduction pathways, and are generated in low concentrations (fM) during metabolic activity (Droge, 2002). They have been implicated to defend against infectious agents and protect from cell injury (Droge, 2002; Valko *et al.*, 2007). However, increased $[Ca^{2+}]_i$ and elevated mitochondrial Ca^{2+} concentrations can stimulate over-production of ROS (Kruman and Mattson, 1999), which can induce oxidative stress by sensitising IP_3R and RyR to Ca^{2+} activation. This subsequently can lead to the generation of the permeability transition pore (PTP) and initiation of apoptotic signalling cascades (Hajnoczky *et al.*, 2006). In addition, ROS also function as second messengers, mediating intercellular signal transduction through binding to cell surface receptors such as the receptor tyrosine kinase family (Zent *et al.*, 1999; Chiarugi and Cirri, 2003). This function is facilitated by the dynamic modulation imposed by ROS on many cellular proteins and receptors, and their generation during multiple signalling cascades (Adler *et al.*, 1999; Griendling *et al.*, 2000; Cakir and Ballinger, 2005). More recently, ROS release from damaged cells has been implicated to induce apoptosis in neighbouring cells, via the 'bystander effect' (Das *et al.*, 2007), see Section 7.1.1.

7.1.3. Direct cell-to-cell coupling via gap junctions

Most cells have the inherent capacity to communicate with each other via specialised intracellular junctions, termed gap junctions. Gap junctions are formed by the association of two hemichannels (or connexons) of neighbouring cells. Connexin hemichannels are composed of six connexin subunits, which are the fundamental components of gap junctions. Connexins are a family of ~20 proteins of molecular weights ranging from 20 to 62kDa. Collectively they exhibit a wide tissue distribution, and although some tissues can express over four types of connexin (Stauffer and Unwin, 1992; Sosinsky and Nicholson, 2005), some are characterised by tissue segregation, e.g. connexin 26 is distributed in tissues that include liver and skin, whereas connexin 43 is expressed more abundantly in tissues such as brain and heart. Heterogeneous connexin expression can result in the formation of both homo- and heterotypic gap junctions (composed of either homo- or heteromeric hemichannels (Laird, 2006) (Figure 7.1). The pore formed by gap junctions is between 6 and 15Å wide, which allows the passage of molecules <2kDa such as ions Na^+, K^+ and Ca^{2+}, second messengers IP_3 and cAMP, as well as small peptides and amino acids (Veenstra, 1996; Gong and Nicholson, 2001; Veenstra, 2001; Weber *et al.*, 2004).

7.1.4. Cell signalling mediated by connexin hemichannels

The role of gap junctions in transducing signals to regulate critical processes such as differentiation, and proliferation has been previously reported (Pitts *et al.*, 1988; Charles *et al.*, 1992; Neveu *et al.*, 1995; Cronier *et al.*, 1997; Yamori, 1998; Gramsch *et al.*, 2001; Kojima *et al.*, 2001; Princen *et al.*, 2001). However, more recently, connexins have been shown to have critical cellular functions that are independent of their role in mediating direct cell-to-cell communication (Verselis *et al.*, 2000; Jiang and Gu, 2005; Rodriguez-Sinovas *et al.*, 2007). The signal transducing function of connexins, distinct from gap junctions occurs either by the formation of unopposed hemichannels or the independent activity of individual connexins (Jiang and Gu, 2005) (Figure 7.1). To maintain homeostasis and cellular integrity, physiological conditions favour the closed state of hemichannels. In pathological states, for

example, during metabolic suppression (Kondo *et al.*, 2000; Contreras *et al.*, 2002) or a decrease in extracellular Ca^{2+} via an extracellular Ca^{2+} binding site (Li *et al.*, 1996; Gomez-Hernandez *et al.*, 2003; Ye *et al.*, 2003; Thimm *et al.*, 2005) hemichannel opening can be triggered. In addition, rapid changes in intracellular Ca^{2+} (in the range of 0.2-1μM) have also been proposed to activate hemichannel opening (De Vuyst *et al.*, 2006). Hemichannels have been associated with the release of regulatory molecules that may be involved in the promotion of cell death in neighbouring cells (Contreras *et al.*, 2004; Garcia-Dorado *et al.*, 2004).

7.1.5. Objective

Gap junctions provide a means by which I-domain-expressing cells can transmit signals to neighbouring cells triggering their demise. However, a central tenet of this chapter is the previous finding that neighbouring cells still exhibited phenotypic alterations despite not being physically coupled to an I-domain expressing cell (Figures 4.5 and 5.15). Consequently, this chapter reports upon the role that unopposed hemichannels may play in cellular signalling in the experiments presented in this thesis (Contreras *et al.*, 2002; Contreras *et al.*, 2004; De Vuyst *et al.*, 2006).

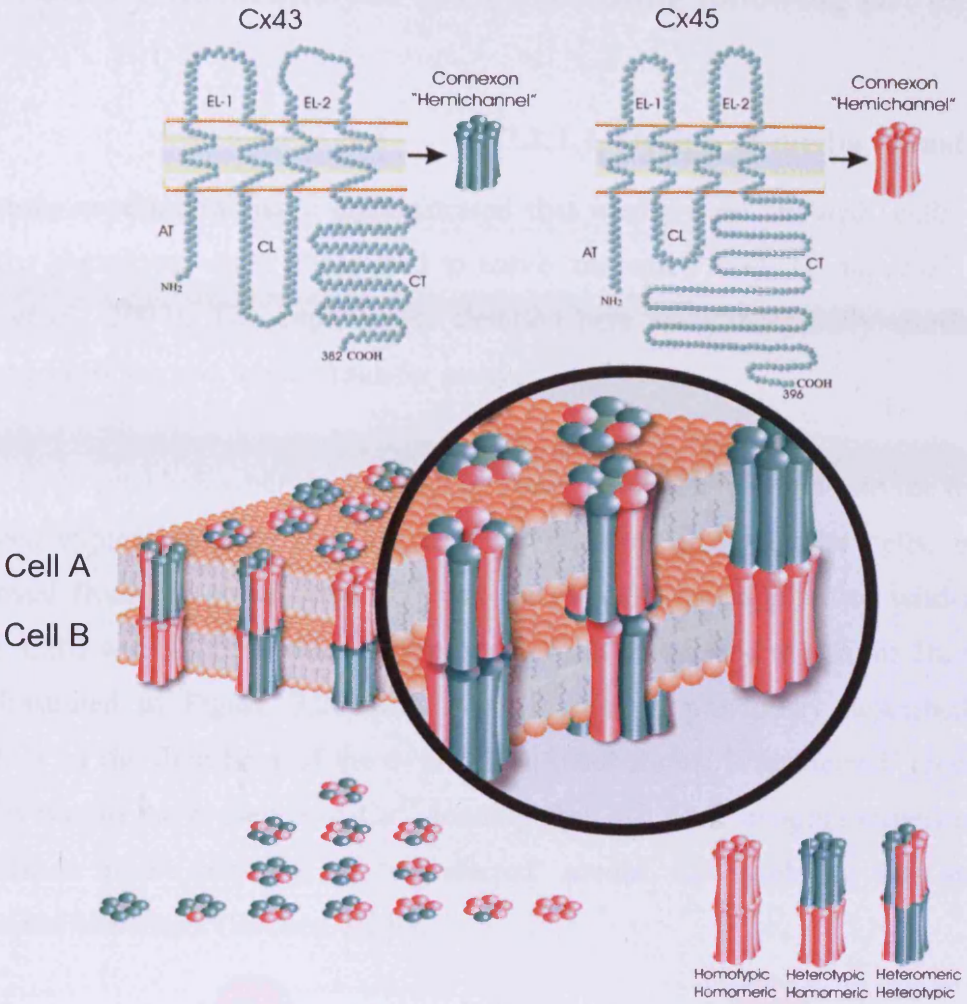

Figure 7.1. Gap junction and hemichannel formation

Association of plasma membrane hemichannels in the formation of gap junctions between adjacent cells (A and B). Each cell contributes a hemichannel to the junction, which is composed of six connexin subunits (in this case connexin 43 or 45). Hemichannels can be formed by the association of the same connexin type (homomeric) or different connexins (heteromeric), and similarly gap junctions can be composed of two hemichannels formed by the same type of connexin (homotypic) or by more than one type (heterotypic). Each connexin subunit is comprised of 4 TM domains and a long cytoplasmic domain that plays a role in intracellular signalling, as illustrated in the top schematics

Adapted from Laird, 2006

7.2. Methods

7.2.1. Confocal analysis of Ca^{2+} handling following ID^B expression

7.2.1.1. Design of media transfer assays

Previous experiments have demonstrated that media from 'treated' cells induced a similar phenotype when transferred to naïve 'untreated' cells (Lyng *et al.*, 2002a, b; Das *et al.*, 2007). The experiments detailed here are conceptually similar and are subsequently termed 'media transfer assays'.

In order to establish whether a signalling messenger was released into the media by I-domain expressing cells that altered Ca^{2+} handling in bystander cells, media was removed from 24h-transfected ID^B and mRFP cells and applied to wild-type HEK cells. Cells were incubated in the presence of the transferred media for 1h, 6h or 24h, as illustrated in Figure 7.2. Cells were loaded as previously described (Section 2.2.8.3) for the final hour of the 6- and 24-h incubations. 'Transferred' media applied for 1h was in the presence of Ca^{2+} loading dye. All Ca^{2+} imaging experiments were performed in the presence of 'transferred' media. Cell viability was assessed as described elsewhere (Section 3.2.4).

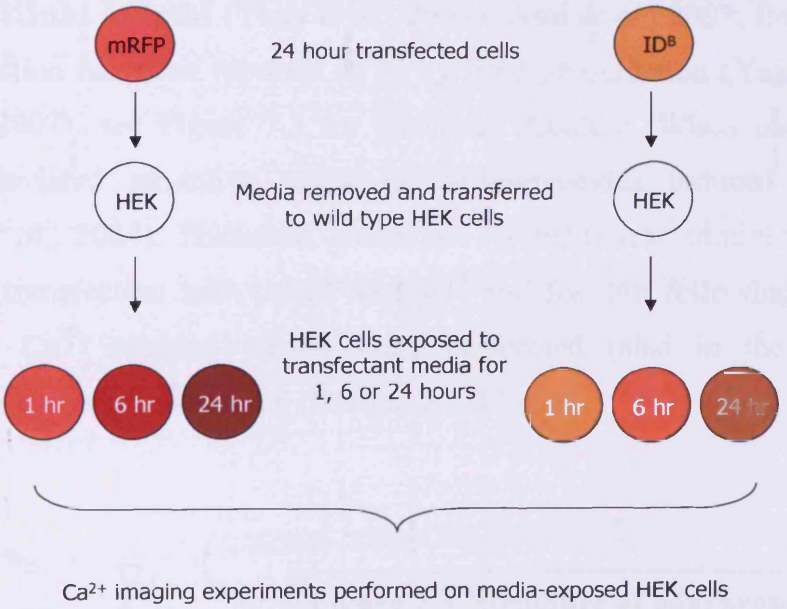

Figure 7.2. Schematic of media transfer experiments

Media was transferred from mRFP and ID^B transfected cells to wild-type HEK for 1, 6 or 24h prior to Ca^{2+} imaging experiments.

7.2.1.2. Hydrolysis of extracellular ATP using apyrase

Apyrase is an ATP hydrolase isolated from potato that converts ATP to ADP. It was used in this project to hydrolyse extracellular ATP to prevent ATP-driven signalling between cells. Apyrase has been used in similar experiments at concentrations between 0.1 U/ml and 30U/ml both transiently and for up to three days (Ostrom *et al.*, 2000; Gallagher and Salter, 2003; Ahmad *et al.*, 2004; Eltzschig *et al.*, 2006). In accordance with these studies, cells expressing mRFP and ID^B were exposed to 10U/ml apyrase during transfection and for 24h following transfection. All cellular manipulations including Ca^{2+} imaging were performed in the presence of apyrase. Cells were then imaged using CLSM as described in section 2.2.8.3 and data was analysed as described in section 6.2.1.1.1.

7.2.1.3. Scavenging reactive oxygen species (ROS) using edaravone

As detailed above, ROS can act as an intercellular messenger, conveying death signals to neighbouring cells (Bulanova *et al.*, 2005; Noguchi *et al.*, 2008). Edaravone (also termed MCI-186) is proposed to be a potent free-radical scavenger at concentrations ranging from 1.5μM to 1mM (Yano *et al.*, 2005a; Asai *et al.*, 2007; Ito *et al.*, 2008). Its mode of action has been reported to be by lipid peroxidation (Yagi *et al.*, 2005; Noor *et al.*, 2007), see Figure 7.3 for chemical structure. When used at 0.1mM, edaravone alleviated oxidative stress in cardiomyocytes induced by ischemia (Yamawaki *et al.*, 2004). Therefore, edaravone (0.1mM) was administered to HEK cells prior to transfection with mRFP and ID^B and for 24h following transfection. Subsequently, Ca^{2+} imaging studies were performed (also in the presence of Edaravone) as previously described (Section 2.2.8.3).

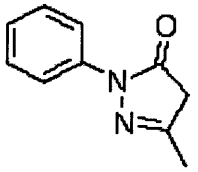

Figure 7.3. Structure of edaravone

7.2.2. Measurement of extracellular ATP

ATP released from metabolically active cells participates in signal transduction pathways (Ahmad *et al.*, 2004; Bulanova *et al.*, 2005). In light of this, extracellular ATP concentrations were assessed to determine if I-domain transfection altered the efflux of ATP from cells. The chemiluminescent-based ENLITEN assay (Promega) utilises the ATP-dependence of the luciferase-catalysed reaction between D-luciferin and molecular oxygen to produce light in proportion to the levels of ATP. Released light rapidly decreases when ATP is the limiting factor. ENLITEN® has a sensitivity to measure ATP in the range of 1pM to 100nM. The lyophilised rLuciferin/Luciferase (rL/L) was combined with the supplied reconstitution buffer (stable at RT for up to 24h, or up to 14 days when stored at -20°C). Light output was measured using a Turner Designs 20/20 Luminometer.

An ATP standard curve was constructed using 10µl of 1pM to 100nM ATP that was incubated with 100µl ENLITEN reagent for one min at RT. Light output was then measured in a Turner Designs 20/20 Luminometer using the programmed settings of delay (5s), integration (10s) and 60% sensitivity. Cells expressing mRFP and ID^B were seeded in 12 well plates 6h after transfection for analysis on consecutive days (Day 1-4). Cells were incubated for 1h with 1ml pre-warmed serum-free DMEM (as serum adversely effects the luciferase reaction). After 1h, media was removed from the cells and snap-frozen for storage at -80°C prior to assay. The total cells per well were counted to correlate the ATP produced with cell number. All assays were performed in triplicate and the entire experiment was performed three times. Both mRFP and ID^B data were normalised to mean number of cells expressing mRFP per day.

7.3. Results

7.3.1. ID^B media transfer did not alter Ca^{2+} handling

Previous studies have demonstrated an increase in apoptosis in naïve cells receiving media transferred from cells treated with an apoptosis-inducing factor (Lyng *et al.*, 2002b; Lyng *et al.*, 2006; Das *et al.*, 2007). This, together with the occurrence of apoptosis in cells that were not physically coupled (Figure 4.5), prompted the study as to whether a signalling molecule released from ID^B transfected cells underpinned the 'bystander effect'.

Confocal analysis of mRFP and ID^B 'transferred' media exposed cells showed no differences in resting Ca^{2+} dynamics at any of the time periods (Figure 7.4). In addition, cell viability was not significantly different in ID^B and mRFP media transfer experiments at the same time periods, despite there being a clear trend toward a lower viability in cells exposed to ID^B media (Figure 7.5). Cell viability was also comparable to HEK and mRFP cell viability at 24 and 48h (1-2%) while non-viable populations of ID^B were about 3% and 6% at 24 and 48h respectively (see Figure 3.21).

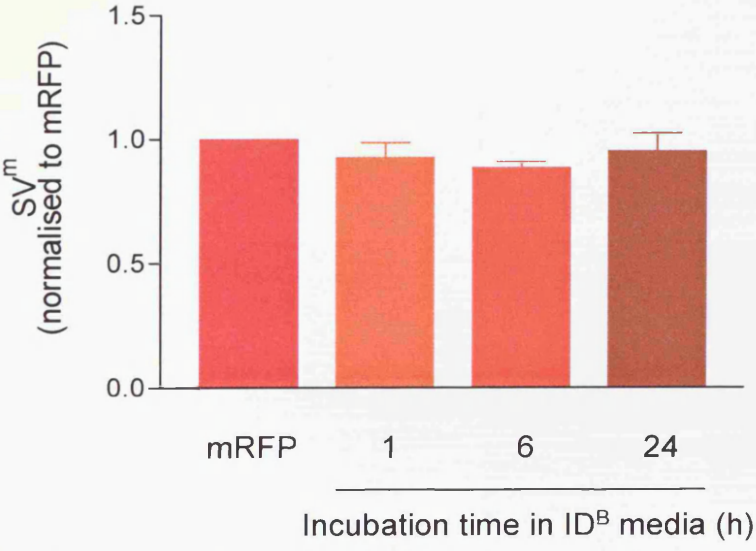

Figure 7.4. SV^m of cells exposed to 24h ID^B media for 1, 6 and 24h

HEK cells were exposed to media transferred from 24h transfected ID^B and mRFP cells for 1, 6 and 24h. Cells were analysed for Ca^{2+} handling using SV^m. Data were obtained from at least 11 separate experiments per condition, and ID^B SV^m data were normalised to mRFP SV^m data at the same time intervals.

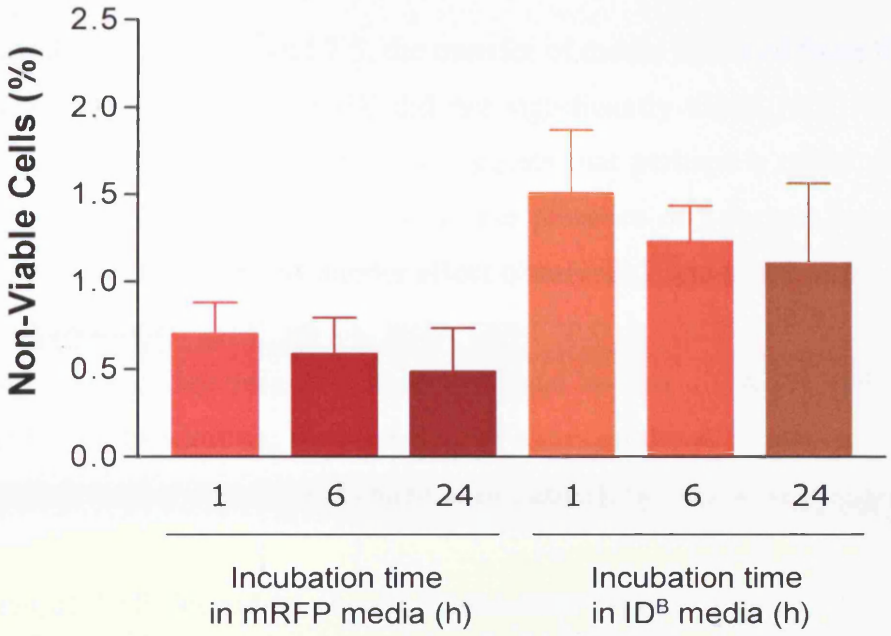

Figure 7.5. Cell viability following mRFP and ID^B media transfer

Cell viability of HEK cells exposed to media transferred from mRFP and ID^B cells 24h post-transfection for durations of 1, 6 and 24h. Data was an average of two individual measurements obtained from 6 separate experiments per condition.

7.3.2. Extracellular ATP was unaltered in cells expressing ID^B

As displayed in Figures 7.4 and 7.5, the transfer of media removed from ID^B cells 24h post-transfection to wild type HEK did not significantly affect NUC Ca^{2+} handling using the assays described above. This suggests that perhaps a rather short-lived or transiently-released molecule that requires the presence of I-domain transfected cells may have contributed to the bystander effect observed (Figures 4.5 and 5.15). In view of this, extracellular ATP levels were monitored in both mRFP and I-domain expressing cells to determine whether continual release of ATP could induce the bystander effect. In addition, measurement of extracellular ATP also serves as a good index of hemichannel opening (Leybaert *et al.*, 2003).

Calibration of ATP-dependent chemiluminescence (1pM – 100nM) (Figure 7.6) was used to determine ATP levels in media from mRFP and ID^B expressing cells (Figure 7.7). At days 1-4 extracellular ATP was no different between mRFP and ID^B expressing cells, which suggests that hemichannels were not persistently open following transfection with ID^B, however, this does not exclude the possibility that hemichannels are transiently opened. From Figure 7.7 it is difficult to believe that day 1 and day 4 ATP measurements are NOT statistically different in mRFP-expressing cells.

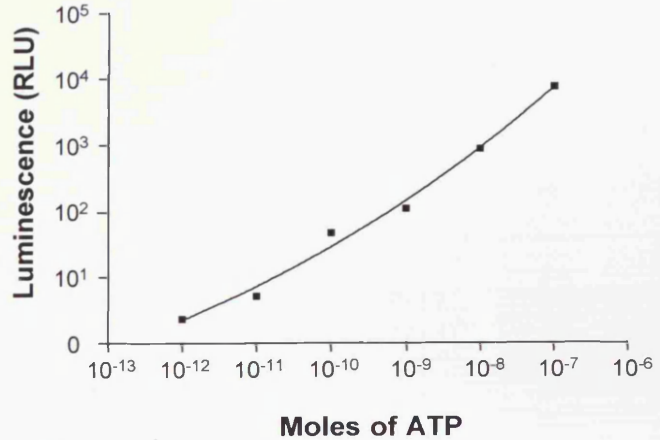

Figure 7.6. ATP standard Curve

Calibration of ATP in media assessed using ENLITEN luciferin/luciferase reagent. n=3 for each ATP concentration. SEM was calculated but was less than the dimensions of each point.

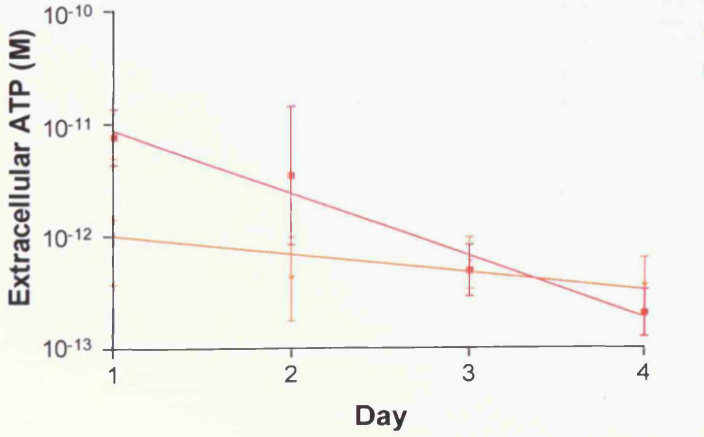

Figure 7.7. ATP released by ID^B expressing cells normalised to mRFP cell number

Data was acquired from triplicate experiments for each day and is given as mean±SEM.

7.3.2.1. Hydrolysis of extracellular ATP did not affect intracellular Ca^{2+} handling in bystander cells

Given the proposed role of ATP as an extracellular signalling molecule in the promotion of cell death cascades (Ahmad *et al.*, 2004; Eltzschig *et al.*, 2006; Noguchi *et al.*, 2008), cells were exposed to apyrase to hydrolyse extracellular ATP, thus preventing ATP-driven cell-to-cell signalling. SV^m of apyrase-treated mRFP and respective $mRFP_{NUC}$ were normalised to untreated mRFP and $mRFP_{NUC}$ cells respectively. Likewise, SV^m of ID^B and $ID^B{}_{NUC}$ apyrase-treated cells were normalised to ID^B and $ID^B{}_{NUC}$ untreated cells. Treated cells were normalised to control cells, which in this instance were their untreated counterparts, in line with previous studies. SV^m was comparable between $ID^B{}_{NUC}$ and apyrase treated $ID^B{}_{NUC}$ (Figure 7.8). However, mRFP cells treated with apyrase displayed a pronounced reduction in SV^m compared to untreated mRFP expressing cells (Figure 7.8). Although ID^B and $ID^B{}_{NUC}$ exhibited SV^m comparable to their untreated counterparts, these were still significantly different from the normalised SV^m of mRFP and $mRFP_{NUC}$.

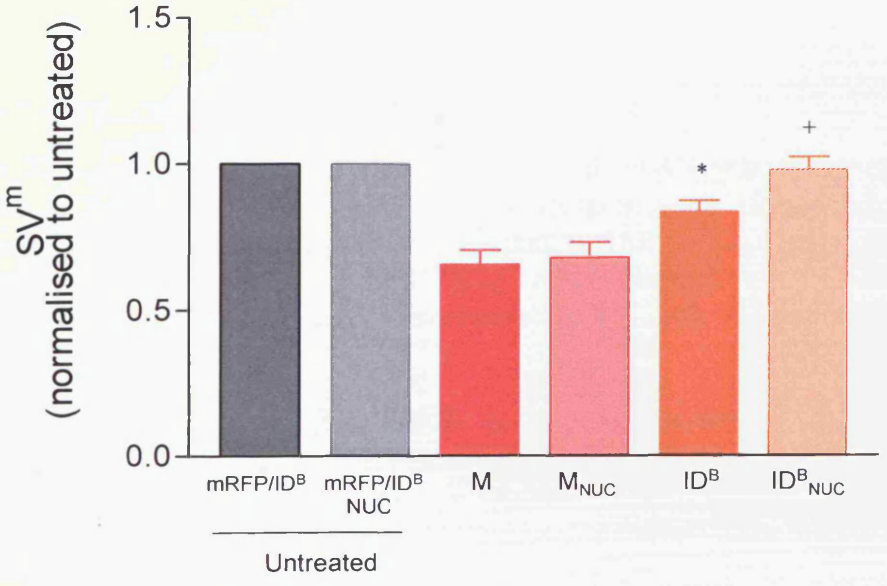

Figure 7.8. Apyrase exposed mRFP and ID^B cells

ID^B and mRFP (M) expressing cells were exposed to apyrase for 24h and analysed by confocal microscopy. Data were obtained from 10 separate experiments and assessed using SV^m. Treated mRFP/ID^B and mRFP/$ID^B{}_{NUC}$ cells were normalised to untreated mRFP/ID^B and mRFP/$ID^B{}_{NUC}$ cells respectively. Untreated cells were consequently expressed as 1. $^*p<0.05$ compared to M, $^+p<0.001$ compared to M_{NUC}.

7.3.3. Scavenging free radicals did not rescue dysfunctional Ca^{2+} handling in ID^B transfected cells

Edaravone was administered to cells in view of its anti-oxidant qualities to investigate whether it could correct dysfunctional Ca^{2+} cycling in NUCs. The addition of edaravone did not alter the SV^m in mRFP cells when compared to unexposed cells transfected with mRFP (Figure 7.9). However, ID^B expressing cells and $ID^B{}_{NUC}$ displayed a significantly higher SV^m to untreated cells indicating that edaravone altered resting Ca^{2+} handling in these cells.

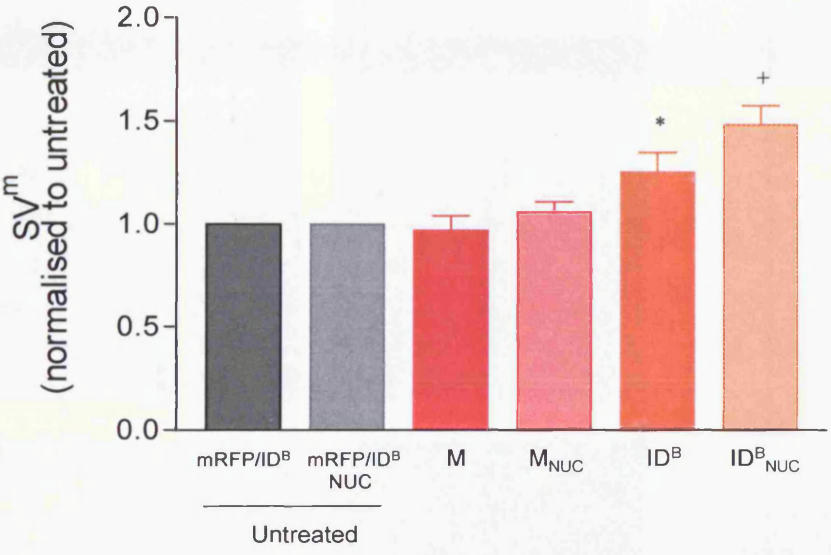

Figure 7.9. Edaravone exposed mRFP and ID^B cells

SV^m in ID^B and mRFP (M) expressing cells and NUCs was analysed following a 24h exposure to edaravone. Data were obtained from at least 10 separate experiments and assessed using SV^m. Treated mRFP/ID^B and mRFP/$ID^B{}_{NUC}$ cells were normalised to untreated mRFP/ID^B and mRFP/$ID^B{}_{NUC}$ cells respectively. Untreated cells were consequently expressed as 1 $^*p<0.05$ compared to M, $^+p<0.001$ compared to M_{NUC}.

7.3.4. HEK cells communicate via gap junctions

In order to determine whether HEK cells possessed functional gap junctions that would permit cell-to-cell communication, Lucifer yellow was injected into a single HEK cell and assessed for subsequent dye transfer (Figure 7.10). Although HEK cells displayed dye coupling, the transfer of Lucifer yellow was extremely slow ($t_{1/2}$ ~7 min). Nevertheless, these findings corroborate the existence of functional gap junctions in HEK, and should be viewed in light of low cell surface area contact between neighbouring cells (phase panel).

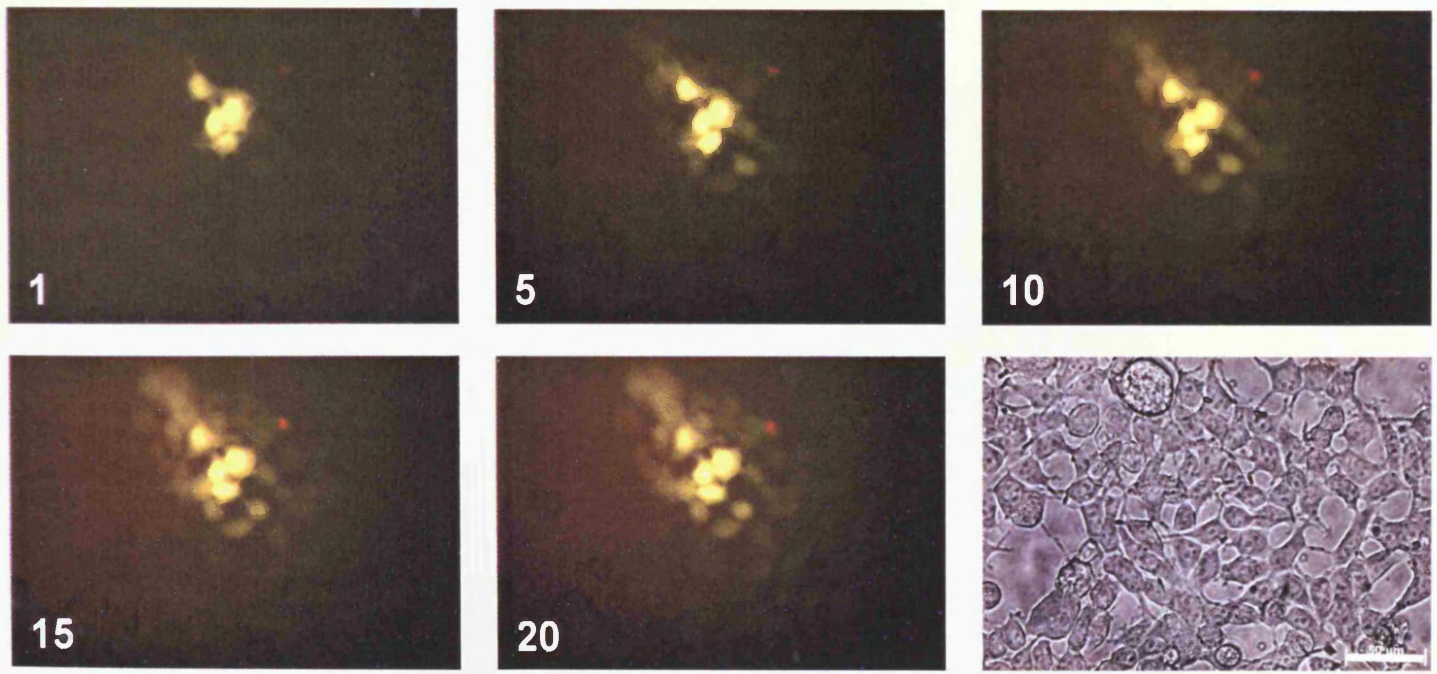

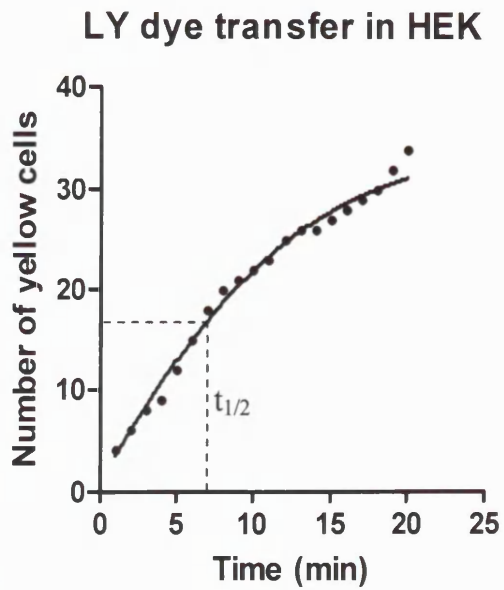

Figure 7.10. Lucifer yellow (LY) dye transfer in HEK cells

Microinjection of a single WT HEK cell and the consequent dye transfer was monitored to assess the presence of functional gap junctions. Images were obtained between 1 and 20 min following microinjection and the number of cells fluorescing yellow were quantified. Scale bar represents 50µm.

Images taken by Hala Jundi

7.4. Discussion

7.4.1. Bystander cell death was not mediated by ATP

Given that oxidative stress and Ca^{2+} signalling have been implicated in the occurrence of cell damage induced by neighbouring cells, this chapter explored whether either pathway was responsible for I-domain linked apoptosis in NUCs. As discussed in Chapter 5, the occurrence of the bystander effect was not dependent on cell-to-cell contact (Figure 5.15). In addition, the present experiments were carried out in view of the findings of Mothersill and Seymour, whereby irradiated cells released a factor into the media that was transduced to surrounding cells by a mechanism independent of gap junctions (Mothersill *et al.*, 2005). Furthermore, an accumulating number of studies report that media exchange from irradiated cells to non-irradiated cells resulted in apoptosis and reduced cell viability (Lyng *et al.*, 2002a, b; Das *et al.*, 2007; Grifalconi *et al.*, 2007). However, the data presented here showed that Ca^{2+} handling and cell phenotype of wild type HEK was not altered when exposed to media from ID^B expressing cells. Nevertheless, this approach was subject to time limitations, and for a more comprehensive insight, media transfer experiments should also be considered both at prolonged intervals (i.e. > 36h post-transfection) or within the first few hours following the appearance of recombinant I-domain protein.

Considering that cellular release of ATP can be triggered by both physical and chemical means, and its critical involvement in signal transduction processes (Ahmad *et al.*, 2004; Eltzschig *et al.*, 2006; Stamatakis and Mantzaris, 2006), it was vital that extracellular ATP concentrations were determined. In line with previous experiments, both mRFP and ID^B were assessed, and although there appeared to be a trend toward lower extracellular ATP released from ID^B cells, this was not significant. Furthermore, the finding that extracellular ATP concentrations were more comparable between mRFP and ID^B on day 3 (Figure 7.7), yet apoptosis at this time-point was still very high (Figure 4.5) strongly suggests that extracellular ATP does not mediate the bystander effect. Hydrolysis of extracellular ATP gave conflicting results; it considerably reduced Ca^{2+} signal variability in mRFP cells, an effect that was not observed in ID^B cells. An explanation for this finding has not yet been determined, however, since ID^B exhibited a higher basal Ca^{2+} signal variability than mRFP cells, it is likely that apyrase may have suppressed SV^m proportionally in both cells. It is also important to note that apyrase does not alter intracellular ATP concentrations (Cotrina *et al.*, 1998) and therefore should not effect intracellular Ca^{2+} handing. Nevertheless, this is at odds with the reduced

SV^m measured in mRFP cells following apyrase treatment. Alternatively, there is the possibility that HEK cells can sense extracellular ATP, which models intracellular Ca^{2+} handling accordingly.

7.4.2. ROS did not mediate the bystander effect

Scavenging ROS using edaravone failed to alleviate dysfunctional Ca^{2+} handling in ID^B cells. Instead it was associated with higher SV^m in both mRFP and ID^B cells (Figure 7.9), in line with a recent report that demonstrated its involvement in the promotion of oxidative stress and cell death (Arai *et al.*, 2008).

The studies performed in this chapter are consistent with previous research on the bystander effect, and suggest that I-domain expression mediates cell death via two pathways: 1) cells expressing recombinant protein are rapidly eliminated due to disrupted Ca^{2+} homeostasis and 2) NUCs are exposed to a soluble factor transiently released into the media by transfected cells, which alters Ca^{2+} homeostasis and commits cells to either apoptotic or necrotic cell death. The data presented in this chapter suggest that neither ATP nor ROS are likely candidates for mediating the bystander effects observed but it is acknowledged that this preliminary data does require further investigation. However, the data does allow the speculation that the bystander effect is probably mediated by a potent, transiently released, or short lived extracellular signalling molecule.

Chapter 8
General Discussion

Chapter 8 General Discussion

8.1. Localisation of I-domain constructs is not dependent on cellular expression of RyR2

Cellular expression of ID was consistent with the localisation of full-length RyR (Bhat and Ma, 2002b; Rossi et al., 2002) (Chapter 3). The comparable targeting of I-domain fragments in HEK and HL-1 cells irrespective of RyR2 background (Claycomb *et al.*, 1998; Tong *et al.*, 1999), indicates that RyR2 is not necessary for the intracellular localisation of the I-domain. These findings also provided the first evidence that suggested the I-domain may interact with IP_3R Ca^{2+} channels, which is in line with the hypothesis detailed in Chapter 1. Although the distinct localisation of ID and ID^C supports the concept that the ER retention signal lies within the first two predicted TM spanning regions (aa4499-4519, 4572-4593) (Meur *et al.*, 2007), it is still to be determined whether I-domain constructs exist as integral membrane proteins or are only associated with intracellular membranes. Further work is needed to address this issue.

8.2. I-domain expression induced apoptosis

Phenotypic observations of HEK cells transfected with I-domain sections revealed elevated levels of apoptosis 2-3 days post-transfection (Figure 4.5), which returned to normal levels following rapid elimination of recombinant I-domain protein (Figure 3.24). This phenomenon was also observed in studies using an alternative expression vector (Figure 3.25). The precise molecular pathways involved in I-domain mediated cell death were not fully characterised, however the results presented here strongly support the concept that I-domain expression interfered with IP_3R-dependent Ca^{2+} signalling (Figure 8.1, Chapter 5). It is speculated that these cytotoxic events triggered by I-domain expression also involved mitochondria, consistent with other studies (Hajnoczky *et al.*, 1995; Szalai *et al.*, 1999; Wang and El-Deiry, 2004; Mendes *et al.*, 2005; Hajnoczky *et al.*, 2006).

Ultimately the cytotoxicity associated with I-domain expression precluded the generation of stable cell lines. The successful enrichment of other cell populations (e.g. CHO cells) that expressed low levels of RyR2 (George *et al.*, 2003c), which was not achievable with I-domain (Chapter 4), suggests that I-domain expression is more toxic to cells than expression of the

whole, fully functional tetrameric protein. This unexpected and profound cytotoxicity presents limitations for chronically expressing I-domain constructs. The ramifications of these findings on the potential therapeutic use of I-domain in modulating intracellular Ca^{2+} signalling are substantial.

8.3. IP_3R agonist-induced responses are profoundly diminished by I-domain constructs

Most I-domain constructs reduced endogenous IP_3R responses to carbachol compared to mRFP. The data presented in this thesis suggests that the inhibitory effect of I-domain constructs on IP_3R-dependent agonist responses may be due to subtle changes in ER Ca^{2+} store loading that manifested as increased basal cytoplasmic Ca^{2+} fluxes (i.e. elevated SV^m) (Figure 8.1, Chapters 5 and 6). It is possible that I-domain expression locks the IP_3R in a subconductance state thus inducing a steady leak of Ca^{2+} from the ER leaving less free Ca^{2+} available for agonist-induced Ca^{2+} release. This may subsequently result in lower ER Ca^{2+} stores by reducing the Ca^{2+} available for resequestration into the ER via SERCA (Figure 8.1). It could be speculated that elevated SV^m in cells expressing I-domain may be a consequence of an increased rate of Ca^{2+} cycling between cytosolic and SR compartments, which maintained a temporary state of equilibrium, and may explain why these changes did not manifest as an increase in $[Ca^{2+}]_i$ (Figure 8.1). Cells were only able to temporarily compensate for the disruption in cellular Ca^{2+} handling induced by I-domain expression, which subsequently was responsible for their demise (Section 8.2).

It is feasible that the interaction of I-domain sections with the IP_3R modulated channel activity as a consequence of the striking structural homology between RyR and IP_3R (Appendix I). The data supports the regulation of IP_3R and RyR2 channel activity by interdomain interaction, which appears to be a common feature of both Ca^{2+} channel families. This phenomenon is consistent with the studies of Varnai and colleagues who found that recombinant domains of IP_3R were able to interact with and modify endogenous IP_3R channels by means of their precise spatial localisation (Varnai *et al.*, 2005). Nevertheless, despite similar sequence and structural homology between all I-domain sections with both IP_3R1 and 2 (Appendix I), lower co-localisation of I-domain constructs was observed with IP_3R2 than IP_3R1, which suggests that other factors probably contributed to the findings presented here. However, some effects could arise as a result of the lower expression levels

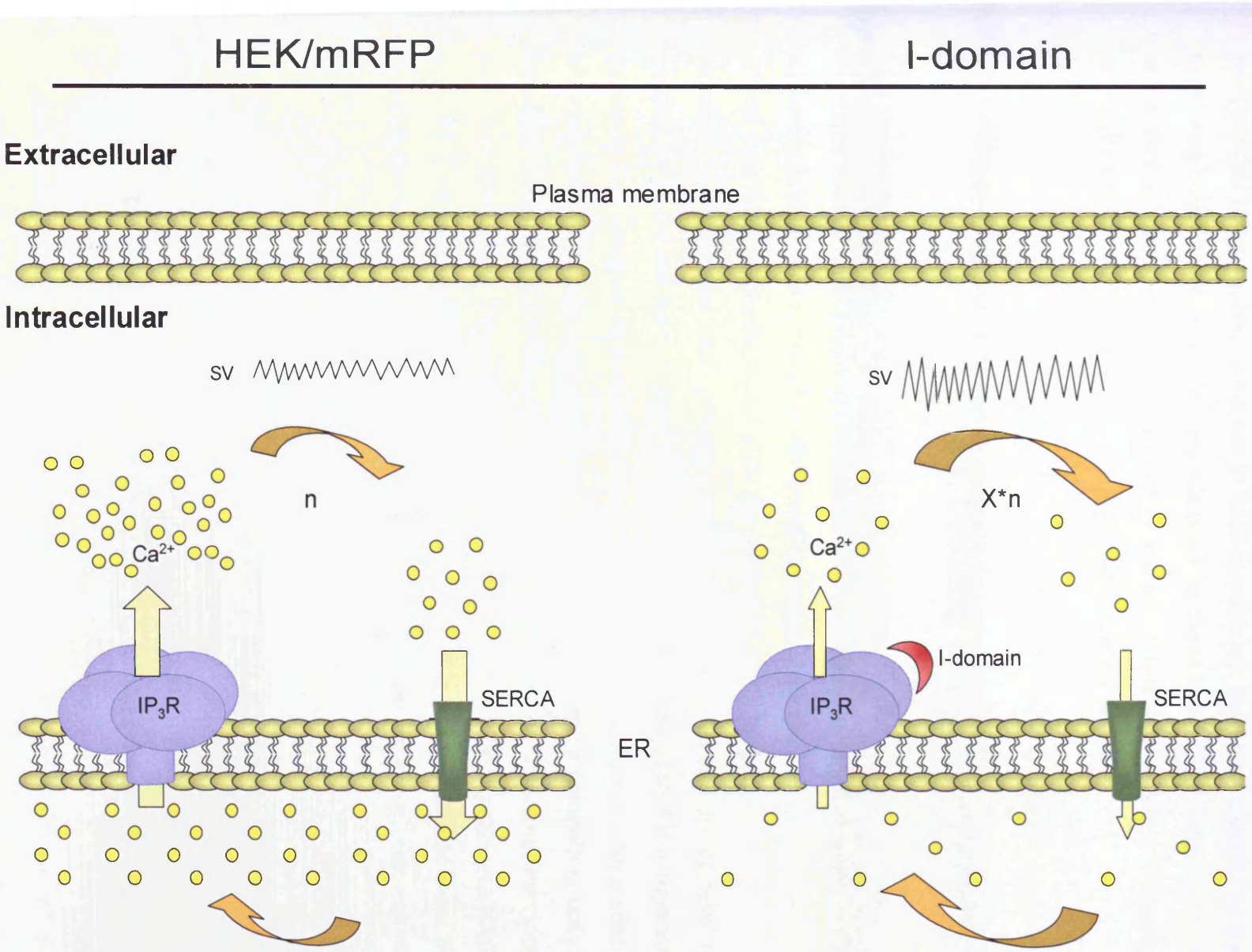

Figure 8.1. Schematical representation of I-domain-induced intracellular Ca^{2+} dysregulation

Left and right panels depict Ca^{2+} signalling in HEK/mRFP cells and in cells expressing I-domain constructs respectively. ER Ca^{2+} is lower in I-domain cells, as is Ca^{2+} release via IP_3R. The absence of an increase in $[Ca^{2+}]_i$ in I-domain expressing cells suggests that cells compensate by increasing Ca^{2+} cycling through the cell, this is shown in the figure as n in HEK and mRFP cells, which is increased to X*n in I-domain cells, where X is the coefficient by which Ca^{2+} cycling is increased. Increased Ca^{2+} cycling could lead to an increase in signal variability (SV).

and greater cytoplasmic localisation of IP_3R1 than IP_3R2 (Chapter 5). Furthermore, IP_3R1 rather than IP_3R2 is more centrally involved in apoptosis cascades (Assefa *et al.*, 2004; Oakes *et al.*, 2005). Although I-domain expression induced cell death, this data provides proof-of-principle that I-domain fragments can be used to modulate local Ca^{2+} signals (such as those in expressing cells) and remote Ca^{2+} signals (such as those in NUCs). Analytical tools such as single channel experiments may provide a greater insight into whether I-domain sections physically interact with the IP_3R to modulate channel function.

8.4. Decoding of intracellular Ca^{2+} handling

This thesis described the use of SV^m, a new parameter for the analysis of basal Ca^{2+} signal variability. Notably, the robust application of SV^m in measuring small changes in Ca^{2+} signals was made possible due to the powerful imaging system used (512x512 resolution, imaging at 200ms intervals) in combination with the optimised Ca^{2+} indicator fluo-4. Ca^{2+} imaging techniques have become more refined over the past decade, on account of developments in imaging hardware and the evolution of new Ca^{2+} indicator dyes. Fluo-4 is a superior Ca^{2+} dye for use in Ca^{2+} imaging experiments due to its 'brighter' fluorescence (compared to fluo-3) when excited with an argon laser. The use of SV^m has permitted a compelling insight into the biological (downstream) consequences of small changes in Ca^{2+} handling. Previous research has demonstrated how large Ca^{2+} oscillations shape various cellular processes (Dolmetsch *et al.*, 1997; Dolmetsch *et al.*, 1998), and the current project has now extended these findings by revealing that small, dynamic fluctuations in cellular Ca^{2+} can dictate cell fate and phenotype.

8.5. I-domain expression and the bystander effect

Remarkably, the profoundly altered phenotype and cell death induced by I-domain constructs was also a prominent feature of neighbouring non-expressing cells (see Chapters 5 and 6). A possible explanation for this striking and consistent finding is that Ca^{2+} store depletion or increased basal Ca^{2+} fluxes in I-domain-expressing cells initiated a cascade of signals that were transduced to neighbouring cells. This transduction may be considered to occur via points of cell-to-cell contact (e.g. gap junctions), but as indicated in Chapters 4 and 5, such a bystander effect was determined where the cells were not physically coupled. In view of this, experiments were designed to determine if a trans-cellular exchange of diffusible mediators

contributed to the bystander effect. The numbers of potential mediators are extensive and include ROS, ATP, lipids, amino acids and many other molecules. As discussed in Chapter 7, the bystander effect, in which targeted changes in cellular phenotype are conveyed to surrounding cells, has been well documented in other areas of research (e.g. cancer). However there are few mechanistic insights as to the transductory mechanisms involved. The data presented in this thesis provides important clues that altered cellular Ca^{2+} handling via manipulation of IP_3R may underlie the bystander effect.

The toxic nature of transient I-domain expression indicated that chronic expression would not be a viable therapeutic strategy in normalising aberrant RyR2 Ca^{2+} release. Therapeutically these findings could provide a route for targeted cell eradication, but this concept requires far more substantial investigation.

8.6. Pathways underlying ID^B induced cytotoxicity

This project aimed to elucidate the pathways and signalling molecules underpinning I-domain cytotoxicity in neighbouring untransfected cells (NUCs). As discussed above, the data suggests a link between cytotoxicity and the altered Ca^{2+} cycling induced by I-domain fragments. Given the well documented relationship between altered Ca^{2+} handling and efflux of ATP and ROS from cells, the study was extended to explore whether ATP and/or ROS release from I-domain expressing cells underlined the observed cytotoxicity and altered agonist responses. The results presented in this thesis suggest that ATP released from ID^B expressing cells did not mediate bystander cell death (Figure 7.7). Further studies using a ROS scavenger (edaravone) also failed to alleviate perturbations in Ca^{2+} signalling induced by I-domain expression (Figure 7.9), and actually increased basal Ca^{2+} signal variability. However, the inability of edaravone to reduce dysfunctional Ca^{2+} cycling in the present experiments does not rule out ROS as mediators of death signals to bystander cells. Additional experiments would need to assess extracellular concentrations of ROS in order to fully determine its involvement. Time limitations precluded these further investigations. The increased perturbed Ca^{2+} signalling following edaravone exposure may actually question the therapeutic qualities of edaravone, which is consistent with recent reports of its cytotoxic effects (Arai *et al.*, 2008).

8.7. Further work and future direction

The work described in this thesis has revealed that fragments of the I-domain can modulate intracellular Ca^{2+} handling. However, further work is required in order to determine the ramifications of expressing recombinant fragments of the cardiac RyR in diseased myocardium.

The findings of this project suggest that I-domain expression resulted in IP_3R down-regulation, however this was not confirmed. Further experiments such as increasing n number of both IP_3R type 1 and type 2 immunoblots are required to establish whether this was in fact the case. Similarly, in order to determine whether high I-domain expression correlates with reduced IP_3R expression, it would be useful to quantify total IP_3R and I-domain protein in individual cells.

In addition, further experiments are necessary to fully assess the functional effect of expressing I-domain constructs on both IP_3R and RyR activity, particularly via the use of lipid bi-layers. In view of the cytotoxicity of I-domain expression, it would also be interesting to construct smaller sub-fragments of the I-domain (especially ID^B) and assess the functional implications of these on IP_3R and RyR activity in whole cells and lipid bi-layers, specifically to determine whether they are less toxic and if they would pose a greater therapeutic strategy. Finally, in order to fully determine the implications of this work on the regulation of intracellular Ca^{2+} release channels in normal and diseased myocardium, it is essential that these studies be carried out in cells of a cardiomyocyte lineage.

8.8 Practical limitations

HEK cells were used throughout this project for a number of reasons. Firstly, they represent an RyR2-null background that permits the study of I-domain fragments on IP_3R-dependent Ca^{2+} signalling. Secondly, HEK cells are widely employed as the cell line of choice for heterologous expression of recombinant RyR2 (Thomas *et al.*, 2005; Jiang *et al.*, 2007; Jones *et al.*, 2007) and thus could be used as an experimental model for investigating the effects of I-domain on RyR2. To this end, HEK cells have been used in diagnosing perturbations in Ca^{2+} handling mediated by recombinant mutant RyR2 channels (Jiang *et al.*, 2002a; Thomas *et al.*, 2004; Paavola *et al.*, 2007). However, it is acknowledged that the effects of I-domain

fragments on RyR2 in an IP_3R-null cell context were not investigated. Although cells do exist that lack all IP_3R subtypes (DT40 chicken lymphocytes (Miyakawa *et al.*, 1999)) these are non-mammalian cells that compensate for lack of homeostatic IP_3R-mediated signalling by abnormal changes in other facets of the Ca^{2+} signalling machinery.

Similarly, HL-1 cells were used as a model for endogenous RyR2 expression, and these cells are equipped with a full complement of accessory proteins (including CSQ and FKBP12.6). However, HL-1s, although characterised by adult cardiomyocyte phenotype and contractility (Claycomb *et al.*, 1998) are an immortalised cell line that do not possess T-tubules. Thus, again it is recognised that these cells may not be the ideal choice for studying the effects of I-domain expression on RyR2. An RyR2-deficient cardiac cell line that expresses a full complement of accessory proteins similar to the 1B5 skeletal myotubes used for RyR1 and RyR3 studies (Moore *et al.*, 1998) would be valuable, but no such model has so far been developed. Given the central role of RyR2 in cardiac cell function, it is also presumed that an RyR2-null cardiac cell would lack cardiac cell phenotype.

Other limitations of this thesis include the use of thapsigargin to deplete ER stores. Thapsigargin only provides an estimation of ER load and cannot be used to assess dynamic changes in the ER store. However, since thapsigargin has been routinely implemented in similar studies (Jiang *et al.*, 1994; Tong *et al.*, 1999; Gerasimenko *et al.*, 2003; Thomas *et al.*, 2005), it is considered a useful tool for studying ER Ca^{2+} status.

Cells were monitored on a daily basis in accordance with initial phenotypic observations. However, in view of the findings of this project, a more detailed analysis of I-domain expressing cells between 1 and 2 days post-transfection is now warranted.

Finally, the use of mRFP, although a robust fluorescent fusion tag that enabled the unequivocal identification of I-domain expressing cells (which led to the observation of the bystander effect) may have some effect on the functionality of I-domain constructs. However, the data presented in this thesis has shown that different mRFP-tagged I-domain fragments exhibited distinct functionality, consistent with previous reports that mRFP in most circumstances does not compromise the function of the protein to which it is fused (Campbell *et al.*, 2002).

Appendices

Appendix I

Bioinformatic analysis of RyR2 and IP_3R I-domains

	RyR2 ID fragment characteristics						Structural motifs [A]				Sequence homology [B]				Predicted structural homology [C]	
	Locus (a.a.)	Residues	MW (kD)	pI	Hydropathy index (HI) [D]	HI per residue	α-helix (%)	β-turn (%)	Extended strand (%)	Coiled (%)	vs. RyR1 (%)	vs. RyR3 (%)	vs. IP_3R-1 (%) [E]	vs. IP_3R-2 (%) [E]	vs. IP_3R-1 (%)	vs. IP_3R-2 (%)
ID	3722-4610	889	101.65	5.1	122.51	0.14	59.96	5.62	9.45	24.97	59	66	12 (832-2385)[F]	13 (844-2934)	ND[G]	ND
ID^A	3722-4353	630	71.93	5.0	43.76	0.07	63.33	5.08	7.62	23.97	69	75	15 (1736-2650)	17 (1741-2656)	67	65
ID^B	4353-4499	147	16.97	4.6	105.74	0.76	57.14	3.40	6.12	33.33	15	35	17 (1972-2219)	10 (1979-2227)	64	64
ID^C	4353-4610	261	29.74	5.2	69.56	0.27	57.53	3.09	10.81	28.57	33	45	14 (1972-2385)	10 (1979-2394)	67	69

Table i. Bioinformatic analysis of I-Domain sequences

[A] Structural predictions based on primary amino acid sequences were obtained via the SOPMA algorithm (Combet C., Blanchet C., Geourjon C. and Deléage G. (2000) TIBS 25:147-150) operated through a web-based server (http://npsa-pbil.ibcp.fr/cgi-bin/npsa_automat.pl?page=/NPSA/npsa_sopma.html). **See also Table ii**

[B] The extent of sequence homology (where 100% represents identical sequence match) was determined by sequence alignment using the ClustalW program available at http://www.ebi.ac.uk/Tools/clustalw2/index.html

[C] SOPMA output files corresponding to structural predictions for I-Domain fragments (RyR2) and ID-like regions (IP_3R) respectively were aligned using the ClustalW program. See **Figure iii-v** for detailed analysis.

[D] Hydropathic indices were calculated using the Hopp-Wood algorithm (Hopp TR., and Woods KR. (1981) PNAS 78:3824-3828) operated through the ExPaSy molecular biology server (http://www.**expasy**.org/tools/protscale.html). **See Figures i and ii.**

[E] The GenBank accession numbers for the human IP_3R sequences are NP_002213 (*IP3R-1*; 2695aa, 306.8kDa) and NP_002214 (*IP3R-2*; 2701aa, 308.06kDa).

[F] Residues in parentheses represent IP_3R regions that exhibited the greatest degree of sequence homology with RyR2 I-Domain fragments.

[G] ND= not determined. There was insufficient homology between RyR2 ID and IP_3R-1 and IP_3R-2 to perform reliable structural homology modelling.

	α-helix (%)	β-turn (%)	Extended strand (%)	Coil (%)
RyR2				
ID	59.96	5.62	9.45	24.97
ID^A	63.33	5.08	7.62	23.97
ID^B	57.14	3.4	6.12	33.33
ID^C	57.53	3.09	10.81	28.57
IP_3R1				
ID^A-like	54.54	4.25	11.15	30.05
ID^B-like	51.82	3.64	10.93	33.60
ID^C-like	56.90	5.08	11.14	26.88
IP_3R2				
ID^A-like	54.21	3.95	11.45	30.39
ID^B-like	48.39	4.44	12.90	34.27
ID^C-like	56.14	5.06	12.29	26.51

Table Y. Predicted structural motifs in RyR2 I-domains and the I-domain-like regions in IP_3R.

Motifs were predicted using the SOPMA algorithm as described in Table X. The detailed organisation of these motifs within the RyR2 and IP_3R is shown in Figure AA to AC.

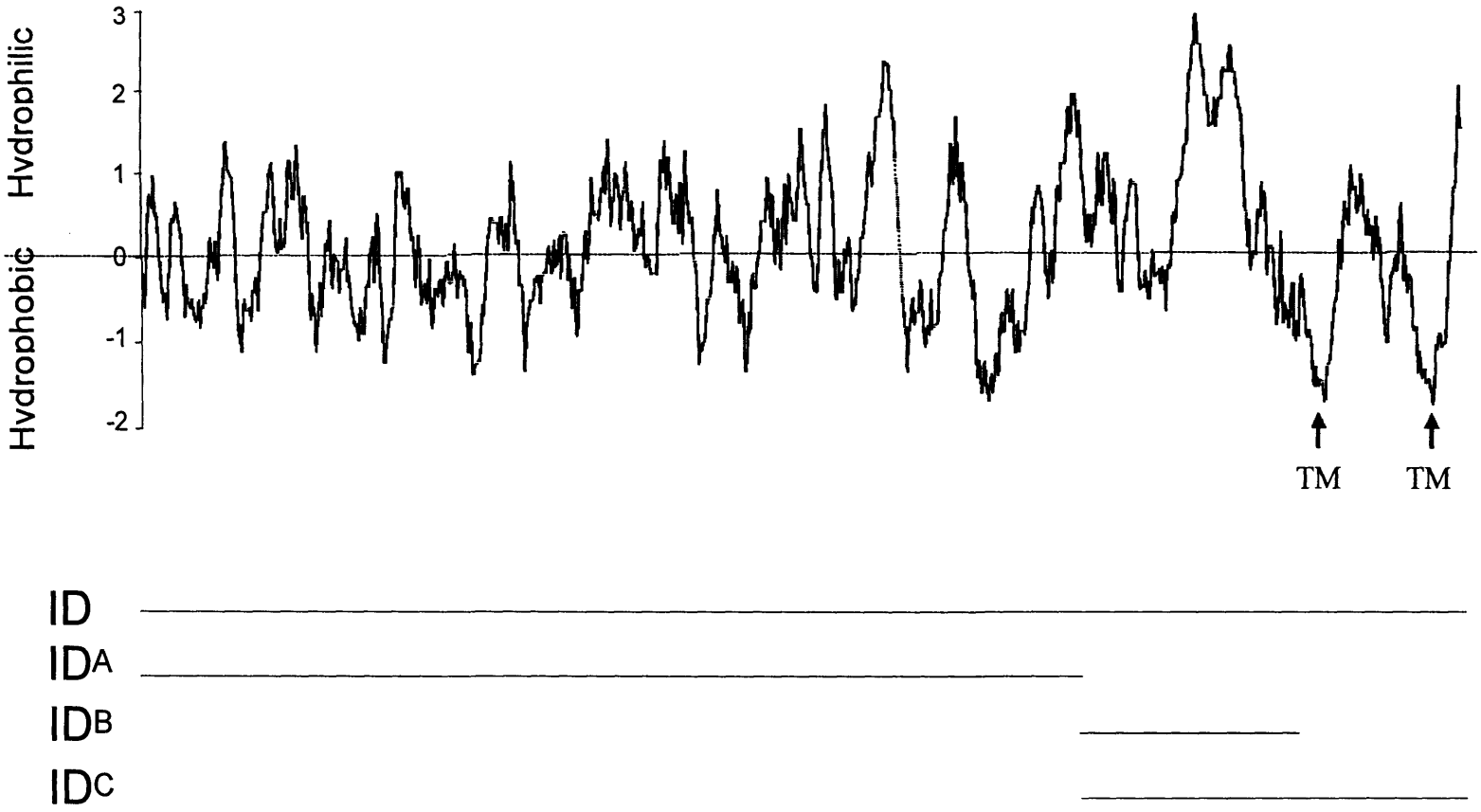

Figure Y. Hydropathy analysis of the human RyR2 I-Domain

Hydropathy analysis of the human RyR2 I-domain (residues 3722-4610) was performed using the Hopp-Woods algorithm as described in Table X. The hydrophobic scale is given in Figure Z. Positive and negative ranges correspond to hydrophilic and hydrophobic residues, respectively. The two TM regions (arrowed) correspond to TM1 and 2 according to the model of Tunwell *et al.*

Using the scale Hphob. / Hopp & Woods, the individual values for the 20 amino acids are:

```
Ala: -0.500
Arg:  3.000
Asn:  0.200
Asp:  3.000
Cys: -1.000
Gln:  0.200
Glu:  3.000
Gly:  0.000
His: -0.500
Ile: -1.800
Leu: -1.800
Lys:  3.000
Met: -1.300
Phe: -2.500
Pro:  0.000
Ser:  0.300
Thr: -0.400
Trp: -3.400
Tyr: -2.300
Val: -1.500
```

Figure Z. Hydrophobic scale

H= alpha helix / T= beta turn / E= extended strand / C=coil

Homology between RyR2 and IP_3R-1 / IP_3R-2

Homology between RyR2 and IP_3R-1

Homology between RyR2 and IP_3R-2

Figure iii- IDA-like region homology

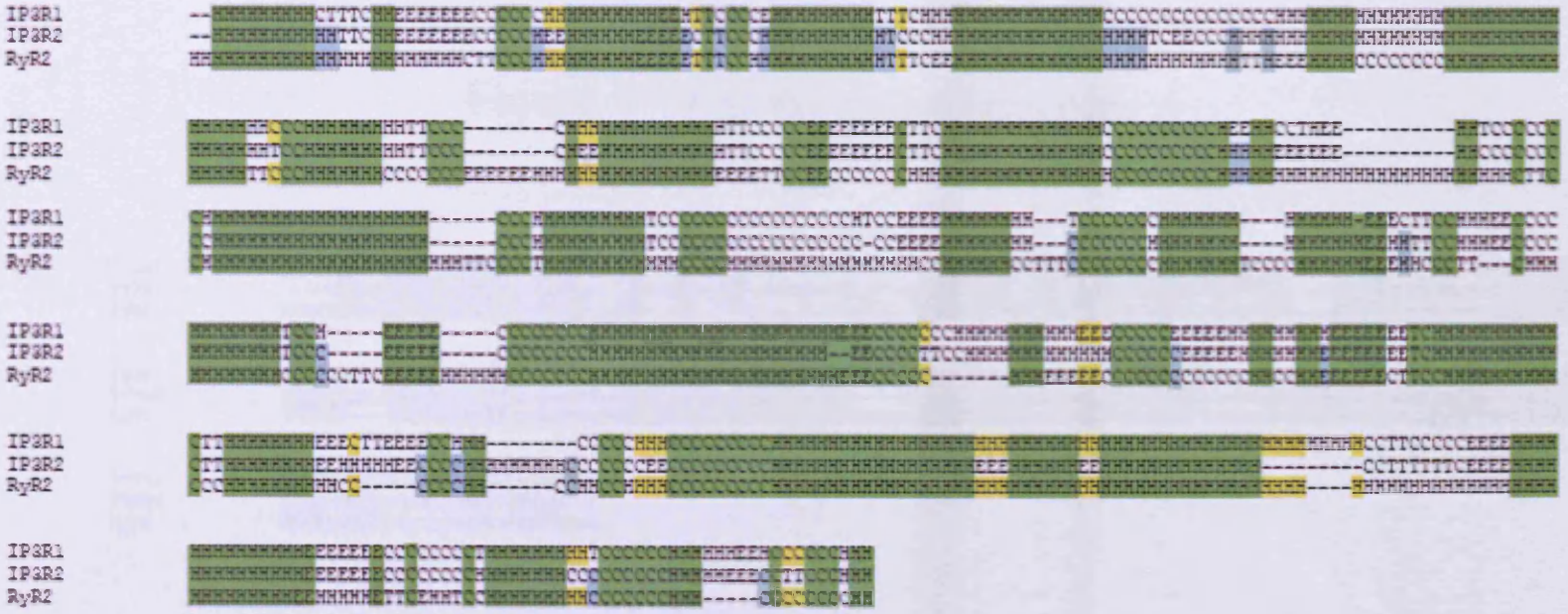

Figure iv - IDB-like region homology

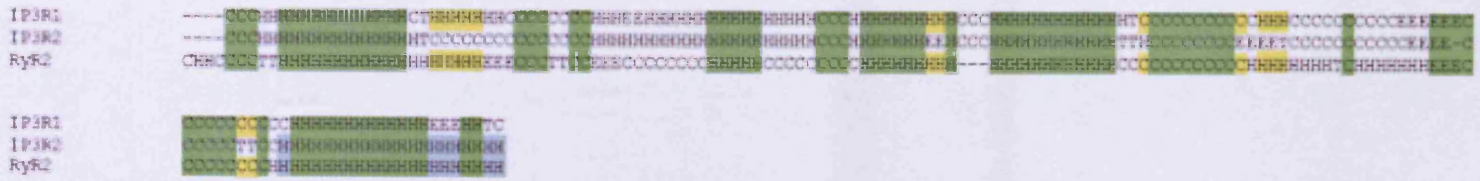

Figure v - IDC-like region homology

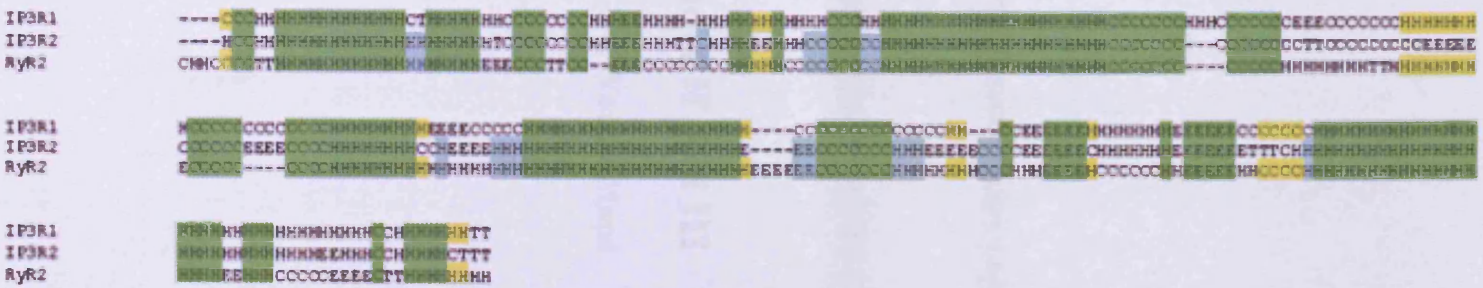

Appendix II and III

Vector Maps

Appendix II

pmRFP-C1 map

CTAGCGCCACC**ATGGCCTCCTCCGAGGACGTCATCAAGGAGTTCATGCGCTTCAAGGTGCGC**
ATGGAGGGCTCCGTGAACGGCCACGAGTTCGAGATCGAGGGCGAGGGCGAGGGCCGCCCCTA
CGAGGGCACCCAGACCGCCAAGCTGAAGGTGACCAAGGGCGGCCCCCTGCCCTTCGCCTGGG
ACATCCTGTCCCCTCAGTTCCAGTACGGCTCCAAGGCCTACGTGAAGCACCCCGCCGACATC
CCCGACTACTTGAAGCTGTCCTTCCCCGAGGGCTTCAAGTGGGAGCGCGTGATGAACTTCGA
GGACGGCGGCGTGGTGACCGTGACCCAGGACTCCTCCCTGCAGGACGGCGAGTTCATCTACA
AGGTGAAGCTGCGCGGCACCAACTTCCCCTCCGACGGCCCCGTAATGCAGAAGAAGACCATG
GGCTGGGAGGCCTCCACCGAGCGGATGTACCCCGAGGACGGCGCCCTGAAGGGCGAGATCAA
GATGAGGCTGAAGCTGAAGGACGGCGGCCACTACGACGCCGAGGTCAAGACCACCTACATGG
CCAAGAAGCCCGTGCAGCTGCCCGGCGCCTACAAGACCGACATCAAGCTGGACATCACCTCC
CACAACGAGGACTACACCATCGTGGAACAGTACGAGCGCGCCGAGGGCCGCCACTCCACCGG
CGCCCAAGCTTCGAATTCTGCAGTCGACGGTACCGCGGGCCCGGGATCCACCGGATCTAGAT
AACTGATCATAATCAGCCATACCACATTTGTAGAGGTTTTACTTGCTTTAAAAAACCTCCCA
CACCTCCCCCTGAACCTGAAACATAAAATGAATGCAATTGTTGTTGTTAACTTGTTTATTGC
AGCTTATAATGGTTACAAATAAAGCAATAGCATCACAAATTTCACAAATAAAGCATTTTTTT
CACTGCATTCTAGTTGTGGTTTGTCCAAACTCATCAATGTATCTTAAGGCGTAAATTGTAAG
CGTTAATATTTTGTTAAAATTCGCGTTAAATTTTTGTTAAATCAGCTCATTTTTTAACCAAT
AGGCCGAAATCGGCAAAATCCCTTATAAATCAAAAGAATAGACCGAGATAGGGTTGAGTGTT
GTTCCAGTTTGGAACAAGAGTCCACTATTAAAGAACGTGGACTCCAACGTCAAAGGGCGAAA
AACCGTCTATCAGGGCGATGGCCCACTACGTGAACCATCACCCTAATCAAGTTTTTTGGGGT
CGAGGTGCCGTAAAGCACTAAATCGGAACCCTAAAGGGAGCCCCCGATTTAGAGCTTGACGG
GGAAAGCCGGCGAACGTGGCGAGAAAGGAAGGGAAGAAAGCGAAAGGAGCGGGCGCTAGGGC
GCTGGCAAGTGTAGCGGTCACGCTGCGCGTAACCACCACACCCGCCGCGCTTAATGCGCCGC
TACAGGGCGCGTCAGGTGGCACTTTTCGGGGAAATGTGCGCGGAACCCCTATTTGTTTATTT
TTCTAAATACATTCAAATATGTATCCGCTCATGAGACAATAACCCTGATAAATGCTTCAATA
ATATTGAAAAAGGAAGAGTCCTGAGGCGGAAAGAACCAGCTGTGGAATGTGTGTCAGTTAGG
GTGTGGAAAGTCCCCAGGCTCCCCAGCAGGCAGAAGTATGCAAAGCATGCATCTCAATTAGT
CAGCAACCAGGTGTGGAAAGTCCCCAGGCTCCCCAGCAGGCAGAAGTATGCAAAGCATGCAT
CTCAATTAGTCAGCAACCATAGTCCCGCCCCTAACTCCGCCCATCCCGCCCCTAACTCCGCC
CAGTTCCGCCCATTCTCCGCCCCATGGCTGACTAATTTTTTTTATTTATGCAGAGGCCGAGG
CCGCCTCGGCCTCTGAGCTATTCCAGAAGTAGTGAGGAGGCTTTTTTGGAGGCCTAGGCTTT
TGCAAAGATCGATCAAGAGACAGGATGAGGATCGTTTCGC**ATGATTGAACAAGATGGATTGC**
ACGCAGGTTCTCCGGCCGCTTGGGTGGAGAGGCTATTCGGCTATGACTGGGCACAACAGACA
ATCGGCTGCTCTGATGCCGCCGTGTTCCGGCTGTCAGCGCAGGGGCGCCCGGTTCTTTTTGT
CAAGACCGACCTGTCCGGTGCCCTGAATGAACTGCAAGACGAGGCAGCGCGGCTATCGTGGC
TGGCCACGACGGGCGTTCCTTGCGCAGCTGTGCTCGACGTTGTCACTGAAGCGGGAAGGGAC
TGGCTGCTATTGGGCGAAGTGCCGGGGCAGGATCTCCTGTCATCTCACCTTGCTCCTGCCGA
GAAAGTATCCATCATGGCTGATGCAATGCGGCGGCTGCATACGCTTGATCCGGCTACCTGCC
CATTCGACCACCAAGCGAAACATCGCATCGAGCGAGCACGTACTCGGATGGAAGCCGGTCTT
GTCGATCAGGATGATCTGGACGAAGAGCATCAGGGGCTCGCGCCAGCCGAACTGTTCGCCAG
GCTCAAGGCGAGCATGCCCGACGGCGAGGATCTCGTCGTGACCCATGGCGATGCCTGCTTGC
CGAATATCATGGTGGAAAATGGCCGCTTTTCTGGATTCATCGACTGTGGCCGGCTGGGTGTG
GCGGACCGCTATCAGGACATAGCGTTGGCTACCCGTGATATTGCTGAAGAGCTTGGCGGCGA
ATGGGCTGACCGCTTCCTCGTGCTTTACGGTATCGCCGCTCCCGATTCGCAGCGCATCGCCT
TCTATCGCCTTCTTGACGAGTTCTTCTGAGCGGGACTCTGGGGTTCGAAATGACCGACCAAG
CGACGCCCAACCTGCCATCACGAGATTTCGATTCCACCGCCGCCTTCTATGAAAGGTTGGGC
TTCGGAATCGTTTTCCGGGACGCCGGCTGGATGATCCTCCAGCGCGGGGATCTCATGCTGGA

GTTCTTCGCCCACCCTAGGGGGAGGCTAACTGAAACACGGAAGGAGACAATACCGGAAGGAA
CCCGCGCTATGACGGCAATAAAAAGACAGAATAAAACGCACGGTGTTGGGTCGTTTGTTCAT
AAACGCGGGGTTCGGTCCCAGGGCTGGCACTCTGTCGATACCCCACCGAGACCCCATTGGGG
CCAATACGCCCGCGTTTCTTCCTTTTCCCCACCCCACCCCCCAAGTTCGGGTGAAGGCCCAG
GGCTCGCAGCCAACGTCGGGGCGGCAGGCCCTGCCATAGCCTCAGGTTACTCATATATACTT
TAGATTGATTTAAAACTTCATTTTTAATTTAAAAGGATCTAGGTGAAGATCCTTTTTGATAA
TCTCATGACCAAAATCCCTTAACGTGAGTTTTCGTTCCACTGAGCGTCAGACCCCGTAGAAA
AGATCAAAGGATCTTCTTGAGATCCTTTTTTTCTGCGCGTAATCTGCTGCTTGCAAACAAAA
AAACCACCGCTACCAGCGGTGGTTTGTTTGCCGGATCAAGAGCTACCAACTCTTTTTCCGAA
GGTAACTGGCTTCAGCAGAGCGCAGATACCAAATACTGTCCTTCTAGTGTAGCCGTAGTTAG
GCCACCACTTCAAGAACTCTGTAGCACCGCCTACATACCTCGCTCTGCTAATCCTGTTACCA
GTGGCTGCTGCCAGTGGCGATAAGTCGTGTCTTACCGGGTTGGACTCAAGACGATAGTTACC
GGATAAGGCGCAGCGGTCGGGCTGAACGGGGGGTTCGTGCACACAGCCCAGCTTGGAGCGAA
CGACCTACACCGAACTGAGATACCTACAGCGTGAGCTATGAGAAAGCGCCACGCTTCCCGAA
GGGAGAAAGGCGGACAGGTATCCGGTAAGCGGCAGGGTCGGAACAGGAGAGCGCACGAGGGA
GCTTCCAGGGGGAAACGCCTGGTATCTTTATAGTCCTGTCGGGTTTCGCCACCTCTGACTTG
AGCGTCGATTTTTGTGATGCTCGTCAGGGGGGCGGAGCCTATGGAAAAACGCCAGCAACGCG
GCCTTTTTACGGTTCCTGGCCTTTTGCTGGCCTTTTGCTCACATGTTCTTTCCTGCGTTATC
CCCTGATTCTGTGGATAACCGTATTACCGCCATGCAT**TAGTTATTAATAGTAATCAATTACG**
GGGTCATTAGTTCATAGCCCATATATGGAGTTCCGCGTTACATAACTTACGGTAAATGGCCC
GCCTGGCTGACCGCCCAACGACCCCCGCCCATTGACGTCAATAATGACGTATGTTCCCATAG
TAACGCCAATAGGGACTTTCCATTGACGTCAATGGGTGGAGTATTTACGGTAAACTGCCCAC
TTGGCAGTACATCAAGTGTATCATATGCCAAGTACGCCCCCTATTGACGTCAATGACGGTAA
ATGGCCCGCCTGGCATTATGCCCAGTACATGACCTTATGGGACTTTCCTACTTGGCAGTACA
TCTACGTATTAGTCATCGCTATTACCATGGTGATGCGGTTTTGGCAGTACATCAATGGGCGT
GGATAGCGGTTTGACTCACGGGGATTTCCAAGTCTCCACCCCATTGACGTCAATGGGAGTTT
GTTTTGGCACCAAAATCAACGGGACTTTCCAAAATGTCGTAACAACTCCGCCCCATTGACGC
AAATGGGCGGTAGGCGTGTACGGTGGGAGGTCTATATAAGCAGAGCTGGTTTAGTGAACCGT
CAGATCCG

Red	**open reading frame encoding mRFP**
Orange	**cassette encoding kanamycin resistance**
Green	**cassette containing the immediate early promoter region of CMV**

Appendix III

pcDNA3.1 hygromycin map

GACGGATCGGGAGATCTCCCGATCCCCTATGGTGCACTCTCAGTACAATCTGCTCTGATGCC
GCATAGTTAAGCCAGTATCTGCTCCCTGCTTGTGTGTTGGAGGTCGCTGAGTAGTGCGCGAG
CAAAATTTAAGCTACAACAAGGCAAGGCTTGACCGACAATTGCATGAAGAATCTGCTTAGGG
TTAGGCGTTTTGCGCTGCTTCGCGATGTACGGGCCAGATATACGCGTTGACATTGATTATTG
AC**TAGTTATTAATAGTAATCAATTACGGGGTCATTAGTTCATAGCCCATATATGGAGTTCCG**
CGTTACATAACTTACGGTAAATGGCCCGCCTGGCTGACCGCCCAACGACCCCCGCCCATTGA
CGTCAATAATGACGTATGTTCCCATAGTAACGCCAATAGGGACTTTCCATTGACGTCAATGG
GTGGAGTATTTACGGTAAACTGCCCACTTGGCAGTACATCAAGTGTATCATATGCCAAGTAC
GCCCCCTATTGACGTCAATGACGGTAAATGGCCCGCCTGGCATTATGCCCAGTACATGACCT
TATGGGACTTTCCTACTTGGCAGTACATCTACGTATTAGTCATCGCTATTACCATGGTGATG
CGGTTTTGGCAGTACATCAATGGGCGTGGATAGCGGTTTGACTCACGGGGATTTCCAAGTCT
CCACCCCATTGACGTCAATGGGAGTTTGTTTTGGCACCAAAATCAACGGGACTTTCCAAAAT
GTCGTAACAACTCCGCCCCATTGACGCAAATGGGCGGTAGGCGTGTACGGTGGGAGGTCTAT
ATAAGCAGAGCTCTCTGGCTAACTAGAGAACCCACTGCTTACTGGCTTATCGAAATTAATAC
GACTCACTATAGGGAGACCCAAGCTG**GCTAGCGTTTAAACTTAAGCTTGGTACCGAGCTCGG**
ATCCACTAGTCCAGTGTGGTGGAATTCTGCAGATATCCAGCACAGTGGCGGCCGCTCGAGTC
TAGAGGGCCCGTTTAAACCCGCTGATCAGCCTCGACTGTGCCTTCTAGTTGCCAGCCATCTG
TTGTTTGCCCCTCCCCCGTGCCTTCCTTGACCCTGGAAGGTGCCACTCCCACTGTCCTTTCC
TAATAAAATGAGGAAATTGCATCGCATTGTCTGAGTAGGTGTCATTCTATTCTGGGGGGTGG
GGTGGGGCAGGACAGCAAGGGGGAGGATTGGGAAGACAATAGCAGGCATGCTGGGGATGCGG
TGGGCTCTATGGCTTCTGAGGCGGAAAGAACCAGCTGGGGCTCTAGGGGGTATCCCCACGCG
CCCTGTAGCGGCGCATTAAGCGCGGCGGGTGTGGTGGTTACGCGCAGCGTGACCGCTACACT
TGCCAGCGCCCTAGCGCCCGCTCCTTTCGCTTTCTTCCCTTCCTTTCTCGCCACGTTCGCCG
GCTTTCCCCGTCAAGCTCTAAATCGGGGGCTCCCTTTAGGGTTCCGATTTAGTGCTTTACGG
CACCTCGACCCCAAAAAACTTGATTAGGGTGATGGTTCACGTAGTGGGCCATCGCCCTGATA
GACGGTTTTTCGCCCTTTGACGTTGGAGTCCACGTTCTTTAATAGTGGACTCTTGTTCCAAA
CTGGAACAACACTCAACCCTATCTCGGTCTATTCTTTTGATTTATAAGGGATTTTGCCGATT
TCGGCCTATTGGTTAAAAAATGAGCTGATTTAACAAAAATTTAACGCGAATTAATTCTGTGG
AATGTGTGTCAGTTAGGGTGTGGAAAGTCCCCAGGCTCCCCAGCAGGCAGAAGTATGCAAAG
CATGCATCTCAATTAGTCAGCAACCAGGTGTGGAAAGTCCCCAGGCTCCCCAGCAGGCAGAA
GTATGCAAAGCATGCATCTCAATTAGTCAGCAACCATAGTCCCGCCCCTAACTCCGCCCATC
CCGCCCCTAACTCCGCCCAGTTCCGCCCATTCTCCGCCCCATGGCTGACTAATTTTTTTTAT
TTATGCAGAGGCCGAGGCCGCCTCTGCCTCTGAGCTATTCCAGAAGTAGTGAGGAGGCTTTT
TTGGAGGCCTAGGCTTTTGCAAAAAGCTCCCGGGAGCTTGTATATCCATTTTCGGATCTGAT
CAGCACGTGATGAAAAAGCCTGAACTCACCGCGACGTCTGTCGAGAAGTTTCTGATCGAAAA
GTTCGACAGCGTCTCCGACCTGATGCAGCTCTCGGAGGGCGAAGAATCTCGTGCTTTCAGCT
TCGATGTAGGAGGGCGTGGATATGTCCTGCGGGTAAATAGCTGCGCCGATGGTTTCTACAAA
GATCGTTATGTTTATCGGCACTTTGCATCGGCCGCGCTCCCGATTCCGGAAGTGCTTGACAT
TGGGGAATTCAGCGAGAGCCTGACCTATTGCATCTCCCGCCGTGCACAGGGTGTCACGTTGC
AAGACCTGCCTGAAACCGAACTGCCCGCTGTTCTGCAGCCGGTCGCGGAGGCCATGGATGCG
ATCGCTGCGGCCGATCTTAGCCAGACGAGCGGGTTCGGCCCATTCGGACCGCAAGGAATCGG
TCAATACACTACATGGCGTGATTTCATATGCGCGATTGCTGATCCCCATGTGTATCACTGGC
AAACTGTGATGGACGACACCGTCAGTGCGTCCGTCGCGCAGGCTCTCGATGAGCTGATGCTT
TGGGCCGAGGACTGCCCCGAAGTCCGGCACCTCGTGCACGCGGATTTCGGCTCCAACAATGT
CCTGACGGACAATGGCCGCATAACAGCGGTCATTGACTGGAGCGAGGCGATGTTCGGGGATT
CCCAATACGAGGTCGCCAACATCTTCTTCTGGAGGCCGTGGTTGGCTTGTATGGAGCAGCAG

ACGCGCTACTTCGAGCGGAGGCATCCGGAGCTTGCAGGATCGCCGCGGCTCCGGGCGTATAT
GCTCCGCATTGGTCTTGACCAACTCTATCAGAGCTTGGTTGACGGCAATTTCGATGATGCAG
CTTGGGCGCAGGGTCGATGCGACGCAATCGTCCGATCCGGAGCCGGGACTGTCGGGCGTACA
CAAATCGCCCGCAGAAGCGCGGCCGTCTGGACCGATGGCTGTGTAGAAGTACTCGCCGATAG
TGGAAACCGACGCCCCAGCACTCGTCCGAGGGCAAAGGAATAGCACGTGCTACGAGATTTCG
ATTCCACCGCCGCCTTCTATGAAAGGTTGGGCTTCGGAATCGTTTTCCGGGACGCCGGCTGG
ATGATCCTCCAGCGCGGGGATCTCATGCTGGAGTTCTTCGCCCACCCCAACTTGTTTATTGC
AGCTTATAATGGTTACAAATAAAGCAATAGCATCACAAATTTCACAAATAAAGCATTTTTTT
CACTGCATTCTAGTTGTGGTTTGTCCAAACTCATCAATGTATCTTATCATGTCTGTATACCG
TCGACCTCTAGCTAGAGCTTGGCGTAATCATGGTCATAGCTGTTTCCTGTGTGAAATTGTTA
TCCGCTCACAATTCCACACAACATACGAGCCGGAAGCATAAAGTGTAAAGCCTGGGGTGCCT
AATGAGTGAGCTAACTCACATTAATTGCGTTGCGCTCACTGCCCGCTTTCCAGTCGGGAAAC
CTGTCGTGCCAGCTGCATTAATGAATCGGCCAACGCGCGGGGAGAGGCGGTTTGCGTATTGG
GCGCTCTTCCGCTTCCTCGCTCACTGACTCGCTGCGCTCGGTCGTTCGGCTGCGGCGAGCGG
TATCAGCTCACTCAAAGGCGGTAATACGGTTATCCACAGAATCAGGGGATAACGCAGGAAAG
AACATGTGAGCAAAAGGCCAGCAAAAGGCCAGGAACCGTAAAAAGGCCGCGTTGCTGGCGTT
TTTCCATAGGCTCCGCCCCCCTGACGAGCATCACAAAAATCGACGCTCAAGTCAGAGGTGGC
GAAACCCGACAGGACTATAAAGATACCAGGCGTTTCCCCCTGGAAGCTCCCTCGTGCGCTCT
CCTGTTCCGACCCTGCCGCTTACCGGATACCTGTCCGCCTTTCTCCCTTCGGGAAGCGTGGC
GCTTTCTCATAGCTCACGCTGTAGGTATCTCAGTTCGGTGTAGGTCGTTCGCTCCAAGCTGG
GCTGTGTGCACGAACCCCCCGTTCAGCCCGACCGCTGCGCCTTATCCGGTAACTATCGTCTT
GAGTCCAACCCGGTAAGACACGACTTATCGCCACTGGCAGCAGCCACTGGTAACAGGATTAG
CAGAGCGAGGTATGTAGGCGGTGCTACAGAGTTCTTGAAGTGGTGGCCTAACTACGGCTACA
CTAGAAGAACAGTATTTGGTATCTGCGCTCTGCTGAAGCCAGTTACCTTCGGAAAAAGAGTT
GGTAGCTCTTGATCCGGCAAACAAACCACCGCTGGTAGCGGTTTTTTTGTTTGCAAGCAGCA
GATTACGCGCAGAAAAAAAGGATCTCAAGAAGATCCTTTGATCTTTTCTACGGGGTCTGACG
CTCAGTGGAACGAAAACTCACGTTAAGGGATTTTGGTCATGAGATTATCAAAAAGGATCTTC
ACCTAGATCCTTTTAAATTAAAAATGAAGTTTTAAATCAATCTAAAGTATATATGAGTAAAC
TTGGTCTGACAG**TTACCAATGCTTAATCAGTGAGGCACCTATCTCAGCGATCTGTCTATTTC**
GTTCATCCATAGTTGCCTGACTCCCCGTCGTGTAGATAACTACGATACGGGAGGGCTTACCA
TCTGGCCCCAGTGCTGCAATGATACCGCGAGACCCACGCTCACCGGCTCCAGATTTATCAGC
AATAAACCAGCCAGCCGGAAGGGCCGAGCGCAGAAGTGGTCCTGCAACTTTATCCGCCTCCA
TCCAGTCTATTAATTGTTGCCGGGAAGCTAGAGTAAGTAGTTCGCCAGTTAATAGTTTGCGC
AACGTTGTTGCCATTGCTACAGGCATCGTGGTGTCACGCTCGTCGTTTGGTATGGCTTCATT
CAGCTCCGGTTCCCAACGATCAAGGCGAGTTACATGATCCCCCATGTTGTGCAAAAAAGCGG
TTAGCTCCTTCGGTCCTCCGATCGTTGTCAGAAGTAAGTTGGCCGCAGTGTTATCACTCATG
GTTATGGCAGCACTGCATAATTCTCTTACTGTCATGCCATCCGTAAGATGCTTTTCTGTGAC
TGGTGAGTACTCAACCAAGTCATTCTGAGAATAGTGTATGCGGCGACCGAGTTGCTCTTGCC
CGGCGTCAATACGGGATAATACCGCGCCACATAGCAGAACTTTAAAAGTGCTCATCATTGGA
AAACGTTCTTCGGGGCGAAAACTCTCAAGGATCTTACCGCTGTTGAGATCCAGTTCGATGTA
ACCCACTCGTGCACCCAACTGATCTTCAGCATCTTTTACTTTCACCAGCGTTTCTGGGTGAG
CAAAAACAGGAAGGCAAAATGCCGCAAAAAAGGGAATAAGGGCGACACGGAAATGTTGAATA
CTCATACTCTTCCTTTTTCAATATTATTGAAGCATTTATCAGGGTTATTGTCTCATGAGCGG
ATACATATTTGAATGTATTTAGAAAAATAAACAAATAGGGGTTCCGCGCACATTTCCCCGAA
AAGTGCCACCTGACGTC

Green	**cassette containing the immediate early promoter region of CMV**
Purple	**multiple cloning site**
Cyan	**cassette encoding the resistance gene to ampicillin**

Bibliography

Bibliography

Adkins, C.E., Morris, S.A., De Smedt, H., Sienaert, I., Torok, K., and Taylor, C.W. 2000. Ca^{2+}-calmodulin inhibits Ca^{2+} release mediated by type-1, -2 and -3 inositol trisphosphate receptors. *Biochem J.* 345 Pt 2:357-363.

Adler, V., Yin, Z., Tew, K.D., and Ronai, Z. 1999. Role of redox potential and reactive oxygen species in stress signaling. *Oncogene.* 18:6104-6111.

Ahmad, S., Ahmad, A., Ghosh, M., Leslie, C.C., and White, C.W. 2004. Extracellular ATP-mediated signaling for survival in hyperoxia-induced oxidative stress. *J Biol Chem.* 279:16317-16325.

Ai, X., Curran, J.W., Shannon, T.R., Bers, D.M., and Pogwizd, S.M. 2005. Ca^{2+}/calmodulin-dependent protein kinase modulates cardiac ryanodine receptor phosphorylation and sarcoplasmic reticulum Ca^{2+} leak in heart failure. *Circ Res.* 97:1314-1322.

Anderson, A.A., Brown, R.L., Polster, B., Pollock, N., and Stowell, K.M. 2008. Identification and biochemical characterization of a novel ryanodine receptor gene mutation associated with malignant hyperthermia. *Anesthesiology.* 108:208-215.

Ando, H., Mizutani, A., Kiefer, H., Tsuzurugi, D., Michikawa, T., and Mikoshiba, K. 2006. IRBIT suppresses IP_3 receptor activity by competing with IP_3 for the common binding site on the IP_3 receptor. *Mol Cell.* 22:795-806.

Ando, H., Mizutani, A., Matsu-ura, T., and Mikoshiba, K. 2003. IRBIT, a novel inositol 1,4,5-trisphosphate (IP_3) receptor-binding protein, is released from the IP_3 receptor upon IP_3 binding to the receptor. *J Biol Chem.* 278:10602-10612.

Anzai, K., Ogawa, K., Ozawa, T., and Yamamoto, H. 2000. Oxidative modification of ion channel activity of ryanodine receptor. *Antioxid Redox Signal.* 2:35-40.

Aracena-Parks, P., Goonasekera, S.A., Gilman, C.P., Dirksen, R.T., Hidalgo, C., and Hamilton, S.L. 2006. Identification of cysteines involved in S-nitrosylation, S-glutathionylation, and oxidation to disulfides in ryanodine receptor type 1. *J Biol Chem.* 281:40354-40368.

Arai, T., Nonogawa, M., Makino, K., Endo, N., Mori, H., Miyoshi, T., Yamashita, K., Sasada, M., Kakuyama, M., and Fukuda, K. 2008. The radical scavenger edaravone (3-methyl-1-phenyl-2-pyrazolin-5-one) reacts with a pterin derivative and produces a cytotoxic substance that induces intracellular reactive oxygen species generation and cell death. *J Pharmacol Exp Ther.* 324:529-538.

Arguin, G., Regimbald-Dumas, Y., Fregeau, M.O., Caron, A.Z., and Guillemette, G. 2007. Protein kinase C phosphorylates the inositol 1,4,5-trisphosphate receptor type 2 and decreases the mobilization of Ca^{2+} in pancreatoma AR4-2J cells. *J Endocrinol.* 192:659-668.

Arnaudeau, S., Kelley, W.L., Walsh, J.V., Jr., and Demaurex, N. 2001. Mitochondria recycle Ca^{2+} to the endoplasmic reticulum and prevent the depletion of neighboring endoplasmic reticulum regions. *J Biol Chem.* 276:29430-29439.

Asai, T., Ohno, Y., Minatoguchi, S., Funaguchi, N., Yuhgetsu, H., Sawada, M., Takemura, G., Komada, A., Fujiwara, T., and Fujiwara, H. 2007. The specific free radical scavenger edaravone suppresses bleomycin-induced acute pulmonary injury in rabbits. *Clin Exp Pharmacol Physiol.* 34:22-26.

Assefa, Z., Bultynck, G., Szlufcik, K., Nadif Kasri, N., Vermassen, E., Goris, J., Missiaen, L., Callewaert, G., Parys, J.B., and De Smedt, H. 2004. Caspase-3-induced truncation of type 1 inositol trisphosphate receptor accelerates apoptotic cell death and induces inositol trisphosphate-independent calcium release during apoptosis. *J Biol Chem.* 279:43227-43236.

Ayettey, A.S., and Navaratnam, V. 1978. The T-tubule system in the specialized and general myocardium of the rat. *J Anat.* 127:125-140.

Baird, G.S., Zacharias, D.A., and Tsien, R.Y. 2000. Biochemistry, mutagenesis, and oligomerization of DsRed, a red fluorescent protein from coral. *Proc Natl Acad Sci U S A.* 97:11984-11989.

Balshaw, D., Gao, L., and Meissner, G. 1999. Luminal loop of the ryanodine receptor: a pore-forming segment? *Proc Natl Acad Sci U S A.* 96:3345-3347.

Balshaw, D.M., Xu, L., Yamaguchi, N., Pasek, D.A., and Meissner, G. 2001. Calmodulin binding and inhibition of cardiac muscle calcium release channel (ryanodine receptor). *J Biol Chem.* 276:20144-20153.

Bannister, M.L., Hamada, T., Murayama, T., Harvey, P.J., Casarotto, M.G., Dulhunty, A.F., and Ikemoto, N. 2007. Malignant hyperthermia mutation sites in the Leu2442-Pro2477 (DP4) region of RyR1 (ryanodine receptor 1) are clustered in a structurally and functionally definable area. *Biochem J.* 401:333-339.

Bano, D., Munarriz, E., Chen, H.L., Ziviani, E., Lippi, G., Young, K.W., and Nicotera, P. 2007. The plasma membrane Na^+/Ca^{2+} exchanger is cleaved by distinct protease families in neuronal cell death. *Ann N Y Acad Sci.* 1099:451-455.

Bare, D.J., Kettlun, C.S., Liang, M., Bers, D.M., and Mignery, G.A. 2005. Cardiac type 2 inositol 1,4,5-trisphosphate receptor: interaction and modulation by calcium/calmodulin-dependent protein kinase II. *J Biol Chem.* 280:15912-15920.

Basu, A., and Miura, A. 2002. Differential regulation of extrinsic and intrinsic cell death pathways by protein kinase C. *Int J Mol Med.* 10:541-545.

Beard, N.A., Casarotto, M.G., Wei, L., Varsanyi, M., Laver, D.R., and Dulhunty, A.F. 2005. Regulation of ryanodine receptors by calsequestrin: effect of high luminal Ca^{2+} and phosphorylation. *Biophys J.* 88:3444-3454.

Beard, N.A., Laver, D.R., and Dulhunty, A.F. 2004. Calsequestrin and the calcium release channel of skeletal and cardiac muscle. *Prog Biophys Mol Biol.* 85:33-69.

Benkusky, N.A., Weber, C.S., Scherman, J.A., Farrell, E.F., Hacker, T.A., John, M.C., Powers, P.A., and Valdivia, H.H. 2007. Intact beta-adrenergic response and unmodified progression toward heart failure in mice with genetic ablation of a major protein kinase A phosphorylation site in the cardiac ryanodine receptor. *Circ Res.* 101:819-829.

Berrebi-Bertrand, I., Souchet, M., Camelin, J.C., Laville, M.P., Calmels, T., and Bril, A. 1998. Biophysical interaction between phospholamban and protein phosphatase 1 regulatory subunit GM. *FEBS Lett.* 439:224-230.

Berridge, M.J. 1993. Inositol trisphosphate and calcium signalling. *Nature.* 361:315-325.

Berridge, M.J., Bootman, M.D., and Lipp, P. 1998. Calcium--a life and death signal. *Nature.* 395:645-648.

Berridge, M.J., Bootman, M.D., and Roderick, H.L. 2003. Calcium signalling: dynamics, homeostasis and remodelling. *Nat. Rev. Mol. Cell Biol.* 4:517-529.

Bers, D.M. 2002. Cardiac excitation-contraction coupling. *Nature.* 415:198 - 205.

Bers, D.M. 2004. Macromolecular complexes regulating cardiac ryanodine receptor function. *J Mol Cell Cardiol.* 37:417-429.

Bers, D.M. 2008. Calcium cycling and signaling in cardiac myocytes. *Annu Rev Physiol.* 70:23-49.

Bers, D.M., and Despa, S. 2006. Cardiac myocytes Ca^{2+} and Na^+ regulation in normal and failing hearts. *J Pharmacol Sci.* 100:315-322.

Bers, D.M., and Perez-Reyes, E. 1999. Ca^{2+} channels in cardiac myocytes: structure and function in Ca^{2+} influx and intracellular Ca^{2+} release. *Cardiovasc Res.* 42:339-360.

Bers, D.M., and Weber, C.R. 2002. Na^+/Ca^{2+} exchange function in intact ventricular myocytes. *Ann N Y Acad Sci.* 976:500-512.

Bhat, M.B., Hayek, S.M., Zhao, J., Zang, W., Takeshima, H., Wier, W.G., and Ma, J. 1999. Expression and functional characterization of the cardiac muscle ryanodine receptor Ca^{2+} release channel in Chinese hamster ovary cells. *Biophys J.* 77:808-816.

Bhat, M.B., and Ma, J. 2002a. The transmembrane segment of ryanodine receptor contains an intracellular membrane retention signal for Ca^{2+} release channel. *J. Biol. Chem.* 277:8597-8601.

Bhat, M.B., and Ma, J. 2002b. The transmembrane segment of ryanodine receptor contains an intracellular membrane retention signal for Ca^{2+} release channel. *J Biol Chem.* 277:8597-8601.

Bhat, M.B., Zhao, J., Takeshima, H., and Ma, J. 1997. Functional calcium release channel formed by the carboxyl-terminal portion of ryanodine receptor. *Biophys J.* 73:1329-1336.

Bhuiyan, Z.A., Hamdan, M.A., Shamsi, E.T., Postma, A.V., Mannens, M.M., Wilde, A.A., and Al-Gazali, L. 2007a. A novel early onset lethal form of catecholaminergic polymorphic ventricular tachycardia maps to chromosome 7p14-p22. *J Cardiovasc Electrophysiol.* 18:1060-1066.

Bhuiyan, Z.A., van den Berg, M.P., van Tintelen, J.P., Bink-Boelkens, M.T., Wiesfeld, A.C., Alders, M., Postma, A.V., van Langen, I., Mannens, M.M., and Wilde, A.A. 2007b. Expanding spectrum of human RYR2-related disease: new electrocardiographic, structural, and genetic features. *Circulation.* 116:1569-1576.

Block, B.A., Imagawa, T., Campbell, K.P., and Franzini-Armstrong, C. 1988. Structural evidence for direct interaction between the molecular components of the transverse tubule/sarcoplasmic reticulum junction in skeletal muscle. *J Cell Biol.* 107:2587-2600.

Bobe, R., Bredoux, R., Corvazier, E., Andersen, J.P., Clausen, J.D., Dode, L., Kovacs, T., and Enouf, J. 2004. Identification, expression, function, and localization of a novel (sixth) isoform of the human sarco/endoplasmic reticulum Ca^{2+}ATPase 3 gene. *J Biol Chem.* 279:24297-24306.

Bodalina, U.M., Hammond, K.D., and Gilbert, D.A. 2005. Temporal changes in the expression of protein phosphatase 1 and protein phosphatase 2A in proliferating and differentiating murine erythroleukaemia cells. *Cell Biol Int.* 29:287-299.

Boehning, D., and Joseph, S.K. 2000. Direct association of ligand-binding and pore domains in homo- and heterotetrameric inositol 1,4,5-trisphosphate receptors. *Embo J.* 19:5450-5459.

Boehning, D., Patterson, R.L., Sedaghat, L., Glebova, N.O., Kurosaki, T., and Snyder, S.H. 2003. Cytochrome c binds to inositol (1,4,5) trisphosphate receptors, amplifying calcium-dependent apoptosis. *Nat Cell Biol.* 5:1051-1061.

Boehning, D., van Rossum, D.B., Patterson, R.L., and Snyder, S.H. 2005. A peptide inhibitor of cytochrome c/inositol 1,4,5-trisphosphate receptor binding blocks intrinsic and extrinsic cell death pathways. *Proc Natl Acad Sci U S A.* 102:1466-1471.

Bosanac, I., Alattia, J.R., Mal, T.K., Chan, J., Talarico, S., Tong, F.K., Tong, K.I., Yoshikawa, F., Furuichi, T., Iwai, M., Michikawa, T., Mikoshiba, K., and Ikura, M. 2002. Structure of the inositol 1,4,5-trisphosphate receptor binding core in complex with its ligand. *Nature.* 420:696-700.

Bosanac, I., Yamazaki, H., Matsu-Ura, T., Michikawa, T., Mikoshiba, K., and Ikura, M. 2005. Crystal structure of the ligand binding suppressor domain of type 1 inositol 1,4,5-trisphosphate receptor. *Mol Cell.* 17:193-203.

Braet, K., Mabilde, C., Cabooter, L., Rapp, G., and Leybaert, L. 2004. Electroporation loading and photoactivation of caged IP_3: tools to investigate the relation between cellular ATP release in response to intracellular IP_3 elevation. *J Neurosci Methods.* 132:81-89.

Bray, M.A., Geisse, N.A., and Parker, K.K. 2007. Multidimensional detection and analysis of Ca^{2+} sparks in cardiac myocytes. *Biophys J.* 92:4433-4443.

Brillantes, A.M., Allen, P., Takahashi, T., Izumo, S., and Marks, A.R. 1992. Differences in cardiac calcium release channel (ryanodine receptor) expression in myocardium from patients with end-stage heart failure caused by ischemic versus dilated cardiomyopathy. *Circ Res.* 71:18-26.

Brini, M. 2004. Ryanodine receptor defects in muscle genetic diseases. *Biochem. Biophys. Res. Commun.* 322:1245-1255.

Brouckaert, G., Kalai, M., Krysko, D.V., Saelens, X., Vercammen, D., Ndlovu, M., Haegeman, G., D'Herde, K., and Vandenabeele, P. 2004. Phagocytosis of necrotic cells by macrophages is phosphatidylserine dependent and does not induce inflammatory cytokine production. *Mol Biol Cell.* 15:1089-1100.

Bulanova, E., Budagian, V., Orinska, Z., Hein, M., Petersen, F., Thon, L., Adam, D., and Bulfone-Paus, S. 2005. Extracellular ATP induces cytokine expression and apoptosis through P2X7 receptor in murine mast cells. *J Immunol.* 174:3880-3890.

Bull, R., Finkelstein, J.P., Humeres, A., Behrens, M.I., and Hidalgo, C. 2007. Effects of ATP, Mg^{2+}, and redox agents on the Ca^{2+} dependence of RyR channels from rat brain cortex. *Am J Physiol Cell Physiol.* 293:C162-171.

Bultynck, G., De Smet, P., Rossi, D., Callewaert, G., Missiaen, L., Sorrentino, V., De Smedt, H., and Parys, J.B. 2001. Characterization and mapping of the 12 kDa FK506-binding protein (FKBP12)-binding site on different isoforms of the ryanodine receptor and of the inositol 1,4,5-trisphosphate receptor. *Biochem J.* 354:413-422.

Burnette, W.N. 1981. "Western blotting": electrophoretic transfer of proteins from sodium dodecyl sulfate--polyacrylamide gels to unmodified nitrocellulose and radiographic detection with antibody and radioiodinated protein A. *Anal Biochem.* 112:195-203.

Butanda-Ochoa, A., Hojer, G., Morales-Tlalpan, V., and Diaz-Munoz, M. 2006. Recognition and activation of ryanodine receptors by purines. *Curr Med Chem.* 13:647-657.

Butcher, R.W., and Sutherland, E.W. 1962. Adenosine 3',5'-phosphate in biological materials. I. Purification and properties of cyclic 3',5'-nucleotide phosphodiesterase and use of this enzyme to characterize adenosine 3',5'-phosphate in human urine. *J Biol Chem.* 237:1244-1250.

Cakir, Y., and Ballinger, S.W. 2005. Reactive species-mediated regulation of cell signaling and the cell cycle: the role of MAPK. *Antioxid Redox Signal.* 7:726-740.

Cameron, A.M., Nucifora, F.C., Jr., Fung, E.T., Livingston, D.J., Aldape, R.A., Ross, C.A., and Snyder, S.H. 1997. FKBP12 binds the inositol 1,4,5-trisphosphate receptor at leucine-proline (1400-1401) and anchors calcineurin to this FK506-like domain. *J Biol Chem.* 272:27582-27588.

Campbell, K.P., Franzini-Armstrong, C., and Shamoo, A.E. 1980. Further characterization of light and heavy sarcoplasmic reticulum vesicles. Identification of the 'sarcoplasmic reticulum feet' associated with heavy sarcoplasmic reticulum vesicles. *Biochim Biophys Acta.* 602:97-116.

Campbell, R.E., Tour, O., Palmer, A.E., Steinbach, P.A., Baird, G.S., Zacharias, D.A., and Tsien, R.Y. 2002. A monomeric red fluorescent protein. *PNAS.* 99:7877-7882.

Carafoli, E. 2002. Calcium signaling: a tale for all seasons. *Proc Natl Acad Sci U S A.* 99:1115-1122.

Cardenas, C., Liberona, J.L., Molgo, J., Colasante, C., Mignery, G.A., and Jaimovich, E. 2005. Nuclear inositol 1,4,5-trisphosphate receptors regulate local Ca^{2+} transients and modulate cAMP response element binding protein phosphorylation. *J Cell Sci.* 118:3131-3140.

Cardozo, A.K., Ortis, F., Storling, J., Feng, Y.M., Rasschaert, J., Tonnesen, M., Van Eylen, F., Mandrup-Poulsen, T., Herchuelz, A., and Eizirik, D.L. 2005. Cytokines downregulate the sarcoendoplasmic reticulum pump Ca^{2+} ATPase 2b and deplete endoplasmic reticulum Ca^{2+}, leading to induction of endoplasmic reticulum stress in pancreatic beta-cells. *Diabetes.* 54:452-461.

Caron, A.Z., Chaloux, B., Arguin, G., and Guillemette, G. 2007. Protein kinase C decreases the apparent affinity of the inositol 1,4,5-trisphosphate receptor type 3 in RINm5F cells. *Cell Calcium*. 42:323-331.

Carr, A.N., Schmidt, A.G., Suzuki, Y., del Monte, F., Sato, Y., Lanner, C., Breeden, K., Jing, S.L., Allen, P.B., Greengard, P., Yatani, A., Hoit, B.D., Grupp, I.L., Hajjar, R.J., DePaoli-Roach, A.A., and Kranias, E.G. 2002. Type 1 phosphatase, a negative regulator of cardiac function. *Mol Cell Biol*. 22:4124-4135.

Carter, S., Colyer, J., and Sitsapesan, R. 2006. Maximum phosphorylation of the cardiac ryanodine receptor at serine-2809 by protein kinase a produces unique modifications to channel gating and conductance not observed at lower levels of phosphorylation. *Circ Res*. 98:1506-1513.

Cerrone, M., Colombi, B., Santoro, M., di Barletta, M.R., Scelsi, M., Villani, L., Napolitano, C., and Priori, S.G. 2005. Bidirectional ventricular tachycardia and fibrillation elicited in a knock-in mouse model carrier of a mutation in the cardiac ryanodine receptor. *Circ Res*. 96:e77-82.

Chaabane, C., Corvazier, E., Bredoux, R., Dally, S., Raies, A., Villemain, A., Dupuy, E., Enouf, J., and Bobe, R. 2006. Sarco/endoplasmic reticulum Ca^{2+}ATPase type 3 isoforms (SERCA3b and SERCA3f): distinct roles in cell adhesion and ER stress. *Biochem Biophys Res Commun*. 345:1377-1385.

Chalfie, M., Tu, Y., Euskirchen, G., Ward, W.W., and Prasher, D.C. 1994. Green fluorescent protein as a marker for gene expression. *Science*. 263:802-805.

Chalmers, M., Schell, M.J., and Thorn, P. 2006. Agonist-evoked inositol trisphosphate receptor (IP_3R) clustering is not dependent on changes in the structure of the endoplasmic reticulum. *Biochem J*. 394:57-66.

Chaloux, B., Caron, A.Z., and Guillemette, G. 2007. Protein kinase A increases the binding affinity and the Ca^{2+} release activity of the inositol 1,4,5-trisphosphate receptor type 3 in RINm5F cells. *Biol Cell*. 99:379-388.

Chan, W.M., Welch, W., and Sitsapesan, R. 2003. Structural characteristics that govern binding to, and modulation through, the cardiac ryanodine receptor nucleotide binding site. *Mol Pharmacol*. 63:174-182.

Chapman, H., Ramstrom, C., Korhonen, L., Laine, M., Wann, K.T., Lindholm, D., Pasternack, M., and Tornquist, K. 2005. Downregulation of the HERG (KCNH2) K^+ channel by ceramide: evidence for ubiquitin-mediated lysosomal degradation. *J Cell Sci*. 118:5325-5334.

Charles, A.C., Naus, C.C., Zhu, D., Kidder, G.M., Dirksen, E.R., and Sanderson, M.J. 1992. Intercellular calcium signaling via gap junctions in glioma cells. *J Cell Biol*. 118:195-201.

Chautan, M., Chazal, G., Cecconi, F., Gruss, P., and Golstein, P. 1999. Interdigital cell death can occur through a necrotic and caspase-independent pathway. *Curr Biol*. 9:967-970.

Chelu, M.G., Goonasekera, S.A., Durham, W.J., Tang, W., Lueck, J.D., Riehl, J., Pessah, I.N., Zhang, P., Bhattacharjee, M.B., Dirksen, R.T., and Hamilton, S.L. 2006. Heat- and anesthesia-induced malignant hyperthermia in an RyR1 knock-in mouse. *Faseb J*. 20:329-330.

Chen, C., and Okayama, H. 1987. High-efficiency transformation of mammalian cells by plasmid DNA. *Mol. Biol. Cell*. 7:2745-2752.

Chen, C.C., Chang, J., and Lin, W.W. 1995a. Differential expression of protein kinase C isoforms in glial and neuronal cells. Translocation and down-regulation of PKC isoforms in C6 glioma and NG 108-15 hybrid cells: effects of extracellular Ca^{2+}-depletion. *Neurochem Int*. 26:455-464.

Chen, S.R., Airey, J.A., and MacLennan, D.H. 1993. Positioning of major tryptic fragments in the Ca^{2+} release channel (ryanodine receptor) resulting from partial digestion of rabbit skeletal muscle sarcoplasmic reticulum. *J Biol Chem*. 268:22642-22649.

Chen, S.R., Leong, P., Imredy, J.P., Bartlett, C., Zhang, L., and MacLennan, D.H. 1997. Single-channel properties of the recombinant skeletal muscle Ca^{2+} release channel (ryanodine receptor). *Biophys J.* 73:1904-1912.

Chen, Z.P., Levy, A., and Lightman, S.L. 1995b. Nucleotides as extracellular signalling molecules. *J Neuroendocrinol.* 7:83-96.

Cheng, W., Altafaj, X., Ronjat, M., and Coronado, R. 2005. Interaction between the dihydropyridine receptor Ca^{2+} channel beta-subunit and ryanodine receptor type 1 strengthens excitation-contraction coupling. *Proc Natl Acad Sci U S A.* 102:19225-19230.

Chiarugi, P., and Cirri, P. 2003. Redox regulation of protein tyrosine phosphatases during receptor tyrosine kinase signal transduction. *Trends Biochem Sci.* 28:509-514.

Ching, L.L., Williams, A.J., and Sitsapesan, R. 2000. Evidence for Ca^{2+} activation and inactivation sites on the luminal side of the cardiac ryanodine receptor complex. *Circ Res.* 87:201-206.

Choe, C.U., and Ehrlich, B.E. 2006. The inositol 1,4,5-trisphosphate receptor (IP_3R) and its regulators: sometimes good and sometimes bad teamwork. *Sci STKE.* 2006:re15.

Chu, G., Ferguson, D.G., Edes, I., Kiss, E., Sato, Y., and Kranias, E.G. 1998. Phospholamban ablation and compensatory responses in the mammalian heart. *Ann N Y Acad Sci.* 853:49-62.

Claycomb, W.C., Lanson, N.A., Jr., Stallworth, B.S., Egeland, D.B., Delcarpio, J.B., Bahinski, A., and Izzo, N.J., Jr. 1998. HL-1 cells: a cardiac muscle cell line that contracts and retains phenotypic characteristics of the adult cardiomyocyte. *Proc Natl Acad Sci U S A.* 95:2979-2984.

Cohen, J.J., Duke, R.C., Fadok, V.A., and Sellins, K.S. 1992. Apoptosis and programmed cell death in immunity. *Annu Rev Immunol.* 10:267-293.

Colbran, R.J., Schworer, C.M., Hashimoto, Y., Fong, Y.L., Rich, D.P., Smith, M.K., and Soderling, T.R. 1989. Calcium/calmodulin-dependent protein kinase II. *Biochem J.* 258:313-325.

Colella, M., Grisan, F., Robert, V., Turner, J.D., Thomas, A.P., and Pozzan, T. 2008. Ca^{2+} oscillation frequency decoding in cardiac cell hypertrophy: role of calcineurin/NFAT as Ca^{2+} signal integrators. *Proc Natl Acad Sci U S A.* 105:2859-2864.

Collier, M.L., Ji, G., Wang, Y., and Kotlikoff, M.I. 2000. Calcium-induced calcium release in smooth muscle: loose coupling between the action potential and calcium release. *J Gen Physiol.* 115:653-662.

Colyer, J. 1998. Phosphorylation states of phospholamban. *Ann N Y Acad Sci.* 853:79-91.

Conklin, B.R., Chabre, O., Wong, Y.H., Federman, A.D., and Bourne, H.R. 1992. Recombinant Gq alpha. Mutational activation and coupling to receptors and phospholipase C. *J Biol Chem.* 267:31-34.

Contreras, J.E., Sanchez, H.A., Eugenin, E.A., Speidel, D., Theis, M., Willecke, K., Bukauskas, F.F., Bennett, M.V., and Saez, J.C. 2002. Metabolic inhibition induces opening of unapposed connexin 43 gap junction hemichannels and reduces gap junctional communication in cortical astrocytes in culture. *Proc Natl Acad Sci U S A.* 99:495-500.

Contreras, J.E., Sanchez, H.A., Veliz, L.P., Bukauskas, F.F., Bennett, M.V., and Saez, J.C. 2004. Role of connexin-based gap junction channels and hemichannels in ischemia-induced cell death in nervous tissue. *Brain Res Brain Res Rev.* 47:290-303.

Copello, J.A., Barg, S., Sonnleitner, A., Porta, M., Diaz-Sylvester, P., Fill, M., Schindler, H., and Fleischer, S. 2002. Differential activation by Ca^{2+}, ATP and caffeine of cardiac and skeletal muscle ryanodine receptors after block by Mg^{2+}. *J Membr Biol.* 187:51-64.

Copello, J.A., Qi, Y., Jeyakumar, L.H., Ogunbunmi, E., and Fleischer, S. 2001. Lack of effect of cADP-ribose and NAADP on the activity of skeletal muscle and heart ryanodine receptors. *Cell Calcium.* 30:269-284.

Coronado, R., Morrissette, J., Sukhareva, M., and Vaughan, D.M. 1994. Structure and function of ryanodine receptors. *Am J Physiol.* 266:C1485-1504.

Cotrina, M.L., Lin, J.H., and Nedergaard, M. 1998. Cytoskeletal assembly and ATP release regulate astrocytic calcium signaling. *J Neurosci.* 18:8794-8804.

Cronier, L., Herve, J.C., Deleze, J., and Malassine, A. 1997. Regulation of gap junctional communication during human trophoblast differentiation. *Microsc Res Tech.* 38:21-28.

Csordas, G., Renken, C., Varnai, P., Walter, L., Weaver, D., Buttle, K.F., Balla, T., Mannella, C.A., and Hajnoczky, G. 2006. Structural and functional features and significance of the physical linkage between ER and mitochondria. *J Cell Biol.* 174:915-921.

Curran, J., Hinton, M.J., Rios, E., Bers, D.M., and Shannon, T.R. 2007. Beta-adrenergic enhancement of sarcoplasmic reticulum calcium leak in cardiac myocytes is mediated by calcium/calmodulin-dependent protein kinase. *Circ Res.* 100:391-398.

Currie, S., Loughrey, C.M., Craig, M.A., and Smith, G.L. 2004. Calcium/calmodulin-dependent protein kinase IIdelta associates with the ryanodine receptor complex and regulates channel function in rabbit heart. *Biochem J.* 377:357-366.

Cusato, K., Ripps, H., Zakevicius, J., and Spray, D.C. 2006. Gap junctions remain open during cytochrome c-induced cell death: relationship of conductance to 'bystander' cell killing. *Cell Death Differ.* 13:1707-1714.

Cusato, K., Zakevicius, J., and Ripps, H. 2003. An experimental approach to the study of gap-junction-mediated cell death. *Biol Bull.* 205:197-199.

Dai, D.-z., and Yu, F. 2005. Ion channelopathy and hyperphosphorylation contributing to cardiac arrhythmias. *Acta Pharmacologica Sinica.* 26:918-925.

Das, S., Nwachukwu, J.C., Li, D., Vulin, A.I., Martinez-Caballero, S., Kinnally, K.W., and Samuels, H.H. 2007. The nuclear receptor interacting factor-3 transcriptional coregulator mediates rapid apoptosis in breast cancer cells through direct and bystander-mediated events. *Cancer Res.* 67:1775-1782.

Dassanayake, R.P., Maheswaran, S.K., and Srikumaran, S. 2007. Monomeric expression of bovine beta2-integrin subunits reveals their role in Mannheimia haemolytica leukotoxin-induced biological effects. *Infect Immun.* 75:5004-5010.

Davia, K., Bernobich, E., Ranu, H.K., del Monte, F., Terracciano, C.M., MacLeod, K.T., Adamson, D.L., Chaudhri, B., Hajjar, R.J., and Harding, S.E. 2001. SERCA2A overexpression decreases the incidence of aftercontractions in adult rabbit ventricular myocytes. *J Mol Cell Cardiol.* 33:1005-1015.

Davia, K., Hajjar, R.J., Terracciano, C.M., Kent, N.S., Ranu, H.K., O'Gara, P., Rosenzweig, A., and Harding, S.E. 1999. Functional alterations in adult rat myocytes after overexpression of phospholamban with use of adenovirus. *Physiol Genomics.* 1:41-50.

Davidson, S.M., and Duchen, M.R. 2006. Effects of NO on mitochondrial function in cardiomyocytes: Pathophysiological relevance. *Cardiovasc Res.* 71:10-21.

Davis, J.P., Norman, C., Kobayashi, T., Solaro, R.J., Swartz, D.R., and Tikunova, S.B. 2007. Effects of thin and thick filament proteins on calcium binding and exchange with cardiac troponin C. *Biophys J.* 92:3195-3206.

De Vuyst, E., Decrock, E., Cabooter, L., Dubyak, G.R., Naus, C.C., Evans, W.H., and Leybaert, L. 2006. Intracellular calcium changes trigger connexin 32 hemichannel opening. *Embo J.* 25:34-44.

Deitmer, J.W., Brockhaus, J., and Casel, D. 2006. Modulation of synaptic activity in Purkinje neurons by ATP. *Cerebellum.* 5:49-54.

del Monte, F., Harding, S.E., Schmidt, U., Matsui, T., Kang, Z.B., Dec, G.W., Gwathmey, J.K., Rosenzweig, A., and Hajjar, R.J. 1999. Restoration of contractile function in

isolated cardiomyocytes from failing human hearts by gene transfer of SERCA2a. *Circulation.* 100:2308-2311.

Demaurex, N., and Distelhorst, C. 2003. Cell biology. Apoptosis--the calcium connection. *Science.* 300:65-67.

Dettling, M., Sander, T., Weber, M., and Steinlein, O.K. 2004. Mutation analysis of the ryanodine receptor gene isoform 3 (RYR3) in recurrent neuroleptic malignant syndrome. *J Clin Psychopharmacol.* 24:471-473.

Devogelaere, B., Beullens, M., Sammels, E., Derua, R., Waelkens, E., van Lint, J., Parys, J.B., Missiaen, L., Bollen, M., and De Smedt, H. 2007. Protein phosphatase-1 is a novel regulator of the interaction between IRBIT and the inositol 1,4,5-trisphosphate receptor. *Biochem J.* 407:303-311.

Didenko, V.V., Ngo, H., Minchew, C.L., Boudreaux, D.J., Widmayer, M.A., and Baskin, D.S. 2002. Caspase-3-dependent and -independent apoptosis in focal brain ischemia. *Mol Med.* 8:347-352.

Dillmann, W.H. 1998. Influences of increased expression of the Ca^{2+} ATPase of the sarcoplasmic reticulum by a transgenic approach on cardiac contractility. *Ann N Y Acad Sci.* 853:43-48.

Ding, W.X., Ni, H.M., DiFrancesca, D., Stolz, D.B., and Yin, X.M. 2004. Bid-dependent generation of oxygen radicals promotes death receptor activation-induced apoptosis in murine hepatocytes. *Hepatology.* 40:403-413.

Dirksen, W.P., Lacombe, V.A., Chi, M., Kalyanasundaram, A., Viatchenko-Karpinski, S., Terentyev, D., Zhou, Z., Vedamoorthyrao, S., Li, N., Chiamvimonvat, N., Carnes, C.A., Franzini-Armstrong, C., Gyorke, S., and Periasamy, M. 2007. A mutation in calsequestrin, CASQ2 D307H, impairs Sarcoplasmic Reticulum Ca^{2+} handling and causes complex ventricular arrhythmias in mice. *Cardiovasc Res.* 75:69-78.

Doi, M., Yano, M., Kobayashi, S., Kohno, M., Tokuhisa, T., Okuda, S., Suetsugu, M., Hisamatsu, Y., Ohkusa, T., Kohno, M., and Matsuzaki, M. 2002. Propranolol prevents the development of heart failure by restoring FKBP12.6-mediated stabilization of ryanodine receptor. *Circulation.* 105:1374-1379.

Dolmetsch, R.E., Lewis, R.S., Goodnow, C.C., and Healy, J.I. 1997. Differential activation of transcription factors induced by Ca^{2+} response amplitude and duration. *Nature.* 386:855-858.

Dolmetsch, R.E., Xu, K., and Lewis, R.S. 1998. Calcium oscillations increase the efficiency and specificity of gene expression. *Nature.* 392:933-936.

Domeier, T.L., Zima, A.V., Maxwell, J.T., Huke, S., Mignery, G.A., and Blatter, L.A. 2008. IP_3 receptor-dependent Ca^{2+} release modulates excitation-contraction coupling in rabbit ventricular myocytes. *Am J Physiol Heart Circ Physiol.* 294:H596-604.

Droge, W. 2002. Free radicals in the physiological control of cell function. *Physiol Rev.* 82:47-95.

Du, G.G., Avila, G., Sharma, P., Khanna, V.K., Dirksen, R.T., and MacLennan, D.H. 2004. Role of the sequence surrounding predicted transmembrane helix M4 in membrane association and function of the Ca^{2+} release channel of skeletal muscle sarcoplasmic reticulum (ryanodine receptor isoform 1). *J Biol Chem.* 279:37566-37574.

Du, G.G., Guo, X., Khanna, V.K., and MacLennan, D.H. 2001. Ryanodine sensitizes the cardiac Ca^{2+} release channel (ryanodine receptor isoform 2) to Ca^{2+} activation and dissociates as the channel is closed by Ca^{2+} depletion. *Proc Natl Acad Sci U S A.* 98:13625-13630.

Du, G.G., and MacLennan, D.H. 1998. Functional consequences of mutations of conserved, polar amino acids in transmembrane sequences of the Ca^{2+} release channel (ryanodine receptor) of rabbit skeletal muscle sarcoplasmic reticulum. *J Biol Chem.* 273:31867-31872.

Du, G.G., Sandhu, B., Khanna, V.K., Guo, X.H., and MacLennan, D.H. 2002a. Topology of the Ca^{2+} release channel of skeletal muscle sarcoplasmic reticulum (RyR1). *PNAS.* 99:16725-16730.

Du, G.G., Sandhu, B., Khanna, V.K., Guo, X.H., and MacLennan, D.H. 2002b. Topology of the Ca^{2+} release channel of skeletal muscle sarcoplasmic reticulum (RyR1). *Proc Natl Acad Sci U S A.* 99:16725-16730.

Durham, W.J., Aracena-Parks, P., Long, C., Rossi, A.E., Goonasekera, S.A., Boncompagni, S., Galvan, D.L., Gilman, C.P., Baker, M.R., Shirokova, N., Protasi, F., Dirksen, R., and Hamilton, S.L. 2008. RyR1 S-nitrosylation underlies environmental heat stroke and sudden death in Y522S RyR1 knockin mice. *Cell.* 133:53-65.

Earnshaw, W.C., Martins, L.M., and Kaufmann, S.H. 1999. Mammalian caspases: structure, activation, substrates, and functions during apoptosis. *Annu Rev Biochem.* 68:383-424.

Echt, D.S., Liebson, P.R., Mitchell, L.B., Peters, R.W., Obias-Manno, D., Barker, A.H., Arensberg, D., Baker, A., Friedman, L., Greene, H.L., and et al. 1991. Mortality and morbidity in patients receiving encainide, flecainide, or placebo. The Cardiac Arrhythmia Suppression Trial. *N Engl J Med.* 324:781-788.

Eguchi, Y., Shimizu, S., and Tsujimoto, Y. 1997. Intracellular ATP levels determine cell death fate by apoptosis or necrosis. *Cancer Res.* 57:1835-1840.

Eisner, D.A., Venetucci, L.A., and Trafford, A.W. 2006. Life, sudden death, and intracellular calcium. *Circ Res.* 99:223-224.

El-Hayek, R., Saiki, Y., Yamamoto, T., and Ikemoto, N. 1999. A postulated role of the near amino-terminal domain of the ryanodine receptor in the regulation of the sarcoplasmic reticulum Ca^{2+} channel. *J Biol Chem.* 274:33341-33347.

Eldar, M., Pras, E., and Lahat, H. 2002. A missense mutation in a highly conserved region of CASQ2 is associated with autosomal recessive catecholamine-induced polymorphic ventricular tachycardia in Bedouin families from Israel. *Cold Spring Harb Symp Quant Biol.* 67:333-337.

Eltzschig, H.K., Eckle, T., Mager, A., Kuper, N., Karcher, C., Weissmuller, T., Boengler, K., Schulz, R., Robson, S.C., and Colgan, S.P. 2006. ATP release from activated neutrophils occurs via connexin 43 and modulates adenosine-dependent endothelial cell function. *Circ Res.* 99:1100-1108.

Fabiato, A. 1983. Calcium-induced release of calcium from the cardiac sarcoplasmic reticulum. *Am J Physiol.* 245:C1-14.

Fedorov, V.I., and Cherkasova, O.P. 1997. The effect of a stable acetylcholine analog on angiotensin-converting enzyme activity in the lung, kidney and arterial blood plasma of rats with increased sympathetic activity. *Ross Fiziol Zh Im I M Sechenova.* 83:76-83.

Felgner, P.L., Gadek, T.R., Holm, M., Roman, R., Chan, H.W., Wenz, M., Northrop, J.P., Ringold, G.M., and Danielsen, M. 1987. Lipofection: a highly efficient, lipid-mediated DNA-transfection procedure. *Proc Natl Acad Sci U S A.* 84:7413-7417.

Ferreiro, E., Oliveira, C.R., and Pereira, C.M. 2008. The release of calcium from the endoplasmic reticulum induced by amyloid-beta and prion peptides activates the mitochondrial apoptotic pathway. *Neurobiol Dis.* 30:331-342.

Ferrero, P., Said, M., Sanchez, G., Vittone, L., Valverde, C., Donoso, P., Mattiazzi, A., and Mundina-Weilenmann, C. 2007. Ca^{2+}/calmodulin kinase II increases ryanodine binding and Ca^{2+}-induced sarcoplasmic reticulum Ca^{2+} release kinetics during beta-adrenergic stimulation. *J Mol Cell Cardiol.* 43:281-291.

Ferris, C.D., Huganir, R.L., Bredt, D.S., Cameron, A.M., and Snyder, S.H. 1991. Inositol trisphosphate receptor: phosphorylation by protein kinase C and calcium calmodulin-dependent protein kinases in reconstituted lipid vesicles. *Proc Natl Acad Sci U S A.* 88:2232-2235.

Fessenden, J.D., Chen, L., Wang, Y., Paolini, C., Franzini-Armstrong, C., Allen, P.D., and Pessah, I.N. 2001. Ryanodine receptor point mutant E4032A reveals an allosteric interaction with ryanodine. *Proc Natl Acad Sci U S A.* 98:2865-2870.

Fill, M., and Copello, J.A. 2002. Ryanodine receptor calcium release channels. *Physiol. Rev.* 82:893-922.

Fleischer, S., and Inui, M. 1989. Biochemistry and biophysics of excitation-contraction coupling. *Annu Rev Biophys Biophys Chem.* 18:333-364.

Flucher, B.E., and Franzini-Armstrong, C. 1996. Formation of junctions involved in excitation-contraction coupling in skeletal and cardiac muscle. *Proc Natl Acad Sci U S A.* 93:8101-8106.

Foss, K.B., Landmark, B., Skalhegg, B.S., Tasken, K., Jellum, E., Hansson, V., and Jahnsen, T. 1994. Characterization of in-vitro-translated human regulatory and catalytic subunits of cAMP-dependent protein kinases. *Eur J Biochem.* 220:217-223.

Fradkov, A.F., Chen, Y., Ding, L., Barsova, E.V., Matz, M.V., and Lukyanov, S.A. 2000. Novel fluorescent protein from Discosoma coral and its mutants possesses a unique far-red fluorescence. *FEBS Lett.* 479:127-130.

Francis, J., Sankar, V., Nair, V.K., and Priori, S.G. 2005. Catecholaminergic polymorphic ventricular tachycardia. *Heart Rhythm.* 2:550-554.

Franzini-Armstrong, C. 1980. Structure of sarcoplasmic reticulum. *Fed Proc.* 39:2403-2409.

Fujino, I., Yamada, N., Miyawaki, A., Hasegawa, M., Furuichi, T., and Mikoshiba, K. 1995. Differential expression of type 2 and type 3 inositol 1,4,5-trisphosphate receptor mRNAs in various mouse tissues: in situ hybridization study. *Cell Tissue Res.* 280:201-210.

Furuichi, T., Simon-Chazottes, D., Fujino, I., Yamada, N., Hasegawa, M., Miyawaki, A., Yoshikawa, S., Guenet, J.L., and Mikoshiba, K. 1993. Widespread expression of inositol 1,4,5-trisphosphate receptor type 1 gene (IP_3R1) in the mouse central nervous system. *Receptors Channels.* 1:11-24.

Futatsugi, A., Nakamura, T., Yamada, M.K., Ebisui, E., Nakamura, K., Uchida, K., Kitaguchi, T., Takahashi-Iwanaga, H., Noda, T., Aruga, J., and Mikoshiba, K. 2005. IP_3 receptor types 2 and 3 mediate exocrine secretion underlying energy metabolism. *Science.* 309:2232-2234.

Gaburjakova, J., and Gaburjakova, M. 2008. Effect of luminal Ca^{2+} on the stability of coupled gating between ryanodine receptors from the rat heart. *Acta Physiol (Oxf).*

Gaburjakova, M., Gaburjakova, J., Reiken, S., Huang, F., Marx, S.O., Rosemblit, N., and Marks, A.R. 2001. FKBP12 binding modulates ryanodine receptor channel gating. *J Biol Chem.* 276:16931-16935.

Gallagher, C.J., and Salter, M.W. 2003. Differential properties of astrocyte calcium waves mediated by P2Y1 and P2Y2 receptors. *J Neurosci.* 23:6728-6739.

Galvan, D.L., Borrego-Diaz, E., Perez, P.J., and Mignery, G.A. 1999. Subunit oligomerization, and topology of the inositol 1,4, 5-trisphosphate receptor. *J Biol Chem.* 274:29483-29492.

Gangopadhyay, J.P., and Ikemoto, N. 2008. Interaction of the Lys^{3614}-Asn^{3643} calmodulin-binding domain with the Cys^{4114}-Asn^{4142} region of the type 1 ryanodine receptor is involved in the mechanism of Ca^{2+}/agonist-induced channel activation. *Biochem J.* 411:415-423.

Gao, L., Tripathy, A., Lu, X., and Meissner, G. 1997. Evidence for a role of C-terminal amino acid residues in skeletal muscle Ca^{2+} release channel (ryanodine receptor) function. *FEBS Lett.* 412:223-226.

Garcia-Dorado, D., Rodriguez-Sinovas, A., and Ruiz-Meana, M. 2004. Gap junction-mediated spread of cell injury and death during myocardial ischemia-reperfusion. *Cardiovasc Res.* 61:386-401.

Garcia, M.L., Usachev, Y.M., Thayer, S.A., Strehler, E.E., and Windebank, A.J. 2001. Plasma membrane calcium ATPase plays a role in reducing Ca^{2+}-mediated cytotoxicity in PC12 cells. *J Neurosci Res.* 64:661-669.

Gee, K.R., Brown, K.A., Chen, W.N., Bishop-Stewart, J., Gray, D., and Johnson, I. 2000. Chemical and physiological characterization of fluo-4 Ca^{2+}-indicator dyes. *Cell Calcium.* 27:97-106.

George, C.H. 2008. Sarcoplasmic reticulum Ca^{2+} leak in heart failure: mere observation or functional relevance? *Cardiovasc Res.* 77:302-314.

George, C.H., Higgs, G.V., and Lai, F.A. 2003a. Ryanodine receptor mutations associated with stress-induced ventricular tachycardia mediate increased calcium release in stimulated cardiomyocytes. *Circ Res.* 93:531-540.

George, C.H., Higgs, G.V., Mackrill, J.J., and Lai, F.A. 2003b. Dysregulated ryanodine receptors mediate cellular toxicity: restoration of normal phenotype by FKBP12.6. *J Biol Chem.* 278:28856-28864.

George, C.H., Jundi, H., Thomas, N.L., Scoote, M., Walters, N., Williams, A.J., and Lai, F.A. 2004. Ryanodine receptor regulation by intramolecular interaction between cytoplasmic and transmembrane domains. *Mol Biol Cell.* 15:2627-2638.

George, C.H., Jundi, H., Walters, N., Thomas, N.L., West, R.R., and Lai, F.A. 2006. Arrhythmogenic mutation-linked defects in ryanodine receptor autoregulation reveal a novel mechanism of Ca^{2+} release channel dysfunction. *Circ Res.* 98:88-97.

George, C.H., Rogers, S.A., Bertrand, B.M., Tunwell, R.E., Thomas, N.L., Steele, D.S., Cox, E.V., Pepper, C., Hazeel, C.J., Claycomb, W.C., and Lai, F.A. 2007. Alternative splicing of ryanodine receptors modulates cardiomyocyte Ca^{2+} signaling and susceptibility to apoptosis. *Circ Res.* 100:874-883.

George, C.H., Sorathia, R., Bertrand, B.M., and Lai, F.A. 2003c. In situ modulation of the human cardiac ryanodine receptor (hRyR2) by FKBP12.6. *Biochem J.* 370:579-589.

George, C.H., Thomas, N.L., and Lai, F.A. 2005. Ryanodine receptor dysfunction in arrhythmia and sudden cardiac death. *Future Cardiology.* 1:531-541.

Gerasimenko, J.V., Maruyama, Y., Yano, K., Dolman, N.J., Tepikin, A.V., Petersen, O.H., and Gerasimenko, O.V. 2003. NAADP mobilizes Ca^{2+} from a thapsigargin-sensitive store in the nuclear envelope by activating ryanodine receptors. *J Cell Biol.* 163:271-282.

Gergs, U., Berndt, T., Buskase, J., Jones, L.R., Kirchhefer, U., Muller, F.U., Schluter, K.D., Schmitz, W., and Neumann, J. 2007. On the role of junctin in cardiac Ca^{2+} handling, contractility, and heart failure. *Am J Physiol Heart Circ Physiol.* 293:H728-734.

Gergs, U., Boknik, P., Buchwalow, I., Fabritz, L., Matus, M., Justus, I., Hanske, G., Schmitz, W., and Neumann, J. 2004. Overexpression of the catalytic subunit of protein phosphatase 2A impairs cardiac function. *J Biol Chem.* 279:40827-40834.

Giannini, G., Conti, A., Mammarella, S., Scrobogna, M., and Sorrentino, V. 1995. The ryanodine receptor/calcium channel genes are widely and differentially expressed in murine brain and peripheral tissues. *J Cell Biol.* 128:893-904.

Goddard, C.A., Ghais, N.S., Zhang, Y., Williams, A.J., Colledge, W.H., Grace, A.A., and Huang, C.L. 2008. Physiological consequences of the P2328S mutation in the ryanodine receptor (RyR2) gene in genetically modified murine hearts. *Acta Physiol (Oxf).*

Gomez-Hernandez, J.M., de Miguel, M., Larrosa, B., Gonzalez, D., and Barrio, L.C. 2003. Molecular basis of calcium regulation in connexin-32 hemichannels. *Proc Natl Acad Sci U S A.* 100:16030-16035.

Gong, X.Q., and Nicholson, B.J. 2001. Size selectivity between gap junction channels composed of different connexins. *Cell Commun Adhes.* 8:187-192.

Gonzalez, D.R., Beigi, F., Treuer, A.V., and Hare, J.M. 2007. Deficient ryanodine receptor S-nitrosylation increases sarcoplasmic reticulum calcium leak and arrhythmogenesis in cardiomyocytes. *Proc Natl Acad Sci U S A.* 104:20612-20617.

Gordon, J.L. 1986. Extracellular ATP: effects, sources and fate. *Biochem J.* 233:309-319.

Gorza, L., Schiaffino, S., and Volpe, P. 1993. Inositol 1,4,5-trisphosphate receptor in heart: evidence for its concentration in Purkinje myocytes of the conduction system. *J Cell Biol.* 121:345-353.

Govindaraju, V., Martin, J.G., Maghni, K., Ferraro, P., and Michoud, M.C. 2005. The effects of extracellular purines and pyrimidines on human airway smooth muscle cells. *J Pharmacol Exp Ther.* 315:941-948.

Graham, F.L., Smiley, J., Russell, W.C., and Nairn, R. 1977. Characteristics of a human cell line transformed by DNA from human adenovirus type 5. *J Gen Virol.* 36:59-74.

Gramolini, A.O., Kislinger, T., Alikhani-Koopaei, R., Fong, V., Thompson, N.J., Isserlin, R., Sharma, P., Oudit, G.Y., Trivieri, M.G., Fagan, A., Kannan, A., Higgins, D., Huedig, H., Hess, G., Arab, S., Seidman, J.G., Seidman, C.E., Frey, B., Perry, M., Backx, P.H., Liu, P.P., Maclennan, D.H., and Emili, A. 2007. Comparative proteomic profiling of a phospholamban mutant mouse model of dilated cardiomyopathy reveals progressive intracellular stress responses. *Mol Cell Proteomics.*

Gramsch, B., Gabriel, H.D., Wiemann, M., Grummer, R., Winterhager, E., Bingmann, D., and Schirrmacher, K. 2001. Enhancement of connexin 43 expression increases proliferation and differentiation of an osteoblast-like cell line. *Exp Cell Res.* 264:397-407.

Griendling, K.K., Sorescu, D., Lassegue, B., and Ushio-Fukai, M. 2000. Modulation of protein kinase activity and gene expression by reactive oxygen species and their role in vascular physiology and pathophysiology. *Arterioscler Thromb Vasc Biol.* 20:2175-2183.

Grifalconi, M., Celotti, L., and Mognato, M. 2007. Bystander response in human lymphoblastoid TK6 cells. *Mutat Res.* 625:102-111.

Griffiths, E.J. 1999. Species dependence of mitochondrial calcium transients during excitation-contraction coupling in isolated cardiomyocytes. *Biochem Biophys Res Commun.* 263:554-559.

Groner, F., Rubio, M., Schulte-Euler, P., Matthes, J., Khan, I.F., Bodi, I., Koch, S.E., Schwartz, A., and Herzig, S. 2004. Single-channel gating and regulation of human L-type calcium channels in cardiomyocytes of transgenic mice. *Biochem Biophys Res Commun.* 314:878-884.

Groschner, K., Schuhmann, K., Mieskes, G., Baumgartner, W., and Romanin, C. 1996. A type 2A phosphatase-sensitive phosphorylation site controls modal gating of L-type Ca^{2+} channels in human vascular smooth-muscle cells. *Biochem J.* 318 (Pt 2):513-517.

Grueter, C.E., Abiria, S.A., Dzhura, I., Wu, Y., Ham, A.J., Mohler, P.J., Anderson, M.E., and Colbran, R.J. 2006. L-type Ca^{2+} channel facilitation mediated by phosphorylation of the beta subunit by CaMKII. *Mol Cell.* 23:641-650.

Grynkiewicz, G., Poenie, M., and Tsien, R.Y. 1985. A new generation of Ca^{2+} indicators with greatly improved fluorescence properties. *J Biol Chem.* 260:3440-3450.

Guatimosim, S., Amaya, M.J., Guerra, M.T., Aguiar, C.J., Goes, A.M., Gomez-Viquez, N.L., Rodrigues, M.A., Gomes, D.A., Martins-Cruz, J., Lederer, W.J., and Leite, M.F. 2008. Nuclear Ca^{2+} regulates cardiomyocyte function. *Cell Calcium.* 44:230-242.

Guo, J.H., Liu, Y.S., Zhang, H.C., Li, X.B., Xu, Y., Zhang, Y.Y., and Yuan, L. 2004. [Expression and function changes of ryanodine receptors and inositol 1,4,5-triphosphate receptors of atrial myocytes during atrial fibrillation]. *Zhonghua Yi Xue Za Zhi.* 84:1196-1199.

Guo, T., Zhang, T., Mestril, R., and Bers, D.M. 2006. Ca^{2+}/Calmodulin-dependent protein kinase II phosphorylation of ryanodine receptor does affect calcium sparks in mouse ventricular myocytes. *Circ Res.* 99:398-406.

Gutcher, I., Webb, P.R., and Anderson, N.G. 2003. The isoform-specific regulation of apoptosis by protein kinase C. *Cell Mol Life Sci.* 60:1061-1070.

Gutstein, D.E., and Marks, A.R. 1997. Role of inositol 1,4,5-trisphosphate receptors in regulating apoptotic signaling and heart failure. *Heart Vessels.* Suppl 12:53-57.

Gyorke, I., and Gyorke, S. 1998. Regulation of the cardiac ryanodine receptor channel by luminal Ca^{2+} involves luminal Ca^{2+} sensing sites. *Biophys. J.* 75:2801-2810.

Haase, H., Karczewski, P., Beckert, R., and Krause, E.G. 1993. Phosphorylation of the L-type calcium channel beta subunit is involved in beta-adrenergic signal transduction in canine myocardium. *FEBS Lett.* 335:217-222.

Haghighi, K., Kolokathis, F., Gramolini, A.O., Waggoner, J.R., Pater, L., Lynch, R.A., Fan, G.C., Tsiapras, D., Parekh, R.R., Dorn, G.W., 2nd, MacLennan, D.H., Kremastinos, D.T., and Kranias, E.G. 2006. A mutation in the human phospholamban gene, deleting arginine 14, results in lethal, hereditary cardiomyopathy. *Proc Natl Acad Sci U S A.* 103:1388-1393.

Haghighi, K., Kolokathis, F., Pater, L., Lynch, R.A., Asahi, M., Gramolini, A.O., Fan, G.C., Tsiapras, D., Hahn, H.S., Adamopoulos, S., Liggett, S.B., Dorn, G.W., 2nd, MacLennan, D.H., Kremastinos, D.T., and Kranias, E.G. 2003. Human phospholamban null results in lethal dilated cardiomyopathy revealing a critical difference between mouse and human. *J Clin Invest.* 111:869-876.

Haghighi, K., Schmidt, A.G., Hoit, B.D., Brittsan, A.G., Yatani, A., Lester, J.W., Zhai, J., Kimura, Y., Dorn, G.W., 2nd, MacLennan, D.H., and Kranias, E.G. 2001. Superinhibition of sarcoplasmic reticulum function by phospholamban induces cardiac contractile failure. *J Biol Chem.* 276:24145-24152.

Hain, J., Onoue, H., Mayrleitner, M., Fleischer, S., and Schindler, H. 1995. Phosphorylation modulates the function of the calcium release channel of sarcoplasmic reticulum from cardiac muscle. *J Biol Chem.* 270:2074-2081.

Hajjar, R.J., Schmidt, U., Kang, J.X., Matsui, T., and Rosenzweig, A. 1997. Adenoviral gene transfer of phospholamban in isolated rat cardiomyocytes. Rescue effects by concomitant gene transfer of sarcoplasmic reticulum Ca^{2+}-ATPase. *Circ Res.* 81:145-153.

Hajnoczky, G., Csordas, G., Das, S., Garcia-Perez, C., Saotome, M., Sinha Roy, S., and Yi, M. 2006. Mitochondrial calcium signalling and cell death: approaches for assessing the role of mitochondrial Ca^{2+} uptake in apoptosis. *Cell Calcium.* 40:553-560.

Hajnoczky, G., Csordas, G., Madesh, M., and Pacher, P. 2000. Control of apoptosis by IP_3 and ryanodine receptor driven calcium signals. *Cell Calcium.* 28:349-363.

Hajnoczky, G., Robb-Gaspers, L.D., Seitz, M.B., and Thomas, A.P. 1995. Decoding of cytosolic calcium oscillations in the mitochondria. *Cell.* 82:415-424.

Hakamata, Y., Nakai, J., Takeshima, H., and Imoto, K. 1992. Primary structure and distribution of a novel ryanodine receptor/calcium release channel from rabbit brain. *FEBS Lett.* 312:229-235.

Hamada, N., Matsumoto, H., Hara, T., and Kobayashi, Y. 2007a. Intercellular and intracellular signaling pathways mediating ionizing radiation-induced bystander effects. *J Radiat Res (Tokyo).* 48:87-95.

Hamada, T., Bannister, M.L., and Ikemoto, N. 2007b. Peptide probe study of the role of interaction between the cytoplasmic and transmembrane domains of the ryanodine receptor in the channel regulation mechanism. *Biochemistry.* 46:4272-4279.

Hanson, C.J., Bootman, M.D., Distelhorst, C.W., Maraldi, T., and Roderick, H.L. 2008a. The cellular concentration of Bcl-2 determines its pro- or anti-apoptotic effect. *Cell Calcium.*

Hanson, C.J., Bootman, M.D., Distelhorst, C.W., Wojcikiewicz, R.J., and Roderick, H.L. 2008b. Bcl-2 suppresses Ca^{2+} release through inositol 1,4,5-trisphosphate receptors and inhibits Ca^{2+} uptake by mitochondria without affecting ER calcium store content. *Cell Calcium.*

Hasko, G., Kuhel, D.G., Salzman, A.L., and Szabo, C. 2000. ATP suppression of interleukin-12 and tumour necrosis factor-alpha release from macrophages. *Br J Pharmacol.* 129:909-914.

Henderson, S.A., Goldhaber, J.I., So, J.M., Han, T., Motter, C., Ngo, A., Chantawansri, C., Ritter, M.R., Friedlander, M., Nicoll, D.A., Frank, J.S., Jordan, M.C., Roos, K.P., Ross, R.S., and Philipson, K.D. 2004. Functional adult myocardium in the absence of Na^{+}-Ca^{2+} exchange: cardiac-specific knockout of NCX1. *Circ Res.* 95:604-611.

Henriquez, M., Armisen, R., Stutzin, A., and Quest, A.F. 2008. Cell death by necrosis, a regulated way to go. *Curr Mol Med.* 8:187-206.

Hentati, M., Ben Ameur, I., Kechida, Z., Charfeddine, H., Hached, L., Grati, Z., and Kammoun, S. 2003. Use of an implantable defibrillator for the prevention of sudden death in hypertrophic cardiomyopathy. *Tunis Med.* 81 Suppl 8:675-679.

Herrmann-Frank, A., and Lehmann-Horn, F. 1996. Regulation of the purified Ca^{2+} release channel/ryanodine receptor complex of skeletal muscle sarcoplasmic reticulum by luminal calcium. *Pflugers Arch.* 432:155-157.

Hess, S.T., Sheets, E.D., Wagenknecht-Wiesner, A., and Heikal, A.A. 2003. Quantitative analysis of the fluorescence properties of intrinsically fluorescent proteins in living cells. *Biophys J.* 85:2566-2580.

Higo, T., Hattori, M., Nakamura, T., Natsume, T., Michikawa, T., and Mikoshiba, K. 2005. Subtype-specific and ER lumenal environment-dependent regulation of inositol 1,4,5-trisphosphate receptor type 1 by ERp44. *Cell.* 120:85-98.

Hintz, K.K., Norby, F.L., Duan, J., Cinnamon, M.A., Doze, V.A., and Ren, J. 2002. Comparison of cardiac excitation-contraction coupling in isolated ventricular myocytes between rat and mouse. *Comp Biochem Physiol A Mol Integr Physiol.* 133:191-198.

Hirota, J., Ando, H., Hamada, K., and Mikoshiba, K. 2003. Carbonic anhydrase-related protein is a novel binding protein for inositol 1,4,5-trisphosphate receptor type 1. *Biochem J.* 372:435-441.

Hisatsune, C., Yasumatsu, K., Takahashi-Iwanaga, H., Ogawa, N., Kuroda, Y., Yoshida, R., Ninomiya, Y., and Mikoshiba, K. 2007. Abnormal taste perception in mice lacking the type 3 inositol 1, 4, 5-trisphosphate receptor. *J Biol Chem.*

Hohenegger, M., and Suko, J. 1993. Phosphorylation of the purified cardiac ryanodine receptor by exogenous and endogenous protein kinases. *Biochem J.* 296 (Pt 2):303-308.

Honda, K., Takano, Y., and Kamiya, H. 1994. The mechanism of muscarinic agonist-stimulated inositol phosphate formation in permeabilized ileal smooth muscle. *Jpn J Pharmacol.* 65:275-280.

Hong, C.S., Cho, M.C., Kwak, Y.G., Song, C.H., Lee, Y.H., Lim, J.S., Kwon, Y.K., Chae, S.W., and Kim, D.H. 2002. Cardiac remodeling and atrial fibrillation in transgenic mice overexpressing junctin. *Faseb J.* 16:1310-1312.

Hool, L.C. 2006. Reactive oxygen species in cardiac signalling: from mitochondria to plasma membrane ion channels. *Clin Exp Pharmacol Physiol.* 33:146-151.

Hool, L.C. 2008. Evidence for the regulation of L-type Ca^{2+} channels in the heart by reactive oxygen species: mechanism for mediating pathology. *Clin Exp Pharmacol Physiol.* 35:229-234.

Hoshijima, M. 2005. Gene therapy targeted at calcium handling as an approach to the treatment of heart failure. *Pharmacol Ther.* 105:211-228.

Hu, X.F., Liang, X., Chen, K.Y., Xie, H., Xu, Y., Zhu, P.H., and Hu, J. 2005a. Modulation of the oligomerization of isolated ryanodine receptors by their functional states. *Biophys J.* 89:1692-1699.

Hu, X.F., Liang, X., Chen, K.Y., Zhu, P.H., and Hu, J. 2005b. Depletion of FKBP does not affect the interaction between isolated ryanodine receptors. *Biochem Biophys Res Commun.* 336:128-133.

Hymel, L., Schindler, H., Inui, M., and Fleischer, S. 1988. Reconstitution of purified cardiac muscle calcium release channel (ryanodine receptor) in planar bilayers. *Biochem Biophys Res Commun.* 152:308-314.

Ikemoto, N., and Yamamoto, T. 2002. Regulation of calcium release by interdomain interaction within ryanodine receptors. *Front Biosci.* 7:d671-683.

Imahashi, K., Pott, C., Goldhaber, J.I., Steenbergen, C., Philipson, K.D., and Murphy, E. 2005. Cardiac-specific ablation of the Na^{+}-Ca^{2+} exchanger confers protection against ischemia/reperfusion injury. *Circ Res.* 97:916-921.

Inoue, T., Kato, K., Kohda, K., and Mikoshiba, K. 1998. Type 1 inositol 1,4,5-trisphosphate receptor is required for induction of long-term depression in cerebellar Purkinje neurons. *J Neurosci.* 18:5366-5373.

Ito, K., Ozasa, H., and Horikawa, S. 2005. Edaravone protects against lung injury induced by intestinal ischemia/reperfusion in rat. *Free Radic Biol Med.* 38:369-374.

Ito, K., Ozasa, H., Noda, Y., Arii, S., and Horikawa, S. 2008. Effects of free radical scavenger on acute liver injury induced by d-galactosamine and lipopolysaccharide in rats. *Hepatol Res.* 38:194-201.

Iwata, A., Stys, P.K., Wolf, J.A., Chen, X.H., Taylor, A.G., Meaney, D.F., and Smith, D.H. 2004. Traumatic axonal injury induces proteolytic cleavage of the voltage-gated sodium channels modulated by tetrodotoxin and protease inhibitors. *J Neurosci.* 24:4605-4613.

James, A.F. 2007. Inhibition of SR Ca^{2+} uptake: A novel action of the RyR2-FKBP12.6 antagonist K201. *Cardiovasc Res.*

Jeyakumar, L.H., Copello, J.A., O'Malley, A.M., Wu, G.M., Grassucci, R., Wagenknecht, T., and Fleischer, S. 1998. Purification and characterization of ryanodine receptor 3 from mammalian tissue. *J Biol Chem.* 273:16011-16020.

Jiang, D., Chen, W., Wang, R., Zhang, L., and Chen, S.R. 2007. Loss of luminal Ca^{2+} activation in the cardiac ryanodine receptor is associated with ventricular fibrillation and sudden death. *Proc Natl Acad Sci U S A.* 104:18309-18314.

Jiang, D., Wang, R., Xiao, B., Kong, H., Hunt, D.J., Choi, P., Zhang, L., and Chen, S.R. 2005. Enhanced store overload-induced Ca^{2+} release and channel sensitivity to luminal Ca^{2+} activation are common defects of RyR2 mutations linked to ventricular tachycardia and sudden death. *Circ Res.* 97:1173-1181.

Jiang, D., Xiao, B., Yang, D., Wang, R., Choi, P., Zhang, L., Cheng, H., and Chen, S.R. 2004a. RyR2 mutations linked to ventricular tachycardia and sudden death reduce the threshold for store-overload-induced Ca^{2+} release (SOICR). *Proc Natl Acad Sci U S A.* 101:13062-13067.

Jiang, D., Xiao, B., Yang, D., Wang, R., Choi, P., Zhang, L., Cheng, H., and Chen, S.R.W. 2004b. RyR2 mutations linked to ventricular tachycardia and sudden death reduce the threshold for store-overload-induced Ca^{2+} release (SOICR). *PNAS.* 101:13062-13067.

Jiang, D., Xiao, B., Zhang, L., and Chen, S.R.W. 2002a. Enhanced basal activity of a cardiac Ca^{2+} release channel (ryanodine receptor) mutant associated with ventricular tachycardia and sudden death. *Circ Res.* 91:218-225.

Jiang, J.X., and Gu, S. 2005. Gap junction- and hemichannel-independent actions of connexins. *Biochim Biophys Acta.* 1711:208-214.

Jiang, M.T., Lokuta, A.J., Farrell, E.F., Wolff, M.R., Haworth, R.A., and Valdivia, H.H. 2002b. Abnormal Ca^{2+} release, but normal ryanodine receptors, in canine and human heart failure. *Circ Res.* 91:1015-1022.

Jiang, S., Chow, S.C., Nicotera, P., and Orrenius, S. 1994. Intracellular Ca^{2+} signals activate apoptosis in thymocytes: studies using the Ca^{2+}-ATPase inhibitor thapsigargin. *Exp Cell Res.* 212:84-92.

Jones, L.R., Suzuki, Y.J., Wang, W., Kobayashi, Y.M., Ramesh, V., Franzini-Armstrong, C., Cleemann, L., and Morad, M. 1998. Regulation of Ca^{2+} signaling in transgenic mouse cardiac myocytes overexpressing calsequestrin. *J Clin Invest.* 101:1385-1393.

Jones, P.P., Meng, X., Xiao, B., Cai, S., Bolstad, J., Wagenknecht, T., Liu, Z., and Chen, S.R. 2007. Localization of PKA phosphorylation site, serine-2030, in the three-dimensional structure of cardiac ryanodine receptor. *Biochem J.*

Joseph, S.K., Nakao, S.K., and Sukumvanich, S. 2006. Reactivity of free thiol groups in type-I inositol trisphosphate receptors. *Biochem J.* 393:575-582.

Kaneko, N., Matsuda, R., Toda, M., and Shimamoto, K. 1997. Inhibition of annexin V-dependent Ca^{2+} movement in large unilamellar vesicles by K201, a new 1,4-benzothiazepine derivative. *Biochim Biophys Acta.* 1330:1-7.

Kang, J., Kang, S., Yoo, S.H., and Park, S. 2007. Identification of residues participating in the interaction between an intraluminal loop of inositol 1,4,5-trisphosphate receptor and a conserved N-terminal region of chromogranin B. *Biochim Biophys Acta.* 1774:502-509.

Kannankeril, P.J., Mitchell, B.M., Goonasekera, S.A., Chelu, M.G., Zhang, W., Sood, S., Kearney, D.L., Danila, C.I., De Biasi, M., Wehrens, X.H., Pautler, R.G., Roden, D.M., Taffet, G.E., Dirksen, R.T., Anderson, M.E., and Hamilton, S.L. 2006. Mice with the R176Q cardiac ryanodine receptor mutation exhibit catecholamine-induced ventricular tachycardia and cardiomyopathy. *Proc Natl Acad Sci U S A.* 103:12179-12184.

Kasri, N.N., Holmes, A.M., Bultynck, G., Parys, J.B., Bootman, M.D., Rietdorf, K., Missiaen, L., McDonald, F., De Smedt, H., Conway, S.J., Holmes, A.B., Berridge, M.J., and Roderick, H.L. 2004. Regulation of IP_3 receptor activity by neuronal Ca^{2+}-binding proteins. *Embo J.* 23:312-321.

Katsuragi, T., Sato, C., Usune, S., Ueno, S., Segawa, M., and Migita, K. 2008. Caffeine-inducible ATP release is mediated by Ca^{2+}-signal transducing system from the endoplasmic reticulum to mitochondria. *Naunyn Schmiedebergs Arch Pharmacol.*

Kawano, S. 1998. Dual mechanisms of Mg^{2+} block of ryanodine receptor Ca^{2+} release channel from cardiac sarcoplasmic reticulum. *Receptors Channels.* 5:405-416.

Kaznacheyeva, E., Lupu, V.D., and Bezprozvanny, I. 1998. Single-channel properties of inositol (1,4,5)-trisphosphate receptor heterologously expressed in HEK-293 cells. *J Gen Physiol.* 111:847-856.

Keating, M.T., and Sanguinetti, M.C. 2001. Molecular and cellular mechanisms of cardiac arrhythmias. *Cell.* 104:569-580.

Keizer, J., and Smith, G.D. 1998. Spark-to-wave transition: saltatory transmission of calcium waves in cardiac myocytes. *Biophys Chem.* 72:87-100.

Kelliher, M., Fastbom, J., Cowburn, R.F., Bonkale, W., Ohm, T.G., Ravid, R., Sorrentino, V., and O'Neill, C. 1999. Alterations in the ryanodine receptor calcium release channel correlate with Alzheimer's disease neurofibrillary and beta-amyloid pathologies. *Neuroscience.* 92:499-513.

Kettman, J., and Skarvall, H. 1974. The allogeneic effect: bystander effect in the primary immune response in vitro. *Eur J Immunol.* 4:641-645.

Khan, M.T., Wagner, L., 2nd, Yule, D.I., Bhanumathy, C., and Joseph, S.K. 2006. Akt kinase phosphorylation of inositol 1,4,5-trisphosphate receptors. *J Biol Chem.* 281:3731-3737.

Kim, S., Ahn, T., and Park, C. 2005. The Pro335 --> Leu polymorphism of type 3 inositol 1,4,5-trisphosphate receptor found in mouse inbred lines results in functional change. *J Biol Chem.* 280:26024-26031.

Kim, Y.S., Ko, J., Kim, I.S., Jang, S.W., Sung, H.J., Lee, H.J., Lee, S.Y., Kim, Y., and Na, D.S. 2003. PKCdelta-dependent cleavage and nuclear translocation of annexin A1 by phorbol 12-myristate 13-acetate. *Eur J Biochem.* 270:4089-4094.

Kirchhefer, U., Hanske, G., Jones, L.R., Justus, I., Kaestner, L., Lipp, P., Schmitz, W., and Neumann, J. 2006. Overexpression of junctin causes adaptive changes in cardiac myocyte Ca^{2+} signaling. *Cell Calcium.* 39:131-142.

Kirchhefer, U., Jones, L.R., Begrow, F., Boknik, P., Hein, L., Lohse, M.J., Riemann, B., Schmitz, W., Stypmann, J., and Neumann, J. 2004. Transgenic triadin 1 overexpression alters SR Ca^{2+} handling and leads to a blunted contractile response to [beta]-adrenergic agonists. *Cardiovasc Res.* 62:122-134.

Kirchhefer, U., Neumann, J., Baba, H.A., Begrow, F., Kobayashi, Y.M., Reinke, U., Schmitz, W., and Jones, L.R. 2001. Cardiac hypertrophy and impaired relaxation in transgenic mice overexpressing triadin 1. *J Biol Chem.* 276:4142-4149.

Kirchhof, P., Klimas, J., Fabritz, L., Zwiener, M., Jones, L.R., Schafers, M., Hermann, S., Boknik, P., Schmitz, W., Breithardt, G., Kirchhefer, U., and Neumann, J. 2007. Stress and high heart rate provoke ventricular tachycardia in mice expressing triadin. *J Mol Cell Cardiol.* 42:962-971.

Kiselyov, K., Xu, X., Mozhayeva, G., Kuo, T., Pessah, I., Mignery, G., Zhu, X., Birnbaumer, L., and Muallem, S. 1998. Functional interaction between IP_3 receptors and store-operated Htrp3 channels. *Nature.* 396:478-482.

Knollmann, B.C., Chopra, N., Hlaing, T., Akin, B., Yang, T., Ettensohn, K., Knollmann, B.E., Horton, K.D., Weissman, N.J., Holinstat, I., Zhang, W., Roden, D.M., Jones, L.R., Franzini-Armstrong, C., and Pfeifer, K. 2006. Casq2 deletion causes sarcoplasmic reticulum volume increase, premature Ca^{2+} release, and catecholaminergic polymorphic ventricular tachycardia. *J Clin Invest.* 116:2510-2520.

Knollmann, B.C., Knollmann-Ritschel, B.E., Weissman, N.J., Jones, L.R., and Morad, M. 2000. Remodelling of ionic currents in hypertrophied and failing hearts of transgenic mice overexpressing calsequestrin. *J Physiol.* 525 Pt 2:483-498.

Kobayashi, S., Yamamoto, T., Parness, J., and Ikemoto, N. 2004. Antibody probe study of Ca^{2+} channel regulation by interdomain interaction within the ryanodine receptor. *Biochem J.* 380:561-569.

Kohlhaas, M., Zhang, T., Seidler, T., Zibrova, D., Dybkova, N., Steen, A., Wagner, S., Chen, L., Brown, J.H., Bers, D.M., and Maier, L.S. 2006. Increased sarcoplasmic reticulum calcium leak but unaltered contractility by acute CaMKII overexpression in isolated rabbit cardiac myocytes. *Circ Res.* 98:235-244.

Kohno, M., Yano, M., Kobayashi, S., Doi, M., Oda, T., Tokuhisa, T., Okuda, S., Ohkusa, T., and Matsuzaki, M. 2003. A new cardioprotective agent, JTV519, improves defective channel gating of ryanodine receptor in heart failure. *Am J Physiol Heart Circ Physiol.* 284:H1035-1042.

Kojima, T., Fort, A., Tao, M., Yamamoto, M., and Spray, D.C. 2001. Gap junction expression and cell proliferation in differentiating cultures of Cx43 KO mouse hepatocytes. *Am J Physiol Gastrointest Liver Physiol.* 281:G1004-1013.

Kondo, R.P., Wang, S.Y., John, S.A., Weiss, J.N., and Goldhaber, J.I. 2000. Metabolic inhibition activates a non-selective current through connexin hemichannels in isolated ventricular myocytes. *J Mol Cell Cardiol.* 32:1859-1872.

Kong, H., Wang, R., Chen, W., Zhang, L., Chen, K., Shimoni, Y., Duff, H.J., and Chen, S.R. 2007. Skeletal and cardiac ryanodine receptors exhibit different responses to Ca^{2+} overload and luminal Ca^{2+}. *Biophys J.* 92:2757-2770.

Kranias, E.G., and Bers, D.M. 2007. Calcium and cardiomyopathies. *Subcell Biochem.* 45:523-537.

Kruman, II, and Mattson, M.P. 1999. Pivotal role of mitochondrial calcium uptake in neural cell apoptosis and necrosis. *J Neurochem.* 72:529-540.

Kubalova, Z., Gyorke, I., Terentyeva, R., Viatchenko-Karpinski, S., Terentyev, D., Williams, S.C., and Gyorke, S. 2004. Modulation of cytosolic and intra-sarcoplasmic reticulum calcium waves by calsequestrin in rat cardiac myocytes. *J Physiol.* 561:515-524.

Kubalova, Z., Terentyev, D., Viatchenko-Karpinski, S., Nishijima, Y., Gyorke, I., Terentyeva, R., da Cunha, D.N., Sridhar, A., Feldman, D.S., Hamlin, R.L., Carnes, C.A., and Gyorke, S. 2005. Abnormal intrastore calcium signaling in chronic heart failure. *Proc Natl Acad Sci U S A.* 102:14104-14109.

Kumasaka, S., Shoji, H., and Okabe, E. 1999. Novel mechanisms involved in superoxide anion radical-triggered Ca^{2+} release from cardiac sarcoplasmic reticulum linked to cyclic ADP-ribose stimulation. *Antioxid Redox Signal.* 1:55-69.

Kunapuli, P., Lawson, J.A., Rokach, J., and FitzGerald, G.A. 1997. Functional characterization of the ocular prostaglandin f2alpha (PGF2alpha) receptor. Activation by the isoprostane, 12-iso-PGF2alpha. *J Biol Chem.* 272:27147-27154.

Laemmli, U.K. 1970. Cleavage of structural proteins during the assembly of the head of bacteriophage T4. *Nature.* 227:680-685.

Laemmli, U.K., and Quittner, S.F. 1974. Maturation of the head of bacteriophage T4. IV. The proteins of the core of the tubular polyheads and in vitro cleavage of the head proteins. *Virology.* 62:483-499.

Lahat, H., and Eldar, M. 2002. Autosomal recessive catecholamine-induced polymorphic ventricular tachycardia. *Isr Med Assoc J.* 4:1095-1096.

Lahat, H., Pras, E., and Eldar, M. 2004. A missense mutation in CASQ2 is associated with autosomal recessive catecholamine-induced polymorphic ventricular tachycardia in Bedouin families from Israel. *Ann Med.* 36 Suppl 1:87-91.

Lahat, H., Pras, E., Olender, T., Avidan, N., Ben-Asher, E., Man, O., Levy-Nissenbaum, E., Khoury, A., Lorber, A., Goldman, B., Lancet, D., and Eldar, M. 2001. A missense mutation in a highly conserved region of CASQ2 is associated with autosomal recessive catecholamine-induced polymorphic ventricular tachycardia in Bedouin families from Israel. *Am J Hum Genet.* 69:1378-1384.

Lai, F.A., Anderson, K., Rousseau, E., Liu, Q.Y., and Meissner, G. 1988. Evidence for a Ca^{2+} channel within the ryanodine receptor complex from cardiac sarcoplasmic reticulum. *Biochem Biophys Res Commun.* 151:441-449.

Lai, F.A., Dent, M., Wickenden, C., Xu, L., Kumari, G., Misra, M., Lee, H.B., Sar, M., and Meissner, G. 1992. Expression of a cardiac Ca^{2+}-release channel isoform in mammalian brain. *Biochem J.* 288 (Pt 2):553-564.

Lai, F.A., Erickson, H., Block, B.A., and Meissner, G. 1987. Evidence for a junctional feet-ryanodine receptor complex from sarcoplasmic reticulum. *Biochem Biophys Res Commun.* 143:704-709.

Laird, D.W. 2006. Life cycle of connexins in health and disease. *Biochem J.* 394:527-543.

Laitinen, P.J., Brown, K.M., Piippo, K., Swan, H., Devaney, J.M., Brahmbhatt, B., Donarum, E.A., Marino, M., Tiso, N., Viitasalo, M., Toivonen, L., Stephan, D.A., and Kontula, K. 2001. Mutations of the cardiac ryanodine receptor (RyR2) gene in familial polymorphic ventricular tachycardia. *Circulation.* 103:485-490.

Laitinen, P.J., Swan, H., and Kontula, K. 2003. Molecular genetics of exercise-induced polymorphic ventricular tachycardia: identification of three novel cardiac ryanodine receptor mutations and two common calsequestrin 2 amino-acid polymorphisms. *Eur J Hum Genet.* 11:888-891.

Laver, D.R. 2007. Ca^{2+} stores regulate ryanodine receptor Ca^{2+} release channels via luminal and cytosolic Ca^{2+} sites. *Clin Exp Pharmacol Physiol.* 34:889-896.

Laver, D.R., Baynes, T.M., and Dulhunty, A.F. 1997. Magnesium inhibition of ryanodine-receptor calcium channels: evidence for two independent mechanisms. *J Membr Biol.* 156:213-229.

Laver, D.R., Hamada, T., Fessenden, J.D., and Ikemoto, N. 2007a. The ryanodine receptor pore blocker neomycin also inhibits channel activity via a previously undescribed high-affinity Ca^{2+} binding site. *J Membr Biol.* 220:11-20.

Laver, D.R., Honen, B.N., Lamb, G.D., and Ikemoto, N. 2007b. A domain peptide of the cardiac ryanodine receptor regulates channel sensitivity to luminal Ca^{2+} via cytoplasmic Ca^{2+} sites. *Eur Biophys J.*

Laver, D.R., O'Neill, E.R., and Lamb, G.D. 2004. Luminal Ca^{2+}-regulated Mg^{2+} inhibition of skeletal RyRs reconstituted as isolated channels or coupled clusters. *J Gen Physiol.* 124:741-758.

Lebkowski, J.S., Clancy, S., and Calos, M.P. 1985. Simian virus 40 replication in adenovirus-transformed human cells antagonizes gene expression. *Nature.* 317:169-171.

Lee, T.S., Karl, R., Moosmang, S., Lenhardt, P., Klugbauer, N., Hofmann, F., Kleppisch, T., and Welling, A. 2006. Calmodulin kinase II is involved in voltage-dependent facilitation of the L-type Cav1.2 calcium channel: Identification of the phosphorylation sites. *J Biol Chem.* 281:25560-25567.

Leeb, T., and Brenig, B. 1998. cDNA cloning and sequencing of the human ryanodine receptor type 3 (RYR3) reveals a novel alternative splice site in the RYR3 gene. *FEBS Lett.* 423:367-370.

Lehnart, S.E. 2007. Novel targets for treating heart and muscle disease: stabilizing ryanodine receptors and preventing intracellular calcium leak. *Curr Opin Pharmacol.* 7:225-232.

Lehnart, S.E., Mongillo, M., Bellinger, A., Lindegger, N., Chen, B.X., Hsueh, W., Reiken, S., Wronska, A., Drew, L.J., Ward, C.W., Lederer, W.J., Kass, R.S., Morley, G., and Marks, A.R. 2008. Leaky Ca^{2+} release channel/ryanodine receptor 2 causes seizures and sudden cardiac death in mice. *J Clin Invest.*

Lehnart, S.E., Wehrens, X.H., and Marks, A.R. 2005. Defective ryanodine receptor interdomain interactions may contribute to intracellular Ca^{2+} leak: a novel therapeutic target in heart failure. *Circulation.* 111:3342-3346.

Lehnart, S.E., Wehrens, X.H.T., Laitinen, P.J., Reiken, S.R., Deng, S.-X., Cheng, Z., Landry, D.W., Kontula, K., Swan, H., and Marks, A.R. 2004. Sudden death in familial polymorphic ventricular tachycardia associated with calcium release channel (ryanodine receptor) leak. *Circulation.* 109:3208-3214.

Leist, M., and Jaattela, M. 2001. Four deaths and a funeral: from caspases to alternative mechanisms. *Nat Rev Mol Cell Biol.* 2:589-598.

Leist, M., Single, B., Castoldi, A.F., Kuhnle, S., and Nicotera, P. 1997. Intracellular adenosine triphosphate (ATP) concentration: a switch in the decision between apoptosis and necrosis. *J Exp Med.* 185:1481-1486.

Leist, M., Single, B., Naumann, H., Fava, E., Simon, B., Kuhnle, S., and Nicotera, P. 1999. Inhibition of mitochondrial ATP generation by nitric oxide switches apoptosis to necrosis. *Exp Cell Res.* 249:396-403.

Leybaert, L., Braet, K., Vandamme, W., Cabooter, L., Martin, P.E., and Evans, W.H. 2003. Connexin channels, connexin mimetic peptides and ATP release. *Cell Commun Adhes.* 10:251-257.

Li, H., Liu, T.F., Lazrak, A., Peracchia, C., Goldberg, G.S., Lampe, P.D., and Johnson, R.G. 1996. Properties and regulation of gap junctional hemichannels in the plasma membranes of cultured cells. *J Cell Biol.* 134:1019-1030.

Li, J., Marionneau, C., Zhang, R., Shah, V., Hell, J.W., Nerbonne, J.M., and Anderson, M.E. 2006. Calmodulin kinase II inhibition shortens action potential duration by upregulation of K^+ currents. *Circ Res.* 99:1092-1099.

Li, L., Chu, G., Kranias, E.G., and Bers, D.M. 1998. Cardiac myocyte calcium transport in phospholamban knockout mouse: relaxation and endogenous CaMKII effects. *Am J Physiol.* 274:H1335-1347.

Li, X., Zima, A.V., Sheikh, F., Blatter, L.A., and Chen, J. 2005. Endothelin-1-induced arrhythmogenic Ca^{2+} signaling is abolished in atrial myocytes of inositol-1,4,5-trisphosphate(IP_3)-receptor type 2-deficient mice. *Circ Res.* 96:1274-1281.

Liang, X., Hu, X., and Hu, J. 2006. Dynamic inter-receptor coupling: a novel working mechanism of 2-D ryanodine receptor array. *Biophys J.*

Lim, S., Chang, W., Lee, B.K., Song, H., Hong, J.H., Lee, S., Song, B.W., Kim, H.J., Cha, M.J., Jang, Y., Chung, N.S., Choi, S.Y., and Hwang, K.C. 2008. Enhanced calreticulin expression promotes calcium-dependent apoptosis in postnatal cardiomyocytes. *Mol Cells.* 25:390-396.

Lin, J.H., Weigel, H., Cotrina, M.L., Liu, S., Bueno, E., Hansen, A.J., Hansen, T.W., Goldman, S., and Nedergaard, M. 1998. Gap-junction-mediated propagation and amplification of cell injury. *Nat Neurosci.* 1:494-500.

Lin, W.W., and Chen, B.C. 1998. Distinct PKC isoforms mediate the activation of cPLA2 and adenylyl cyclase by phorbol ester in RAW264.7 macrophages. *Br J Pharmacol.* 125:1601-1609.

Lipp, P., Laine, M., Tovey, S.C., Burrell, K.M., Berridge, M.J., Li, W., and Bootman, M.D. 2000. Functional IP_3 receptors that may modulate excitation-contraction coupling in the heart. *Curr Biol.* 10:939-942.

Lipp, P., and Niggli, E. 1996. Submicroscopic calcium signals as fundamental events of excitation--contraction coupling in guinea-pig cardiac myocytes. *J Physiol.* 492 (Pt 1):31-38.

Liu, N., Colombi, B., Memmi, M., Zissimopoulos, S., Rizzi, N., Negri, S., Imbriani, M., Napolitano, C., Lai, F.A., and Priori, S.G. 2006. Arrhythmogenesis in catecholaminergic polymorphic ventricular tachycardia: insights from a RyR2 R4496C knock-in mouse model. *Circ Res.* 99:292-298.

Liu, Z., Zhang, J., Li, P., Chen, S.R., and Wagenknecht, T. 2002. Three-dimensional reconstruction of the recombinant type 2 ryanodine receptor and localization of its divergent region 1. *J Biol Chem.* 277:46712-46719.

Liu, Z., Zhang, J., Wang, R., Wayne Chen, S.R., and Wagenknecht, T. 2004. Location of divergent region 2 on the three-dimensional structure of cardiac muscle ryanodine receptor/calcium release channel. *J Mol Biol.* 338:533-545.

Lokuta, A.J., Meyers, M.B., Sander, P.R., Fishman, G.I., and Valdivia, H.H. 1997. Modulation of cardiac ryanodine receptors by sorcin. *J Biol Chem.* 272:25333-25338.

Lokuta, A.J., Rogers, T.B., Lederer, W.J., and Valdivia, H.H. 1995. Modulation of cardiac ryanodine receptors of swine and rabbit by a phosphorylation-dephosphorylation mechanism. *J Physiol.* 487 (Pt 3):609-622.

Louis, N., Evelegh, C., and Graham, F.L. 1997. Cloning and sequencing of the cellular-viral junctions from the human adenovirus type 5 transformed 293 cell line. *Virology.* 233:423-429.

Lu, X., Xu, L., and Meissner, G. 1994. Activation of the skeletal muscle calcium release channel by a cytoplasmic loop of the dihydropyridine receptor. *J Biol Chem.* 269:6511-6516.

Ludtke, S.J., Serysheva, II, Hamilton, S.L., and Chiu, W. 2005. The pore structure of the closed RyR1 channel. *Structure.* 13:1203-1211.

Luo, D., Broad, L.M., Bird, G.S., and Putney, J.W., Jr. 2001. Signaling pathways underlying muscarinic receptor-induced [Ca2+]i oscillations in HEK293 cells. *J Biol Chem.* 276:5613-5621.

Luo, D., Sun, H., Xiao, R.P., and Han, Q. 2005. Caffeine induced Ca^{2+} release and capacitative Ca^{2+} entry in human embryonic kidney (HEK293) cells. *Eur J Pharmacol.* 509:109-115.

Luo, W., Grupp, I.L., Harrer, J., Ponniah, S., Grupp, G., Duffy, J.J., Doetschman, T., and Kranias, E.G. 1994. Targeted ablation of the phospholamban gene is associated with markedly enhanced myocardial contractility and loss of beta-agonist stimulation. *Circ Res.* 75:401-409.

Lyng, F.M., Maguire, P., McClean, B., Seymour, C., and Mothersill, C. 2006. The involvement of calcium and MAP kinase signaling pathways in the production of radiation-induced bystander effects. *Radiat Res.* 165:400-409.

Lyng, F.M., Seymour, C.B., and Mothersill, C. 2000. Production of a signal by irradiated cells which leads to a response in unirradiated cells characteristic of initiation of apoptosis. *Br J Cancer.* 83:1223-1230.

Lyng, F.M., Seymour, C.B., and Mothersill, C. 2002a. Early events in the apoptotic cascade initiated in cells treated with medium from the progeny of irradiated cells. *Radiat Prot Dosimetry.* 99:169-172.

Lyng, F.M., Seymour, C.B., and Mothersill, C. 2002b. Initiation of apoptosis in cells exposed to medium from the progeny of irradiated cells: a possible mechanism for bystander-induced genomic instability? *Radiat Res.* 157:365-370.

MacDougall, L.K., Jones, L.R., and Cohen, P. 1991. Identification of the major protein phosphatases in mammalian cardiac muscle which dephosphorylate phospholamban. *Eur J Biochem.* 196:725-734.

MacKenzie, A.E., Korneluk, R.G., Zorzato, F., Fujii, J., Phillips, M., Iles, D., Wieringa, B., Leblond, S., Bailly, J., Willard, H.F., and et al. 1990. The human ryanodine receptor gene: its mapping to 19q13.1, placement in a chromosome 19 linkage group, and exclusion as the gene causing myotonic dystrophy. *Am J Hum Genet.* 46:1082-1089.

Mackenzie, L., Bootman, M.D., Laine, M., Berridge, M.J., Thuring, J., Holmes, A., Li, W.H., and Lipp, P. 2002. The role of inositol 1,4,5-trisphosphate receptors in Ca^{2+} signalling and the generation of arrhythmias in rat atrial myocytes. *J Physiol.* 541:395-409.

MacKrill, J.J. 1999. Protein-protein interactions in intracellular Ca^{2+}-release channel function. *Biochem J.* 337 (Pt 3):345-361.

Mackrill, J.J., Challiss, R.A., O'Connell D, A., Lai, F.A., and Nahorski, S.R. 1997. Differential expression and regulation of ryanodine receptor and myo-inositol 1,4,5-trisphosphate receptor Ca^{2+} release channels in mammalian tissues and cell lines. *Biochem J.* 327 (Pt 1):251-258.

MacLennan, D.H., Duff, C., Zorzato, F., Fujii, J., Phillips, M., Korneluk, R.G., Frodis, W., Britt, B.A., and Worton, R.G. 1990. Ryanodine receptor gene is a candidate for predisposition to malignant hyperthermia. *Nature.* 343:559-561.

MacLennan, D.H., Toyofuku, T., and Kimura, Y. 1997. Sites of regulatory interaction between calcium ATPases and phospholamban. *Basic Res Cardiol.* 92 Suppl 1:11-15.

MacMillan, D., Chalmers, S., Muir, T.C., and McCarron, J.G. 2005. IP_3-mediated Ca^{2+} increases do not involve the ryanodine receptor, but ryanodine receptor antagonists reduce IP_3-mediated Ca^{2+} increases in guinea-pig colonic smooth muscle cells. *J Physiol.* 569:533-544.

Maes, K., Missiaen, L., De Smet, P., Vanlingen, S., Callewaert, G., Parys, J.B., and De Smedt, H. 2000. Differential modulation of inositol 1,4,5-trisphosphate receptor type 1 and type 3 by ATP. *Cell Calcium.* 27:257-267.

Magnino, F., Schmidt, K., Mery, L., and Dufour, J.F. 2001. Rat inositol 1,4,5-trisphosphate receptor isoform 2 interacts with itself in its C-terminal portion and upstream of the first transmembrane domain. *Eur J Biochem.* 268:5981-5988.

Maier, L.S., Wahl-Schott, C., Horn, W., Weichert, S., Pagel, C., Wagner, S., Dybkova, N., Muller, O.J., Nabauer, M., Franz, W.M., and Pieske, B. 2005. Increased SR Ca^{2+}

cycling contributes to improved contractile performance in SERCA2a-overexpressing transgenic rats. *Cardiovasc Res.* 67:636-646.

Mandi, M., and Bak, J. 2008. Nicotinic Acid Adenine Dinucleotide Phosphate (NAADP) and Ca^{2+} Mobilization. *J Recept Signal Transduct Res.* 28:163-184.

Mandil, R., Ashkenazi, E., Blass, M., Kronfeld, I., Kazimirsky, G., Rosenthal, G., Umansky, F., Lorenzo, P.S., Blumberg, P.M., and Brodie, C. 2001. Protein kinase Calpha and protein kinase Cdelta play opposite roles in the proliferation and apoptosis of glioma cells. *Cancer Res.* 61:4612-4619.

Marban, E. 2002. Cardiac channelopathies. *Nature.* 415:213-218.

Marx, S.O., Gaburjakova, J., Gaburjakova, M., Henrikson, C., Ondrias, K., and Marks, A.R. 2001a. Coupled gating between cardiac calcium release channels (ryanodine receptors). *Circ Res.* 88:1151-1158.

Marx, S.O., Reiken, S., Hisamatsu, Y., Gaburjakova, M., Gaburjakova, J., Yang, Y.M., Rosemblit, N., and Marks, A.R. 2001b. Phosphorylation-dependent regulation of ryanodine receptors: a novel role for leucine/isoleucine zippers. *J Cell Biol.* 153:699-708.

Marx, S.O., Reiken, S., Hisamatsu, Y., Jayaraman, T., Burkhoff, D., Rosemblit, N., and Marks, A.R. 2000. PKA phosphorylation dissociates FKBP12.6 from the calcium release channel (ryanodine receptor): defective regulation in failing hearts. *Cell.* 101:365-376.

Marziali, G., Rossi, D., Giannini, G., Charlesworth, A., and Sorrentino, V. 1996. cDNA cloning reveals a tissue specific expression of alternatively spliced transcripts of the ryanodine receptor type 3 (RyR3) calcium release channel. *FEBS Lett.* 394:76-82.

Masumiya, H., Li, P., Zhang, L., and Chen, S.R. 2001. Ryanodine sensitizes the Ca^{2+} release channel (ryanodine receptor) to Ca^{2+} activation. *J Biol Chem.* 276:39727-39735.

Matsumoto, M., and Nagata, E. 1999. Type 1 inositol 1,4,5-trisphosphate receptor knock-out mice: their phenotypes and their meaning in neuroscience and clinical practice. *J Mol Med.* 77:406-411.

Matsumoto, M., Nakagawa, T., Inoue, T., Nagata, E., Tanaka, K., Takano, H., Minowa, O., Kuno, J., Sakakibara, S., Yamada, M., Yoneshima, H., Miyawaki, A., Fukuuchi, Y., Furuichi, T., Okano, H., Mikoshiba, K., and Noda, T. 1996. Ataxia and epileptic seizures in mice lacking type 1 inositol 1,4,5-trisphosphate receptor. *Nature.* 379:168-171.

Mattei, M.G., Giannini, G., Moscatelli, F., and Sorrentino, V. 1994. Chromosomal localization of murine ryanodine receptor genes RYR1, RYR2, and RYR3 by in situ hybridization. *Genomics.* 22:202-204.

Mattson, M.P., and Chan, S.L. 2003. Calcium orchestrates apoptosis. *Nat Cell Biol.* 5:1041-1043.

McCarron, J.G., Bradley, K.N., MacMillan, D., and Muir, T.C. 2003. Sarcolemma agonist-induced interactions between IP_3 and ryanodine receptors in Ca^{2+} oscillations and waves in smooth muscle. *Biochem Soc Trans.* 31:920-924.

Meissner, G. 1994. Ryanodine receptor/Ca^{2+} release channels and their regulation by endogenous effectors. *Annu Rev Physiol.* 56:485-508.

Meissner, G. 2004. Molecular regulation of cardiac ryanodine receptor ion channel. *Cell Calcium.* 35:621-628.

Melino, G., Bernassola, F., Knight, R.A., Corasaniti, M.T., Nistico, G., and Finazzi-Agro, A. 1997. S-nitrosylation regulates apoptosis. *Nature.* 388:432-433.

Mendes, C.C., Gomes, D.A., Thompson, M., Souto, N.C., Goes, T.S., Goes, A.M., Rodrigues, M.A., Gomez, M.V., Nathanson, M.H., and Leite, M.F. 2005. The type III inositol 1,4,5-trisphosphate receptor preferentially transmits apoptotic Ca^{2+} signals into mitochondria. *J Biol Chem.* 280:40892-40900.

Mercan, D., and Malaisse, W.J. 1996. Pancreatic islet B-cell individual variability rather than subpopulation heterogeneity. *Mol Cell Endocrinol.* 118:163-171.

Meur, G., Parker, A.K., Gergely, F.V., and Taylor, C.W. 2007. Targeting and retention of type 1 ryanodine receptors to the endoplasmic reticulum. *J Biol Chem.* 282:23096-23103.

Meyers, M.B., Fischer, A., Sun, Y.J., Lopes, C.M., Rohacs, T., Nakamura, T.Y., Zhou, Y.Y., Lee, P.C., Altschuld, R.A., McCune, S.A., Coetzee, W.A., and Fishman, G.I. 2003. Sorcin regulates excitation-contraction coupling in the heart. *J Biol Chem.* 278:28865-28871.

Michalak, M., Dupraz, P., and Shoshan-Barmatz, V. 1988. Ryanodine binding to sarcoplasmic reticulum membrane; comparison between cardiac and skeletal muscle. *Biochim Biophys Acta.* 939:587-594.

Mignery, G.A., Newton, C.L., Archer, B.T., 3rd, and Sudhof, T.C. 1990. Structure and expression of the rat inositol 1,4,5-trisphosphate receptor. *J Biol Chem.* 265:12679-12685.

Mignery, G.A., Sudhof, T.C., Takei, K., and De Camilli, P. 1989. Putative receptor for inositol 1,4,5-trisphosphate similar to ryanodine receptor. *Nature.* 342:192-195.

Mikoshiba, K. 2007. IP_3 receptor/Ca^{2+} channel: from discovery to new signaling concepts. *J Neurochem.* 102:1426-1446.

Mikoshiba, K., Furuichi, T., and Miyawaki, A. 1994. Structure and function of IP_3 receptors. *Semin Cell Biol.* 5:273-281.

Miller, S.L., Currie, S., Loughrey, C.M., Kettlewell, S., Seidler, T., Reynolds, D.F., Hasenfuss, G., and Smith, G.L. 2005. Effects of calsequestrin over-expression on excitation-contraction coupling in isolated rabbit cardiomyocytes. *Cardiovasc Res.* 67:667-677.

Milner, R.E., Famulski, K.S., and Michalak, M. 1992. Calcium binding proteins in the sarcoplasmic/endoplasmic reticulum of muscle and nonmuscle cells. *Mol Cell Biochem.* 112:1-13.

Milting, H., Janssen, P.M., Wangemann, T., Kogler, H., Domeier, E., Seidler, T., Hakim, K., Grapow, M., Zeitz, O., Prestle, J., and Zerkowski, H.R. 2001. FK506 does not affect cardiac contractility and adrenergic response in vitro. *Eur J Pharmacol.* 430:299-304.

Missiaen, L., Parys, J.B., De Smedt, H., Sienaert, I., Sipma, H., Vanlingen, S., Maes, K., Kunzelmann, K., and Casteels, R. 1998. Inhibition of inositol trisphosphate-induced calcium release by cyclic ADP-ribose in A7r5 smooth-muscle cells and in 16HBE14o-bronchial mucosal cells. *Biochem J.* 329 (Pt 3):489-495.

Miyakawa, T., Maeda, A., Yamazawa, T., Hirose, K., Kurosaki, T., and Iino, M. 1999. Encoding of Ca^{2+} signals by differential expression of IP_3 receptor subtypes. *Embo J.* 18:1303-1308.

Miyamoto, S., Howes, A.L., Adams, J.W., Dorn, G.W., 2nd, and Brown, J.H. 2005. Ca^{2+} dysregulation induces mitochondrial depolarization and apoptosis: role of Na^{+}/Ca^{2+} exchanger and AKT. *J Biol Chem.* 280:38505-38512.

Miyazaki, S., Yuzaki, M., Nakada, K., Shirakawa, H., Nakanishi, S., Nakade, S., and Mikoshiba, K. 1992. Block of Ca^{2+} wave and Ca^{2+} oscillation by antibody to the inositol 1,4,5-trisphosphate receptor in fertilized hamster eggs. *Science.* 257:251-255.

Mochizuki, M., Yano, M., Oda, T., Tateishi, H., Kobayashi, S., Yamamoto, T., Ikeda, Y., Ohkusa, T., Ikemoto, N., and Matsuzaki, M. 2007. Scavenging free radicals by low-dose carvedilol prevents redox-dependent Ca^{2+} leak via stabilization of ryanodine receptor in heart failure. *J Am Coll Cardiol.* 49:1722-1732.

Moore, R.A., Nguyen, H., Galceran, J., Pessah, I.N., and Allen, P.D. 1998. A transgenic myogenic cell line lacking ryanodine receptor protein for homologous expression studies: reconstitution of Ry1R protein and function. *J Cell Biol.* 140:843-851.

Mori, F., Fukaya, M., Abe, H., Wakabayashi, K., and Watanabe, M. 2000. Developmental changes in expression of the three ryanodine receptor mRNAs in the mouse brain. *Neurosci Lett.* 285:57-60.

Moschella, M.C., and Marks, A.R. 1993. Inositol 1,4,5-trisphosphate receptor expression in cardiac myocytes. *J Cell Biol.* 120:1137-1146.

Mothersill, C., Lyng, F., Seymour, C., Maguire, P., Lorimore, S., and Wright, E. 2005. Genetic factors influencing bystander signaling in murine bladder epithelium after low-dose irradiation in vivo. *Radiat Res.* 163:391-399.

Muller-Taubenberger, A., Vos, M.J., Bottger, A., Lasi, M., Lai, F.P., Fischer, M., and Rottner, K. 2006. Monomeric red fluorescent protein variants used for imaging studies in different species. *Eur J Cell Biol.* 85:1119-1129.

Mundell, S.J., and Benovic, J.L. 2000. Selective regulation of endogenous G protein-coupled receptors by arrestins in HEK293 cells. *J Biol Chem.* 275:12900-12908.

Murayama, T., Oba, T., Hara, H., Wakebe, K., Ikemoto, N., and Ogawa, Y. 2006. Postulated role of interdomain interaction between regions 1 and 2 within type 1 ryanodine receptor in the pathogenesis of porcine malignant hyperthermia. *Biochem J.*

Murthy, K.S., and Zhou, H. 2003. Selective phosphorylation of the IP_3R1 in vivo by cGMP-dependent protein kinase in smooth muscle. *Am J Physiol Gastrointest Liver Physiol.* 284:G221-230.

Nakamura, K., Robertson, M., Liu, G., Dickie, P., Nakamura, K., Guo, J.Q., Duff, H.J., Opas, M., Kavanagh, K., and Michalak, M. 2001. Complete heart block and sudden death in mice overexpressing calreticulin. *J Clin Invest.* 107:1245-1253.

Nakaya, H., Furusawa, Y., Ogura, T., Tamagawa, M., and Uemura, H. 2000. Inhibitory effects of JTV-519, a novel cardioprotective drug, on potassium currents and experimental atrial fibrillation in guinea-pig hearts. *Br J Pharmacol.* 131:1363-1372.

Nakayama, T., Hattori, M., Uchida, K., Nakamura, T., Tateishi, Y., Bannai, H., Iwai, M., Michikawa, T., Inoue, T., and Mikoshiba, K. 2004. The regulatory domain of the inositol 1,4,5-trisphosphate receptor is necessary to keep the channel domain closed: possible physiological significance of specific cleavage by caspase 3. *Biochem J.* 377:299-307.

Nanavaty, U.B., Pawliczak, R., Doniger, J., Gladwin, M.T., Cowan, M.J., Logun, C., and Shelhamer, J.H. 2002. Oxidant-induced cell death in respiratory epithelial cells is due to DNA damage and loss of ATP. *Exp Lung Res.* 28:591-607.

Napolitano, C., and Priori, S.G. 2006. Brugada syndrome. *Orphanet J Rare Dis.* 1:35.

Nathanson, N.M., Klein, W.L., and Nirenberg, M. 1978. Regulation of adenylate cyclase activity mediated by muscarinic acetylcholine receptors. *Proc Natl Acad Sci U S A.* 75:1788-1791.

Neveu, M.J., Hully, J.R., Babcock, K.L., Vaughan, J., Hertzberg, E.L., Nicholson, B.J., Paul, D.L., and Pitot, H.C. 1995. Proliferation-associated differences in the spatial and temporal expression of gap junction genes in rat liver. *Hepatology.* 22:202-212.

Newton, C.L., Mignery, G.A., and Sudhof, T.C. 1994. Co-expression in vertebrate tissues and cell lines of multiple inositol 1,4,5-trisphosphate (IP_3) receptors with distinct affinities for IP_3. *J Biol Chem.* 269:28613-28619.

Nicotera, P., Leist, M., and Ferrando-May, E. 1998. Intracellular ATP, a switch in the decision between apoptosis and necrosis. *Toxicol Lett.* 102-103:139-142.

Nicotera, P., and Melino, G. 2004. Regulation of the apoptosis-necrosis switch. *Oncogene.* 23:2757-2765.

Niggli, E., Piston, D.W., Kirby, M.S., Cheng, H., Sandison, D.R., Webb, W.W., and Lederer, W.J. 1994. A confocal laser scanning microscope designed for indicators with ultraviolet excitation wavelengths. *Am J Physiol.* 266:C303-310.

Nishio, H., Iwata, M., Tamura, A., Miyazaki, T., Tsuboi, K., and Suzuki, K. 2008. Identification of a novel mutation V2321M of the cardiac ryanodine receptor gene of

sudden unexplained death and a phenotypic study of the gene mutations. *Leg Med (Tokyo)*.

Niyaz, M., Numakawa, T., Matsuki, Y., Kumamaru, E., Adachi, N., Kitazawa, H., Kunugi, H., and Kudo, M. 2007. MCI-186 prevents brain tissue from neuronal damage in cerebral infarction through the activation of intracellular signaling. *J Neurosci Res.* 85:2933-2942.

Noguchi, T., Ishii, K., Fukutomi, H., Naguro, I., Matsuzawa, A., Takeda, K., and Ichijo, H. 2008. Requirement of reactive oxygen species-dependent activation of ASK1-p38 MAPK pathway for extracellular ATP-induced apoptosis in macrophage. *J Biol Chem.* 283:7657-7665.

Noor, J.I., Ueda, Y., Ikeda, T., and Ikenoue, T. 2007. Edaravone inhibits lipid peroxidation in neonatal hypoxic-ischemic rats: an in vivo microdialysis study. *Neurosci Lett.* 414:5-9.

North, R.A., and Verkhratsky, A. 2006. Purinergic transmission in the central nervous system. *Pflugers Arch.* 452:479-485.

Novak, E.J., and Rabinovitch, P.S. 1994. Improved sensitivity in flow cytometric intracellular ionized calcium measurement using fluo-3/Fura Red fluorescence ratios. *Cytometry.* 17:135-141.

O'Neill, C., Cowburn, R.F., Bonkale, W.L., Ohm, T.G., Fastbom, J., Carmody, M., and Kelliher, M. 2001. Dysfunctional intracellular calcium homoeostasis: a central cause of neurodegeneration in Alzheimer's disease. *Biochem Soc Symp.* 177-194.

Oakes, S.A., Scorrano, L., Opferman, J.T., Bassik, M.C., Nishino, M., Pozzan, T., and Korsmeyer, S.J. 2005. Proapoptotic BAX and BAK regulate the type 1 inositol trisphosphate receptor and calcium leak from the endoplasmic reticulum. *Proc Natl Acad Sci U S A.* 102:105-110.

Oda, T., Yano, M., Yamamoto, T., Tokuhisa, T., Okuda, S., Doi, M., Ohkusa, T., Ikeda, Y., Kobayashi, S., Ikemoto, N., and Matsuzaki, M. 2005. Defective regulation of interdomain interactions within the ryanodine receptor plays a key role in the pathogenesis of heart failure. *Circulation.* 111:3400-3410.

Ondrias, K., Marx, S.O., Gaburjakova, M., and Marks, A.R. 1998. FKBP12 modulates gating of the ryanodine receptor/calcium release channel. *Ann N Y Acad Sci.* 853:149-156.

Onogi, H., Minatoguchi, S., Chen, X.H., Bao, N., Kobayashi, H., Misao, Y., Yasuda, S., Yamaki, T., Maruyama, R., Uno, Y., Arai, M., Takemura, G., and Fujiwara, H. 2006. Edaravone reduces myocardial infarct size and improves cardiac function and remodelling in rabbits. *Clin Exp Pharmacol Physiol.* 33:1035-1041.

Orrenius, S., Zhivotovsky, B., and Nicotera, P. 2003. Regulation of cell death: the calcium-apoptosis link. *Nat Rev Mol Cell Biol.* 4:552-565.

Ostrom, R.S., Gregorian, C., and Insel, P.A. 2000. Cellular release of and response to ATP as key determinants of the set-point of signal transduction pathways. *J Biol Chem.* 275:11735-11739.

Otsu, K., Fujii, J., Periasamy, M., Difilippantonio, M., Uppender, M., Ward, D.C., and MacLennan, D.H. 1993. Chromosome mapping of five human cardiac and skeletal muscle sarcoplasmic reticulum protein genes. *Genomics.* 17:507-509.

Otsu, K., Willard, H.F., Khanna, V.K., Zorzato, F., Green, N.M., and MacLennan, D.H. 1990. Molecular cloning of cDNA encoding the Ca^{2+} release channel (ryanodine receptor) of rabbit cardiac muscle sarcoplasmic reticulum. *J Biol Chem.* 265:13472-13483.

Paavola, J., Viitasalo, M., Laitinen-Forsblom, P.J., Pasternack, M., Swan, H., Tikkanen, I., Toivonen, L., Kontula, K., and Laine, M. 2007. Mutant ryanodine receptors in catecholaminergic polymorphic ventricular tachycardia generate delayed afterdepolarizations due to increased propensity to Ca^{2+} waves. *Eur Heart J.* 28:1135-1142.

Pan, Z., Damron, D., Nieminen, A.L., Bhat, M.B., and Ma, J. 2000. Depletion of intracellular Ca^{2+} by caffeine and ryanodine induces apoptosis of chinese hamster ovary cells transfected with ryanodine receptor. *J Biol Chem.* 275:19978-19984.

Paolini, C., Fessenden, J.D., Pessah, I.N., and Franzini-Armstrong, C. 2004. Evidence for conformational coupling between two calcium channels. *Proc Natl Acad Sci U S A.* 101:12748-12752.

Park, I.C., Park, M.J., Rhee, C.H., Lee, J.I., Choe, T.B., Jang, J.J., Lee, S.H., and Hong, S.I. 2001. Protein kinase C activation by PMA rapidly induces apoptosis through caspase-3/CPP32 and serine protease(s) in a gastric cancer cell line. *Int J Oncol.* 18:1077-1083.

Parker, A.K., Gergely, F.V., and Taylor, C.W. 2004. Targeting of inositol 1,4,5-trisphosphate receptors to the endoplasmic reticulum by multiple signals within their transmembrane domains. *J Biol Chem.* 279:23797-23805.

Paszty, K., Antalffy, G., Hegedus, L., Padanyi, R., Penheiter, A.R., Filoteo, A.G., Penniston, J.T., and Enyedi, A. 2007. Cleavage of the plasma membrane Ca^{2+}ATPase during apoptosis. *Ann N Y Acad Sci.* 1099:440-450.

Paszty, K., Verma, A.K., Padanyi, R., Filoteo, A.G., Penniston, J.T., and Enyedi, A. 2002. Plasma membrane Ca^{2+}ATPase isoform 4b is cleaved and activated by caspase-3 during the early phase of apoptosis. *J Biol Chem.* 277:6822-6829.

Patel, S., Joseph, S.K., and Thomas, A.P. 1999. Molecular properties of inositol 1,4,5-trisphosphate receptors. *Cell Calcium.* 25:247-264.

Peluso, J.J., Pappalardo, A., and Fernandez, G. 2001. Basic fibroblast growth factor maintains calcium homeostasis and granulosa cell viability by stimulating calcium efflux via a PKC delta-dependent pathway. *Endocrinology.* 142:4203-4211.

Pepper, C., Hoy, T., and Bentley, P. 1998. Elevated Bcl-2/Bax are a consistent feature of apoptosis resistance in B-cell chronic lymphocytic leukaemia and are correlated with in vivo chemoresistance. *Leuk Lymphoma.* 28:355-361.

Pessah, I.N., Waterhouse, A.L., and Casida, J.E. 1985. The calcium-ryanodine receptor complex of skeletal and cardiac muscle. *Biochem Biophys Res Commun.* 128:449-456.

Petersen, O.H., and Burdakova, N. 2002. The specificity of Ca^{2+} signalling. *Acta Physiol Hung.* 89:439-450.

Pettit, R.K., Weber, C.A., Kean, M.J., Hoffmann, H., Pettit, G.R., Tan, R., Franks, K.S., and Horton, M.L. 2005. Microplate Alamar blue assay for *Staphylococcus epidermidis* biofilm susceptibility testing. *Antimicrob Agents Chemother.* 49:2612-2617.

Picht, E., DeSantiago, J., Huke, S., Kaetzel, M.A., Dedman, J.R., and Bers, D.M. 2007. CaMKII inhibition targeted to the sarcoplasmic reticulum inhibits frequency-dependent acceleration of relaxation and Ca^{2+} current facilitation. *J Mol Cell Cardiol.* 42:196-205.

Pitt, G.S. 2007. Calmodulin and CaMKII as molecular switches for cardiac ion channels. *Cardiovasc Res.* 73:641-647.

Pitts, J.D., Finbow, M.E., and Kam, E. 1988. Junctional communication and cellular differentiation. *Br J Cancer Suppl.* 9:52-57.

Pizzuto, M.F., Valverde, A.M., Heavey, B.M., Banas, M.D., Michelakis, N., Suzuki, G., Fallavollita, J.A., and Canty, J.M., Jr. 2006. Brief sympathetic activation precedes the development of ventricular tachycardia and ventricular fibrillation in hibernating myocardium. *J Electrocardiol.* 39:S140-145.

Postma, A.V., Denjoy, I., Hoorntje, T.M., Lupoglazoff, J.-M., Da Costa, A., Sebillon, P., Mannens, M.M.A.M., Wilde, A.A.M., and Guicheney, P. 2002. Absence of calsequestrin 2 causes severe forms of catecholaminergic polymorphic ventricular tachycardia. *Circ Res.* 91:21e-26.

Postma, A.V., Denjoy, I., Kamblock, J., Alders, M., Lupoglazoff, J.M., Vaksmann, G., Dubosq-Bidot, L., Sebillon, P., Mannens, M.M., Guicheney, P., and Wilde, A.A.

2005. Catecholaminergic polymorphic ventricular tachycardia: RYR2 mutations, bradycardia, and follow up of the patients. *J Med Genet.* 42:863-870.

Pott, C., Goldhaber, J.I., and Philipson, K.D. 2007a. Homozygous overexpression of the Na^+/Ca^{2+} exchanger in mice: evidence for increased transsarcolemmal Ca^{2+} fluxes. *Ann N Y Acad Sci.* 1099:310-314.

Pott, C., Henderson, S.A., Goldhaber, J.I., and Philipson, K.D. 2007b. Na^+/Ca^{2+} exchanger knockout mice: plasticity of cardiac excitation-contraction coupling. *Ann N Y Acad Sci.* 1099:270-275.

Pott, C., Philipson, K.D., and Goldhaber, J.I. 2005. Excitation-contraction coupling in Na^+/Ca^{2+} exchanger knockout mice: reduced transsarcolemmal Ca^{2+} flux. *Circ Res.* 97:1288-1295.

Pott, C., Ren, X., Tran, D.X., Yang, M.J., Henderson, S., Jordan, M.C., Roos, K.P., Garfinkel, A., Philipson, K.D., and Goldhaber, J.I. 2007c. Mechanism of shortened action potential duration in Na^+/Ca^{2+} exchanger knockout mice. *Am J Physiol Cell Physiol.* 292:C968-973.

Pott, C., Yip, M., Goldhaber, J.I., and Philipson, K.D. 2007d. Regulation of cardiac L-type Ca^{2+} current in Na^+/Ca^{2+} exchanger knockout mice: functional coupling of the Ca^{2+} channel and the Na^+/Ca^{2+} exchanger. *Biophys J.* 92:1431-1437.

Powell, J.A., Carrasco, M.A., Adams, D.S., Drouet, B., Rios, J., Muller, M., Estrada, M., and Jaimovich, E. 2001. IP_3 receptor function and localization in myotubes: an unexplored Ca^{2+} signaling pathway in skeletal muscle. *J Cell Sci.* 114:3673-3683.

Princen, F., Robe, P., Gros, D., Jarry-Guichard, T., Gielen, J., Merville, M.P., and Bours, V. 2001. Rat gap junction connexin-30 inhibits proliferation of glioma cell lines. *Carcinogenesis.* 22:507-513.

Priori, S.G., and Corr, P.B. 1990. Mechanisms underlying early and delayed afterdepolarizations induced by catecholamines. *Am J Physiol.* 258:H1796-1805.

Priori, S.G., Napolitano, C., Memmi, M., Colombi, B., Drago, F., Gasparini, M., DeSimone, L., Coltorti, F., Bloise, R., Keegan, R., Cruz Filho, F.E., Vignati, G., Benatar, A., and DeLogu, A. 2002. Clinical and molecular characterization of patients with catecholaminergic polymorphic ventricular tachycardia. *Circulation.* 106:69-74.

Priori, S.G., Napolitano, C., Tiso, N., Memmi, M., Vignati, G., Bloise, R., Sorrentino, V., and Danieli, G.A. 2001. Mutations in the cardiac ryanodine receptor gene (hRyR2) underlie catecholaminergic polymorphic ventricular tachycardia. *Circulation.* 103:196-200.

Proven, A., Roderick, H.L., Conway, S.J., Berridge, M.J., Horton, J.K., Capper, S.J., and Bootman, M.D. 2006. Inositol 1,4,5-trisphosphate supports the arrhythmogenic action of endothelin-1 on ventricular cardiac myocytes. *J Cell Sci.* 119:3363-3375.

Quane, K.A., Healy, J.M., Keating, K.E., Manning, B.M., Couch, F.J., Palmucci, L.M., Doriguzzi, C., Fagerlund, T.H., Berg, K., Ording, H., and et al. 1993. Mutations in the ryanodine receptor gene in central core disease and malignant hyperthermia. *Nat Genet.* 5:51-55.

Querfurth, H.W., Haughey, N.J., Greenway, S.C., Yacono, P.W., Golan, D.E., and Geiger, J.D. 1998. Expression of ryanodine receptors in human embryonic kidney (HEK293) cells. *Biochem J.* 334 (Pt 1):79-86.

Radermacher, M., Rao, V., Grassucci, R., Frank, J., Timerman, A.P., Fleischer, S., and Wagenknecht, T. 1994. Cryo-electron microscopy and three-dimensional reconstruction of the calcium release channel/ryanodine receptor from skeletal muscle. *J Cell Biol.* 127:411-423.

Ramos-Franco, J., Fill, M., and Mignery, G.A. 1998. Isoform-specific function of single inositol 1,4,5-trisphosphate receptor channels. *Biophys J.* 75:834-839.

Ranu, H.K., Terracciano, C.M., Davia, K., Bernobich, E., Chaudhri, B., Robinson, S.E., Bin Kang, Z., Hajjar, R.J., MacLeod, K.T., and Harding, S.E. 2002. Effects of Na^+/Ca^{2+}-

exchanger overexpression on excitation-contraction coupling in adult rabbit ventricular myocytes. *J Mol Cell Cardiol.* 34:389-400.

Regimbald-Dumas, Y., Arguin, G., Fregeau, M.O., and Guillemette, G. 2007. cAMP-dependent protein kinase enhances inositol 1,4,5-trisphosphate-induced Ca^{2+} release in AR4-2J cells. *J Cell Biochem.* 101:609-618.

Reiken, S., Gaburjakova, M., Guatimosim, S., Gomez, A.M., D'Armiento, J., Burkhoff, D., Wang, J., Vassort, G., Lederer, W.J., and Marks, A.R. 2003a. Protein kinase A phosphorylation of the cardiac calcium release channel (ryanodine receptor) in normal and failing hearts. Role of phosphatases and response to isoproterenol. *J Biol Chem.* 278:444-453.

Reiken, S., Lacampagne, A., Zhou, H., Kherani, A., Lehnart, S.E., Ward, C., Huang, F., Gaburjakova, M., Gaburjakova, J., Rosemblit, N., Warren, M.S., He, K.L., Yi, G.H., Wang, J., Burkhoff, D., Vassort, G., and Marks, A.R. 2003b. PKA phosphorylation activates the calcium release channel (ryanodine receptor) in skeletal muscle: defective regulation in heart failure. *J Cell Biol.* 160:919-928.

Reiken, S., Wehrens, X.H., Vest, J.A., Barbone, A., Klotz, S., Mancini, D., Burkhoff, D., and Marks, A.R. 2003c. Beta-blockers restore calcium release channel function and improve cardiac muscle performance in human heart failure. *Circulation.* 107:2459-2466.

Reilly, A.M., Petrou, S., Panchal, R.G., and Williams, D.A. 2001. Restoration of calcium handling properties of adult cardiac myocytes from hypertrophied hearts. *Cell Calcium.* 30:59-66.

Reuter, H., Han, T., Motter, C., Philipson, K.D., and Goldhaber, J.I. 2004. Mice overexpressing the cardiac sodium-calcium exchanger: defects in excitation-contraction coupling. *J Physiol.* 554:779-789.

Reuter, H., Henderson, S.A., Han, T., Mottino, G.A., Frank, J.S., Ross, R.S., Goldhaber, J.I., and Philipson, K.D. 2003. Cardiac excitation-contraction coupling in the absence of Na^{+}/Ca^{2+} exchange. *Cell Calcium.* 34:19-26.

Rintoul, G.L., Raymond, L.A., and Baimbridge, K.G. 2001. Calcium buffering and protection from excitotoxic cell death by exogenous calbindin-D28k in HEK293 cells. *Cell Calcium.* 29:277-287.

Rizzuto, R., Brini, M., Murgia, M., and Pozzan, T. 1993. Microdomains with high Ca^{2+} close to IP_3-sensitive channels that are sensed by neighboring mitochondria. *Science.* 262:744-747.

Rodriguez-Sinovas, A., Cabestrero, A., Lopez, D., Torre, I., Morente, M., Abellan, A., Miro, E., Ruiz-Meana, M., and Garcia-Dorado, D. 2007. The modulatory effects of connexin 43 on cell death/survival beyond cell coupling. *Prog Biophys Mol Biol.* 94:219-232.

Rodriguez, P., Bhogal, M.S., and Colyer, J. 2003. Stoichiometric phosphorylation of cardiac ryanodine receptor on serine 2809 by calmodulin-dependent kinase II and protein kinase A. *J.Biol. Chem.* 278:38593-38600.

Rossi, D., Simeoni, I., Micheli, M., Bootman, M., Lipp, P., Allen, P.D., and Sorrentino, V. 2002. RyR1 and RyR3 isoforms provide distinct intracellular Ca^{2+} signals in HEK 293 cells. *J Cell Sci.* 115:2497-2504.

Rosso, R., Kalman, J.M., Rogowski, O., Diamant, S., Birger, A., Biner, S., Belhassen, B., and Viskin, S. 2007. Calcium channel blockers and beta-blockers versus beta-blockers alone for preventing exercise-induced arrhythmias in catecholaminergic polymorphic ventricular tachycardia. *Heart Rhythm.* 4:1149-1154.

Ruegg, J.C. 1990. Towards a molecular understanding of contractility. *Cardioscience.* 1:163-168.

Sako, Y., Sekihata, A., Yanagisawa, Y., Yamamoto, M., Shimada, Y., Ozaki, K., and Kusumi, A. 1997. Comparison of two-photon excitation laser scanning microscopy with UV-

confocal laser scanning microscopy in three-dimensional calcium imaging using the fluorescence indicator Indo-1. *J Microsc.* 185:9-20.

Samso, M., Wagenknecht, T., and Allen, P.D. 2005. Internal structure and visualization of transmembrane domains of the RyR1 calcium release channel by cryo-EM. *Nat Struct Mol Biol.* 12:539-544.

Sanchez, G., Escobar, M., Pedrozo, Z., Macho, P., Domenech, R., Hartel, S., Hidalgo, C., and Donoso, P. 2008. Exercise and tachycardia increase NADPH oxidase and ryanodine receptor-2 activity: possible role in cardioprotection. *Cardiovasc Res.* 77:380-386.

Sande, J.B., Sjaastad, I., Hoen, I.B., Bokenes, J., Tonnessen, T., Holt, E., Lunde, P.K., and Christensen, G. 2002. Reduced level of serine(16) phosphorylated phospholamban in the failing rat myocardium: a major contributor to reduced SERCA2 activity. *Cardiovasc Res.* 53:382-391.

Sandstrom, K., Hakansson, L., Lukinius, A., and Venge, P. 2000. A method to study apoptosis in eosinophils by flow cytometry. *J Immunol Methods.* 240:55-68.

Sanger, F., Nicklen, S., and Coulson, A.R. 1977. DNA sequencing with chain-terminating inhibitors. *Proc Natl Acad Sci U S A.* 74:5463-5467.

Santana, L.F., Kranias, E.G., and Lederer, W.J. 1997. Calcium sparks and excitation-contraction coupling in phospholamban-deficient mouse ventricular myocytes. *J Physiol.* 503 (Pt 1):21-29.

Sato, Y., Ferguson, D.G., Sako, H., Dorn, G.W., 2nd, Kadambi, V.J., Yatani, A., Hoit, B.D., Walsh, R.A., and Kranias, E.G. 1998. Cardiac-specific overexpression of mouse cardiac calsequestrin is associated with depressed cardiovascular function and hypertrophy in transgenic mice. *J Biol Chem.* 273:28470-28477.

Schachter, J.B., Sromek, S.M., Nicholas, R.A., and Harden, T.K. 1997. HEK293 human embryonic kidney cells endogenously express the P2Y1 and P2Y2 receptors. *Neuropharmacology.* 36:1181-1187.

Scheinman, M.M., and Lam, J. 2006. Exercise-induced ventricular arrhythmias in patients with no structural cardiac disease. *Annu Rev Med.* 57:473-484.

Schillinger, W., Janssen, P.M., Emami, S., Henderson, S.A., Ross, R.S., Teucher, N., Zeitz, O., Philipson, K.D., Prestle, J., and Hasenfuss, G. 2000. Impaired contractile performance of cultured rabbit ventricular myocytes after adenoviral gene transfer of Na^+/Ca^{2+} exchanger. *Circ Res.* 87:581-587.

Schug, Z.T., da Fonseca, P.C., Bhanumathy, C.D., Wagner, L., 2nd, Zhang, X., Bailey, B., Morris, E.P., Yule, D.I., and Joseph, S.K. 2008. Molecular Characterization of the Inositol 1,4,5-Trisphosphate Receptor Pore-forming Segment. *J Biol Chem.* 283:2939-2948.

Schug, Z.T., and Joseph, S.K. 2006. The role of the S4-S5 linker and C-terminal tail in inositol 1,4,5-trisphosphate receptor function. *J Biol Chem.* 281:24431-24440.

Schulteis, C.T., Nagaya, N., and Papazian, D.M. 1996. Intersubunit interaction between amino- and carboxyl-terminal cysteine residues in tetrameric shaker K^+ channels. *Biochemistry.* 35:12133-12140.

Schumacher, C., Konigs, B., Sigmund, M., Kohne, B., Schondube, F., Vob, M., Stein, B., Weil, J., and Hanrath, P. 1995. The ryanodine binding sarcoplasmic reticulum calcium release channel in nonfailing and in failing human myocardium. *Naunyn Schmiedebergs Arch Pharmacol.* 353:80-85.

Schuster, S., Knoke, B., and Marhl, M. 2005. Differential regulation of proteins by bursting calcium oscillations--a theoretical study. *Biosystems.* 81:49-63.

Schuster, S., Marhl, M., and Hofer, T. 2002. Modelling of simple and complex calcium oscillations. From single-cell responses to intercellular signalling. *Eur J Biochem.* 269:1333-1355.

Schwab, B.L., Guerini, D., Didszun, C., Bano, D., Ferrando-May, E., Fava, E., Tam, J., Xu, D., Xanthoudakis, S., Nicholson, D.W., Carafoli, E., and Nicotera, P. 2002. Cleavage

of plasma membrane calcium pumps by caspases: a link between apoptosis and necrosis. *Cell Death Differ.* 9:818-831.

Sedlak, T.W., and Snyder, S.H. 2006. Messenger molecules and cell death: therapeutic implications. *Jama.* 295:81-89.

Seisenberger, C., Specht, V., Welling, A., Platzer, J., Pfeifer, A., Kuhbandner, S., Striessnig, J., Klugbauer, N., Feil, R., and Hofmann, F. 2000. Functional embryonic cardiomyocytes after disruption of the L-type alpha1C (Cav1.2) calcium channel gene in the mouse. *J Biol Chem.* 275:39193-39199.

Shaner, N.C., Campbell, R.E., Steinbach, P.A., Giepmans, B.N.G., Palmer, A.E., and Tsien, R.Y. 2004. Improved monomeric red, orange and yellow fluorescent proteins derived from *Discosoma sp.* red fluorescent protein. *Nat. Biotechnol.* 22:1567-1572.

Shaner, N.C., Patterson, G.H., and Davidson, M.W. 2007. Advances in fluorescent protein technology. *J Cell Sci.* 120:4247-4260.

Shannon, T.R., Pogwizd, S.M., and Bers, D.M. 2003. Elevated sarcoplasmic reticulum Ca^{2+} leak in intact ventricular myocytes from rabbits in heart failure. *Circ Res.* 93:592-594.

Sharma, M.R., Jeyakumar, L.H., Fleischer, S., and Wagenknecht, T. 2006. Three-dimensional visualization of FKBP12.6 binding to an open conformation of cardiac ryanodine receptor. *Biophys J.* 90:164-172.

Shen, X., Franzini-Armstrong, C., Lopez, J.R., Jones, L.R., Kobayashi, Y.M., Wang, Y., Kerrick, W.G., Caswell, A.H., Potter, J.D., Miller, T., Allen, P.D., and Perez, C.F. 2007. Triadins modulate intracellular Ca^{2+} homeostasis but are not essential for excitation-contraction coupling in skeletal muscle. *J Biol Chem.*

Shimomura, O., Johnson, F.H., and Saiga, Y. 1962. Extraction, purification and properties of aequorin, a bioluminescent protein from the luminous hydromedusan, Aequorea. *J Cell Comp Physiol.* 59:223-239.

Shimomura, O., Johnson, F.H., and Saiga, Y. 1963. Further Data on the Bioluminescent Protein, Aequorin. *J Cell Physiol.* 62:1-8.

Shtifman, A., Ward, C.W., Yamamoto, T., Wang, J., Olbinski, B., Valdivia, H.H., Ikemoto, N., and Schneider, M.F. 2002. Interdomain interactions within ryanodine receptors regulate Ca^{2+} spark frequency in skeletal muscle. *J Gen Physiol.* 119:15-32.

Shuba Ia, M. 2007. [Calcium signaling in carcinogenesis]. *Fiziol Zh.* 53:110-128.

Sitsapesan, R., McGarry, S.J., and Williams, A.J. 1994. Cyclic ADP-ribose competes with ATP for the adenine nucleotide binding site on the cardiac ryanodine receptor Ca^{2+}-release channel. *Circ Res.* 75:596-600.

Sitsapesan, R., and Williams, A.J. 1994. Regulation of the gating of the sheep cardiac sarcoplasmic reticulum Ca^{2+}-release channel by luminal Ca^{2+}. *J Membr Biol.* 137:215-226.

Smith, G.D., Keizer, J.E., Stern, M.D., Lederer, W.J., and Cheng, H. 1998. A simple numerical model of calcium spark formation and detection in cardiac myocytes. *Biophys J.* 75:15-32.

Sobie, E.A., Guatimosim, S., Gomez-Viquez, L., Song, L.S., Hartmann, H., Saleet Jafri, M., and Lederer, W.J. 2006. The Ca^{2+} leak paradox and rogue ryanodine receptors: SR Ca^{2+} efflux theory and practice. *Prog Biophys Mol Biol.* 90:172-185.

Song, L., Alcalai, R., Arad, M., Wolf, C.M., Toka, O., Conner, D.A., Berul, C.I., Eldar, M., Seidman, C.E., and Seidman, J.G. 2007. Calsequestrin 2 (CASQ2) mutations increase expression of calreticulin and ryanodine receptors, causing catecholaminergic polymorphic ventricular tachycardia. *J Clin Invest.* 117:1814-1823.

Song, L.S., Guia, A., Muth, J.N., Rubio, M., Wang, S.Q., Xiao, R.P., Josephson, I.R., Lakatta, E.G., Schwartz, A., and Cheng, H. 2002. Ca^{2+} signaling in cardiac myocytes overexpressing the alpha(1) subunit of L-type Ca^{2+} channel. *Circ Res.* 90:174-181.

Song, L.S., Sobie, E.A., McCulle, S., Lederer, W.J., Balke, C.W., and Cheng, H. 2006. Orphaned ryanodine receptors in the failing heart. *Proc Natl Acad Sci U S A.* 103:4305-4310.

Sorrentino, V., Giannini, G., Malzac, P., and Mattei, M.G. 1993. Localization of a novel ryanodine receptor gene (RYR3) to human chromosome 15q14-q15 by in situ hybridization. *Genomics.* 18:163-165.

Sorrentino, V., and Volpe, P. 1993. Ryanodine receptors: how many, where and why? *Trends Pharmacol Sci.* 14:98-103.

Sosinsky, G.E., and Nicholson, B.J. 2005. Structural organization of gap junction channels. *Biochim Biophys Acta.* 1711:99-125.

Splawski, I., Timothy, K.W., Decher, N., Kumar, P., Sachse, F.B., Beggs, A.H., Sanguinetti, M.C., and Keating, M.T. 2005. Severe arrhythmia disorder caused by cardiac L-type calcium channel mutations. *Proc Natl Acad Sci U S A.* 102:8089-8096; discussion 8086-8088.

Splawski, I., Timothy, K.W., Sharpe, L.M., Decher, N., Kumar, P., Bloise, R., Napolitano, C., Schwartz, P.J., Joseph, R.M., Condouris, K., Tager-Flusberg, H., Priori, S.G., Sanguinetti, M.C., and Keating, M.T. 2004. $Ca_V1.2$ calcium channel dysfunction causes a multisystem disorder including arrhythmia and autism. *Cell.* 119:19-31.

Stamatakis, M., and Mantzaris, N.V. 2006. Modeling of ATP-mediated signal transduction and wave propagation in astrocytic cellular networks. *J Theor Biol.* 241:649-668.

Stange, M., Xu, L., Balshaw, D., Yamaguchi, N., and Meissner, G. 2003. Characterization of recombinant skeletal muscle (ser-2843) and cardiac muscle (ser-2809) ryanodine receptor phosphorylation mutants. *J. Biol. Chem.* 278:51693-51702.

Starmer, C.F., Lastra, A.A., Nesterenko, V.V., and Grant, A.O. 1991. Proarrhythmic response to sodium channel blockade. Theoretical model and numerical experiments. *Circulation.* 84:1364-1377.

Stauffer, K.A., and Unwin, N. 1992. Structure of gap junction channels. *Semin Cell Biol.* 3:17-20.

Steele, D.S., and Duke, A.M. 2007. Defective Mg^{2+} regulation of RyR1 as a causal factor in malignant hyperthermia. *Arch Biochem Biophys.* 458:57-64.

Stetzer, E., Ebbinghaus, U., Storch, A., Poteur, L., Schrattenholz, A., Kramer, G., Methfessel, C., and Maelicke, A. 1996. Stable expression in HEK-293 cells of the rat alpha3/beta4 subtype of neuronal nicotinic acetylcholine receptor. *FEBS Lett.* 397:39-44.

Stewart, N., and Bacchetti, S. 1991. Expression of SV40 large T antigen, but not small t antigen, is required for the induction of chromosomal aberrations in transformed human cells. *Virology.* 180:49-57.

Stewart, R., Song, L., Carter, S.M., Sigalas, C., Zaccai, N.R., Kanamarlapudi, V., Bhat, M.B., Takeshima, H., and Sitsapesan, R. 2008. Single-Channel Characterization of the Rabbit Recombinant RyR2 Reveals a Novel Inactivation Property of Physiological Concentrations of ATP. *J Membr Biol.*

Stoyanovsky, D., Murphy, T., Anno, P.R., Kim, Y.M., and Salama, G. 1997. Nitric oxide activates skeletal and cardiac ryanodine receptors. *Cell Calcium.* 21:19-29.

Sudhof, T.C., Newton, C.L., Archer, B.T., 3rd, Ushkaryov, Y.A., and Mignery, G.A. 1991. Structure of a novel IP_3 receptor. *Embo J.* 10:3199-3206.

Sugawara, H., Kurosaki, M., Takata, M., and Kurosaki, T. 1997. Genetic evidence for involvement of type 1, type 2 and type 3 inositol 1,4,5-trisphosphate receptors in signal transduction through the B-cell antigen receptor. *Embo J.* 16:3078-3088.

Sumitomo, N., Harada, K., Nagashima, M., Yasuda, T., Nakamura, Y., Aragaki, Y., Saito, A., Kurosaki, K., Jouo, K., Koujiro, M., Konishi, S., Matsuoka, S., Oono, T., Hayakawa, S., Miura, M., Ushinohama, H., Shibata, T., and Niimura, I. 2003. Catecholaminergic polymorphic ventricular tachycardia: electrocardiographic characteristics and optimal therapeutic strategies to prevent sudden death. *Heart.* 89:66-70.

Sun, J., Xin, C., Eu, J.P., Stamler, J.S., and Meissner, G. 2001. Cysteine-3635 is responsible for skeletal muscle ryanodine receptor modulation by NO. *Proc Natl Acad Sci U S A.* 98:11158-11162.

Suzuki, Y., Imai, Y., Nakayama, H., Takahashi, K., Takio, K., and Takahashi, R. 2001. A serine protease, HtrA2, is released from the mitochondria and interacts with XIAP, inducing cell death. *Mol Cell.* 8:613-621.

Swan, H., Laitinen, P., Kontula, K., and Toivonen, L. 2005. Calcium channel antagonism reduces exercise-induced ventricular arrhythmias in catecholaminergic polymorphic ventricular tachycardia patients with RyR2 mutations. *J Cardiovasc Electrophysiol.* 16:162-166.

Swan, H., Piippo, K., Viitasalo, M., Heikkila, P., Paavonen, T., Kainulainen, K., Kere, J., Keto, P., Kontula, K., and Toivonen, L. 1999. Arrhythmic disorder mapped to chromosome 1q42-q43 causes malignant polymorphic ventricular tachycardia in structurally normal hearts. *J Am Coll Cardiol.* 34:2035-2042.

Szado, T., Vanderheyden, V., Parys, J.B., De Smedt, H., Rietdorf, K., Kotelevets, L., Chastre, E., Khan, F., Landegren, U., Soderberg, O., Bootman, M.D., and Roderick, H.L. 2008. Phosphorylation of inositol 1,4,5-trisphosphate receptors by protein kinase B/Akt inhibits Ca^{2+} release and apoptosis. *Proc Natl Acad Sci U S A.* 105:2427-2432.

Szalai, G., Krishnamurthy, R., and Hajnoczky, G. 1999. Apoptosis driven by IP_3-linked mitochondrial calcium signals. *Embo J.* 18:6349-6361.

Takagishi, Y., Yasui, K., Severs, N.J., and Murata, Y. 2000. Species-specific difference in distribution of voltage-gated L-type Ca^{2+} channels of cardiac myocytes. *Am J Physiol Cell Physiol.* 279:C1963-1969.

Takasago, T., Imagawa, T., Furukawa, K., Ogurusu, T., and Shigekawa, M. 1991. Regulation of the cardiac ryanodine receptor by protein kinase-dependent phosphorylation. *J Biochem (Tokyo).* 109:163-170.

Takekura, H., Paolini, C., Franzini-Armstrong, C., Kugler, G., Grabner, M., and Flucher, B.E. 2004. Differential contribution of skeletal and cardiac II-III loop sequences to the assembly of dihydropyridine-receptor arrays in skeletal muscle. *Mol Biol Cell.* 15:5408-5419.

Takeshima, H., Iino, M., Takekura, H., Nishi, M., Kuno, J., Minowa, O., Takano, H., and Noda, T. 1994a. Excitation-contraction uncoupling and muscular degeneration in mice lacking functional skeletal muscle ryanodine-receptor gene. *Nature.* 369:556-559.

Takeshima, H., Ikemoto, T., Nishi, M., Nishiyama, N., Shimuta, M., Sugitani, Y., Kuno, J., Saito, I., Saito, H., Endo, M., Iino, M., and Noda, T. 1996. Generation and characterization of mutant mice lacking ryanodine receptor type 3. *J Biol Chem.* 271:19649-19652.

Takeshima, H., Komazaki, S., Hirose, K., Nishi, M., Noda, T., and Iino, M. 1998. Embryonic lethality and abnormal cardiac myocytes in mice lacking ryanodine receptor type 2. *Embo J.* 17:3309-3316.

Takeshima, H., Nishi, M., Iwabe, N., Miyata, T., Hosoya, T., Masai, I., and Hotta, Y. 1994b. Isolation and characterization of a gene for a ryanodine receptor/calcium release channel in Drosophila melanogaster. *FEBS Lett.* 337:81-87.

Takeshima, H., Nishimura, S., Matsumoto, T., Ishida, H., Kangawa, K., Minamino, N., Matsuo, H., Ueda, M., Hanaoka, M., Hirose, T., and et al. 1989. Primary structure and expression from complementary DNA of skeletal muscle ryanodine receptor. *Nature.* 339:439-445.

Talukder, M.A., Kalyanasundaram, A., Zuo, L., Velayutham, M., Nishijima, Y., Periasamy, M., and Zweier, J.L. 2008. Is Reduced SERCA2a Expression Detrimental or Beneficial to Postischemic Cardiac Function and Injury? Evidence from Heterozygous SERCA2a Knockout Mice. *Am J Physiol Heart Circ Physiol.*

Tanabe, T., Fukusaki, M., Terao, Y., Yamashita, K., Sumikawa, K., Mukaida, K., Ibarra, C.A., and Nishino, I. 2008. Malignant hyperthermia susceptibility diagnosed with a family-specific ryanodine receptor gene type 1 mutation. *J Anesth.* 22:70-73.

Tang, T.S., Tu, H., Wang, Z., and Bezprozvanny, I. 2003. Modulation of type 1 inositol (1,4,5)-trisphosphate receptor function by protein kinase a and protein phosphatase 1alpha. *J Neurosci.* 23:403-415.

Tantral, L., Malathi, K., Kohyama, S., Silane, M., Berenstein, A., and Jayaraman, T. 2004. Intracellular calcium release is required for caspase-3 and -9 activation. *Cell Biochem Funct.* 22:35-40.

Tateishi, Y., Hattori, M., Nakayama, T., Iwai, M., Bannai, H., Nakamura, T., Michikawa, T., Inoue, T., and Mikoshiba, K. 2005. Cluster formation of inositol 1,4,5-trisphosphate receptor requires its transition to open state. *J Biol Chem.* 280:6816-6822.

Taylor, C.W., and Richardson, A. 1991. Structure and function of inositol trisphosphate receptors. *Pharmacol Ther.* 51:97-137.

Terentyev, D., Cala, S.E., Houle, T.D., Viatchenko-Karpinski, S., Gyorke, I., Terentyeva, R., Williams, S.C., and Gyorke, S. 2005. Triadin overexpression stimulates excitation-contraction coupling and increases predisposition to cellular arrhythmia in cardiac myocytes. *Circ Res.* 96:651-658.

Terentyev, D., Nori, A., Santoro, M., Viatchenko-Karpinski, S., Kubalova, Z., Gyorke, I., Terentyeva, R., Vedamoorthyrao, S., Blom, N.A., Valle, G., Napolitano, C., Williams, S.C., Volpe, P., Priori, S.G., and Gyorke, S. 2006. Abnormal interactions of calsequestrin with the ryanodine receptor calcium release channel complex linked to exercise-induced sudden cardiac death. *Circ Res.* 98:1151-1158.

Terentyev, D., Viatchenko-Karpinski, S., Gyorke, I., Terentyeva, R., and Gyorke, S. 2003. Protein phosphatases decrease sarcoplasmic reticulum calcium content by stimulating calcium release in cardiac myocytes. *J Physiol.* 552:109-118.

Terracciano, C.M., Hajjar, R.J., and Harding, S.E. 2002. Overexpression of SERCA2a accelerates repolarisation in rabbit ventricular myocytes. *Cell Calcium.* 31:299-305.

Terracciano, C.M., Souza, A.I., Philipson, K.D., and MacLeod, K.T. 1998. Na^+/Ca^{2+} exchange and sarcoplasmic reticular Ca^{2+} regulation in ventricular myocytes from transgenic mice overexpressing the Na^+/Ca^{2+} exchanger. *J Physiol.* 512 (Pt 3):651-667.

Tester, D.J., Dura, M., Carturan, E., Reiken, S., Wronska, A., Marks, A.R., and Ackerman, M.J. 2007. A mechanism for sudden infant death syndrome (SIDS): stress-induced leak via ryanodine receptors. *Heart Rhythm.* 4:733-739.

Tester, D.J., Spoon, D.B., Valdivia, H.H., Makielski, J.C., and Ackerman, M.J. 2004. Targeted mutational analysis of the RyR2-encoded cardiac ryanodine receptor in sudden unexplained death: a molecular autopsy of 49 medical examiner/coroner's cases. *Mayo Clin Proc.* 79:1380-1384.

Thannickal, V.J., and Fanburg, B.L. 2000. Reactive oxygen species in cell signaling. *Am J Physiol Lung Cell Mol Physiol.* 279:L1005-1028.

Thastrup, O., Cullen, P.J., Drobak, B.K., Hanley, M.R., and Dawson, A.P. 1990. Thapsigargin, a tumor promoter, discharges intracellular Ca^{2+} stores by specific inhibition of the endoplasmic reticulum Ca^{2+}-ATPase. *Proc Natl Acad Sci U S A.* 87:2466-2470.

Thimm, J., Mechler, A., Lin, H., Rhee, S., and Lal, R. 2005. Calcium-dependent open/closed conformations and interfacial energy maps of reconstituted hemichannels. *J Biol Chem.* 280:10646-10654.

Thomas, D., Tovey, S.C., Collins, T.J., Bootman, M.D., Berridge, M.J., and Lipp, P. 2000. A comparison of fluorescent Ca^{2+} indicator properties and their use in measuring elementary and global Ca^{2+} signals. *Cell Calcium.* 28:213-223.

Thomas, N.L., George, C.H., and Lai, F.A. 2004. Functional heterogeneity of ryanodine receptor mutations associated with sudden cardiac death. *Cardiovasc. Res.* 64:52-60.

Thomas, N.L., George, C.H., Williams, A.J., and Lai, F.A. 2007. Ryanodine receptor mutations in arrhythmias: advances in understanding the mechanisms of channel dysfunction. *Biochem Soc Trans.* 35:946-951.

Thomas, N.L., Lai, F.A., and George, C.H. 2005. Differential Ca^{2+} sensitivity of RyR2 mutations reveals distinct mechanisms of channel dysfunction in sudden cardiac death. *Biochem Biophys Res Commun.* 331:231-238.

Thrower, E.C., Choe, C.U., So, S.H., Jeon, S.H., Ehrlich, B.E., and Yoo, S.H. 2003. A functional interaction between chromogranin B and the inositol 1,4,5-trisphosphate receptor/Ca^{2+} channel. *J Biol Chem.* 278:49699-49706.

Timerman, A.P., Onoue, H., Xin, H.B., Barg, S., Copello, J., Wiederrecht, G., and Fleischer, S. 1996. Selective binding of FKBP12.6 by the cardiac ryanodine receptor. *J Biol Chem.* 271:20385-20391.

Tinker, A., and Williams, A.J. 1995. Measuring the length of the pore of the sheep cardiac sarcoplasmic reticulum calcium-release channel using related trimethylammonium ions as molecular calipers. *Biophys J.* 68:111-120.

Tiso, N., Stephan, D.A., Nava, A., Bagattin, A., Devaney, J.M., Stanchi, F., Larderet, G., Brahmbhatt, B., Brown, K., Bauce, B., Muriago, M., Basso, C., Thiene, G., Danieli, G.A., and Rampazzo, A. 2001. Identification of mutations in the cardiac ryanodine receptor gene in families affected with arrhythmogenic right ventricular cardiomyopathy type 2 (ARVD2). *Hum Mol Genet.* 10:189-194.

Tojyo, Y., Tanimura, A., and Matsumoto, Y. 1997. Imaging of intracellular Ca^{2+} waves induced by muscarinic receptor stimulation in rat parotid acinar cells. *Cell Calcium.* 22:455-462.

Tokuhisa, T., Yano, M., Obayashi, M., Noma, T., Mochizuki, M., Oda, T., Okuda, S., Doi, M., Liu, J., Ikeda, Y., Yamamoto, T., Ohkusa, T., and Matsuzaki, M. 2006. AT1 receptor antagonist restores cardiac ryanodine receptor function, rendering isoproterenol-induced failing heart less susceptible to Ca^{2+} -leak induced by oxidative stress. *Circ J.* 70:777-786.

Tong, J., Du, G.G., Chen, S.R., and MacLennan, D.H. 1999. HEK-293 cells possess a carbachol- and thapsigargin-sensitive intracellular Ca^{2+} store that is responsive to stop-flow medium changes and insensitive to caffeine and ryanodine. *Biochem J.* 343 Pt 1:39-44.

Toyofuku, T., Kurzydlowski, K., Tada, M., and MacLennan, D.H. 1994. Amino acids Glu2 to Ile18 in the cytoplasmic domain of phospholamban are essential for functional association with the Ca^{2+}-ATPase of sarcoplasmic reticulum. *J Biol Chem.* 269:3088-3094.

Treves, S., De Mattei, M., Landfredi, M., Villa, A., Green, N.M., MacLennan, D.H., Meldolesi, J., and Pozzan, T. 1990. Calreticulin is a candidate for a calsequestrin-like function in Ca2(+)-storage compartments (calciosomes) of liver and brain. *Biochem J.* 271:473-480.

Treves, S., Pouliquin, R., Moccagatta, L., and Zorzato, F. 2002. Functional properties of EGFP-tagged skeletal muscle calcium-release channel (ryanodine receptor) expressed in COS-7 cells: sensitivity to caffeine and 4-chloro-m-cresol. *Cell Calcium.* 31:1-12.

Triantafilou, M., and Triantafilou, K. 2004. Heat-shock protein 70 and heat-shock protein 90 associate with Toll-like receptor 4 in response to bacterial lipopolysaccharide. *Biochem Soc Trans.* 32:636-639.

Tripathy, A., and Meissner, G. 1996. Sarcoplasmic reticulum lumenal Ca^{2+} has access to cytosolic activation and inactivation sites of skeletal muscle Ca^{2+} release channel. *Biophys J.* 70:2600-2615.

Trump, B.F., and Berezesky, I.K. 1992. The role of cytosolic Ca^{2+} in cell injury, necrosis and apoptosis. *Curr Opin Cell Biol.* 4:227-232.

Trump, B.F., and Berezesky, I.K. 1996. The role of altered $[Ca^{2+}]_i$ regulation in apoptosis, oncosis, and necrosis. *Biochim Biophys Acta.* 1313:173-178.

Trump, B.F., Berezesky, I.K., Chang, S.H., and Phelps, P.C. 1997. The pathways of cell death: oncosis, apoptosis, and necrosis. *Toxicol Pathol.* 25:82-88.

Tsien, R.Y. 1980. New calcium indicators and buffers with high selectivity against magnesium and protons: design, synthesis, and properties of prototype structures. *Biochemistry.* 19:2396-2404.

Tsien, R.Y. 1992. Intracellular signal transduction in four dimensions: from molecular design to physiology. *Am J Physiol.* 263:C723-728.

Tsukamoto, A., and Kaneko, Y. 1993. Thapsigargin, a Ca^{2+}-ATPase inhibitor, depletes the intracellular Ca^{2+} pool and induces apoptosis in human hepatoma cells. *Cell Biol Int.* 17:969-970.

Tu, J.C., Xiao, B., Yuan, J.P., Lanahan, A.A., Leoffert, K., Li, M., Linden, D.J., and Worley, P.F. 1998. Homer binds a novel proline-rich motif and links group 1 metabotropic glutamate receptors with IP_3 receptors. *Neuron.* 21:717-726.

Tu, Q., Velez, P., Brodwick, M., and Fill, M. 1994. Streaming potentials reveal a short ryanodine-sensitive selectivity filter in cardiac Ca^{2+} release channel. *Biophys J.* 67:2280-2285.

Tunwell, R.E.A., Wickenden, C., Bertrand, B.M.A., Shevchenko, V.I., Walsh, M.B., Allen, P.D., and Lai, F.A. 1996. The human cardiac muscle ryanodine receptor-calcium release channel: identification, primary structure and topological analysis. *J. Biochem.* 318:477-487.

Uchida, K., Miyauchi, H., Furuichi, T., Michikawa, T., and Mikoshiba, K. 2003. Critical regions for activation gating of the inositol 1,4,5-trisphosphate receptor. *J Biol Chem.* 278:16551-16560.

Udawatte, C., and Ripps, H. 2005. The spread of apoptosis through gap-junctional channels in BHK cells transfected with Cx32. *Apoptosis.* 10:1019-1029.

Uehara, A., Yasukochi, M., Mejia-Alvarez, R., Fill, M., and Imanaga, I. 2002. Gating kinetics and ligand sensitivity modified by phosphorylation of cardiac ryanodine receptors. *Pflugers Arch.* 444:202-212.

Uhlen, P. 2004. Spectral analysis of calcium oscillations. *Sci STKE.* 2004:pl15.

Valdivia, H.H., Kaplan, J.H., Ellis-Davies, G.C., and Lederer, W.J. 1995. Rapid adaptation of cardiac ryanodine receptors: modulation by Mg^{2+} and phosphorylation. *Science.* 267:1997-2000.

Valko, M., Leibfritz, D., Moncol, J., Cronin, M.T., Mazur, M., and Telser, J. 2007. Free radicals and antioxidants in normal physiological functions and human disease. *Int J Biochem Cell Biol.* 39:44-84.

Van Delden, C., Foti, M., Lew, D.P., and Krause, K.H. 1993. Ca^{2+} and Mg^{2+} regulation of inositol 1,4,5-triphosphate binding in myeloid cells. *J Biol Chem.* 268:12443-12448.

Vangheluwe, P., Tjwa, M., Van Den Bergh, A., Louch, W.E., Beullens, M., Dode, L., Carmeliet, P., Kranias, E., Herijgers, P., Sipido, K.R., Raeymaekers, L., and Wuytack, F. 2006. A SERCA2 pump with an increased Ca^{2+} affinity can lead to severe cardiac hypertrophy, stress intolerance and reduced life span. *J Mol Cell Cardiol.* 41:308-317.

Varnai, P., Balla, A., Hunyady, L., and Balla, T. 2005. Targeted expression of the inositol 1,4,5-triphosphate receptor (IP_3R) ligand-binding domain releases Ca^{2+} via endogenous IP_3R channels. *Proc Natl Acad Sci U S A.* 102:7859-7864.

Veenstra, R.D. 1996. Size and selectivity of gap junction channels formed from different connexins. *J Bioenerg Biomembr.* 28:327-337.

Veenstra, R.D. 2001. Determining ionic permeabilities of gap junction channels. *Methods Mol Biol.* 154:293-311.

Verhoven, B., Schlegel, R.A., and Williamson, P. 1995. Mechanisms of phosphatidylserine exposure, a phagocyte recognition signal, on apoptotic T lymphocytes. *J Exp Med.* 182:1597-1601.

Vermassen, E., Parys, J.B., and Mauger, J.P. 2004. Subcellular distribution of the inositol 1,4,5-trisphosphate receptors: functional relevance and molecular determinants. *Biol Cell.* 96:3-17.

Verselis, V.K., Trexler, E.B., and Bukauskas, F.F. 2000. Connexin hemichannels and cell-cell channels: comparison of properties. *Braz J Med Biol Res.* 33:379-389.

Vest, J.A., Wehrens, X.H.T., Reiken, S.R., Lehnart, S.E., Dobrev, D., Chandra, P., Danilo, P., Ravens, U., Rosen, M.R., and Marks, A.R. 2005. Defective cardiac ryanodine receptor regulation during atrial fibrillation. *Circulation.* 111:2025-2032.

Viatchenko-Karpinski, S., Terentyev, D., Gyorke, I., Terentyeva, R., Volpe, P., Priori, S.G., Napolitano, C., Nori, A., Williams, S.C., and Gyorke, S. 2004. Abnormal calcium signaling and sudden cardiac death associated with mutation of calsequestrin. *Circ Res.* 94:471-477.

Vila-Petroff, M., Salas, M.A., Said, M., Valverde, C.A., Sapia, L., Portiansky, E., Hajjar, R.J., Kranias, E.G., Mundina-Weilenmann, C., and Mattiazzi, A. 2007. CaMKII inhibition protects against necrosis and apoptosis in irreversible ischemia-reperfusion injury. *Cardiovasc Res.* 73:689-698.

Vines, A.M., Lyng, F.M., McClean, B., Seymour, C., and Mothersill, C.E. 2008. Bystander signal production and response are independent processes which are cell line dependent. *Int J Radiat Biol.* 84:83-90.

Volpe, P., and Vezu, L. 1993. Intracellular magnesium and inositol 1,4,5-trisphosphate receptor: molecular mechanisms of interaction, physiology and pharmacology. *Magnes Res.* 6:267-274.

Wagenknecht, T., Grassucci, R., Berkowitz, J., Wiederrecht, G.J., Xin, H.B., and Fleischer, S. 1996. Cryoelectron microscopy resolves FK506-binding protein sites on the skeletal muscle ryanodine receptor. *Biophys J.* 70:1709-1715.

Wakimoto, K., Kobayashi, K., Kuro, O.M., Yao, A., Iwamoto, T., Yanaka, N., Kita, S., Nishida, A., Azuma, S., Toyoda, Y., Omori, K., Imahie, H., Oka, T., Kudoh, S., Kohmoto, O., Yazaki, Y., Shigekawa, M., Imai, Y., Nabeshima, Y., and Komuro, I. 2000. Targeted disruption of Na^+/Ca^{2+} exchanger gene leads to cardiomyocyte apoptosis and defects in heartbeat. *J Biol Chem.* 275:36991-36998.

Walsh, K.B., Zhang, J., Fuseler, J.W., Hilliard, N., and Hockerman, G.H. 2007. Adenoviral-mediated expression of dihydropyridine-insensitive L-type calcium channels in cardiac ventricular myocytes and fibroblasts. *Eur J Pharmacol.* 565:7-16.

Wang, J.P., Needleman, D.H., Seryshev, A.B., Aghdasi, B., Slavik, K.J., Liu, S.Q., Pedersen, S.E., and Hamilton, S.L. 1996. Interaction between ryanodine and neomycin binding sites on Ca^{2+} release channel from skeletal muscle sarcoplasmic reticulum. *J Biol Chem.* 271:8387-8393.

Wang, R., Bolstad, J., Kong, H., Zhang, L., Brown, C., and Chen, S.R. 2004. The predicted TM10 transmembrane sequence of the cardiac Ca^{2+} release channel (ryanodine receptor) is crucial for channel activation and gating. *J Biol Chem.* 279:3635-3642.

Wang, R., Zhang, L., Bolstad, J., Diao, N., Brown, C., Ruest, L., Welch, W., Williams, A.J., and Chen, S.R. 2003. Residue Gln4863 within a predicted transmembrane sequence of the Ca^{2+} release channel (ryanodine receptor) is critical for ryanodine interaction. *J Biol Chem.* 278:51557-51565.

Wang, S., and El-Deiry, W.S. 2004. Cytochrome C: a crosslink between the mitochondria and the endoplasmic reticulum in calcium-dependent apoptosis. *Cancer Biol Ther.* 3:44-46.

Wang, X.J. 1998. Calcium coding and adaptive temporal computation in cortical pyramidal neurons. *J Neurophysiol.* 79:1549-1566.

Waring, P. 2005. Redox active calcium ion channels and cell death. *Arch Biochem Biophys.* 434:33-42.

Weber, P.A., Chang, H.C., Spaeth, K.E., Nitsche, J.M., and Nicholson, B.J. 2004. The permeability of gap junction channels to probes of different size is dependent on connexin composition and permeant-pore affinities. *Biophys J.* 87:958-973.

Wehrens, X.H., Lehnart, S.E., Huang, F., Vest, J.A., Reiken, S.R., Mohler, P.J., Sun, J., Guatimosim, S., Song, L.S., Rosemblit, N., D'Armiento, J.M., Napolitano, C., Memmi, M., Priori, S.G., Lederer, W.J., and Marks, A.R. 2003. FKBP12.6 deficiency and defective calcium release channel (ryanodine receptor) function linked to exercise-induced sudden cardiac death. *Cell.* 113:829-840.

Wehrens, X.H., Lehnart, S.E., and Marks, A.R. 2005a. Ryanodine receptor-targeted anti-arrhythmic therapy. *Ann N Y Acad Sci.* 1047:366-375.

Wehrens, X.H., Lehnart, S.E., Reiken, S., Vest, J.A., Wronska, A., and Marks, A.R. 2006. Ryanodine receptor/calcium release channel PKA phosphorylation: a critical mediator of heart failure progression. *Proc Natl Acad Sci U S A.* 103:511-518.

Wehrens, X.H., Lehnart, S.E., Reiken, S.R., Deng, S.X., Vest, J.A., Cervantes, D., Coromilas, J., Landry, D.W., and Marks, A.R. 2004a. Protection from cardiac arrhythmia through ryanodine receptor-stabilizing protein calstabin2. *Science.* 304:292-296.

Wehrens, X.H., Lehnart, S.E., Reiken, S.R., and Marks, A.R. 2004b. Ca^{2+}/calmodulin-dependent protein kinase II phosphorylation regulates the cardiac ryanodine receptor. *Circ Res.* 94:e61-70.

Wehrens, X.H., and Marks, A.R. 2002. Myocardial disease in failing hearts: defective excitation-contraction coupling. *Cold Spring Harb Symp Quant Biol.* 67:533-541.

Wehrens, X.H.T., Lehnart, S.E., Reiken, S., van der Nagel, R., Morales, R., Sun, J., Cheng, Z., Deng, S.-X., de Windt, L.J., Landry, D.W., and Marks, A.R. 2005b. Enhancing calstabin binding to ryanodine receptors improves cardiac and skeletal muscle function in heart failure. *PNAS.* 102:9607-9612.

Wehrens, X.H.T., and Marks, A.R. 2004. Novel therapeutic approaches for heart failure by normalizing calcium cycling. *Nat. Rev. Drug. Discov.* 3:1-8.

Wei, S.K., Colecraft, H.M., DeMaria, C.D., Peterson, B.Z., Zhang, R., Kohout, T.A., Rogers, T.B., and Yue, D.T. 2000. Ca^{2+} channel modulation by recombinant auxiliary beta subunits expressed in young adult heart cells. *Circ Res.* 86:175-184.

Weisleder, N., and Ma, J.J. 2006. Ca^{2+} sparks as a plastic signal for skeletal muscle health, aging, and dystrophy. *Acta Pharmacol Sin.* 27:791-798.

Werner, B., Przybylski, A., Kucinska, B., Lewandowski, M., Szwed, H., and Wroblewska-Kaluzewska, M. 2004. Implantable cardioverter-defibrillators in children. *Kardiol Pol.* 60:239-246.

White, A.M., Varney, M.A., Maeda, N., Mikoshiba, K., and Watson, S.P. 1993. Comparison of Ins(1,4,5)P_3 receptors from rat cerebellum and bovine adrenal cortex. *Biochim Biophys Acta.* 1175:307-311.

White, C., and McGeown, J.G. 2002. Carbachol triggers RyR-dependent Ca^{2+} release via activation of IP_3 receptors in isolated rat gastric myocytes. *J Physiol.* 542:725-733.

Wier, W.G., and Balke, C.W. 1999. Ca^{2+} release mechanisms, Ca^{2+} sparks, and local control of excitation-contraction coupling in normal heart muscle. *Circ Res.* 85:770-776.

Williams, A.J. 1992. Ion conduction and discrimination in the sarcoplasmic reticulum ryanodine receptor/calcium-release channel. *J Muscle Res Cell Motil.* 13:7-26.

Williams, A.J., West, D.J., and Sitsapesan, R. 2001. Light at the end of the Ca^{2+}-release channel tunnel: structures and mechanisms involved in ion translocation in ryanodine receptor channels. *Q Rev Biophys.* 34:61-104.

Wilson, M.R., Close, T.W., and Trosko, J.E. 2000. Cell population dynamics (apoptosis, mitosis, and cell-cell communication) during disruption of homeostasis. *Exp Cell Res.* 254:257-268.

Witcher, D.R., Kovacs, R.J., Schulman, H., Cefali, D.C., and Jones, L.R. 1991. Unique phosphorylation site on the cardiac ryanodine receptor regulates calcium channel activity. *J Biol Chem.* 266:11144-11152.

Wojcikiewicz, R.J. 1995. Type I, II, and III inositol 1,4,5-trisphosphate receptors are unequally susceptible to down-regulation and are expressed in markedly different proportions in different cell types. *J Biol Chem.* 270:11678-11683.

Wood, A.W., and Cadusch, P.J. 2005. Cell calcium oscillations: the origin of their variability. *Med Biol Eng Comput.* 43:200-205.

Wu, G., Long, X., and Marin-Garcia, J. 2004. Adenoviral SERCA1 overexpression triggers an apoptotic response in cultured neonatal but not in adult rat cardiomyocytes. *Mol Cell Biochem.* 267:123-132.

Wu, Y., Aghdasi, B., Dou, S.J., Zhang, J.Z., Liu, S.Q., and Hamilton, S.L. 1997. Functional interactions between cytoplasmic domains of the skeletal muscle Ca^{2+} release channel. *J Biol Chem.* 272:25051-25061.

Xiao, B., Jiang, M.T., Zhao, M., Yang, D., Sutherland, C., Lai, F.A., Walsh, M.P., Warltier, D.C., Cheng, H., and Chen, S.R. 2005. Characterization of a novel PKA phosphorylation site, serine-2030, reveals no PKA hyperphosphorylation of the cardiac ryanodine receptor in canine heart failure. *Circ Res.* 96:847-855.

Xiao, B., Masumiya, H., Jiang, D., Wang, R., Sei, Y., Zhang, L., Murayama, T., Ogawa, Y., Lai, F.A., Wagenknecht, T., and Chen, S.R. 2002. Isoform-dependent formation of heteromeric Ca^{2+} release channels (ryanodine receptors). *J Biol Chem.* 277:41778-41785.

Xiao, B., Sutherland, C., Walsh, M.P., and Chen, S.R. 2004. Protein kinase A phosphorylation at serine-2808 of the cardiac Ca^{2+}-release channel (ryanodine receptor) does not dissociate 12.6-kDa FK506-binding protein (FKBP12.6). *Circ Res.* 94:487-495.

Xiao, B., Zhong, G., Obayashi, M., Yang, D., Chen, K., Walsh, M.P., Shimoni, Y., Cheng, H., Ter Keurs, H., and Chen, S.R. 2006. Ser-2030, but not Ser-2808, is the major phosphorylation site in cardiac ryanodine receptors responding to protein kinase A activation upon beta-adrenergic stimulation in normal and failing hearts. *Biochem J.* 396:7-16.

Xiao, J., Tian, X., Jones, P.P., Bolstad, J., Kong, H., Wang, R., Zhang, L., Duff, H.J., Gillis, A.M., Fleischer, S., Kotlikoff, M., Copello, J.A., and Chen, S.R. 2007. Removal of FKBP12.6 does not alter the conductance and activation of the cardiac ryanodine receptor or the susceptibility to stress-induced ventricular arrhythmias. *J Biol Chem.* 282:34828-34838.

Xiong, L., Zhang, J.Z., He, R., and Hamilton, S.L. 2006. A Ca^{2+}-binding domain in RyR1 that interacts with the calmodulin binding site and modulates channel activity. *Biophys J.* 90:173-182.

Xu, L., Eu, J.P., Meissner, G., and Stamler, J.S. 1998. Activation of the cardiac calcium release channel (ryanodine receptor) by poly-S-nitrosylation. *Science.* 279:234-237.

Xu, L., and Meissner, G. 1998. Regulation of cardiac muscle Ca^{2+} release channel by sarcoplasmic reticulum lumenal Ca^{2+}. *Biophys J.* 75:2302-2312.

Xu, L., and Meissner, G. 2004. Mechanism of calmodulin inhibition of cardiac sarcoplasmic reticulum Ca^{2+} release channel (ryanodine receptor). *Biophys J.* 86:797-804.

Yagi, H., Horinaka, S., and Matsuoka, H. 2005. Edaravone prevented deteriorated cardiac function after myocardial ischemia-reperfusion via inhibiting lipid peroxidation in rat. *J Cardiovasc Pharmacol.* 46:46-51.

Yamada, N., Makino, Y., Clark, R.A., Pearson, D.W., Mattei, M.G., Guenet, J.L., Ohama, E., Fujino, I., Miyawaki, A., Furuichi, T., and et al. 1994. Human inositol 1,4,5-trisphosphate type-1 receptor, IP_3R1: structure, function, regulation of expression and chromosomal localization. *Biochem J.* 302 (Pt 3):781-790.

Yamaguchi, N., Takahashi, N., Xu, L., Smithies, O., and Meissner, G. 2007. Early cardiac hypertrophy in mice with impaired calmodulin regulation of cardiac muscle Ca^{2+} release channel. *J Clin Invest.* 117:1344-1353.

Yamamoto-Hino, M., Miyawaki, A., Kawano, H., Sugiyama, T., Furuichi, T., Hasegawa, M., and Mikoshiba, K. 1995. Immunohistochemical study of inositol 1,4,5-trisphosphate receptor type 3 in rat central nervous system. *Neuroreport.* 6:273-276.

Yamamoto-Hino, M., Sugiyama, T., Hikichi, K., Mattei, M.G., Hasegawa, K., Sekine, S., Sakurada, K., Miyawaki, A., Furuichi, T., Hasegawa, M., and et al. 1994. Cloning and characterization of human type 2 and type 3 inositol 1,4,5-trisphosphate receptors. *Receptors Channels.* 2:9-22.

Yamamoto, T., El-Hayek, R., and Ikemoto, N. 2000. Postulated role of interdomain interaction within the ryanodine receptor in Ca^{2+} channel regulation. *J Biol Chem.* 275:11618-11625.

Yamawaki, M., Sasaki, N., Shimoyama, M., Miake, J., Ogino, K., Igawa, O., Tajima, F., Shigemasa, C., and Hisatome, I. 2004. Protective effect of edaravone against hypoxia-reoxygenation injury in rabbit cardiomyocytes. *Br J Pharmacol.* 142:618-626.

Yamori, Y. 1998. The correlation between gap junction-mediated communication and cell proliferation among retinal pigment epithelial cells. *Nippon Ganka Gakkai Zasshi.* 102:481-486.

Yan, Y., Liu, J., Wei, C., Li, K., Xie, W., Wang, Y., and Cheng, H. 2008. Bidirectional regulation of Ca2+ sparks by mitochondria-derived reactive oxygen species in cardiac myocytes. *Cardiovasc Res.* 77:432-441.

Yang, J., McBride, S., Mak, D.O., Vardi, N., Palczewski, K., Haeseleer, F., and Foskett, J.K. 2002. Identification of a family of calcium sensors as protein ligands of inositol trisphosphate receptor Ca^{2+} release channels. *Proc Natl Acad Sci U S A.* 99:7711-7716.

Yang, T., Riehl, J., Esteve, E., Matthaei, K.I., Goth, S., Allen, P.D., Pessah, I.N., and Lopez, J.R. 2006a. Pharmacologic and functional characterization of malignant hyperthermia in the R163C RyR1 knock-in mouse. *Anesthesiology.* 105:1164-1175.

Yang, Z., Ikemoto, N., Lamb, G.D., and Steele, D.S. 2006b. The RyR2 central domain peptide DPc10 lowers the threshold for spontaneous Ca^{2+} release in permeabilized cardiomyocytes. *Cardiovasc Res.* 70:475-485.

Yano, M., Okuda, S., Oda, T., Tokuhisa, T., Tateishi, H., Mochizuki, M., Noma, T., Doi, M., Kobayashi, S., Yamamoto, T., Ikeda, Y., Ohkusa, T., Ikemoto, N., and Matsuzaki, M. 2005a. Correction of defective interdomain interaction within ryanodine receptor by antioxidant is a new therapeutic strategy against heart failure. *Circulation.* 112:3633-3643.

Yano, M., Yamamoto, T., Ikeda, Y., and Matsuzaki, M. 2006. Mechanisms of Disease: ryanodine receptor defects in heart failure and fatal arrhythmia. *Nat Clin Pract Cardiovasc Med.* 3:43-52.

Yano, M., Yamamoto, T., Ikemoto, N., and Matsuzaki, M. 2005b. Abnormal ryanodine receptor function in heart failure. *Pharmacol Ther.* 107:377-391.

Yao, X., Liu, W., Tian, S., Rafi, H., Segal, A.S., and Desir, G.V. 2000. Close association of the N terminus of $K_v1.3$ with the pore region. *J Biol Chem.* 275:10859-10863.

Ye, Z.C., Wyeth, M.S., Baltan-Tekkok, S., and Ransom, B.R. 2003. Functional hemichannels in astrocytes: a novel mechanism of glutamate release. *J Neurosci.* 23:3588-3596.

Yeung, H.M., Kravtsov, G.M., Ng, K.M., Wong, T.M., and Fung, M.L. 2007. Chronic intermittent hypoxia alters Ca^{2+} handling in rat cardiomyocytes by augmented Na^{+}/Ca^{2+} exchange and ryanodine receptor activities in ischemia-reperfusion. *Am J Physiol Cell Physiol.* 292:C2046-2056.

Yin, C.C., Blayney, L.M., and Lai, F.A. 2005a. Physical coupling between ryanodine receptor-calcium release channels. *J Mol Biol.* 349:538-546.

Yin, C.C., Han, H., Wei, R., and Lai, F.A. 2005b. Two-dimensional crystallization of the ryanodine receptor Ca^{2+} release channel on lipid membranes. *J Struct Biol.* 149:219-224.

Yoshida, Y., and Imai, S. 1997. Structure and function of inositol 1,4,5-trisphosphate receptor. *Jpn J Pharmacol.* 74:125-137.

Yoshikawa, F., Iwasaki, H., Michikawa, T., Furuichi, T., and Mikoshiba, K. 1999. Cooperative formation of the ligand-binding site of the inositol 1,4, 5-trisphosphate receptor by two separable domains. *J Biol Chem.* 274:328-334.

Yoshikawa, F., Morita, M., Monkawa, T., Michikawa, T., Furuichi, T., and Mikoshiba, K. 1996. Mutational analysis of the ligand binding site of the inositol 1,4,5-trisphosphate receptor. *J Biol Chem.* 271:18277-18284.

Yuan, Q., Fan, G.C., Dong, M., Altschafl, B., Diwan, A., Ren, X., Hahn, H.H., Zhao, W., Waggoner, J.R., Jones, L.R., Jones, W.K., Bers, D.M., Dorn, G.W., 2nd, Wang, H.S., Valdivia, H.H., Chu, G., and Kranias, E.G. 2007. Sarcoplasmic reticulum calcium overloading in junctin deficiency enhances cardiac contractility but increases ventricular automaticity. *Circulation.* 115:300-309.

Zaffaroni, N., Pennati, M., and Daidone, M.G. 2005. Survivin as a target for new anticancer interventions. *J Cell Mol Med.* 9:360-372.

Zent, R., Ailenberg, M., Downey, G.P., and Silverman, M. 1999. ROS stimulate reorganization of mesangial cell-collagen gels by tyrosine kinase signaling. *Am J Physiol.* 276:F278-287.

Zhang, G., Gurtu, V., and Kain, S.R. 1996. An enhanced green fluorescent protein allows sensitive detection of gene transfer in mammalian cells. *Biochem Biophys Res Commun.* 227:707-711.

Zhang, J., Liu, Z., Masumiya, H., Wang, R., Jiang, D., Li, F., Wagenknecht, T., and Chen, S.R. 2003. Three-dimensional localization of divergent region 3 of the ryanodine receptor to the clamp-shaped structures adjacent to the FKBP binding sites. *J Biol Chem.* 278:14211-14218.

Zhang, L., Franzini-Armstrong, C., Ramesh, V., and Jones, L.R. 2001. Structural alterations in cardiac calcium release units resulting from overexpression of junctin. *J Mol Cell Cardiol.* 33:233-247.

Zhang, L., Kelley, J., Schmeisser, G., Kobayashi, Y.M., and Jones, L.R. 1997. Complex formation between junctin, triadin, calsequestrin, and the ryanodine receptor. Proteins of the cardiac junctional sarcoplasmic reticulum membrane. *J Biol Chem.* 272:23389-23397.

Zhang, S., Liu, W., He, P., Gong, F., and Yang, D. 2006. Establishment of stable high expression cell line with green fluorescent protein and resistance genes. *J Huazhong Univ Sci Technolog Med Sci.* 26:298-300.

Zhang, Y., Chen, H.S., Khanna, V.K., De Leon, S., Phillips, M.S., Schappert, K., Britt, B.A., Browell, A.K., and MacLennan, D.H. 1993. A mutation in the human ryanodine receptor gene associated with central core disease. *Nat Genet.* 5:46-50.

Zhao, W., Meiri, N., Xu, H., Cavallaro, S., Quattrone, A., Zhang, L., and Alkon, D.L. 2000. Spatial learning induced changes in expression of the ryanodine type II receptor in the rat hippocampus. *Faseb J.* 14:290-300.

Zhou, H., Jungbluth, H., Sewry, C.A., Feng, L., Bertini, E., Bushby, K., Straub, V., Roper, H., Rose, M.R., Brockington, M., Kinali, M., Manzur, A., Robb, S., Appleton, R., Messina, S., D'Amico, A., Quinlivan, R., Swash, M., Muller, C.R., Brown, S., Treves, S., and Muntoni, F. 2007. Molecular mechanisms and phenotypic variation in RYR1-related congenital myopathies. *Brain.* 130:2024-2036.

Zhou, H., Yamaguchi, N., Xu, L., Wang, Y., Sewry, C., Jungbluth, H., Zorzato, F., Bertini, E., Muntoni, F., Meissner, G., and Treves, S. 2006. Characterization of recessive RYR1 mutations in core myopathies. *Hum Mol Genet.* 15:2791-2803.

Zhu, D.M., Tekle, E., Chock, P.B., and Huang, C.Y. 1996. Reversible phosphorylation as a controlling factor for sustaining calcium oscillations in HeLa cells: Involvement of calmodulin-dependent kinase II and a calyculin A-inhibitable phosphatase. *Biochemistry*. 35:7214-7223.

Zima, A.V., Bare, D.J., Mignery, G.A., and Blatter, L.A. 2007. IP_3-dependent nuclear Ca^{2+} signaling in the heart. *J Physiol.*

Zima, A.V., and Blatter, L.A. 2004. Inositol-1,4,5-trisphosphate-dependent Ca^{2+} signalling in cat atrial excitation-contraction coupling and arrhythmias. *J Physiol.* 555:607-615.

Zima, A.V., and Blatter, L.A. 2006. Redox regulation of cardiac calcium channels and transporters. *Cardiovasc Res.* 71:310-321.

Zima, A.V., Copello, J.A., and Blatter, L.A. 2004. Effects of cytosolic NADH/NAD^+ levels on sarcoplasmic reticulum Ca^{2+} release in permeabilized rat ventricular myocytes. *J Physiol.* 555:727-741.

Zimanyi, I., Buck, E., Abramson, J.J., Mack, M.M., and Pessah, I.N. 1992. Ryanodine induces persistent inactivation of the Ca^{2+} release channel from skeletal muscle sarcoplasmic reticulum. *Mol Pharmacol.* 42:1049-1057.

Zimanyi, I., and Pessah, I.N. 1991. Comparison of [3H]ryanodine receptors and Ca^{2+} release from rat cardiac and rabbit skeletal muscle sarcoplasmic reticulum. *J Pharmacol Exp Ther.* 256:938-946.

Ziolo, M.T., Martin, J.L., Bossuyt, J., Bers, D.M., and Pogwizd, S.M. 2005. Adenoviral gene transfer of mutant phospholamban rescues contractile dysfunction in failing rabbit myocytes with relatively preserved SERCA function. *Circ Res.* 96:815-817.

Zong, Z.P., Matsui, S., Katsuda, S., Han, J.F., and Fujikawa-Yamamoto, K. 2004. Phorbol myristate induces apoptosis of taxol-resistant sarcoma cells in vitro. *Eur J Pharmacol.* 489:3-11.

Zorzato, F., Fujii, J., Otsu, K., Phillips, M., Green, N.M., Lai, F.A., Meissner, G., and MacLennan, D.H. 1990. Molecular cloning of cDNA encoding human and rabbit forms of the Ca^{2+} release channel (ryanodine receptor) of skeletal muscle sarcoplasmic reticulum. *J Biol Chem.* 265:2244-2256.

Zorzato, F., Menegazzi, P., Treves, S., and Ronjat, M. 1996. Role of malignant hyperthermia domain in the regulation of Ca^{2+} release channel (ryanodine receptor) of skeletal muscle sarcoplasmic reticulum. *J Biol Chem.* 271:22759-22763.